Production of fine and platform chemicals from microalgae

The Chemicalgal plant concept

Yann Lie

PhD

University of York
Department of Chemistry – Green Chemistry Centre of Excellence

December 2020

Abstract

Climate change, related ecological catastrophes, and fossil-resource depletion are now pushing all actors of society to find solutions to pressing sustainability issues. Green chemistry was born at the end of the 20th century and contributed to the rise in ecological awareness amongst chemists. Biorefinery concepts, and metrics intimately associated with green chemistry, have evolved over the years to adapt and perfect their design to current problems. However, most metrics lack a visual representation, and none of them quantifies the logic of chemical routes. In addition, current biorefinery concepts rely on lignocellulosic feedstocks whose usage potentially disrupts natural geochemical cycles and agricultural systems.

Herein, a computational tool offering a visual representation of chemical routes and assessing the rationality of such was designed. Modifications of the van Krevelen diagram led to the so-called *BioLogicTool,* providing a visual and quantitative tool to determine the logic of chemical pathways. Emphasis is being made to compare bio-derived routes to drop-in replacements or alternatives to fossil-derived chemicals. Throughout this work, examples are given to demonstrate the use of the *BioLogicTool*.

Secondly, a concept for a third-phase and third-generation microalgal biorefinery is developed (*Chemicalgal plant*). The CMF reaction, central to the concept, was successfully applied to microalgae allowing the valorisation of microalgal carbohydrates into CMF. This compound and other potential microalgae-derivable platform molecules were then used to synthesise UV-filters, photopolymers, and surfactants, the latter using fatty alcohols obtainable from microalgal fatty acids. Lastly, the two most abundant amino acids in these microalgae, glutamic acid and lysine, were thermally decarboxylated to γ-aminobutyric acid and 1,5-pentanediamine, respectively. The latter was used for the production of a bio-based non-isocyanate polyurethane with self-blowing behaviour.

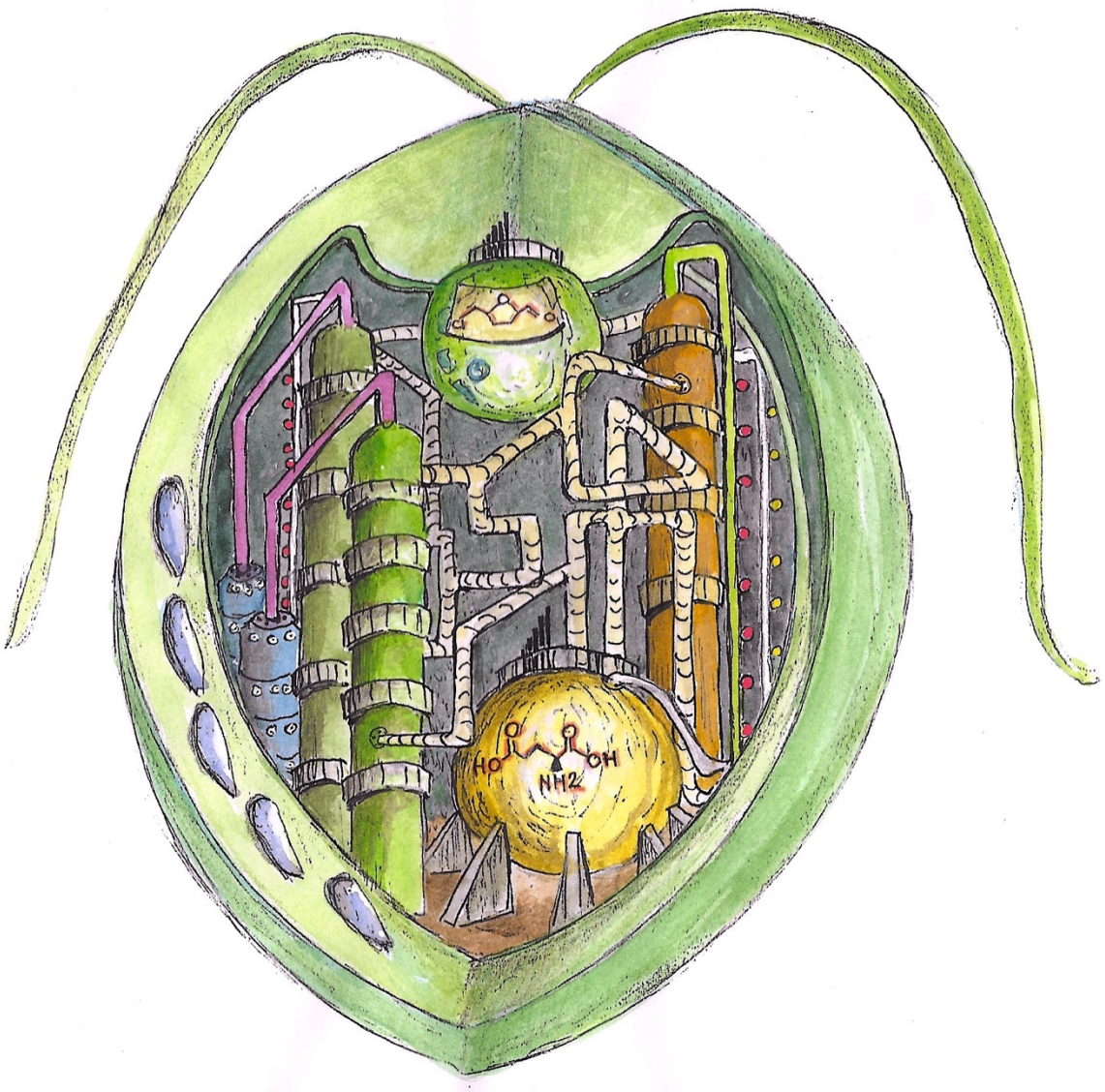

The Chemicalgal plant

artist view by Julia Ardaillon

Acknowledgements

First and foremost, I want to thank my supervisors Dr. Thomas J. Farmer and Dr. Duncan J. Macquarrie, for their guidance and support during this PhD. You pushed me to be a better scientist and gave me the confidence, autonomy and support I needed to grow as a chemist. For this, I cannot be thankful enough.

I want to thank all the administration team of the University of York especially, Alison Edmons, Sophie Palmer and Katy Brooke for the amazing job they've done and keep doing for the students and academics in the GCCE. I praise the work done by Paul Elliot without whom I'd have lost half of my PhD time trying to fix vacuum pumps, looking for mysteriously hidden tools or chemicals and much more. Thanks to Dr. Hannah Briers for teaching me how to tame the HPLC and all the work she does in the GCCE. To Dr. Tabitha Petchey, thank you for your help and the great time in York.

To Jonny Ruffell, thank you for the great, sometimes productive, talks we had (at the Blue Bell, Derry, Charles or at work) and for helping me pack my ridiculously huge columns. To Dinah, my desk (and home) closest neighbour, thanks for allowing me to put my feet on your chair, help with the porosimeter and letting me do my laundry at yours, you are the best. I want to thank all my PhD fellows: Alisa, Andy, Allyn, Ben, Han, Majed, Parul, Rebecca, Roxanna, Ryan, Yang, Jaspreet and, all others.

I am grateful for the collaboration with the post-doctoral researchers in this group especially, Dr. Jimmy Comerford for his help with the polymerisation, Intron machine and for the delicious beverages he produces, Dr. Fergal Byrne for teaching me the way of TMO, Dr. Ale Pellis, for the Yanmers polymerisation, Dr. Ian Ingram for making polymers with smelly diamines, and Dr. Katie Lamb for her help during the UV-filter project. I also want to thank Dr. Tom Attard, Dr. Rob McElroy and Dr. James Sherwood.

Thanks to my family for their moral and financial support during this time in England, none of this would have been possible without you. To all my secondary and high-school science teachers and mentors, you made me the scientist I am today, thank you. Lastly, to Emilie thank you for supporting me, for calming me down when I thought I had breathed something toxic in the lab and above all for your love and who you are. I love you.

Author's declaration

I declare that this thesis is a presentation of original work, and I am the sole author. This work has not previously been presented for an award at this, or any other, university. All sources are acknowledged as References.
List of publications associated with the relevant chapters:

- **Lie, Y**., Ortiz, P., Vendamme, R., Vanbroekhoven, K. & Farmer, T. J. *BioLogicTool* : A Simple Visual Tool For Assisting In The Logical Selection Of Pathways From Biomass To Products. *Ind. Eng. Chem. Res.* **58**, 15945–15957 (2019), is associated with **chapter II**
- Comerford, J., Gray T.; **Lie, Y.** *et al. Laminaria digitata* And *Palmaria palmata* Seaweeds As Natural Source Of Catalysts For The Cycloaddition Of CO_2 To Epoxides. *Molecules* **24**, 269 (2019), is associated with the microwave-based amino acid analysis developed **chapter III.1-part. 1**
- **Lie, Y.** *et al.* Work-hardening Photopolymer From Renewable Photoactive 3,3'-(2,5-Furandiyl)Bisacrylic Acid. *ChemSusChem* cssc.202000842 (2020), is associated with **chapter III.3**
- **Lie, Y.,** Farmer, T. J. & Macquarrie, D. J. Facile And Rapid Decarboxylation Of Glutamic Acid To γ-Aminobutyric Acid Via Microwave-Assisted Reaction: Towards Valorisation Of Waste Gluten. *J. Clean. Prod.* **205**, (2018), is associated with **chapter IV part. 1**
- Clark, J. H., Farmer, T. J., Ingram, I. D. V., **Lie, Y**. & North, M. Renewable Self-Blowing Non-Isocyanate Poly(urethane) Foams From Lysine And Sorbitol. *European J. Org. Chem.* **2018**, 4265–4271 (2018), is associated with **chapter IV part. 2.**

Chapter III.2 was part of a collaborative industrial project with BASF laboratory (Basel, Germany). Chapter III.4 was part of an industrial project with Unilever R&D (Liverpool, UK). Further details of individual contributions are given at the beginning of each chapter.

The tool presented in chapter II was designed in collaboration with Dr. Pablo Ortiz, Dr. Richard Vendamme and Dr. Karolien Vanbroekhoven (VITO, Belgium) who helped test the tool. Chapter III.2 was part of a collaborative competition organised by BASF and I.Know.Who which also involved several European universities. Enzymatic polymerisations presented in chapter III.3, were performed by Dr. Alessandro Pellis and the characterisation of the obtained polymers. TD-DFT calculations were realised by Dr. Ignacio Funès and Dr. Diego Sampedro. Chapter III.4 was part of a project mandated by Unilever PLC Ltd (UK) for the obtention of furan derived sulfonated surfactants. Dr. Craig Fairgrieve (Unilever) realised the physical and performance testing of synthesised surfactants. Finally, polymerisation and synthesis of bis-cyclic carbonate presented in chapter IV.2 were done by Dr. Ian Ingram. Collaboration with large chemical and home & personal care companies further highlights the significant commercial promise of this work.

List of Contents

List of tables

List of figures

List of schemes

List of appendices

Chapter I
General introduction

1.1 Context and birth of the sustainability concept

Environmental issues are at the forefront of attention in media and public debates. The weekly "school strikes for climate" that started in 2018, the creation of the more radical Extinction Rebellion group or the publication of a bio-based economy agenda in the UK and the rest of Europe are testifying that a rise of awareness about climate change issues is germinating.[1,2] The SARS-CoV-2 virus impacted our society in unprecedented proportions. Although the entire aftermath of this pandemic is yet to be measured, opportunities to favour green incentives and initiate a decarbonised society should be taken when the recovery comes.

Efforts to tackle the ecological crisis had started half a century ago. The first glimpse of environmental awareness in the political sphere can be traced back to the 1970s when the Stockholm conference was held in 1972 (considered the first Earth Summit) and later when "Our common future" (or Brundtland report) was published in 1987. This report settled the most widely accepted definition of sustainability and made it an unavoidable topic in the future political debate.[3] Sustainability, according to the Brundtland report, is defined as:

> *"[…] to make development sustainable to ensure that it meets the needs of the present without compromising the ability of future generations to meet their own needs."*

To achieve this state of development, all actors of society have to take drastic and coercive measures. Recently, policymakers and scientists have developed rules and targets for the

promotion of sustainable technologies. Most notably, the United Nations for Sustainable Development Program (UNSDP) published in September 2015, a set of 17 sustainable development goals (SDGs, Figure 1).[4]

Figure 1 Infographic of the 17 sustainable development goals published by the UNPD. *Reproduced from https://commons.wikimedia.org/wiki/File:Sustainable_Development_Goals.jpg (accessed 25/05/20)*

These 17 targets, which are supposed to be reached by 2030, are guidelines for nations worldwide to implement new policies for a better, more sustainable society.

1.2 Role of the chemical industry in a sustainable society

In this context, the chemical industry has an essential role to play to ensure that the comfort level of society is preserved and its development, made sustainably. Chemistry has made a significant contribution to the dramatic demographic expansion and the globally

increasing standards of living, which is observed at the beginning of the 20th century. For instance, the Haber-Bosch process, which allowed the synthesis of fertilisers from atmospheric N_2 and dihydrogen from methane steam reforming, helped to impressively increase crop yields and contributed to the third agricultural revolution.[5] Due to the high energy requirement of this process employing temperatures around 400-500 °C and dependence on natural gas, the greenness of this reaction is poor.[6] Simultaneously, the chemical industry quickly became dependent on non-renewable resources, namely, oil, natural gas and coal as those were cheap and abundant.

Nowadays, the majority of chemically derived commodities are produced from non-renewable resources. By cracking crude oil, at elevated temperature and pressure, base-chemicals are produced (Scheme 1) which are the fundamental petrochemical building-blocks of the more complicated molecules used in plastics, cosmetics, pharmaceuticals, surfactants, etc.

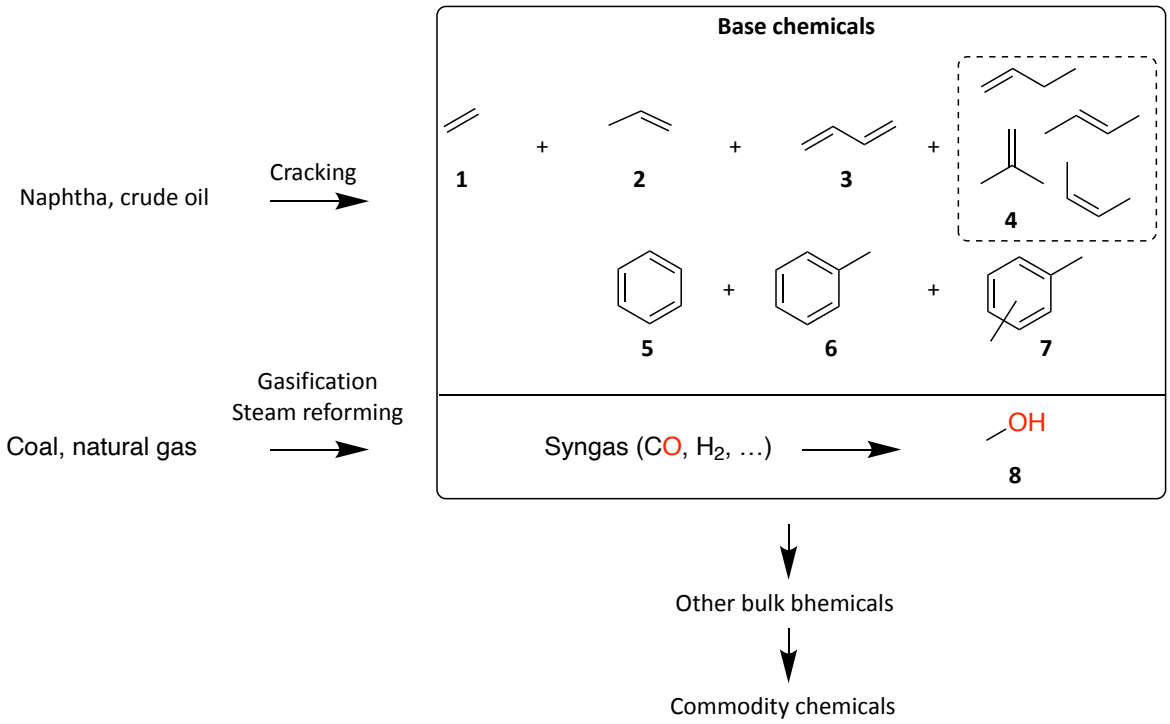

*Scheme 1 Base chemical production from naphtha (crude oil), coal or natural gas. ethene **1**; propene, **2**; butadiene, **3**; butene (3 isomers), **4**; benzene, **5**, methylbenzene **6**; dimethylbenzene (3 isomers), **7**; methanol, **8***

Approximately 14% of primary oil and 8% of natural gas demands are attributable to the production of petrochemicals (including process energy) every year.[7] However, the primary demand for oil remains controlled by the transportation sector (56%), whereas power generation represents the largest sector for natural gas demand (40%). Hence, the production of non-renewable feedstocks is governed by a synergistic relationship between the different sectors of society. Indeed, transportation of petrochemicals across the globe, and energy, is an inherent part of petrochemical production. Likewise, transport and power generation depend on the demand of other sectors to guarantee their profitability.

However, it is worth noting that their roles may reverse. The oil demand growth is projected to be mainly imputable to the petrochemical sector, accounting for half of it by

2050. On the other hand, the transportation sector may see a reduction in its role for oil demand as better fuel economy and new technologies are being implemented.[8]

Unfortunately, the ecological impact caused by the use of such resources, mostly due to greenhouse gas (GHG) emissions led to a dramatic increase in global temperature, ocean acidification, loss of biodiversity, disruption of geochemical cycles etc. Scientists proposed to define this period of rapid environmental mutations the *Anthropocene* epoch, to highlight the role of human behaviour on their environment on a geological timescale.[9]

Only a finite amount of oil, coal and gas is available for extraction, which is embodied in the concept of peak oil. Typically, an individual oil reservoir has a limited lifetime (decades, depending on its size) with an initially high output followed by a peak of production, decreasing over time. With the primary demand for oil growing, new reserves have to be discovered and exploited to compensate the diminishing older reservoirs. The first oil reservoirs were easily extracted and did not require expensive methods. Today, more technically and financially demanding extraction techniques are being deployed for the exploitation of novel reservoirs. When global oil production no longer meets demands, we'll have reached peak oil. Large reserves will remain, but the global output can no longer increase. Thus, the cost would likely dramatically increase, as seen for peak US-oil in the 1970s (also influenced by political decisions). Many attempts to estimate the moment when peak oil is going to happen were made. However, due to the technology improving and allowing new reserves to be discovered and extracted, most predictions were invariably wrong. If governments implement new coercive policies in order to meet the Paris agreement, the demand should peak before the production.

Commonly, two distinct approaches are considered to tackle these issues and meet the SDGs: transmaterialisation and dematerialisation.[10]

Dematerialism (Figure 2**B**) has been pursued since the Industrial Revolution by producing more goods with fewer resources. A natural extension of this concept is the use of fewer resources per person, thus reducing generated wastes. Economists and sociologists have proposed a deeper interpretation of the dematerialism concept and suggested that only a "degrowth" or "steady growth" society vision can lead to a sustainable future.[11,12]

Transmaterialism (Figure 2**C**), the preferred approach by chemists, is using alternative resources to produce similar (*drop-in compounds*) or functionally equivalent goods (*alternative molecules*). Taking into account the SDGs, the resources used must be renewable (SDG 12 & 13), not compete with food (SDG 2), and respect the natural geochemical cycles (SDG 13, 14 & 15). In this concept, a circular scheme replaces the linear approach in the petrochemical production currently in place. Cheap oil and thus cheap petrochemicals have led to a consumer-driven society with a linear focus. Goods were produced, used and discarded, generating an immense amount of wastes. In an ideal circular approach, no waste is generated thanks to the efficient use of the resources where wastes are converted into useful products.

Assuming that a resource meeting the SDGs exists, it seems only logical to replace the fossil resources used in traditional refineries, by renewable resources to produce fuel and chemicals in the so-called biorefineries.

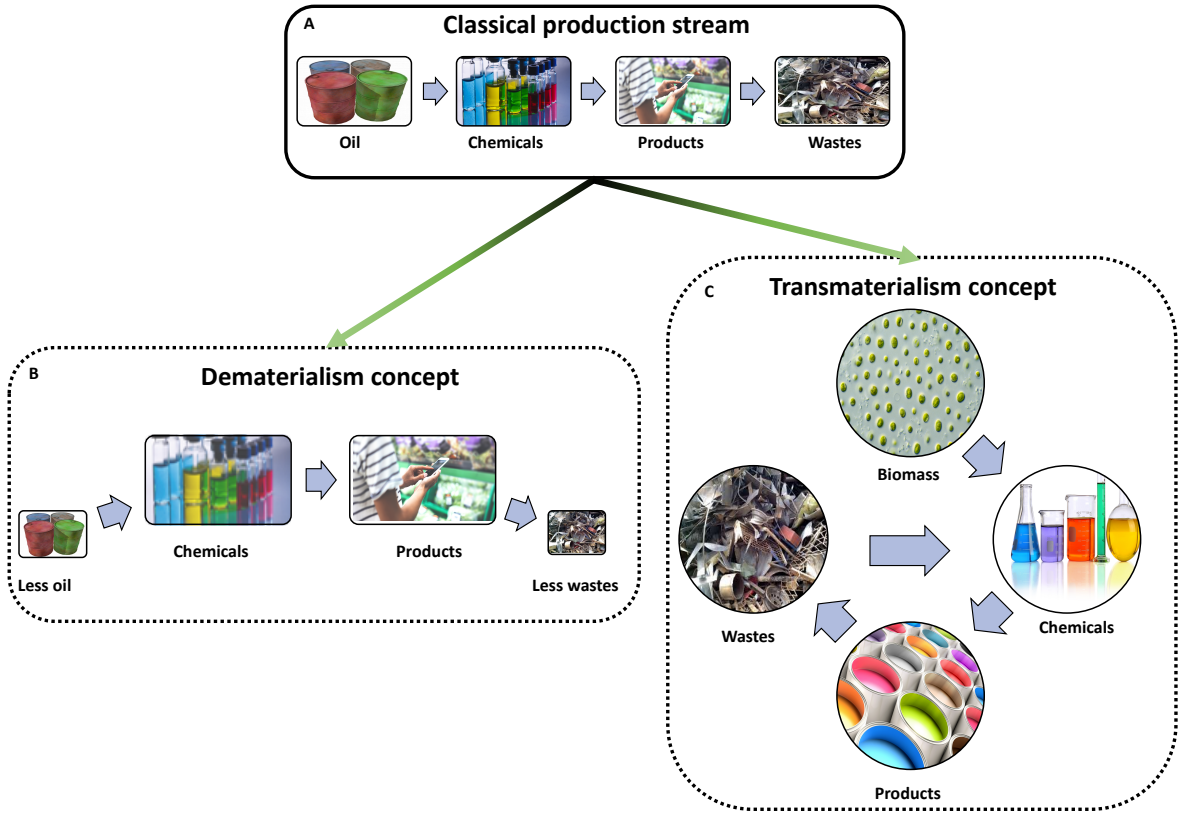

Figure 2 Different productivity stream approaches. ***A****: Classical production stream;* ***B****: Dematerialism using oil as feedstock;* ***C****: Transmaterialism employing biomass as feedstock.*

1.3 Green Chemistry and the biorefinery concept

1.3.1 Biorefineries phases and generations

A biorefinery can be defined as a facility where renewable biomass feedstock or "wastes" (*i.e.* a substance *previously* unexploited and generally discarded) is processed to produce chemicals, materials, fuel or energy. Essential to successful biorefineries will be the production of several products/outputs. In this way, they are somewhat analogous to a crude oil refinery (producing base chemicals, materials, fuel and energy).

Numerous renewable feedstocks have been considered in biorefineries depending on their location, the seasonality and the target products (corn in North America for starch, sugar cane in South America for sugars, jatropha in Africa for oil etc.). Most fossil-based

refineries are huge, centralised hubs which import feedstocks and export produced chemicals. Because of the physical nature of renewable feedstocks (high water content, large volume, changing composition over seasons and transportation time), bio-refineries must be small, rural units close to the feedstock production field.

Over the last two decades, major concerns over a potential competition between the land use for food or feedstock for biorefineries arose. Specifically, when (edible) crop products such as corn or sugar cane (Figure 3, Ist generation biorefinery), were used to produce bio-ethanol, a "food/fuel" competition was of major concern. These early biorefineries, using one type of feedstock and making one type of chemical are referred to as first-phase biorefineries (Figure 3). Currently, research focuses on the second and third-phase biorefineries. Second-phase biorefineries also use single feedstocks but can produce a variety of chemicals while third-phase biorefineries will accept different feedstocks and generate a wide array of products.[13]

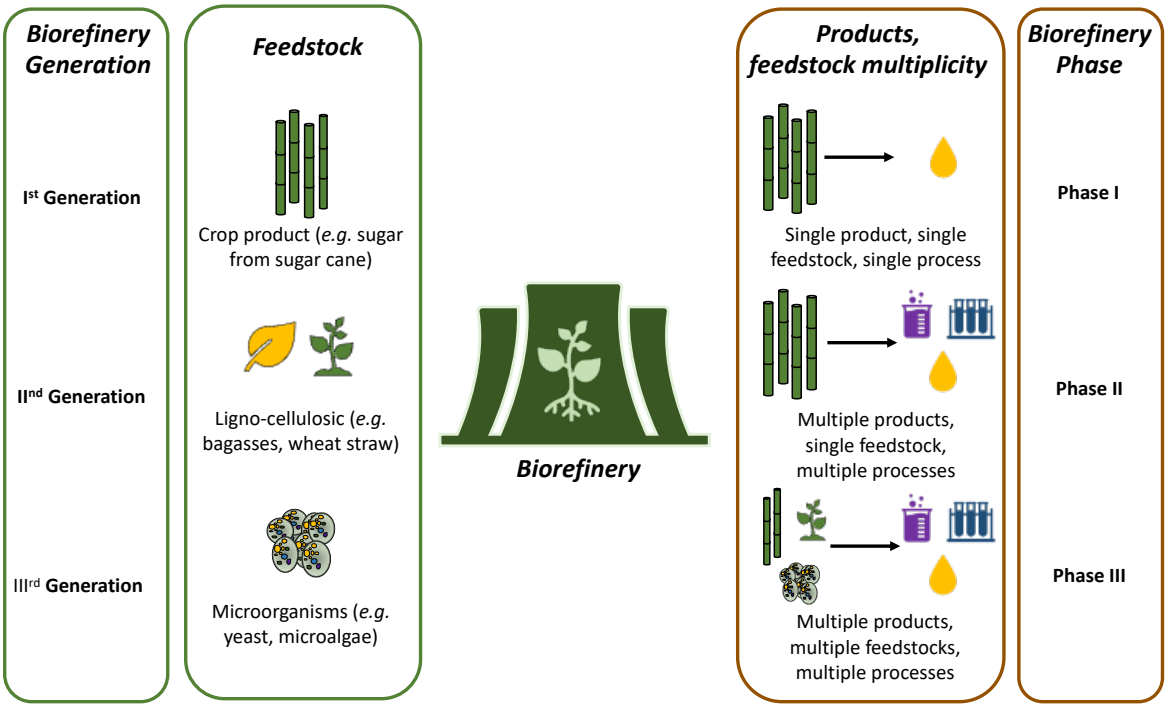

Figure 3 Different generations and phases of biorefinery

Second-generation feedstocks (lignocellulosics) were used to answer concerns over a potential food/fuel competition. Because this feedstock is commonly obtained from crop residues, competition with edible crop products no longer exists. However, the presence of lignin renders the access to cellulose difficult, which complicates its breakdown into glucose units, as commonly required before any chemicals/fuels can be obtained. Furthermore, crop residues are necessary for a sustainable agricultural system since they are usually buried back into the soil to release the remaining nutrients used during the growth and participate in the soil structure.

Hence, a last generation of feedstock is currently considered: microorganisms, and particularly, microalgae. Microalgae are fast-growing photosynthetic microorganisms that can produce an impressive biomass quantity in a short amount of time. Chisti *et al*. estimated that a yield of 39 $kL.ha^{-1}$ of oil from microalgae could be achieved with organisms

containing 30% dry weight of triglycerides.[14] Comparatively, a typical palm oil crop produces 6 $kL.ha^{-1}$. Also, no arable lands are required to grow microalgae as they are typically cultivated in open-pond systems or closed photobioreactors. Finally, the impressive variety of microalgae allows the selection of particular species with a specific biochemical composition to optimise yields of the biorefinery's target molecules. More details on microalgae cultivation and remaining challenges will be discussed in chapter III.1.

Due to the difference in composition between renewable and fossil resources, the chemicals issued from bio- and traditional refineries will likely differ. Indeed, the chemicals produced by biorefineries, later called platform chemicals, may impose the need to redesign processes, reactions and mindsets acquired in the 20th century.

1.3.2 Platform molecules: a comparison to base chemicals

In 2014, Farmer and Mascal defined platform molecules as:

> *"A bio-based (or bio-derived) platform molecule is a chemical compound whose constituent elements originate wholly from biomass (material of biological origin, excluding fossil carbon sources), and that can be utilised as a building block for the production of other chemicals."* [15]

That definition encompasses a much larger proportion of molecules than the dozens of base chemicals utilised today. Sugars, fats, proteins or other metabolites possess a high degree of functionalisation and complexity, leading to various platform molecules represented in Figure 4. Molecules containing a majority of biomass-derived atoms, and not solely *wholly bio-derived* as defined above, were included as well. These chemicals

were selected based on the possibility to produce them at large scale. As the biorefinery technology matures, this list may eventually be reduced to only a dozen platform chemicals being synthesised at low cost and scale.

A wide array of different processes is used to obtain platform molecules such as biological (fermentation), thermal or thermochemical (hydrothermal liquefaction, pyrolysis), chemocatalytic and extraction. Ideally, one or several of these processes are employed in a fully integrated manner to the biorefinery downstream.

The majority of platform molecules represented in Figure 4 are derived from cellulose, hemicellulose or sugars which can be explained by the abundance of these biocomponents and the possibility to use either thermal, chemocatalytic, extraction or biological processes — fermentation – to convert sugars into platform molecules. Indeed, the utilisation of sugars to feed genetically modified fermenting microorganism offers a range of platform molecules challenging to obtain otherwise (*e.g.* itaconic acid, **25**).

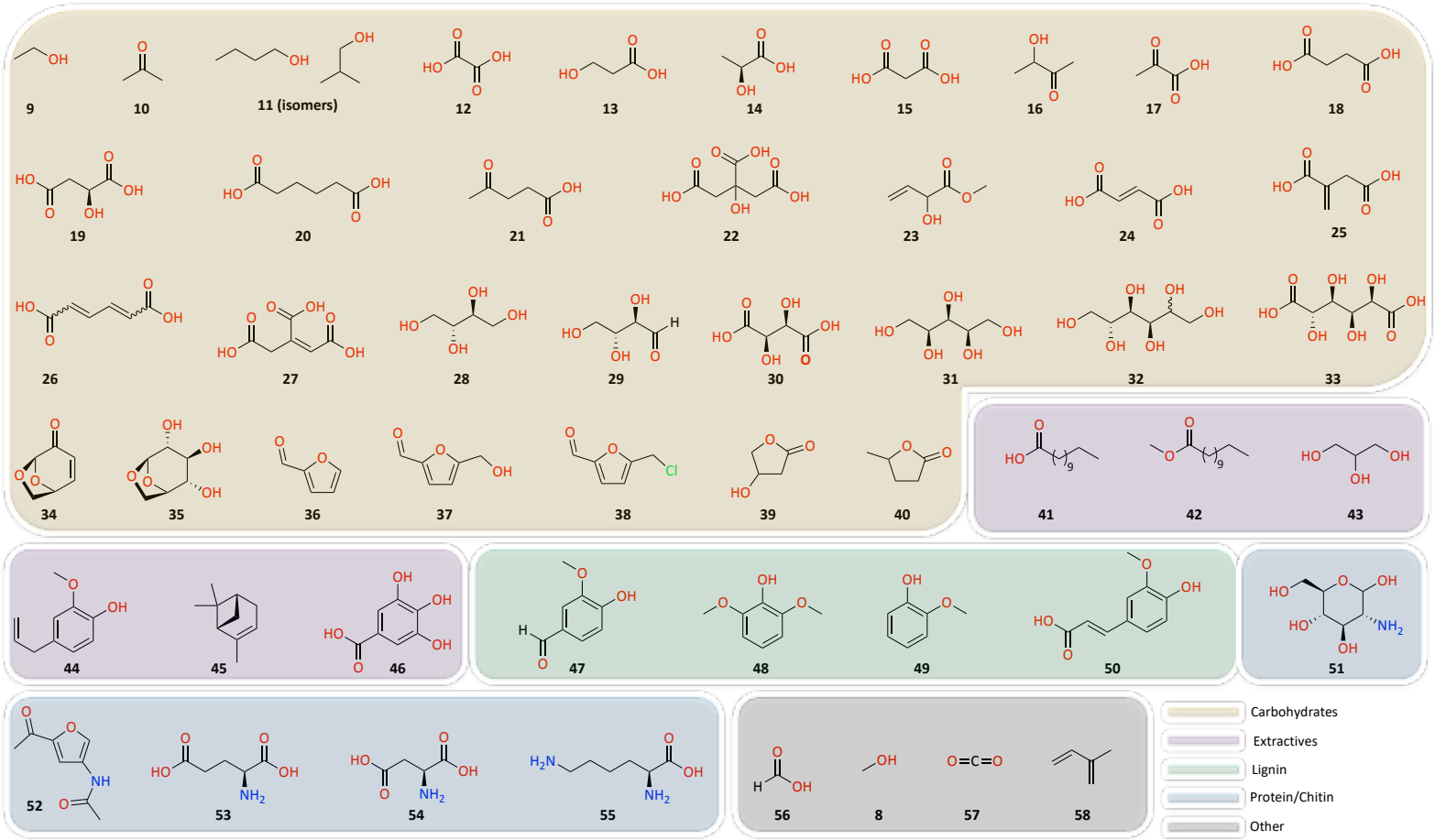

*Figure 4 Structures of chemicals considered as platform molecules in this work. ethanol, **9**; acetone, **10**; butanol (n-, iso-), **11**; oxalic acid, **12**; 3-hydroxypropionic acid, **13**; (S)-lactic acid, **14**; malonic acid, **15**; acetoin, **16**; pyruvic acid, **17**; malic acid, **18**; succinic acid, **19**; adipic acid, **20**; levulinic acid, **21**; citric acid, **22**; methyl vinyl glycolate, **23**; fumaric acid, **24**; itaconic acid, **25**; muconic acid, **26**; aconitic acid, **27**; erythritol, **28**; erythrose, **29**; tartaric acid, **30**; xylitol and arabitinol, **31**; sorbitol and mannitol, **32**; glucaric acid, **33**; levoglucosenone, **34**; levoglucosan, **35**; furfural, **36**; 5-(hydroxymethyl)furfural, **37**; 5-(chloromethyl)furfural, **38**; 3-hydroxybutyrolactone, **39**; γ-valerolactone, **40**; fatty acids (e.g., lauric acid), **41**; fatty acid alkyl esters (e.g., methyl laurate), **42**; glycerol, **43**; eugenol, **44**; D-limonene and pinenes, **45**; gallic acid, **46**; vanillin, **47**; syringol, **48**; guaiacol, **49**; ferulic acid, **50**; glucosamine, **51**; 3-acetamido-5-acetylfuran **52**; L- glutamic acid, **53**; L-aspartic acid, **54**; L-lysine, **55**; formic acid, **56**; carbon dioxide, **57**; isoprene, **58**.*

Extractives are directly utilised (eugenol, **44**, pinene **45**) or after simple chemocatalytic treatment (fatty acid methyl ester, FAME, **42**). Unsaturated fatty acids, also obtained by extraction, have been used to produce polyols and used in polycondensation reactions, as discussed in chapter IV.2.

Lignin harbours a multitude of polyphenolic compounds and represents a formidable source of aromatic molecules. Unfortunately, the high stability and recalcitrance of lignin towards most treatment (chemical/thermal/biological) prevents this resource from being exploited to the fullest. Thus, most studies focused on model compounds such as guaiacol or syringol (**48** and **47** respectively), but few reports make use of lignin from biomass.[16] Recently, Liao *et al.* managed to convert up to 78% (by weight) of birch wood (rich in lignin) into xylochemicals representing a significant advancement in lignin-valorisation.[17]

Proteins and chitins are the primary sources of bio-derived nitrogen-containing compounds. Research on the utilisation of proteins from biorefinery side-streams starts to gain attention from the green chemistry community.[18] However, the higher complexity of protein structure compared to polysaccharides renders their valorisation more tedious as discussed in chapter IV.1. The quantity of generated shellfish wastes containing chitin is estimated between 6 and 8 million tonnes per year globally.[19] Chitin may be converted to 3-acetamido-5-acetyl furan (**52**), a motif commonly found in pharmaceuticals (*e.g.* antibiotic proximicin A). Deacetylation of chitin leads to chitosan (used as a thickener for food) while further depolymerisation of chitosan leads to glucosamine (**51**), another potential platform molecule containing nitrogen.

Finally, the last category of platform molecules may be obtained from syngas produced using almost any carbonaceous material. Under controlled thermal treatment

(>700 °C), a mixture of CO and H_2 is synthesised from which a broad range of chemicals may be obtained (MeOH, formaldehyde etc.). Despite the high energy demand for this process, virtually any carbon-containing feedstock may be used, which is the principal asset of this thermal gasification method.

Platform molecules are destined to be utilised as building blocks for a multitude of bulk chemicals and eventually commodity chemicals, mimicking the fossil-based refineries. Reaching the current multi-million-tonne production volume of petrol-based chemicals with platform molecules represents another significant challenge to be tackled. The multiple reactions which lead to the commodity chemicals must be carefully designed and monitored to ensure their environmental friendliness. For this reason, a set of principles were published as guidelines for chemists who wish to improve a reaction sustainability.

1.3.3 Green principles and metrics

In 1998, Paul Anastas and John Warner published the book "*Green chemistry: theory and practice"* which introduced the twelve principles of green chemistry (Figure 5).[20] These principles have been the steppingstones of the green chemistry field and profoundly helped raise awareness amongst industries and academia.

Throughout the last 30 years, an increasing number of metrics and guidelines have been used, designed or repurposed to help assess reactions against the twelve principles. The atom economy, developed in 1991 by Barry Trost, has often been used in a green chemistry context to quantify the first green chemistry principle (waste prevention).[21] It estimates the amount of the reactants remaining as a constitutive part of the final product, by dividing the molar mass of the product by the molar mass(es) of reagent(s). The E-factor

designed by Sheldon in 1992 focuses more specifically on waste generated in a process.[22] Depending on the industries, E-factors can range from <0.1 (oil refining, bulk chemicals industry, high production volume, minimum waste generation) to >100 in pharmaceutical industries (low production volume, increased waste generation).[23] In 2002, Curzons *et al.* from GSK published an extensive list of green metrics taking into account more principles, for example, less hazardous synthesis/design safer chemicals (Figure 5 principle 3 & 5, **HuEx** index) or energy efficiency (principle 6, $\mathbf{E_{process}}$ index). In recent years, governments and industries have developed more "hybrid" metrics to combine both environmental and mass considerations in one analytical tool, such as Green Motion, GREENSCOPE and EcoScale. [24–26] The ease of using the first metrics (AE, E-factors, yield) explain their popularity amongst chemists. More accurate/exhaustive metrics (hybrid metrics, BUE etc.) may not be used often due to their higher complexity.

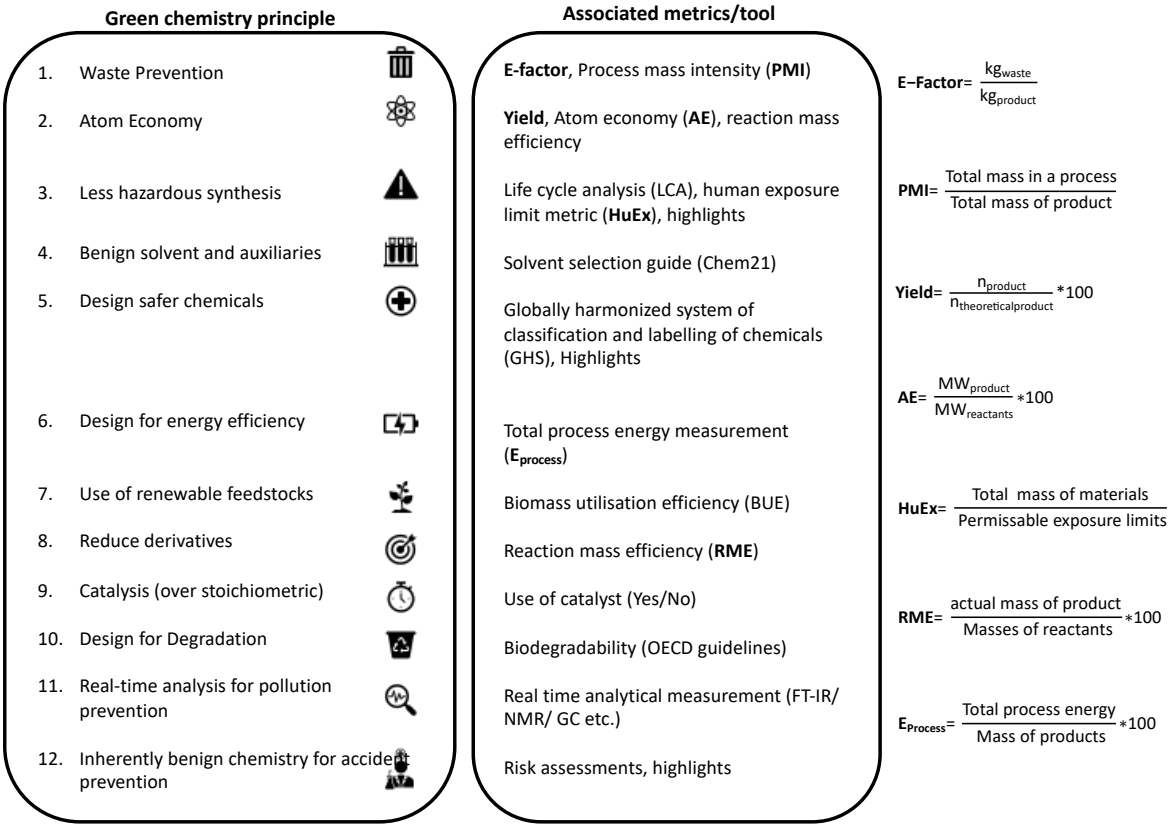

Figure 5 12 green chemistry principles and corresponding metrics

Despite the necessary frame of work that Anastas and Warner brought, some of the green chemistry principles as originally presented left aside essential aspects of sustainability or led to misinterpretation.[27,28]

For example, principle 1 does not take into account the nature of wastes being generated. Some wastes might be of particular concerns (toxic, environmental, radioactive) while others might be benign or even become a reagent for another reaction hence contributing to the circular economy.

Some principles might be incompatible with one another. For instance, criticisms might be raised regarding the promotion of less hazardous chemistry (principles 3,4,5 & 12). Inherently safer molecules are more often than not difficult to react. They may then

require additional catalyst or energy to increase their reactivity hence going against principles 2, 6 and 8. It is evident that a safer chemistry is paramount for scientists, workers and society, but one must find the right balance between reactivity and safety. Furthermore, depending on the scale at which the reaction is carried out, hazards might not be the same. For instance, HCN is a highly poisonous reagent typically avoided or generated in situ at laboratory scale. Industrially, however, hydrogen cyanide is used daily in tonne quantities.

The design for energy efficiency (principle 6) does not include the source of energy nor the scope where processes must be made energy-efficient. Necessarily, fossil-fuel depletion should lead to using renewables, leaving a myriad of potential energy sources available (electric, thermal, chemical, biomass). One should also ensure that making a chemical reaction more energy efficient is not compensated by an increase in another side of the production chain (transport, treatment etc.).

As highlighted in the previous section, not all renewable resources are equivalent (principle 7). For example, while some plants may take months to grow fully and provide usable feedstock, trees may require years or decades. The applicability of a greener reaction/process should always be considered at a larger scale. As ironically pointed out by Winterton in 2016, replacing the amount of PET produced from one fossil-based plant (producing 500 000 tonnes per year of PET) with wool would require a surface the Netherlands' size only to feed the sheep.[28]

The pursuit of catalytic reactions (principle 9) must also be designed with careful choice of the transition metals often associated in a metal-based catalyst. Indeed, many of the most reactive metal elements (Ru, Rh, Pd, etc.) are becoming scarce due to their increasing extraction rate for electronics and low recovery/recycling rate.[29] Chemists may

consider developing recyclable catalysts based on widely available metals such as Fe, Ni, Cu with comparable reactivity to critical element-based catalysts. However, due to the low volume and low-impact on overall process green credentials, this aspect is often ignored in green chemistry publications.

Lastly, designing chemicals for degradation (principle 10) may be overruled by the design of chemicals for reuse or repurpose. Indeed, while many products may end-up in the environment, their degradation products might turn out to be toxic or bioaccumulate. Reusing or repurposing chemicals may prevent these issues while promoting a circular economy.

By wrongly interpreting the principles as independent targets rather than synergistic goals, some authors may have overlooked important factors of chemical reactions/routes studied. The above criticisms usually found against the green chemistry principles often come down to scalability issues. The seemingly significant improvements made on a chemical reaction at a laboratory scale must also be applicable at some point at an industrial scale whilst taking all aspects of sustainability into account.

Finally, it would be delusional to believe that a simple increase in the AE of a reaction, or the development of a highly active critical element-free catalyst would reverse the ecological crisis alone. The Twelve Principles have had tremendous repercussions on academia and industries but without strong, demanding and holistic changes from all actors of society (researchers, industries, policymakers, public etc.) green chemistry discoveries may just remain a silent revolution.

1.4 Aims of this project

The work presented here revolves around two principal axes:

- The development of a tool to help assess the rationality of a chemical route with a focus on the comparison between fossil-based and bio-based routes
- The design of a concept for a 3rd generation, 3rd phase bio-refinery using microalgae as a feedstock.

The first goal emerged from the observation that no green metrics offered a visual representation of the chemical routes studied. Besides, it was of interest to provide a tool which does not require prior experimental work nor extensive mechanistic knowledge to employ. The advantage of having visual aids to help in decision-making processes is undeniable. For this reason, the possibility to graphically map chemicals based on their heteroatom atom content and molar mass led to represent chemical reactions in the so-called *BioLogicTool plots* in **chapter II**. This tool offers the possibility to visually and quantitatively assess the logic of a chemical route thanks to rationality scores given with the plots. Through the different chapters of this thesis, examples of the use of this tool are provided to reflect on the rationality of the routes employed and to compare them with other published or hypothetical pathways.

The second axiom of this thesis originates from the will to demonstrate the remaining potential that microalgal biomass represents for green chemistry. Indeed, while an increasing number of authors are advocates for the development of “multi-component

microalgal biorefineries", most reports only focus on a single biocomponent (either lipids or sugars) usually for the sole production of bioenergy. Yet, the impressive diversity of microalgae and even more exciting capacity to accumulate a chosen biochemical should have led to more reports using this feedstock.

First, the current bottlenecks of microalgal cultivation are discussed in **chapter III.1-*part 1***. Three different species of microalgae were characterised via proximate and amino acid analysis. Next, sugars derived from these microalgae were the first class of biomolecules to be valorised. In **chapter III.1-*part 2***, the CMF process was identified as a potential solution to alleviate several microalgae cultivation challenges. The simultaneous extraction and valorisation of sugars into CMF was proven possible with the microalgae tested. Thus, efforts were being made from chapters III.2 to IV to demonstrate the synthesis of different commodity chemicals from microalgae-derivable molecules.

Chapter III.2 presents work on the synthesis of furan derived UV-filters to replace molecules of concern for the aquatic environment. A series of UV-active compounds could be synthesised and were tested for their potential application in sunscreen formulations.

A particularly UV-reactive bi-functional compound was then used to produce a work-hardening photopolymer as presented in **chapter III.3**. Under optimised enzymatic conditions, a film displaying work-hardening behaviour after UV-curing could be obtained with potential uses in photolithography or 3D applications.

Different families of furan-derived sulfonated surfactants were designed in **chapter III.4** as potential alternatives to current fossil-based linear alkylbenzene sulfonates (LAS). In the pursuit of employing more microalgae-derived biocomponents, a mixture of surfactants using a theoretically obtainable mixture of fatty alcohols from *Spirulina sp.*'s

lipid was made. A family of surfactants was further tested and characterised for their detergency and presented excellent properties compared to benchmark substances.

Finally, **chapters IV.1** and **IV.2** focused on using the two most abundant amino acids in the microalgae tested: glutamic acid and lysine, respectively. First, a protocol for the thermal carbonyl-induced decarboxylation of glutamic acid was developed. This protocol avoided the reported isomerisation of glutamic acid to its lactam equivalent and afforded γ-aminobutyric acid in up to 63% yield. Glutamic acid isolated from the protein-rich fractions left after the CMF process (using gluten) could also be decarboxylated in lower yield.

The decarboxylation product of lysine namely, 1,5-pentanediamine, was used for the aminolysis of a sorbitol-derived bis-cyclic carbonate to produce a non-isocyanate polyurethanes (NIPU), in this case, a polyhydroxyurethane (PHU). The foamy appearance of the obtained polymer was attributed to the emission of CO_2 during the polymerisation reaction. This side-reaction further increased the polymer's sustainable character by avoiding any additional blowing agent for foam formation and could be useful for insulation applications. Figure 6 summarises the different sections of this thesis and will be shown in a more detailed version in Chapter V (Conclusion).

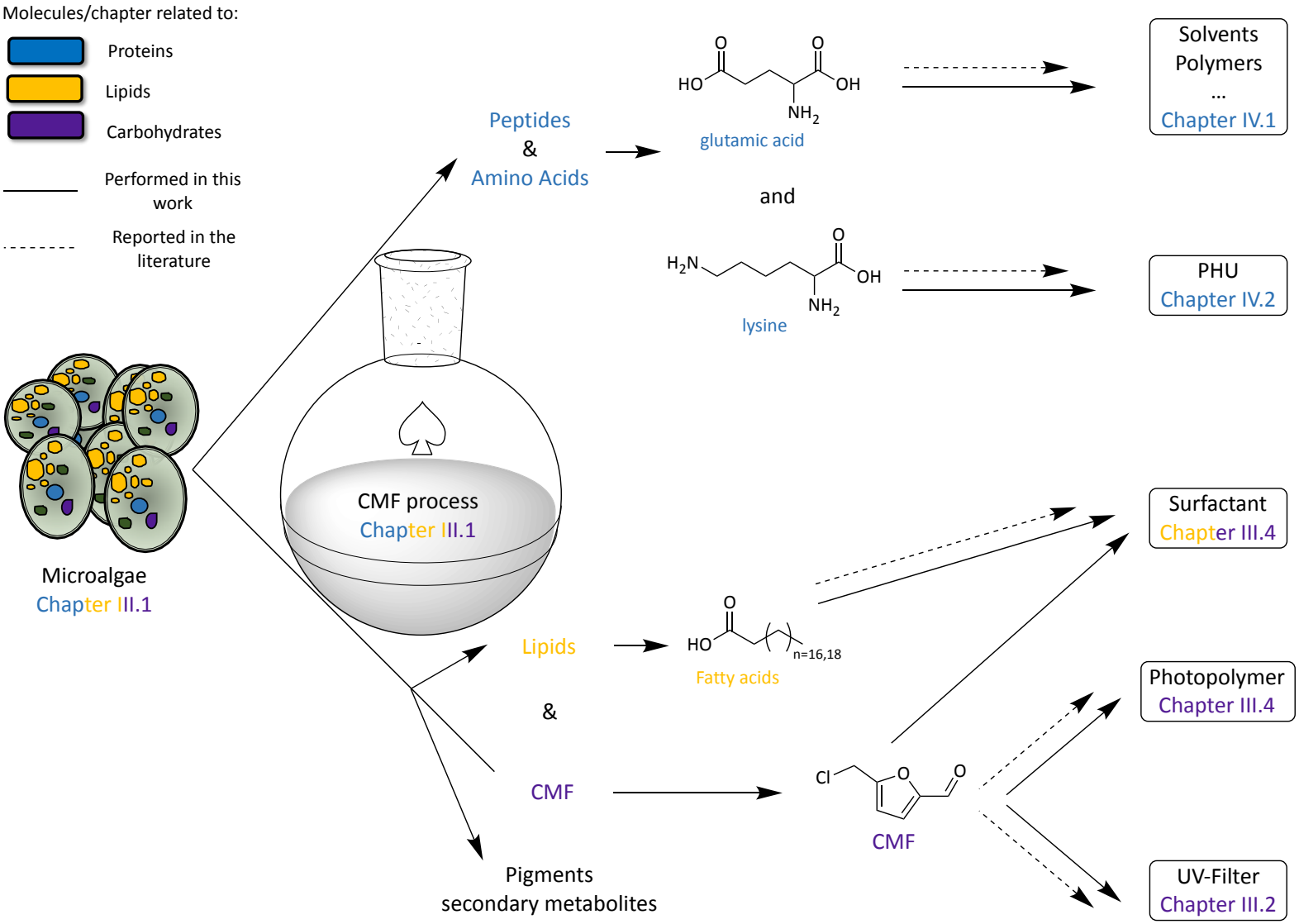

Figure 6 Summary of the different chapters presented in this thesis, approach to the Chemicalgal plant concept

Chapter II
Development of a tool to assess the rationality of reaction pathways: *BioLogicTool*[*]

[*] This chapter is based on a published article: Lie, Y., Ortiz, P., Vendamme, R., Vanbroekhoven, K. & Farmer, T. J. BioLogicTool : A Simple Visual Tool For Assisting In The Logical Selection Of Pathways From Biomass To Products. *Ind. Eng. Chem. Res.* acs.iecr.9b00575 (2019) Yann Lie designed the *BiologicTool* and wrote the section of the article "*BioLogicTool: Assessing Pathways From Feedstock To Products By Summation Of Route Vector Lengths*" which was used and extended to write the section II.4, Thomas Farmer designed the initial concept of the tool and wrote the sections "*Mapping The Heteroatom Content Of Platform Molecules*", "*Low/No Heteroatom Content Products*" of the article which were modified and extended to write the section II.1 and the end of II.3 of this chapter respectively.

2.1 Introduction: deciding on bio-based drop-in replacements or alternative molecules

As presented in the introductory chapter, platform molecules differ from base chemicals mostly by their multiple functional groups associated with a higher heteroatom content and molar mass (Figure 4, p. 33). Only CO (syngas, Scheme 1, p. 25) and thus methanol produced from syngas (Figure 4, p. 33, **8** both platform molecule and base chemical) possesses a heteroatom (oxygen) while all other base chemicals are hydrocarbons.

The 20th-century chemical industry has been optimised to incorporate functionalities into simple hydrocarbon-based building blocks. Thus heteroatoms (mostly oxygen, nitrogen and halogens) are added thanks to an oxidative-oriented chemistry (Figure 7**A**, key petrochemicals product are above base chemicals on the plot). On the other hand, molecules obtained from biomass are typically rich in heteroatoms and, if drop-in replacements to oil-based goods are targeted, it will require removal of heteroatoms from platform molecules (sometimes reincorporating them later) and thus favour a more reductive chemistry (Figure 7**B**, key petrochemicals product are under platform molecules on the plot).[30] Yet, from a mass efficiency perspective, stripping off heteroatoms from the starting material may not be optimal, and certainly not on the scale that bulk and commodity chemicals are produced globally. It would indeed be preferable to preserve these heteroatoms in the final products or even when possible, design alternative molecules with similar if not better properties that would keep the pre-existing heteroatoms originating from the platform molecules.

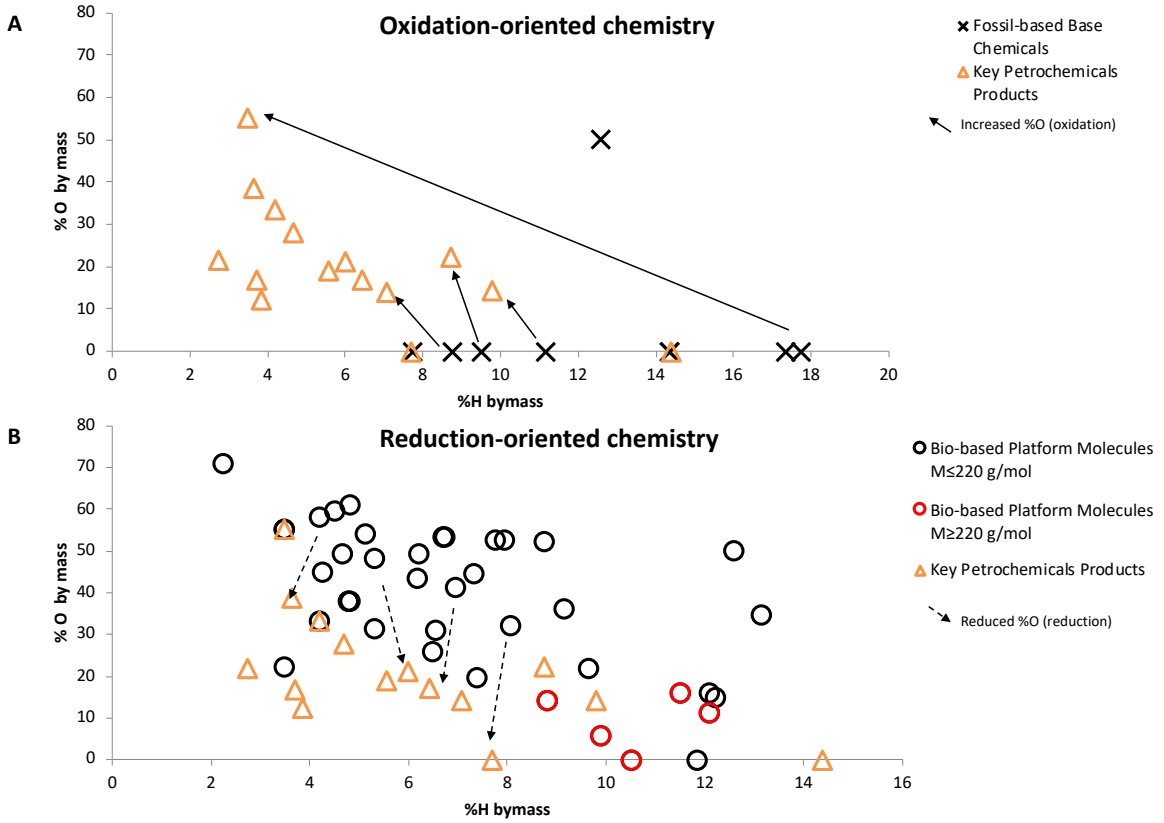

*Figure 7 Representation of the oxidative oriented chemistry using base chemicals **A** and the reductive oriented chemistry using platform molecules **B**. The %O by mass in chosen chemicals is plotted against the %H to illustrate the gain/loss of O*

For instance, NMP (Scheme 2, **64**), which is currently produced from acetylene (**59**) via the route represented in Scheme 2, contains both oxygen and nitrogen as heteroatoms. These O and N atoms are added via reaction with formaldehyde, O_2 oxidation and methylamine to form the end product **64** (as discussed in greater details in the following section). Since industrial processes and infrastructures are already in place using acetylene, is it genuinely rational to entirely strip off heteroatoms from platform molecules to produce acetylene? Should a bio-based alternative product with similar or even better properties be developed instead? Clearly, the decision to either focus one's efforts on producing drop-in replacements from platform molecules or develop novel, possibly better compounds, must be made.

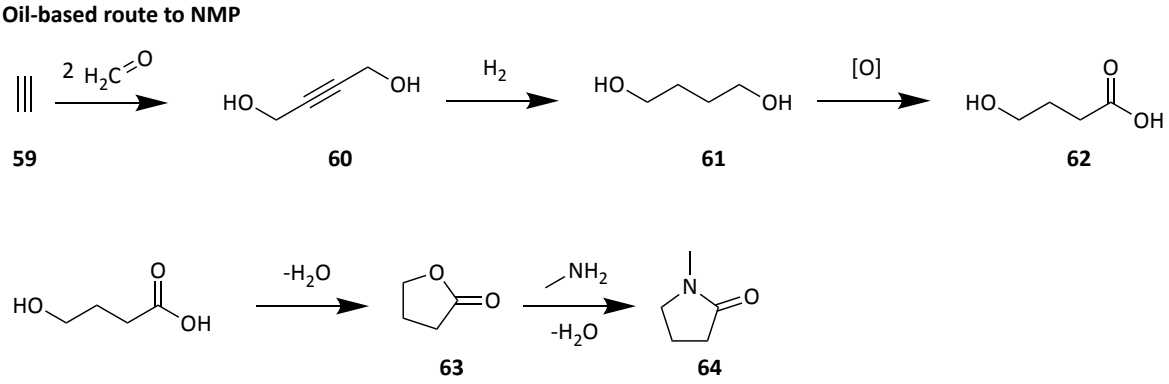

*Scheme 2 Oil-based route to NMP (**64**)*

The previous questions led to the search for simple calculations or tools that could help assess the rationality of chemical routes without the need for experimental work. Metrics such as atom economy (AE) already exist and are commonly used. As previously explained (Chapter 1.3.3), AE only requires an understanding of the reaction scheme and what reactants come into play. In the case of NMP, the atom economy (taking only the oxygen atomic mass into account for the oxidant during the calculation) is 73%. Without performing a calculation, it appears evident that stripping off heteroatoms from platform molecules to produce acetylene can only decrease the AE of the route and is less logical. Despite the widespread use of AE and ease of utilisation, AE does suffer from some drawbacks:

1) It does not consider what reactants are bioderived or not.
2) It requires a good understanding of the reaction mechanism so that the stoichiometric equivalents can be correctly determined
3) Experimental work is needed to obtain reliable figures
4) It does not offer a visual representation of a synthetic pathway.

2.2 Aims of chapter II

The development of a tool allowing rapid visual representation of a planned synthetic pathway and designed to assess the rationality thereof is the goal of this chapter. This tool should provide answers to the limitations of other metrics such as 2), 3) or 4) mentioned in the above list (p.46).

First, a visual representation to map chemicals was selected. This graphical object had to highlight discrepancies between atomic compositions of different compounds to allow widespread distribution of starting material, intermediates or target molecules. The van Krevelen diagram was chosen as a starting point for this new tool development. After different modifications, the representation of chemical routes on a single plot was possible and provided qualitative information on their complexity. However, qualitative analysis of a synthetic pathway's intricacy was not sufficient on its own. In order to adequately compare and help the decision-making process between two routes, a quantitative measurement accounting for the complexity of such routes needed to be provided. Two numbers were chosen to describe the length and tortuosity of a plotted synthetic pathway. Lastly, a demonstration of the tool was made by comparing routes to a photoactive monomer (pentaerythritol tetraacrylate) or alternative compounds. Examples primarily focused on comparing bio-derived routes (employing heteroatom-rich platform molecules) with petrol-derived ones (using base chemicals devoid of heteroatoms). Another critical aspect to consider was the ease of utilisation of this tool. As such, a freely available Excel spreadsheet requiring minimal input from the users (compound names, atomic compositions, molar masses and yields (optional)) was designed. This tool, named

BioLogicTool, may become part of the chemist toolbox and complement other well-established metrics.

2.3 Representation of the heteroatom content in platform molecules and base chemicals

As a first approach, the van Krevelen diagram (Figure 8**A**) appeared to be a good starting point for representing the heteroatom content in platform and base molecules. The van Krevelen diagram is a graphic plot of the atomic ratios of H:C (represented on the y-axis) versus O:C (plotted on the x-axis) and was initially developed as a mean of comparing the composition of kerogen (solid, insoluble organic matter in sediments) and petroleum.[31] Its use has since been extended to other research fields, such as the analysis of compounds obtained from natural organic matter (NOM) and the partition thereof into protein, cellulose, lipid or lignin-like groups.[32]

However, as Dusselier *et al.* noticed, the van Krevelen representation had limitations when platform molecules and chemical routes were considered.[33] This led to a first modification of the diagram, replacing the O:C ratio by a *functionality to carbon ratio*: F:C.

In 2018, another modification of the van-Krevelen diagram was done by Rivas-Ubach *et al*.[34] The need to assess the importance of other heteroatoms such as nitrogen or phosphorus, omnipresent in living organisms, led this group to change the traditionally employed O:C atomic ratios on the y-axis with N:C, P:C or even N:P to help their classification. Yet, atomic ratios were still employed, which did not account for the necessary change in molar mass as a result of these heteroatoms being present.

Nonetheless, these steppingstones in the refinement of the van Krevelen diagram for bio-based chemicals inspired the further changes presented here.

First, the x- and y-axes were changed to a percentage of H and O content, respectively (as %weight, Figure 8**B**) rather than atomic ratios. This change resulted in the widening of the points on each axis and reversed all the previously ordinate-aligned base chemicals on the abscissa. Moreover, the use of % by weight further highlights the contribution of heteroatoms in the overall molar mass of the molecules relative to that of hydrogen. Thus, the next natural modification was to replace the *x*-axis with the molar mass (M in $g.mol^{-1}$, Figure 8**C**). Throughout a synthetic pathway, the molar mass of the intermediates and product changes, *e.g.* elimination reactions will decrease the molar mass, and additions will increase it. Thus, when a chemical pathway is studied plotting the change in molar mass helps visualise both heteroatom content changes and the general increase in complexity from initial building blocks.

The last modification performed here was to replace the % oxygen by mass represented on the ordinate with the % heteroatom by mass to include other heteroatoms such as nitrogen, halogens or sulfur which regularly occur in bio-derived chemicals and platform molecules.[19] The resulting plot did not fundamentally change the compound locations since oxygen was essentially the only heteroatom present in most molecules considered here. However, some platform molecules such as glucosamine (**50**, see Figure 4, p. 33) or amino acids (**53-55,** see Figure 4, p. 33) contain nitrogen as heteroatoms and are expected to be particularly relevant in the bio-based society for sourcing bio-derived nitrogen-containing compounds.[35] Furthermore, 5-(chloromethyl)furfural (**38** see Figure 4,

p. 33), contains a chlorine atom and is a promising platform molecule the versatility of which to produce compounds of interest had repeatedly been reported.[36–40]

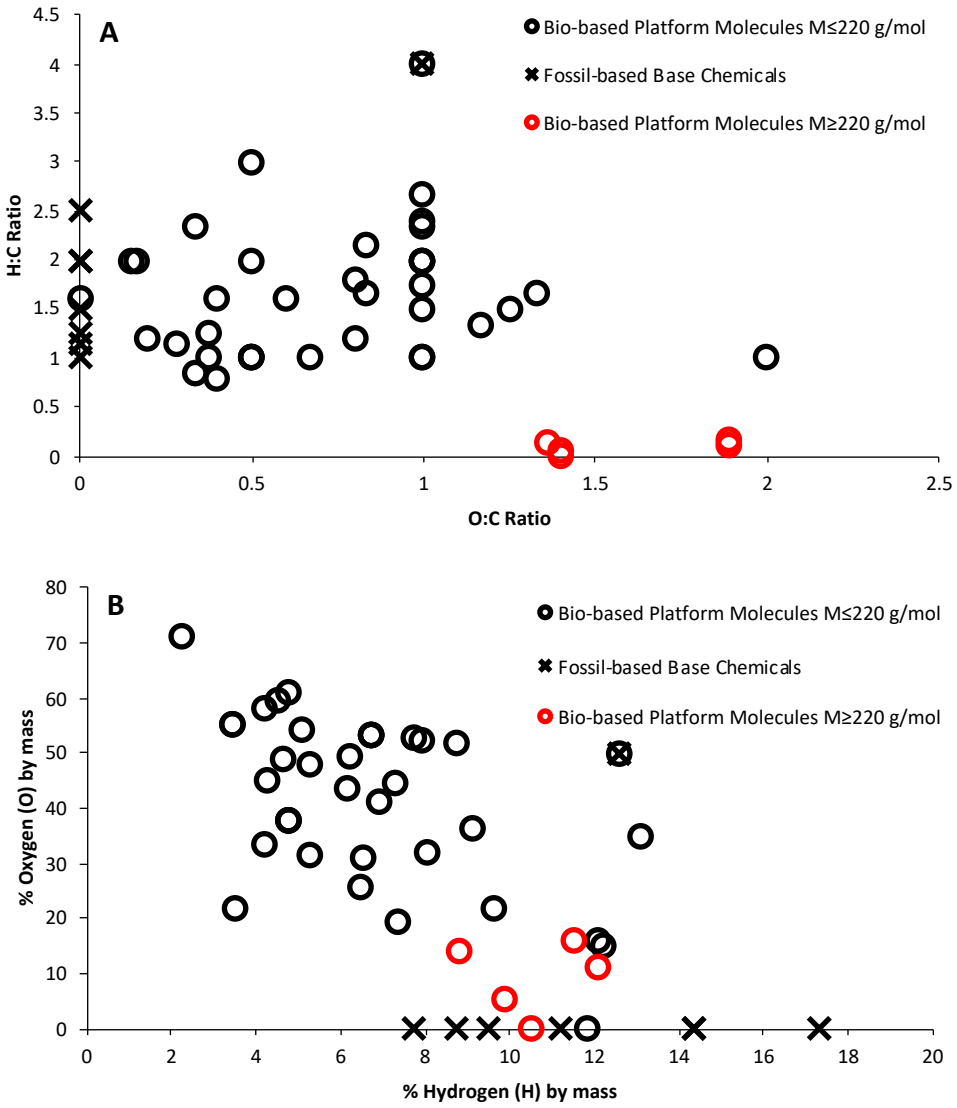

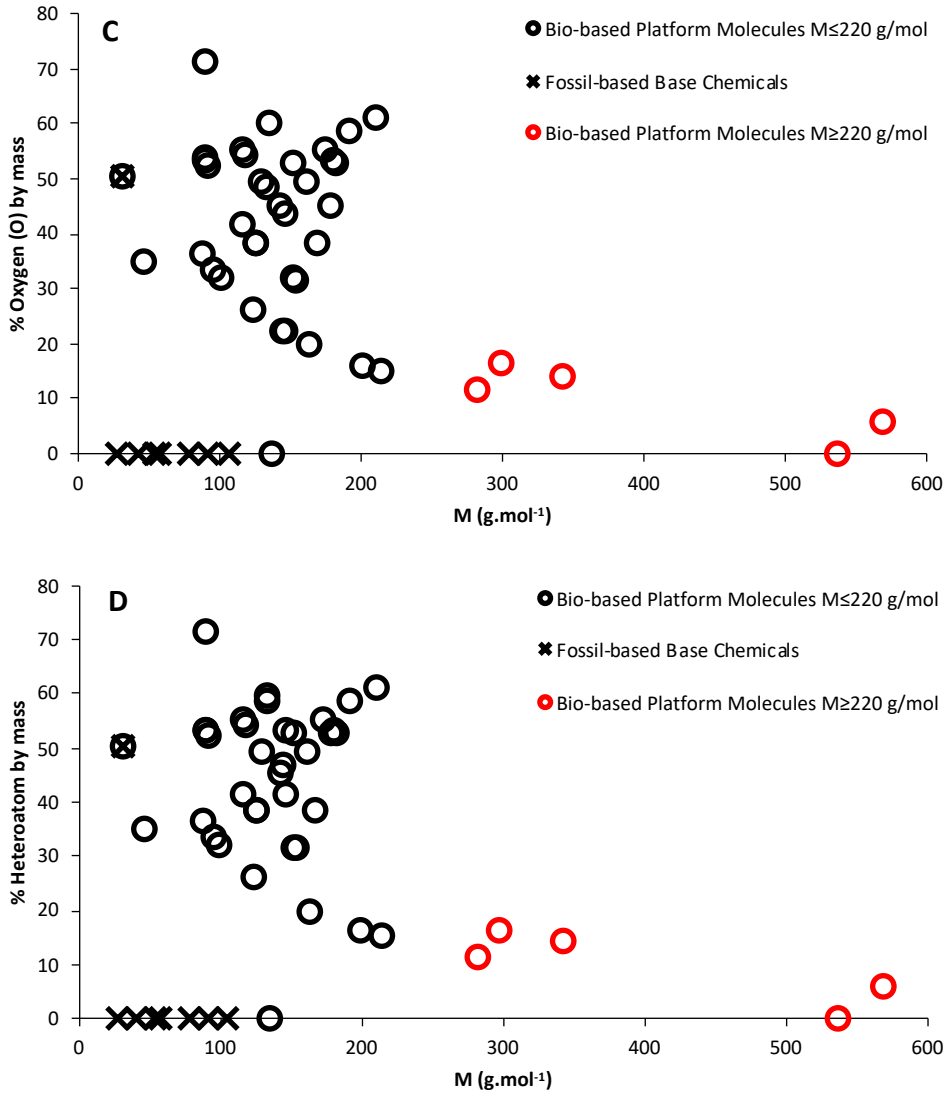

*Figure 8 Different modifications of the van Krevelen diagram with base chemicals (✕) and platform molecules (○ for M≤ 220 g/mol and ○ for M≥ 200 g/mol). **A**: Original van Krevelen diagram of platform molecules and base chemicals (full list available in Appendix 1); **B**: First modification of the van Krevelen diagram replacing the y-axis by %O by mass and %H by mass; **C**: Second modification of the diagram replacing the %H by mass with the molar mass M (g.mol^{-1}); **D**: BioLogicTool plot advantageously replacing the %O by mass in the previous plot with the %Heteroatom by mass. A fully labelled version of plot C is available in Appendix 1.*

A plot where base chemicals, platform molecules and a selection of 14 petrochemical consumer products (dye, surfactant, polymers, herbicide etc.) is represented in Figure 9. It is apparent from this plot that most products from the petrochemistry are far away from their starting material, namely the base chemicals. This observation demonstrates how the current oxidative-driven chemical industry primarily consists in introducing heteroatoms

(leading to products higher relative to the y-axis) while concomitantly increasing their molar mass (more to the right relative to the x-axis).

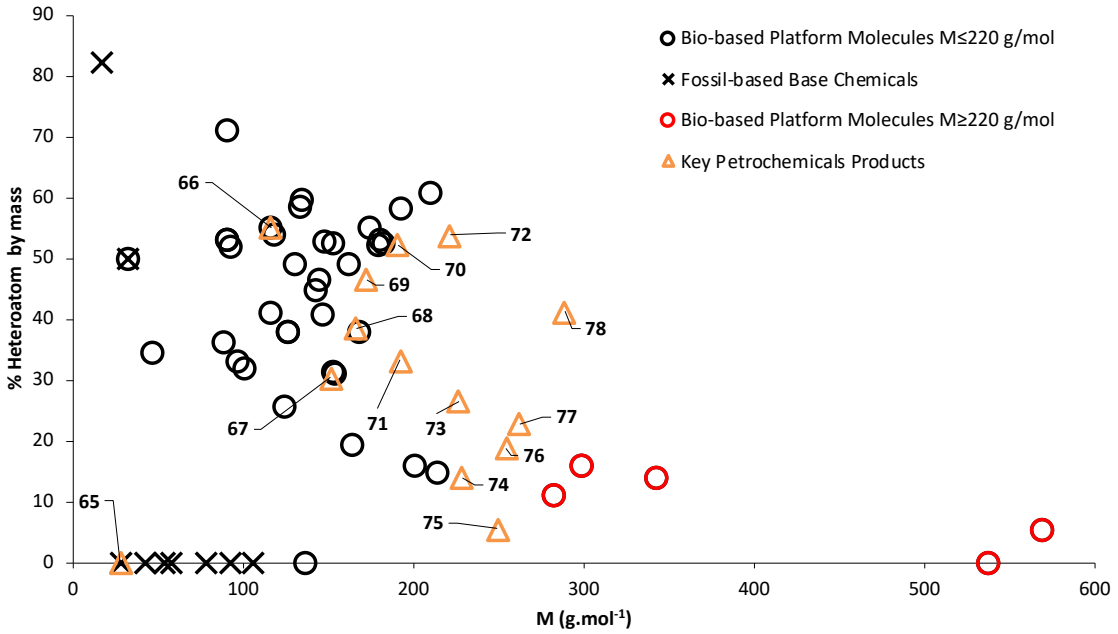

*Figure 9 Plot of platform and base chemicals as represented Figure 8**D** p. 52 including 14 key petrochemical products. Poly(ethene) (polyalkane) **65**, maleic acid (monomer) **66**, N-acetyl-p-aminophenol (paracetamol, pharmaceutical) **67**, Terephthalic acid (monomer) **68**, para-toluenesulfonic acid (Catalyst) **69**, para-toluenesulfonyl chloride (Activating agent) **70**, PET **71**, 2,4-dichlorophenoxyethanoic acid (herbicide) **72**, nylon-6,6 (polyamide) **73**, bis-phenol A (BPA, monomer) **74**, 4-cyano-4'-penylbiphenyl (nematic liquid crystal) **75**, poly(bisphenol-A) carbonate (polycarbonate) **76**, 2,2'-Bis(2,3-dihydro-3- oxoindolyliden) (indigo blue, dye) **77**, sodium dodecylsulfate (surfactant) **78** mass of the monomer was used in case of polymers.*

From these selected exemplary petrochemical products, only poly(ethene) is devoid of heteroatoms. Besides, from the examples taken above, 8 of the products possess at least one heteroatom other than oxygen, further supporting the importance of using the %heteroatom by mass for the ordinate. From Figure 9, it is also clear that, while base chemicals systematically lie on the x-axis, products formed from them are dispersed over the plot, much like platform chemicals. Hence, this plot qualitatively indicates that the most rational route to obtain drop-in replacements from platform chemicals would be to

preserve the heteroatoms already present. This different approach requires preservation of the already high oxidation state carbons in platform molecules, if not decreasing it, through a more reductive-driven approach.

Yet, the sole qualitative assessment of the proximity of a final product with its starting material on the plot is not sufficient to assess the rationality of a synthesis. Intermediates involved in a chemical route must be taken into account as it is them which will determine the tortuosity of such a route. Having a quantitative measure of the complexity (tortuosity) of a chemical pathway is thus essential to assess its rationality. Also, an appreciation of the yields of each reaction step would be of interest, as it remains the first (and sometimes only) metric used by chemists to assess the success of a reaction.

The last modification of the van Krevelen diagram presented above (Figure 8**D**, p. 52) may not only be used to compare bio-based and fossil-based (target) molecules but can also help to assess the rationality of the chemical routes designed to synthesise these compounds. A user-friendly Excel-based tool, named *BioLogicTool,* was thus developed to visualise a chemical route (using the modified van Krevelen diagram in Figure 8**D**) and give rationality scores to assess the logic thereof as detailed in the following section.

2.4 Introduction to *BioLogicTool* plots and scores

The *BioLogicTool* allows all feedstock (Figure 10, A), intermediates (Figure 10, B, C) and final products (Figure 10, D) of a synthetic route to be plotted on the same graphical object. This new plot gives the opportunity to *visualise* individual reactions of a whole synthesis by plotting vectors beginning from starting materials (or intermediates) and ending at products (or intermediates) (Figure 10).

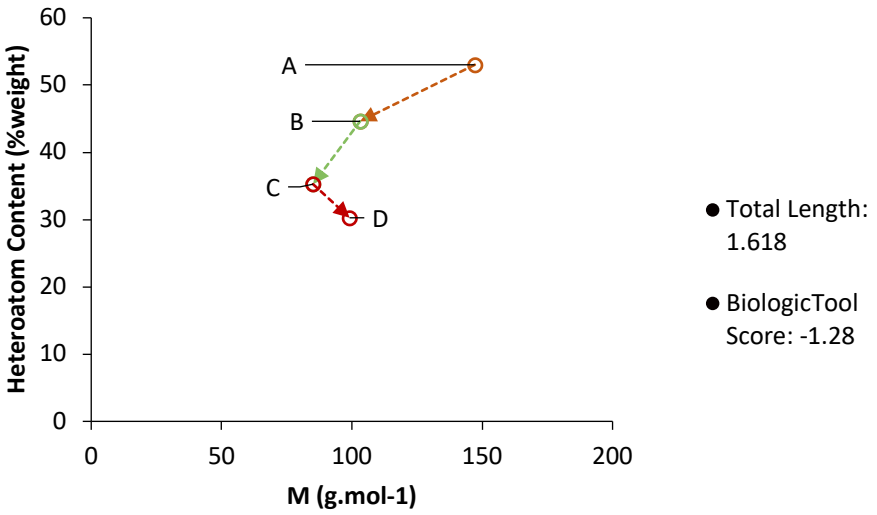

Figure 10 Visualisation of a synthetic route starting from feedstock (A) and ending at the product (D) via intermediates (B & C) using the heteroatom content (%weight) for the y-axis and the molecular mass M (g.mol^{-1}) for the x-axis.

The tortuosity of the route formed by the vectors was deemed a good representation of the logic of said synthetic path (within the limits of the variables used here). However, tortuosity can be laborious to calculate. Instead, the lengths (norms) of all individual vectors were calculated (l_i, eq. ii) and summed (eq. iii) to give the *Total length* of a synthesis (based on its vectorial representation). In the example Figure 10, l_1 would be the length of the vector formed by points A and B, l_2 the length of the vector created by points B & C and so on. Prior to any calculation, data units were removed by normalising them following equation (i). This step was necessary to prevent the addition of different unit values in equation (ii). Simultaneously, normalisation tends to harmonise different data sets and reduces the differences between them considerably.

$$X_{std} = \frac{X - X_{min}}{X_{max} - X_{min}} \qquad \text{(eq. i)}$$

$$l_i = \sqrt{(x_{ib} - x_{ia})^2 + (y_{ib} - y_{ia})^2} \quad \text{(eq. ii)}$$

$$\forall i, n \in \mathbb{N}, Total\ length = \sum_{i=1}^{n} l_i \quad \text{(eq. iii)}$$

Where X_{std} is the standardised value of the coordinate X (%heteroatom (y_i) or molar mass (x_i)) of a point (compound), X_{min} and X_{max} the minimum and maximum values respectively amongst all %heteroatom (y_i) or molar mass (x_i) being computed, and l_i the length of a vector corresponding to the i^{th} chemical step.

The *Total length* alone was not sufficient to give an approximation of the tortuosity of a reaction pathway. A final vector was taken into account during the computation: starting from the feedstock and going directly to the final product, this vector was called the *direct vector*. In the above example, the *direct vector* would begin from A and end at D but not proceed via B or C. This direct vector was also given a positive sign if the difference in %heteroatom was positive (i.e. heteroatom content increased) or a negative sign in the other case (i.e. heteroatom content is reduced). Signs were not attributed to other usual vectors.

Dividing the *Total length* of a reaction route by the length of the *direct vector* gives the *BioLogicTool scores* representing the rationality of a synthetic pathway. The more "logical" a reaction is, the less tortuous its vector path and the closer to 1 the *BioLogicTool score* should be. Explanations for interpreting the *BioLogicTool score* values and signs are given in Table 1.

Table 1 Interpretation of high/low BioLogicTool score values and positive or negative signs

		***BioLogicTool score* sign**	
		+	-
***BioLogicTool score* value**	>>1	Gain of heteroatoms, more tortuous route	Loss of heteroatoms, more tortuous route
	~1	Gain of heteroatoms, more direct route	Loss of heteroatoms, more direct route

A spreadsheet tool was designed to allow any researcher interested in mapping a reaction pathway and calculating its *BioLogicTool score* (See Appendix 2 for screenshots of the spreadsheet). For example, the comparison between the bio-based and the oil-based route to NMP (**64**) is given (Scheme 3). NMP is a polar aprotic solvent widely used to formulate and process paints and coatings, pharmaceuticals, plastics etc. NMP's global production is estimated to be 200-300 $kt.year^{-1}$. As mentioned previously, the current industrial production pathway uses acetylene (**59**) as feedstock which is condensed with formaldehyde to 1,4-butynediol (**60**). A hydrogenation step forms 1,4-butanediol (**61**), which is oxidised to γ-hydroxybutyric acid (**62**). **62** is cyclised to form the γ-butyrolactone (**63**), and a lactone-lactam conversion with methylamine converts **64** to NMP (Scheme 3).

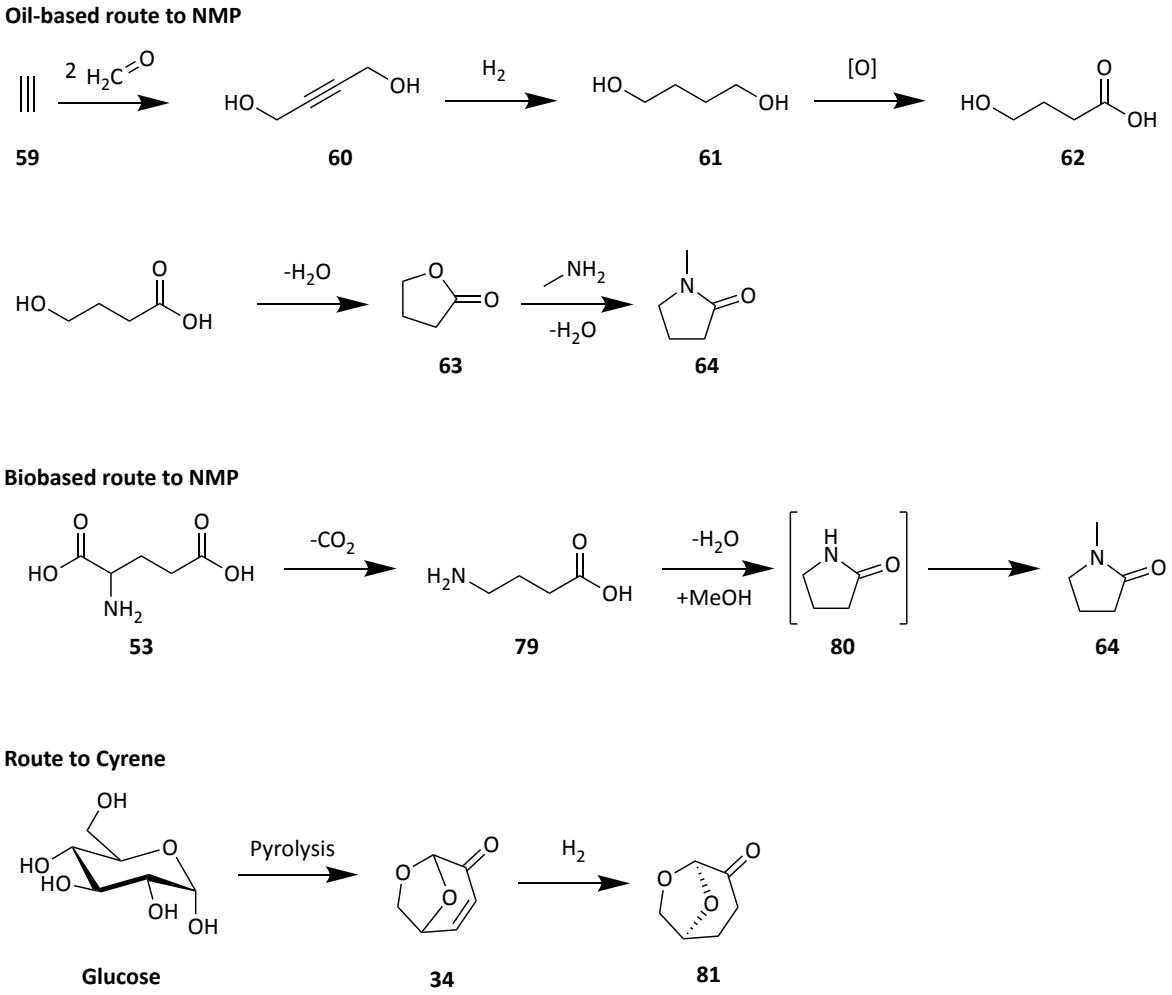

*Scheme 3 Oil and bio-based routes to NMP (**64**) and route to NMP alternative solvent, Cyrene® (**81**).*

The bio-based route to NMP starts from L-glutamic acid (**53**), one of the most abundant amino acids in nature currently produced on a massive scale by fermentation (2 million tonnes per year globally).[41,42] The first step to **64** involves the decarboxylation of glutamic acid to γ-aminobutyric acid (GABA, **79**). This reaction is explored in greater depth in chapter IV.1. GABA is then cyclised to 2-pyrrolidone (**80**) which is subsequently methylated to form NMP. Alternatively, 2-pyrrolidone may not be isolated but instead, NMP can be directly generated by a one-pot cyclisation/methylation of GABA. [42]

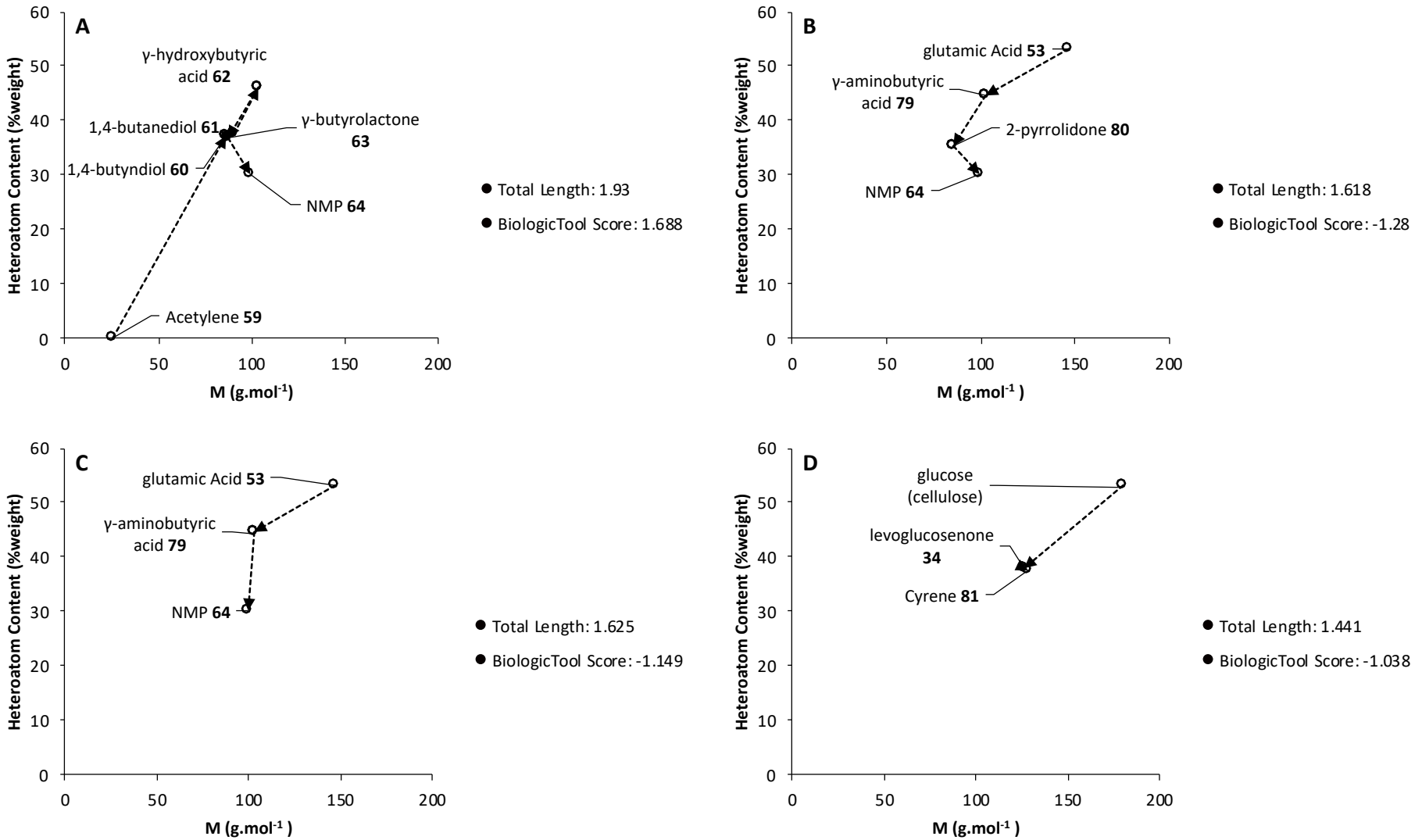

*Figure 11 BioLogicTool plot of different routes to NMP (**64**) and route to Cyrene (**81**). **A**: Petrol based route from acetylene; **B**: Bio-based route from glutamic acid via 2-pyrrolidone; **C**: Bio-based route from glutamic acid without 2-pyrrolidone as intermediate **D**: Route to NMP alternative solvent Cyrene*

Using the *BioLogicTool* to visualise these pathways highlights the differences in complexity and rationality (Figure 11**A-C**). Many intermediates with close M/%weight heteroatom are involved in the oil-based route which necessarily increases the *Total length* of the reaction (1.93) and thus, its *BioLogicTool score* (+1.69) (Figure 11**A**). On the other hand, the bio-based route, with only 3 reaction steps, has a cumulative vector length of 1.62 and a *BioLogicTool score of* -1.28 (Figure 11**B**). If the isolation is avoided and GABA is directly cyclised and methylated the cumulative vector length does not change (1.62 due to the normalisation of data). Still, the *BioLogicTool* scores drop to -1.15 (Figure 11**C**). Despite the seemingly small difference between these scores, they illustrate how the *BioLogicTool* can be used as a tool to discriminate between two routes to an identical product. Nevertheless, to make an informed decision, all three indicators (cumulative vector length, *BioLogicTool score and* visualisation) should be taken considered.

The bio-based route to NMP does not overcome many of the initial issues caused by this solvent. Indeed, despite its good biodegradability and low aquatic life toxicity, NMP is a reprotoxic, irritant solvent. Hence, using a safer, greener replacement would be preferable. An alternative solvent, Cyrene®, was recently developed, which is likely an excellent alternative for polar aprotic solvents such as NMP. Cyrene® is produced from cellulose in raw biomass via pyrolysis, forming levoglucosenone (**34**) and single-step hydrogenation produces Cyrene® (Scheme 3, **81**).[43,44] Because of the simple synthetic route (Figure 11**D**), with the only intermediate **34** almost being on the *direct vector* (from glucose (cellulose) to Cyrene®), the *BioLogicTool score* of this pathway is -1.038, showing very low tortuosity.

These chosen examples demonstrate how the *BioLogicTool* presented here can help assess the rationality of a reaction scheme using readily available data. The high-heteroatom

content of bio-derived molecules makes them attractive to use as raw materials for commodity products. Nonetheless, it is evident that in some cases, the bio-based route to a product might not always be the preferred one, especially when few/no heteroatoms are present in the final product.

Indeed, many chemicals produced on a large scale are devoid of heteroatoms (surfactants (hydrophobic part), lubricants, solvents etc.). As such, alternatives from heteroatom-rich platform molecules should be found. For instance, fatty acids produced by oleaginous plants such as lauric (**41**, Figure 4 p. 33), myristic, palmitic or oleic acid are well-known compounds used in cosmetic (oil component of emulsion) or detergent applications (hydrophobic chains of surfactant as discussed chapter III.4).[45] However, as most of these compounds are currently obtained from food crops, the competition arising from these product usages for food or chemicals must be avoided. Fortunately, other means of production of these oleo-chemicals exist. For instance, research on microalgae has been striving to enhance the ability of these microorganisms to accumulate lipids (mainly triglycerides).[46–48] Fermentation is also considered a possible way of producing oleo-chemicals using oleaginous yeast, bacteria or fungi species.[49]

Terpenes are also bio-derivable compounds widely used for fragrances in cosmetics or cleaning products (*e.g.* limonene, **45** Figure 4 p. 33), or solvents (turpentine oil). However, the current scale of production of terpenes and other bio-derived few/no heteroatom content molecules is currently not high enough (360-370 kt in 2017 for turpentine oil globally) to provide for few/no heteroatom content products at a comparable level as fossil-derived base chemicals do.[50]

2.5 Photoresist case study: turning the light on pentaerythritol tetraacrylate

A widely used polymer class are photopolymers, *i.e.* polymers, whose physicochemical properties change under light (commonly UV) irradiation. One type of photopolymer, namely **Type I**, are made of monomers, or short oligomers constituted of photoactive units which undergo polymerisation in the presence of a photoinitiator.[51] A more in-depth, introduction on photopolymers is presented chapter III.3.

Here, the example of pentaerythritol tetraacrylate (Scheme 4, **84**), an acrylate monomer used in photolithography as a negative photoresist, will be taken to demonstrate the use of the *BioLogicTool.*[51] Industrially, **84** is produced from ethene, which is oxidised to acetaldehyde (Scheme 4, **82**, route **A**) via the Wacker process.[52,53] High yields can be achieved as unreacted ethene is fed back in the reacting vessel and the reduced catalyst (usually $PdCl_2$) regenerated with copper salts ($CuCl_2$). Base-catalysed aldol condensation of acetaldehyde and formaldehyde followed by Cannizzaro reaction with an additional equivalent of formaldehyde leads to pentaerythritol (**83**). Yields up to 88% have been reported in patents.[54] Esterification using acryloyl chloride forms **84** in excellent yields (97%).[55]

The possibility to account for the yield of a step was added in the *BioLogicTool* design. A colour code (Table 2) from red (poor yield) to bright green (excellent yield) was used according to an extended Vogel classification.[56] This add-on was used in the case study, as represented in Figure 12.

Table 2 Colour code used in the BioLogicTool plots to account for chemical step yields

Arrow colour:	Yield
Very clear green	**>98%**
Clear Green	**>90%**
Green	**>80%**
Orange	**>70%**
Dark Orange	**>50%**
Red	**>40 %**
Dark Red	**< 40%**

The *BioLogicTool score* of this route is excellent (1.46) together with a low *Total length* (1.84) due to the relatively small number of steps and average heteroatom content of the final product. Values for the routes represented in Scheme 4 and Figure 12 are summarised Table 3. Nonetheless, from a sustainability perspective, using ethene derived from fossil-resources is not logical.

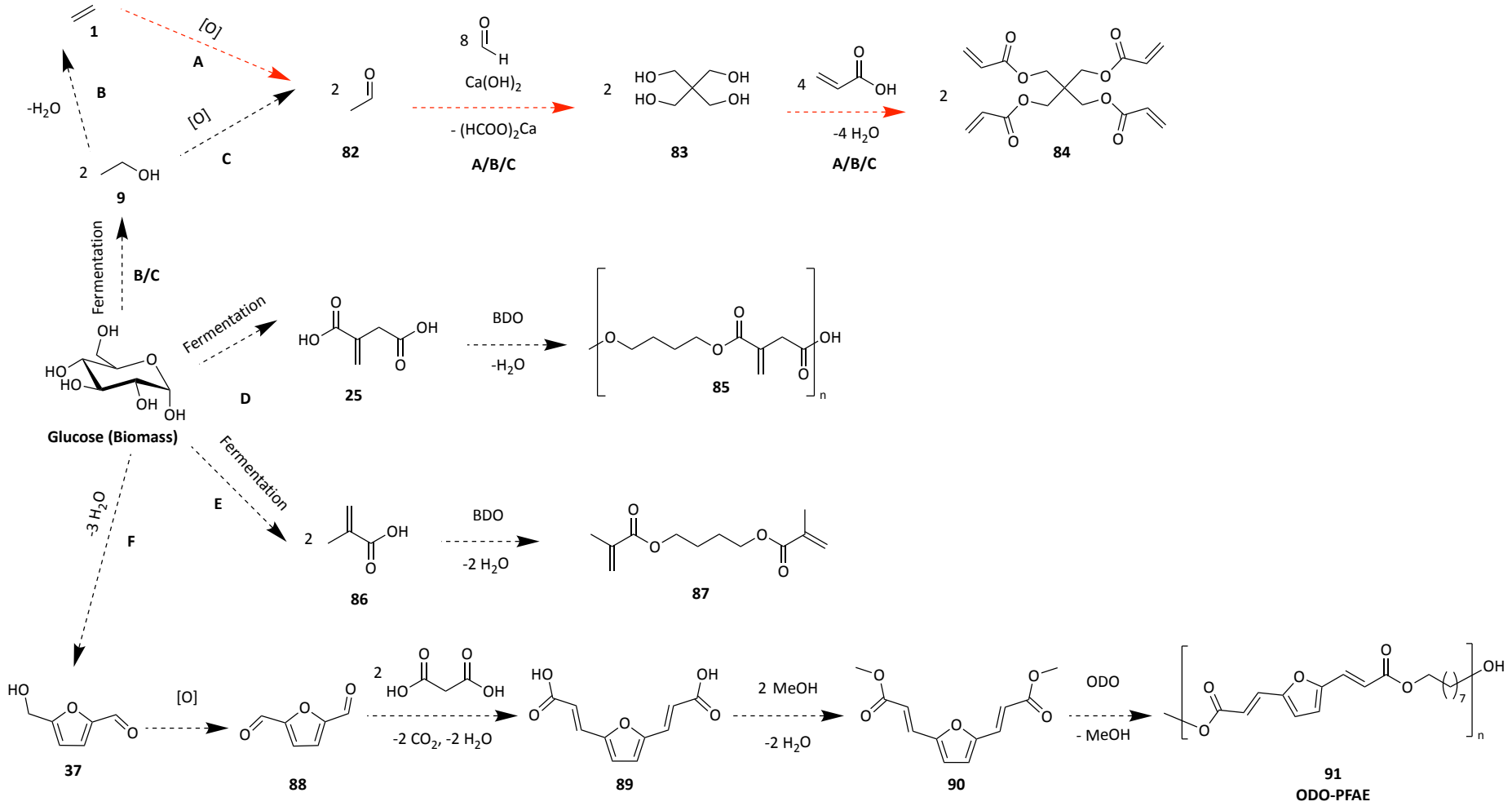

*Scheme 4 Routes studied for BioLogicTool case study. Fossil-based route to pentaerythritol tetraacrylate (**84**, red arrows, **A**), bio-based route to **84**, via ethene (black dashed arrows, **B**), bio-based route to **84** via ethanol oxidation [O] (black dashed arrows, **C**), route to poly(butylene)itaconate **85** (black dashed arrows, **D**), bio-based route to butanediol dimethacrylate, **87** (black dashed arrows, **E**), route to 1,8-octanediol (ODO)- poly(ester) of furandiyl diacrylic ester, ODO-PFAE **91**, (black dashed arrows, **F**). BDO: 1,4-butanediol. [O]: Oxidation*

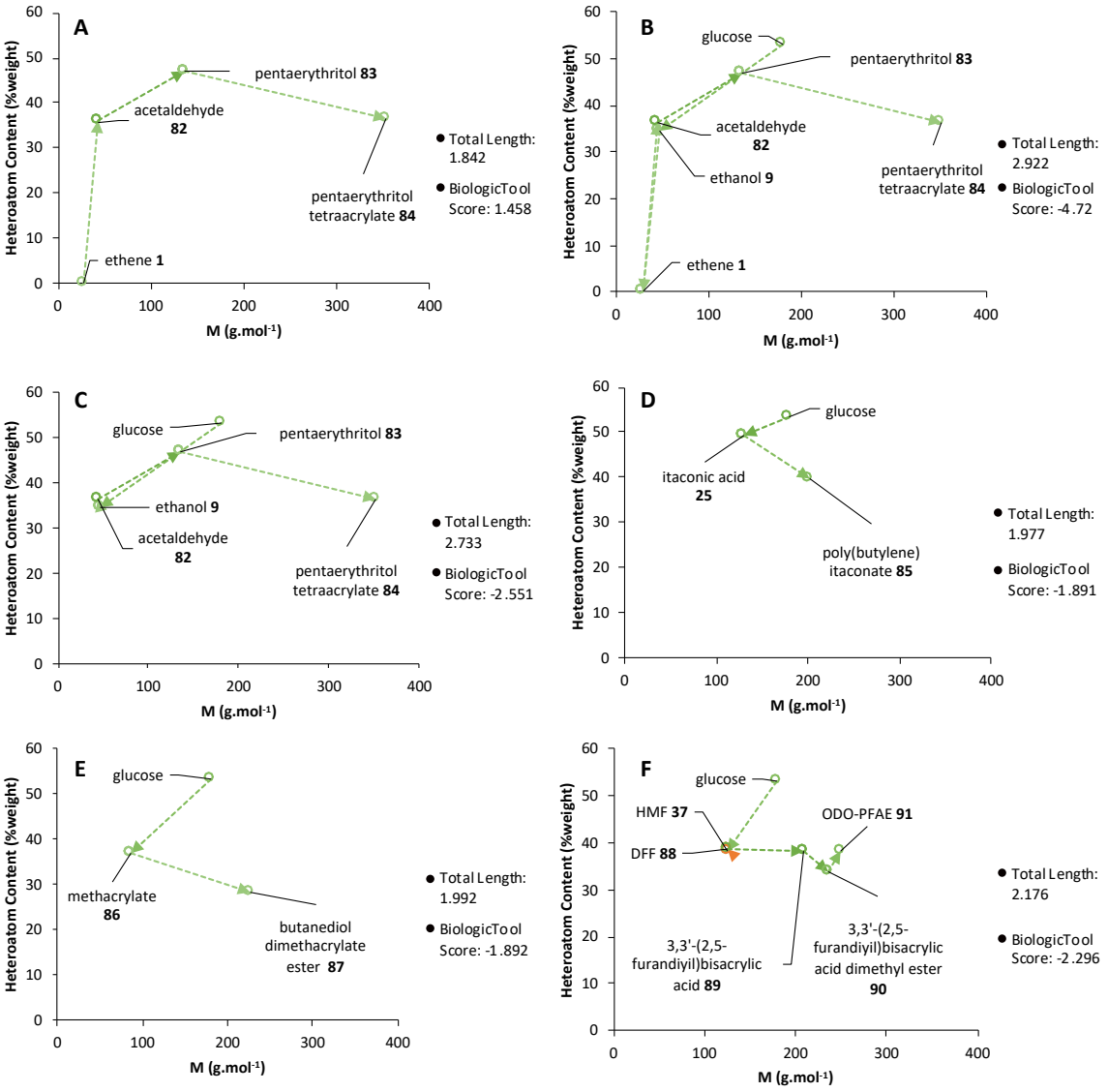

Figure 12 BioLogicTool plots of the different routes represented in Scheme 4. ***A:*** *Fossil-based route to pentaerythritol tetraacrylate (**84**),* ***B:*** *bio-based route to **84**, via ethene,* ***C:*** *bio-based route to **84** via ethanol,* ***D:*** *route to poly(butylene)itaconate **85*** ***E:*** *bio-based route to butanediol dimethacrylate, **87**,* ***F:*** *route to 1,8-octanediol (ODO)- poly(ester) of furandiyl diacrylic ester, ODO-PFAE **90***

Many efforts to produce bio-derived ethene have been made in the past decades (Scheme 4 and Figure 12, route **B**). Ethene is currently produced by cracking naphtha at very high temperature (>800 °C). To make this base chemical from bio-derived molecules, the removal of all heteroatoms is necessary. Bio-ethene is mainly obtained from ethanol (**9**) dehydration and high yields have been reported (up to 99%).[57] Ethanol is in turn previously obtained by fermentation also in high yield (95%).[58] The following steps in this route are

similar to the ones employing fossil-derived ethene. As illustrated by the much higher *Total length* (2.92) and *BioLogicTool score* absolute value (-4.72), stripping off the heteroatoms present in the biomass (here glucose), to produce drop-in replacements of fossil-derived molecules greatly decreases the rationality scores. Moreover, ethene is currently produced on a multi-million-tonne scale (~255 Mt in 2017 globally with propylene).[7] The production of bio-ethene at such scale would require enormous surfaces of arable land (for 1st generation biorefineries) to produce the necessary substrate for fermentation and would generate large quantities of water and CO_2 (Scheme 4**B/C**). It is possible to preserve the oxygen atom present in ethanol by directly oxidising it to acetaldehyde (Scheme 4 and Figure 12, route **C**). Excellent yields were reported for this reaction (up to 95%).[59] Preserving the existing heteroatom already improves the bio-based route's rationality as shown by the lower *Total length* (2.733) and *BioLogicTool score* absolute value (-2.55), now almost half of route **B**'s (-4.72). *Perstorp,* a Swedish speciality chemical company, commercialised a bio-derived pentaerythritol product named Voxtar M100, which is based on bio-derived acetaldehyde from ethanol and bio-derived formaldehyde from methanol.[60]

Table 3 Summary of the Total length and BioLogicTool score values for the different routes depicted Scheme 4 and Figure 12. Non-normalised values are also given

Route	Feedstock	key Intermediate	Number of steps	Total Length	*BioLogicTool* score	Total length (non-normalised)	*BioLogicTool* score (non-normalised)
A	petroleum	ethene	3	1.84	1.46	350	1.07
B	glucose	bio-ethene	5	2.92	-4.72	523	-3.02
C	glucose	bio-ethene	4	2.73	-2.55	447	-2.58
D	glucose	itaconic acid	2	1.98	-1.89	123	-4.73
E	glucose	methacrylate	2	1.99	-1.89	236	-4.50
F	glucose	HMF	5	2.18	-2.30	185	-2.59

These scores remain comparatively high against the fossil-based route. Instead, if alternative bio-derived products to **84** are targeted, the rationality scores improve significantly. For instance, poly(butylene itaconate) (**85**, Scheme 4 and Figure 12, route **D**), a potential **Type I** bio-derived photopolymer, can be obtained via polycondensation of itaconic acid (**25**) and 1,4 butanediol (BDO) in excellent yield (92%).[61] Itaconic acid is a platform molecule obtained by fermentation in yields close to 85%, which preserves most of the heteroatoms present in the fermentable sugars (glucose, xylose).[62] The scores obtained for this pathway are excellent with a *Total length* of 1.98 and a *BioLogicTool score* of -1.89. These rationality scores come close to the fossil-based route. When plotted data (%heteroatom by mass and M) are not normalised (Table 3), this route has the smallest *Total length* value of all (122.97). However, this reduced *Total length* value is compensated in the *BioLogicTool score* value, which is now the highest due to the proximity of both starting material and final product.

An even closer bio-derived replacement to **84** could be butanediol dimethacrylate ester (**87**, Scheme 4 and Figure 12, route **E**). It is obtained from the esterification of methacrylic acid with 1,4-butanediol in 98% yield.[63] In 2012, methacrylate (**86**) production by fermentation was described in a patent, claiming yields up to 95% based on fermentable sugar input.[64] The photoactivity of this monomer has already been reported. Merck patented its use in photoresist application in 2009.[65] The potentially bio-derived route also has comparable *Total length* and *BioLogicTool* values as the previous route: 1.99 and -1.89 respectively.

Finally, the work-hardening photopolymer developed during this work (see chapter III.3) is compared to the other photopolymers in route **F** (Scheme 4 and Figure 12, route **F**). Due to the many steps involved in this polymer synthesis, the *Total Length* and *BioLogicTool*

score values are higher than in route **D** and **E** (2.18 and -2.30). Nevertheless, this represents an improvement when compared to the bio-ethene/bio-ethanol routes **B** and **C**. In addition, it appears that qualitatively, this route is the one that preserves most of the heteroatoms already available in the starting material (vector for each step almost horizontally aligned). As illustrated by the non-normalised scores (Table 3, p. 67), the *Total length* non-normalised is 185, the second-best after route **D**. Unlike route **D** however, the non-normalised *BioLogicTool score* does not increase dramatically (-2.59).

This tool does suffer from some limitations and in no case was the *BioLogicTool* intended to replace other metrics already in place. On the contrary, it proves more useful when a rapid or complementary assessment must be done without prior knowledge of the mechanism, stoichiometry or environmental friendliness of the synthesis. Some of the main limitations of this tool are listed here:

- The tool does not highlight where excess reagents or reactants are required. Other metrics such as PMI are more appropriate for this, but they require the reaction to be performed in the first instance and for the user to gather data for the mass of each reagent used
- The tool does not consider the energetics of the reaction steps and overall pathways. Hence, a chemical route with a higher rationality score (low *Total Length* and *BioLogicTool score* absolute value*)* but that is much more efficient energetically will always be favoured. It is possible that a third axis could address this issue, but this approach would require additional computational work and complicate the tool utilisation.

- The tool does not give direct information on whether one process is more or less environmentally friendly or economically viable. Many additional parameters are required to make such judgements. However, there is likely to be some correlation between improved resource efficiency and a reduction in the number of steps to lower cost and environmental impact. Therefore the tool may offer some initial general assessment of these considerations.

2.6 Conclusion for chapter II

The development of metrics to assess a reaction or chemical route in terms of mass efficiency, financial viability, or sustainability is now an essential part of chemistry. Although the yield remains the most used metric of all, a rise in environmental awareness in the chemistry community has led other parameters to be used. The atom economy, E-factor, and biomass utilisation efficiency or the many hybrid metrics such as Green Motion or Green-scope scale demonstrate the efforts that industries, academia and governments make to put sustainability at the forefront of their research/policy. However, many of these metrics require a sound grasp of either the reaction mechanism, stoichiometries or extensive experimental work and do not offer a visual representation.

Iterative modifications of the van Krevelen diagram (O:C against H:C) led to the development of the *BioLogicTool* plots (%heteroatoms by mass against molar mass). From it, mapping molecules on these plots permitted easy and rapid visualisation of a chemical route. This visualisation, together with the scores given, was designed to assess the rationality of a chemical route, emphasising on bio-based pathways. A case study on a

photopolymer constitutive unit, pentaerythritol tetraacrylate, showed an example as to how the *BioLogicTool* can be used to assess the logic of a proposed route. From this instance, the removal of heteroatoms in platform molecules to produce few/no-heteroatom drop-in replacements of fossil-derived products was clearly not the best solution to adopt. Instead, alternative, functionally similar, products were shown to have a close rationality score.

Like other green metrics, this tool was not designed to be a stand-alone metric that can replace the use of life-cycle analysis, E-factor or others due to its intrinsic limitations. The *BioLogicTool* does benefit from a complementary study on the environmental friendliness of the studied reactions, as well as an energetic and financial evaluation.

Throughout the rest of the work presented here, the *BioLogicTool* will be utilised to compare the different routes undertaken during the synthesis of bio-derived UV-filters, surfactants or polymers. When possible, the comparison of fossil-based products with their bio-derived alternatives will be made and continue to illustrate how the *BioLogicTool* can be used in real-laboratory scenarios.

Chapter III.1
Microalgal characterisation and production of CMF from microalgal biomass

Part 1: Microalgae characterisation

3.1.1 Introduction: microalgal biomass, culture and biochemical composition

Microalgae are fast-growing microorganisms capable of photosynthesis. From a phylogenetic point of view, an immense diversity of microalgae exists.[66] For ease of understanding, both eukaryotic (Haptophytes, Diatoms, Chlorophyceae, etc.) and prokaryotic cells (Cyanobacteria) will further be referred to as *microalgae.* They are found in almost every known aquatic environment, from the Arctic cold water to hot volcanic springs.[67] Their outstanding adaptability and ability to reproduce at a very fast pace (commonly between 0.001 and 0.05 $kg.m^{-2}.d^{-1}$ in open pond reactors), swiftly producing a large amount of biomass, have pushed researchers to consider using them as feedstock for biorefineries.[68,69] Besides, arable lands are not required to cultivate microalgae, avoiding any competition with land utilisation for food crops. Indeed, these microorganisms can grow in fresh, saline, brown water (rich in N and P), or metal-contaminated drainage water (*e.g.* from Ru mining) which is currently being studied as a mean of remediating or recycling these elements.[67,70]

Microalgae are commonly cultivated in two different culturing systems: open-pond (or raceway, open systems Figure 13**A**) and photobioreactor (closed systems Figure 13**B** and **C**). [14,69]

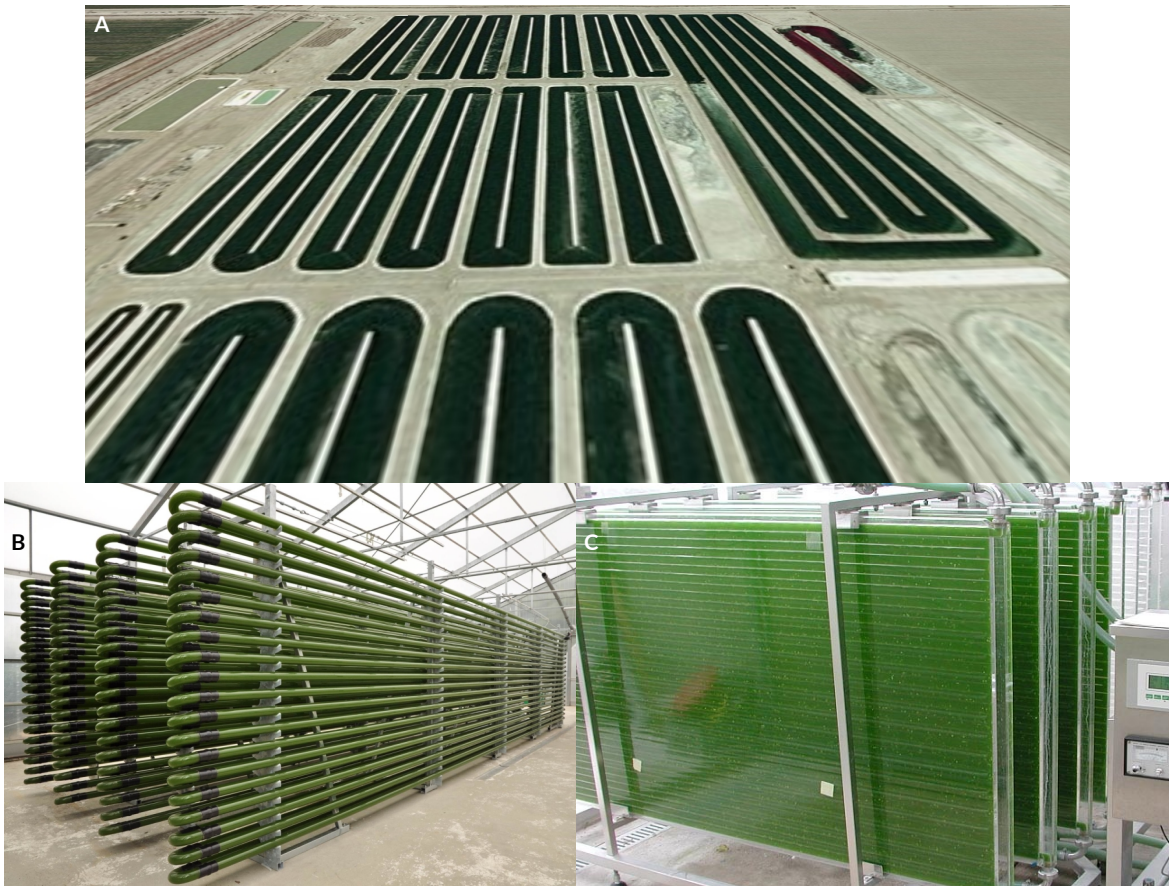

Figure 13 Two main types of culture systems for microalgae. ***A:*** *Open-pond (raceways) system.* ***B*** *and* ***C****: Photobioreactor with tubular (****B****) and panel (****C****) design.* *Photo reproduced from: https://bit.ly/33pytil, https://bit.ly/3hD0mbT and https://bit.ly/2ZD43b7. (accessed 21/07/20).*

Raceways are cheap to implement (*c.a.* $145,000 per ha) compared to other systems (see below) and currently the preferred method employed at a larger scale (hundreds of kilograms). [68] On the other hand, the culturing conditions in these open-systems (temperature, light, pH etc.) are hard to control and submitted to the vicissitudes of the climate. In addition, contaminations (bacterial, or other microalgae species) are practically unavoidable without further inputs.

Alternatively, photobioreactors offer the possibility to regulate most culture parameters closely and, because they are closed systems, contaminations can be controlled and avoided. Unfortunately, these systems require a high initial capital

investment (over €1,000,000 for 1 ha) and are currently reserved for laboratory/pilot-scale projects.[71]

Classically, microorganisms can be grown in two modes, namely the batch mode and the continuous mode. In a batch mode, microalgae are produced in one of the above systems until they reach a growth plateau (due to nutrient or light limitation). The biomass is then harvested, and the process is repeated. In this approach, culturing conditions are changing, and the culture cannot reach steady states. In continuous mode, the cultivation medium containing microalgae is continuously diluted. When it reaches a defined threshold (e.g. pH, nutrient concentration or turbidity of the cultivation medium) a fresh nutrient solution is simultaneously pumped into the reactor at a specific dilution rate. In these stable culturing conditions, the culture reaches steady states and can be studied more accurately. As microalgae reproduce, the turbidity of the culturing medium increases, making the turbidity a parameter of choice to select as a threshold in continuous mode. This type of growth method is then called turbidostat.[72]

Originally, microalgae were used for human consumption: Incas used to harvest green deposit (most likely *Spirulina sp.*) at the water surface and dry it before eating it as a pancake.[69] *Spirulina sp.* is today known for its high protein content (>50% dry weight) and is currently cultivated for food supplements.[73] In the 1960s, microalgae were considered for energy production (H_2, bioethanol or biodiesel) in the American *Aquatic Species Program.*[74] Indeed, when microalgae are under stressful conditions, typically nutrient – nitrogen– starvation, high irradiance etc., they can accumulate key molecules such as starch or triglycerides. These compounds are then facilely transformed into biofuels (*e.g*.

bioethanol and biodiesel).[74] The amount and type of accumulated biomolecules will depend on the induced stress, species and strains. When grown under normal non-stressful conditions, microalgae typically accumulate proteins.

In the last 20 years, many reviews have been dedicated to the untapped potential for chemical production that microalgae represent.[74–79] However, no industrial-scale microalgal biorefinery has emerged due to the many unsolved challenges. These issues have been highlighted multiples times in the literature, some of which are summarised in Table 4.[74,80–83]

Table 4 Current challenges for a microalgal biorefinery, proposed solutions, advantages and limitations

Current main challenges	Proposed solutions	Advantages	Limitation
High initial capital expenditures (CAPEX)	Culture in open-ponds preferred over photobioreactors	Cheap and already available	Water evaporation Culture contamination[68,79]
	Reduced use of inputs (fertilisers, light, additives) by cultivation on wastewater	Recycling of nutrients Waste remediation	Less controlled growing medium, Lower yield[84] Only for non-food/feed and cosmetic applications
Light penetration limitation in culturing systems	Reduction of antenna size for more "transparent" culture	Culture at higher concentration possible Higher light intensity can be used	Strains more sensitive to photoinhibition Reduced photosynthetic yield[85,86]
	Growth in dilute environments Growth in photobioreactor, novel photobioreactor designs	Better light distribution, no "dark-zone"	Lower biomass yield
Energy demanding and costly harvesting, cell wall disruption, dewatering of algae	Hydrothermal liquefaction treatment	No dewatering, No disruption	Loss of valuable compounds
	Cultivation in gel or biofilm	Harvest by melting gel Recycling of culturing medium easy	Only available at laboratory scale
Stress required for biomolecule accumulation (requiring two-stage cultivation and growth inhibition)	Genetic engineering of more productive strains	Selective choice of phenotype traits to enhance productivity	Costly, genetic drift, often outcompeted by native species Only demonstrated on few species[87]
	Continuous selection pressure	Mimic natural selection likely better resistance of natural species	Long (>6 months) Uncertain outcomes[72]
Uncertain upscaling from laboratory to industry scales	Growth in photobioreactor	Closed system, better monitoring	Very high cost of manufacturing (98% of total cost)[88]
	Standardised data and cultivation practice	More comparable data between experiments Better understanding of algae biology	Traceability difficult to guarantee[74]
CO_2 transportation to microalgae culture	Proximity next to CO_2 source	Reduce cost of transportation, allow integration in industrial processes	Limits localisation of microalgae culture

Most solutions proposed to address these bottlenecks also have limitations that usually prevent their implementation on a large scale due to technological constraint (*e.g.* novel gel cultivation not developed on a large scale) or high CAPEX/OPEX (growth in photobioreactors representing high CAPEX).[80] However, many lessons have been learnt from the last decades of research on microalgae, and some dogmas were challenged. For instance, the cultivation in open-pond, despite the low-cost associated with its implementation, may not be the sole profitable means of cultivation.[71] Genetic engineering, usually seen as the pinnacle for strain selection, may be replaced by other selection methods such as flow cytometry sorter or continuous selection pressure.[72,89]

On the other hand, some certitudes have been ascertained or acquired. It now appears clear that the source of nutrient (CO_2, N, P) plays a significant role in the economic and ecological viability of a microalgae biorefinery. For instance, CO_2, necessary for microalgae to perform photosynthesis, must come from industrial operations (ammonia plant, ethanol fermentation plant, power station etc.). The culturing medium must either be recycled or originate from a waste stream.[74,80]

Also evident from previous data is the necessary development of multi-component microalgal biorefineries (Figure 14).[81,82] Contrary to the initially developed concept where only one microalgae-derived biochemical is used to produce one low value-added product (*e.g.* biodiesel, bioethanol, H_2, Figure 14 green boxes); the multi-component biorefinery strives to use most of the chemicals contained in the biomass to produce value-added products and energy (Figure 14 red and green boxes).

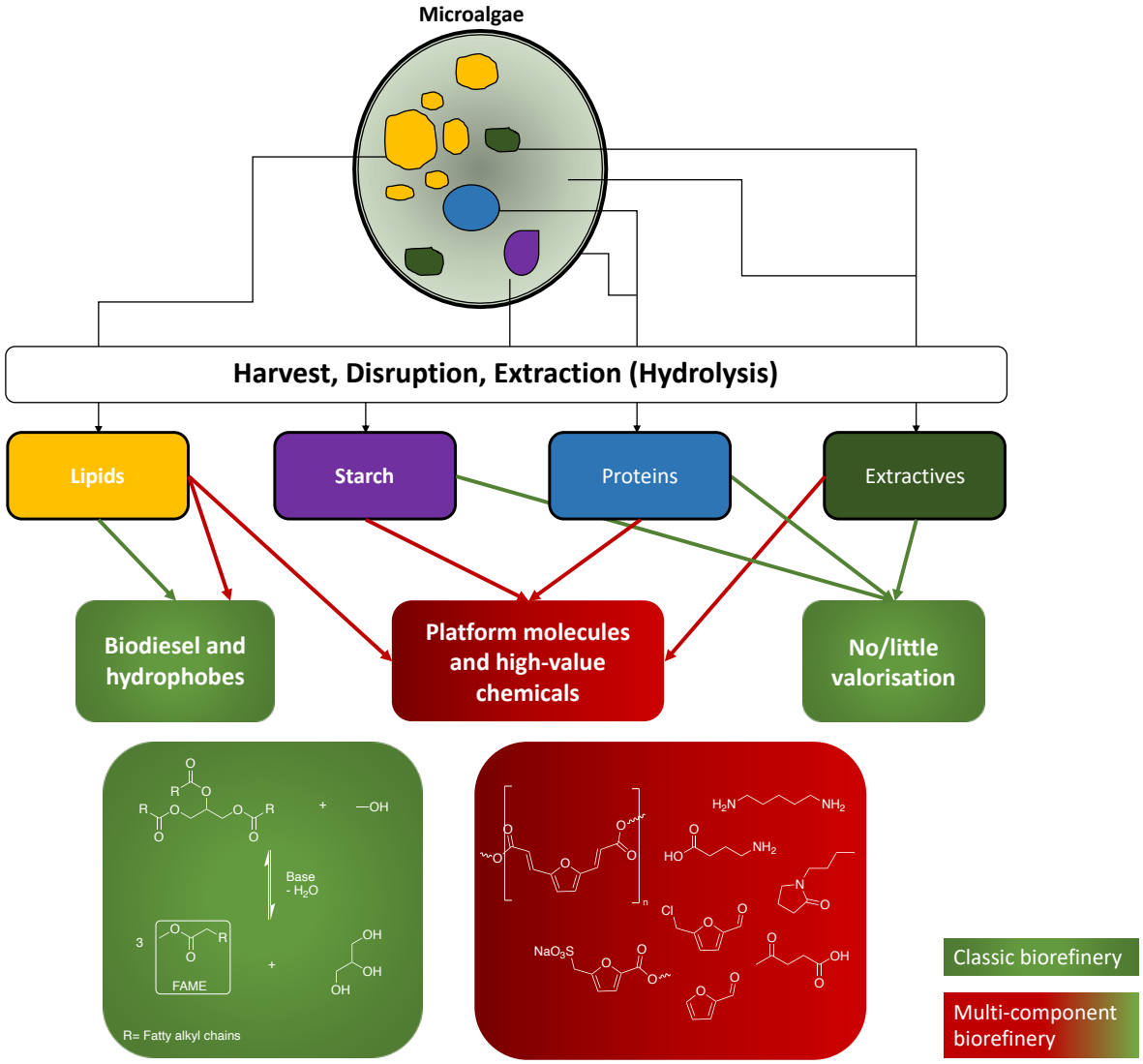

Figure 14 Diagram of a classic microalgae biorefinery (green) and potential multicomponent-microalgal biorefinery (red)

Nonetheless, many microalgae farms currently on the market focus on the sole production of high-value chemicals such as carotenoids, polyunsaturated fatty acids (PUFAs) or antioxidants. The financial pressure that microalgae farms are under forced this trend to settle until the demand for bio-derived, lower-value chemicals increases. Thus, microalgae farms must be ready to face this demand and switch their production from high-value low yielding compounds only, to a combination with low-value high yielding chemicals which they were initially developed for. However, unless an appreciable knowledge of the

biochemical composition of the biomass is built, the yield of expected biofuels, platform chemicals or any valorised products cannot be predicted or calculated adequately.

3.1.2 Aims of chapter III.1 - part. 1 and 2

Microalgae represent a formidable feedstock for 3rd generation biorefineries. However, the currently high cost of this biomass (~40 €.kg^{-1}) largely due to its cultivation requires further improvements both upstream and downstream. Furthermore, a scientific consensus has emerged, and it appears clear that only a multi-component microalgal biorefinery can be profitable.[81,82]

This chapter focuses on optimising a key reaction that could simultaneously extract/use major microalgal biocomponents while alleviating the main challenges as listed in Table 4 (p. 77). The CMF process was considered as an excellent reaction candidate fulfilling these criteria. In the first part, proximate analysis of the different microalgal species used in this work was carried out. This step was essential to determine the biochemical composition of this feedstock and select value-added target molecules incorporating such molecules. In the second part of this chapter, the optimisation of the CMF process and the use of microalgae as a starting material is presented. Being a well-established reaction, it appeared that the solvent remained the principal aspect to optimise. Indeed, CMF production commonly requires the use of toxic chlorinated solvents which severely undermines the sustainable character of this reaction. Hansen Solubility Parameters of selected solvents and pairs of solvents were modelled, and the most promising ones were tried experimentally. Microalgae were then used as a starting material for the reaction.

Due to their low carbohydrate content, only poor mass yields of CMF/lipids could be obtained. Nevertheless, with all three different species, CMF could be produced in moderate quantity, thus proving the possibility to use this reaction for a multi-component microalgal biorefinery later called, *Chemicalgal plant*.

3.1.3 Proximate analysis of microalgal biomass

The characterisation of microalgal biomass is essential to assess its potential use as feedstock. In an attempt to provide standardised data, and thus comparable results, the National Renewable Energy Laboratory (NREL) released a series of laboratory analytical procedures (LAP) which were used in this work to characterise the biomass.[90,91] Despite efforts to provide robust and accurate analytical procedures, large discrepancies in the chemical composition of a similar microalga species may be observed. For instance, Tokuşoglu *et al.* reported a 7.4% ash content, a 7.1% lipid content, a 63.3% protein content and a 15.2% carbohydrate content for *Spirulina platensis.*[92] For the same species, Agustini *et al.* reported an ash content of 10.7% (+2.7%), a lipid content of 2.6% (-4.5%), a protein content of 67.2% (+3.9%) and a carbohydrate content of 11.7 (-3.5%).[93] The observed differences are likely due to the different farming methods (photobioreactor in the first/open ponds in the second) which do not allow the same control on cultivation conditions. Moreover, phases of harvest (exponential-growth or stable/plateau stage), light regimes (continuous/cyclic) or weather conditions also profoundly impact the biomass composition. Still, no standards for these parameters currently exists. Thus, care must be taken when one compares previously reported values, and definitive conclusions should

only be drawn with results obtained from microalgae harvested and grown in the same manner.

The proximate analysis of three different microalgae is shown in Table 5. The total solid content (TSC) is calculated from the moisture content according to equation iv. This number includes both the biomass organic matter and the residual inorganic salts. During the drying procedure, some volatile compounds are also removed.

$$TSC = \frac{Weight_{crucible+dry\ sample} - Weight_{crucible}}{Weight_{sample\ before\ drying}} * 100 \qquad \text{(eq. iv)}$$

Table 5 Proximate analysis of three different microalgae

	Nannochloropsis occulata	***Spirulina sp.***	***Tetraselmis suecica***
Total Solid (%)	98.29 ± 0.05	94.59 ± 0.54	94.39 ± 0.49
Moisture Content (%)	1.71 ± 0.05	5.41 ± 0.54	5.61 ± 0.49
Total Ash (+ char) (%)	26.25	5.53	41.19
Total Lipids (%)	29.00 ± 5.62	28.00 ± 10. 59	24.00 ± 4.69
Total Protein N-factor 4.78 (%DW)	31.05 ± 0.17	54.40 ± 0.00	15.61 ± 0.12
Total Protein N-factor 6.25 (%DW)	40.59 ± 0.22	71.13 ± 0.00	20.41 ± 0.16
Total Protein HPLC (%DW)	39.58 ± 5.10	61.65 ± 2.63	19.62 ± 2.66
Total Carbohydrate (%DW)	5.15	<1	9.57

Both (pre-)freeze-dried microalgae species (*Tetraselmis s.* and *Spirulina sp.*) contain a similar amount of total solids (94.4% and 94.6% respectively) whereas the (pre-) oven-dried *Nannochloropsis o.* biomass TSC is estimated to be 98.3%. This difference may be explained

by the propensity of freeze-dried samples to take up the moisture from the air, which will decrease their TSC.

The TSC value permits the calculation of the oven-dry weight (ODW) of the samples according to equation v. The ODW will be further used to specify yields or dry weight content of a biochemical unless specified.

$$ODW = \frac{Weight_{air\ dried\ sample} \times \%TotalSolids}{100} \qquad \text{(eq. v)}$$

The total ash content (TAC) is measured by thermogravimetric analysis under N_2, following the ramp established by van Wychen and Laurens for furnace calcination of microalgae, to estimate inorganic matter in the biomass.[94]

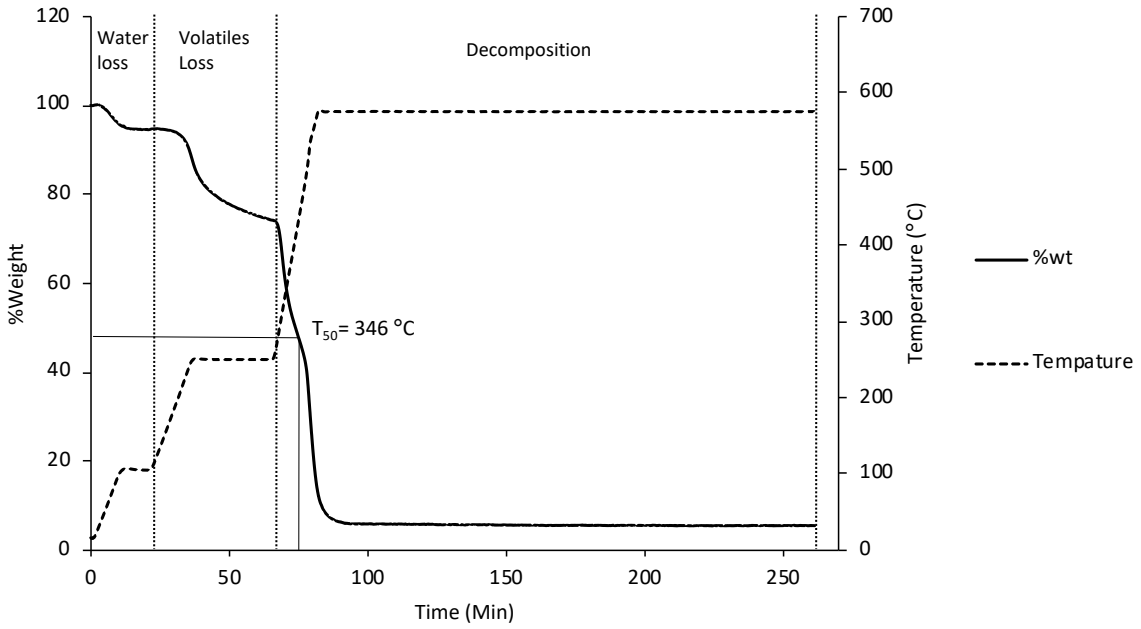

Figure 15 STA plot for Spirulina sp.

A typical Simultaneous Thermogravimetric Analysis (STA) trace obtained for the thermogravimetric analysis of *Spirulina sp.* is represented in Figure 15. During the first heating ramp from 0 to 105 °C, the remaining water in the sample is evaporated, and this typically corresponds to less than 5% of the original weight. During the second temperature ramp, from 105 °C to 250 °C (held for 30 min), most of the volatile compounds are removed. In this example, an additional ~20% loss of the original weight is observed. The last heating event from 250 °C to 575 °C (held for 3 h) corresponds to the decomposition of most organic material and loss of higher boiling point material (terpene, fats, etc.). The %weight remaining at the end of this pyrolysis will further be considered as the TAC of the samples.

Results show a significant difference between the algae species. *Tetraselmis s.* sample contains 41% of inorganic material/decomposed organic matter whereas the TAC is 26.5% and 5.53% for *Nannochloropsis o.* and *Spirulina sp.* respectively. Unsurprisingly, the lowest ash and char content was found in the freshwater microalga *Spirulina sp.* possibly due to the lower salt concentration of the culture medium. Both sea water-cultivated microalgae had a higher amount of inorganic material, up to 8 times *Spirulina sp.*'s TAC, illustrating how the microalgae species and the cultivating environment can influence the composition in this type of biomass. Studies on the difference in salt/ions absorption between freshwater and marine microalgae are scarce. One review by Wilde and Bennemann mentions that no significant difference was reported between them regarding heavy metal absorption.[95] The high TAC in *Tetraselmis s.* was likely due to the harvesting method employed (biofilm formation) which seemed to promote salt accumulation for this microalga.

According to this value, one can expect a higher yield of organic compounds from *Nannochloropsis o.* and *Spirulina sp.* than from *Tetraselmis s.*. This difference in TAC values

between species was also observed in the biomass elemental CHN analysis (Rest, Figure 16).

The CHN analysis of *Nannochloropsis o.* and *Spirulina sp.* showed that both had higher C content, 39.8% and 48.8% respectively, whereas *Tetraselmis s.* only had 24.6%. This discrepancy could indicate that the high TAC obtained previously for *Tetraselmis s.* was indeed inorganic salts and that both *Nannochloropsis o.* and *Spirulina sp.* have a higher organic matter content.

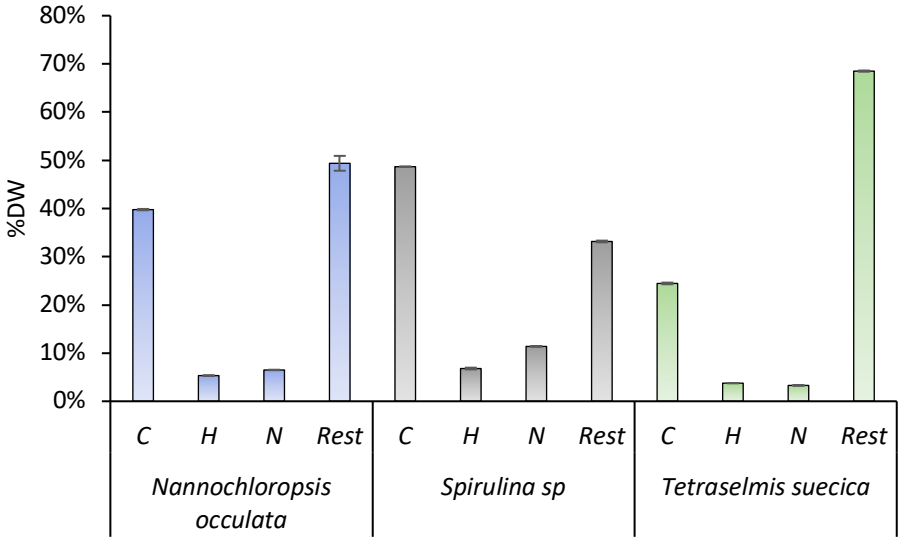

Figure 16 CHN analysis of three microalgae species error bars represent the standard deviation from duplicates.

Commonly the total %N content is multiplied by a fixed factor, either 4.78 or 6.25, to evaluate the total protein content (TPC) present in the material. [96,97] These %N to protein factors were obtained by measuring the total amount of amino acids present in a wide range of biomasses and dividing it by the amount of nitrogen these amino acids (in anhydrous form) represent.[96] Although debatable, a common N-factor of 6.25 (or rarely employed 4.78) has been used for decades by the scientific community. [98,99] This 6.25 factor

usually tends to over-estimate the protein content of a sample due to the presence of other N-containing biomolecules (*e.g.* chlorophyll, nucleic acids) and inorganic N accumulation into microalgae vacuoles. More accurate N-to protein conversions factors have also been reported for various biomasses.[97] Nevertheless, it remains a quick and convenient way to estimate the TPC when more accurate methods are not available.

The TPC value was estimated between 54.4% and 71.0% for *Spirulina sp.* using the 4.78 or 6.25 %N to protein conversion factor respectively. The value of 65% advertised on the retailer's website (MyProtein.com accessed 13/11/19) is within the range of TPC values obtained here using the 4.78 and 6.25 N to proteins conversion factor.[100] A previous TPC as high as 69% (measured by HPLC) was reported in 2002 by Campanella *et al.* for this species.[101] The TPC for *Nannochloropsis o.* was evaluated between 31.0% and 40.6%. In 1991, Brown reported a TPC of 35% (measured by HPLC) for the same microalga species, which falls within the CHN-derived values reported here.[102] Finally, the measured TPC for *Tetraselmis s.*, between 15.6% and 20.4%, was the lowest of all. For this microalga species, a value of 31% (measured by HPLC) was previously recorded.[102] As mentioned above, many parameters, such as cultivation condition or time of harvest, influence the biochemical composition of microalgae. Likely, one or both of these parameters may account for the different values obtained here.

The total amino acid analysis (TAA) of a biomass sample is considered the most accurate way to measure the TPC. It measures the respective abundance of all the 20 commonly naturally occurring amino acids (Figure 17) and does not include other nitrogen-containing biomolecules. Although some amino acids may be present as "free amino acids" in the cell cytoplasm, their quantity is negligible compared to proteogenic ones.

The most widespread method to break down proteins into amino acids is a 6 M HCl hydrolysis at 110°C for 24 h in the presence of a chlorine radical scavenger (phenol).[103] This long reaction time was significantly reduced to 30 min using microwaves as a heating method and was thus used instead.[104–106] Before elution through the HPLC column (C_{18}), a derivatisation step is necessary to detect amino acids by the diode array detector to be possible. Several derivatisation agents exist (*e*.g. Ninhydrin, PITC, Dansyl chloride, Figure 17). However, the combination of fluorenylmethyloxycarbonyl and *o*-phthalaldehyde (FMOC/OPA) is amongst the most popular method. It can be done in the auto-sampler needle, which prevents experimental bias in the procedure and facilitates the analysis.[107,108]

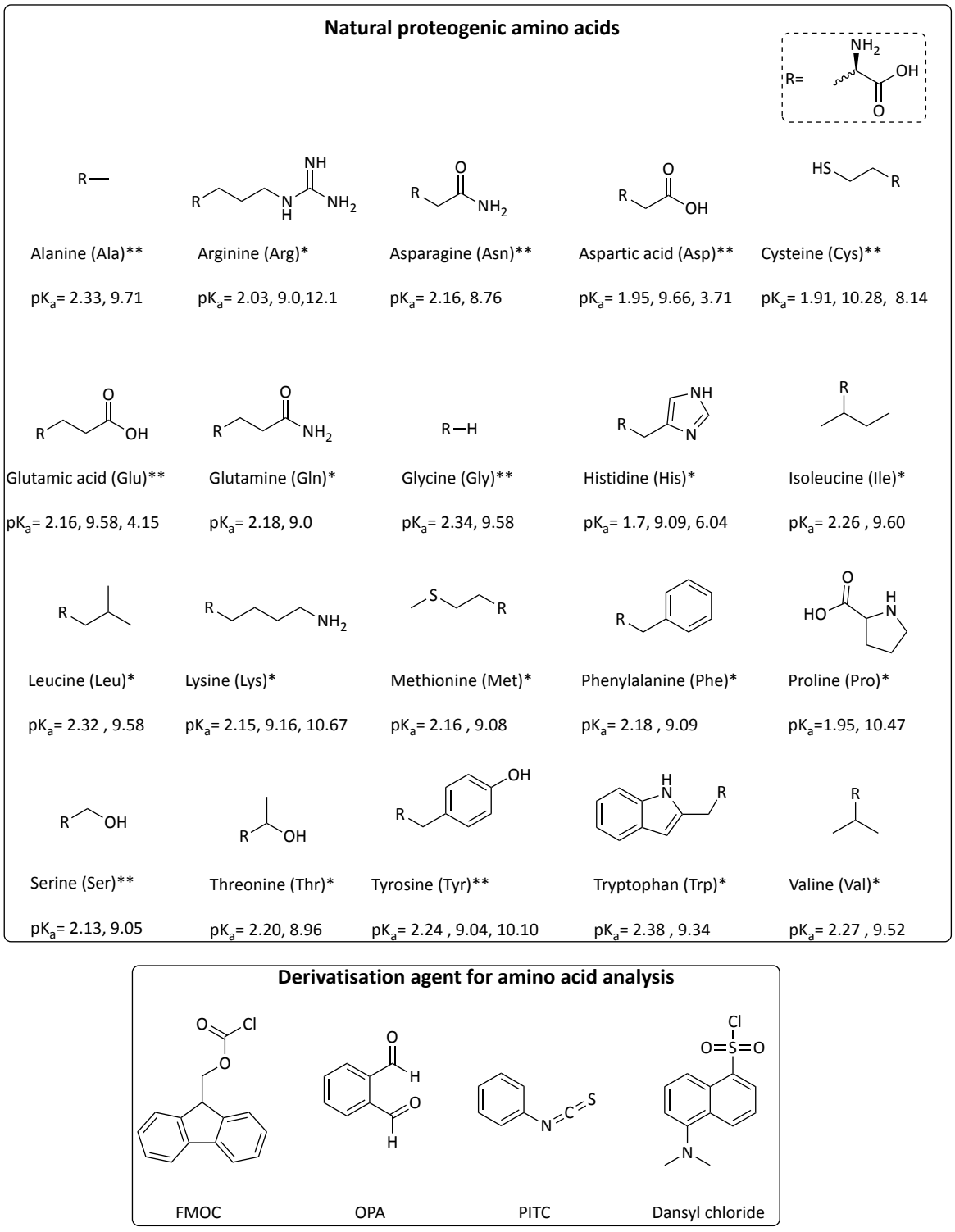

*Figure 17 Natural proteogenic amino acids (L- form) and examples of derivatisation agents. *Essential amino acid **Non-essential amino acid*

A typical HPLC chromatogram of an amino acid standard solution (0.2 mM) is presented in Appendix 3. The quantitative analysis of 20 naturally occurring amino acids can be

performed in a single run. 19 amino acids are detected as their OPA derivatives at 338 nm, whereas proline was detected as its FMOC derivative at 263 nm. Elution order was determined by comparing the retention time of single amino acids.

First, validation of the HPLC method and hydrolysis protocol was carried out using bovine serum albumin (BSA) as a protein standard. A comparison of the BSA amino acid profile (measured as %weight of the total amino acids) reported by Spahr and the microwave-hydrolysed sample in this report is comparatively presented in Figure 18.[109]

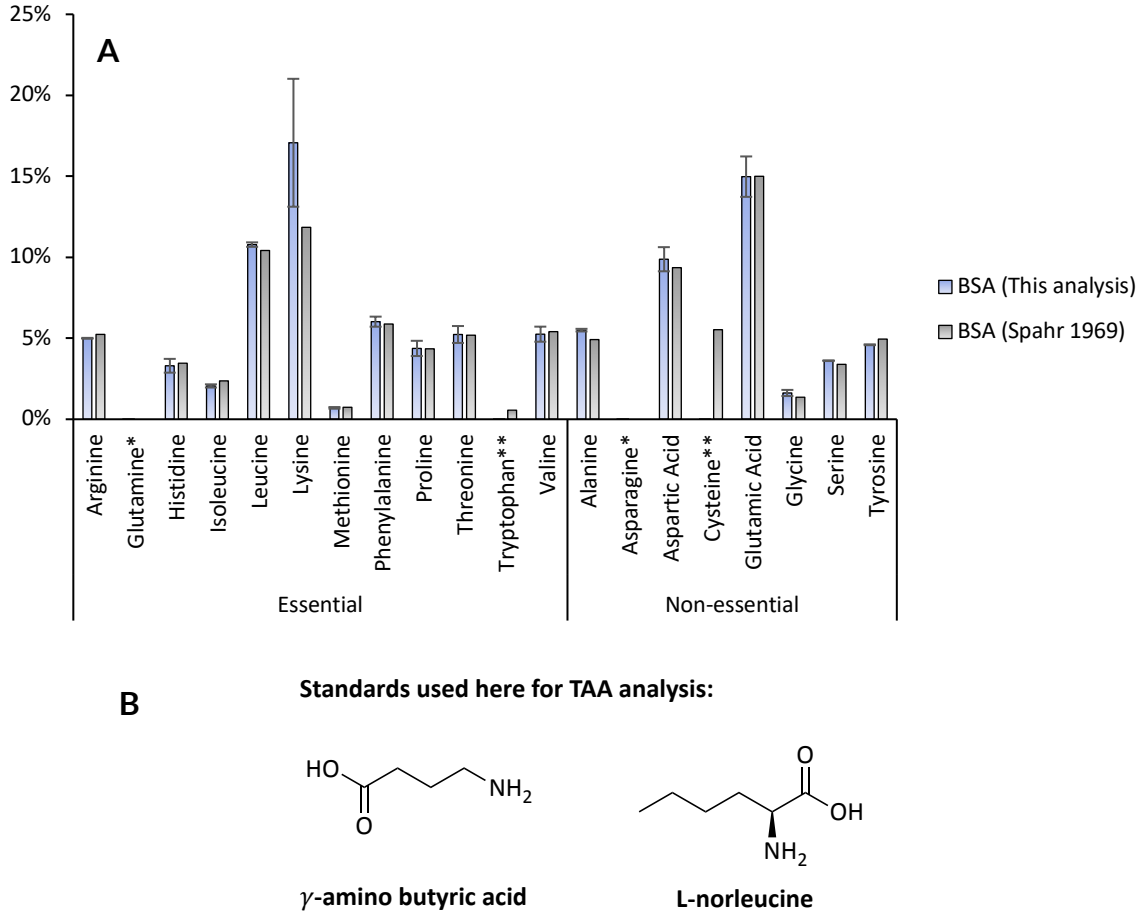

Figure 18 ***A:*** *BSA amino acid profile (in %weight) comparison with Spahr's previous report. Error bars indicate the standard deviation between two samples analysed with different internal standard (GABA and L-norleucine). *glutamine and asparagine are converted to glutamic acid and aspartic acid respectively during acid hydrolysis. **cysteine and tryptophan decompose during acid hydrolysis and were analysed separately by Spahr;* ***B****: Amino acid internal standards used for TAA analysis*

The correlation factor between Spahr's reported value and the one evaluated herein is R^2= 0.99 when tryptophan, cysteine (decomposed during the HCl hydrolysis) and lysine are not included and 0.95 when lysine is included. The values represented in Figure 18 are the average of two TAA analysis employing two different internal standards, namely GABA and L-norleucine (Figure 18**B**). The high standard deviation observed for lysine (Figure 18) and the lower correlation with the value reported by Spahr are suspected to be caused by the use of GABA as an internal standard (R^2 of 0.96 for lysine calibration curve). Indeed, the terminal amine group at GABA's γ-position may compete with lysine's terminal amine group during pre-column derivatisation. Thus, the utilisation of this internal standard may underestimate the lysine content of a sample. When norleucine was used instead as an internal standard, a calibration curve with an R^2 of 0.99 for lysine was obtained. Nevertheless, the good to excellent correlation factor with the previously reported value validated the hydrolysis and HPLC methods developed here.

Hence, the TAA protocol was applied to the different microalgae samples used in this work. Results are summarised in Figure 19 and compared with previously reported values.[101,102] Glutamic acid was the most abundant amino acid, usually followed by aspartic acid and lysine. This result agrees with previous works which concluded that glutamic acid is likely the most abundant amino acid in nature.[110] Hence, the work in chapter IV will be dedicated to the synthesis of higher value chemicals from glutamic acid and lysine; aspartic acid, being structurally similar to glutamic acid, was not considered.

In both *Nannochloropsis o.* and *Tetraselmis s.*, the arginine content was systematically higher (7.3% and 13.2% respectively in Brown's reported values against 4.8% and 4.9% reported here). In contrast, aspartic, glutamic acid, and lysine contents were ~0.7

times lower.[102] The use of methanesulfonic acid for the sample hydrolysis and phenyl isothiocyanate (PITC) for the derivatisation in the 1990 report may explain this difference.

Moreover, another step employed by Brown, consisting of a cation-exchange resin purification, may explain the discrepancy found in basic and acidic amino acids levels (glutamic acid, aspartic acid, lysine, arginine and histidine).[102] Indeed, these amino acids are more likely to be retained by the resin than the others leading to underestimating their level in the amino acid profile.[102] Finally, the use of microwave (30 min at 150 °C or 10 min at 180 °C) is known to improve the recovery of some amino acids such as threonine, tyrosine and serine. Aspartic acid, glutamic acid or lysine recovery may also benefit from this heating method.[105,111,112] Values reported by Campanella *et al.* agree with the measurements completed here, R^2= 0.93.[101]

The TAA obtained allowed the TPC calculation, which should be within the range of CHN-derived values. Indeed, the HPLC-derived TPC were found to be 39.6% for *Nannochloropsis o.* (31.1% - 40.6% by CHN), 61.6% for *Spirulina sp.* (54.4% - 71.1% by CHN) and 19.6% for *Tetraselmis s.* (15.6% and 20.4% by CHN). As expected, the 6.25 factor did overestimate the protein content in all microalgae. Thus, it was possible to calculate a corrected %N to protein factor.[96,97] Corrected N-to protein factors of 5.8 for *Tetraselmis s.*, 5.64 for *Spirulina sp.* and 5.85 for *Nannochloropsis o.* were found and considered more appropriate for these microalgae species.

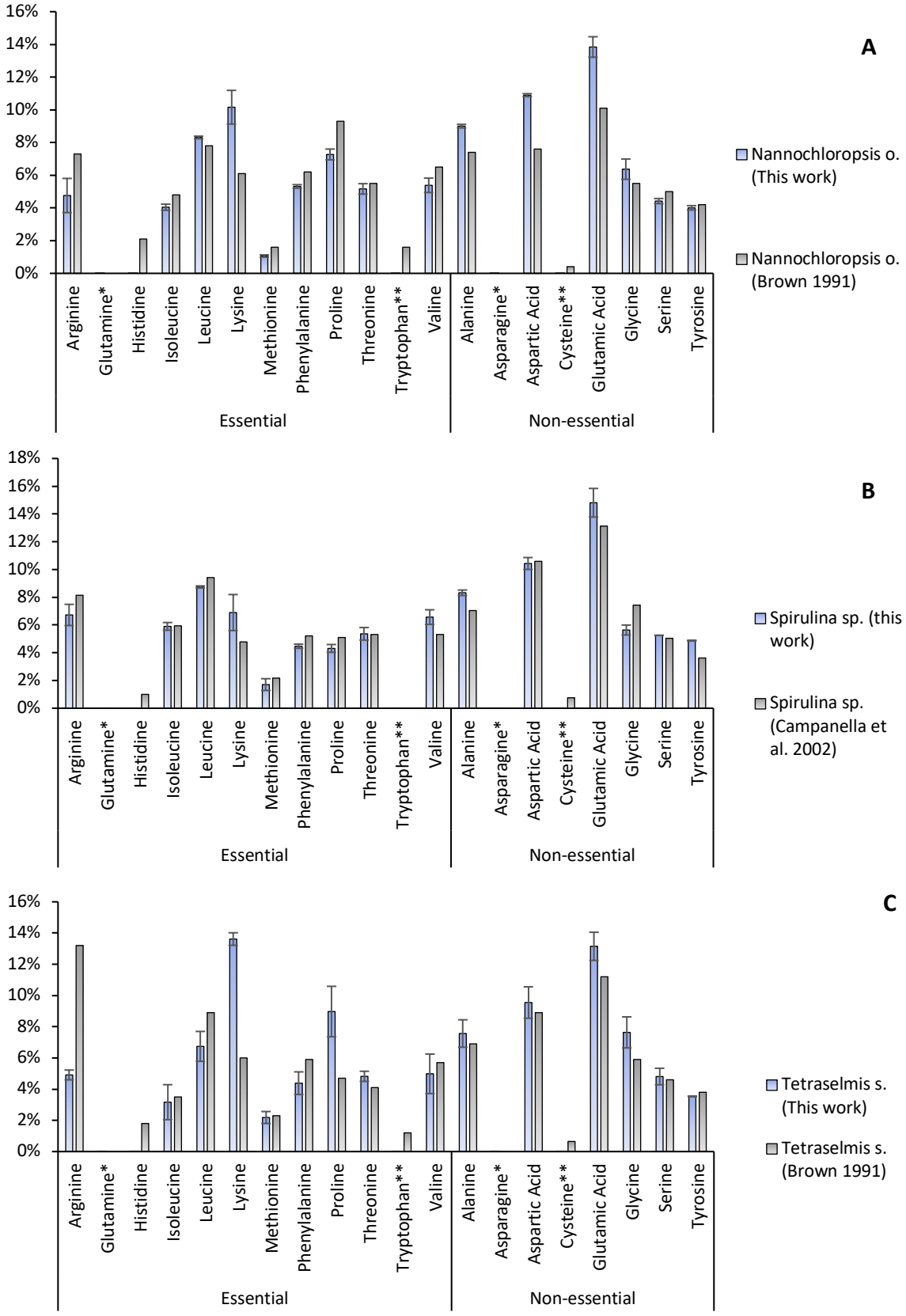

*Figure 19 Amino acid profile of three different microalgae and comparison with previously reported values. Error bars indicate the standard deviation between two samples analysed with different internal standard (GABA and L-norleucine). *glutamine and asparagine are converted to glutamic acid and aspartic acid respectively during acid hydrolysis. **cysteine and tryptophan decomposed during acid hydrolysis and were analysed separately by Spahr.*

The total lipids content (TLiC) was determined using soxhlet extraction employing $CHCl_3$:MeOH (2:1). The solvent was removed under reduced pressure, and TLiC was obtained by calculating the ratio of the thus obtained lipid residue mass with the respective microalgae ODW before extraction. This solvent system usually provides the highest TLiC by extracting both less polar biomolecules such as triglycerides, carotenoids and more polar compounds, phospholipids or glycolipids for instance.[113]

The TLiC of *Nannochloropsis o.* is 29%, *Spirulina sp.* 28% and *Tetraselmis s.* 24%. Analysis of the extract by GC-MS was conducted and revealed the presence of mainly C_{16}, C_{18} fatty acids together with phytol (identification of compounds with NIST library).

Total carbohydrate content (TCC) was initially determined by HPLC analysis. However, the required two-step hydrolysis with sulfuric acid did not yield exploitable results consistent with obtained values for TSC, TPC, TLiC etc. Different temperatures were tried for the hydrolysis step: 121 °C, 150 °C and 180 °C. Unfortunately, most of the sugars remained in oligomeric form after all temperatures tried (Figure 20). Despite a consistent decrease in the oligomer peak area (highlighted by the blue rectangle): $2.8*10^5$ a.u for 121 °C, $2.2*10^5$ for 150 °C and $1.8*10^5$ for 180 °C, the glucose or other sugars content did not increase proportionally.

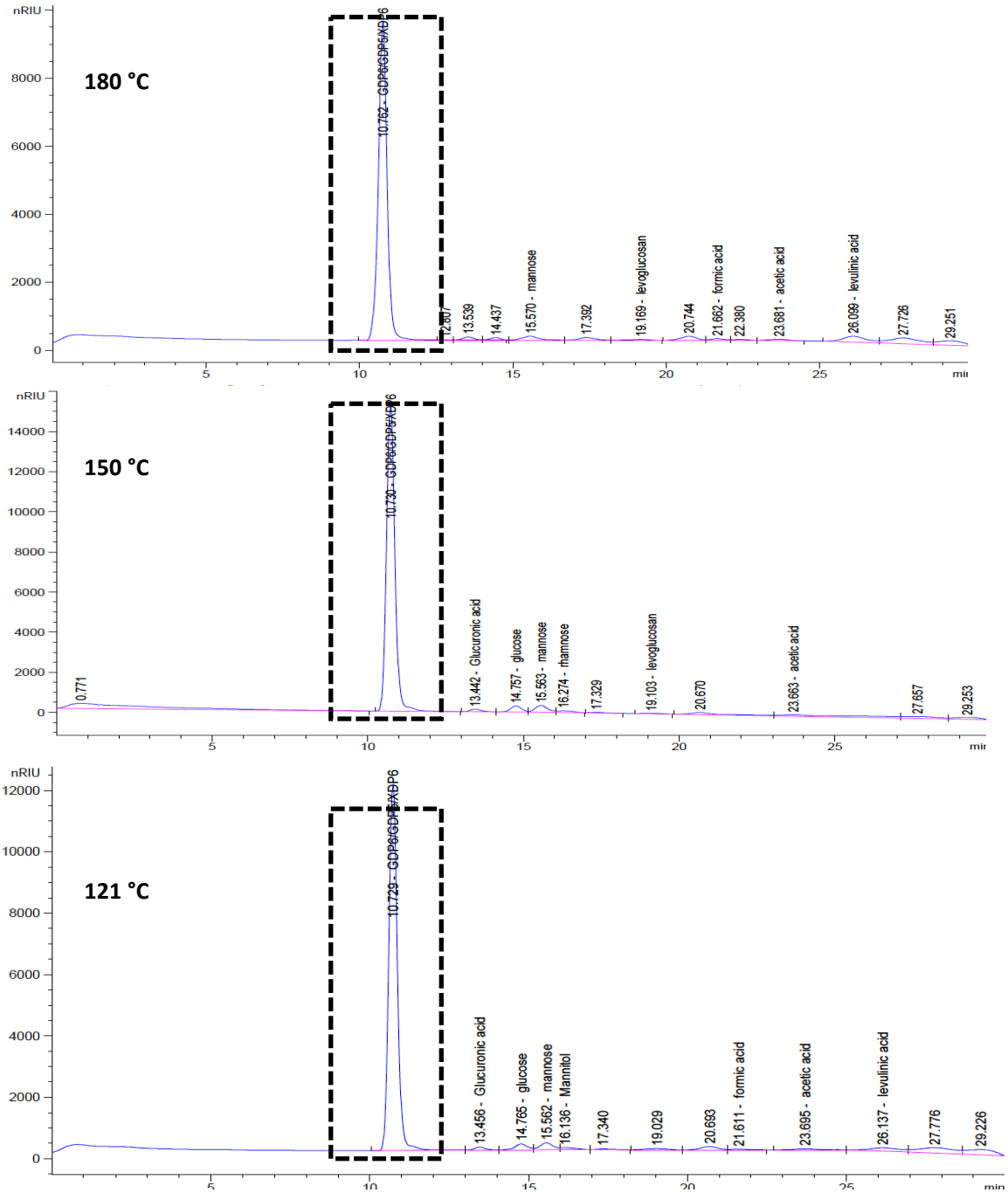

Figure 20 Chromatogram obtained for Nannochloropsis o. after 2-step hydrolysis (with microwave) at 121 °C (bottom) 150 °C (middle) and 180 °C (top) for 1 h. Dashed rectangle highlights the polysaccharide oligomer peak.

TCC was subsequently obtained by subtraction with the other values according to the equation vi. Unsurprisingly, the TCC of this biomass was low (less than 10% DW for all three). These microalgae were cultivated for animal feed (*Tetraselmis s.*), food supplement

(*Spirulina sp.*) or oyster farming (*Nannochloropsis o.*) thus, protein and lipids were the primary biomolecules targeted for accumulation, and not carbohydrates.

$$TCC = TSC - (TAC + TLiC + TPC) \qquad \text{(eq. vi)}$$

3.1.4 Conclusion for chapter III.1 - part.1

The characterisation of 3 different microalgae was performed via proximate analysis. Various parameters such as TSC or ODW were obtained and further used to determine the biomass composition. It appeared that *Nannochloropsis o.* and *Spirulina sp.* had the highest TLiC (29% and 28% respectively) and TPC (40% and 62% by HPLC respectively). The CHN and STA analysis of the samples showed a significantly high TAC in *Tetraselmis s.* when compared to the other two, likely due to the higher inorganic salt content of its culture medium and culturing method.

The amino acid profile revealed that glutamic acid, aspartic acid and lysine are the most abundant in these organisms. At the same time, GC-MS mainly showed the presence of C_{16} and C_{18} fatty acids in the lipids extracts. For these reasons, chapter III.4 and chapter IV will strive to implement these extractable biomolecules in value-added compounds.

Lastly, TCC was low in almost all microalgae tested here (<10% DW of all microalgae). The organisms analysed were destined to be used as a food supplement for human or animal consumption which explained the prevalence of proteins and lipids instead of carbohydrate in their composition.

In the following section, the CMF reaction –that converts carbohydrates into CMF and extract lipophilic compounds simultaneously– was explored as a potential essential reaction for the *Chemicalgal plant* concept. The low TCC and TLiC of these microalgae will likely result in a small CMF-lipid mass yield. However, considering their impressive biocomposition tunability, it is no doubt that a carbohydrate-rich microalga species can result in excellent CMF mass yields as previously reported.

Chapter III.1
Microalgal characterisation and production of CMF from microalgal biomass

Part 2. CMF a versatile platform molecule derivable from microalgae

3.1.5 Introduction: CMF, a more stable HMF alternative

5-(Chloromethyl)furfural (CMF, **38**, Scheme 5) was synthesised and accurately characterised as early as 1901 by Fenton and Gostling.[114] During their study on methylfurfural derivatives they treated hexoses (fructose) and cellulose with HCl gas in diethyl ether which afforded a "[…] *yellow oil or syrup which (remains) generally refuses to crystallise, […]"* and was rightly identified as CMF.

The rise of green chemistry at the end of the 20th century pushed chemists to seek possible platform chemicals from biomass, particularly those accessible on an industrial scale. In 2008, Mascal and Nikitin demonstrated the facile one-pot preparation of CMF from cellulose via a biphasic reaction involving concentrated HCl, an organic solvent (usually 1,2-dichloroethane, DCE) and a catalytic amount of lithium chloride (LiCl).[115] The following year, the same group showed that the use of LiCl was not necessary for their process to proceed in high-yields starting from polysaccharides.[116]

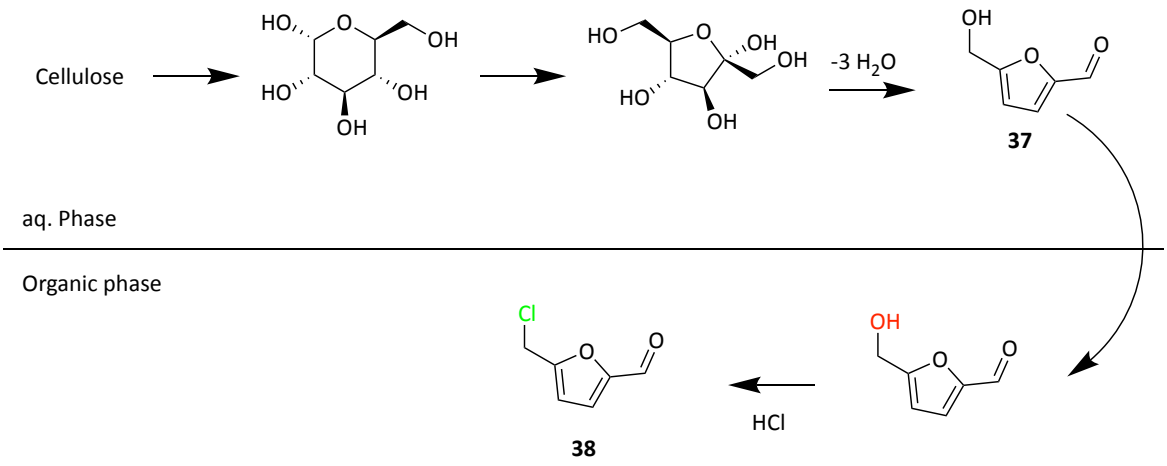

Scheme 5 CMF process in a biphasic reaction

CMF (**38**) is structurally closely related to the better known 5-(hydroxymethyl) furfural (HMF, Scheme 5, **37**). A chloromethyl group in CMF simply replaces the hydroxymethyl moiety attached on the furan ring in HMF. This seemingly small difference gives CMF its superior stability in the production process and grants synthetic possibilities that HMF does not offer.

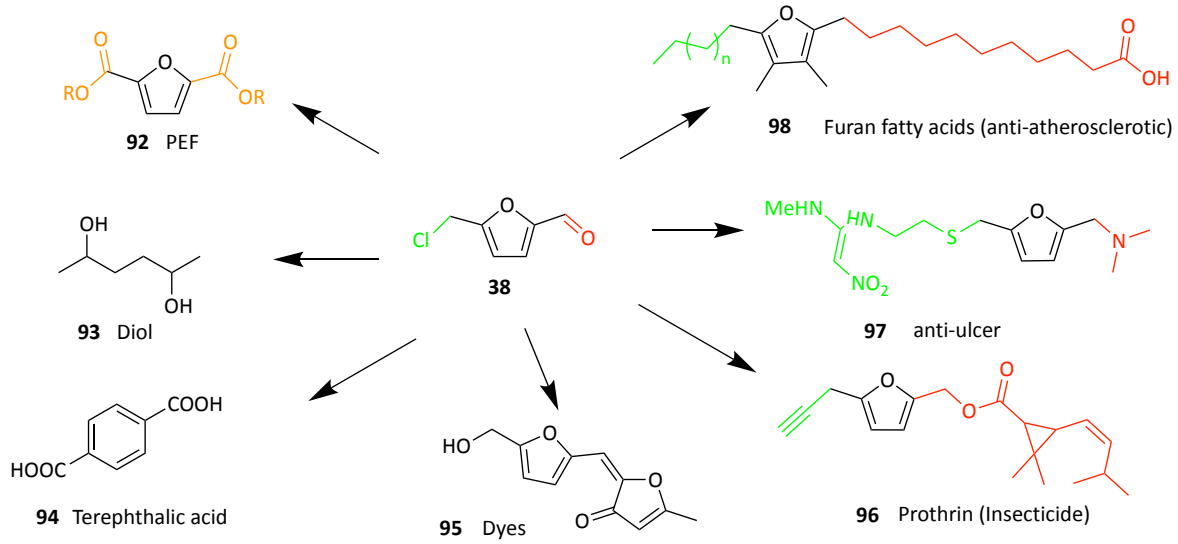

*Figure 21 Reported uses of CMF (**38**). Green: chloromethyl manifold used, Red: aldehyde manifold is used, Orange: both are used. Modified Figure from* 117.

For instance, Chang *et al.* made use of the chloromethyl- manifold in a Ni-catalysed Kumada coupling between a protected CMF and EtMgCl for the synthesis of furan fatty acids (Figure 21. **98**), which are used as anti-atherosclerotic drugs.[36] The use of the chloromethyl- moiety was also illustrated in the total synthesis of Prothrin (Figure 21 **96**), a powerful insecticide.[39] Here, the acetal-protected CMF is coupled to TMS-acetylene mediated by CuI. Recently, Mascal's group published a novel route to 100% biobased dyes based on CMF derived butenolides (Figure 21 **95**).[40]

Besides, one can also obtain products synthesised from HMF using CMF. For example, poly(ethylene furanoate) (PEF, Figure 21 **92**) can be obtained from CMF after the formation of diformyl furan (DFF) via Kornblum oxidation, subsequent synthesis of the diacyl chloride with t-BuOCl and esterification.[117] Likewise, CMF possesses the same ability as HMF to be converted to another platform molecule, levulinic acid. The latter also permits the synthesis of high-value chemicals such as δ-aminolevulinic acid (for photodynamic therapy), or lower value chemicals such as γ-valerolactone (GVL) used as solvent, fuel or monomer.[118]

One of the main advantages of CMF (**38**) over HMF (**37**) resides in the former's preference to stay in the organic phase during the synthesis due to its higher hydrophobicity as illustrated by their different cLogP values $cLogP_{CMF}$= 1.4 and $cLogP_{HMF}$= 0.2383 (Computed using DataWarrior software). This "trapping" of **38** in the organic phase dramatically increases its stability since less CMF is hydrolysed to levulinic, formic acids or other decomposition products, which generally occurs in an acidic aqueous environment with HMF. A higher **38** yield of up to 80% can be achieved from cellulose-rich biomass such as corn stover whereas **37** is rarely isolated.[119,120]

In many aspects, the CMF process provides answers to the current challenges that a multi-component microalgal biorefinery has:

1. Harvest is no longer required in the CMF process since HCl gas would be used in pilot/industrial-scale plant, bubbled directly into the culturing medium containing the biomass to keep a constant titre.

2. Likewise, disruption is not necessary since the strongly acidic environment disrupts microalgae without the need for any expensive pre-treatment (ultrasound, microwave, osmotic shock etc.)
3. Dewatering is not mandatory during the treatment of the biomass by the gas. Water can later be recycled and reconditioned for another culturing medium.
4. Triglycerides and carbohydrates are directly extracted and converted to fatty acids and **38,** respectively. The separation of the CMF-lipid mixture being possible by vacuum distillation or chromatography.
5. The aqueous phase left behind should contain inorganic salts (Si, K, Ca, P oxides etc.) and humin residue potentially used in soil amendment.[117] The protein can be hydrolysed to single amino acids and valorised as platform molecules.

As a central part of a microalgal biorefinery, this reaction can address many of the challenges currently existing. The following section presents the computation of solvent alternative, experimental trials and the study of microalgal biomass behaviour in the CMF process.

3.1.6 Solvent selection alternative for the CMF process

3.1.6.1 Parameters influencing the CMF process and use of the Hansen solubility parameters

6 parameters may be taken into account to optimise the CMF reaction, namely: the temperature of the reaction (T_{CMF} in °C), stirring rate (SR, rotations per second), biomass

(sugar) loading (B_L, w/V), reaction time (RaT, min), aqueous/organic solvent ratio and solvent used. Amongst all these parameters, it was found that T_{CMF} and SR were dependent on the used substrate and should be optimised based on a case by case scenario.[117]

For instance, in the case of microalgae, a moderate stirring rate was better as to avoid loss of the biomass to the side of the vessel. This observation goes against the results by Lane *et al*., which suggested that a high stirring was better to prevent decomposition of CMF in levulinic acid and increase mass transfer (using pure glucose).[121] To compensate, a large magnetic stirrer flea was used. Also, a lower temperature is used for microalgae, 75 °C rather than >100 °C for pure glucose or fructose. This change is due to the reaction of unsaturated lipids and other metabolites with conc. HCl (chlorination) which is detrimental if lipids are to be further processed.

From the studies by Lane *et al.*, and to a lesser extent by Szmant and Chundury, B_L, RaT and aqueous/ organic solvent ratio optima can be obtained. A high biomass loading (in their cases glucose or high fructose corn syrup respectively), had a deleterious effect on CMF yield. Thus, the lower the initial B_L, the higher the CMF yield. Typically, a concentration of less than 0.5 M glucose was considered optimal (for a constant combined aqueous HCl and organic solvent volume of 210 mL).[121] Likewise, the RaT optimum was found to be 3 hours with regular extraction of the organic phase every hour.[116] Finally, the organic/aqueous solvent ratio was established to be optimum at higher than 1 values. However, it also appeared that water had a positive impact on the CMF yield since first synthesises of CMF, conducted with dry HCl gas in ether, only led to poor yields.[114] It was thus decided to use a 2/1 organic solvent to conc. (37%) HCl ratio in this work.

The last parameter that could be optimised was the choice of organic solvent. In that regard, 1,2 dichloroethane (DCE) is commonly the organic solvent of choice for the

CMF process. Its immiscibility with water and higher boiling point (bp= 80 °C) than dichloromethane (DCM, bp= 40 °C) made DCE the ideal solvent as a "next in the shelf" alternative to DCM. Unfortunately, this solvent is also a known carcinogen and is now restricted under REACH regulations.[122] Thus, to promote safer practices in chemistry, it is of interest to find an alternative to DCE for the CMF reaction.

The method employed here to find the optimum organic solvent(s) made use of the Hansen Solubility Parameters (HSP). HSPs are used to describe solvent and solute interactions in terms of dispersity (δ_D), polarity (δ_P) and hydrogen bonding (δ_H). These parameters are obtained from the postulate that the total cohesive energy (E) energy can be described as a sum of three individual terms.[123] The dispersion energy term (E_D) arises from attractive atomic forces, such as London forces. The polarity energy term (E_P) is a molecular force that comes from the permanent dipole-permanent dipole interactions molecules can have with each other. Finally, the hydrogen bonding energy term (E_H) is due to the electron exchange that occurs when hydrogen bond donors/acceptors are present. This postulate gives rise to equation vii:

$$E = E_D + E_P + E_H \qquad \text{(eq. vii)}$$

When divided by the molar volume (V_m), the total cohesive energy E becomes the square of a parameter known as the solubility parameter or Hildebrand parameter δ:

$$E/V_m = E_D/V_m + E_P/V_m + E_H/V_m \quad \text{(eq. viii)}$$

$$\delta^2 = \delta^2{}_D + \delta^2{}_P + \delta^2{}_H \qquad \text{(eq. ix)}$$

One can directly measure the Hildebrand parameter since it correlates to the energy of vaporisation, which corresponds to the energy required for the complete conversion of a solvent to a gas.

The HSPs may be obtained by 3 methods, namely the chart method (only for δ_D), calculation, or experimental trial and error. Amongst all the HSPs, δ_D is the one that received the most attention, as the other parameters were (and sometimes still are) derived from it. Originally, the chart method was used to estimate δ_D. For a polar molecule, this method consists of calculating the energy of vapourisation of the homomorph, *i.e.* the non-polar equivalent of the studied molecule with similar size (and "shape") at the same reduced temperature ($T_r = T/T_c$, where T_c is the critical temperature).[124] For instance, the homomorph of pentanol would be *n*-hexane.

The Hansen polarity parameter δ_P and hydrogen bonding parameter δ_H arise from the intrinsic polarity of a molecule and hydrogen bonding ability respectively. These are hence null in non-polar compounds. The energy of vaporisation (thus the solubility parameter δ) of an apolar molecule is equal to the dispersion energy parameter δ_D (equation ix).[125] If the polar molecule is not constituted of a linear carbon chain only, the homomorph will be the closest non-polar equivalent in terms of shape and molar volume. For example, the homomorph of chlorobenzene will be toluene.

It is then possible to plot the energy of vaporisation (thus dispersion energy E_D) as a function of the molar volume for the different reduced temperature for different types of homomorph (straight carbon chains, cyclic carbon, aromatics etc.). It follows that if considered at the same reduced temperature the molar volume of the polar molecule and its homomorph are the same and the E_D, (thus the δ_D) of the polar compound can be

extrapolated from the chart. When substituted compounds such as octylbenzene are used as homomorph, it becomes necessary to evaluate both the aromatic moiety and octyl moiety separately and calculate a weighted average of the E_D for the whole homomorph (group contribution method). The E_D for octylbenzene would then be the arithmetic average of benzene and octane for the molar volume of octylbenzene.

Originally, the two other parameters δ_P and δ_H were obtained experimentally by trial and error, *i.e.* placing solvents in a 3-coordinates space knowing the δ_D value and the vector sum of δ_P and δ_H according to equation x and xi:

$$E_a = E - \delta_D = \delta_P + \delta_H \qquad \text{(eq. x)}$$

$$\delta_a{}^2 = \delta_P{}^2 + \delta_H{}^2 \qquad \text{(eq. xi)}$$

Where $\delta_a = \left(\frac{E_a}{V_m}\right)^{\frac{1}{2}}$ (eq. xii)

Solvents were placed according to their ability to solubilise a set of 33 polymers, *i.e.* solvents that could dissolve the same polymers were clustered. This original approach allowed Hansen to estimate the HSP of 90 solvents. Later, Yamamoto *et al.* proposed to calculate the δ_D parameter using the refractive index (ηD) according to equation xiii:

$$\delta_D = (\eta\mathrm{D} - 0.784)/0.0395 \quad \text{(eq. xiii)}$$

Where the different factors were obtained from a data set of 540 points. In 2017, it was also proposed to separate the dispersion parameter in two related terms: van der Waals

dispersion parameter δ_{vdw} and the functional group dispersion parameter δ_{fg} (equation xiv).[126]

$$\delta_D{}^2 = \delta_{vdw}{}^2 + \delta_{fg}{}^2 \quad \text{(eq. xiv)}$$

The calculation of the Hansen polarity parameter, δ_P, was also proposed by using the dipole moment (μ) following equation xv:

$$\delta_P = \frac{37.4\mu}{V^{1/2}} \qquad \text{(eq. xv)}$$

This equation was primarily used to account for polarity changes in function of a temperature or pressure change as this form can be integrated according to equation xvi:

$$\frac{\partial \delta_P}{\delta_P} = \frac{\partial V}{2V} \qquad \text{(eq. xvi)}$$

Finally, the Hansen hydrogen bonding parameter is obtained by subtracting the polar and dispersion energy from the total vaporisation energy. This calculation remains the method of choice for the obtention of δ_H.

Once the Hansen parameters of the solute (a) and solvent (b) have been estimated, the relative "distance" (Ra) between them is calculated according to equation xvii:

$$Ra^2 = 4(\delta_{Db} - \delta_{Da})^2 + (\delta_{Pb} - \delta_{Pa})^2 + (\delta_{Hb} - \delta_{Ha})^2 \qquad \text{(eq. xvii)}$$

The 4 factor before the Hansen dispersion energy is here to account for the difference between the atomic dispersion forces versus the polarity and hydrogen bonding forces, molecular in nature.[126] The factor also helps the visual representation of the target molecule become a sphere rather than a box when all $\delta_{D,}$ δ_{P} and δ_{H} axis are the same lengths.

This representation is based on the theory that "like dissolves like", *i.e.* compounds with similar solubility parameters will be miscible. Interestingly, when the definition for δ_{D} in terms of van der Waals δ_{vdw} and functional group δ_{fg} is used, the factor 4 is no longer needed.[126]

The study by Lane *et al.* suggested that the capacity of an organic solvent to extract HMF during the CMF process is key to obtain higher CMF yield. Thus, the HMF's HSPs were computed using the built-in HSP calculator in the HSPip software.

Subsequently, a list of solvents satisfying the CMF process conditions was created. For a solvent to be used in the CMF-process, it had to be:

a) immiscible with water/aqueous phase
b) tolerant to concentrated HCl
c) chemically inert relative to the final CMF product
d) volatile enough to be removed under vacuum at practical temperature (typically boiling point < 120 °C at atmospheric pressure).

A list of water-immiscible solvents, their HSP parameters and relative distance from the HMF or CMF HSPs computed by equation xvii is summarised in Table 6. The solvents are

listed in descending order based on their “proximity” to the HMF partial solubility parameters (R_{aHMF}). The smaller the R_{aHMF}, the more likely the solvent to dissolve HMF.

Table 6 List of all water-immiscible solvents used in the analysis

	Target molecules	δ_D	δ_P	δ_H	Distance HMF (R_{aHMF})	Distance CMF (R_{aCMF})	
	HMF	**18.8**	**15.2**	**14.2**	-	-	-
	CMF	**18.6**	**14.1**	**7.3**	-	-	-
entry	**Solvents**						**Bp (°C)**
1	*n*-butyl pyrrolidone	17.5	9.9	5.8	10.3	4.9	241
2	butan-1-ol	16.0	5.7	15.8	11.1	13.0	118
3	methylene dichloride (dichloromethane)	17.0	7.3	7.1	11.2	7.5	40
4	butan-2-ol	15.8	5.7	14.5	11.2	12.4	100
5	methyl ethyl ketone (MEK)	16.0	9.0	5.1	12.3	7.6	80
6	ethylene dichloride	18.0	7.4	4.1	12.9	7.5	83
7	ethyl acetate	15.8	5.3	7.2	13.5	10.4	77
8	chloroform	17.8	3.1	5.7	14.9	11.2	61
9	trichloroethylene	18.0	3.1	5.3	15.1	11.2	87
10	*n*-butyl acetate	15.8	3.7	6.3	15.2	11.8	126
11	cyclopentyl methyl ether (Cpme)	16.7	4.3	4.3	15.3	10.9	106
12	chlorobenzene	19.0	4.3	2.0	16.4	11.2	132
13	methyl-t-butyl ether (MTBE)	14.8	4.3	5.0	16.3	12.6	55
14	carbon tetrachloride (p by group cont.)	16.1	8.3	0.0	16.7	10.6	77
15	diethyl ether	14.5	2.9	4.6	17.8	14.1	35
16	isopropyl ether	15.1	3.2	3.2	17.9	13.6	69
17	*p*-xylene	17.8	1.0	3.1	18.1	13.8	138
18	toluene	18.0	1.4	2.0	18.5	13.8	110
19	2,2,5,5-tetramethyloxalane (TMO)	15.6	2.3	2.4	18.6	14.1	110
20	benzene	18.4	0.0	2.0	19.5	15.1	80
21	carbon tetrachloride (0 dipole moment)	17.8	0.0	0.6	20.5	15.7	77
22	triethylamine	15.5	0.4	1.0	20.9	16.3	89
23	cyclohexane	16.8	0.0	0.2	21.0	16.2	81
24	*n*-heptane	15.3	0.0	0.0	21.9	17.2	98
25	*n* hexane	14.9	0.0	0.0	22.2	17.5	68
26	*n*-pentane	14.5	0.0	0.0	22.5	17.9	36

3.1.6.2 Assessing the alternative solvent options.

The first entry in Table 6, N-butyl-2-pyrrolidone (NBP, Scheme 6, **99**) is a recently reported greener alternative for NMP.[127] It seemed the solvent most apt to dissolve HMF in this list (entry 1. R_{aHMF} = 10.27). However, its high boiling point is likely to require a high amount of energy (heating or vacuum) to remove.

Next in the table is the polar protic solvent butan-1-ol (Scheme 6, **101**) with a distance from HMF R_{aHMF} = 11.14. As previously reported in the literature, the solvent hydrogen bonding parameter is determinant for the dissolution of HMF.[121] Indeed, unlike CMF, HMF's hydroxymethyl moiety grants hydrogen bond donating properties to this compound as illustrated by the δ_H being almost twice that of CMF. Thus, it was expected to find a polar protic solvent such as butan-1-ol, high in the list. With a boiling point of 118 °C this solvent could be a potential replacement for chlorinated solvents.

DCM is third in the table with a distance from HMF R_{aHMF} of 11.22. DCM is widely used in reactions involving HMF and was known to dissolve it well. Because of its higher hydrogen bonding properties than DCE, DCM has a higher R_a than the usual solvent used for the CMF reaction. However, the higher boiling point of DCE made it the solvent of choice.

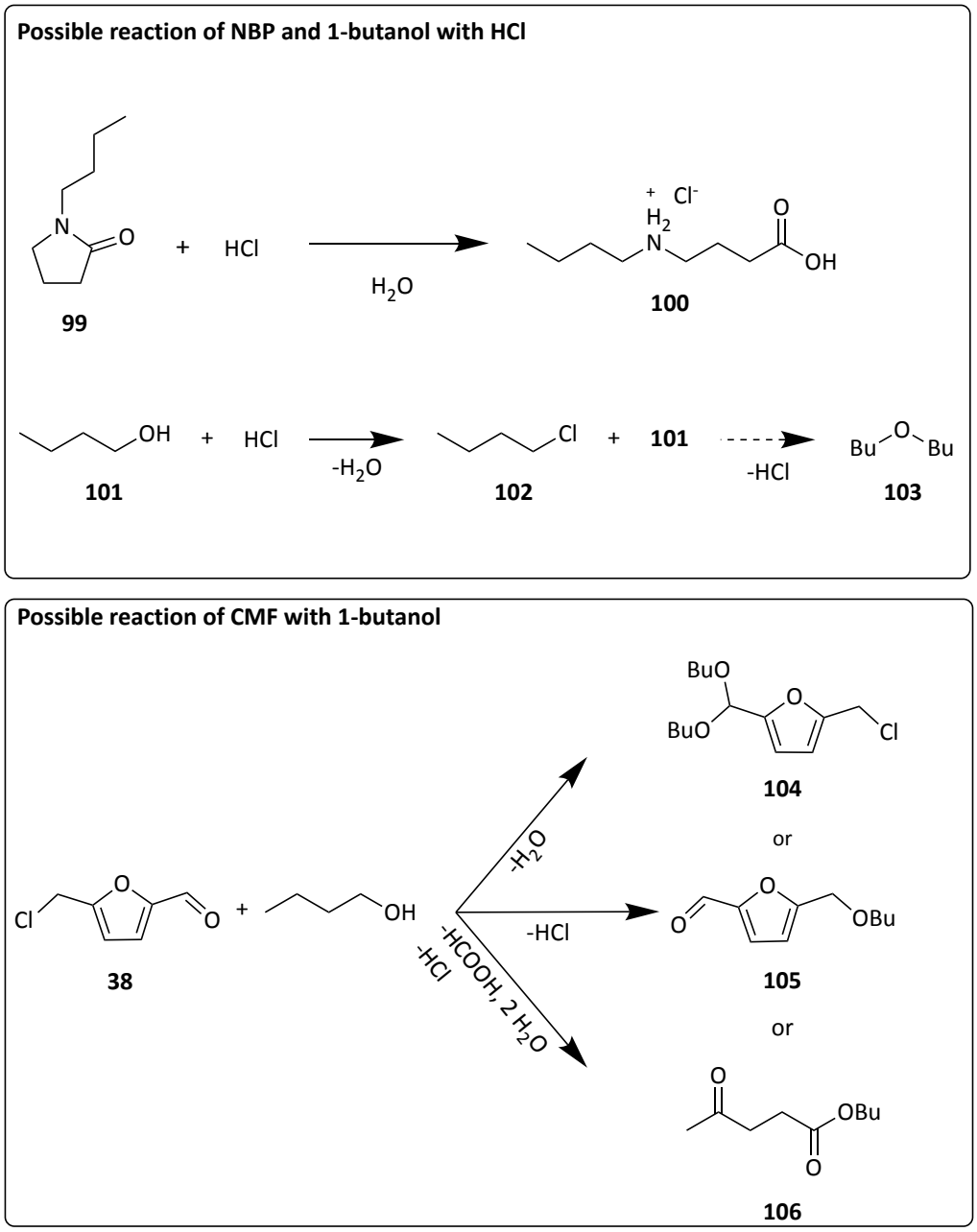

*Scheme 6 Possible reaction of some selected solvents with HCl and of CMF (**38**) with butan-1-ol*

Notably, the ability of a solvent to keep CMF in the organic phase (*i.e.* with the higher R_{aCMF} possible) is also essential to avoid the decomposition of CMF once formed. In this regard, butan-1-ol has a high R_{aCMF} of 13.03 and is thus less likely to "trap" CMF in the organic phase compared to NBP (R_{aCMF} = 4.97) or DCM (R_{aCMF}= 7.52). Hence, the best compromise for both

HMF and CMF dissolution appeared to be NBP. Unfortunately, in the presence of 37% conc. HCl, NBP will likely be hydrolysed to 4-butyl-amino-butyric acid (Scheme 6, **100**).[128,129]

Similarly, butan-1-ol could react with HCl to form 1-chlorobutane (Scheme 6, **102**), which may further react with **101** to dibutylether (Scheme 6, **103). 101** can also react with CMF forming 2-(chloromethyl)-5-(dibutoxymethyl)furan (Scheme 6, **104**) butoxy-methyl furfural (Scheme 6, **105**) or butyl levulinate (Scheme 6, **106**). [130,131] It is worth noting that these distances remain relatively "far" from the HSP of HMF as can be visualised in Figure 22.

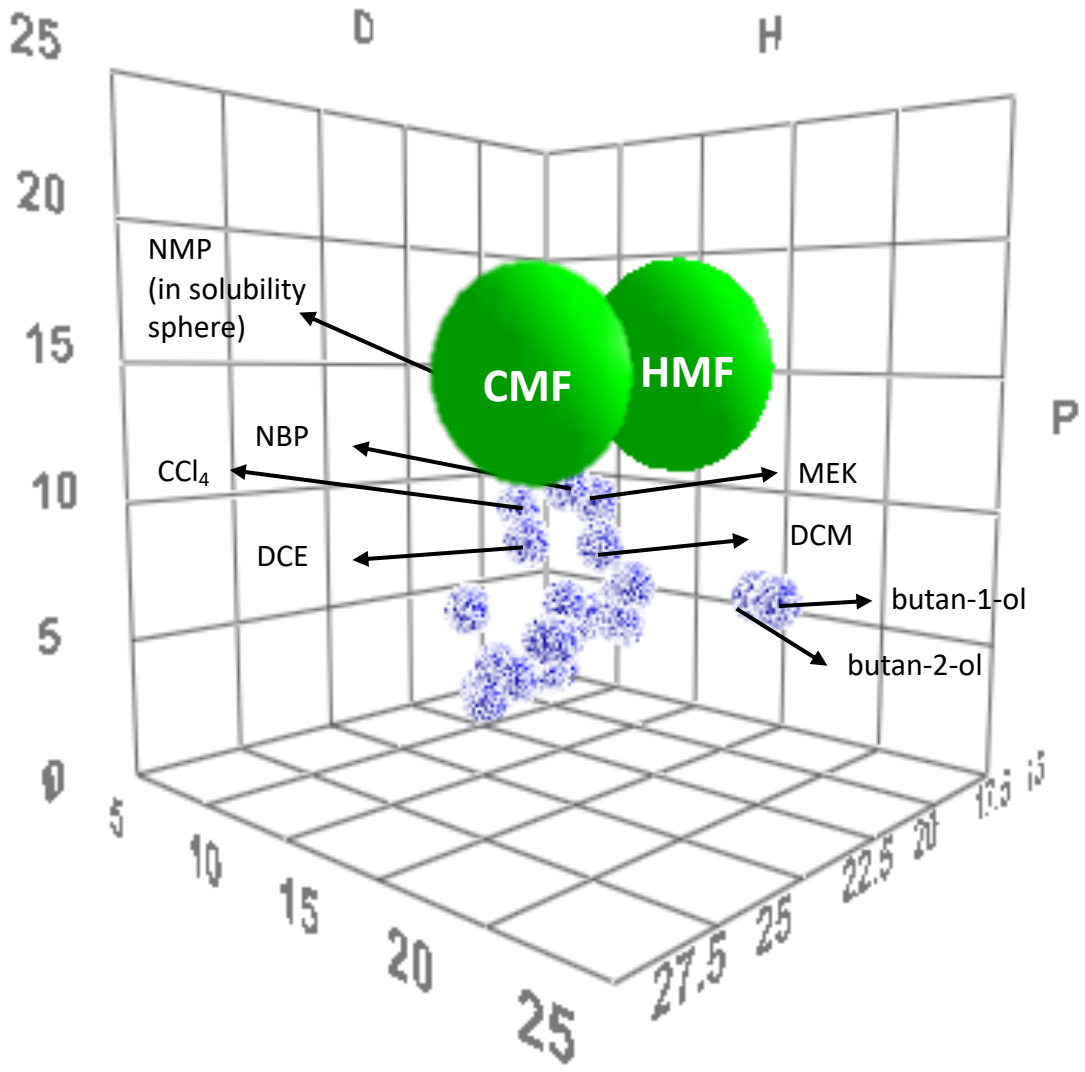

*Figure 22 HMF (**37**) and CMF (**38**) solubility spheres represented in a d(D,P,H) space. Water immiscible solvents from Table 6 p. 109 are shown as blue spheres.*

Greener solvent suggested by the Chem21 solvent selection guide such as MEK, ethyl acetate or 2,2,5,5-tetramethyloxolane (TMO) were also expected to decompose on contact with concentrated HCl.[132] For instance, when TMO was tried experimentally, the only isolable product was 2,5-dichloro-2,5-dimethyl hexane, resulting from the ring opening of TMO and further chlorination. CPME was used by Breeden *et al.* in a microwave-heated CMF reaction and resulted in a 70% yield.[133]

Eventually, DCM seemed to be the solvent of choice that would extract HMF and CMF ($\delta_{H\text{-}HMF}$= 11.22 and $\delta_{H\text{-}CMF}$= 7.52) and satisfy the reaction conditions. However, DCM does not represent a significant improvement in greenness and is classed “Hazardous” in the Chem21 selection guide.[132]

The possibility to use a binary solvent mixture was considered to circumvent this issue. The HSPip software offers the possibility to compute optimal binary (or tertiary) solvent blends to match the HSP of the target molecules. The solvent blends created were then selected based on their miscibility with each other. Hence, a list of 325 solvent pairs was made, and the 4 combinations with the smallest distance from HMF are listed in Table 7 (full list in Appendix 4), an additional entry (entry.5) was added as an easy potentially better solvent blend candidate for the CMF process to try. The miscibility between the solvents used for the combination was also further used to discriminate the potentially right combination: only solvents miscible with one another were considered.

*Table 7. Selection of the best solvent blends computed with HSPip for HMF (**37**) HSPs*

Entry	Solvent 1	Solvent 2	Vol% 1	Vol% 2	δ_{Dmix}	δ_{Pmix}	δ_{Hmix}	R_{aHMF}	R_{aCMF}
1	*N*-butyl pyrrolidone	butan-1-ol	57	43	16.9	8.1	10.1	9.08	7.50
2	butan-2-ol	N-butyl pyrrolidone	40	60	16.8	8.2	9.3	9.41	7.24
3	ethylene dichloride	butan-1-ol	37	63	16.7	6.3	11.5	10.15	9.68
4	dichloromethane	butan-1-ol	49	51	16.5	6.5	11.5	10.22	9.70
5	dichloromethane	ethylene dichloride	50	50	17.5	7.4	5.6	11.76	7.30

The use of binary solvent blends allowed the reduction of the distance from the HSP sphere of HMF. Indeed, it appeared that all entries systematically had a lower distance from HMF than when used alone (except for NBP). An exception is entry 5 (DCM:DCE mix) whose distance from HMF is greater than DCM alone (11.22) but is significantly closer to CMF (distance of 7.3) and is a combination of the solvent already used in the CMF process, hence, easy to apply.

The blends involving NBP and butan-1 or 2-ol were not investigated as they would certainly react in contact with conc. HCl. However, despite the expected reactions of 1- or butan-2-ol, entries 3, 4 and 5 of Table 7 were attempted in a microwave reaction using fructose as starting material. As expected, butan-1 or 2-ol did not tolerate the CMF process conditions. Unfortunately, the mixtures employing butan-1 or 2-ol afforded a dark resin-like product, only partially soluble in deuterated chloroform or methanol. The presence of polymeric material likely resulted from the humin formation together with other butanol-derived polymers. Unsurprisingly, the DCM:DCE blend gave a clean ^{1}H-NMR spectrum showing only CMF as a final product (Appendix 5). However, no significant improvement in terms of isolated CMF yield was observed.

Despite the computational analysis realised here, it appeared that DCE remained the ideal solvent to be used in this reaction in terms of the polarity and stability. However, due to REACH regulation in the EU, it is necessary to find safer, better solutions for this particular reaction. The approach using solvent blends considered here, although theoretically promising, must be refined to smooth the transition from the *in-silico* analysis to the laboratory application. Notably, the construction of a solubility sphere for HMF could help discriminate solvents and design a solvent solution for this reaction. Although water-immiscible, selected solvents can absorb water to a varying degree. For instance, DCE is 0.13M in water at saturation. This property is likely a critical parameter to consider when computing an alternative solvent for the CMF process. Hence, to assess the potential of microalgal biomass for the CMF reaction DCE was further used as a solvent. The use of DCE may be acceptable if a complete recovery and reuse are made.

3.1.7 Use of microalgae in the CMF process

The proximate analysis results described previously showed a low carbohydrate content in the microalgae selected in this work. Hence, this biomass was not expected to yield a high amount of CMF. Nevertheless, a carbohydrate residue would be left if not effectively utilised. Thus, it was decided to assess the possibility of producing CMF from microalgae based on the ^{1}H-NMR spectrum of the crude CMF-lipids mixture obtained after the reaction.

Initial biomass loadings of 250, 500 and 1000 mg were attempted with *Spirulina sp*. powder with a constant amount of conc. HCl and DCE (35 mL and 70 mL respectively, B_L

~2%, 4%, 8% w/v). Despite the inferior carbohydrate content of *Spirulina sp.,* it was decided to try to optimise the reaction parameter with this microalga due to its wider availability.

Phase separation between the organic and aqueous layers was more tedious at loading higher than 2% w/v. As previously mentioned, *Lane et al.* demonstrated that the higher the starting material loading, the lower the CMF yield. Hence, in the context of this study, the initial loading of 2% was considered optimal.

The ^{1}H-NMR spectra of the CMF-lipid mixture obtained after the reaction with 3 different microalgae species are presented in Figure 23. Using the spectrum of pure CMF synthesised from HMF as a reference, the characteristic signals for CMF appeared clearly in all 3 products obtained from microalgae. Shift values reported here are consistent with the CMF shift values found in the literature.[133]

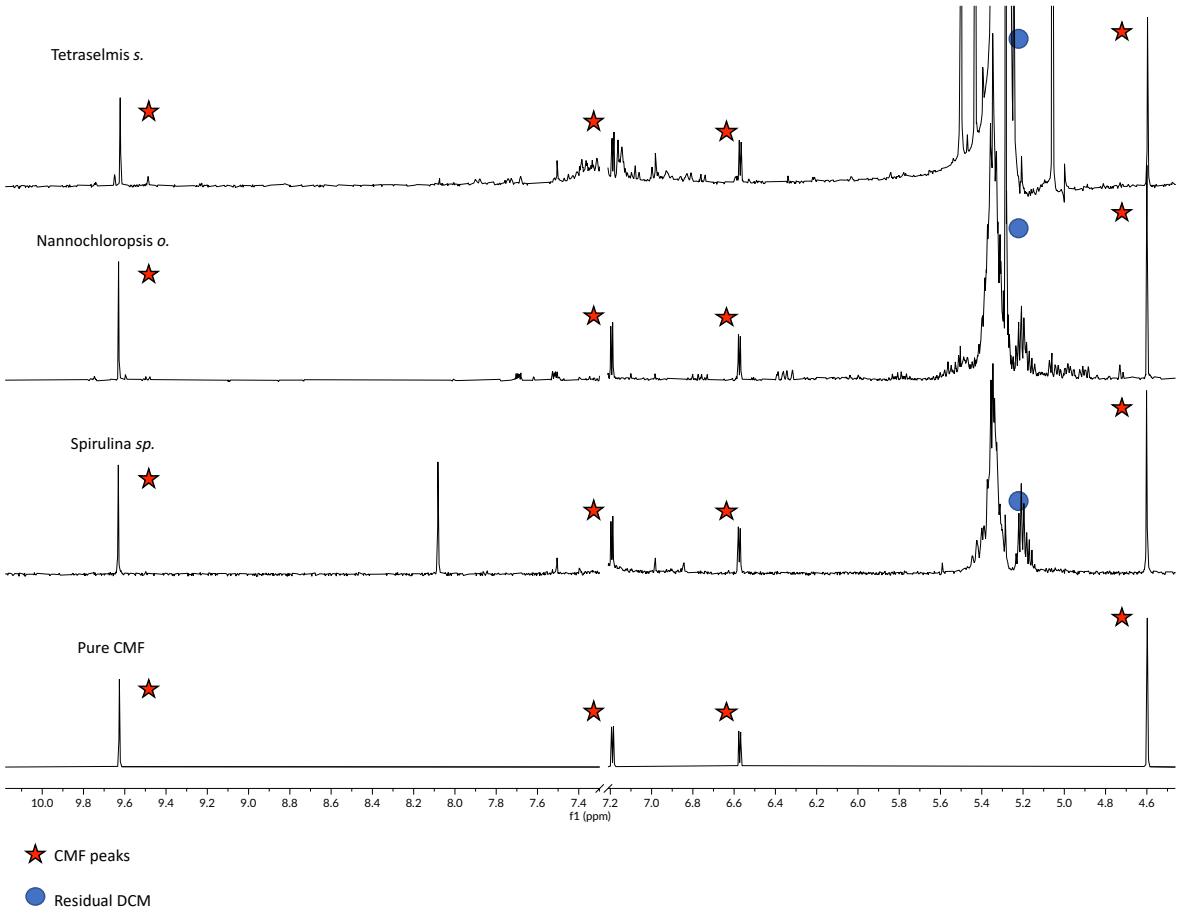

Figure 23 Overlay of ^{1}H-NMR spectra obtained after CMF reaction with 3 different microalgae species. ^{1}H-NMR spectrum of pure CMF is shown at the bottom for comparison. Signal for $CDCl_3$ (7.2-7.4 ppm) was cut for ease of reading.

The mass yield obtained of CMF-lipid for *Tetraselmis s.* was 23% whereas the mass yield was 7% and 10% for *Spirulina sp.* and *Nannochloropsis o.* respectively. However, the strong signal at ~5.1 ppm present in *Tetraselmis s.'s* NMR spectrum and to a lesser extent in *Nannochloropsis o.* spectrum likely indicate the presence of DCM (in ratio 1:2223 for *Tetraselmis s.* and 1:19 for *Nannochloropsis o.*, based on the peak area of the CMF aldehyde's signal and the DCM peak area) used during silica filtration step. The remaining DCM prevents any definitive conclusion from being drawn regarding the yield of the reaction depending on the microalgae species. Results of these experiments are summarised Table 8.

It was repeatedly observed that DCM "holds onto" CMF very tightly making it particularly difficult to remove altogether. The close polarity between CMF and DCM (based on their δ_P see Figure 22, p. 113) may explain this observation. The presence of salts in the biomass would increase the ionic strength of the aqueous phase and help the organic layer to pull HMF from it. A recent study on the effect of different Brönsted acids on the formation of HMF from cellulose suggested that phosphoric acid increased HMF yield. [134] The high ash content may indicate a high concentration of salts in *Tetraselmis s.* which can also explain the higher yield.

Table 8 Theoretical total lipid content ($TLiC_{th}$), total carbohydrate content (TCC_{th}) and experimental CMF-Lipid, humins and aqueous residue masses obtained for 3 different microalgae species

Microalgae species	Mass of biomass (mg)	$TLiC_{th}$ (mg)	TCC_{th} (mg)	Organic fraction* (mg)	Mass Yield (%)**	Aq. residues (mg)	Humins (mg)
Spirulina sp.	250	65.5	2.36	27.2	40	385	21.0
*Tetraselmis suecica****	500	111	45.2	109	70	-	-
*Nannochloropsis occulata****	750	215	37.9	94.3	37	764	12.1

*Organic fraction includes CMF, lipid, free fatty acids and glycerol.

**Complete extraction of lipids and conversion of carbohydrates was assumed for yield calculation.

***DCM present in the CMF-lipid mixture.

During the CMF process, the triglycerides present are also hydrolysed to fatty acids and glycerol as previously reported.[117] This was confirmed by the NMR analysis of the CMF reaction product obtained, which showed the presence of fatty acids in the mixture (Figure 24, **107**). The GC-MS analysis of the TLiC did confirm the presence of unsaturated fatty acids (mainly linoleic acid and stearic acid). Hence, the assignment of unsaturated fatty acids protons was realised on the ^{1}H-NMR spectra Figure 24. The presence of glycerol in small quantities (*e.g.* 0.23:1 in *Nannochloropsis o.* and 0.12:1 in *Spirulina sp.* comparing H_c and glycerol multiplets dashed arrows, Figure 24) further confirmed that the hydrolysis of the cellular triglycerides occurred. Both *Nannochloropsis o.* and *Spirulina sp.* contained clear signals for fatty acids and glycerol. However, the ^{1}H-NMR spectrum of *Tetraselmis* displayed a much weaker signal. Some fatty acids are likely in small quantities in solution. This result correlates well with the TLiC results obtained. *Tetraselmis s.* seem to be mostly accumulating a large amount of salt during its cultivation, and other biomolecules are in much less concentration than in other microalgae. Partially hydrolysed proteins lead to free amino acids and short peptides. Under the CMF process conditions, these are likely to protonate and form water-soluble hydrochloride salts. The larger aqueous residues masses than that of starting biomass here obtained were attributed to the presence of these salts.

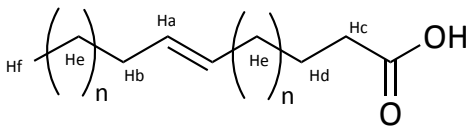

107

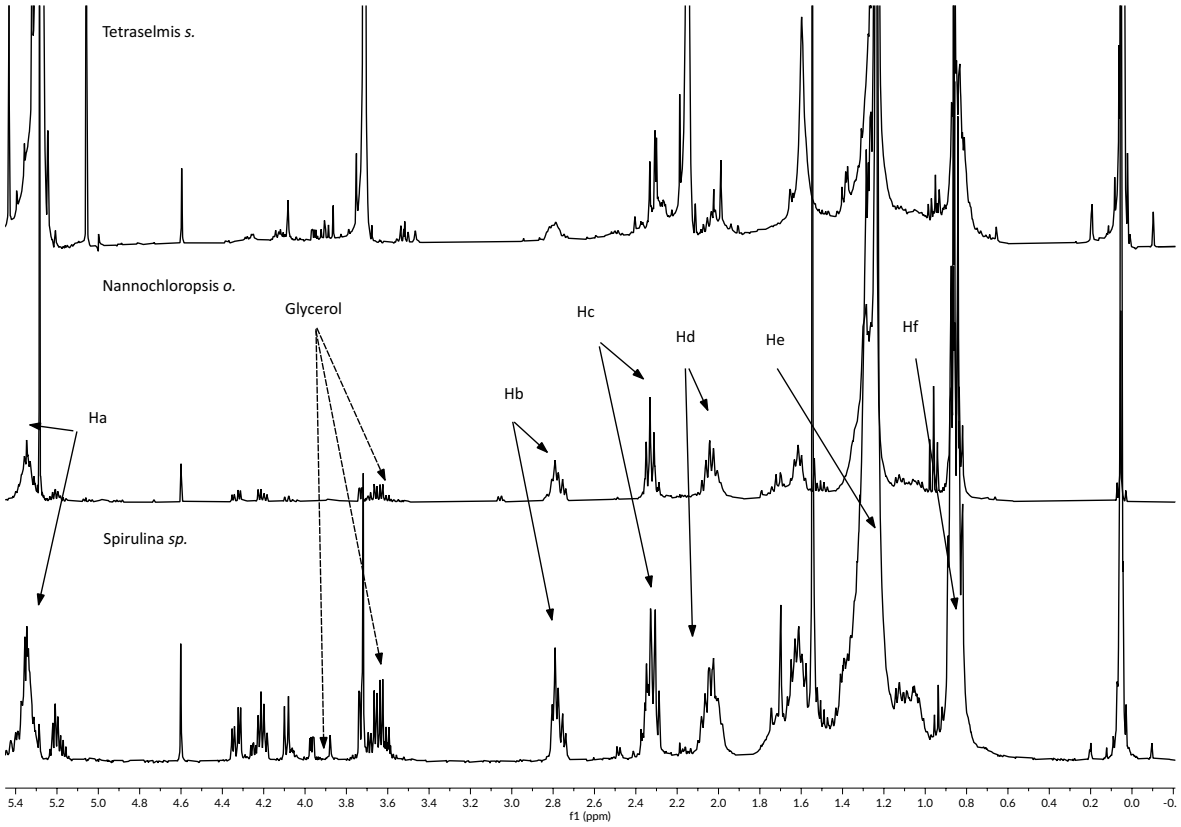

Figure 24 Proton assignment for an unsaturated lipid from CMF-lipid reaction product. Dashed arrows indicate the glycerol signals

3.1.8 Conclusion for chapter III.1 - part.2

From the proximate analysis, it was possible to evaluate the potential of the three microalgae species selected to produce platform molecules. It was expected that the CMF yield from these species would be low. Indeed, with carbohydrate contents between 1 and 10% and considering that a maximum of 80% CMF yield was reported using corn stover, the theoretical maximum yield of CMF for these microalgae would be between 8 – 80 mg

CMF per gram of biomass. Hence, for the optimal loading of ~2%, *i.e.* 250 mg in 105 mL total volume, this would correspond to 2-200 mg of CMF.

None of these microalgae species, or the cultivation method employed, was favourable to accumulate carbohydrates and hence, to produce CMF. Nevertheless, a high-enough conversion of this biomass to CMF to be detected by ^{1}H-NMR spectroscopy was possible. One of the difficulties faced during this work is the current availability microalgae. While lignocellulosics are widely available globally, microalgae require specific biotechnological equipment to be grown under controlled conditions, as discussed in chapter III.1. Some microalgae may be obtained from hatcheries, but their compositions have often been optimised for feeding purposes (*e.g. Nannochloropsis o.* used here) focusing mainly on high protein microalgae.

This study does prove that conceptually, with the appropriate method of cultivation and carbohydrates rich microalgae species, a multi-component bio-refinery based on the CMF process is plausible. Many challenges related to the microalgae cultivation can be addressed using this technology, but novel issues arise.

The use of HCl requires special acid-resistant alloy or coated (typically glass-lined) material, which brings the CAPEX up although standard in the industry. Similarly, the CMF separation from the fatty acids or organic solvent(s) recycling, increase the biorefinery cost. Additionally, it is preferable to recycle the excess HCl used, and fortunately, many technologies such as membrane-assisted pervaporation or electrodialysis exist. Finally, the aqueous medium likely contains a large amount of hydrolysed proteins that represent a promising source of nitrogen-containing molecules. The separation and utilisation of amino acids are discussed in chapter IV, where gluten was also used as an example of protein-rich waste. The remaining inorganic salts may be recycled in a fresh cultivation medium.

These additional costs are likely compensated with the possibility to produce high-value chemicals as previously described or speciality chemicals such as UV-filter for sunscreen application, surfactants or photopolymers. Not only is the production of these chemicals from renewable resources of interest, but their retail price could also simultaneously increase the profitability of a multi-component biorefinery.

The following sections report the work realised on the syntheses of various UV-filters (for beauty and personal care products) from platform molecules potentially extracted from microalgae. The biodegradability of such compounds is discussed together with their fit with the formulations commonly used in the market.

Chapter III.2
Synthesis of bio-derived ultraviolet filters for sunscreen application[†]

[†] Results in this chapter were obtained as part of a collaborative competition organised by I.Know.Who (Sweden) and BASF (Germany). Photo- and chemical stability as well as biodegradability were tested by BASF laboratory. Dr. Ignacio Funes and Prof. Diego Sampedro Ruiz computed the UV-vis absorption of several UV-absorbing candidate compounds. Dr. Julie Grumelard, Dr. Thomas Elis (BASF, Basel, Germany) and Prof. Michael North (University of York, UK) guided and supervised this work.

3.2.1 Introduction: ultraviolet (UV) definitions, UV-absorption in organic compounds and need for bio-based alternatives

3.2.1.1 Theoretical background of UV-filter chemistry

Exposure to sunlight is known to be essential for health. Indeed, the biosynthesis of cholecalciferol (vitamin D_3), is triggered by UV-B-exposure and is a vital pro-hormone which after conversion to calcitriol regulates the body's calcium uptake.[135] It is also established that the production of melatonin and serotonin, essential hormones regulating, for instance, circadian rhythms and mood, is affected by sunlight exposure. When individuals expose to sunlight, melatonin production stops while serotonin (melatonin's precursor) production begins.[136] Other benefits of sunlight exposure on human health include: mood enhancement (endorphin secretion), improved immunological tolerance, promotion of outdoors activities etc.[136]

On the other hand, it is well known that overexposure to sunlight increases skin cancer risks and is famous for provoking sunburns.[137] However, no universally-accepted recommendation regarding sunlight exposure time currently exists. The different skin types, UV levels and sensitivities between one country and one person to another may explain this lack of guidance.[138]

To safely enjoy outdoor activities, whilst preventing the risks mentioned above associated with sunlight exposure, the use of sunscreen containing performant UV filters is recommended. This chapter will focus on organic UV filters, but inorganic compounds such as TiO_2 nanoparticles are routinely used in formulations.

Three types of UV wavelength ranges are distinguished: UV-A, B and C. Typically, the most energetic wavelengths and thus most harmful are the UV-C, ranging from 100 to 280 nm, they are also called the vacuum-UV (Figure 25). These levels of energies commonly correspond to most of the bond dissociation energies in organic molecules (3.6 eV.bond^{-1} for -C-C- bonds to 10 eV.bond^{-1} for -C≡C- bonds at 298 K, 4.5 eV.bond^{-1} for H-C- bonds or 4 eV.bond^{-1} for HO-C- bonds) and are, therefore, particularly dangerous for health.[139] Fortunately, this range of wavelengths is almost entirely filtered by the ozone, water vapour, oxygen and carbon dioxide present in the atmosphere. UV-B range from 280 to 310 nm and 90% of these radiations are also filtered by the molecules present in the atmosphere. UV-B, like UV-C, may as well break bonds found in organic molecules.[140] This type of radiation is known to promote the formation of thymine dimers when absorbed by nucleic acids present in DNA.[141] Finally, UV-A, which composes the largest proportion of UV-light that reaches the Earth, range from 310-390 nm. Although less energetic, UV-A (and UV-B) danger resides in the exposure time and dose during exposure. Hence, skin exposed to UV-A for a prolonged time will show redness called erythema.[142] Although not completely understood, erythema is an inflammation of the skin triggered by UV light absorption. The production of arachidonic acid ($C_{20:4}$ fatty acids) or histamines and other metabolites have been reported to increase after exposure to UV-B and UV-A, which may explain this physiological response.[143] The production of reactive oxygen species ($^1O_2$, peroxides etc.) by UV light and the increase of their concentration after long exposure time may also account for the risks of UV-A/B overexposure.

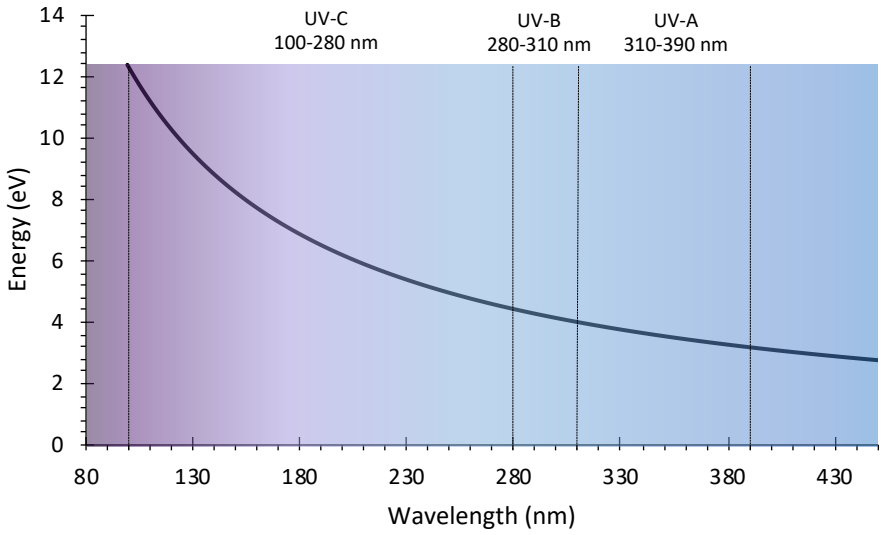

Figure 25. Energy of different wavelengths in the UV region

Consequently, an ideal sunscreen should mostly absorb in the UV-A region but still with some UV-B absorption. Traditionally, the capacity of a formulation to protect from sunlight is measured by the sun protection factor (SPF). The SPF is defined as the ratio of the minimal erythema dose (MED, dose for which first signs of redness on the skin appears) on protected skin over the MED on unprotected skin and ranges in Europe from 15 to 50+.[144,145] Some formulation may be specific for UV-A or UV-B. However, it is common for sunscreens to contain a mixture of UV filters covering both wavelength regions. Sunscreens achieve this UV filtration effect by the absorption of UV of various wavelengths by different molecules present in the formulation.

Organic UV-filters excited to higher energy states may dissipate this energy excess by radiative and non-radiative mechanisms namely: fluorescence or phosphorescence for the radiative processes and vibrational relaxation, internal conversion (IC) or intersystem crossing (ISC) for the non-radiative process (Jablonski's diagram, Figure 26).[140]

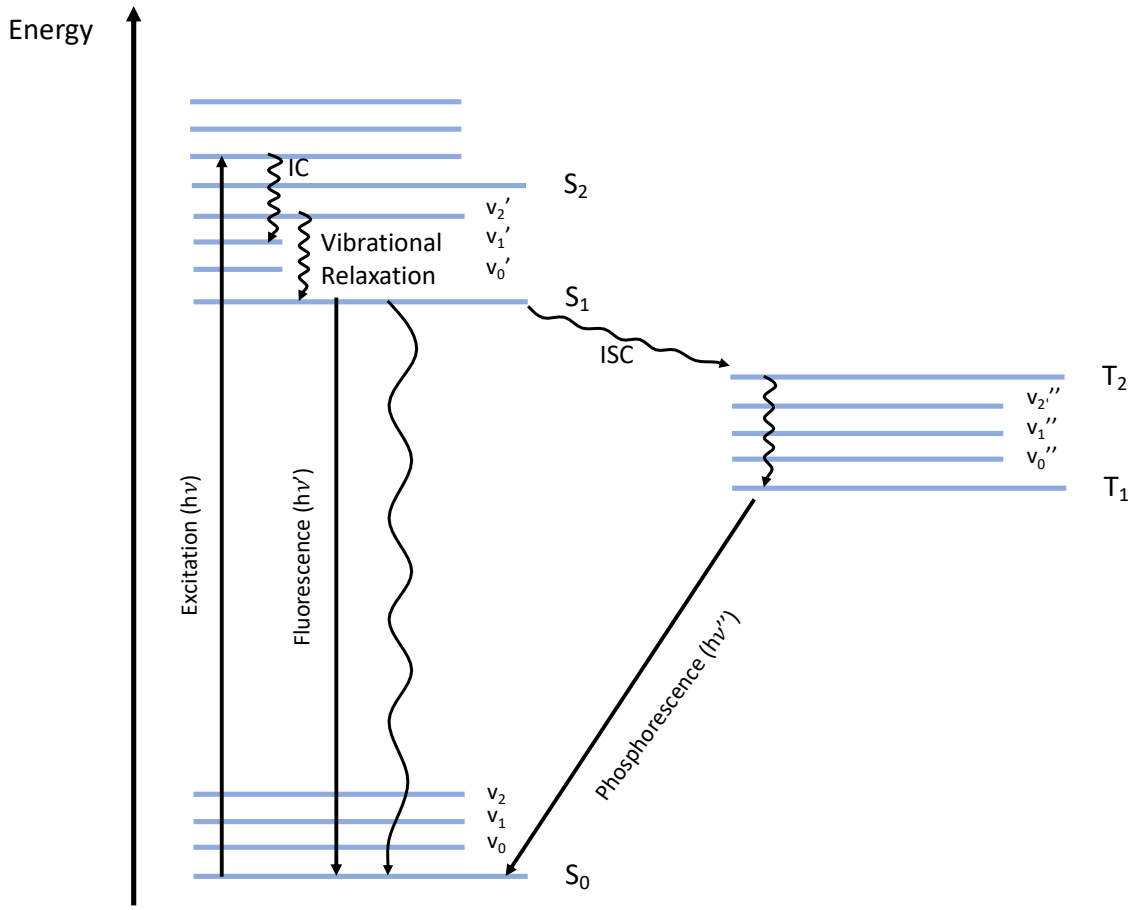

Figure 26 Jablonski's diagram, radiative processes are represented with plain arrows, whereas non-radiative processes are illustrated with wavy arrows. Ground state electrons from bonding orbitals (σ, π) or non-bonding (n) are in the S_0 singlet energy level, whereas excited electrons going to non-bonding (σ^*, π^*) orbitals are in the $S_{1, 2...}$ singlet or triplet (T_1) higher energy level

Electrons in a higher energy state may also partake in an electron transfer mechanism, resulting in covalent bonds or isomer formation. The creation of a bond or isomer in such a mechanism is the photochemistry foundation which is discussed in chapter III.3.

3.2.1.2 Driving forces for the synthesis of bio-derived UV-filters

Most commercial UV-filters currently on the market are derived from petroleum (Figure 27). Recently, compounds contained in many formulations such as 2-hydroxy-4-methoxybenzophenone (Figure 27, **108** oxybenzone), ethylhexyl-4-methoxycinnamate

(Figure 27, **109**), or 4-*tert*-butyl-4'-methoxydibenzoylmethane (Figure 27, **110**, avobenzone), have been associated with coral-bleaching, being potential neurotoxins and of preventing normal development in zebrafish embryos possibly related to their low biodegradability in a marine environment.[146–149]

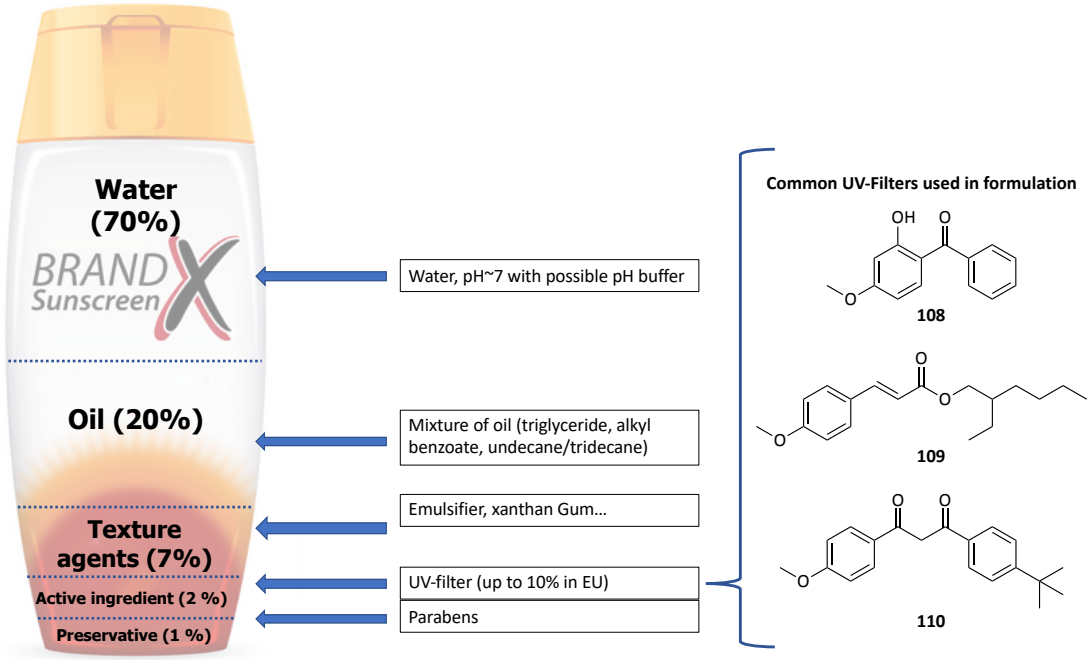

Figure 27 Typical skin-care formulation (oil in water) with examples of UV Filters used in sunscreen

UV filters derived from platform molecules are of interest since all current commercial compounds are made from fossil-resources. Besides, the *BioLogicTool* analysis (Figure 28) realised on some of the currently employed UV filters highlight the need for a more rational solution. Indeed, the tortuous routes for oxybenzone or avobenzone gave a *BioLogicTool* score of 2.41 and 2.12, respectively.

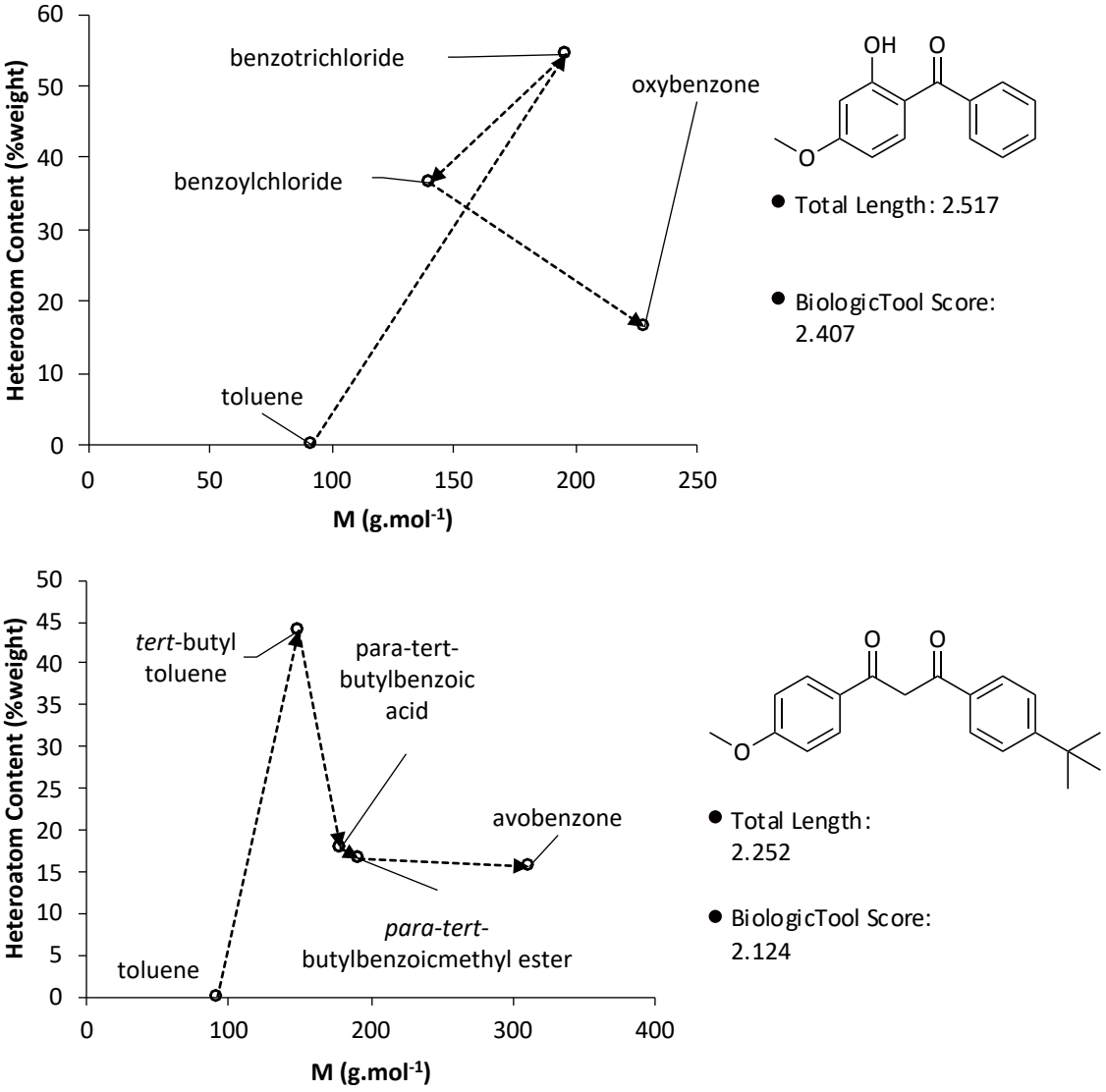

Figure 28 BioLogicTool plots of two currently employed UV-filters in sunscreen formulations

3.2.2 Aims of chapter III.2

The environmental damages imputed to organic UV-filters require changes both upstream– due to the utilisation of fossil resources for their synthesis– and downstream – due to their proven toxicity for corals or fish embryos. It was assumed in this work that biodegradable UV-absorbing compounds would be more innocuous to the environment than the less biodegradable ones.

The goal of this chapter is to develop bioderived and potentially biodegradable UV-absorbing compounds for sunscreen applications. Efforts were made to employ platform molecules obtainable from microalgae via the CMF reaction, as discussed in chapter III.1.

In 2013, it was shown that surfactants derived from platform molecules containing furan groups (for instance, 2,5-furan dicarboxylic acid, FDCA) were potentially biodegradable.[150,151] Furans are also known chromophores that absorb in the UV-B range and are easily accessible from renewable resources. It was thus decided to synthesise UV-absorbing compounds bearing a bio-based furan moiety as a core unit. The hence made molecules were further tested for their suitability in sunscreen formulations and biodegradability according to the BASF laboratory criteria.

3.2.3 Synthesis of UV filters from platform molecules

As a first approach, structures mimicking existing UV filters were explored, replacing benzene rings with more readily bio-derived furan rings (Figure 29), bearing in mind their potential biodegradability.[150] Many of the selected candidates had previously been reported in the literature or patents, but little information could be found on their UV-vis absorption properties.[152,153]

Additionally, for an organic UV filter to be suitable for sunscreen formulation, UV absorption was not the only criteria to take into account. Fundamental properties of a formulation-ready UV filter are summarised in Table 9. Most of the requirements such as UV absorption, solubility in water or cosmetic oils, photostability, or biodegradability were hard to predict without experimental evidence or computational modelisation.[154]

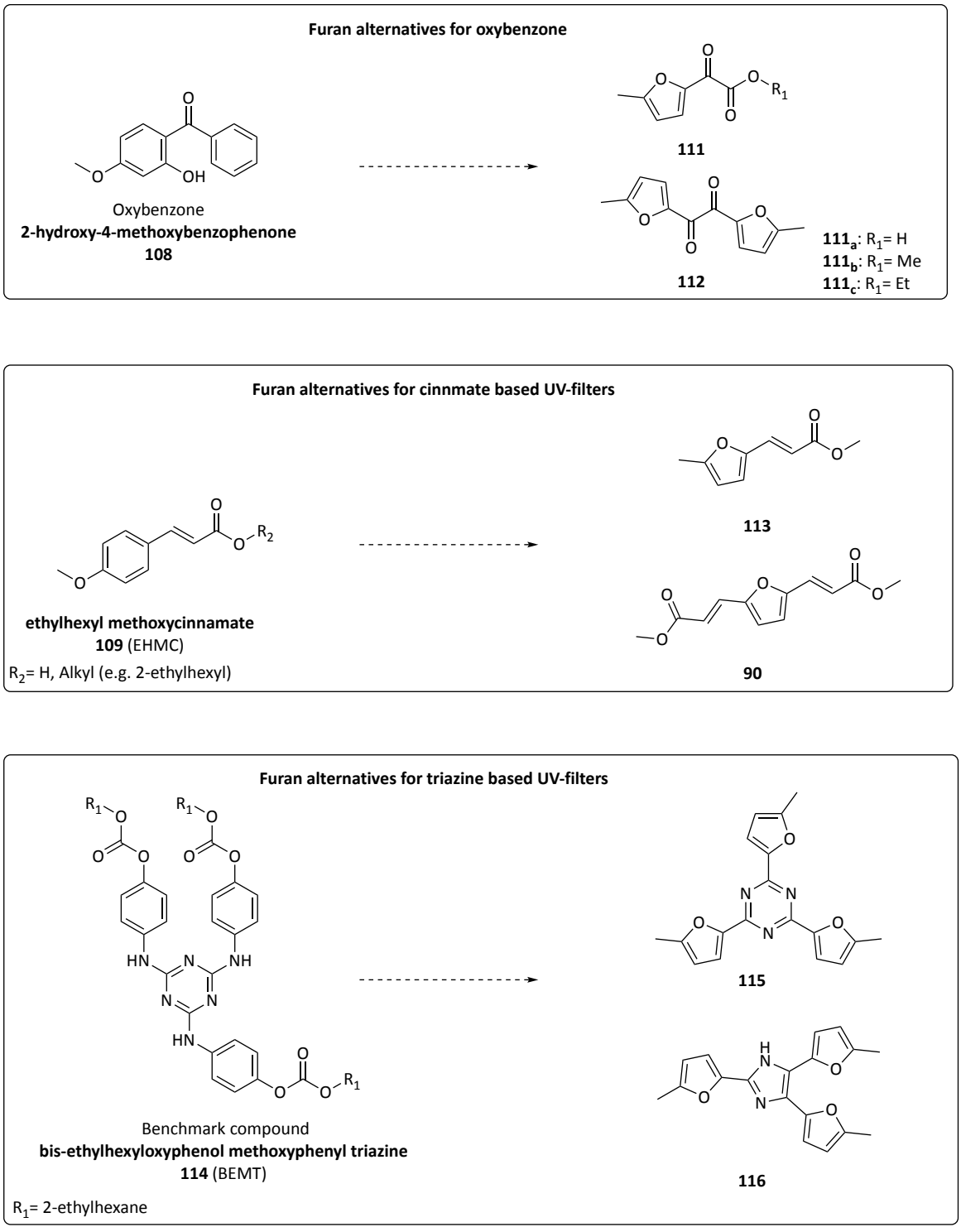

Figure 29 Selected candidates of bio-derived UV-filters based on commercial compounds

Table 9. Evaluation criteria for suitability of an organic UV filter for cosmetic formulation

Criteria	Explanation	Benchmark Molecule (Figure 29, 114)
UV Absorption	1. Initially: E(1,1)[a]>200 in 290-390* nm region	E(1,1) = 500
	2. Area under UV absorbance curve at 290-400nm in solution	
Solubility	>10% solubility minimum in water or cosmetic oils[b]	10% solubility
Photostability**	% recovery in solution	95% after 10 MED & 90% after 30 MED in formulation
	%recovery at 2% in formulation*** after 20 MED, 50MED	
Chemical stability**	% recover at 2% in formulation after 2 weeks at 50 °C	100% after 1 month at 50°C
Biodegradability**	% biodegraded after 28 days in simplified OCDE301 test	to be determined
Availability	Scalable to multi-gram scale	-
Purity	>95% purity	-

[a] $E(1,1) = [\varepsilon\ (L.mol^{-1}.cm^{-1})*10(g.L^{-1})/M(g.mol^{-1})]*l(cm)$. [b] Cosmetic oils tested here were: 1,2 propanediol, C_{12}-C_{15} alkyl benzoate (Cetiol©AB), caprylic/capric triglycerides (Myritol©318), Undecane/Tridecane (Cetiol© Ultimate). **Test realised by BASF, confidential protocol *** Exact formulation available in Appendix 7.

Our collaborators computed the UV-vis spectra of several furan-derived compounds and confirmed the UV-vis absorbing properties of the selected candidates (Appendix 6). Thus, the syntheses were realised first to validate the computed UV-vis spectra. Only if the UV-vis spectra and the solubilities matched the criteria described in Table 9 were the compounds scaled-up and other tests performed. Data related to compounds synthesised are summarised in Table 10.

Table 10 Synthesised bio-derived UV filter candidate compounds

	Compound	Isolated Yield (%)	λ_{max} (nm)	Solubility* (% w/w)	%A UVB§	%A UVA§	%A UVA+B§	E(1,1)
1	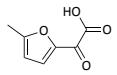 **111_a**	56[a]	302	<5	44.7	32.4	77.2	1051
2	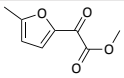 **111_b**	47[a]	305	<5	43.1	39.1	82.2	724
3	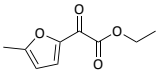 **111_c**	21[a]	305	-	45.4	35.3	80.8	561
4	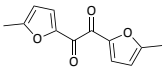 **112**	50[a]	318	<5	29.1	52.8	81.9	836
5	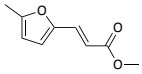 **113****	54[b]	316	>10	42.9	47	89.9	1533
6	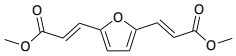 **90**	69[c]	352	<10	9.2	88.7	97.9	1223
7	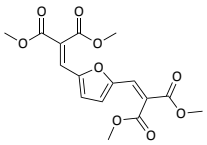 **117**	8[c]	360	<5	6.7	91.8	98.5	1030
8	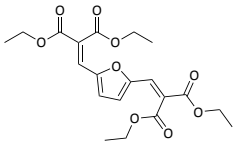 **118**	10[c]	360	<5	5.6	92.9	98.5	869
9	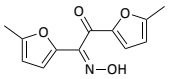 **119**	20%[c]	288	~10	6.7	91.8	98.5	927

a. Isolated yield from 2-methyl furan b. Isolated yield from 2-methyl furfural c. isolated yield reported from 2,5-furandialdehyde

§. Data originally calculated by Prof. M. North

*in 1,2-propanediol

**UV-vis spectroscopy and solubility data recorded by Dr. Katie Lamb

The first class of compounds investigated were related to commercial UV filters containing a cinnamic acid motif (Figure 29, p. 132, EHMC, **109**).

Compound **113** (Table 10, entry 5), obtained after Knoevenagel-Doebner condensation and esterification of 2-methyl furfural, displayed excellent UV-absorbing properties with an impressive E(1,1) value of 1533 and an overall UV-A+B absorbance of

89.9% (of total absorbance). Also, solubility in cosmetic oils was outstanding, with >100% in both Cetiol AB (C_{12}-C_{15} alkyl benzoate) and Myritol 318 (caprylic/capric triglycerides). Scale-up was thus easily performed and purification by Kugelrohr sublimation afforded up to 22 grams of compound **113** (upscaling and testing performed by Dr. Katie Lamb).

Unfortunately, **113** proved to be unstable both chemically and photolytically. Indeed, a ~10% loss of absorption at 316 nm occurred upon storage at 4 °C after one month in air. Besides, after irradiation at 50 MED (1 MED measured for benchmark molecule), only 79% of UV absorption in solution remained, showing this candidate molecule was not photostable either.

It was reported in the early 2000s by Gandini *et al.* that unsaturated furan compounds structurally similar to **113**, **90** or **117** can form [π2+ π2] cycloadduct upon UV irradiation (Figure 30), this is a likely cause of the observed photoinstability.[155–157] These structures are discussed in greater details in chapter III.3. Finally, the biodegradability test showed almost no %biodegradation (test performed by BASF, using a modified confidential OECD 301F protocol: biological oxygen consumption with OxiTop measuring heads) after 18 days by the activated sludge, indicating that this compound was likely not biodegradable (readily biodegradable according to OECD standard 60% after 10% was reached and globally 60% after 28 days).

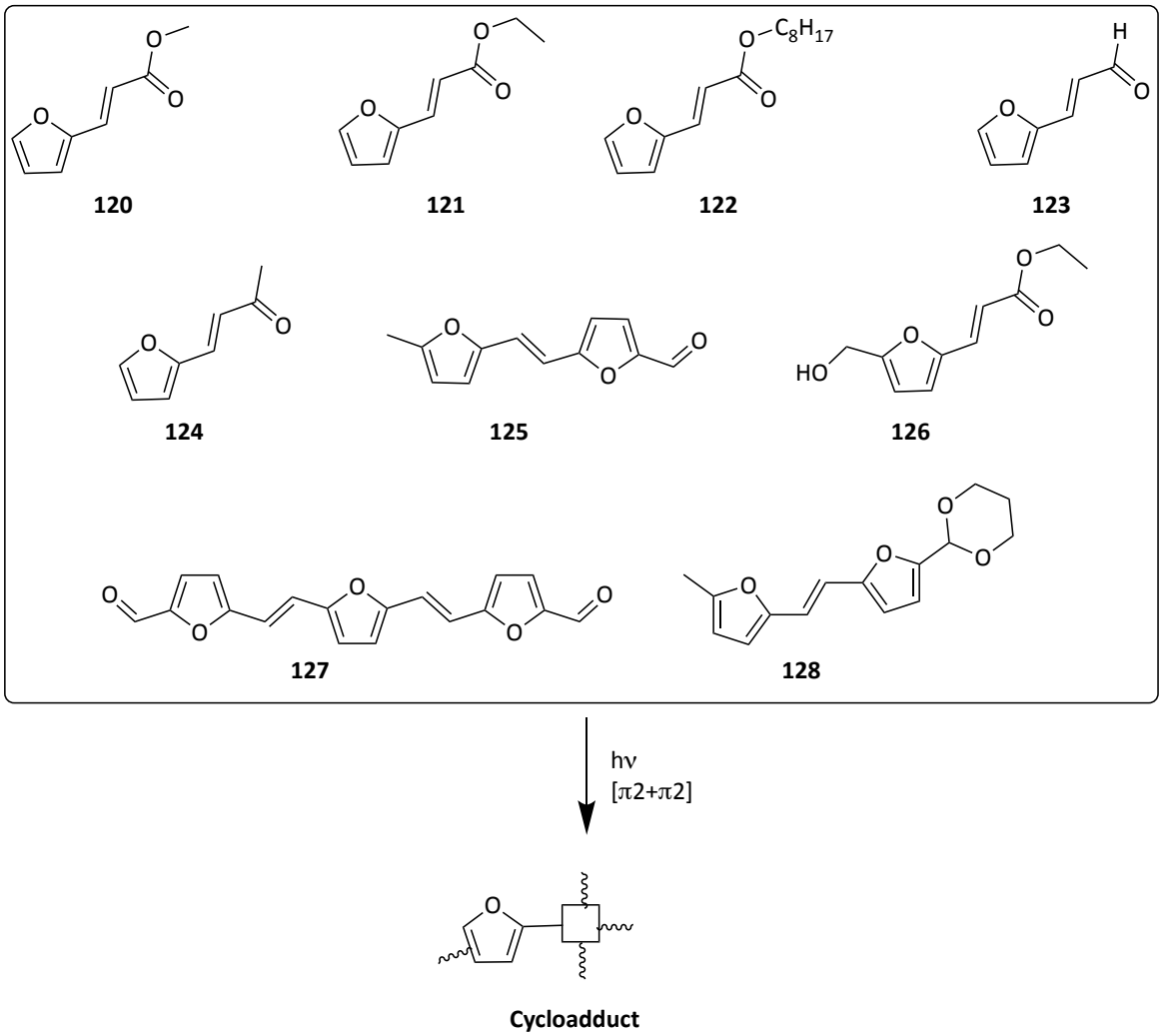

Figure 30 Cycloadduct forming structures with a furan motif as reported by Gandini's group

Since a more conjugated π system in that motif, would decrease the HOMO-LUMO energy gap, increasing the maximum absorption wavelength, the synthesis of compounds **90**, **117** and **118** Table 10, entry 6-8) was performed in parallel to **113**.

Their experimental UV-vis spectra confirmed this hypothesis. With a UV-A absorbance of >97% (of total absorbance) and E(1,1) values between 869 and 1223, these compounds were excellent UV-A absorber. However, their investigation was not pursued because of their poor solubility in cosmetic oils, low yields obtained, and instability of the structurally similar compound **113,** as mentioned earlier.

The second class of compounds prepared were inspired by the commercial UV filters oxybenzone (Figure 27, p. 129, **108**) and avobenzone (Figure 27, p. 129, **110**).

Firstly, compound **112** (Table 10, entry 4) was prepared by reaction of 2-methyl furan with oxalyl chloride following a modified literature procedure (Scheme 7 and see the experimental section, general procedures for chapter III.2).[152] To avoid costly chromatographic separation, the purification of this compound was achieved by repeated recrystallisation which afforded **112** in similar yield than reported previously using chromatographic separation (51% yield reported in the literature).[152] With a UV-B and -A absorbance of 29.1% and 52.9% respectively and an E(1,1) of 836, this compound was deemed of significant interest. Initial tests performed in our laboratory showed solubility of just 10% in 1,2 propanediol at room temperature (test performed by Dr. Katie Lamb). Hence, the synthesis of **112** was up-scaled, and ~20 g was isolated.

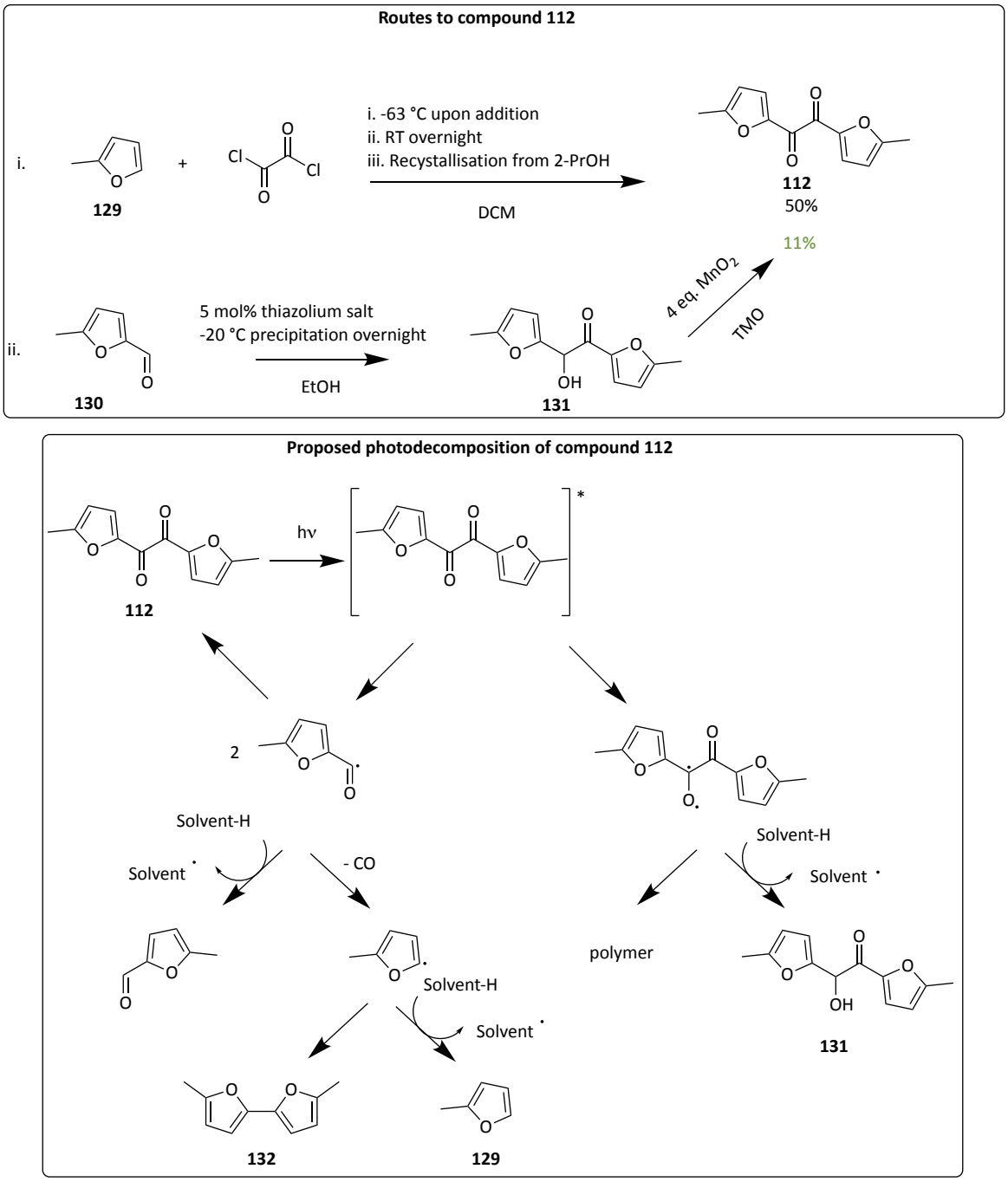

*Scheme 7 Routes to compound **112** and possible degradation route via Norrish type I reaction*

Because this route required chlorinated solvents and reagents prepared from toxic material (oxalyl chloride from phosgene) another route was also explored. Compound **112** was also

obtained via benzoin condensation of 2-methyl furfural (**130**) to furoin (**131**) using a vitamin B_1 analogue catalyst in EtOH, followed by oxidation with MnO_2 in TMO.

The overall yield of 11% (over 2 steps) was low compared to the previous route but had the advantage to use more innocuous solvents and reagents (*i.e.* EtOH, TMO and thiazolium catalyst, MnO_2 respectively). Nevertheless, the solubility of **112** could not be repeated in the photostability and biodegradability testing laboratory: less than 5% of **112** could be dissolved in 1,2 propanediol. In addition, photostability tests showed that after 5 MED, compound's **112** UV absorbance in solution completely disappeared.

A proposed photodecomposition route for **112** is represented in Scheme 7. The excited species [**112**]* likely provides two types of radical species, due to the homolytic cleavage of the -CO-CO- bond (Norrish type I reaction), the first leads to two 2-methylfurfural radicals that may recombine to reform **112** (no net change). Further loss of -CO moieties from the furfural radicals would lead to two 2-methylfuran radicals. Alternatively, hydrogen abstraction from the solvent would produce 2-methylfurfural. The 2-methylfuran radicals can also lead to a dimer (**132**) formation or, after a second hydrogen abstraction from the solvent, 2-methyl furan (**129**). The formation of these species may account the UV-absorbance loss in **112,** and similar reactions have been described during the study of the structurally related Benzil (1,2-diphenylethane-1,2-dione).[158,159]

The other proposed radical species that may form arise from the cleavage of a C=O double bond leading to the biradical compound (**112**$^{\cdot\cdot}$). This bi-radical species likely forms oligomers/polymers in subsequent reactions. Alternatively, **112**$^{\cdot}$ after hydrogen abstraction from the solvent (twice), can produce furoin.

Due to its photoinstability and low solubility, **112** was modified into its oxime derivative, **119**. The presence of an -OH group was expected to increase the solubility in 1,2-propanediol thanks to better hydrogen bonding whilst increasing the photostability via an excited-state proton transfer mechanism, also called photo-tautomerisation (Figure 31).[144,160] Briefly, after photo-excitation, a proton transfer can occur between -OH and =N- group leading to the excited species **119'*** . Release of the excess energy via internal conversion leads to the lower energy level S_0'. Because of the higher energy of the tautomer **119'**, the conversion of **119'** to **119** is, hypothetically, fast, around 10^{-12} s.

As expected, the solubility of the oxime **119** in 1,2-propanediol increased dramatically compared to the diketone derivative. After irradiation at 10 MED, 30 % of the **119**'s UV absorbance was preserved, which is an improvement compared to **112**'s photostability. Unfortunately, this compound's photostability was not deemed good enough to be tested in a formulation despite these improvements.

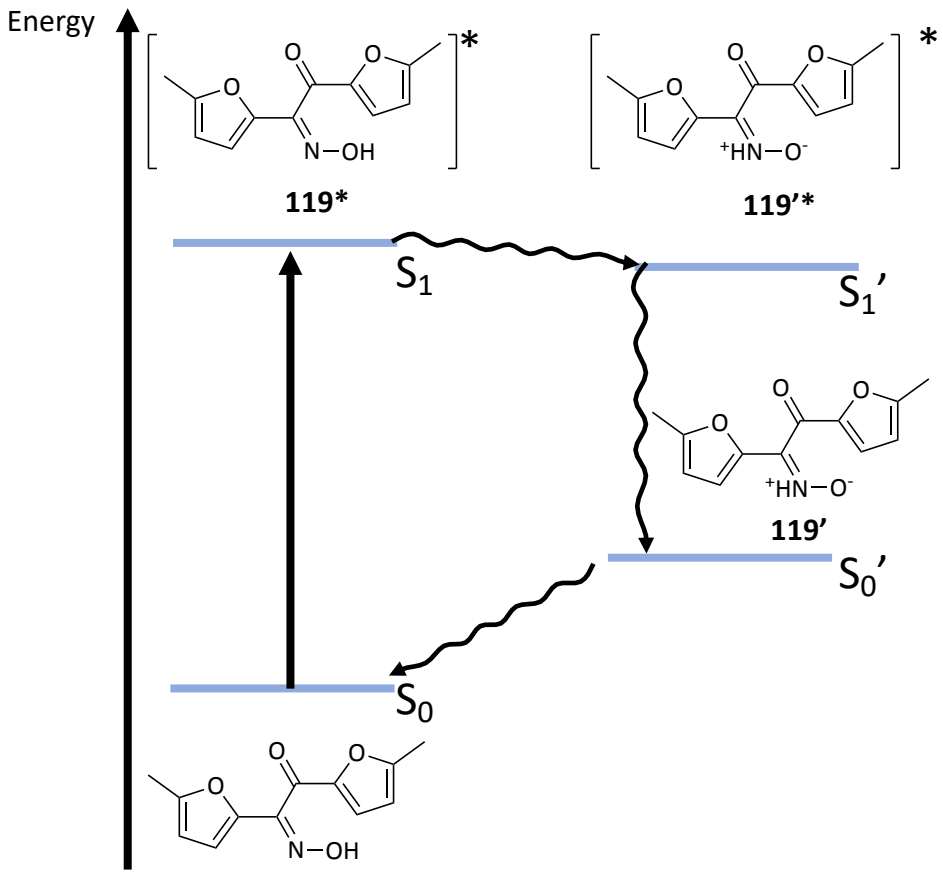

*Figure 31 Possible electronic pathway for the excited state proton transfer of **119***

Interestingly, the replacement of a keto- group for an oxime led to a decrease in the maximum wavelength absorbance (hypsochromic effect), with λ_{max}= 288 nm and an increase in the absorption strength, E(1,1)= 1030.

These two observations may indicate that the HOMO-LUMO energy gap between the diketone **112** and the oxime **119** increased, leading to a lower maximum wavelength absorption. The most plausible explanation for the observed hypsochromic shift is the reduced overlapping of π orbitals in **119**. According to single-crystal XRD analysis, the torsion angle between (C5, C6, C7, C8) in **111** is 129.0 ° and -127.1 ° in **119**. The further away from 180 ° (or 0 °) these angles are, the less likely π orbitals can overlap hence the lower maximum wavelength absorption of **119** (Figure 32).

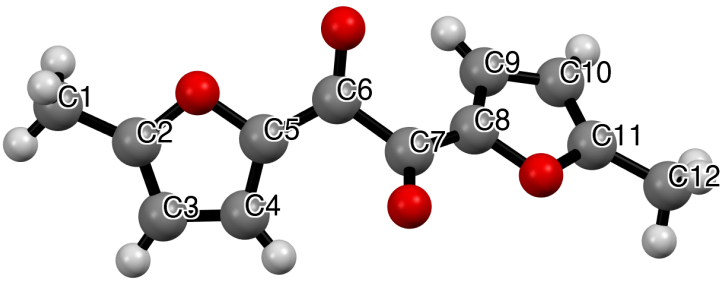

111

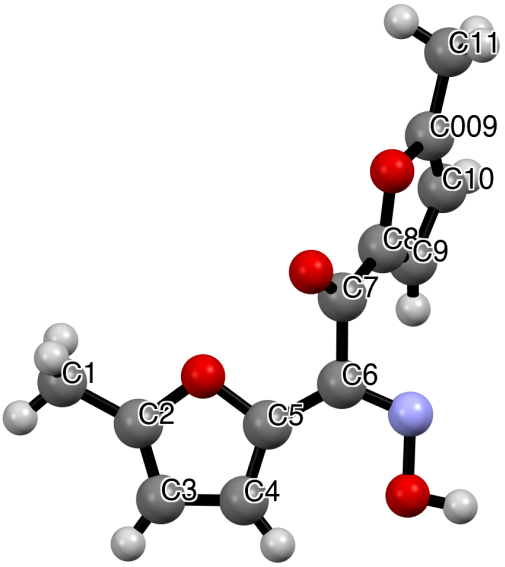

119

*Figure 32 Ball and stick representation of **111** and **119** obtained from single-crystal XRD analysis.*

The excited species **119'*** may also be stabilised by protic solvents such as ethanol (used during UV-vis analysis). The higher stability acquired by hydrogen bonding may lower the n-electrons energy level, thus increasing the HOMO-LUMO energy gap and

consequently shifting the maximum absorption wavelength in the blue region (higher energy).

Another possible explanation for the hypsochromic effect of the oxime group lies in the intramolecular hydrogen bonding of this molecule once in an excited state. Intramolecular bonding (*i.e.* between the -OH group of the oxime and the ketone) may stabilise the '*cis-like* isomer' upon irradiation. Overall, this could result in the locking of this configuration, disruption of the structure due to the proximity of the furan rings and further destabilising the π conjugation of the system (Scheme 8). Despite the poor results of **119** against UV-filter selection criteria, the biodegradability of this compound was tested as well, but no degradation was observed.

Intramolecular H-bonding of 119

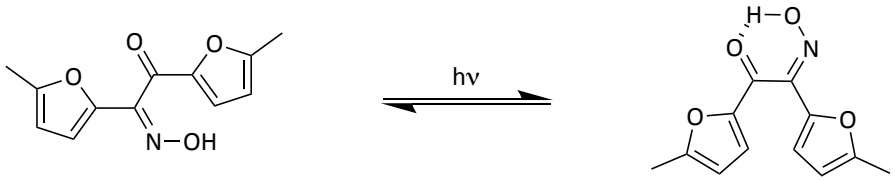

119

*Scheme 8 More favourable "cis-like" structure of **119** due to intramolecular H-bonding*

During the synthesis of the α-diketone compound **112**, another class of keto-derived UV-filters were obtained as a side product.

Using an excess of oxalyl chloride (Scheme 9), **111**$_a$ was obtained in 53% yield. The high E(1,1), 1050, with a maximum absorbance at 302 nm, encouraged further investigation of this α-keto acid compound class. Initially, it was decided to produce the methyl ester **111**$_b$ to slightly increase its solubility while preserving the high E(1,1). Unfortunately, this change had a more significant than expected effect on the E(1,1) which dropped to 724.

Indeed, the higher molar mass was expected to decrease the E(1,1) value to 963 (for a similar ε = 16187.8 L.mol^{-1}.cm^{-1}). The weaker absorption observed may be explained by the lower hydrogen bonding ability of the methyl ester compound **111$_b$**. The excited species of **111$_a$** in [π^1,π^*] state is likely stabilised by hydrogen bonding with the EtOH solvent molecules thus increasing the probability of the electronic transition observed at 302 nm and hence, its intensity.

Route to compound 2-(5-methylfuran-2-yl)-2-oxoacetic acid

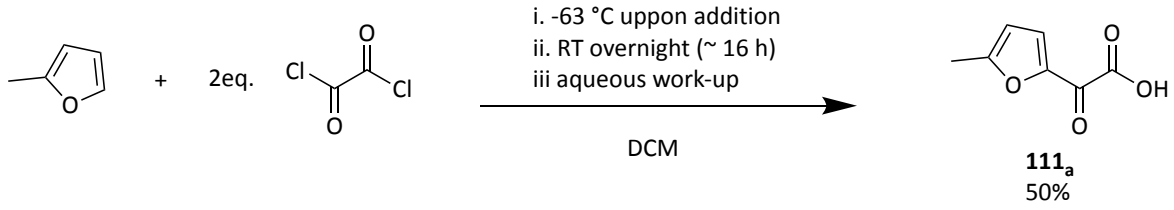

111$_a$
50%

*Scheme 9 Synthesis of 2-(5-methylfuran-2-yl)-2-oxoacetic acid (**111$_a$**)*

For this reason, despite the ease of esterification of this compound, solubility trials with the ethyl ester were not performed nor chemical/photostability/biodegradability trials, and this class of compound was not further studied.

Many factors influence the biodegradable character of a small molecule, such as type of functional group present (*e.g.* esters are famously biodegradable), amount of branching in alkyl chains, molecular geometry and more.[154,161] Although a broad knowledge has now been developed on the biodegradability of polymers, little is known on other, smaller molecules.

According to the results presented here, it appears that furan motifs may not be biodegradable. However, another related compound tested for biodegradability during this

project (made by other collaborators) displayed an excellent biodegradability despite having a furan group. The main difference resided in a hydroxyl group immediately α to the furan ring, likely providing a better degradation pathway for the organism. For instance, it has been shown that the addition of hydroxyl groups on phenyl rings were often the first steps of the aerobic catabolism of *E. Coli* when an aromatic substrate was given to the organism.[162] Furthermore, the presence of hydroxyl groups on catechol derivatives prove essential for *E. Coli* to accept these compounds.[162]

The biodegradability study conducted by BASF only used one activated sludge from the same location, which is a limitation. Indeed, in an ideal study, different types of sludge, fresh and marine water with different microbial composition would be used to represent the many environments in which a compound is susceptible to end up. For instance, since UV filters contained in sunscreen usually end their life in seas and oceans, the sludge to be used should be a sample of marine water from nearby reefs/ beaches containing a similar microbiota, a mock-up of such. However, the high salinity and other marine biology conditions may be particularly hard to replicate in a laboratory for a biodegradability study.

The last aspect to consider is the adaptation factor of a particular sludge for a type of compound. It is not unseen that sludges may sometimes adapt by natural selection, to compounds containing a specific motif (furan, benzene, esters, etc.). For instance, the first report of an organism capable of degrading PET was discovered by Yoshida et al. in PET samples recovered from plastic wastes (PET).[163] This bacterium, *Ideonella sakaiensis,* must have mutated to adapt and consume this substrate for growth. Thus, when a molecule containing unseen functionalities comes in contact with the microorganisms, they likely cannot use it as a metabolite, and will not be biodegradable.

3.2.4 Use of the *BioLogicTool* on existing and proposed UV-filters

The analysis was run on the three primary UV-filter candidates tested for photostability to demonstrate a possible use of the *BioLogicTool* presented in chapter II.

As shown by the qualitative aspect of *BioLogicTool* plots (Figure 33) of some of the selected candidates, the synthesis of bio-derived UV-absorbing compounds is more logical due to the easy access of furan groups from renewable resources. Although the *BioLogicTool* scores do not seem to differ greatly with those of fossil-based compounds, normalisation of data before plotting tends to "erase" the discrepancies between the routes. When normalisation is omitted, the *Total Length* value for Avobenzone becomes 264 against 2.52 with normalisation. Likewise, the *Total Length value* for the diketone **112** becomes 187 without normalisation and 131 for the oxime **119**, highlighting the large difference between the fossil-based routes and the bio-based ones. The development of biorefinery and the larger amount available of furan-derived platform chemicals will likely drive chemical companies to pursue the approach undertaken.

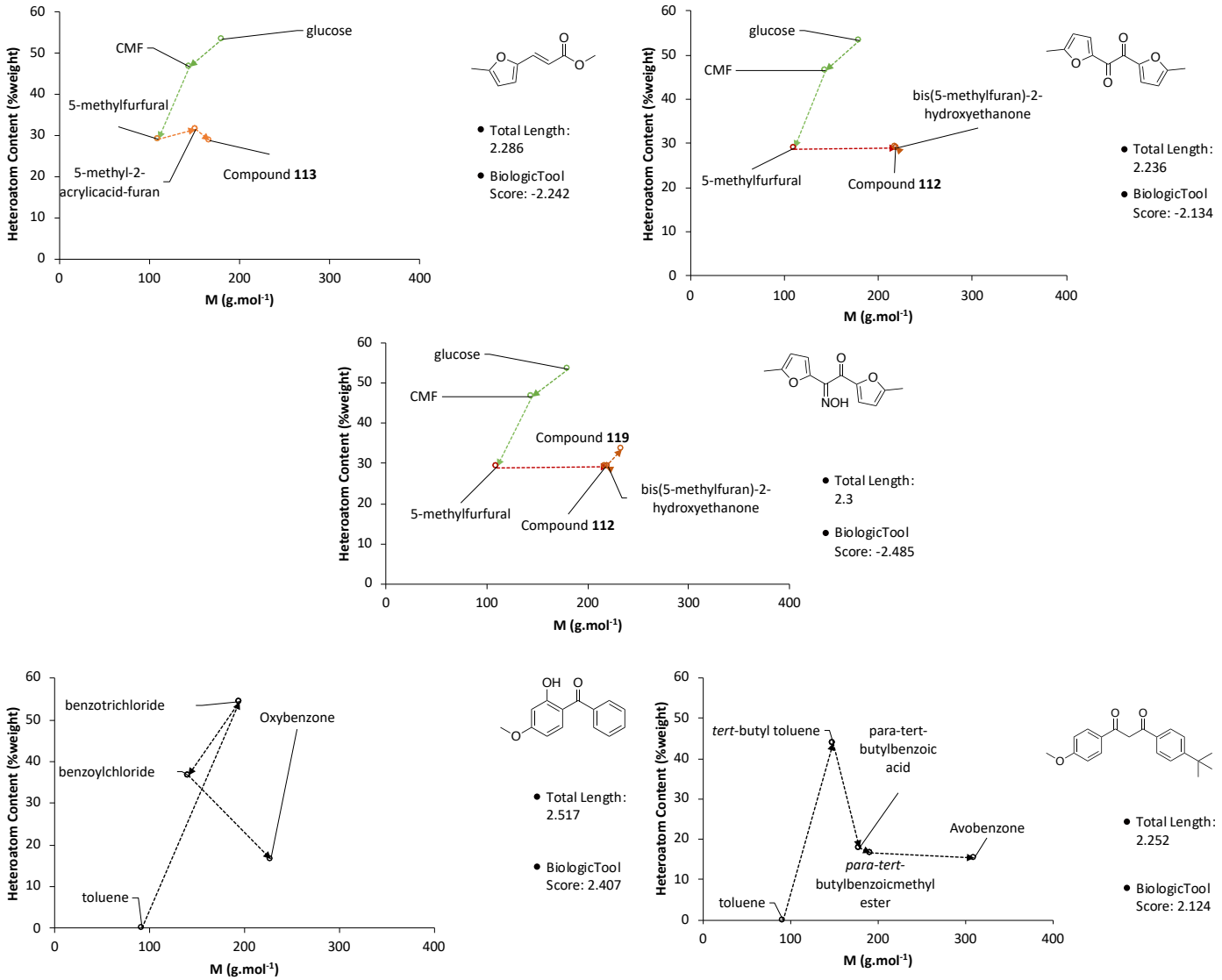

Figure 33 BioLogicTool of selected bio-derived UV filter candidates

3.2.5 Conclusion for chapter III.2

The race for the discovery of biodegradable UV-filters is underway due to the repeated report of the coral toxicity that fossil-based compounds exhibit.[164] Thus, chemical companies and chemists understand the emergency for such compounds to be on the market. For instance, a recent report by Hordbury *et al.* suggested the potential of a lignin derivative used as UV-filters based on cinnamic acid motifs, highlighting the on-going trend settling for renewable UV-filters.[165,166]

Nonetheless, the synthesis of furan-derived UV-absorbing compounds has little been explored. Yet, most of the synthesised molecules in this chapter showed excellent UV-absorbing properties. Additionally, one can easily tune the UV-absorption range of these compounds by employing well-known chemistry rendering the scaling up of these reactions easier. However, the low biodegradability of these molecules revealed that the "biodegradability rules" (presence of O, ester groups, branching, etc.) that apply in different chemistry fields, such as polymers or surfactant, may not be systematically transferable to another. Their insufficient UV-stability also impeded potential sunscreen application.

Finally, the interesting property of unsaturated furans such as compound **90** to form cycloadducts, inspired us to use it as the UV-active monomer for photopolymer. This work is presented in the following section.

Chapter III.3
Production of a bioderived strain-hardening photocurable polymer by enzymatic polymerisation‡

‡ This chapter is adapted from the article: Lie, Y. *et al.* Work-hardening Photopolymer From Renewable Photoactive 3,3'-(2,5-Furandiyl)Bisacrylic Acid. *ChemSusChem* cssc.202000842 (2020) doi:10.1002/cssc.202000842.

Y. Lie performed the monomer synthesis, chemocatalytic polymerisation, MnO_2 characterisation and the photoreaction (curing) on the monomer/polymer and wrote the corresponding sections together with the introduction and conclusion.

Dr. A. Pellis realised the enzymatic polymerisation and characterisation of the polymers pre- and post- curing and wrote the corresponding section of the article. Dr. I. Funès-Ardoiz and Prof. Dr. D. Sampedro performed the TD-DFT calculations and wrote the corresponding section of the article. Dr. T. J. Farmer and Dr. D.J. Macquarrie supervised the work and participated to writing of the article.

3.3.1 Introduction: Photopolymers, definition and global trends

3.3.1.1 Uses and classification of photopolymers

The UV-A absorbing compound, **90**, reported in **chapter III.2** is obtainable from CMF, itself derivable from microalgae (see chapter III.1). The bifunctional nature of this molecule led to investigate its use as a monomer for renewable photopolymer synthesis.

Humanmade polymers such as poly(ethylene terephthalate) (PET), high-density poly(ethylene) (HDPE) and poly(vinyl chloride) (PVC) surround our urban environment and are produced in multi-ton quantities. Synthetic thermoplastic production volume is projected to grow from 350 Mt in 2017 to 590 Mt in 2050.[7] These plastics are used for a wide array of applications ranging from packaging (36%) and construction (16%) to textiles (15%) and others (33%).[7] Unfortunately, most plastics currently produced are derived from the non-renewable base chemicals described in chapter I such as ethene, propylene or benzene/toluene/xylenes (BTX). The depletion of crude oil and natural gas has pushed industries to find polymers derived from renewable resources with similar or better properties successfully exemplified by the development of poly(ethylene furanoate) (PEF).[167] The possible photoactivity of compound **90** described in the previous chapter inspired its use as a monomer in polycondensation reaction to form a photopolymer.

Photopolymers are a class of polymers that are particularly useful in specialised applications such as dentistry, microelectronics or 3D printing.[168] The thermophysical properties of these polymers changes under direct or indirect interaction with light (usually in the UV range). Typically, photopolymers are distinguished according to their reactivity to light. These reactions commonly occur in the presence of photoinitiators such as ketones

(benzil or benzophenone, radical initiator), onium salts (iodonium, ammonium, sulfonium salts, cationic initiator) or nitriles (crystal violet leuconitrile, anionic initiator, Table 11).[169]

Table 11 Example of photoinitiators for photopolymerisation

Photoinitiator type	Structure examples
Radical initiator (ketones)	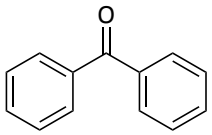 **benzophenone** 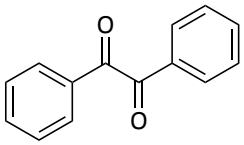 **benzil (1,2-bisphenyletanedione)**
Cationic initiators	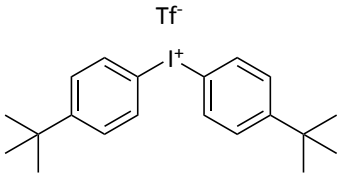 **bis(4-tert-butylphenyl) Iodonium salt** 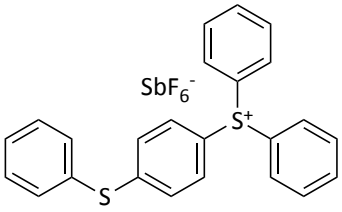 **diphenyl(4-(phenylthio)phenyl)sulfonium salt**
Anionic initiator	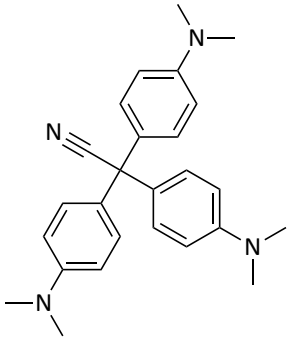 **Cyrstal violet leuconitrile**

In a 2014 review of the area, Crivello and Reichmanis proposed to define five types of photopolymers (Figure 34).[51] **Type I** are monomers or short oligomers bearing two or more functional groups that can undergo chain-growth polymerisation after photoinitiation, leading to a potentially cross-linked network between the polymer chains. These types of photopolymers, such as those based on pentaerythritol tetraacrylate (see chapter II and Figure 34), are particularly useful in 3D printing.[169,170] Upon irradiation, polymerisation or cross-linking occurs, increasing the rigidity of the polymer, which then forms the (stiff) base for another layer of polymer to be applied, making possible the printing of solid 3D objects. **Type II** photopolymers possess intrinsically photoactive moieties which, unlike Type Is, can undergo reactions without the need for a separate initiator. For instance, photopolymers with a constituting unit based on cinnamic acid derivatives (*e.g.* 2,3-diacetoxycinnamic acid) may form a cross-linked network after irradiation without the need for a photoinitiator.[171,172] **Type III** photopolymers possess two complementary moieties susceptible to reacting with each other, one photoactive and another not. After irradiation of the photoactive group (possibly in the presence of a photoinitiator), bond formation occurs between the thus excited moiety and the other. For example, the photoinduced thiol-ene chemistry, where a thiol group and an alkene undergo a coupling reaction after exposure to light in the presence of a suitable radical initiator can be used to produce Type III photopolymers.[173] **Type IV** includes polymers containing a photoreactive moiety which under irradiation converts to another structurally different species but that does not result in chain growth or cross-linking. This property is useful in lithography where the solubility of a photoresist is altered upon irradiation which allows removal (positive photoresist) or retention (negative photoresist) of a specific layer of photopolymer after development with an appropriate solvent. A famous example of Type IV is the diazonaphthoquinone –

Novolac resin combination (Figure 34). Finally, photolysis occurs in the **Type V** photopolymers, where the UV-active sites in the polymer chain are cleaved after exposition to light. For example, the [2+2] cycloaddition between cinnamic acid derivatives may be reversed after irradiation at λ< 260 nm making such photopolymers both type II and V. Polymers such as polyolefinsulfones are also examples of type V photopolymers and considered as potential candidates for extreme UV photolithography applications.[174]

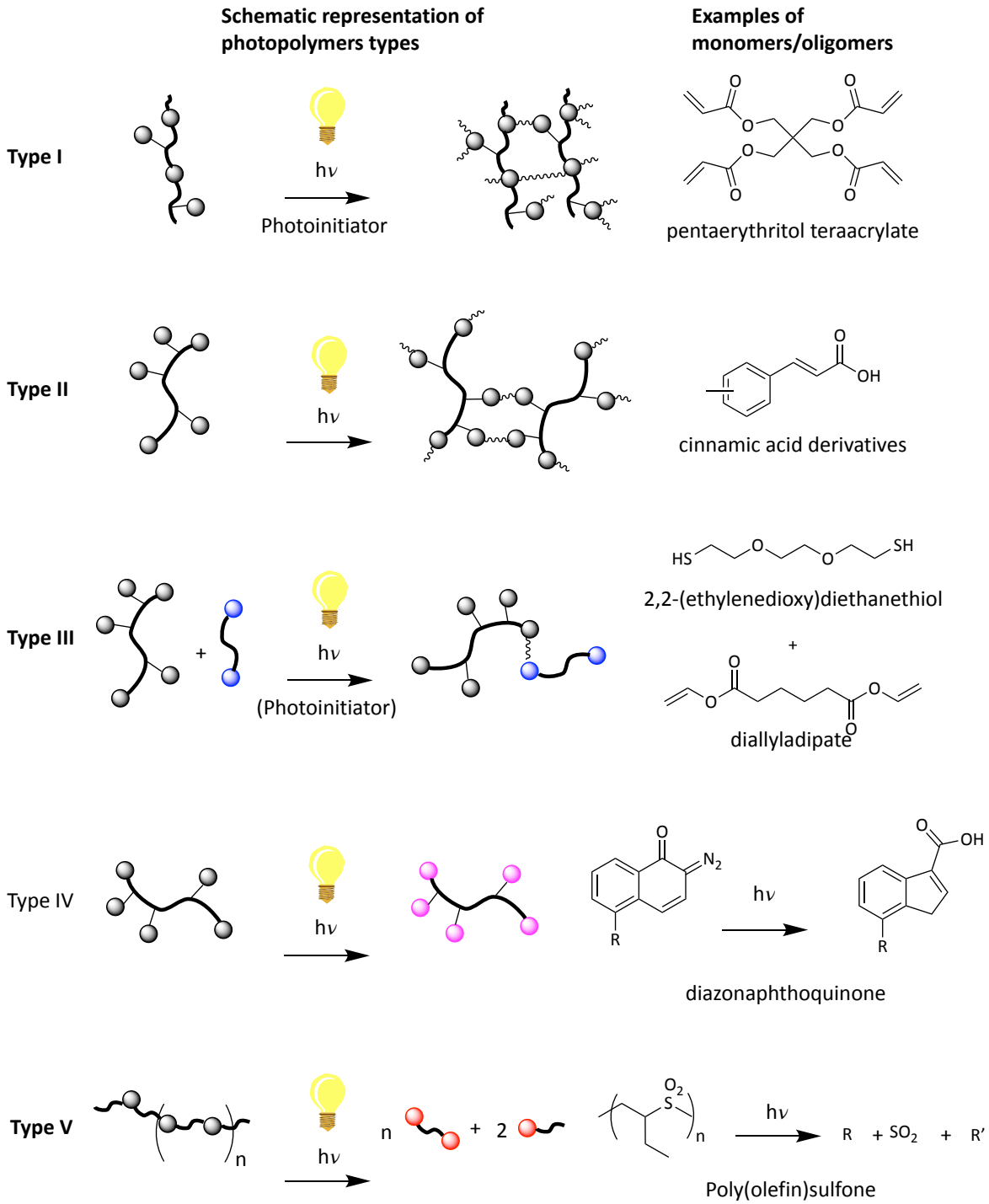

Figure 34 Different types of photopolymer as defined by Crivello and Reichmanis adapted from 51. ***Type I****: polymerisation/cross-linking via multiple functional groups reacting but requiring the use of a separate initiator;* ***Type II****: intrinsically photoactive groups in monomer/polymer undergo polymerisation without the need for a separate initiator;* ***Type III****, two complementary moieties react following photoactivation of one of the moieties and possibly requiring an initiator;* ***Type IV****: Molecular structure of reactive site changes upon irradiation but polymer chain does not extend or break;* ***Type V****: photocleavage of UV-active groups in polymer chain/network.*

3.3.1.2 Current use of bio-derived monomers for photopolymerisation

Most monomers employed to form photopolymers are commonly derived from fossil resources. For example, acrylates and methacrylates derivatives (Figure 35**A**, pentaerythritol tetraacrylate) are formed from ethene, as discussed in chapter II using the *BioLogicTool*.

Alternatively, cinnamic acid or its derivatives, *para*-hydroxycinnamic acids (*p*-coumaric acid or ferulic acid), are interesting monomers bearing a photoactive group (acrylic acid) capable of forming a [2+2] cycloadduct.[175] Although currently produced industrially from benzaldehyde *via* the Perkin reaction, they can also potentially be made from lignin decomposition products or extracted from cinnamon, both renewable resources.[175,176] In 2015, Nguyen *et al.* developed a Sb_2O_3 route towards *p*-hydroxycinnamic acid derivatives (ferulic and coumaric acid) to produce of polyalkyl ferulate or coumarate (Figure 35**B**).[177] However, the authors did not investigate the photochemical properties of these. On the other hand, thermally induced cross-linking of bio-based compounds has been studied in greater depth.[178–180] Notably, a recent different approach by Sousa *et al.* consisted of the copolymerisation of 2,5-furandicarboxylic acid with fumaric, succinic acid and 1,3-propanediol, making use of the fumaric acid unsaturation for thermally induced cross-linking (Figure 35**C**).[181,182] Unfortunately, only low molecular weights could be obtained for these polymers (M_n 1.6-3.2 kDa) and required the presence of a thermal initiator (2-hydroxymethylmethacrylate). The photoactive nature of these polymers was not studied.

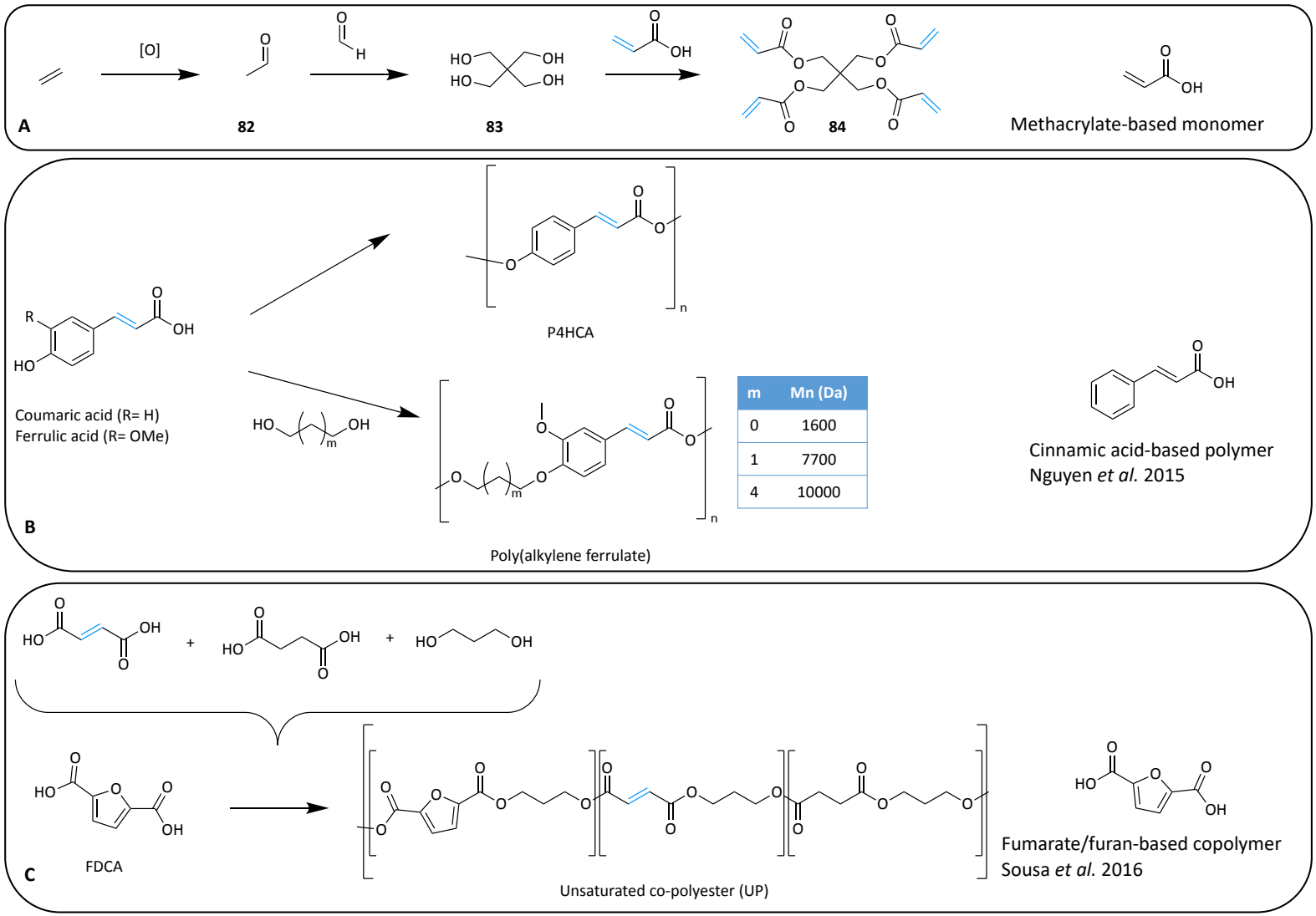

Figure 35 ***A****: Fossil-based route to pentaerythritol methacrylate,* ***B****: Cinnamic acid-containing polymer examples;* ***C****: unsaturated copolyesters containing a poly(ethylene furanoate) unit*

Only a few examples in the literature make use of photoactive bio-derived molecules, such as furan derivatives, to synthesise photopolymers. In the early 2000s, Gandini's group synthesised a series of UV-active furan derivatives to use them as chromophores in photopolymers (as introduced chapter III.2).[155–157] Primarily, Waig Fang *et al.* realised the synthesis of dimers of furfural and 5-methyl furfural (Figure 36, **125-128**). These compounds already displayed promising UV-active properties as their [2+2] cycloadduct could be obtained after irradiation (1-25 h, ~385 nm, 500 W mercury lamp). The further grafting of these compounds on poly(vinyl) alcohol polymers by acetalisation retained the UV-active properties of the chromophores. The use of this photopolymer for lithographic applications was patented in 2002.[183] Lasseuguette *et al.* modified furfural by Knoevenagel-Doebner condensation (Figure 36**C**, **120-122**) or aldol condensation with acetaldehyde or acetone (Figure 36**C**, **123** and **124**) and HMF *via* a Wittig reaction (HMFAE, Figure 36**C**, **126**). The later was copolymerised with ethyl-6-hydroxy hexanoate and hydroxy ethyl esters forming a photopolymer containing up to 10% **126**. Acceptable molecular weights between 3.8-6.9 kDa and M_n between 1.6-2.8 kDa were obtained using K_2CO_3, a mild catalyst employed to preserve the reactive unsaturated furan group.[157] However, the use of co-monomers resulted in low cross-linking levels during the cure, due to the low chromophore content and excessive thickness of the film. Other attempts to use the UV-active properties of unsaturated furan derivatives were described to modify cellulose for biocompatible polymer synthesis or kinetics study.[184,185] However, in the first case, the unsaturated furans moieties were only substituting pendants of the cellulosic polymer, not constitutive unit thereof.[184] Additionally, the in-depth kinetic report employed a methacrylate substituted furan for their study, which takes away the potentially sustainable character of the monomer.[185]

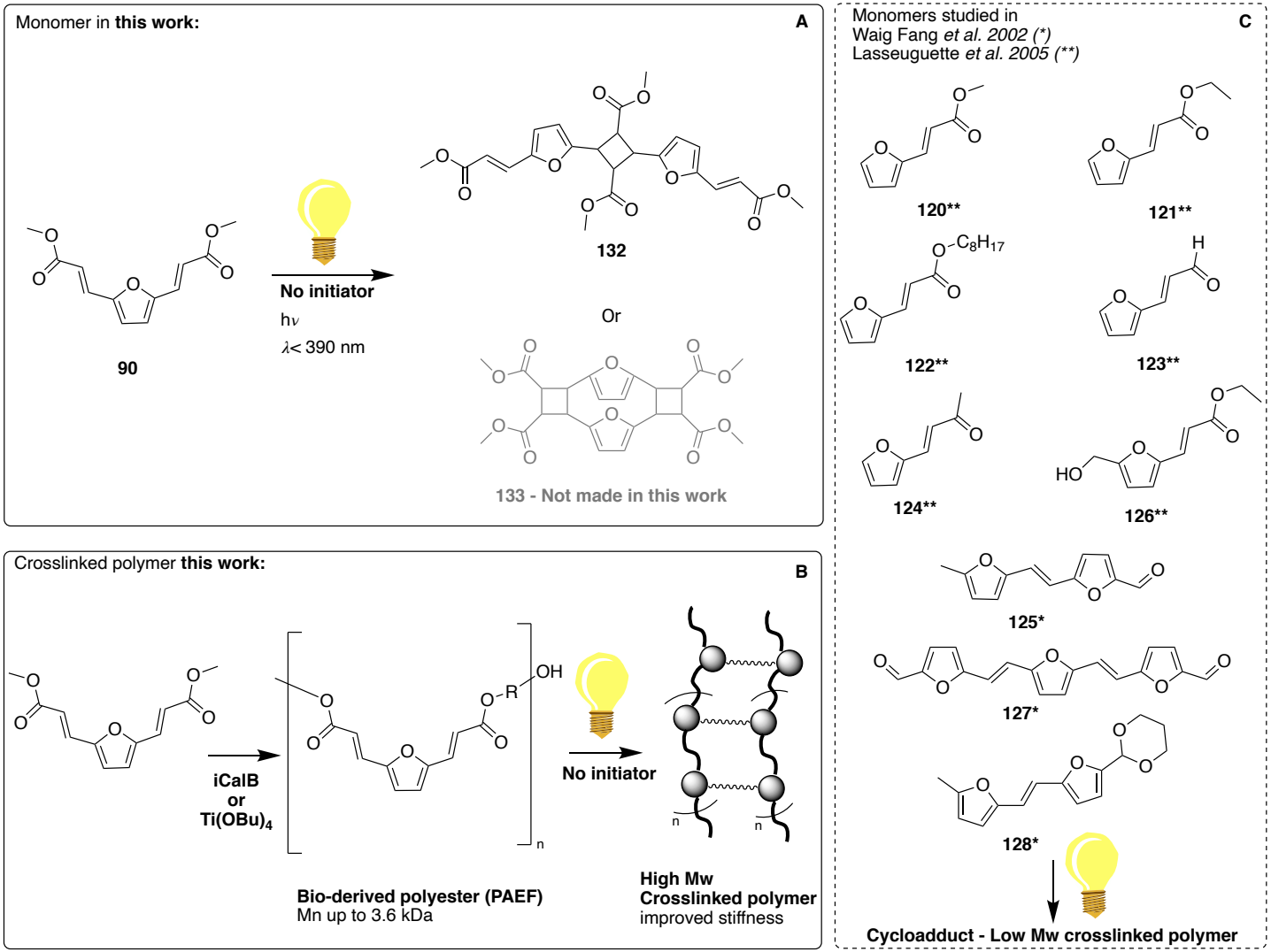

Figure 36 ***A****: Monomer (****90****) used for the enzymatically catalysed transesterification, and possible cycloadduct product;* ***B****: General polycondensation and cross-linking scheme;* ***C****: Previously reported UV-active furan-derived monomers by Lasseuguette et al. and Waig Fang et al.*[156,157]

3.3.2 Aims of chapter III.3

This work presents the development of an alternative photopolymer system based around a renewable furan scaffold, the polyesters of furandiyl diacrylic esters, PFAE. Four principle targets were identified for the successful photopolymer synthesis using **90**.

First, the higher scale synthesis of 2,5-diformylfuran (DFF), a precursor to the highly UV-active compound **90** (see Figure 36**A**, **90**) was carried out. Previously reported methods for DFF synthesis required critical element-containing catalyst (*e.g.* Ru), molecular O_2 or complicated reaction set-up which impeded potential scale-up of the reaction.[186–188] Here, the development of semi-continuous oxidation of HMF with MnO_2 allowed the facile and rapid production of DFF on a multi-gram scale. Due to the reactivity difference between commercial sources of MnO_2 their analysis with powder XRD, SEM-EDX and porosimetry was conducted and revealed structural and compositional variations explaining the different reactivities. Then, the potentially photoactive sites (two exo-furan C=C moieties) were attached to the furan ring core via Knoevenagel-Doebner condensation (and esterification) as described in chapter III.2.

Secondly, photoreactive monomers, such as **90**, are known to be intolerant to classical polycondensation conditions (*e.g.* Ti/Sb salts catalysts, high temperature–180 °C–etc.) explaining the lower M_n obtained previously.[156,157] To test the mechanical properties of such photopolymers, It was essential to develop milder polymerisation conditions that could preserve the monomer's photoactivity and lead to higher M_n. Two different approaches were explored:

- The use of milder catalyst and lower temperatures and

- The polymerisation in high-boiling organic medium using immobilised enzyme catalysts (performed by Dr. Alessandro Pellis).

Thirdly, mechanistic insights of the curing reaction pathway were experimentally obtained using monomer **90** as a model compound, to appreciate the photopolymer's behaviour before and after UV-curing and the resulting structural changes. TD-DFT computational modelling of the proposed mechanism (performed by Dr. Ignacio Funès-Ardoiz) further supported the claims made in this work.

The final aim of this chapter consists of testing the mechanical properties of the synthesised photopolymer before and after curing.

3.3.3 Synthesis of a work-hardening photopolymer with renewable furan repeating units

3.3.3.1 Synthesis of the unsaturated monomer 3,3'-(2,5-furandiyl)bisacrylic acid

Monomer **90** was described as early as 1914 by Cooper & Nuttall during their study on 2,5-diformylfuran and was recently used in reactions with benzyne to produce a potential terephthalate replacement.[187,189] However, no details on **90**'s photoactive properties have thus far been reported in the literature. The precedent chapter showed that this compound was an excellent UV-A absorber and that a structurally related molecule (**113**) was not photostable. This photoinstability was imputed to the formation of a [2+2] cycloadduct although no experimental evidence was collected until now. The synthesis of **90** was

performed according to Scheme 10. It began with the oxidation of HMF to DFF (Scheme 10, **37** and **88** respectively).

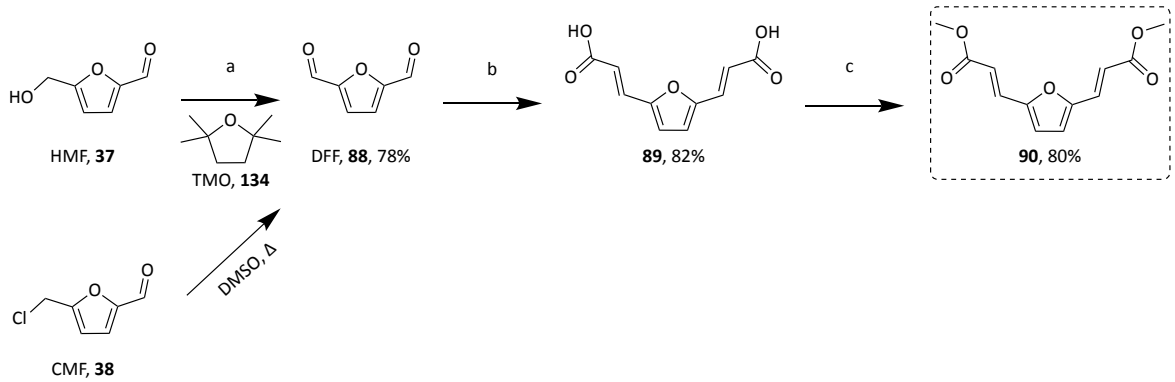

*Scheme 10 Route to monomer **90**. a) HMF (1 g as a 1%w/w solution in TMO), MnO_2 (6.2 g in spent HPLC column), semi continuous flow reaction (see Figure 38) 75 °C residency time of ~2 min, b) DFF (101 mmol), malonic acid (405 mmol), piperidine (20 mmol) and pyridine (150 mL) 85 °C, 16 h then reflux 2 h, c) **89** (43 mmol), NaCl (19 mmol), H_2SO_4 (13 mmol), MeOH (150 mL) reflux 16 h.*

DFF is obtained from HMF (or CMF via Kornblum oxidation in DMSO), as such it is also a platform molecule with high potential for synthetic application for pharmaceuticals (fungicides), electronic (organic metals) or plastics (PEF, imine containing polymer, Figure 37).[190–193]

Although CMF could be obtained from microalgae (as described chapter III.1), HMF was used instead as a starting material due to its commercial availability allowing to scale up the reactions leading to **90**.

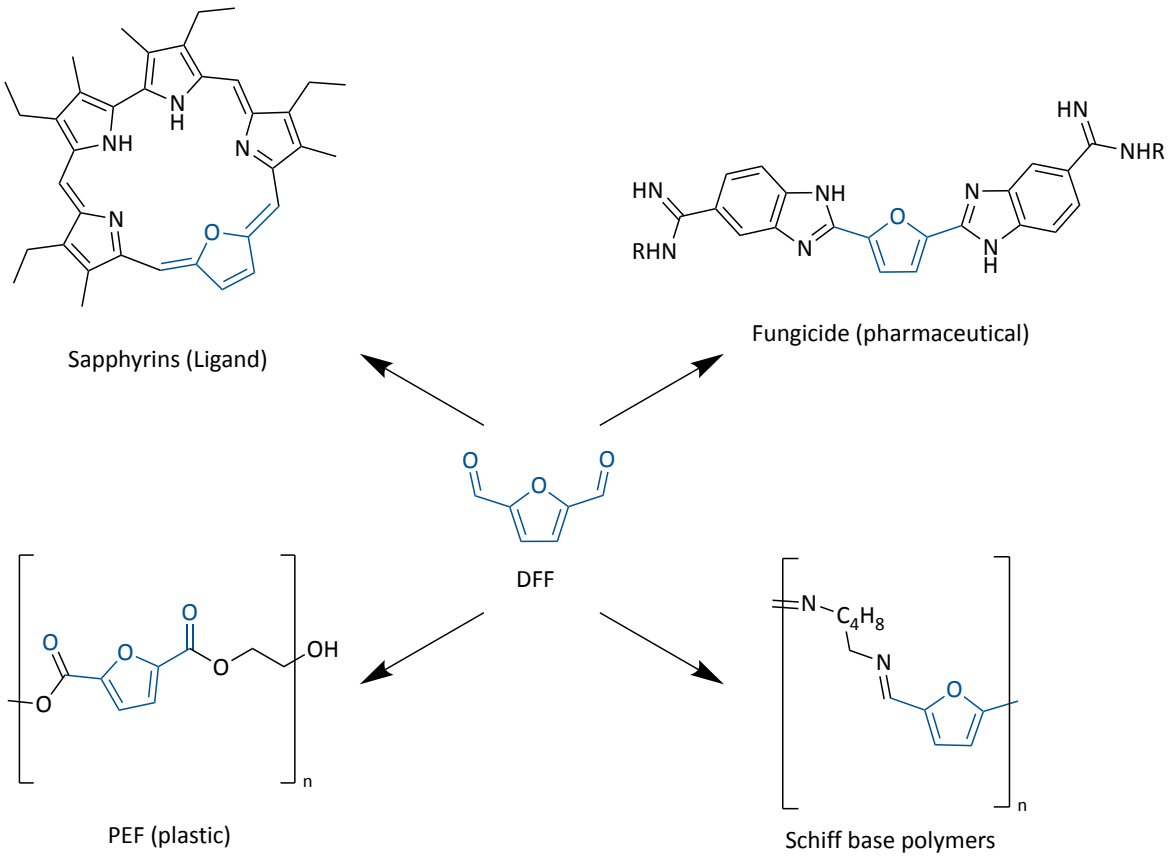

*Figure 37 Different uses of DFF (**88**) for the production of higher-value chemicals*

The presence of two aldehyde groups in DFF offers many possibilities for further modification via Wittig reaction, Schiff bases formation, aldol condensation etc.[194,195] However, despite this promise, few reports make use of this compound partly due to its current high retail price (123 £.g^{-1} Sigma Merck *accessed 14/9/20*) and instability upon prolonged storage. Additionally, the synthesis of DFF from HMF commonly requires expensive critical transition metal (co)-catalyst (*e.g.* Ru) which further reduces green credentials of DFF-derived reaction.[186,188,196,197] Thus, a different method was developed, which avoided the use of critical element containing catalyst. The protocol employed by Serum *et al.* where MnO_2 is used as an oxidant was deemed a good starting point since it did not require any critical element-containing catalyst and was conducted under inert

atmosphere (N_2 avoiding molecular O_2).[187] Yet, from a sustainability perspective, this method suffered from several drawbacks such as:

- Use of dichloromethane as a solvent (carcinogenic hazardous)[198]
- Complicated reaction set-up apparatus (heavier than water dean stark under N_2) also requiring water condenser (high water consumption)
- Prolonged reaction time (14 h)
- Generation of high amounts of solvent wastes (DCM, EtOAc >1 L for 30 g reaction)
- Does not consider reconversion of the reduced MnO to MnO_2.

The heterogeneous nature of the oxidant employed here led to try the oxidation in a semi-continuous manner using a MnO_2-packed spent HPLC column. The reaction system required a pump to pass the HMF through this column. A repurposed HPLC pump (Jasco P980) was thus used to circulate the HMF solution. Although DCM was first used as an ideal solvent to test the reaction system, it was preferable to replace it with a less hazardous solvent. For this reason, 2,2,5,5-tetramethyloxolane (TMO), an alternative solvent to toluene was used instead. Due to the lower solubility of HMF in TMO, pre-heating (75 °C) was necessary before entry into the column and during the contact with MnO_2.

First trials of the reaction system often led to overpressure, resulting in pump shutdown. This problem was later explained by the lower solubility of DFF, which clogged the exit capillary (Figure 38**G**). The issue was remedied using heating tape at the entry (Figure 38**E**) but most importantly at the exit of the column, thus ensuring homogeneous heating all along the circulation path. A picture showing the final optimised version of the system is represented in Figure 38.

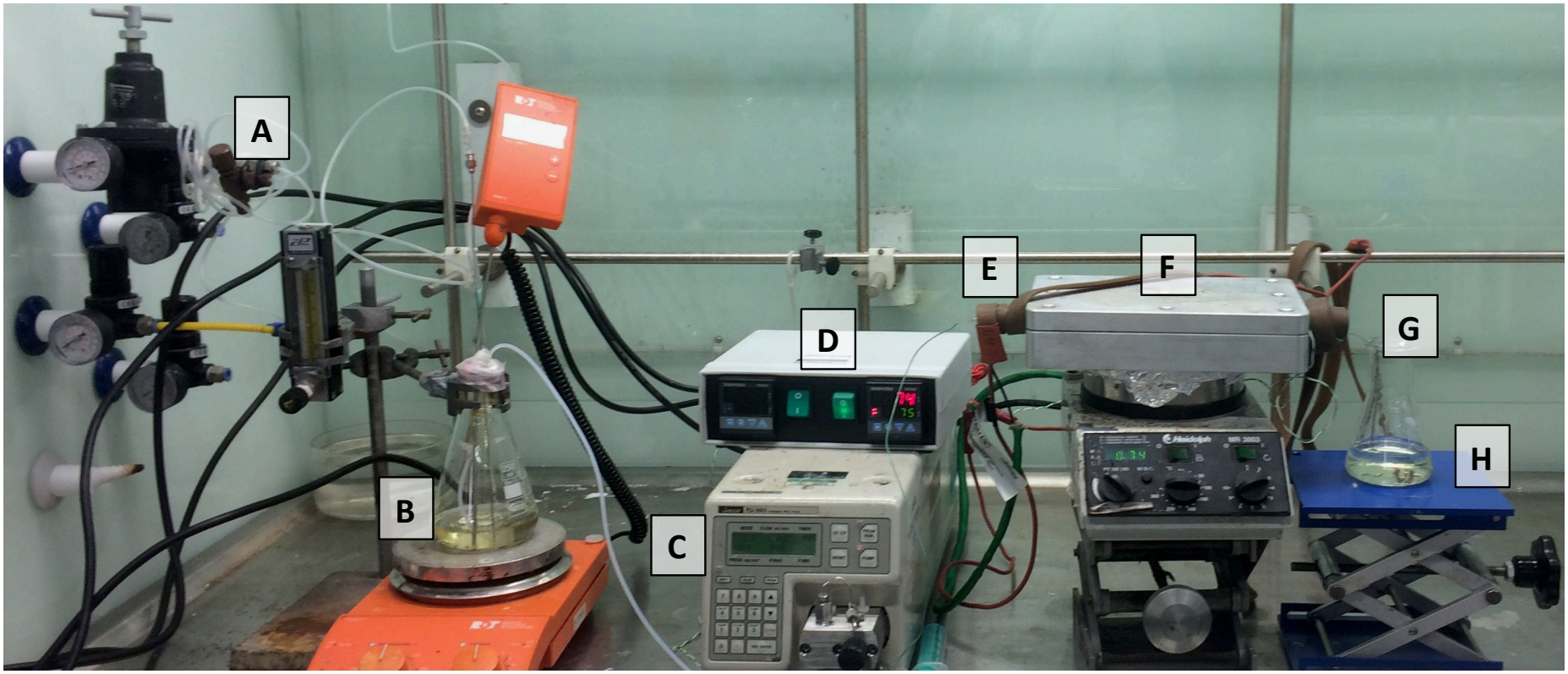

*Figure 38 Semi-continuous oxidation of HMF (**37**) to DFF (**88**) with 88% MnO_2-packed HPLC column **A**: Oxygen input (optional, 2 mL.min^{-1}); **B**: 1% HMF solution in TMO; **C**: JASCO PU-980 HPLC; **D**: Heating tape controller pump; **E**: Heating tape; **F**: MnO_2-packed HPLC column (4 mm internal diameter, 25 mm length) clamped in custom-made heating block; **G**: capillary exit **H**: DFF solution obtained at column exit.*

The solution collected at the exit (Figure 38**H**) after one passage through the column was analysed by GC-FID to assess the conversion of HMF. If the conversion was not complete, the solution was recirculated through the column. When no more HMF conversion was observed, the collected solution was evaporated under reduced pressure. In this manner, DFF could be obtained with very high selectivity and purity after the first passage through the column and was used in the next step without further purification. The first passage through the system yielded up to 78% of pure DFF isolated as a white solid.

The type of commercial manganese dioxide used for the reaction was found to be crucial. Indeed, when using a 99% pure MnO_2, almost no conversion could be observed. Porosimetry analysis showed that the BET surface area of the 88% pure MnO_2 was 6 times higher than the 99% pure MnO_2 (Table 12).

Table 12 Porosimetry analysis of MnO_2

	BET Surface Area ($m^2 \cdot g^{-1}$)	Adsorption average pore width (4V/A by BET, nm)	Desorption average pore width (4V/A by BET, nm)	BJH Adsorption average pore width (4V/A, nm)	BJH Desorption average pore width (4V/A, nm)
MnO_2 99%	19	4.4	4.3	5.3	5.1
MnO_2 88%	108	7.7	7.6	7.8	6.6
MnO_2 88%*	74	8.83	8.7	10.6	8.2
MnO_2 88%**	77	11.6	11.4	10.9	9.7

*Post reaction, no calcination; **Post reaction, with calcination at 300 °C for 1 h.

As demonstrated by the DFT analysis conducted by Hayashi *et al.,* crystal structures of MnO_2 (used in a catalytic amount in their study), are determinant for their activity due to the difference in the vacancy formation energy (VFE) of the oxygen planar sites.[199] Thus, the powder XRD analysis of both oxidants used revealed that the 99% MnO_2 (Figure 39) had a crystalline structure similar to the β-MnO_2 synthesised by Hayashi *et al.* for which they

computed a VFE of 3.25 eV. The domain frame (crystallite size) was calculated using the Scherrer equation, which gave an average value of 28.8 nm. On the other hand, the 88% MnO_2 (Figure 40) had a more amorphous structure, with a domain frame of 5.9 nm, explaining the higher surface area observed by porosimetry, and a crystal structure close to the ε-MnO_2 described before. The smaller domain frame between the two types of MnO_2 may also suggest that more active sites are available in the 88% MnO_2.

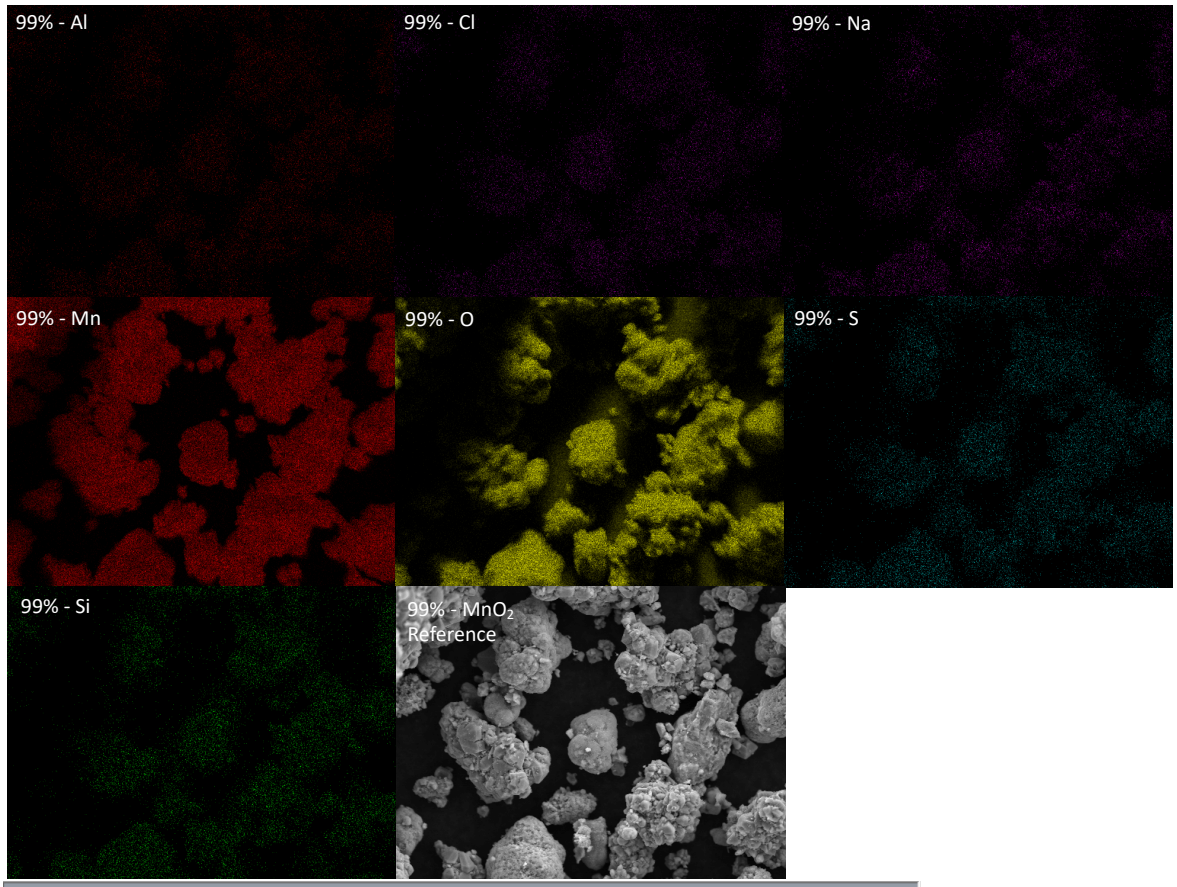

Element	expst(23)		
	Net Counts	Weight %	Atom %
O K	507936	14.61	36.77
Na K	2892	0.19	0.33
Al K	15846	0.42	0.62
Si K	2739	0.06	0.09
S K	4699	0.10	0.13
Cl K	3316	0.08	0.09
Mn K	1193876	84.55	61.98
		100.00	100.00

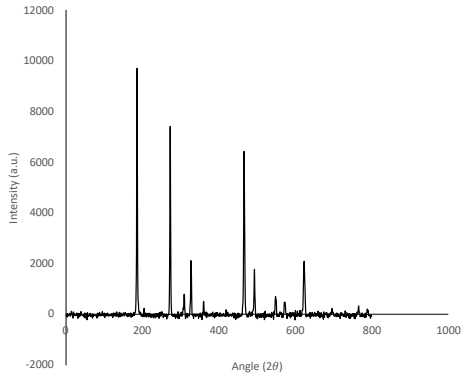

Figure 39 EDX-SEM images and analysis of 99% MnO_2. Powder XRD analysis output is represented below

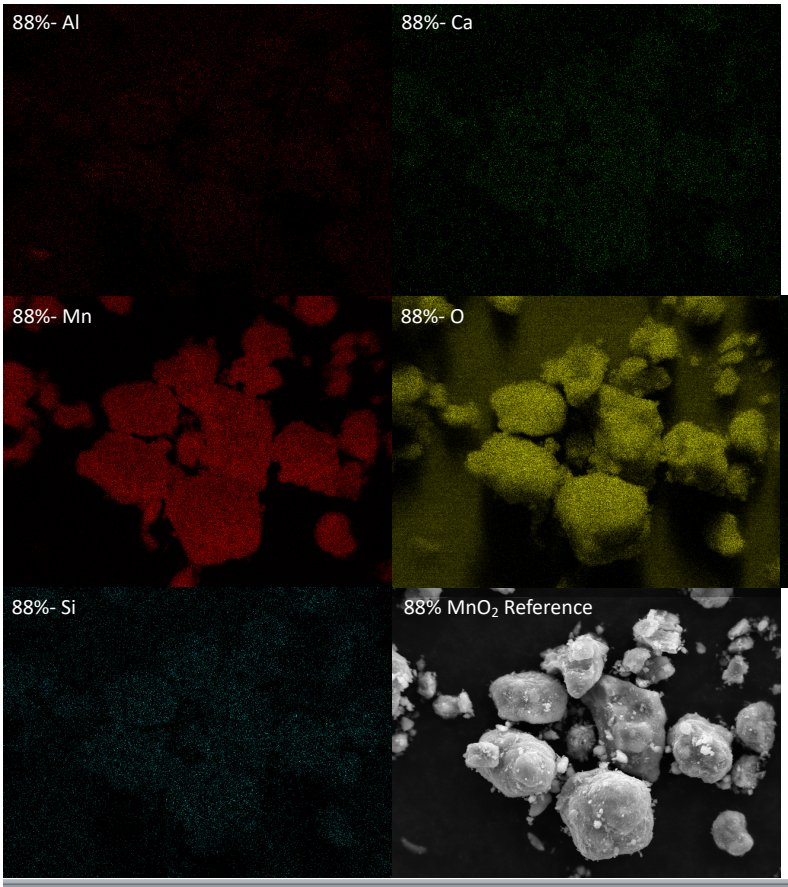

Element	expst(21)		
	Net Counts	Weight %	Atom %
Mn K	739251	74.57	46.75
Ca K	3918	0.16	0.13
S K	10998	0.33	0.35
Si K	6382	0.20	0.24
Al K	14238	0.51	0.65
Na K	5467	0.49	0.73
O K	599381	23.75	51.13
		100.00	100.00

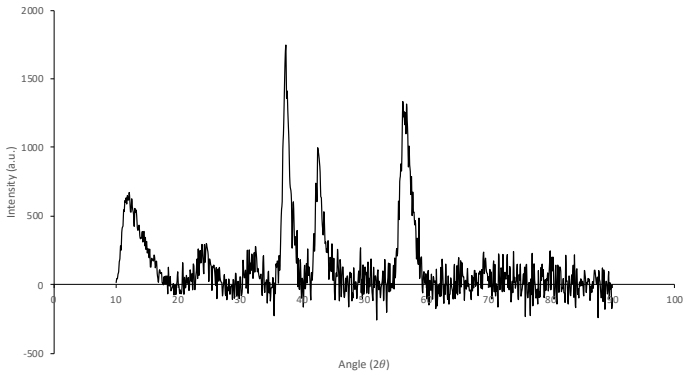

Figure 40 EDX-SEM images and analysis of 88% MnO_2. Powder XRD analysis output is represented below

No oxygen VFE was computed by Hayashi *et al.* for the ε-MnO_2 due to its less defined crystalline system. However, the related γ-MnO_2 had a VFE of 3.84 eV for type α oxygens and 3.15 eV for type β oxygens. The presence of more β oxygens in the 88% MnO_2 may explain its higher oxidative power. EDX-SEM analysis of MnO_2 showed a higher Mn:O ratio in the 99% MnO_2 (84.5:14.6 by weight, Figure 39) corresponding to the empirical formula $MnO_{1.64}$ compared to the 88% (74.6:23.7 by weight, Figure 40) corresponding to a $MnO_{1.1}$ at the surface. Traces of $KMnO_4$ may explain the higher oxidative properties of the 88% MnO_2 and the Mn:O ratio observed in the samples. SEM images (Figure 39-40) did confirm the more amorphous, structure as suggested by powder XRD. Overall, these observations may explain the much higher oxidative property of 88% MnO_2 than 99% MnO_2.

The system developed here for the synthesis of DFF allows facile multiple reuses of the MnO_2-packed column. Indeed, after the first passage of a first 1 %w/v HMF solution, the column was flushed with TMO, and another freshly prepared HMF solution passed through the system. For this novel solution, a conversion of 87% HMF to DFF was reached after 7 passages through the column. This loss of activity was initially thought to be due to the formation of the inactive species MnOOH as suggested previously.[196,200] Hayashi *et al.* suggested that the presence of O_2 in their study allowed the re-oxidation of MnO_{2-d} formed during the reaction.[199] Hence, another system was designed where pure O_2 was bubbled continuously in the HMF solution prior to the column to favour the re-oxidation of the partially reduced MnO_{2-d} to MnO_2 and avoid forming the red-ox inactive species. Unfortunately, no change in the regeneration of the reagent was observed, possibly due to the low solubility of O_2 in TMO.

Calcination of the spent MnO_2 under static air at 300 °C for 1 hour allowed for some recovery in activity and conversion of 30% of HMF to DFF with a fresh HFM in TMO solution. The EDX-SEM analysis of MnO_2 after reaction (Appendix 8) showed a slight reduction in the %O content (Mn:O post-calcination, post-reaction 53.8:44.1 by weight) as well as more crystalline structures after calcination than before (Mn:O pre-calcination, post-reaction 48.1:50.9 by weight). Additionally, porosimetry analysis showed an increase in average pore width of the mesopores, from 8.8 nm to 11.6 nm after calcination (Table 12) which together with the EDX-SEM analysis may account for the regained activity of the 88% MnO_2.

Knoevenagel-Doebner condensation of DFF with malonic acid afforded 3,3'-(2,5-furandiyl)bisacrylic acid (Scheme 11, **89**) in 82% isolated yield with >99% stereoselectivity. Indeed, only the *E-E* isomer of **89** was obtained as confirmed by the high J coupling constant of the alkene protons (δ 7.34 & 6.34 ppm, $J_{c=c}$= 15.8 Hz, experimental section-general synthetic procedures and characterisation, part c). The higher stability of the *E-E* isomer may be due to steric effects, may explain the high stereoselectivity of the Knoevenagel-Doebner reaction.

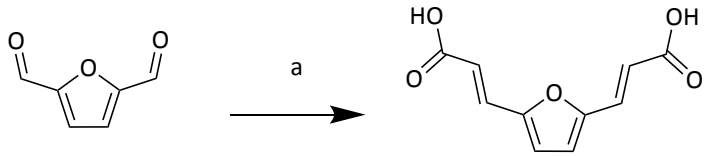

DFF, **88** **89**, 82%

*Scheme 11 Knoevenagel-Doebner reaction of DFF (**88**) with malonic acid. a. DFF (101 mmol), malonic acid (405 mmol), piperidine (20 mmol) and pyridine (150 mL) 85 °C, 16 h then reflux 2 h*

Esterification of this intermediate (Scheme 12) afforded compound **90** in 80% yield giving an overall yield of 51% (over 3 steps). The obtained single-crystal XRD structure (Figure 41**B**) of the esterified product **90** further confirmed the *E-E* configuration, while the ease of crystallisation of **90** as pale brown shiny flakes likely indicated the rigid planar structure this compound sits in.

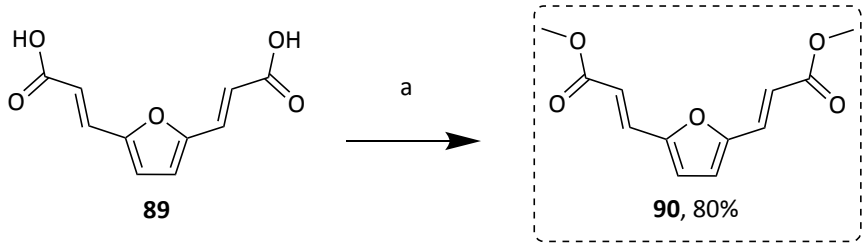

*Scheme 12 Esterification of intermediate **89** with methanol to form **90**. a. **89** (43 mmol), NaCl (19 mmol), H_2SO_4 (13 mmol), MeOH (150 mL) reflux 16 h.*

The intense UV absorbance (Figure 41**A**, ε= 28866 L mol^{-1} cm^{-1}) of **90**, was attributed to the π-π* transition of this compound allowed by the extended π conjugation and symmetry. This strong UV-absorbing property confirmed the possibility to use this monomer as the UV-A active section of a polyester for further UV-curing, assuming the extended conjugation could be preserved from the polycondensation reaction.

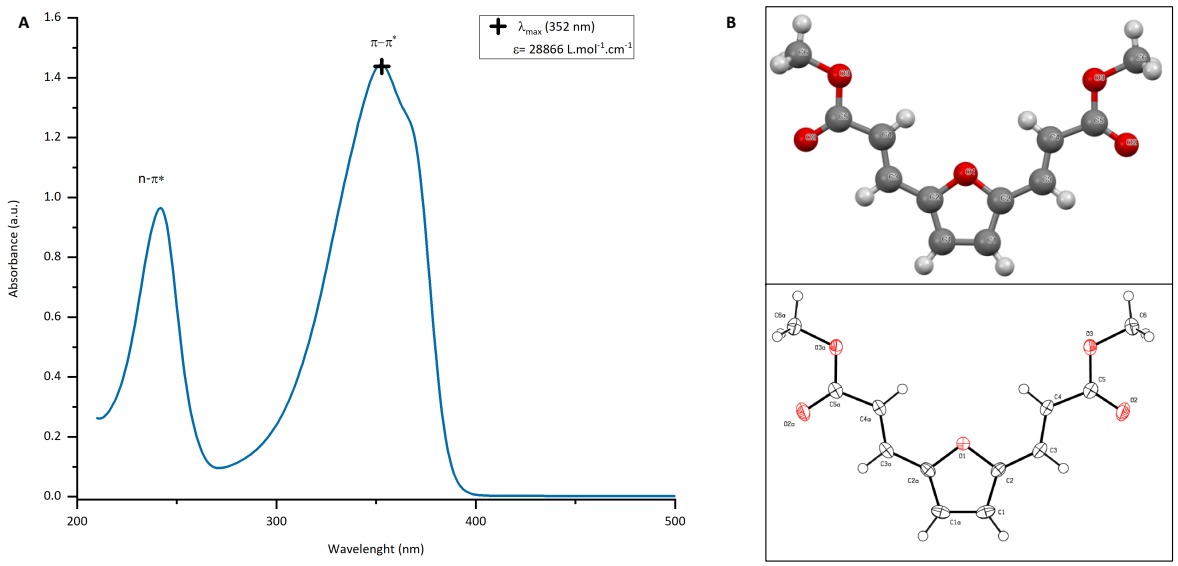

Figure 41 ***A****: UV-vis absorption spectrum (EtOH, 50 µM);* ***B****: Single-crystal XRD results, balls and stick crystal structure representation and 50% probability thermal ellipsoids representation*

3.3.3.2 Polymerisation of renewable UV-A active monomer

In a first instance, **90** was combined with the aliphatic diol 1,8-octanediol (ODO) and the chemo-catalysed (metal salts used: K_2CO_3, Zn(II) acetate, Zr(IV) isopropoxide and Ti(IV) *tert*-butoxide) synthesis of aromatic-aliphatic polyesters was carried out under milder two-stage polycondensation conditions (95 °C under inert atmosphere Ar or N_2 for 24 h with excess (2 eq.) ODO, 5 mol% catalyst, then 4 hours under high vacuum (<1 mbar). Lower temperatures were employed due to the potentially sensitive nature of the acrylic ester units. Unfortunately, with most catalysts, no polymeric product was obtained, only fractions of short oligomers (for the THF-$CHCl_3$ soluble fraction Figure 42 red triangle) residual monomer **90** (specifically Ti(IV), Zr(IV) and Zn(II), Figure 42 green stars) and THF-$CHCl_3$ insoluble cross-linked material.

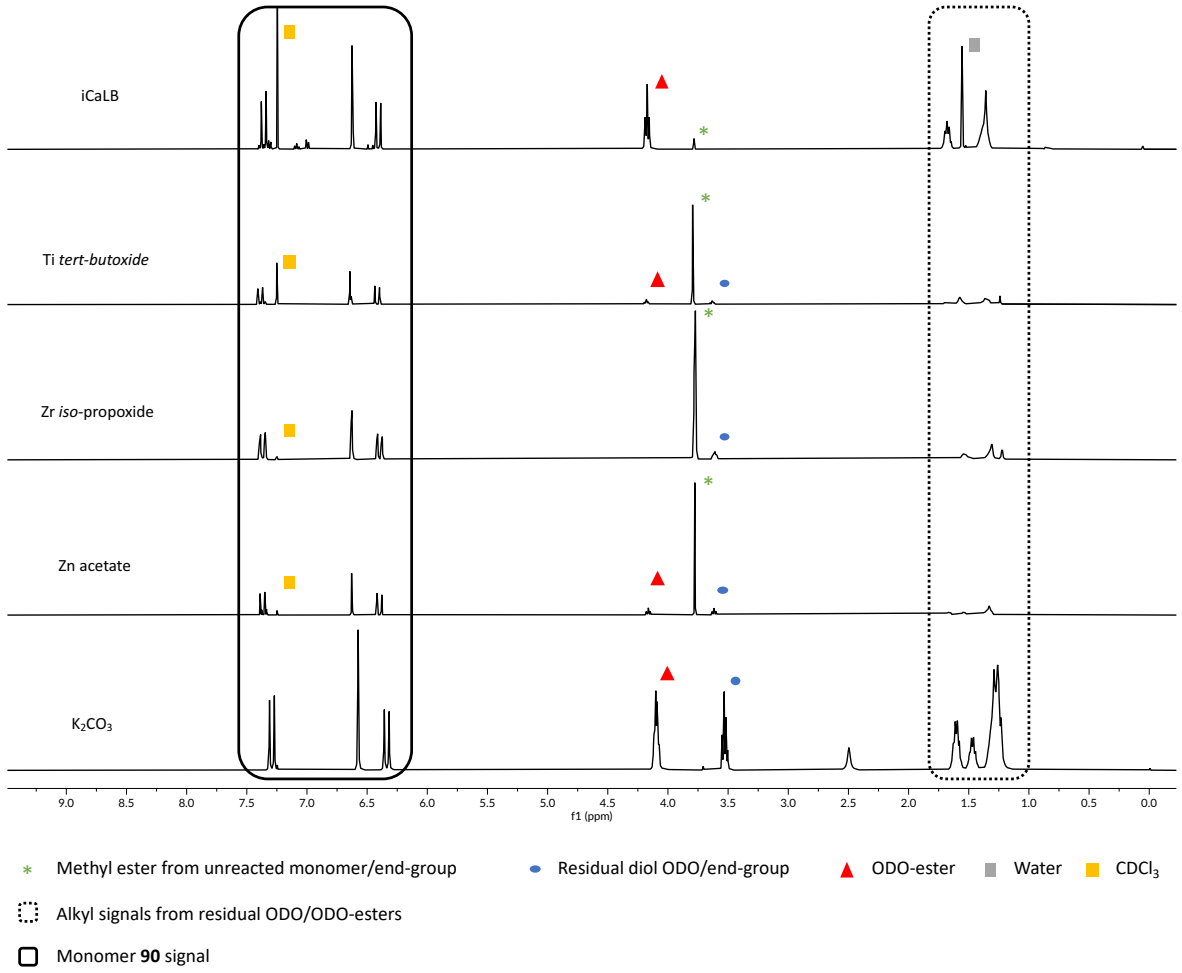

Figure 42 Overlay of ^{1}H-NMR spectra for $CHCl_3$-soluble crude products obtained from chemo-catalysed polycondensations with 1,8-octanediol (ODO)

The absence of methyl ester signals (3.75 ppm) from K_2CO_3-catalysed reaction shows that good conversion was obtained with this catalyst, but only short oligomers with M_n~200 Da could be formed (see GPC results Table 13). This milder catalyst likely avoided branching side reactions which could explain the low M_n. The higher M_n obtained with $Ti(OBu)_4$ might be explained by branching that readily occurred with this catalyst (and Zr isopropoxide and Zn acetate to a lesser extent) increasing M_n in spite of the low conversion observed by ^{1}H-NMR.

Table 13 GPC results for the polymers synthesised using the chemo-catalytic protocols

Catalyst	Formula	M_n [Da]	M_w [Da]	Đ
Potassium carbonate	K_2CO_3	200	400	2.77
Zinc(II) acetate	$Zn(CH_3COO)_2$	100	400	3.42
Zirconium(IV) isopropoxide	$Zr(OCH(CH_3)_2)_4$	>100	100	1.33
Titanium(IV) *tert*-butoxide	$Ti[OC(CH_3)_3]_4$	1200	2400	1.96

Synthesis carried out using Ti(IV) *tert*-butoxide yielded polymers with the highest molecular masses (M_n of 1.2 kDa and M_w of 2.4 kDa) (Table 13). In 2005 Lasseuguette *et al.* reported similar issues while polymerising the furan-based monomer, 2-hydroxymethyl-5-furanacrylic acid ethyl ester (HMFAE, Figure 36, p. 158, **126**), noting that the $Ti(OBu)_4$ catalyst tended to complex with furan rings reducing its catalytic activity.[157] This could explain the low molecular weights obtained in the chemo-catalysed polycondensation despite the mild conditions. The presence of the two exo-furan C=C groups may also increase the ability of **90** to complex with certain metal salts explaining the low catalytic activity of usually very active salts such as $Zn(OAc)_2$ or Zr isopropoxide. In their work, Gandini and co-workers improved the polycondensation reaction co-polymerising HMFAE with ethyl-6-hydroxyhexanoate using K_2CO_3 as the catalyst and temperatures ranging between 95 and 120 °C. In this manner, they obtained polymers of M_n 1.6-2.9 kDa and M_w 3.8-6.8 kDa and yields between 60-85%.[157] In our hands, this K_2CO_3 catalyst only led to short oligomers (M_n ~200 Da, Table 13) despite the good conversion observed by ^{1}H-NMR (Figure 42). Furthermore, a previous study by Krhouf *et al.* on bifuranic polyesters suggested that the presence of labile hydrogens α to the two furan rings lead to radical side reaction, branching and cross-linking.[201–203] The unsaturation (C=C) on both side of

monomer **90** likely reacted in a similar, radical fashion, leading to the insoluble material described above. The higher molecular weight obtained with Ti(IV) might result from its ability to act as a free radical initiator, thus favouring branching and increasing chain length but eventually leading to gelation.[202]

Polycondensation reactions using an enzymatically-catalysed transesterification (made and characterised by Dr. Alessandro Pellis) in organic media perform well at low temperature. Unlike the metal salts used previously, they are also not particularly known to be radical initiators/promoters. Thus, enzymes could potentially reduce the side reactions that were influencing our attempts with chemocatalysts.[204] Based on a recently developed protocol, an immobilised preparation of *Candida antarctica* lipase B (iCaLB) was selected as catalyst and diphenyl ether (DPE) as a solvent.[205–207] The principal advantage of DPE being its high boiling point allowing methanol condensate to be removed from the reaction medium (at polycondensation conditions: 85 °C, 1000 mbar) and thus driving the equilibrium towards longer chain polyesters.

Results from the enzyme-catalysed synthesis were encouraging, with molecular masses ranging from 1.3-3.6 kDa for M_n and 3.3-26 kDa for M_w depending on the used diol. Part of the very high M_w may be attributed to branching that may have started to form prior to the GPC analysis. Nevertheless, isolated yields above 74% were also obtained for all synthesised polymers (Figure 43**A**). As can be observed in Figure 43, the polyesters prepared from ODO as the aliphatic diol were optimum in terms of molecular masses and isolated yields (for the complete series of data on the enzymatic synthesis in DPE see Appendix 9).

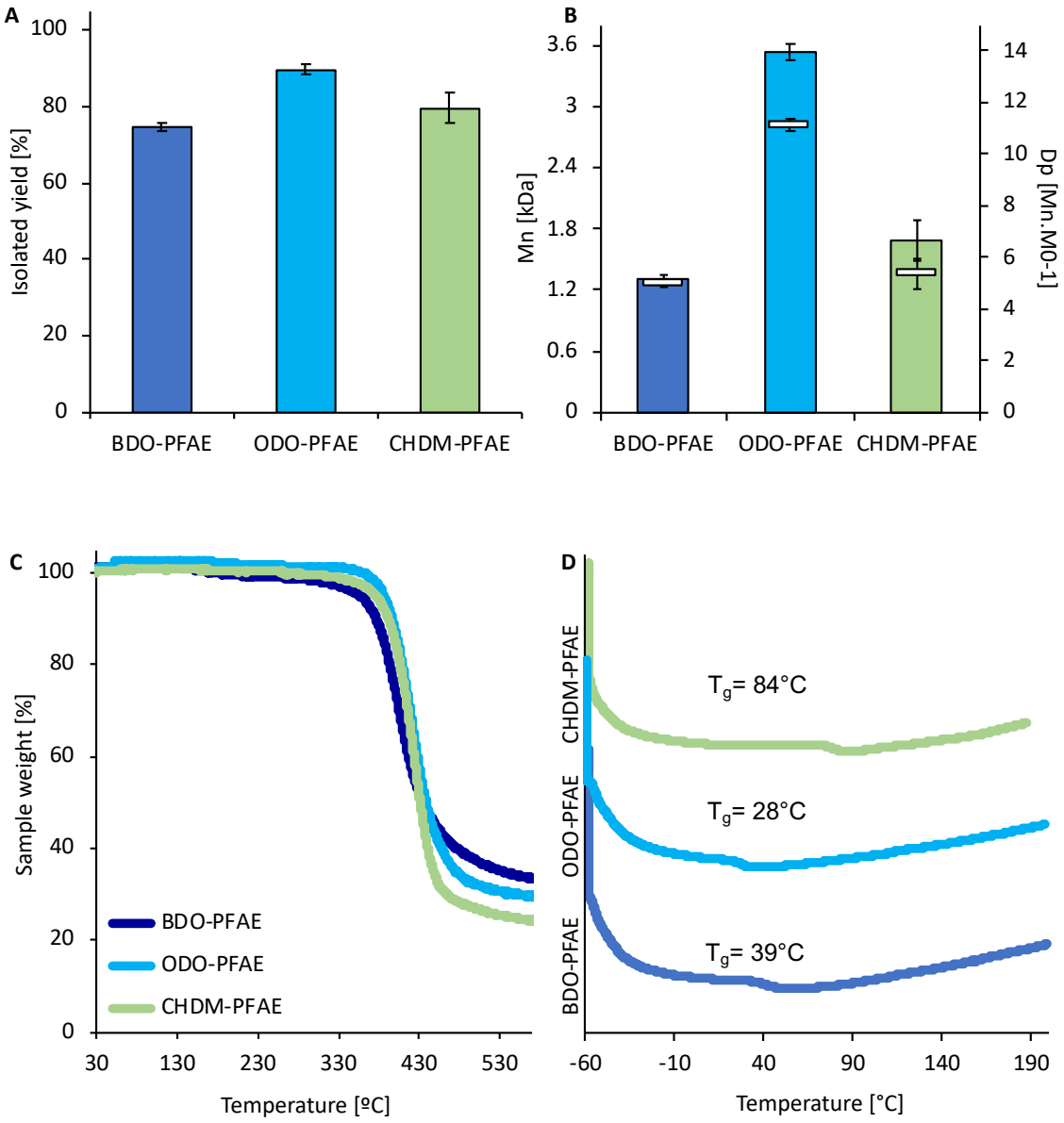

Figure 43 iCaLB-catalysed synthesis of PFAE in DPE as the organic medium at 85 °C and 20 mbar. ***A****: Isolated yield after MeOH precipitation and three washing steps;* ***B****: Number average molecular weight (M_n) calculated via $CHCl_3$ GPC and degree of polymerisation (DP);* ***C****: Thermogravimetric analysis (TGA);* ***D****: Differential scanning calorimetry analysis (DSC). Colours legend: blue= polymers containing 1,4-butanediol (BDO, C4) as the aliphatic, linear diol, red= polymers containing 1,8-octanediol (ODO, C8) as the aliphatic, linear diol and green= polymers containing 1,4-cyclohexanedimethanol (CHDM, C8) as the cyclic, rigid diol. Results obtained by Dr. Alessandro Pellis figure designed by Yann Lie.*

The enzyme employed here belongs to the serine hydrolase superfamily the mechanism of which has previously been investigated.[208] The conjugation of the monomer **90** is

temporarily broken during the formation of a tetrahedral intermediate (Scheme 13, **136**) with a serine residue present in CaLB's active site. The transesterification with the diols then occurs with the attack of the diol on the acyl-enzyme intermediate (Scheme 13, **137**) which formed from **136** after the release of methanol. The elongated product (**139**) is released from the second tetrahedral species formed (Scheme 13, **138**), closing the catalytic cycle by reforming the active site. The relatively low M_n obtained here is possibly due to the need for the highly stable extended conjugation of **90** to be partially broken for the formation of intermediate **136**.[208] The low M_n may also be due to the steric hindrance created by the elongated chains of the polymer. The longer bulky oligomers likely prevent the substrate from entering CaLB's active site (**135**) and thus limit the further growth of the polymer. It is well known that fully aliphatic polyesters can reach far higher molecular weights compared to terephthalate, furan and pyridine-based diesters.[205,209–211]

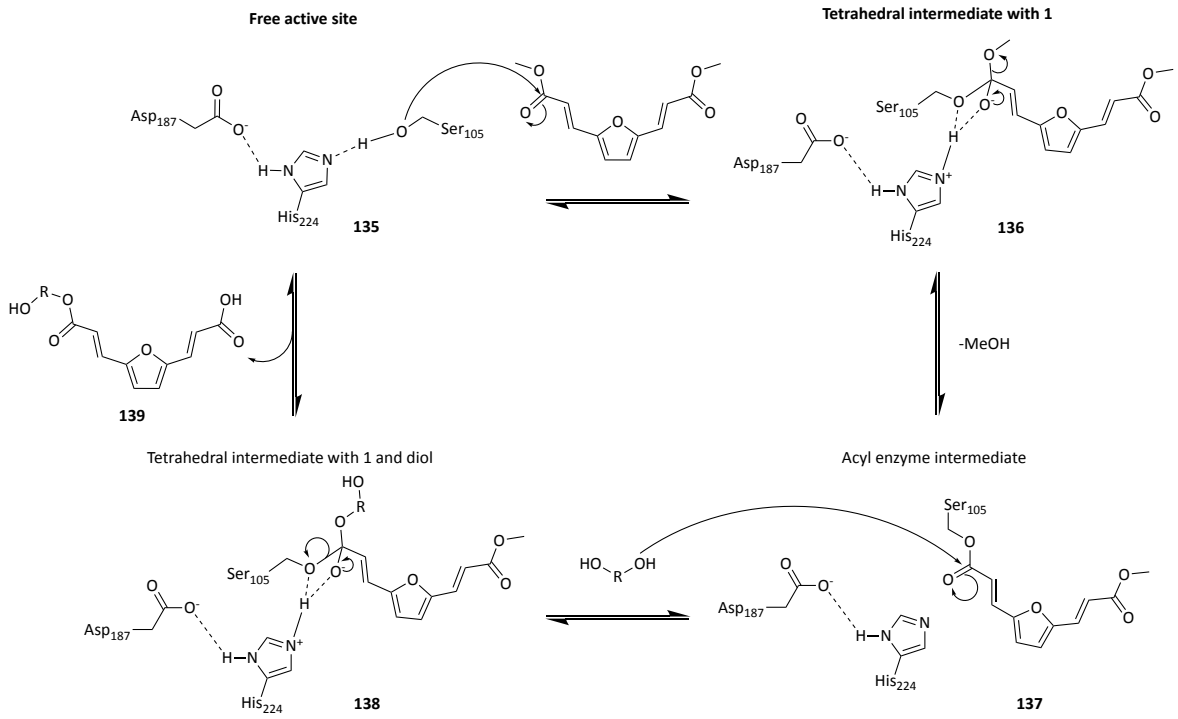

Scheme 13 Mechanism of serine-hydrolase enzymes.

Regarding the thermal analysis data (data collected and analysed by Dr. Alessandro Pellis, Figure 43**C**), all synthesised polymers have a similar T_{d50} between 430 and 438 °C (see Appendix 10 for the complete set of TGA data) indicating good thermal stability. The T_g from the 2nd heating decreases from 39 °C to 28 °C when increasing the aliphatic diol chain length from C4 (1,4-butanediol, BDO, Figure 43**D**, blue line) to C_8 (ODO, Figure 43**D**, red line). The polymers containing the cyclic diol cyclohexanedimethanol (CHDM) have instead a higher T_g of 84 °C (Figure 43**D**, green line, see Appendix 11 for the complete DSC data set). The presence of additional cyclic structure in the repetitive polymer units thus seems to lead to a higher T_g. Due to the more crystalline structure of the polymer, transition to an amorphous state likely requires more energy (therefore higher T_g).

To investigate the thermal behaviour of this newly synthesised class of polyesters, DSC analysis on the ODO-PFAE polymer was repeated for 6 cycles (data collected and analysed by Dr. Alessandro Pellis). Interestingly, a slight increase of the T_g (from 30 °C to 37 °C) and a decrease of the ΔCp (from 0.19 $J.g^{-1}.°C^{-1}$ to 0.13 $J.g^{-1}.°C^{-1}$) were observed (Appendix 11). The observed variation can be due to the shift of the polymer's crystalline/amorphous balance towards a slightly higher crystallinity possibly due to side reaction occurring during the heating/cooling cycles leading to different branched motifs (Diels-Alder addition, radical etc.).

MALDI-TOF analysis (collected and analysed by Dr. Alessandro Pellis) was performed on all samples, confirming the molecular weight distribution observed with the GPC analysis. End group analysis shows the following distribution: major product ester-diol, minor ester-ester, diol-diol and some traces of cyclic polyesters (Table 14 and Appendix 12).[205]

The structures of the polyesters, fully preserving the furan ring, C=C and *E-E* stereochemistry, were confirmed via ^{1}H- and ^{13}C-NMR spectroscopy (experimental section general synthetic procedures and characterisation part c). To ensure the photoactivity of the furan repetitive unit and understand the structural changes of the polymer after irradiation, experimental and computational insights of the photoreaction were gathered.

*Table 14 Summary of MALDI-TOF analysis of the different polyesters obtained by enzymatic catalysis**

		End groups			
Ester	Diol	Ester/diol 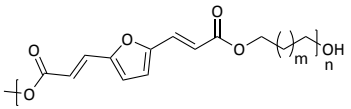	Cyclic 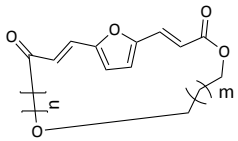	Ester/ester 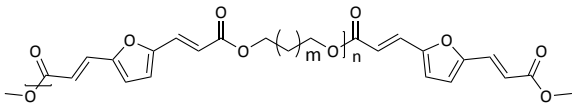	Diol/diol 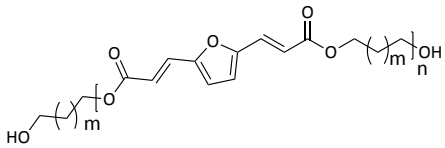
90	BDO	+++	+	+-	+-
	ODO	+++	+	+-	+-
	CHDM	+++	+	+	+

*analysis performed by Dr. Alessandro Pellis. m= 2,6 or C6H10 (cyclic), +: higher peak intensity according to MALDI-TOF analysis -: minor product based on peak intensity

3.3.3.3 Experimental and computational study of the monomer photoreactivity

The photoactive properties of monomer **90** were studied before polycondensation to ascertain that this compound does indeed undergo [2+2] photoinduced cycloaddition and thus is suitable for preparation of Type II photopolymers. Purified compound **90** was subjected to UV-irradiation using a custom-made LED torch (365 nm, 1250 mW flux output, see experimental section-additional equipment, and general synthetic procedures and characterisation, part c.). The reaction was followed by FT-IR spectroscopy (Figure 44**A**), showing the disappearance of the exo-furan C=C signal at 1630 cm^{-1} and C=O shift from 1700 cm^{-1} to 1730 cm^{-1} indicating loss of the conjugation. Also, the presence of an isosbestic point at 1640 cm^{-1} suggests that the photoreaction of monomer **90** follows a single reaction path.[155,212] The conversion of **90** to its photoproducts (Figure 44**B**), seems to follow an exponential trend with a horizontal asymptote at roughly 50% conversion. Limitations due to the experimental set up (*e.g.* LED maximum emission far from maximum absorbance, low power, thickness of monomer layer etc.) and the nature of the irradiated material (crystalline phase) likely limited the complete conversion of monomer **90** crystals to cycloadducts.

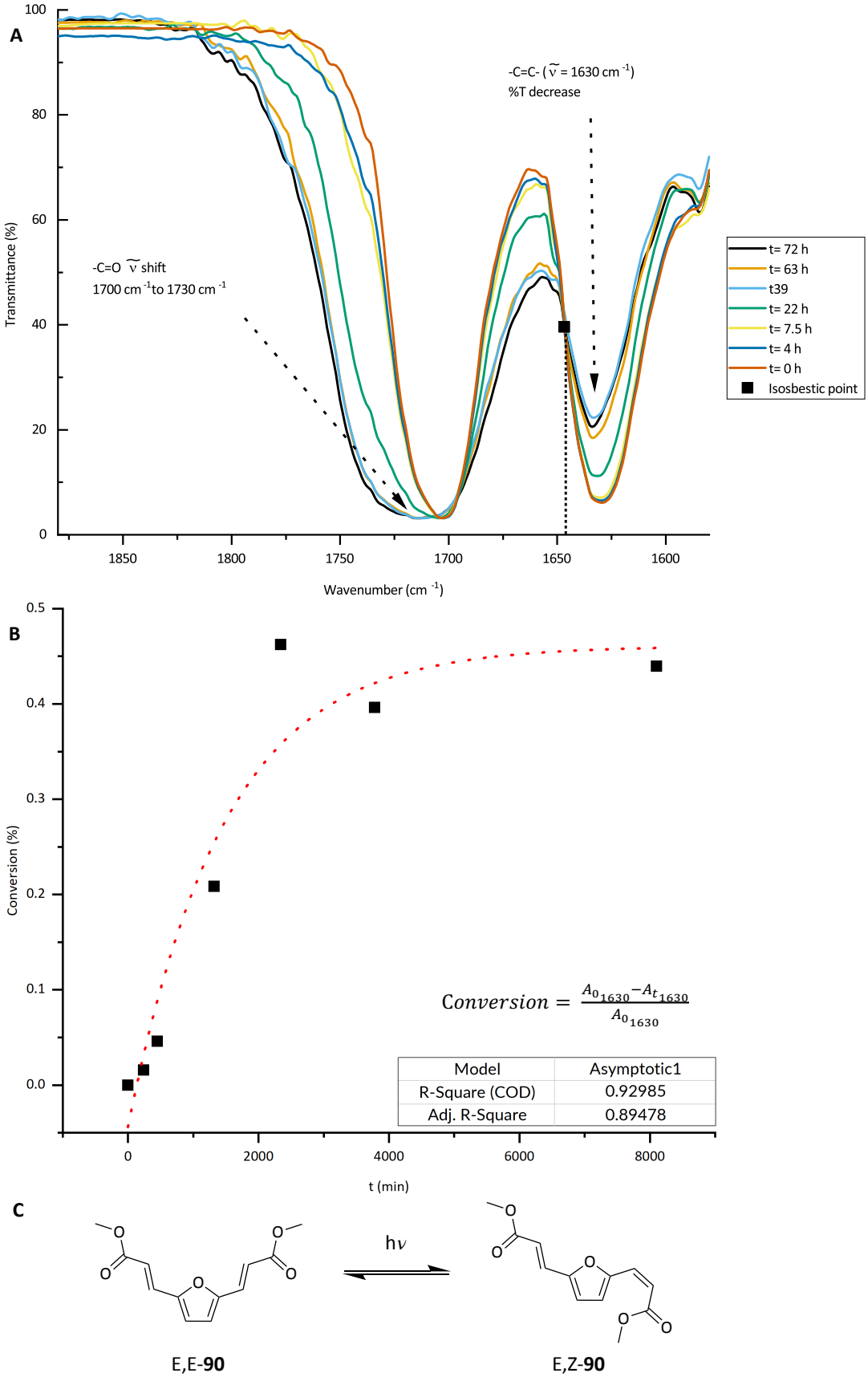

Figure 44 ***A****: FT-IR spectroscopy of UV-active monomer* ***90*** *after different irradiation times between 1580 and 1880 cm^{-1}. Isosbestic point is observable at 1640 cm^{-1};* ***B****: Conversion calculated according to reference [155], at 1630 cm^{-1}. Data were fitted with OriginLab (version 2019) using an exponential model (asymptot1);* ***C****: Proposed E-E to E-Z conversion of* ***90*** *upon irradiation*

Analysis of the ^{1}H-NMR spectra of the material obtained after 24 h of UV irradiation, confirmed the presence of monomer **90** and its single [2+2] cyclo-adduct **132** (Figure 45, head to tail regiochemistry was assumed based on cinnamic esters topochemical dimerisation). However, the presence of the double cycloadduct **133** was not observed. As the UV reaction was conducted in the solid-state, the formation of a single cycloadduct is likely preferred due to the unsaturated side chains orientation in the crystals. Furthermore, after very long exposure to light (>72 hours), the resulting material was no longer completely soluble in $CDCl_3$. The presence of a complicated mixture of oligomers arising from the light-induced self-polymerisation of **90** was still observable by ^{1}H-NMR spectroscopy. This result suggests that a reaction of **132** with another molecule of **90** occurred, and further growth of oligomers in this manner is more likely.

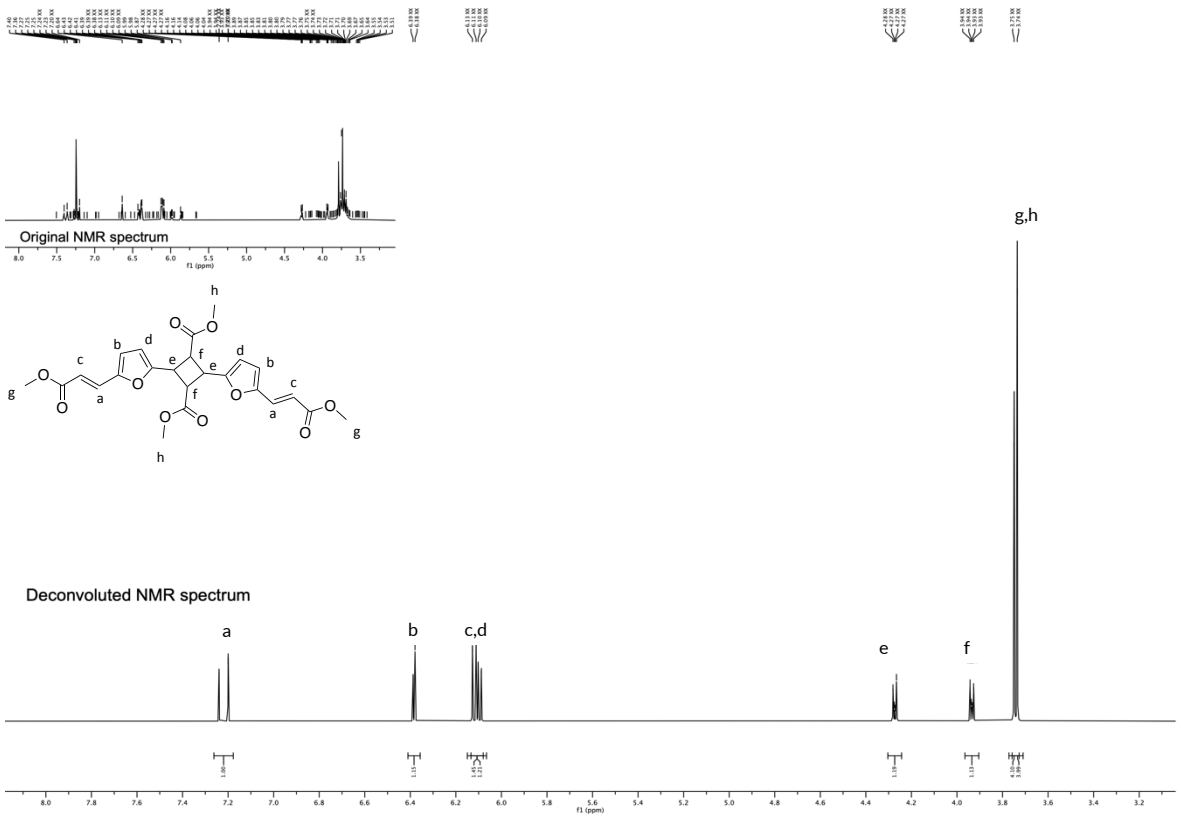

*Figure 45 Deconvoluted [1]H-NMR spectrum for the isolation of cycloadduct **132 (**represented as the head to tail isomer) signals after 24 h of irradiation of **90***

The reverse of the cycloaddition, also known as "crack-healing" for polymers derived from cinnamic acid, proved unsuccessful in our polymer.[213,214] Indeed, attempts to irradiate the cross-linked polymer or **90** with a custom-made UV-lamp (5 W, max emission 253 nm) only led to further cross-linking (followed by FT-IR). The excitation of product **132** was explored by TD-DFT calculation (realised by Dr. Ignacio Funes), and the transition was found to be located in the double bond of **132**. This result implies that the cyclobutane moiety is not in the chromophore, which likely explains the difficulty of reversing the [2+2] cycloaddition photochemically. Further studies are underway to assess the reversibility of the cycloaddition, employing lower UV-range that tried here, with the ambition of also preparing a hybrid **Type II**-**Type V** photopolymer.

3.3.3.4 UV-induced curing of ODO-PFAE and impacts on mechanical behaviour

UV-induced curing of the previously synthesised polymer (ODO-PFAE, **91**) was conducted in the same fashion as monomer **90** (see experimental section general synthetic procedures part c). An almost complete reduction of the alkene signals (Figure 46) confirmed the success of the curing procedure, making this a **Type II** photopolymer.

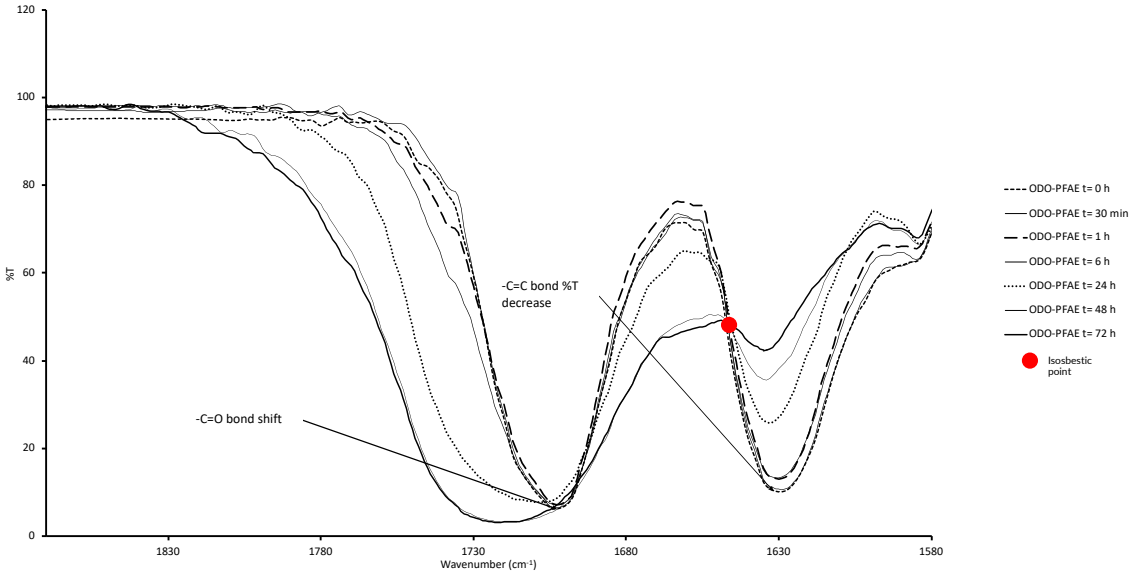

*Figure 46 Overlay of FT-IR spectra of UV-irradiated ODO-PFAE polymer (**91**) after different times*

The thus obtained cured material was neither soluble in THF nor chloroform, suggesting that the desired cross-linking had occurred. ^{13}C solid-state NMR spectroscopy experiments were conducted (Figure 47) to confirm the success of the procedure further, as it was previously suggested to be a method of choice to follow this type of reaction.[181,215] The reduction of the alkene signal (~130 ppm) and appearance of a broad signal corresponding to cyclobutane (40-50 ppm) again confirmed the photoreaction.

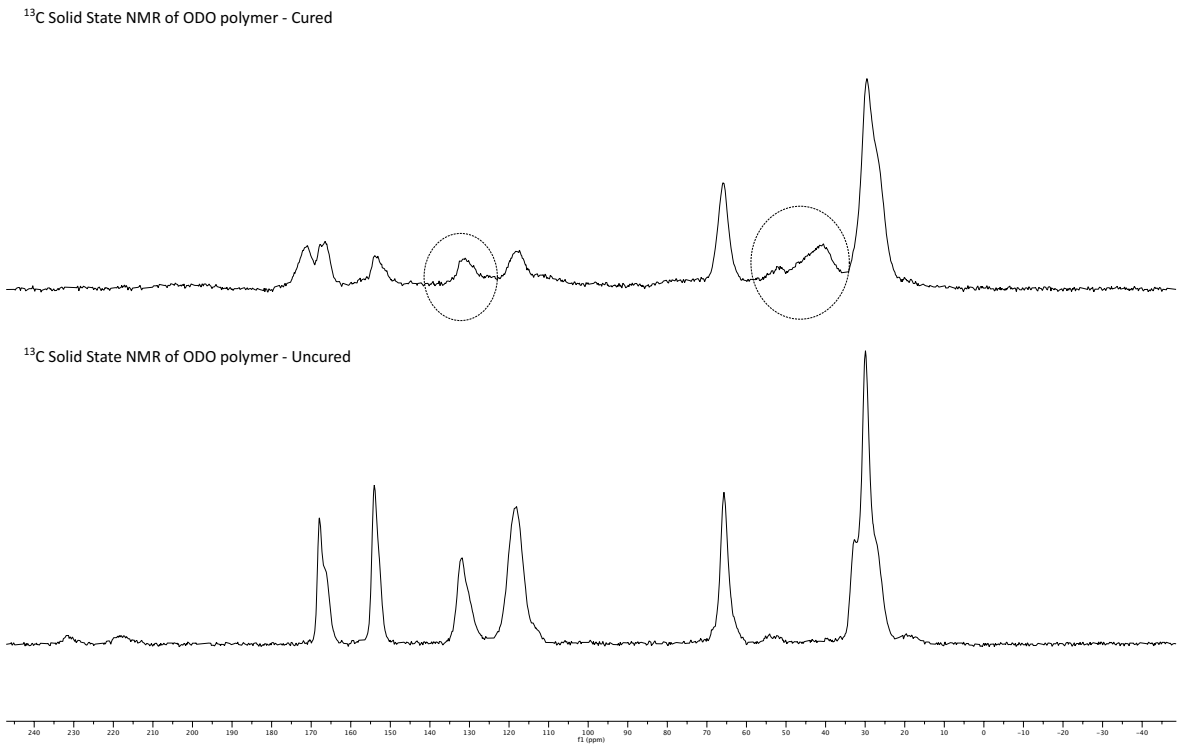

*Figure 47 Solid-state ^{13}C-NMR spectra of the cured (top) and uncured (bottom) ODO-PFAE polymer (**91**).*

A film was solvent cast from $CHCl_3$ (this solvent was selected for ease of removal) to test the mechanical properties of **91**. Before curing, the film's stress-strain curve was measured (Figure 48, left). The un-cured **91** film displayed a flexible, elastic behaviour, as demonstrated by the steady increase in extension and tensile stress resulting in a high extension at break, 46.96 mm ± 1.59 mm and a small modulus 1.42 MPa ± 0.11 MPa. After the test, the strip had an elastic tendency, reforming its original shape.

After curing, noticeable "tanning" of the strips was observed (Figure 48, white dotted square) and stiffness of the material significantly increased. The modulus of the cured polymer increased dramatically to 160.76 MPa ±14.98 MPa whereas its extension at break dropped to 2.68 mm ± 0.1 mm. Comparatively, a furan-based copolymer obtained with acrylated 7,10-dihydroxy-8(E)-octadecenoic acid (DOD) possessed a tensile strength

of up to 19 MPa after UV-curing.[216] Post-test, the herein obtained cured polymer was brittle with no elastic behaviour as observed before.

The cured polymer displayed a strain-hardening behaviour as indicated by the plateau observed on the stress-strain curve (Figure 48 bottom right) around 8.5 MPa followed by a steep increase in tensile stress. This type of strain-hardening behaviour is commonly observed in plastic-like materials such as poly(propylene) or poly(ethylene). It is usually explained on a molecular level by a reorientation of the polymer fibres in the stress direction.

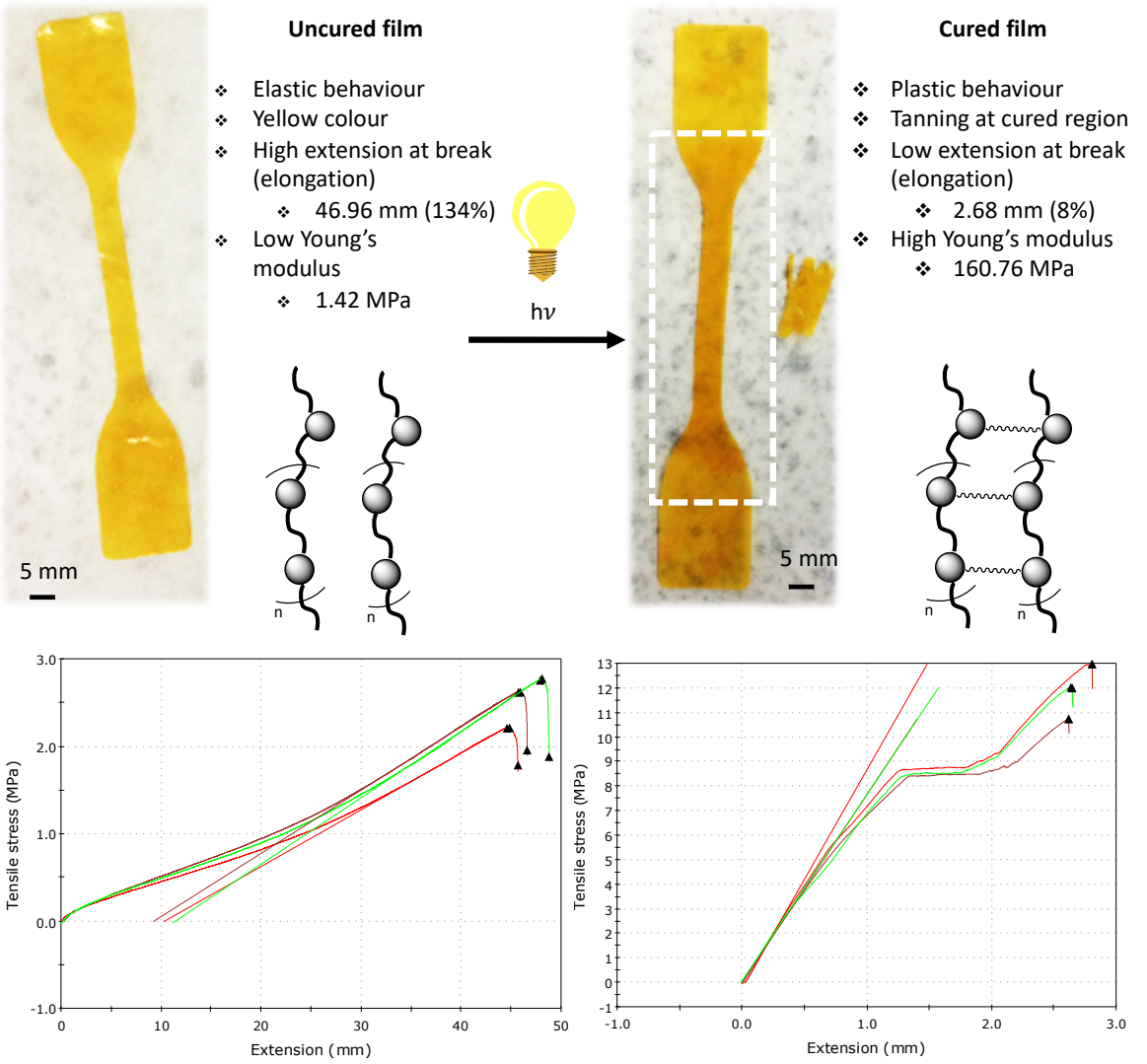

Figure 48 Stress-strain curve of uncured film (left) and UV-cured film (right). Dotted square shows the region where tanning of the polymer occurred. Pictures of the film (with enhanced contrast) shaped for analysis are displayed below the stress-strain curves.

The UV-curing thus had a significant impact on the material properties. The higher stiffness and insolubility resulting from cross-linking between the polymer chains can lead to its use as a negative photoresist or in 3D printing technologies. For instance, the stereolithography of this material may be conducted in the melt (80 °C) using its photoreactivity to harden each layer being printing with the help of a laser.

Alternatively, the highly insoluble character of this polymer following UV-curing may be useful in lithography. Once the surface to be etched is coated with this

photopolymer, a UV-protecting mask may be applied on surfaces to solubilise later. The UV exposed sections are stabilised via cross-linking, and then solvent washing removes un-crosslinked polymer from the UV-protected areas. Microelectronics, for instance, depend heavily on this process for the design of transistors.

3.3.4 Conclusion for chapter III.3

The search for renewable drop-in replacements or alternatives for fossil-derived commodities is actively ongoing. Efforts have been made to find sustainable solutions for the plastics produced on multi-tonnes scales from fossil resources. For similar environmental reasons, finding renewable alternatives to more specialised polymers is also of importance. Indeed, progress in (micro)electronics since the 20th century was partly due to the development of novel photopolymers used as photoresists. The 21st century saw a regained interest for photopolymers due to their potential use in 3D printing applications. Developing photopolymer potentially made from renewable resources under greener conditions is thus more relevant than ever.

The four main targets exposed at the beginning of this chapter to synthesise a renewable photopolymer were successfully achieved.

1. The potentially UV-active compound **90** synthesised initially as a bio-derived UV-filter for sunscreen application was herein employed as a photoactive monomer in a polycondensation reaction. DFF was obtained via semi-continuous MnO_2 oxidation of HMF allowing the multi-gram synthesis of **90** .[117]

2. The polycondensation using enzymatic catalysis proved similar and in some cases superior to the metal salts-catalysed esterification. The preservation of the monomer photoactivity and stereochemistry was possible using this mild catalyst whilst avoiding the use of critical-element containing catalyst (Ti, Zr).[29]
3. Photoreactivity of the repetitive units studied experimentally and by TD-DFT calculations, was confirmed and showed the production of [2+2] cycloadduct as previously described.
4. Finally, the photopolymer obtained by enzymatic catalysis could be solvent cast into a film and cross-linked without the need for a photoinitiator. The cross-linked polymer displayed a greater stiffness and work-hardening behaviour usually reported for plastic-like polymer (PE, PP), making it a **Type II** photopolymer according to Crivello and Reichmanis classification.

The *BioLogicTool* analysis of this compound was studied and compared in chapter II to other photopolymers. Despite the slightly higher scores obtained (-2.30 and 2.18 for the *BioLogicTool score* and *Total length* respectively), these photopolymer scores were in the range of other bio-derived alternatives (itaconic acid, bio-methacrylate). The negative sign also showed that heteroatoms were overall removed from the starting material. Furthermore, this route was a clear improvement on the potential bio-ethene path, as demonstrated by the rationality score difference (-4.72 and 2.92 for the *BioLogicTool score* and *Total length,* respectively).

The physical properties of such photopolymer are likely to be tuneable by a judicious choice of diols or copolymers, showing the versatility of the approach used here. This tuneability

will be of interest for developing renewable photoinduced lithographic, 2/3D printing, coating or adhesive technologies.

So far, only the carbohydrate fraction of microalgae was valorised into value-added chemicals. A surfactant based on both carbohydrate and lipidic portions of microalgae will be presented together with other bio-derived amphiphilic molecules in the following section. Using these additional biocomponents is a necessary step to approach the concept of multi-component microalgal biorefinery discussed previously.

Chapter III.4
Synthesis of bio-derived anionic surfactants for detergent application[§]

[§] This work was done in collaboration with Unilever Ltd. Yann Lie performed the chemical synthesis, characterisation of compounds, reprocessed the surface tension measurements and repeated the computational modelling. Yann Lie and Dr. Thomas J. Farmer designed the chemical routes and help in the selection of the surfactant families. Dr. Craig Fairgrieve (Unilever) performed the surfactant performance testing (Krafft temperature, surface tension measurement, mildness and dynamic interfacial tension), initial computational modelling and helped in the selection of the surfactant families. Dr. David Grainger, Dr. Jane Whittaker, Dr. Sarah Hosking (Unilever) and Dr. Thomas J. Farmer supervised the work. Intermediates in this chapter are numbered with roman lower case numerals.

3.4.1 Introduction: presentation of surfactants, properties and current trends in bio-derived sulfonated surfactants

3.4.1.1 Definition and categories of surfactants

Surface active agents, more commonly named surfactants, are so-called due to their ability to accumulate at the surface of solutions and reduce the surface tension of the medium in which they are. Krister Holmberg defines the surface tension (γ) in 2019 as: *"the surface free energy of a liquid"* or as *"the work required to increase a surface area divided by that area"* by the IUPAC.[217,218] The region between two immiscible liquid phases is called the interface.[218,219]

Surfactants are usually amphiphilic molecules. Their backbone contains at least two different groups, one with a higher affinity for polar environments (*e.g.* water, the hydrophilic group) and one with a higher affinity for apolar environments (*e.g.* hydrocarbons, ethers, the hydrophobic groups). In aqueous solutions, hydrophobic groups of the solvated surfactant, have reduced cohesive interactions with the water molecules due to the absence of hydrogen bonding or ionic groups, electrostatic interaction etc. The water molecules surrounding hydrophobic groups are thus highly ordered to reduce the exposure of the hydrophobic tail to the aqueous solution and maximise hydrogen bonding between the water molecules (Figure 49). This increased ordering reduces the entropy and increases the free energy of the system, rendering the solvation of surfactants unfavourable.

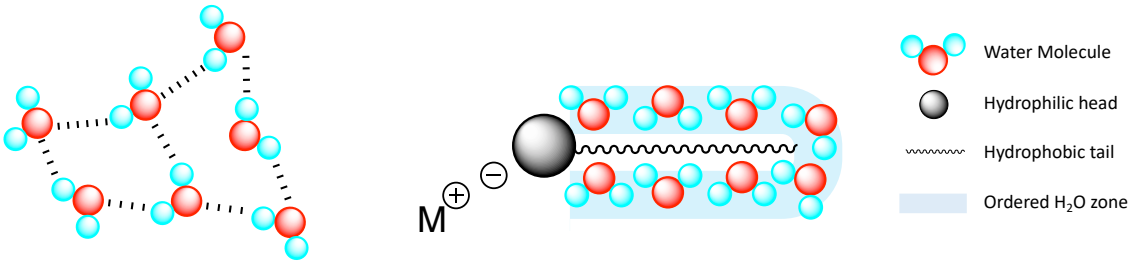

Absence of surfactant
Disordered water
High H-bonding interaction

Presence of surfactant
Highly ordered water around hydrophobic tail

Figure 49 Schematic impact of a surfactant in water with the presence of a "water cage" around the surfactant (right) or absence of surfactant (left)

Hydrophobic groups tend to be expelled out of the solution and aggregate at the surface or form aggregates to reduce the surface exposed to water molecules; this is often called the *hydrophobic effect* (Figure 50, right).[220] This effect was also explained by Kronberg *et al.,* by the positive free energy change required to form a cavity in water to accommodate large hydrophobic chains of surfactants.[220] The accumulation of surfactant at the surface disrupts the cohesive forces between the water molecule, leading to a reduction in the surface tension.[219,221,222]

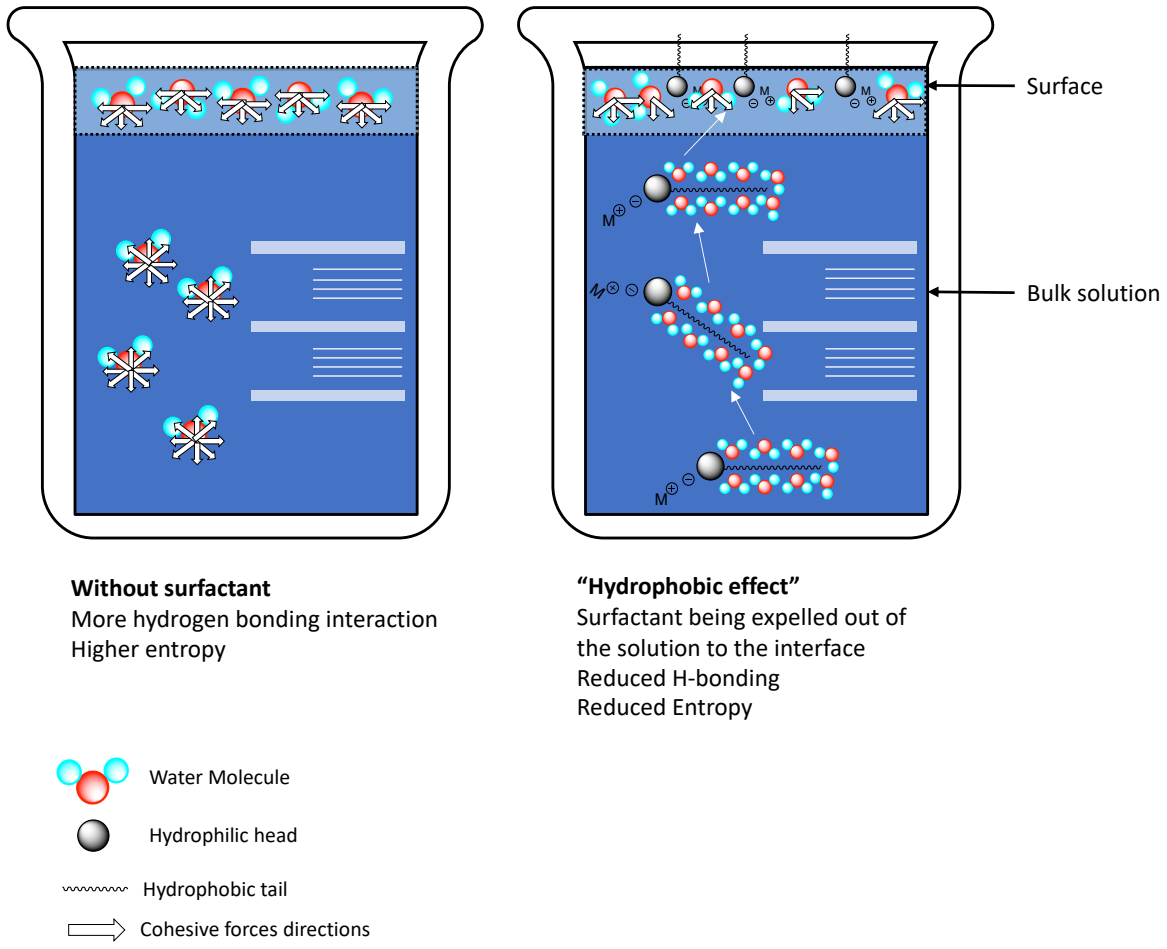

Figure 50 Schematic representation of the hydrophobic effect. In dilute aqueous solutions, surfactant adsorb at the water surface, reducing the surface tension of the solution. Water molecules do not have elements reducing their freedom. Adapted from ref. [222] *and https://bit.ly/2RwwUtl (accessed 29/07/20)*

At a *specific concentration,* the surface cannot host any more surfactant molecules, so any surfactants remaining dispersed in the main volume of the solution non-covalently aggregate to form bigger structures called micelles (Figure 51). This micellisation process is mostly driven by entropy. While surfactants form an ordered structure by positioning their hydrophobic chains close to one another inside the micelle, their hydrophilic moieties interact with the water molecules outside the structure. In this manner, the entropy input of this ordering is lower than the entropy output caused by the release of the water molecules from their conformation of around the hydrophobic groups of the surfactant

molecules in solution. This *specific concentration* is called the *critical micelle concentration* (CMC). It is commonly used, amongst other parameters (such as Krafft temperature, mildness, dynamic interfacial tension, etc.), to assess the suitability of a surfactant for formulations.[218,219,221] The CMC depends on the hydrophilicity to hydrophobicity ratio of the surfactant molecules, called the hydrophilic-lipophilic balance (HLB).[219,221] Typically, for the same hydrophilic group, the longer the fatty chain, the lower the CMC. As micelles can break and take up oily particles within them, it is of interest to have low CMC to have an active surfactant solution with high detergency ability at low concentration. Other types of macromolecular structures (such as lamellar structures, gels etc.) can form at increasing concentration but are out of the scope of the work presented here and will not be further discussed.[221]

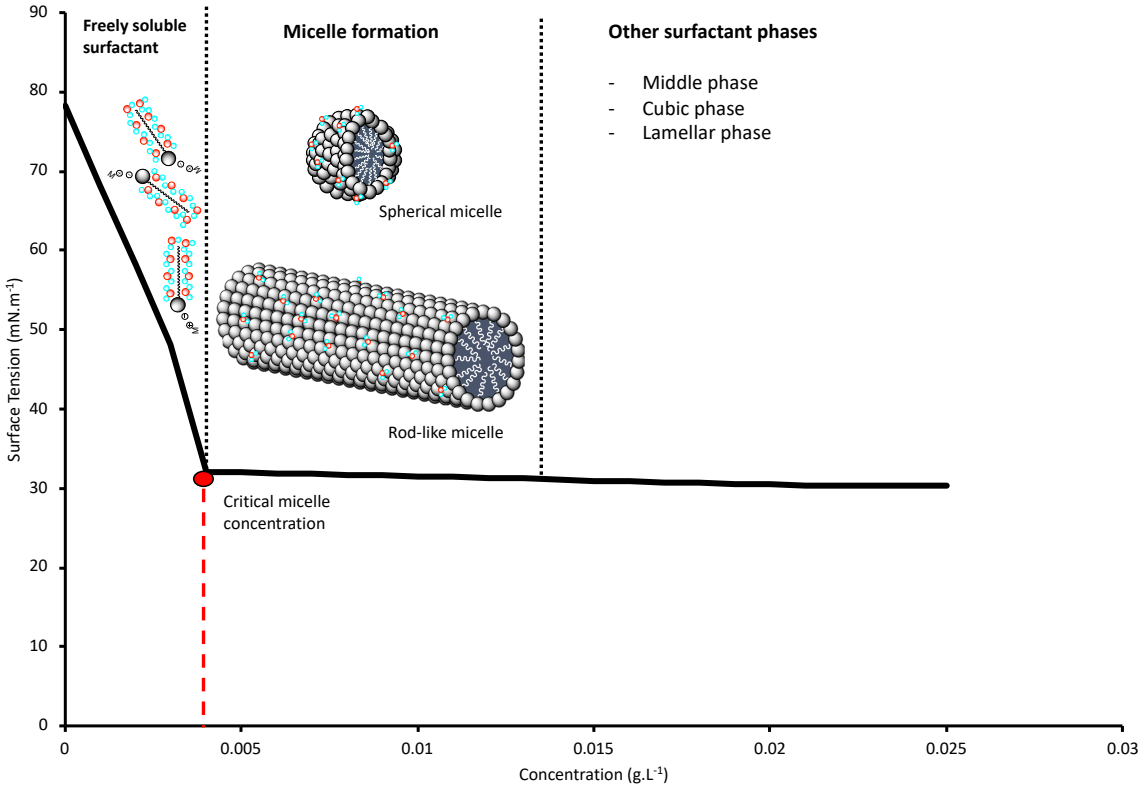

Figure 51 Schematic surface tension against concentration curve with diagrams of the different surfactant states after and before micelle formation. CMC is shown as the red dot. Adapted from [221]

The vast majority of hydrophobic surfactant groups in use today are linear hydrocarbon chains or aromatic groups. For this reason, surfactants are categorised according to the nature of their hydrophilic groups. Four categories are distinguished based on the heads and tails scheme used to described them (Table 15).

Table 15 Four types of surfactant categorised according to their hydrophilic head groups

Surfactant Types	Head-tail diagram	Hydrophilic Group	Commercial surfactants
Anionic	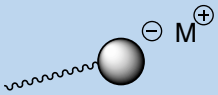	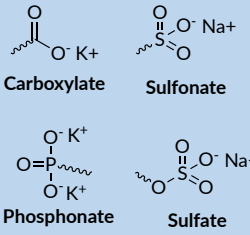 Carboxylate; Sulfonate; Phosphonate; Sulfate	Sodium dodecyl sulfate (SDS), linear alkylbenzene sulfonates (LAS) etc.
Cationic	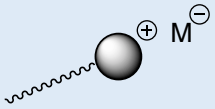	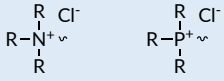 Ammonium; Phosphonium	Triethanolamine quat (TEAQ), Distearyldimethylam monium chloride (DSDMAC) etc.
Non-ionic	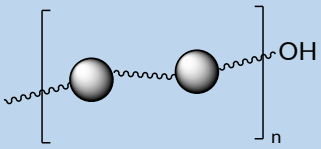	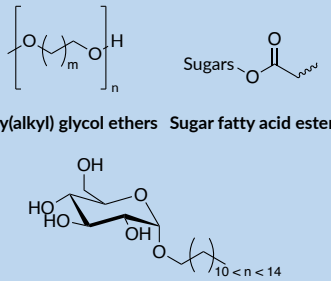 Poly(alkyl) glycol ethers; Sugar fatty acid ester; Alkyl glucosides	Alkyl/alkylphenyl poly(ethylene) glycol, ethers, alkyl glycosides, sugar fatty acid ester etc.
Amphoteric	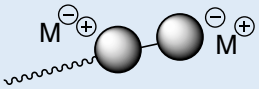	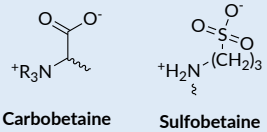 Carbobetaine; Sulfobetaine	Cocoamidopropyl betaine

Anionic surfactants form the largest group of amphiphilic molecules (70% by production volume) used mostly in detergent applications, usually present in formulations between 5-15%wt.[218,219,221] An anionic group, typically $-COO^-$, $-SO_3^-$, $-OSO_3^-$ with small inorganic counterions (e.g. Na^+, K^+, Ca^{2+} and NH_4^+) constitute the hydrophilic moiety of the surfactant.

Cationic surfactants are widely used as bactericides, fabric softeners or hair conditioners. The covalently bound positively charged hydrophilic heads are attracted by the negatively charged fibres, causing the hydrophobic tails to align with the coated material giving a silky soft sensation. Quaternary ammonium salts are traditionally used (-$NR_3^+Cl^-$) in formulations. In cleaning and coating formulation they are typically added between 2.5 up to 10%wt.[223] As a side note, cationic surfactants tend to form insoluble salts with anionic surfactants. As such, this limits their combined use in formulations, but the titration of sulfated/sulfonated surfactants makes use of this reaction.

Non-ionic surfactants are amphiphilic compounds that do not dissociate as ions once in solution. They are typically made of polyalkyl glycol ether chains (m=1-3) or alkyl glycosides with a wide range of application from cosmetics (emulsifier) to pharmaceuticals (drug-encapsulation).

Finally, amphoteric surfactants are the least commonly found. They carry both positively (usually quaternary ammonium groups) and negatively charged (carboxylate, sulfonate) hydrophilic ionic groups covalently bound to the same carbon backbone, making them zwitterionic molecules. Carbo- and sulfo-betaines are the most commonly found groups in amphoteric surfactants.

Surfactants are used in a vast number of water-based formulations for personal and home care applications. They are found in laundry detergent (between 2-28% anionic, 3-4% non-ionic and 2-8% cationic surfactants), shower gel (between 5-30% anionic, 2-3% cationic surfactants, ~10% betaines), shampoos and many more such as liquid hand wash and dishwasher products, surface cleaning detergents, mouth wash, toothpaste etc.[224]

This omnipresence of surfactants in industrial and domestic applications is reflected by their global production which is around 15 Mt.year^{-1}, with salts of fatty acids (soaps) being the most produced surfactants of all, at ~8 Mt.year^{-1}.[219] Sulfated and sulfonated surfactants are produced at a comparable scale and represent an essential class of anionic surfactants.

3.4.1.2 Current synthesis of fossil and bio-based sulfated/sulfonated surfactants

- *Industrial and laboratory-scale sulfation and sulfonation methods*

Industrially, sulfonation is realised using either H_2SO_4, oleum or pure sulfur trioxide, the latter being the preferred method (Scheme 14**A**). SO_3 is a highly potent electrophile and strong oxidant that will form an -SO_3H adduct with almost any organic molecules bearing electron donor groups in an exothermic reaction (around 380 kJ.kg^{-1} SO_3 with linear alkylbenzenes).[225] At large scale, a thin film reactor is used to carry this reaction in which a thin film of reagent, typically linear alkylbenzene, comes in contact with SO_3 carried by a dry inert gas (or air) and falls down the reactor where the product is obtained.[225,226] This method avoids increasing the viscosity of the reaction medium, preventing efficient heat dissipation (which usually occurs in batch processes) as the reaction products are being continuously extracted. Moreover, SO_3 based sulfonation has the advantages of avoiding highly corrosive oleum or H_2SO_4, allowing different feedstocks (linear hydrocarbons, primary alcohols etc.) to be employed and being readily available on a large industrial scale.[226]

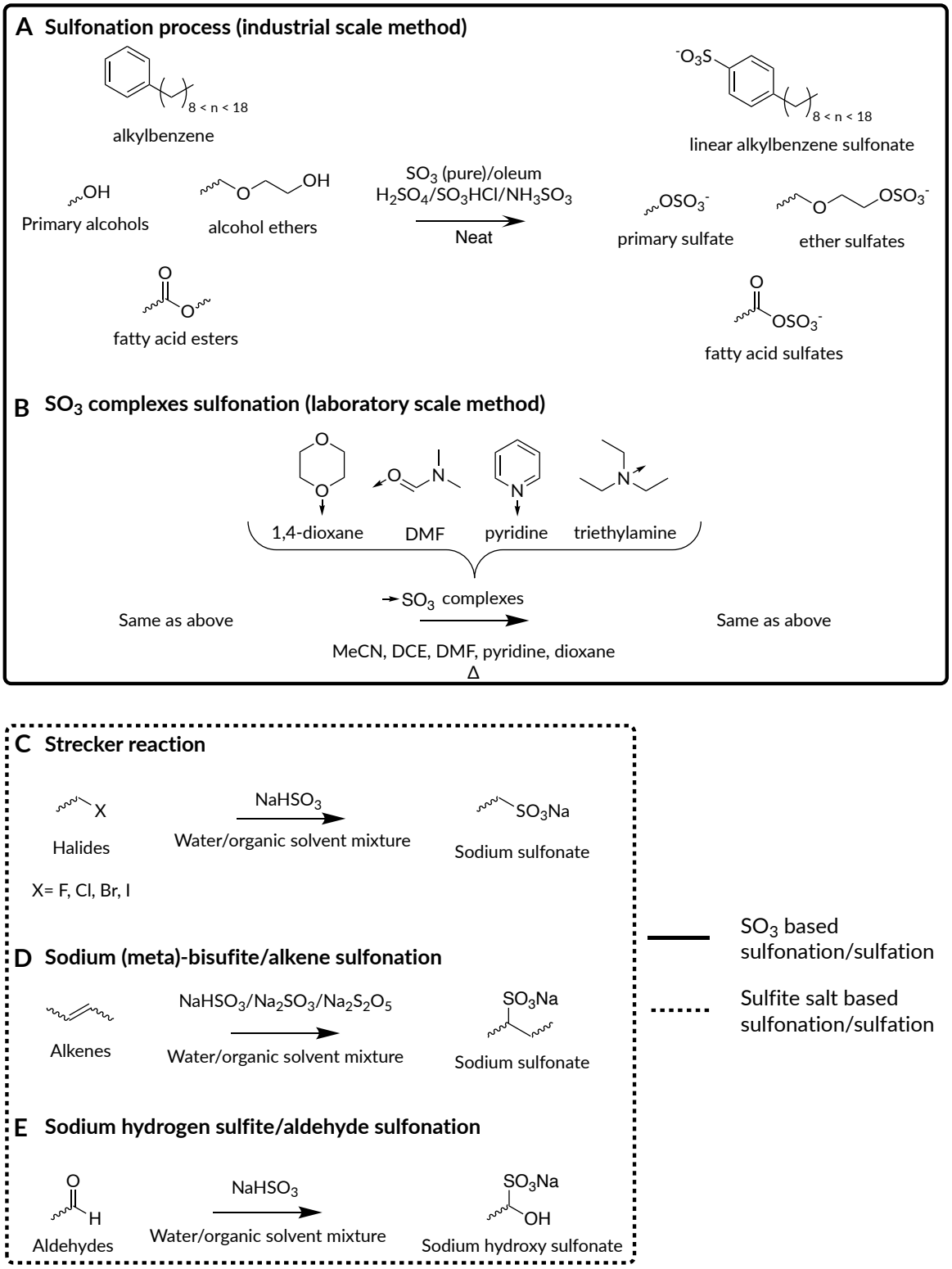

Scheme 14 Different sulfonation reactions with sulfur trioxide or sulfite salts reagents.

Solutions to decrease the high reactivity of SO_3 were developed, allowing higher selectivity and functional group tolerance (Scheme 14**B-E**). These methods/reagents are also more

adapted to classical laboratory techniques as they often do not require specialist equipment (thin-film reactors) to control the reaction conditions. Procedures which rely on cyclic sulfone/sultone-ring opening groups are not presented but represent another potential route to sulfonate/sulfate group.[227]

Sulfamic acid, NH_3SO_3, is an inorganic acid milder (pK_a= ~1) than H_2SO_4 (pK_a= -3 & 2) which may be used for the sulfation of alcohols whilst avoiding sulfonation of aromatic rings.[228–230] Although more susceptible to hydrolysis, sulfate groups are common hydrophilic moieties found in surfactant (*e.g.* sodium dodecyl sulfate, alkylphenol ethoxylate ammonium sulfate).

Reactions using SO_3 complexes, such as SO_3•pyridine, SO_3•triethylamine and SO_3•1,4-dioxane, have found wide application at laboratory scale (Scheme 14**B**).[227,231–233] These complexes present the advantages of being milder than pure SO_3 and offer a wide range of reactivity depending on the complexing group (in order of reactivity: SO_3•1,4-dioxane < SO_3•DMF < SO_3•pyridine < SO_3•triethylamine). However, the basic nature of the complexants commonly forms counter ions with the sulfated/sulfonated molecules (*e.g.* Et_3NH^+, pyridinium sulfates/sulfonates etc.) usually unwanted in the final product. An additional ion-exchange step is thus often required when employing SO_3 complexes. Pyridine•SO_3 complex was used for the sulfation of isosorbide-derived surfactant as reported by Lavergne *et al.* in 2011.[234] The 5-*O*-dodecyl isosorbide thus obtained had a lower CMC than SDS with comparable Krafft temperature making it a potential alternative molecule for sodium dodecyl sulfonate (SDS).

Sulfite (SO_3^{2-}) salts such as sodium hydrogen sulfite (or sodium bisulfite, $NaHSO_3$), sodium sulfite (Na_2SO_3) or sodium metabisulfite ($Na_2S_2O_5$) have all been used in sulfonation reactions (Scheme 14**C**-**F**). For instance, the Strecker reaction employs $NaHSO_3$ or Na_2SO_3

to convert alkyl halides in sulfonate groups (Scheme 14**C**).[235,236] This reaction does not require a counterion exchange (as is the case with SO_3-amines complexes) since the sodium salt of the corresponding product is directly formed. A wide range of functionalities tolerate this sulfation method, and the reaction may proceed in high yield when the halide (X) is an iodine group (*e.g.* via previous Finkelstein reaction).[236] Tomanovà *et al.* reported in 2019 the utilisation of sodium sulfite as an effective reagent for the reductive dehalogenation of aromatic halides, with only chloro- and fluoro-aryl compounds yielding the expected sulfonate product.[237]

Additionally, sulfonates are conveniently formed from alkenes using sodium (meta) bisulfite in aqueous-organic binary solutions (H_2O:n-propanol, H_2O:MeCN etc., Scheme 14**D**).[222,238] Sulfosuccinates-derived surfactants obtained from maleic anhydride and sodium meta-bisulfite are good examples employing this procedure.[239–242] Additionally, maleic anhydride, or its structurally resembling itaconic anhydride, may be obtained from renewable resources which further contributes to the sustainability of this reaction.[222,243]

Aldehydes may also easily be converted to sulfonate hydroxyl groups using sodium hydrogen sulfite (Scheme 14**E**). This reaction is most commonly used to purify aldehydes by selectively forming the aldehyde-sulfite adduct, which typically precipitates from the solution. The solid aldehyde-sulfite adduct is then filtered and converted back to the aldehyde after treatment with a base.[244] Kraus *et al.* in 2013, published a series of sulfonated furans using this method but limited to just short hydrophobic chains (longest being -C_4H_9).[245]

- *Current trends in petroleum-based and bio-derived sulfonated surfactants*

Linear alkylbenzene sulfonates (LAS) are sulfonated anionic surfactants produced at large scale (~3.5 Mt every year.)[218] They consist of a linear alkyl chain attached to a sulfonated benzene ring in the majority at the *para*- position. LAS are produced from fossil resources, employing hazardous chemicals (HF catalysts, SO_3 gas, benzene). Alkylation of the benzene ring is first performed with a linear hydrocarbon derived from ethene oligomerisation (or Fischer-Tropsch process), using hydrogen fluoride or aluminium chloride as catalysts.[218,219] Sulfonation is then realised in a continuous thin film reactor as described in the previous section, followed by a neutralisation step with an alkali (usually NaOH) to form the surface-active (sodium) LAS salt.

The growing demand for surfactants derived from renewable resources is driving the industry to substitute petroleum-based amphiphilic molecules.[219] However, developing greener sulfonated/sulfated anionic surfactants with good detergency; which are safe for the environment (biodegradable); use bio-derived molecules; are producible at large scale and employ sustainable routes represents a significant challenge to be addressed by green chemists.

Fatty acid methyl ester sulfonates (MES, Scheme 15) possess hydrophobic groups issued from renewable resources (oil crops) and is thus considered as *wholly bioderived* according to the EN16440 norm (see chapter I).[246,247]

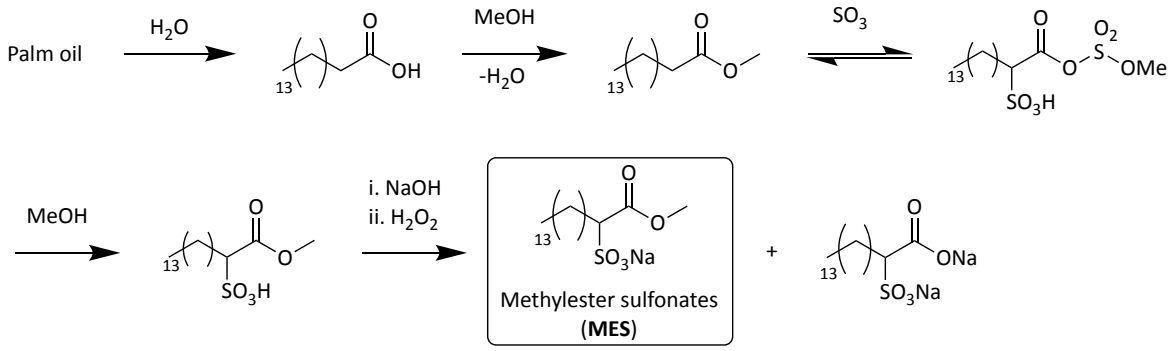

Scheme 15 General synthesis of methyl ester sulfonates as described by Tobori N. and Kakui T.[248]

MES represents the workhorse of bio-based anionic surfactants with a production capacity of over 444,600 t.year^{-1}.[249] Its detergency performance and higher tolerance to hard-water conditions than LAS have made MES the bio-based anionic surfactant of choice for laundry detergent formulation.[248,250] Nevertheless, palm oil, whose production is often associated with deforestation and intensive monoculture, is not ideal for the green credentials of this synthesis. Other bio-based anionic surfactants (non-sulfonated/sulfated) were prepared from fermentation-derived platform molecules such as succinic acid (*e.g.* disodium cocosuccinate) or amino acid (*e.g.* sodium methyl cocoyl taurate).[250]

Furans containing platform molecules (HMF, CMF, furfural) are easily obtained from biomass (as discussed chapter III.1 and III.2). However, furan-derived surfactants are seldom reported. Yet, to substitute LAS, replacing rigid benzene moieties with furan rings appear to be one of the most straightforward solutions.

- *Progress in the development of furan-derived sulfonated surfactants*

The sensitive nature of the furan unit towards the classical sulfonation/sulfation conditions discouraged many researchers from pursuing this route until now.[236,251] In 2016, Park *et al.* reported the synthesis of furan-derived sulfonated surfactant mimicking LAS structures by

replacing the benzene moiety with a furan group (Scheme 16, **140-142**). They demonstrated excellent properties compared to LAS or SDS, which encouraged the patenting of these compounds and method.[45,252] Unfortunately, from a sustainability perspective, their approach suffered from using harsh conditions (trifluoroacetic acid-catalysed anhydride formation of fatty acids at 180 °C) and use of SO_3•pyridine complex for the sulfonation requiring an ion-exchange step. Interestingly, the SO_3•pyridine complex was mild enough to prevent the destruction of the furan motif. A resembling procedure was described in a patent by The Procter and Gamble company in 2015 (Scheme 16, **143**).[253] Here, acetyl furan was reacted with a long hydrocarbon Grignard reagent and subsequently dehydrated, hydrogenated and sulfonated in the same manner, to afford a furan derived surfactant. Their method employed NaOMe to convert the pyridine surfactant salt to the sodium salts which differed from Park's which used Na_2CO_3.

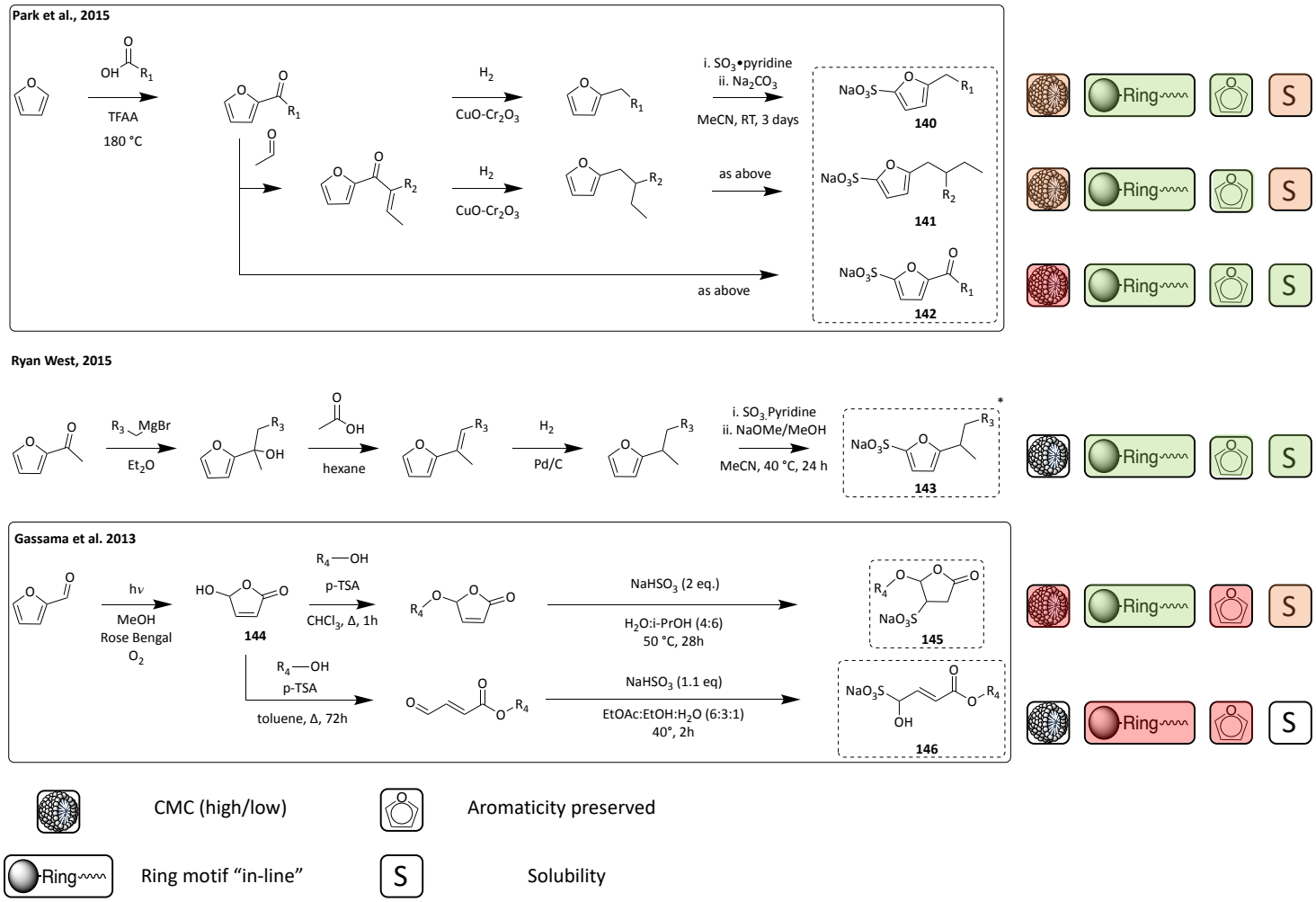

*Scheme 16 Different approaches to the production of sulfonated furan-derived surfactants. Colours indicate qualitatively how the final products match the assessed criteria from good (green) to poor (red), white means that the authors did not assess this criterion. *Sulfonation was also performed on commercial 1-(furan-2-yl)dodecane. R_1= $C_{12}H_{25}$ or $C_{14}H_{29}$ or $C_{18}H_{37}$ or cocinic acid (C_8-C_{18}) hydrocarbon. R_2= $C_{10}H_{21}$. R_3= $C_{12}H_{25}$ or $C_{13}H_{27}$. R_3= C_8H_{17} or C_9H_{19}. R_4= C_8H_{17} or $C_{10}H_{21}$ or $C_{12}H_2$*

In 2013, Gassama *et al.* reported the synthesis of a furan-derived surfactant via the conversion of furfural to 5-hydroxy-2(5*H*)-furanone (Scheme 16, **144**).[238] Acid catalysed etherification with fatty alcohols led to the alkoxy derivatives, which were subsequently sulfonated using the $NaHSO_3$/alkene sulfation reaction (**145**). Upon further heating, the etherification of **144** led to the furan ring-opening forming an unsaturated aldehyde which was further sulfonated with either the previous or the aldehyde/ $NaHSO_3$ sulfation method (Scheme 16, **146**). The ring containing compounds possessed comparable physio-chemical properties to their fossil-derived counterparts (LAS) and biodegradability of up to 78% after 28 days. This biodegradability falls within the definition of "readily biodegradable" compounds according to the OECD standards.[254] However, the aromaticity of the furan ring was not preserved with this approach, potentially impeding even closer LAS-like behaviour.

Recently Kipshagen *et al.* published a novel approach for the synthesis of furan-derived surfactant using the Piancatelli rearrangement from furfural or HMF to produce 1,3-cyclopentanediol (CPD, Scheme 17, **150**).[255] Subsequent Williamson etherification with n-fatty alcohol and sulfation with SO_3•pyridine complex afforded a new class of surfactant bearing a cyclopentane ring "in-line" with the hydrophobic tail (Scheme 17, **151**, **156**), *i.e.* with the cycle between the hydrophilic and the hydrophobic group. Unfortunately, the CMCs of most of these compounds were deemed too high to be of interest. Furthermore, these cyclopentane-containing surfactants were often not soluble enough to measure their CMCs. This study, therefore, reiterates the value of maintaining a furan moiety within the final surfactant structure.

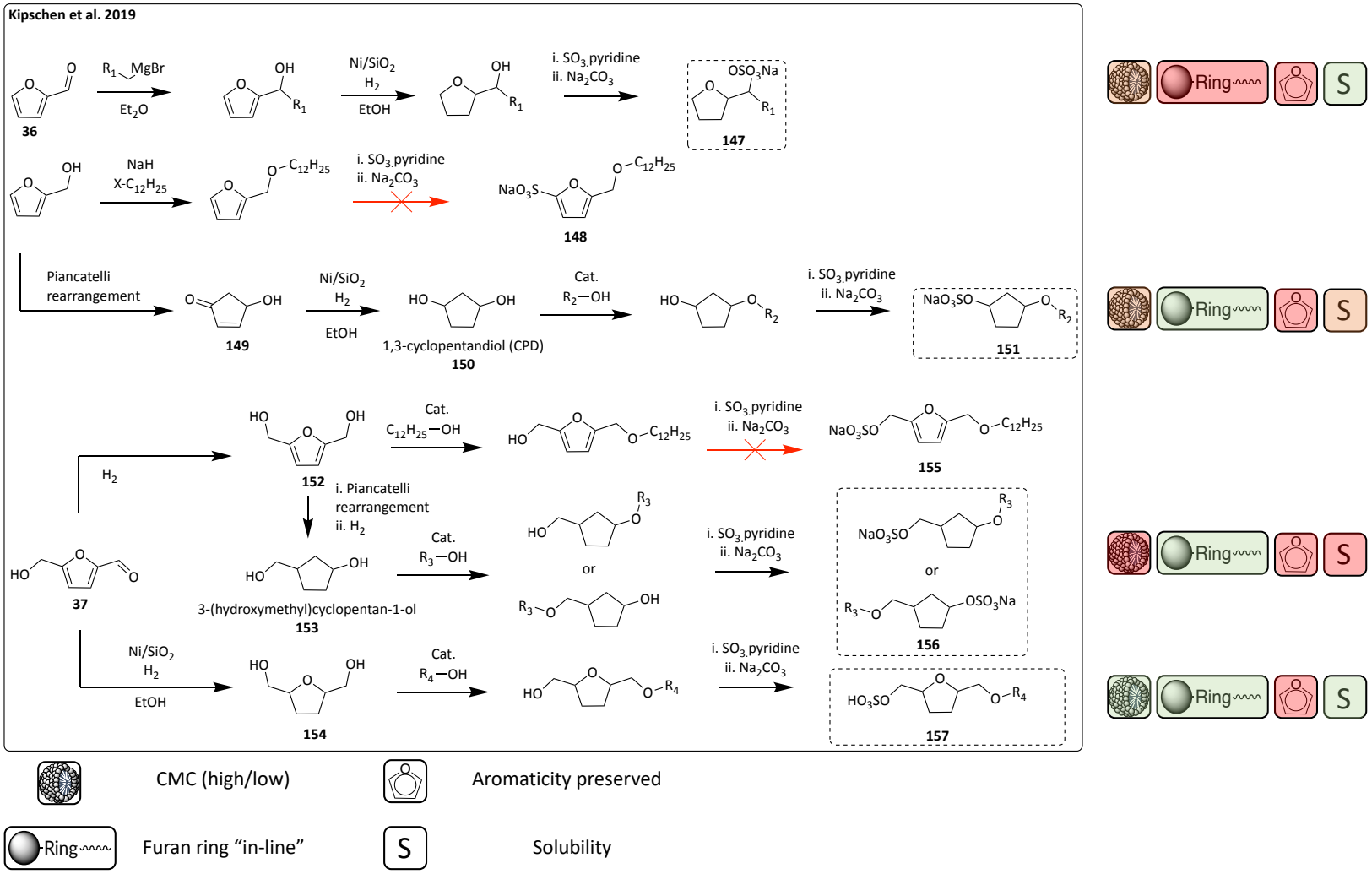

Scheme 17 Summary of the routes to sulfonated furan-derived surfactants by Kipshagen et al..[255] *Colours indicate qualitatively how the final products match the assessed criteria: good match (green) to poor (red), white means that the authors did not assess this criterion. R_1= $C_{12}H_{25}$ or $C_{14}H_{29}$. R_2= $C_{10}H_{21}$ or $C_{12}H_{25}$ or $C_{14}H_{29}$. R_3= $C_{10}H_2$ or $C_{12}H_{25}$. R_4= C_6H_{13} or C_8H_{17} or $C_{10}H_{21}$ or $C_{12}H_{25}$ or $C_{14}H_{29}$ as well as 2-methyl- of C_6H_{13} or C_8H_{17} or $C_{10}H_{21}$ or $C_{12}H_{25}$ or $C_{14}H_{29}$*

Kipshagen proposed other plausible routes to mimic LAS structures. In one example, the Grignard product obtained between n-dodecyl or tetradecyl magnesium bromide and furfural was hydrogenated to the tetrahydrofuran alcohol equivalent and subsequently sulfated with SO_3•pyridine (Scheme 17, **147**). The surfactant bearing the longer C_{14} hydrophobic chain displayed better properties than LAS, although solubility issues arose (insoluble in water at room temperature). This problem was likely due to the length of the hydrophobic chain and the presence of the sulfate group on "the side" of the THF ring and not "in-line" with the alkyl chain. Alternatively, HMF was hydrogenated to 2,5-bis(hydroxymethyl)-tetrahydrofuran (BHMTHF, **154**) which, similar to **150**, was mono-etherified and subsequently sulfonated, affording a THF-containing surfactant with the ring in-line with the hydrophilic and hydrophobic groups (Scheme 17, **157**). This class of surfactant had very low CMC (down to 0.004 $g.L^{-1}$) with a strong surface activity (interfacial tension at CMC between 0.6 and 20.6 $mN.m^{-1}$) surpassing LAS (CMC of 0.08 $g.L^{-1}$ and interfacial tension at CMC of 0.9 $mN.m^{-1}$). The approach applying the Piancatelli rearrangement on 2,5-bis(hydroxymethyl)furan (Scheme 17, **152**) leading to 3-(hydroxymethyl)cyclopentane-1-ol (**153)** and a similar reaction sequence as for **150** only led to a surfactant with poor activity and unclear identification (Scheme 17, **156**). These authors' attempts to sulfonate the furan-containing intermediates led to complete degradation of the expected product (Scheme 17, **148** and **155**), attributed to the excessive reactivity of furans. This result explained why the aromaticity of the furan ring was not kept for subsequent reactions. Nonetheless, a patent by Henkel was published a few weeks after publication of the research article, suggesting Henkel's interest in finding a renewably sourced replacement of common anionic surfactants.

3.4.2 Aims of chapter III.4

The work presented herein pursues the synthesis of innovative new anionic sulfonated furan-containing surfactants. First, a library of furan derived surfactants was modelled, by Unilever R&D, based on their computed cLogP value (partition coefficient between n-octanol and water), relative polar surface area and shape index. These were mapped, and potential target compounds with different functional groups at the 2- and 5- position of the furan ring could be identified based on their predicted efficacy (closeness to LAS according to the model mentioned above), patentability and ease of synthesis. Finally, five families of compounds (Scheme 18) were selected for synthesis based on their potential to be prepared from platform molecules readily available from microalgae such as HMF, CMF, furfural and fatty acids:

- **Family 1** with sulfonate groups directly attached to the furan ring at the 2-position and bearing a hydroxyl group α to the 5- position linked to a fatty carbon chain
- **Family 2** consisted of a furan ring bearing a methyl sulfonate group at the 5- position and a ketone group α to the 2- position linked to a fatty carbon chain
- **Family 3**, furan surfactants with fatty esters at the 2-position and a methyl sulfonate group at the 5-position
- **Family 4** , related to **Family 2** but replacing the ketone with an alcohol group α to the 2- position
- **Family 5**, employing the HMF aldehyde manifold to incorporate a hydrophobic group via Grignard reaction (using 2 eq. of the Grignard reagent to compensate HMF acidic -OH) and a hydrophilic sulfate group added via sulfation of HMF's hydroxyl moiety.

Synthesis of examples of all families depicted Scheme 18 were attempted despite inherent incompatibilities with C-C coupling method (*e.g.* Cl- or HO- groups with Grignard regents) However, the sulfonation steps using SO_3•pyridine complexes often proved unsuccessful. Thus, the Strecker reaction was successfully employed to synthesise four **Family 3** members whose performances were further tested in the Unilever laboratory. An additional compound based on the **Family 3** motif was prepared to link this project with the *Chemicalgal plant* concept (phase III, 3rd generation biorefinery). A mixture of fatty alcohols theoretically obtained by hydrogenation of *Spirulina sp.* fatty acids (based on *Spirulina sp.*'s fatty acid profile) was used as hydrophobic groups, thus getting a step closer a multi-component microalgae biorefinery.

Selected furan derived sulfonated surfactant:

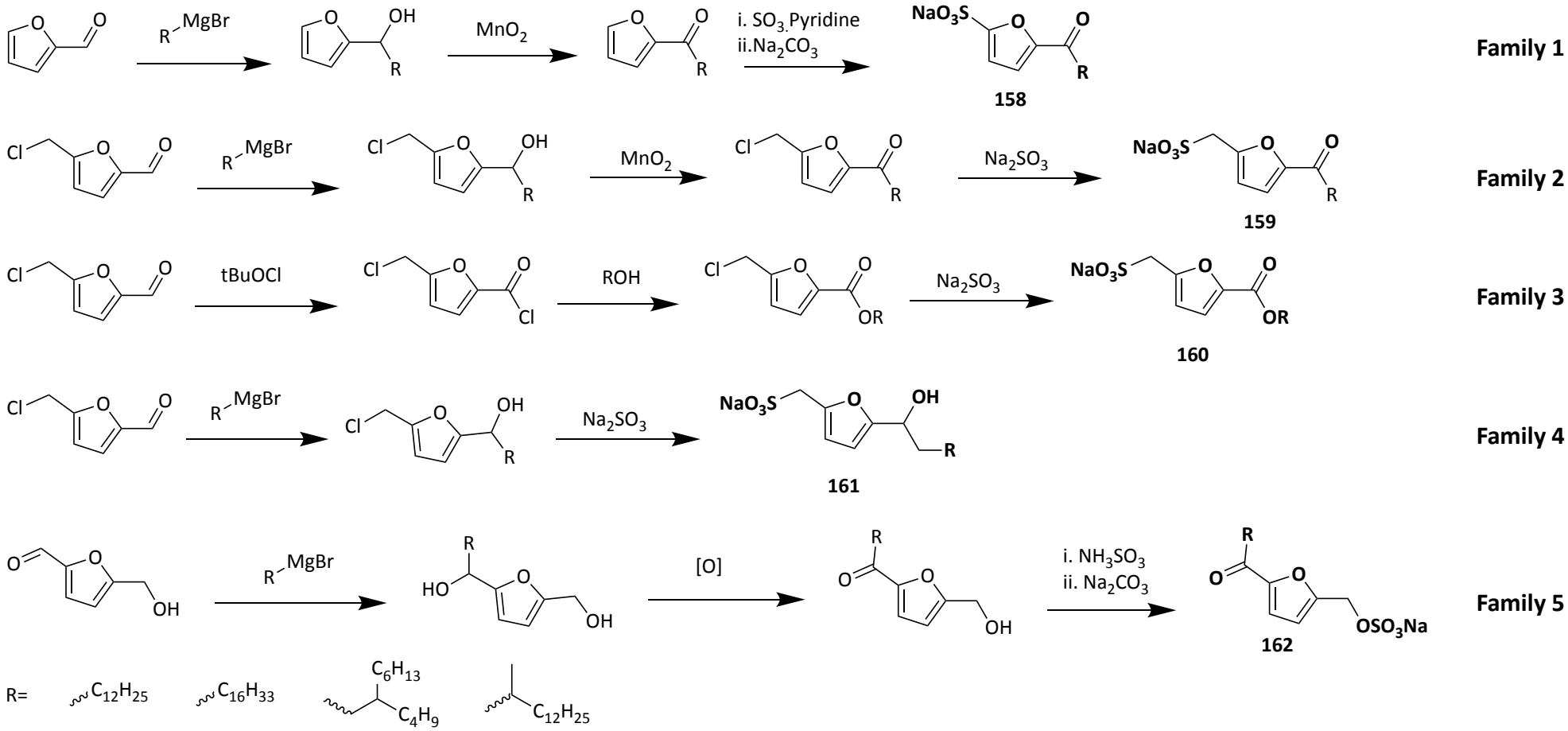

Scheme 18. Selected families for the synthesis of sulfonated/sulfated furan surfactants and proposed routes.

3.4.3 Synthesis and testing of furan-derived sulfonated surfactants

3.4.3.1 Synthesis of Family 1

Synthesis of Family 1, starting from furfural, was selected as the first target. Although these molecules were previously described by Park *et al.*, it was of interest to develop a different approach from furfural and test their performance against other surfactants.

Commercial samples of furfural are usually dark in colour likely due to the presence of polyfuranic compounds as described previously in the case of HMF.[256] Considering the potential impact these impurities may have on yields or colour of the final product, prior vacuum distillation of furfural was performed. The resulting clear to pale-yellow oil was kept at -20 °C under inert atmosphere until further use. The subsequent Grignard reaction using commercially available Grignard reagent such as n-dodecyl magnesium bromide solutions usually proceeded in excellent yield, and over 94% 1-(furan-2-yl)tridecan-1-ol (Scheme 19, **163$_a$**) was obtained. Subsequently, the oxidation using MnO_2 was performed in the toluene alternative solvent TMO. Unfortunately, only a yield of 43% of 1-(furan-2-yl)tridecan-1-one (**164$_a$**) could be obtained, likely due to the bulky character of the substrate preventing access to oxidant sites in MnO_2. Nevertheless, sufficient samples of **164$_a$** were isolated for the remaining step.

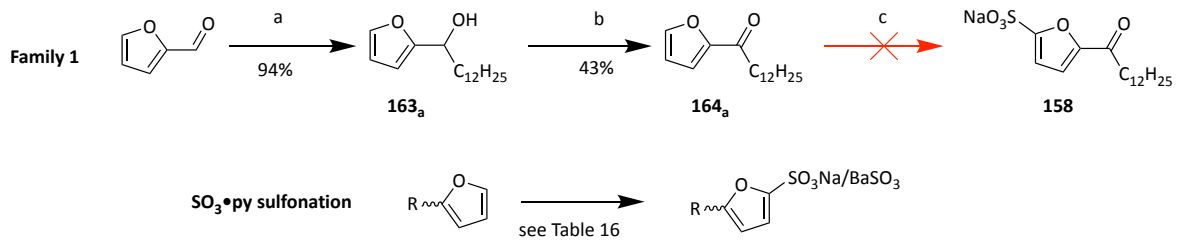

Scheme 19 Route to compound of Family 1 surfactants: sodium 5-alkanoylfuran-2-sulfonates a) furfural (35 mmol), $C_{12}H_{25}MgBr$ (35.5 mmol 0.5 M in 2-MeTHF), 2-MeTHF (30 mL) 0 °C upon addition then room temperature 16 h. b) ***163*** *(5.6 mmol), MnO_2 (9 mmol in 2 portions), 3 Å mol. sieves, TMO (50 mL) 85 °C 8 h then 95 °C, 16 h. c)* ***164*** *(1.9 mmol), SO_3•pyridine (2.8 mmol), MeCN (5 mL), 40 °C 24 h, neutralisation with NaOMe (2.84 mmol in 10 mL MeOH) (see experimental section general synthetic procedures d. for the detailed protocol). SO_3•pyridine sulfonation scheme for Table 16*

Table 16 Summary of different sulfonation conditions reported in the literature and attempted here

Entry[a]	R	Time (h)	SO_3•Py:Furan ratio	T (°C)	Solvent	Neutralisation	Yield (%)	Reference
1	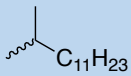	24	1.5:1	40	MeCN	NaOMe/MeOH	36	Ryan West, (2015)[253]
2	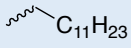	24	1.5:1	40	MeCN	NaOMe/MeOH	75	
3	See Scheme 16, p. 206	72	1:1	RT	MeCN	Na_2CO_3	-	Park *et al.* (2016)[45]
4		8	1:3	95	Neat	$BaCO_3$	20	Scully and Brown (1954)[251]
5		4	3:1	50	DCE	$BaCO_3$	52	
6		72	3:1	RT	DCE	$BaCO_3$	40	
7		72	1:1	RT	DCE	$BaCO_3$	64	
8	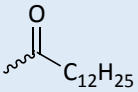 **164_a**	24	1.5:1	40	MeCN	NaOMe/MeOH	-	This work
9		72	1:1	RT	DCE	Na_2CO_3	-	
10		72	2:1	RT	DCE	Na_2CO_3	-	
11	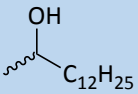 **163_a**	24	2:1	40	MeCN	NaOMe/MeOH	-	
12[b]		24	1.5:1	40	MeCN	NaOMe/MeOH	-	
13		24	1.5:1	40	MeCN	Na_2CO_3	-	
14		72	1:1	RT	MeCN	Na_2CO_3	-	
15		72	1:1	RT	DCE	Na_2CO_3	-	
16		72	2:1	RT	DCE	Na_2CO_3	-	

a. Entry 4-7 were isolated as barium salts

b. Trimethylamine.SO_3 complex was used instead

The sulfonation of **164$_a$** was first attempted following the method described in 2015 by Ryan West in a Procter and Gamble patent at a smaller scale (2 mmol, Table 16, entry 8). However, no reaction occurred, and only the starting material was obtained while an intense green colouration of the reaction medium was observed. Using a different solvent (DCE as reported by Scully and Brown, entries 4-7) did not improve the outcome of the reaction either (entries 9-10).[251] When the neutralisation procedure using Na_2CO_3 (as described by Park *et al.*) was tried using DCE as a solvent, no sulfonated product could be obtained (entries 9-10).[236] These results contradict the previous claim by Park *et al.* that this class of compounds could be sulfonated using SO_3 complexes. No evidence of the successful characterisation of this class of compounds nor yields were found in this article (nor the supplementary information) which may hint at the difficulty of isolating these compounds.

Optimisation of the sulfonation procedure was tried using **163**, which could be synthesised at a larger scale. Unfortunately, repeated attempts with varying conditions (entries 11-16) did not lead to any isolable sulfonated products.

3.4.3.2 Synthesis of Family 5

Considering the successful synthesis of **163** from furfural employing commercial Grignard reagents, the synthesis of **Family 5** (based on HMF) was attempted. Initially, the reaction mixture containing HMF and the Grignard reagent was reacted overnight (~16 h, similar to furfural) after which the reaction medium turned noticeably darker with no Grignard product isolated. Then, careful monitoring of the reaction by TLC (1:4, EtOAc:*n*-hexane) revealed that full conversion was achieved within 50 minutes. However, no expected product could be isolated despite the reduced reaction time. Modification of the aqueous

work-up eventually permitted to isolate some product. Indeed, the HCl acidic work-up commonly conducted after Grignard reactions to convert the Mg-O-R adducts to alcohols was also found to degrade intermediate **165** (Scheme 20). By using a saturated ammonium chloride solution to quench the reaction and convert the Grignard adduct to the expected alcohol, intermediate **165** was obtained in 43% yield by precipitation from *n*-hexane.

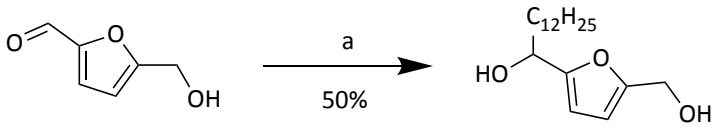

37 **165**

Scheme 20. First synthetic step to compounds of Family 5 surfactants. a) HMF (32 mmol), dodecyl magnesium bromide (65 mmol as 0.5 M solution in 2-MeTHF) 50 min room temperature.)

Attempts were also made to obtain the branched alkyl chain members of **Family 5**. Grignard reagents (2-butyloctyl magnesium bromide, tetradecane-2-yl magnesium bromide and hexadecyl bromide, Scheme 21 $\mathbf{167_a}$, $\mathbf{167_b}$ and $\mathbf{167_c}$ respectively) required for forming the corresponding intermediates **165** were not commercially available, their synthesis from branched alcohols was needed.

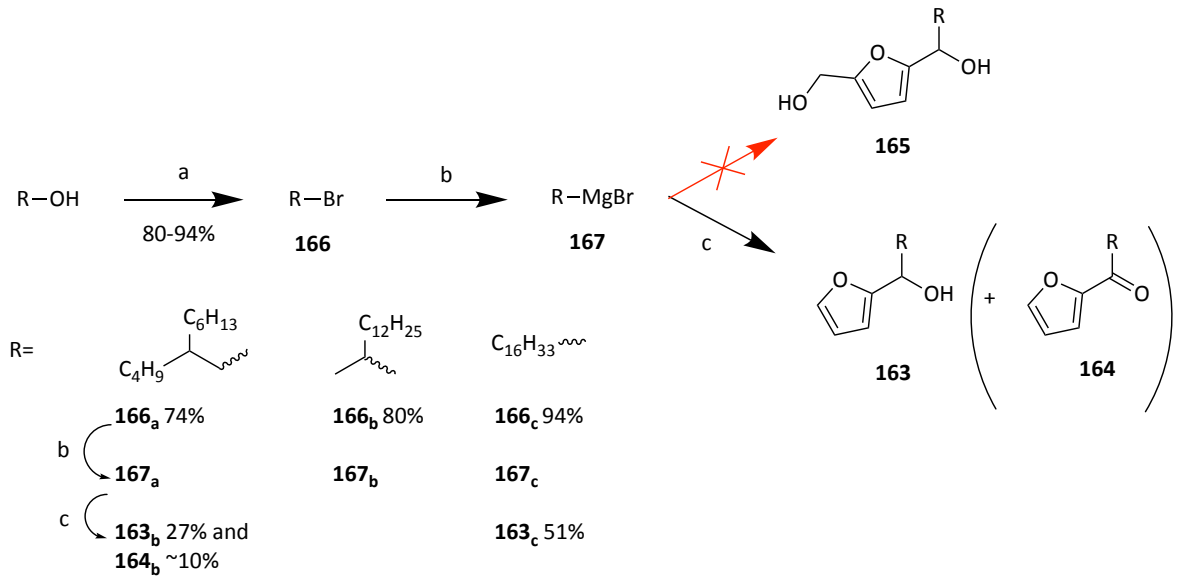

*Scheme 21 Synthesis of **165** and **163** using non-commercially available Grignard reagents and bromo alkyl derivatives. a) alcohol (80.5 mmol), PPh_3 (80.5 mmol), NBS (81 mmol), DCM (200 mL), 0 °C upon addition then 3 h at room temperature; b) **166** (5 mmol), Mg (15 mmol), Et_2O or THF (5 mL), 1,2-dibromoethane (few drops), 1 h stirring; c) furfural (4.5 mmol) in THF or Et_2O (50 mL), 0 °C upon addition, 16 h room temperature (see experimental section general synthetic procedures d. for the detailed protocol and Appendix 13 for different attempted conditions)*

Bromination of the corresponding alcohols with N-bromo succinimide proceeded in good to excellent yields (74% and 80% for **166$_a$** and **166$_b$** respectively). Repeated attempts (see Appendix 13) to convert 2-butyl-1-bromooctane into the corresponding Grignard failed. The bulky nature of these reagents likely reduced their ability to reach the active magnesium surface and form the magnesium bromide group. Due to the higher price of HMF, the reaction was optimised using furfural instead. After many trials (Appendix 13), a small amount of the expected, product **163$_b$** could be obtained in 27% yield using 2-butyl-1-bromooctane and diethyl ether as a solvent. The branched non-brominated hydrocarbon (*i.e.* 2-butyloctane) was also detected in a 1:6 ratio (by ^{1}H-NMR spectroscopy) relative to the product. The same reaction yielded the oxidised compound **164$_b$** in 10% yield as a side product. The presence of 2-butyloctane may suggest that the Schlenck equilibrium (Figure 52) was shifted towards the alkyl magnesium (Figure 52, MgR_2) species possibly due to the

excess magnesium used for the reaction. The basicity of magnesium bromide species in solution may be strong enough to deprotonate the intermediate **163** and form **164** explaining the obtention of this oxo-alkyl furan as a side product.

Figure 52 Schlenck equilibrium between magnesium halide species.

Nevertheless, the successful Grignard formation required Et_2O as a solvent instead of THF. The higher basicity of THF may contribute to stabilise MgR_2 species better, which eventually could drive the equilibrium to the right-hand side (as depicted in Figure 52). The optimised protocol with furfural could not be applied directly to HMF due to its low solubility in diethyl ether, and the branched derivatives of **Family 5** were not further examined. However, the amount of **165** isolated from previous reactions using commercial dodecyl magnesium bromide solution was sufficient to investigate the selective sulfonation of this intermediate.

In the hope of making **168** (Scheme 22), sulfamic acid NH_3SO_3 was initially tried due to previous reports of its preference to sulfate primary alcohols.[228,229] However, this acid remained a strong acid, (pKa ~1.0) and led to the degradation of intermediate **165**. Thus, SO_3•pyridine complex was used in pyridine or DMF since these solvents are known to reduce the activity of the sulfonating agents.[255] Monitoring of the reaction by TLC (DCM:MeOH, 8:2) indicated that full conversion of **165** occurred after 16 hours at 40 °C. Aqueous work-up afforded a brown residue which was chromatographed over silica gel to afford a pale yellow oil which was expected to be **168**. However, no significant chemical

shift of the-CH_2(OH)- signals was observed by ^{1}H nor ^{13}C-NMR spectroscopy (4.57 ppm and 57.66 ppm respectively for **165**). Instead, a 1.5 ppm downfield shift of the triplet signals corresponding to the secondary alcohol (-CH(OH)-CH_2-) of **165** was observed (from 4.63 ppm to 6.13 ppm by ^{1}H-NMR spectroscopy). Additionally, ESI-MS showed the presence of a compound with m/z = 438.2312 which was far from the expected m/z= 398.1739 for **168** or m/z= 453.2185 for the pyridinium salt.

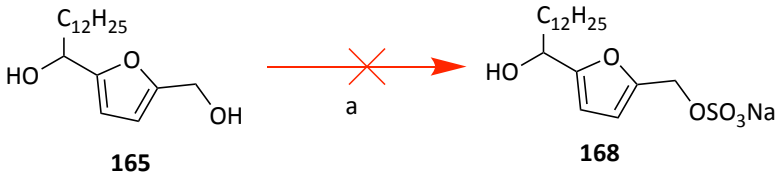

165 **168**

Scheme 22 Sulfonation step of Family 5 surfactants. b) ***165*** *(3.4 mmol), SO_3•pyridine (4.6 mmol in 10 mL DMF), DMF (50 mL), 40 °C 16 h (see experimental section general synthetic procedures d. for the detailed protocol*

Surprisingly, data seemed to indicate that sulfation occurred at the 2-position leaving the primary alcohol intact. Nonetheless, since the hydrophilic group was likely not "in-line" with the furan ring (assumed to provide rigidity to the surfactant molecule and mimicking LAS structure), this class of compound was not studied further.

The outcome of the sulfonation and sulfation reactions using SO_3•pyridine complexes led to explore other methods to incorporate hydrophilic groups. In this regard, using the chloromethyl group in CMF to add a sulfonate moiety via the Strecker reaction appeared as a promising solution.

3.4.3.3 Synthesis of Family 2 and 4

The synthesis of **Families 2** and **4** was pursued next. Unfortunately, the intrinsic incompatibility of CMF with Grignard regents led to an unstable compound (Scheme 23, **169**) which degraded and turned black upon isolation. This result automatically dismissed Families 2 and 4 due to the impracticality for these families to be scaled up.

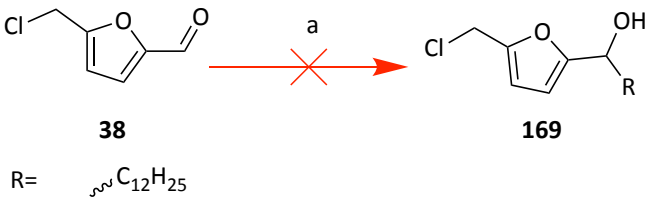

*Scheme 23 Synthesis of the necessary intermediate **169** for Families 3 and 4. a. CMF (1.4 mmol), $C_{12}H_{25}MgBr$ (1.5 mmol from 0.5 M solution in 2-MeTHF), 2-MeTHF (10 mL), 0 °C upon addition, then 50 min at room temperature.*

3.4.3.4 Synthesis of Family 3 and testing

- *Synthesis*

The other selected family based on CMF (**Family 3**) avoided intermediate **169** and was thus attempted for synthesis. The synthetic route to FSS-**Family 3** is depicted in Scheme 24. This route employs the Strecker reaction to incorporate the sulfonate group, thus avoiding SO_3 complexes and ion-exchange.

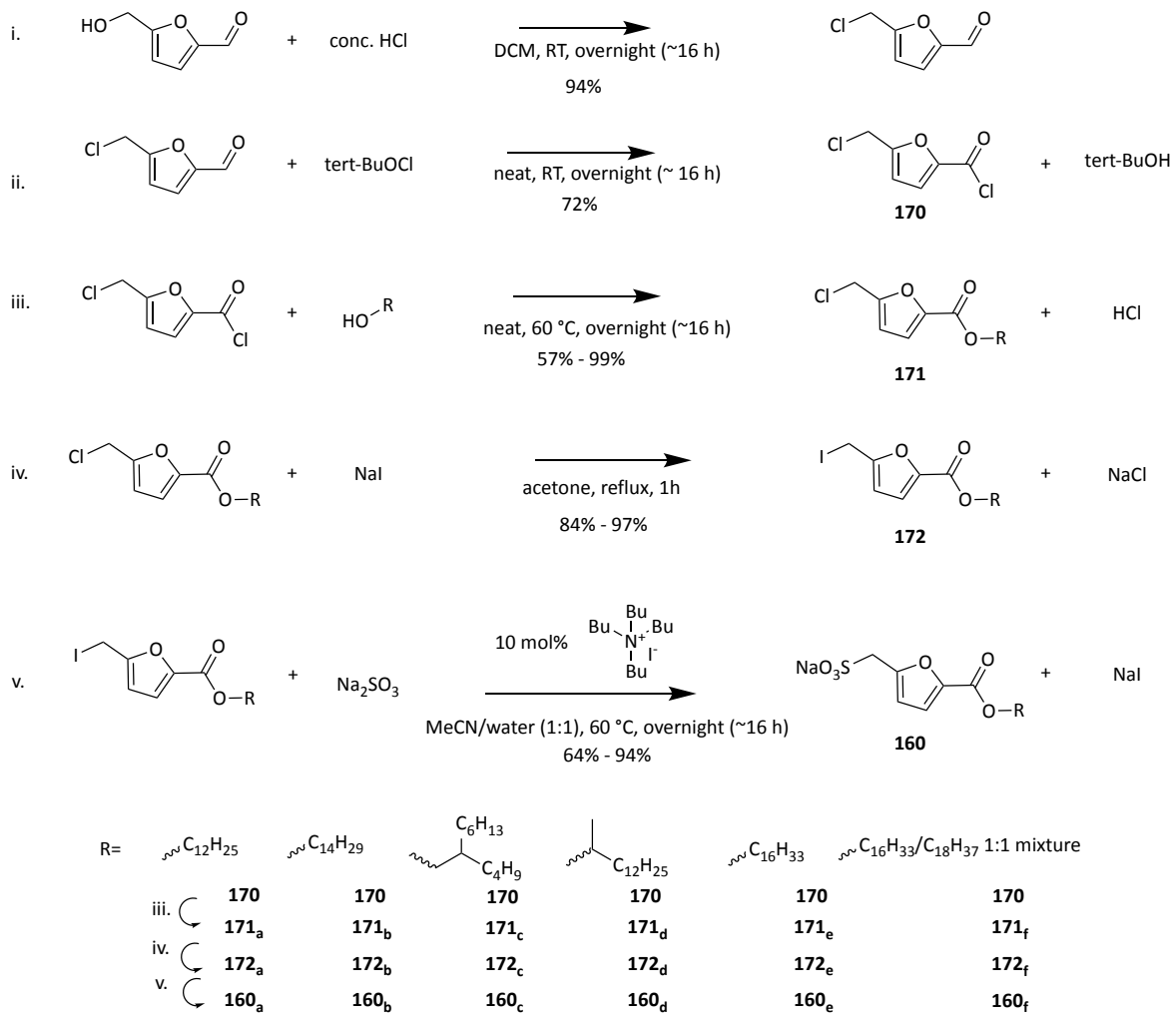

Scheme 24 Synthetic route to FSS-Family 3. i) HMF (198 mmol), 37% HCl (1.5 mol), DCM (250 mL) left to stir overnight (~16 h) at room temperature, ii) CMF (173 mmol), tert-BuOCl (860 mmol), left to stir neat overnight (~16 h). Iii) CMFCC (33 mmol), fatty alcohol (50 mmol), neat 60 °C overnight (~16 h), iv) alkyl 5-(chloromethyl)furan carboxylate (5.2 mmol), NaI (10.4 mmol), acetone (20 mL), reflux 1 h, v) alkyl 5-(iodomethyl)furan carboxylate (20.7 mmo), Na_2SO_3 (31 mmol), tetra-butyl ammonium iodide (2 mmol), MeCN:H_2O (1:1, 50 mL), 60 °C overnight (~16 h). See experimental section general synthetic procedures d. for the detailed protocol

Steps ii and iii were adapted from a previous report by Dutta *et al.*.[192] In this study **170** (5-(chloromethyl)furan-2-carbonyl chloride, CMFCC) was an intermediate in the synthesis of a series of ethyl ester derivatives and poly(ethylene) furanoate monomers. Herein the same route is taken, *tert*-BuOCl could be obtained in 78% from a simple reaction between *tert*-BuOH and 14% NaOCl in just 5 minutes. The desired product *tert*-BuOCl being water-

immiscible is obtained by aqueous work-up further facilitating the scale-up of this reaction. Although CMF could be produced from microalgae (as demonstrated in chapter III.1), the easier production of CMF from HMF was herein undertaken instead to obtain the required quantity for surfactant performance testing.

*Table 17 Summary of the yields obtained for the different alcohols used for FSS-**Family 3** surfactants synthesis on multi-gram (5-10 g) scale*[*]

Entry	Alcohol	Yield (%)			Overall Yield (% From CMF)
	Steps	iii	iv	v	ii - v
1	$C_{12}H_{25}$—OH	99 (77)	84 (90)	72 (86)	43 (48)
2	$C_{14}H_{29}$—OH	99	91	64	41
3	$C_{16}H_{33}$—OH	(73)	(93)	(94)	46
4	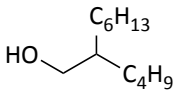	57 (69)	93 (89)	71 (83)	27 (41)
5	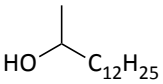	64 (29[**])	97 (85)	63 (89)	28 (17)
6	HO—$C_{16}H_{33}$ HO—$C_{18}H_{37}$ 1:1 mixture	67	93	69	31

*Numbers in brackets indicate the yield obtain for the ~1 gram-scale reactions. **Purification issues arose for this reaction, explaining the low yield obtained.

Esterification of CMFCC and different fatty alcohols was undertaken using 2 equivalents of the neat alcohol (1.5 equivalents for tetradecan-2-ol (entry 5) and 1 equivalent of each alcohol for the mixture (entry 6)). Despite most of these alcohols being solid at room temperature, the temperature at which the reaction was performed allowed the alcohols to melt, thus permitting more industrially relevant solventless systems to be used. Each ester derivative was purified by chromatography and characterised prior to the next steps. Although heating under vacuum may allow removal and recovery of excess alcohol, care

was taken to not over-heat the product considering possible thermal sensitivity. Finkelstein nucleophilic substitution of chlorine with iodine using sodium iodide proceeded in high yield (between 84% and 97%). Although optional, this step was added to ensure the reactivity of intermediate **172** in the following sulfation step, I-R being a better leaving group than Cl-R.[236] Precipitation of NaCl during reaction drives the equilibrium towards the product, hence explaining the high yield herein obtained.

Finally, the Strecker reaction was, so far, the most robust and successful approach for sulfonation of furan-derived surfactant. Although only fair yields (between 60-75%) were obtained, except for **160$_e$** (94%), the scope of this approach regardless of branching or hydrocarbon chain length, must be highlighted. Overall, scaling-up the reactions to multi-gram scale did not lead to a significant yield loss and sometimes an increased yield was even obtained (*e.g.* step ii using n-dodecanol or 2-tetradecanol).

To align with the overall PhD goals, a mixture of fatty alcohol based on the most abundant fatty acids present in *Spirulina sp.* was used for esterification of CMFCC. According to four separate studies the most abundant fatty acids in *Spirulina sp.* are: palmitic (C_{16} between 18 and up to 48% of total fatty acids); palmitoleic ($C_{16:1}$, 1 to 8% of total fatty acids); stearic (C_{18}, 1 to 9% of total fatty acids); oleic ($C_{18:1}$, 2 to 36% of total fatty acids); linoleic ($C_{18:2}$, 6 to 17% of total fatty acids) and γ-linoleic ($C_{18:3}$, 4 to 22% of total fatty acids) acids (Scheme 25 and Appendix 14).[73,92,257,258] On average, regardless of their unsaturation, C_{16} and C_{18} fatty acids make up to 40 and 42% respectively of the total fatty acids present in *Spirulina sp.*, which was approximated to a 1:1 ratio of C_{16}:C_{18} fatty acids. Hydrogenation of fatty acid to fatty alcohols has been extensively studied and is classically performed using H_2 and a supported metal (ReOx-Pd/SiO2, ReOx/TiO_2) or homogenous Ru catalysts (Scheme 25).[259–

[261] After this reaction, fatty acids' carboxylic acid groups (-COOH) can be converted to alcohols (-OH), and unsaturated compounds (bearing -C=C- bonds) are typically reduced to saturated fatty alcohols (bearing only -C-C-, see Scheme 25). Thus, an equimolar mixture of hexadecane-1-ol and octandecan-1-ol mimic the major components that could be obtained from the hydrogenation of fatty acids contained in *Spirulina sp.* The esterification of CMFCC with this fatty alcohol mix successfully occurred. GC-FID and ESI-MS confirmed a 1:1 mixture of the corresponding esters (NMR spectroscopy could not discriminate between the two esters). The following steps could be performed similarly to that previously described, and a 31% overall yield from CMF was obtained. Unfortunately, the mixture of the isolated surfactant was insufficiently soluble in deionised water to be of interest for the application under consideration (liquid detergents and laundry formulations). However, Lin *et al.* reported the genetic engineering of the microalga *Dunaliella tertiolecta* which mutant displayed a sevenfold and a fourfold increase of lauric acid ($C_{12:0}$) and myristic acid ($C_{14:0}$) accumulation respectively compared to the wild type.[262] This combination of fatty acid is more likely to produce a C_{12} and C_{14} enriched fatty alcohol mixture after hydrogenation. Applying the herein developed synthesis with this C_{12}-C_{14} enriched blend will likely lead to more water-soluble surfactant mix. Nevertheless, the C_{16}-C_{18} produced in this work may prove useful for non-aqueous application such as the emulsification of organic phases, or the dispersion of solid particles in oil for the automotive industry.

Compounds corresponding to entry 1 (**160$_a$**), 2 (**160$_b$**), 4 (**160$_c$**) and 5 (**160$_d$**, Table 17, p. 222) were synthesised on a multi-gram scale and their performance as surfactants in aqueous solutions was tested by experts in Unilever R&D, Liverpool. A summary of these tests and

a discussion of their meaning (prepared by Yann Lie and guided by David Grainger and Jane Whittaker from Unilever Ltd) follows.

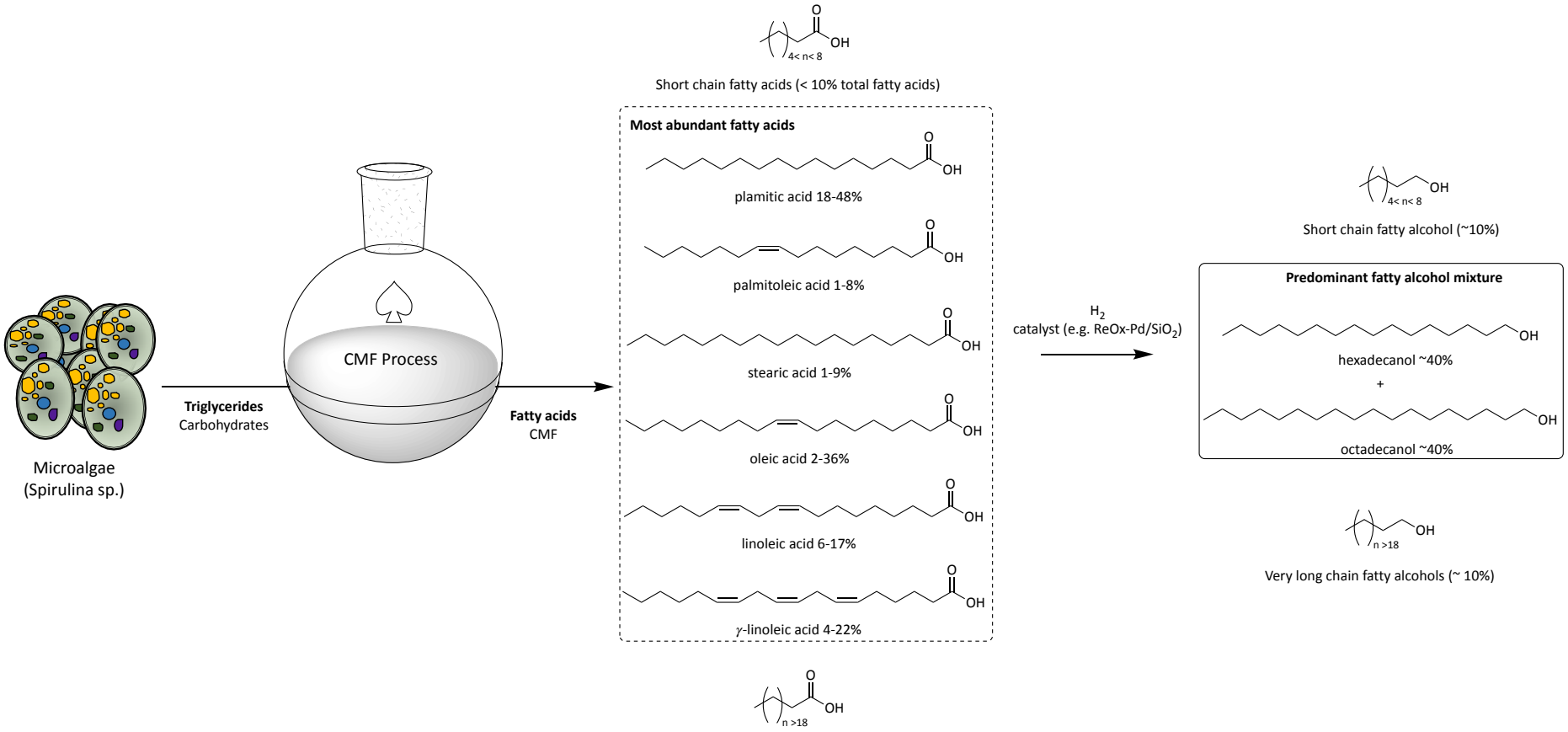

Scheme 25 Production of the theoretical fatty alcohol mixture from fatty acids extracted via CMF process using Spirulina sp. as feedstock

- *Performance testing*

Krafft temperature

The Krafft temperature (or Krafft point) was measured for compounds represented in Figure 53 (see experimental section - analytical instruments and methods, Krafft temperature). Krafft temperature is defined according to the IUPAC as *"the temperature above which the surfactant concentration increases sharply. At this temperature the surfactant concentration becomes equal to the critical micelle concentration. […]"*.[263]

Commonly for detergent application, the lower the Krafft point, the better. Indeed, the Krafft point is often more simply considered as the temperature below which the surfactant will start to precipitate out of the solution. Since most detergents are usually stored at room temperature, the Krafft temperature absolute limit of a surfactant may be considered as 25 °C although 15 °C is likely a more realistic limit to adopt. Besides, the different ingredients present in the final formulated product are likely to alter the physical properties of the amphiphilic molecule. Thus, a surfactant possessing a Krafft temperature above 15 °C may still be relevant for domestic applications. For instance, SDS has a Krafft temperature of 15 °C while that of LAS-C_{12} is 58 °C in deionised water.[234] The Krafft temperatures for the tested surfactant is indicated in Figure 53.

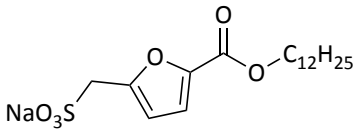

160_a
Krafft Temperature: 10 °C

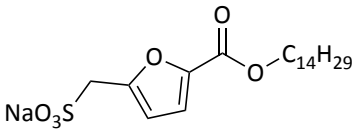

160_b
Krafft Temperature: 36 °C

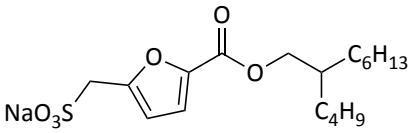

160_c
Krafft Temperature: < 0 °C

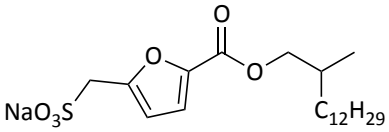

160_d
Krafft Temperature: < 0 °C

Figure 53 Synthesised FSS-Family 3 compounds tested for their performance. Krafft temperature are indicated under their name code

Out of the four candidate compounds, three had Kraft temperatures low enough to be of interest for detergent formulation: **160_a**, **160_c** and **160_d**. As expected, **160_b** had a higher Krafft temperature, 36 °C, than the related candidate **160_a** (10 °C) due to the longer hydrophobic chain. Interestingly, both branched candidate compounds had a Krafft temperature below 0 °C, despite their long aliphatic chains. Compared to previously disclosed furan-derived surfactant Krafft temperatures, the three candidates' values are excellent for the targeted house/personal care application. Indeed, Park *et al.* reported Krafft temperatures below 0 °C only for the OFS-n-1/O (Scheme 16, p. 206, **142**). Simultaneously, most of the other FSS had a Krafft temperature above 20 °C much like Gassama's molecules derived from hydroxyfuranones **145**.

CMC value determination

CMC values of the synthesised molecule were evaluated in varying water hardness (plain 0.1 M NaCl (01S), hashed (3FH), dotted (12FH) and hashed dotted (24FH) lines). Water hardness is defined by the concentration of Ca^{2+} (from $CaCO_3$ or CaO) ion in solution and is reported here, in French hardness degrees (°fH or FH) where 0.10 $mg.L^{-1}$ of Ca^{2+} in solution corresponds to 1 °fH. Soft water is considered to be between 1 and 6 °fH, moderately hard water is between 6.1 and 12 °fH, hard water is between 12.1 and 18 °fH, and very hard water is above 18 °fH. Cations attract anionic surfactants in solution which may reduce their surface activity by preventing them from aggregating at the surface (or form micelles). The cations present in solution (*e.g.* Ca^{2+}) may instead form an insoluble salt with two molecules of anionic surfactants ($R\text{-}SO_3^-$). For this reason, chelators are often added into detergent formulations to prevent a loss of the surfactant performance and selectively chelate polycations.

Surface activity against the surfactant concentration (Figure 54**A**, see experimental section-analytical instruments and methods, CMC determination) was plotted. Data were fitted to a model developed by Al-Soufi *et al.*, and CMC values could be determined for all **Family 3** compounds (Figure 54**B** and comparison of the fitted curve (line) and real data (marker) Figure 54**C**).[264] In this method, the CMC corresponds to the point of inflexion of the curve.

Excellent fit with the model used could be obtained in all but two cases: for compound $\mathbf{160_a}$ in 12 and 24FH water, due to aberrant points obtained at higher concentration. The CMC values obtained in these cases were thus not considered further for interpretation.

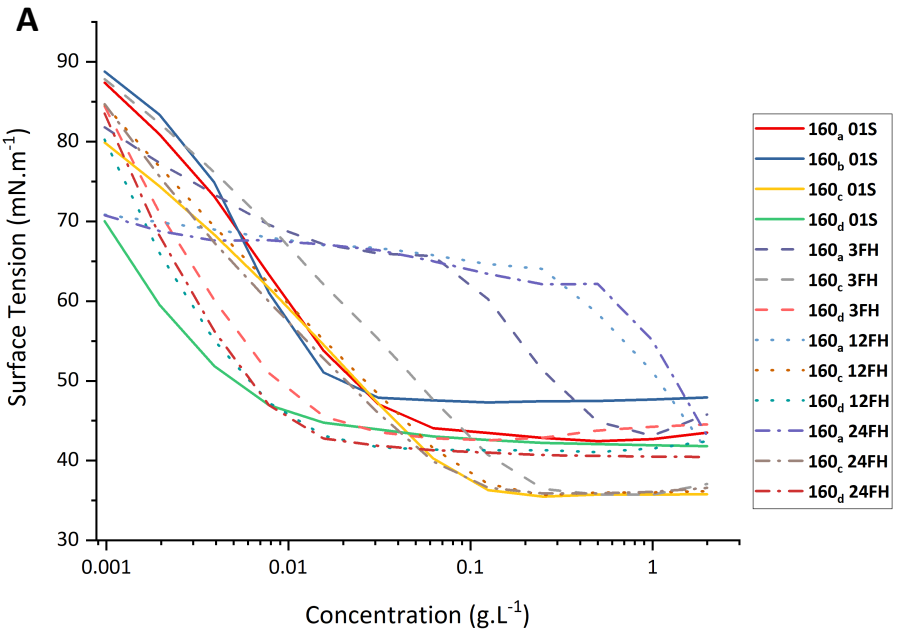
A
Surface Tension (mN.m-1)
90
80
70
60
50
40
30
0.001
0.01
0.1
1
Concentration (g.L-1)
160a 01S
160b 01S
160c 01S
160d 01S
160a 3FH
160c 3FH
160d 3FH
160a 12FH
160c 12FH
160d 12FH
160a 24FH
160c 24FH
160d 24FH

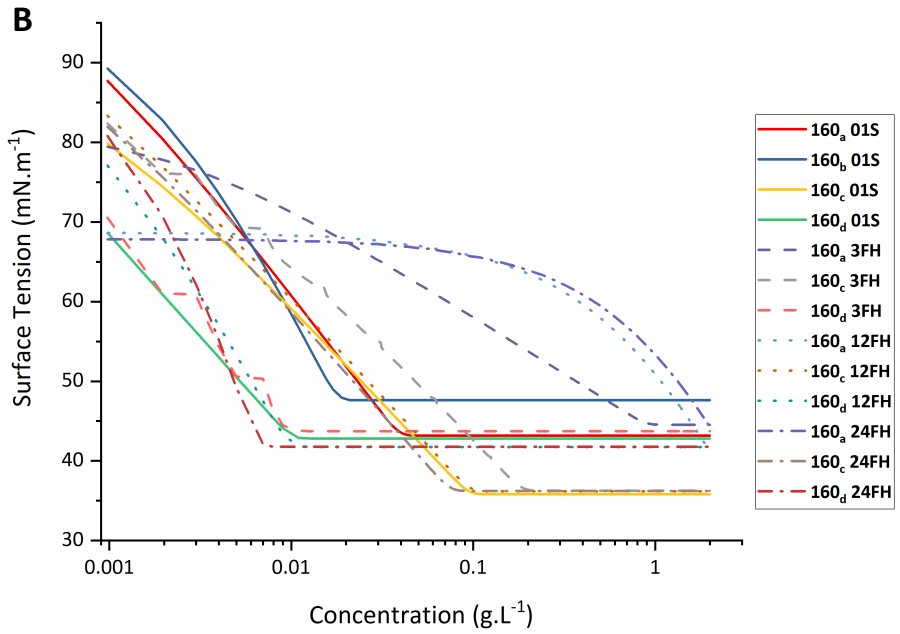
B
Surface Tension (mN.m-1)
90
80
70
60
50
40
30
0.001
0.01
0.1
1
Concentration (g.L-1)
160a 01S
160b 01S
160c 01S
160d 01S
160a 3FH
160c 3FH
160d 3FH
160a 12FH
160c 12FH
160d 12FH
160a 24FH
160c 24FH
160d 24FH

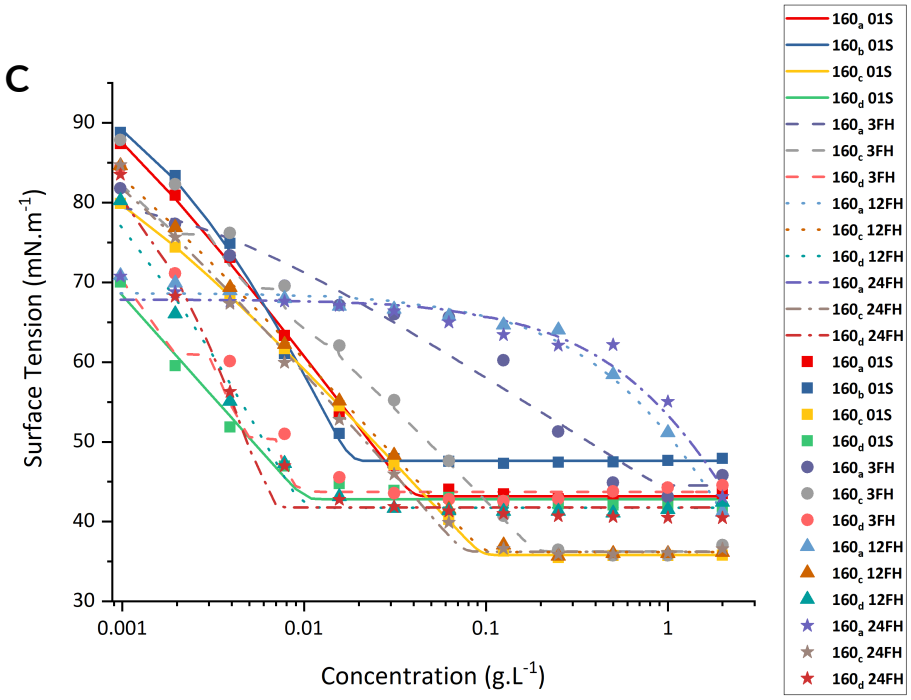

*Figure 54 Surface tension versus concentration plots of the FSS candidate compounds **A**: Raw data smoothed; **B**: Fitted model as developed by Al-Soufi et al.[264]; **C**: Comparison of raw data (marker) and fitted model (lines). Data were processed using OriginLab software 2019 (Version 5.0.0)*

All CMCs of compounds represented in Schemes 16 & 17 (pp. 206 & 208) are collated in Tables 18 & 19 respectively, with the addition of SDS and LAS. The CMCs of the synthesised FSS **Family 3** are represented in Table 20 for different water hardness. In all cases, surfactants synthesised in this study displayed an exceptionally lower CMC than the previously reported FSS (see Table 18 and 19). Indeed, CMC values for **Family 3** between 0.01 and 0.09 $g.L^{-1}$ (for 01S solutions) were observed, whereas few reports were made of furan derived surfactants with a CMC lower than 0.1 $g.L^{-1}$ (see below Table 18-20).

Table 18 CMC values of the structures corresponding to Scheme 16 p. 206 and industrial surfactants LAS and SDS

Surfactant structure	Chain length (n)	Branching	CMC ($g.L^{-1}$)	Ref
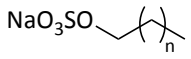 **SDS**	10	No	2.010	45
	10	No	2.365	238
	10	No	2.336	264
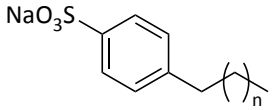 **LAS**	10	No	0.460	45
	10	No	0.418	238
	10	No	0.572	264
	8-12	No	0.080	255
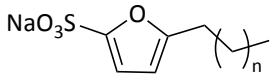 **140**	7	No	2.669	45
	12	No	0.72	
	14	No	0.267	
	18	No	0.316	
	8-18	No	0.512	
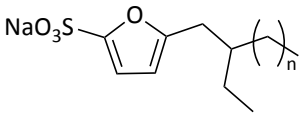 **141**	9	Yes	0.510	
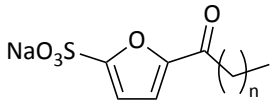 **142**	10	No	11.520	
	12	No	3.127	
	16	No	1.156	
	6-16	No	4.890	
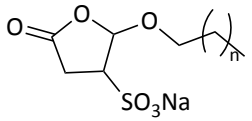 **145**	6	No	9.085	238
	8	No	2.001	
	10	No	0.302	

Table 19 Structure and CMC values of the structure corresponding to Scheme 17, p. 208.

Surfactant structure	Chain length (n)	Branching	CMC ($g.L^{-1}$)	Ref
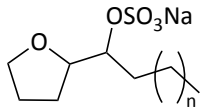 **147**	10	No	0.24	255
	12	No	0.01	
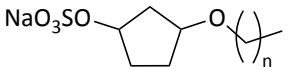 **151**	10	No	0.73	
	12	No	0.13	
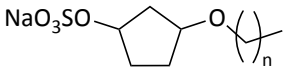 **or** 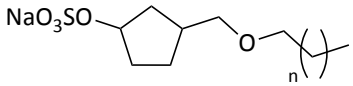 **156**	10	No	0.77	
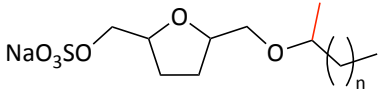 **157**	8	No	0.92	
	10	No	0.05	
	12	No	0.02	
	10	Yes	0.11	
	12	Yes	0.02	
	14	Yes	0.0004	

*Table 20 CMC values of the synthesised **Family 3** surfactants in this work*

Surfactant structure	Sample Number	Chain length (n)	Branching	CMC ($g.L^{-1}$)				Ref
				01S*	3 °fH	12 °fH	24 °fH	
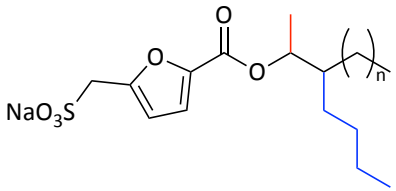 ***160***	**160_a**	9	No	0.032 ± 0.003	0.887 ± 0.527	N.D.	N.D.	This work
	160_b[a]	11	No	0.018 ± 0.001	N.D.	N.D.	N.D.	
	160_c	5	Yes	0.094 ± 0.002	0.187 ± 0.009	0.096 ± 0.006	0.074 ± 0.008	
	160_d	10	Yes	0.010 ± 0.002	0.012 ± 0.001	0.0097 ± 0.001	0.006 ± 0.001	

Different water hardness (expressed in French hardness degrees were tested, 01S corresponds to a 0.1 M NaCl solution). [a]**160_b** was not soluble enough in the 3 °fH for the CMC to be measured

Table 21 Interfacial values at CMC of the synthesised Family 3 surfactants in this work and reported interfacial values for furan derived surfactants

Surfactant structure	Sample Code	Chain length (n)	Branching	Surface tension at CMC ($mN.m^{-1}$)				Ref
				01S*	3 °fH	12 °fH	24 °fH	
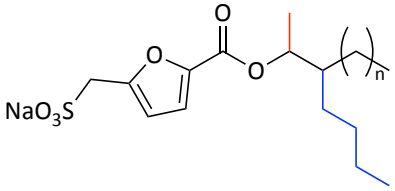 ***160***	**160_a**	9	No	42.5	45.2	N.D.	N.D.	This work
	160_b[a]	11	No	47.2	N.D.	N.D.	N.D.	
	160_c	5	Yes	35.8	36.2	36.1	35.9	
	160_d	10	Yes	42.0	44.5	40.9	40.5	
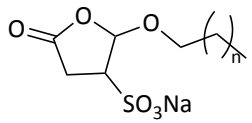 **145**[b]		6	No	29.1	-	-	-	238
		8	No	29.0	-	-	-	
		10	No	28.1	-	-	-	

Different water hardness (expressed in French hardness degrees were tested, *01S corresponds to a 0.1 M NaCl solution). [a]**160_b** was not soluble enough in the 3 °fH for the interfacial tension to be measured. [b]Tests performed utilising a different surface tension measurement apparatus

In comparison, LAS has a CMC between 0.42 and 0.57 $g.L^{-1}$ (bearing in mind that these measures were made at 60 °C, above the Krafft temperature). Only surfactants reported by Kipshagen *et al.* (Table 19, **157**) have values similar to those determined for our furan surfactants. Interestingly, Kipshagen's compounds are those that, structurally, most closely resemble the esters synthesised in this work. The (tetrahydro)furan ring is "in-line" with both a hydrophilic group (in **157** a sulfate and a sulfonate group in **160**) α relative to the 5-position and a linker (ether in **157**, ester in **160**) carrying the hydrophobic chain at the opposite side of the ring. In almost all cases, branching seems to have a positive impact by reducing the CMC values (see **141** Table 18**, 157** Table 19 and **160$_d$**, Table 20). The higher probability of interaction between branched chains during the micelle formation (favoured due to the decrease in entropy) may explain this result. Additionally, branched structures are more likely to cover a larger surface when at the water/air surface than linear structures, thus reducing the CMC, as branched surfactant molecules more rapidly cover the surface. The shape of the hydrophobic chain also influences the stability and structure of micelles. In 1986, Hoffman suggested that branched alkyl chains typically reduce the interface between water and hydrophobic chains which renders less likely the formation of micelles (higher CMC) contrary to the observation herein made.[265] Longer hydrophobic chains usually corresponded to lower CMC, which is also observed in these surfactants.[218,219,221,250,255]

The surface activity of our surfactants was good, with a drop of the surface activity at the CMC concentration down to 35.8 $mN.m^{-1}$ for **160$_c$**, around 42 $mN.m^{-1}$ for **160$_d$**, 42.5 $mN.m^{-1}$ for **160$_a$** and 47.2 $mN.m^{-1}$ for **160$_b$**. These values seem approximately two times higher than other previously disclosed surface tension values at CMC by Gassama *et*

al., but prior studies were often conducted at 25 °C, *i.e.* under the Krafft temperature of these compounds. Nonetheless, the average water surface tension being 72.8 $mN.m^{-1}$, these surfactants effectively decreased it by almost 50%, representing a significant surface activity. Lower surface tension is usually sought after in laundry detergent to increase the wettability of a surface and thus favour lipophilic stains removal by surfactants.

Promisingly, the **Family 3** surfactants appear, when soluble, to be remarkably tolerant towards differing water hardness. The branched surfactants **160_c** and **160_d** seem the least affected by increasing water hardness. Their CMC and surface tension at CMC barely varied when changing water hardness while the linear surfactants could not be solubilised in water hardness above 12 °fH for **160_a** and 3 °fH for **160_b**. Considering that water hardness varies considerably between even very close cities (from 10.3 °fH in York to 4.8 °fH in Leeds), having a surfactant with similar properties regardless of the water hardness is essential.[266,267] Thus far, the branched **160_c** and **160_d** surfactant seem to possess the required properties for detergent applications.

Surfactant mildness test

The mildness of the surfactant was then tested. This test measures the ability of a surfactant to solubilise the proteins present at the surface of human skin. Here, the corn-derived protein zein is used to approximate the structure of skin proteins. The amount of zein solubilised in the solutions containing the test surfactant (optionally with a dye) is measured by UV/vis spectroscopy. The greater the absorbance of the solution, the more zein is dissolved and the harsher the surfactants. A knowingly harsh (non-mild) surfactant (SDS) was used as a positive control, and two negative control were used: rhamnolipids (RL)

and DI water. Different water hardnesses were tested as well, and results are represented in Figure 55.

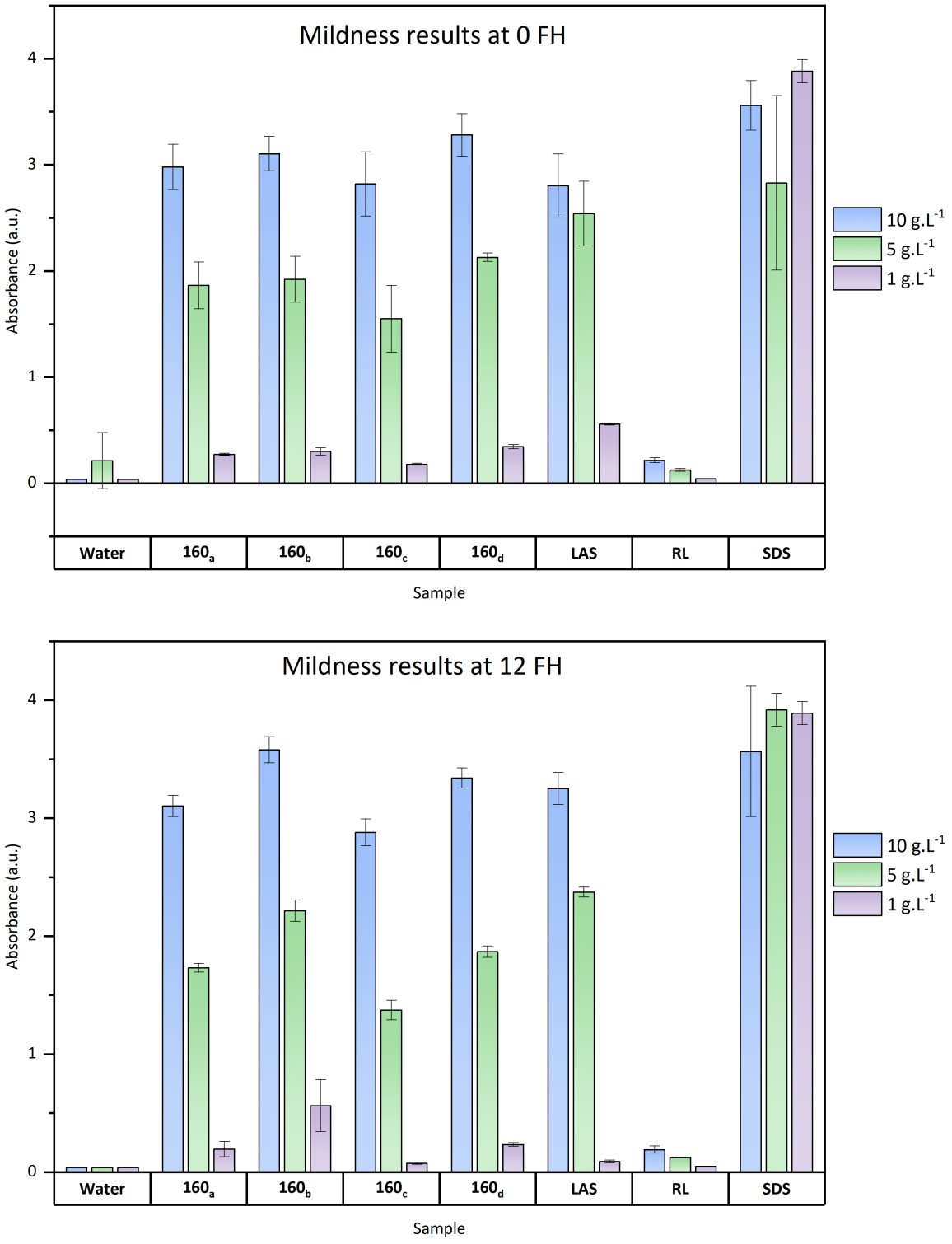

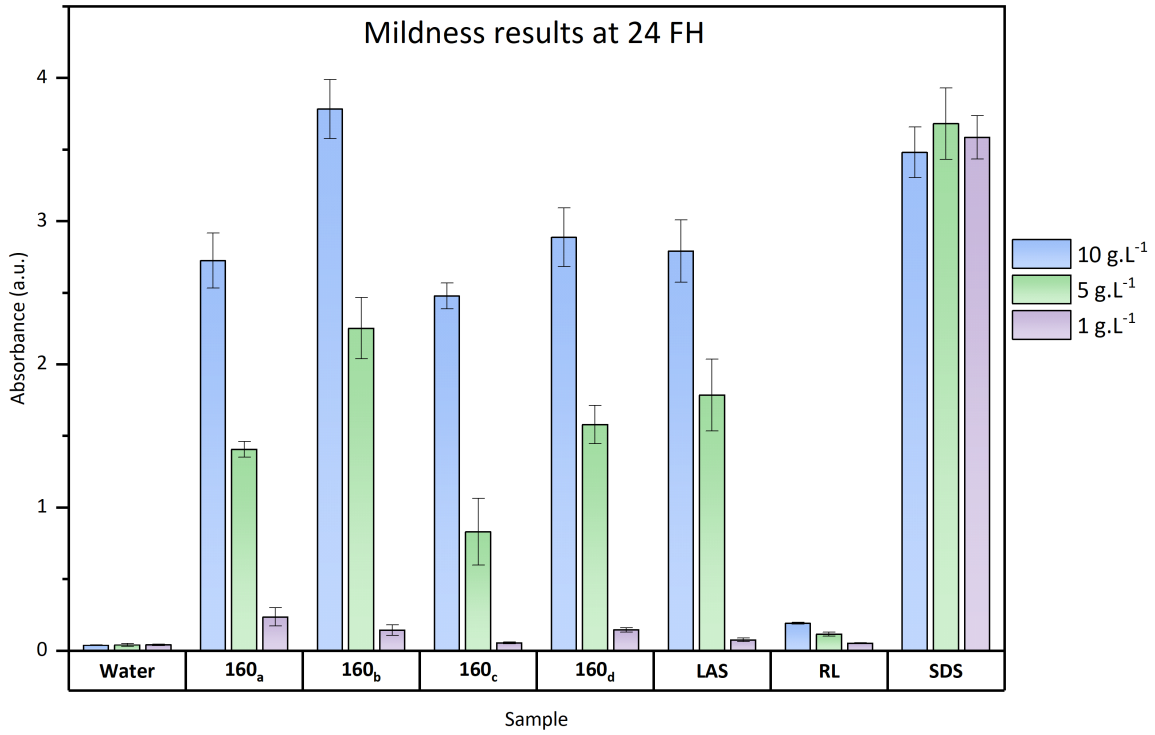

Figure 55 Mildness test results obtained for the FSS-Family 3 surfactants, SDS (positive control), rhamnolipid (RL) and water (negative controls). LAS was used as a comparison point. Different water hardnesses measured in FH (French hardness degrees) were tested

On average, the mildness of **160$_a$**, **160$_c$** and **160$_d$** is lower than that of LAS at 1 and 5 g.L^{-1} and significantly lower than SDS in soft water. At the highest concentration of surfactant, the FSS appear to be dissolving a higher quantity of zein, limiting their applicability for detergent applications. However, SDS is commonly used and is, as confirmed by the results above, a harsh surfactant. Values above the 1 g.L^{-1} concentration for **160$_b$** may be subject to caution due to its low solubility in water harder than 3 °fH.

Concurring with the previous results, the activity of the branched surfactants does not seem to be affected by the water hardness except in very hard water at 24 °fH where the absorbance seems to approximately decrease with a 0.2 factor. The best surfactants in terms of mildness seem to be **160$_c$** and **160$_a$**, having very similar, higher mildness than LAS regardless of the water hardness. At concentration as low as

1 $g.L^{-1}$, well above their CMC, all the FSS seem to be relatively mild, encouraging their formulation at a lower concentration. Considering the previous Krafft temperature, CMC and now, mildness results, the branched candidates **160_c** and **160_d** still appear as promising alternatives to fossil-derived LAS.

3.4.4 *BioLogicTool* analysis of FSS Family 3 and other anionic surfactants

BioLogicTool plots of LAS, **157** and **160_c** were constructed and represented in Figure 56. The highly optimised fossil-derived route of LAS logically gives an excellent *BioLogicTool score of 1.20* and *Total length* of 1.69. Unfortunately, the bio-derived routes necessitate more steps and intermediates to sulfonate the furan-derived compounds. This issue is highlighted by the higher *BioLogicTool scores*, -2.21 and -2.71 for the routes to **157** and **160_a** respectively. Optimisation of the synthesis to **160_a** will be necessary to be applicable on a larger scale and financially viable. For instance, a higher yield of esterification is likely to be obtained by recycling any unreacted material. Additionally, the iodo-intermediate **173_a** is possibly not required for a successful reaction, and these improvements can reduce the *BioLogicTool score* and the *Total Length* to -2.30 and 2.26 respectively (as shown in Figure 56**D**)

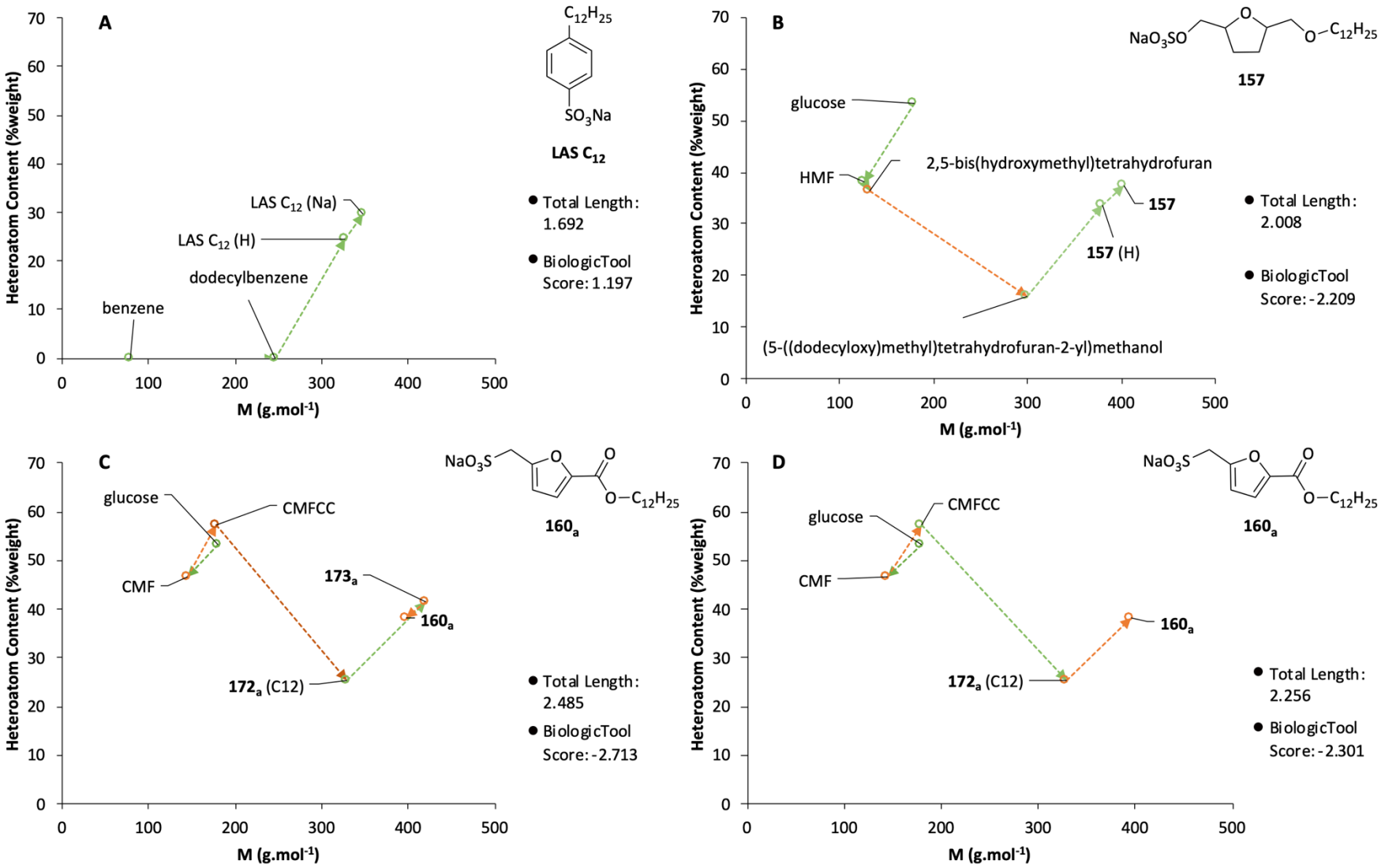

*Figure 56 BioLogicTool plots of the routes to LAS (C_{12}) (**A**), **157** (C_{12}) (**B**) **160$_a$** via **173$_a$** (**C**) **160$_a$** without intermediate **173$_a$** (**D**)*

3.4.5 Conclusion for chapter III.4

The search for FSS with a preserved aromatic furan ring core structure with similar or even better properties than LAS was undertaken. After modelling the cLogP and relative polar surface area of a potential library of FSS, five families were chosen for synthesis (by Unilever R&D). These families were based on platform molecules readily accessible from microalgae (CMF, HMF and furfural). Despite repeated attempts, common sulfonation reactions were unsuccessful with the chosen alkylfurans. More success with alternative sulfonation reactions was found (Strecker reaction), allowing surfactants from one family to be synthesised. The most promising **Family 3** based on an ester hydrophobic chain linker and a sulfonate α to the 5-position was prepared on a multi-gram scale and tested for their performance against LAS. Amongst the 4 members of this series, the two branched candidates **160$_c$** and **160$_d$** appeared to be the best in terms of Krafft temperature, CMC and mildness most of the time surpassing LAS physio-chemical properties. In addition, the presence of an ester hydrophobic chain linker is likely to provide a biodegradability pathway to these compounds, as hinted in previous reports for structurally resembling molecules.[150]

In keeping with the thesis goals, an additional surfactant product was obtained utilising a blend of fatty alcohols. This blend was chosen to represent the potential fatty alcohols obtainable from *Spirulina sp.* according to the fatty acid profile obtained from 4 different studies. Although the synthesis was a success, the insolubility of this product in water did not make it of interest for detergent applications. Instead, this blend of surfactant may be used as dispersants or emulsifiers in a more organic/oil-based medium.

Using the carbohydrate fraction to produce CMF and the fatty acids (as a fatty alcohol blend), gives rise to a potential microalgal multi-component biorefinery. The production of higher value-added products than biofuels alone could potentially render the microalgal technology profitable in a shorter than expected timeline. Yet, to become a truly multi-component biorefinery, a last non-negligible fraction must be used: proteins. The next chapters will focus on utilising this major biocomponent and more precisely the amino acids present in microalgae to produce value-added chemicals, thus completing the concept of a multi-component microalgae biorefinery or *Chemicalgal plant*.

Chapter IV
Use of proteinaceous waste from CMF-process

Part 1. Thermal decarboxylation of glutamic acid to γ-aminobutyric acid via microwave-assisted reaction[**]

[**] This section is adapted from the article: Lie, Y., Farmer, T. J. & Macquarrie, D. J. Facile And Rapid Decarboxylation Of Glutamic Acid To γ-Aminobutyric Acid Via Microwave-Assisted Reaction: Towards Valorisation Of Waste Gluten. *J. Clean. Prod.* **205**, (2018).
Y. Lie performed all experiments and wrote the corresponding article. Dr. T. J. Farmer and D. J. Macquarrie supervised the work and wrote the corresponding article.

4.1 Introduction: possible sources of nitrogen-containing platform chemicals

4.1.1 Current sources of nitrogen-containing molecules

A tremendous amount of speciality chemicals and bulk chemicals contain nitrogen, mostly as an amine or amide functionality. Chosen examples are given in Figure 57, where the volumes produced globally per annum are given for polymers, solvents and agrochemicals. The global market size in US dollars is indicated for pharmaceuticals (due to low production volumes).[7,268–272] These figures highlight further how nitrogen is a ubiquitous heteroatom essential in the chemical industry. Thus, in the perspective of a bioeconomy, sourcing nitrogen is a crucial problem to tackle. Currently, most of the nitrogen contained in these molecules originates from the Haber-Bosch process.[5]

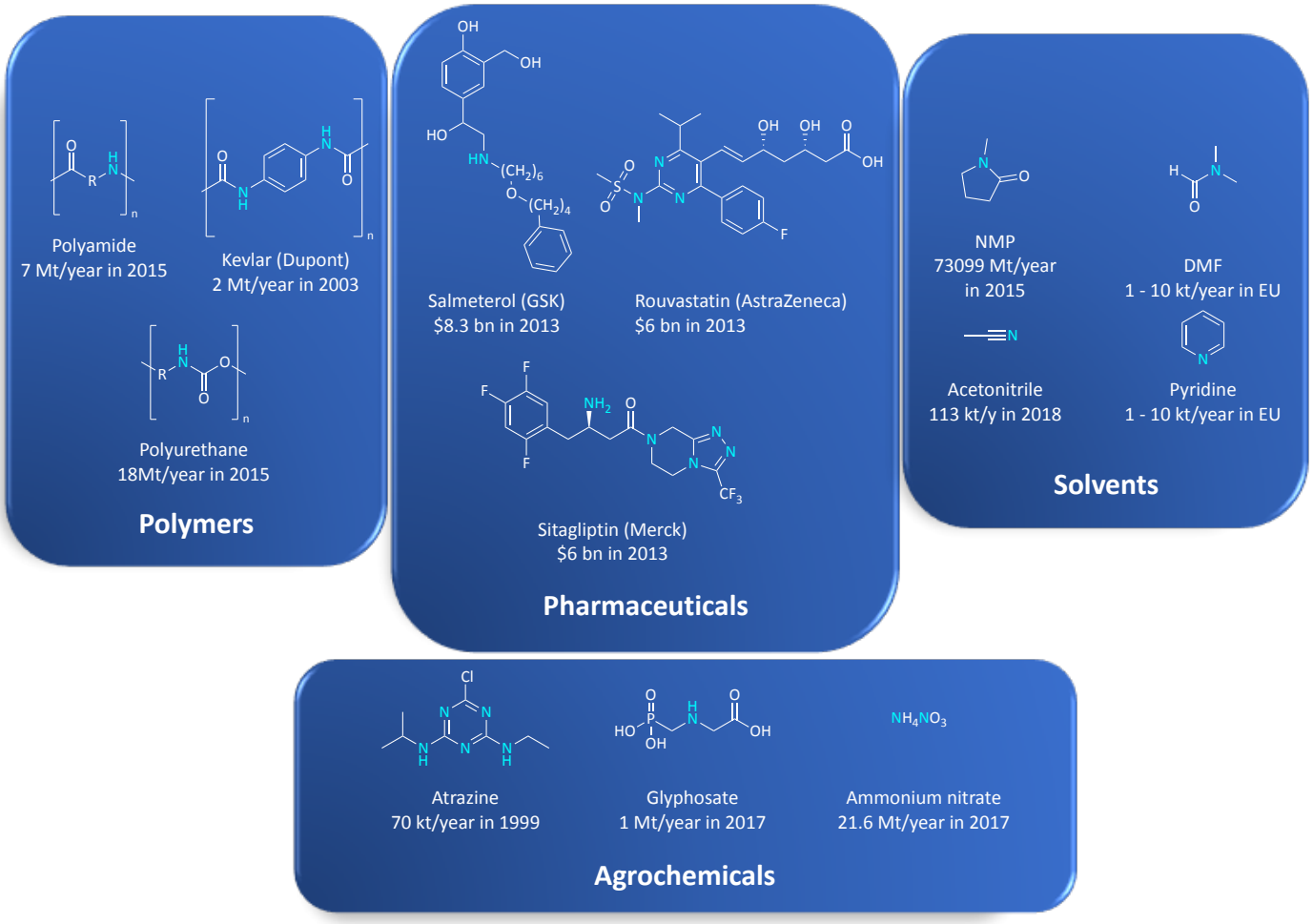

Figure 57 Example of nitrogen-containing molecules amongst polymers, pharmaceuticals, solvents and agrochemicals. Indicated volume of production (in kt or Mt per year) or market size were obtained from 1-6, ranges given for DMF and pyridine are from the ECHA website: https://echa.europa.eu/home (accessed 21/1/20).

Discovered by Haber at the beginning of the 20th century and later developed by Bosch, this process produces ammonia from dinitrogen, sourced from the air, and dihydrogen obtained from natural gas (or other hydrocarbons) via steam reforming (making CO and H_2). Despite the exothermic nature of this reaction (ΔH= -46.22 kJ.mol^{-1}), it commonly requires high pressure and temperature (typically 150 bar, 400-500 °C) and an iron catalyst.[273] These harsh conditions are necessary to activate the otherwise inert dinitrogen. Extensive studies and optimisation of this process over the years permitted to reach excellent ammonia yields (>99%) by feeding back unreacted gases in the reactors.

The importance of this reaction in the exceptional societal development observed from the beginning of the 20th century onward cannot be overstated. The development of the pharmaceutical industry, fertilisers, plastics, cosmetics etc., is intrinsically linked to the Haber-Bosch process. In 2019, the global ammonia production was approximately 170 Mt.[274] Nevertheless, the harsh conditions employed in this synthesis, the current source of dihydrogen (obtained from fossil-resources) and the scale to which it is implemented comes at a cost. It is estimated that ammonia production is solely responsible for over 1% of the global CO_2 emissions.[275] Many other side effects such as the release of fertiliser in oceans or the disruption of N_2 balance in the atmosphere, can also be attributed to the Haber-Bosch process.[5]

Current efforts to ameliorate the greenness of ammonia synthesis is underway. For instance, the use of renewable H_2 and energies can significantly enhance the sustainability of this process. Other technologies such as plasma-induced, electro- and mechanochemical ammonia syntheses were also recently reported.[274,276,277] On the other hand, alternative sources of nitrogen should not be dismissed, in particular when they are considered side-

products or waste of a process. For instance, proteins obtained from biomass are likely to become a promising source of nitrogen-containing molecules.

4.1.2 Potential for bio-derived nitrogen-containing platform chemicals: amino acids

Earlier chapters of this thesis mostly focused on using carbohydrates (chapter III.1-3) and lipids (chapter III.4) both obtained from microalgae during the CMF process. An ideal multi-component algal biorefinery should strive to use all biomolecules available to reduce the generation of waste from the beginning and make more value-added products. This approach is necessary to secure both the financial viability of the biorefinery and its place in a circular bio-society. For this reason, the following sections will focus on nitrogen-containing compounds derivable from proteins.

All types of biorefineries are expected to produce a large amount of proteins as side-products. Scott *et al.* estimated that with 10% of biofuels in the fuel economy, 100 million tons of proteins would be available.[278] Some of these are likely not suitable for human or cattle consumption because of severe pre-treatments (acid hydrolysis, solvent extraction etc.). Yet, proteins and specifically their constituent amino acids, represent a formidable potential source of nitrogen-containing platform molecules.[15]

Synthetic amino acids were first prepared by the Strecker process, where ammonia in the presence of hydrogen cyanide reacts with an aldehyde to form an alpha-amino nitrile. Subsequent acidic hydrolysis leads to the corresponding amino acid in a racemic mixture. This method remains a popular solution for the synthesis of unnatural amino acids, and

many reports of the asymmetric Strecker synthesis have been made.[279,280] Currently, naturally occurring amino acids are predominantly produced by fermentation of sugars (sucrose, glucose etc.), using genetically engineered microorganisms such as *Corynebacterium glutamicum*.[281–283]

These may also be obtained from denatured or partly hydrolysed waste-proteins (*e.g.* from the CMF process) from bio-refineries.[110] Although the direct use of the thus obtained amino acid blend would be desirable, the complexity of this mixture due to the variety of functional groups present commonly requires at least a partial separation and isolation of amino acids. Solutions such as electrodialysis, fractional precipitation or chromatography exist to isolate amino acids and valorise protein wastes.[103,284–291] In particular, most studies have focused on the isolation of glutamic acid, aspartic acid or lysine, due to their abundance in biomass (Figure 58).[110,287,292]

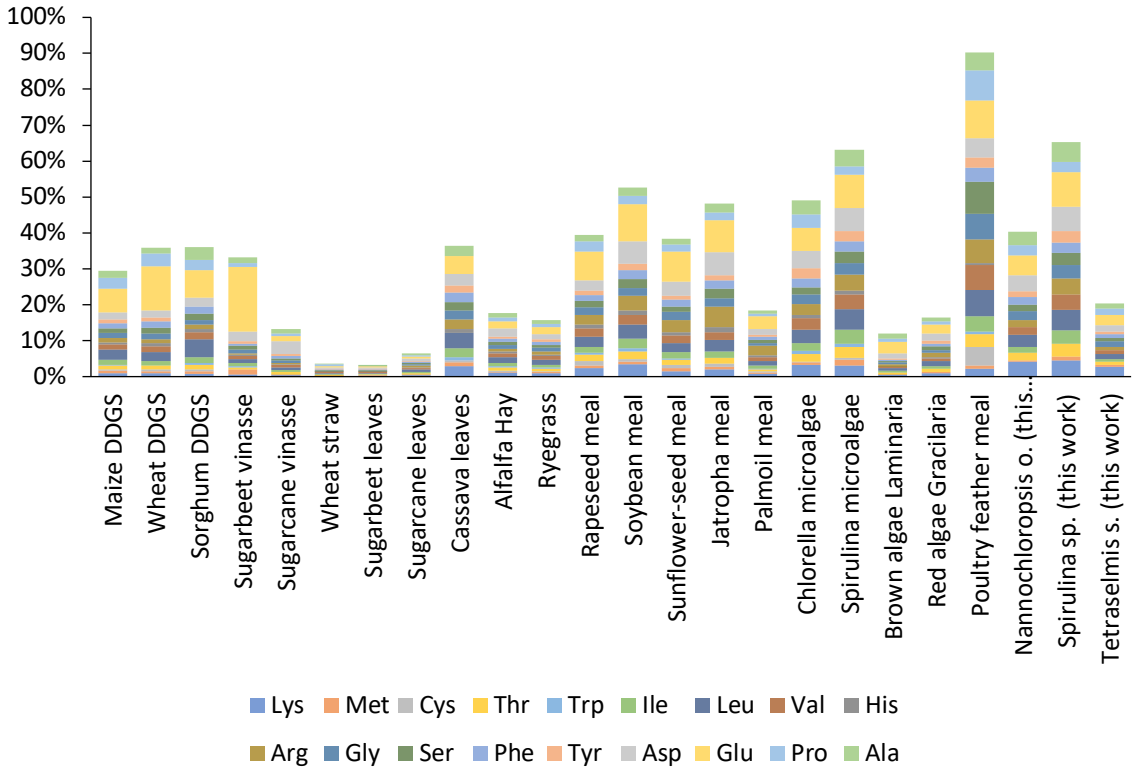

Figure 58 Relative abundance of naturally occurring amino acids (in %weight of amino acids in biomass) in different biomass and biorefinery waste-streams. Data were obtained from 20. Amino acid profile from the microalgae used in this work is also represented (see chapter III.1).

Isolated amino acids possess many functional groups (carboxylic acids, amines and phenyl or alcohols or alkyl etc.). Although valuable, these reactive functionalities may also lead to undesired side reactions (Scheme 26). Instead, selective protection or defunctionalisation may advantageously preserve the most interesting functionalities and allow the use of modified amino acids in well-established synthesis by mimicking the nitrogen-containing fossil-derived chemicals structures.

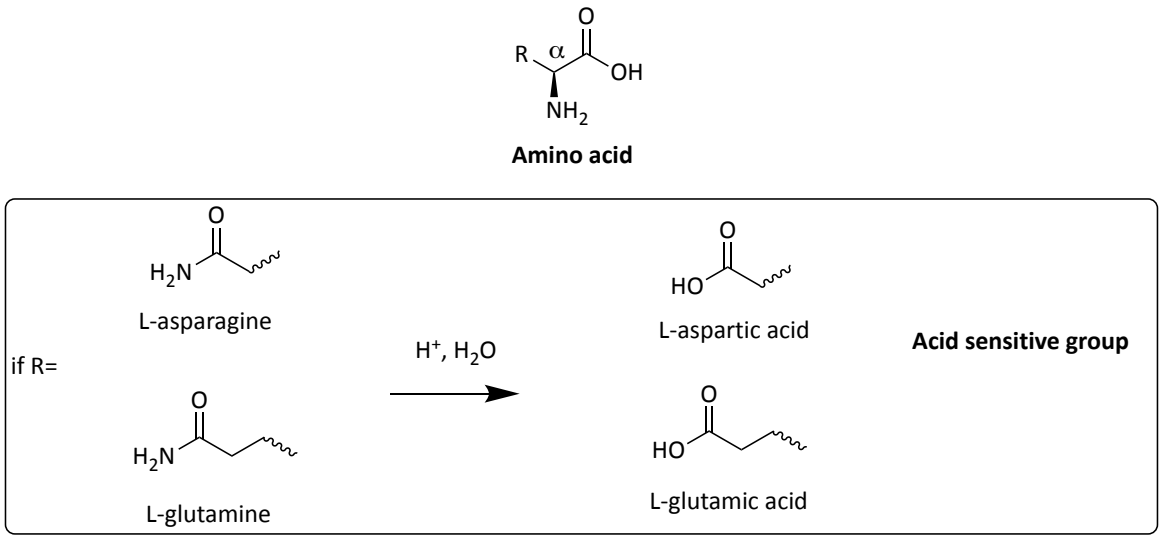

Scheme 26 Examples of sensitive functional groups found in some naturally occurring amino acids

Commonly, amine groups of amino acids are preserved while efforts are focused on the removal/deactivation of the carboxylic acid (Scheme 27). Reductive deamination reactions leading to higher alcohols or alkylamines (Scheme 27) and reduction of amino acids to amino alcohols have also gained interest over the years.[293–296] However, most of the attention focused on decarboxylation reactions, as explained in greater details below (see Scheme 27).

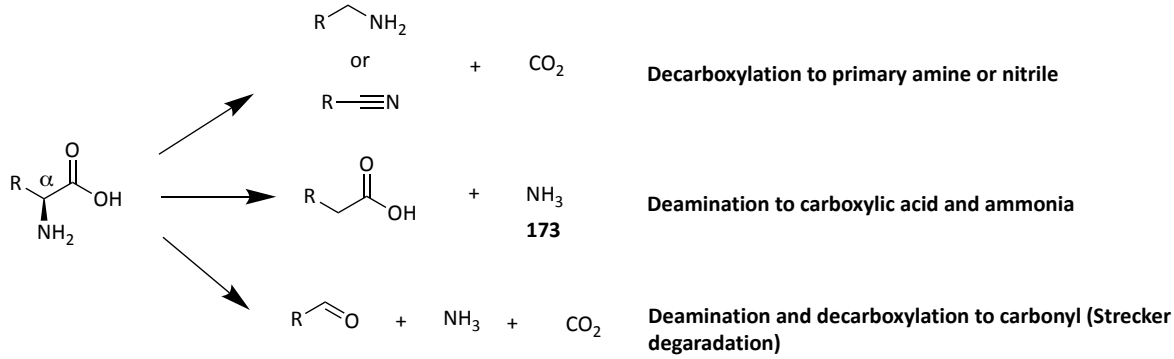

Scheme 27 Examples of selective amino acid defunctionalisation

4.1.3 State of the art on the decarboxylation of amino acids

Two types of amino acid decarboxylation currently exist one oxidative that leads to the nitrile equivalent of the amino acid, the other thermal organocatalysed route, producing the amine equivalent (Scheme 28). [6,297–301]

The oxidative decarboxylation of amino acids typically uses catalysts containing precious metal elements and a halonium source (often generated *in situ* from *N*-bromo succinimide, Br_2, *o*-iodoxybenzoic acid-IBX, Chloramine-T or NaOBr) sometimes in the presence of hydrogen peroxide.[6,297,302–305] The enzymatically catalysed oxidative decarboxylation of amino acid has also been described using vanadium chloroperoxidase.[306,307] Additionally, the electrochemical decarboxylation of amino acids to nitriles was also studied by Matthessen *et al.*.[308] Here, the electrogenerated hypobromite was considered the driving force for the reaction.

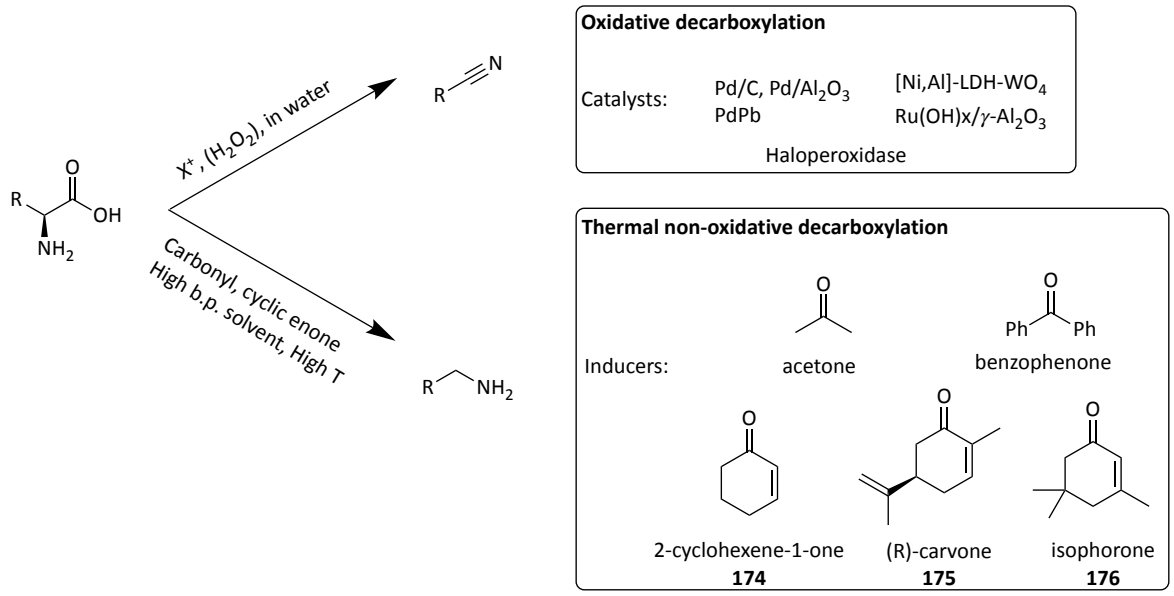

Scheme 28 Two main types of amino acid decarboxylation. Examples of catalysts are given for both types of reaction. R groups, corresponding to the different functional groups occurring in the natural amino acids represented in chapter III.1, Figure 17 p. 88

However, from a green perspective, hydrogen peroxide is a corrosive chemical that readily forms peroxide compounds with organic solvents and may lead to very unstable compound (*e.g.* when reacted with acetone forming explosive peroxides triacetone triperoxide). Besides, most halonium-giving species (NBS, IBX, NaOBr etc.) are corrosive and have potential acute toxicity. The conditions necessary to perform the Pd-catalysed decarboxylation are not ideal: 250 °C, 6 hours under an N_2 atmosphere.[309] Furthermore, the use of expensive and critical metals such as Pt (anode of the electrochemical reaction), Pd or Ru should be avoided on sustainability grounds.[310–312]

The organo-catalysed decarboxylation of amino-acids with carbonyls has been known since the early 20th century. Still, it has been sparsely investigated since initial studies using different carbonyls and select amino acids.[313–317] In a patent titled "*Process for decarboxylation of carboxylic acids*" isophorone (Scheme 28, **176**) was described as a potential organocatalyst for the decarboxylation of amino acids.[300] Isophorone is likely a greener organocatalyst to employ as it is made from acetone and is cheap (4-6 $.kg^{-1}). However, the given examples solely focused on the decarboxylation of lysine, with no evidence that other amino acids were suitable substrates for this method. In 2019, Claes *et al.* reported additional evidence that isophorone was a powerful organocatalyst for the thermal decarboxylation. Using as little as 5 mol% for 24 h at 150 °C in n-propanol yielded up to 99% methylamine hydrochloride from glycine. Unfortunately, this report showed that glutamic acid, the most readily available natural amino acid, did not decarboxylate, yielding only pyroglutamic acid or isopropyl pyroglutamate ester. Other research articles came to a similar conclusion using a structurally resembling carbonyl inducer (R-carvone, Scheme 28, **175**).[318,319] Furthermore, the original paper by Hashimoto *et al.* using a cyclic enone (2-

cyclohexene-1-one, Scheme 28, **174**) inducer did not mention glutamic acid nor pyroglutamic acid as a possible substrate.[299]

4.2 Aims of chapters IV - part. 1 and 2

As discussed in chapter III.1, glutamic acid and lysine are the two most abundant amino acids found in the tested microalgae. In this regard, the *Chemicalgal* biorefinery concept ought to use these molecules. Indeed, the aqueous phase left after the CMF process contains a large amount of small peptide and amino acids arising from the HCl hydrolysis of proteins present in the biomass.[117] The previous section highlighted the need to produce nitrogen-containing platform chemicals and bio-derived speciality chemicals. Proteins, and their amino acid constituents, represent an immense reservoir of such substances.[19] However, the selective separation of amino acids from protein hydrolysates is known to be difficult, and few reports have focused on their valorisation until now.[18,287] In this chapter, the thermal selective decarboxylation of amino acids is seen as a possible way to generate primary amines.

The first part discusses in greater detail the development of a carbonyl-induced decarboxylation protocol using isophorone. Attention was primarily focused on L-glutamic acid due to its reported intolerance to thermal decarboxylation conditions.[42,320,321] In addition, the selective extraction of glutamic acid from CMF-processed proteins waste was studied on gluten and microalgae. The possibility to decarboxylate the obtained biomass-derived glutamic acid was then evaluated.

In the second part, a similar approach was undertaken to optimise the decarboxylation of L-lysine to 1,5-pentanediamine. This aliphatic diamine inspired us to attempt its polymerisation with a bioderived bis-cyclic carbonate to produce a polyhydroxyurethane (PHU). PHUs are considered potential alternative polymers for polyurethanes whose synthesis require particularly toxic reagents (isocyanates).[322] In collaboration with Dr. Ian Ingram (polymerisation and characterisation), a PHU polymer could be obtained, which could find useful for automotive or insulation applications due to its self-blowing behaviour.

4.3 Isophorone-induced thermal decarboxylation of amino acids via microwave-assisted reaction: the case of glutamic acid

4.3.1 Scope of the decarboxylation protocol induced by isophorone

In the first instance, a series of amino acids was investigated using isophorone as an inducer for the decarboxylation. The summary of these reactions is represented in Table 22.

The decarboxylation of phenylalanine occurred in fair yield when 10% of isophorone was used to induce the decarboxylation (Table 22, entry 2) while using 2 equivalents decreased the yield of 2-phenylethylamine HCl (Table 22, entry 1 and 2). Previously, Jackson *et al.* reported an isolated yield of 76% when 2 equivalent of the carbonyl inducer (R)-Carvone was used. Although smaller, the yield reported here was obtained with a catalytic amount of isophorone, thus suggesting the superior inducing capability of isophorone as developed in the next sections.

The aromatic-moiety of phenylalanine likely helps drive the decarboxylation to completion by stabilising intermediates formed during the reaction (see the section below, 4.3.6). Indeed, other aromatic-group containing amino acids: L-histidine (imidazole group, Table 22, entry 4) and DL-tryptophan (indole, Table 21, entry 5) could be decarboxylated in 59% and 69% yield respectively.

Table 22 Series of amino acids tried in the decarboxylation reaction induced by isophorone

Entry	Amino acid	Hold time (min)	Yield (%)	Expected product
1	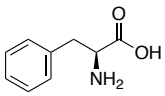 L-phenylalanine	5	47	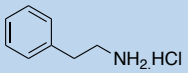 2-phenethylamine HCl, **177**
2[a]		5	68	
3	 glycine	12	47	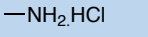 methylamine HCl, **178**
4	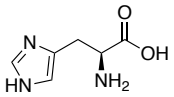 L-histidine	20	59	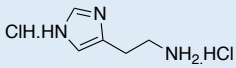 histamine dihydrochloride, **179**
5[b]	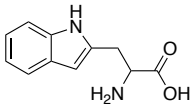 DL-tryptophan	20	69	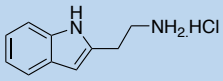 tryptamine HCl, **180**
6[c]	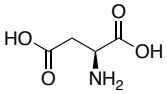 L-aspartic acid	12	-	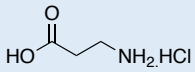 3-aminopropionic acid (β-alanine)
7[d]	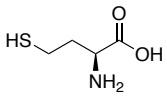 cysteine HCl	12	-	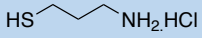 cysteamine HCl
8[d]	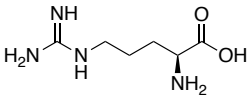 arginine	15	-	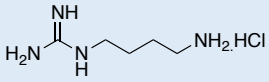 1-(4-aminobutyl)guanidine HCl (agmatine HCl)

General conditions used: amino acid: i) 5 mmol, isophorone: 5 mmol, n-propanol: 3 mL, target temperature: 180 °C. ii) 2 M HCl hydrolysis (10 mL) target temperature: 180 °C, hold time: 5 min. acetone used for trituration.

a) 10 mol% isophorone used (0.3 mmol), phenylalanine: 3 mmol, target temperature not hold for hydrolysis.

b) 20 mol% mmol of isophorone used (1 mmol), 6 mL of n-propanol. EtOH used for trituration

c) only orange brittle solid was obtained.

d) no product could be isolated

The simplest amino acid, glycine, could also be decarboxylated in 47% isolated yield using 2 equivalent of isophorone. Interestingly, some amino acids did not tolerate the conditions employed here, possibly due to a more delicate pendant group in, for instance, L-arginine (guanidino-group). Likewise, the decarboxylation of L-cysteine hydrochloride could not

proceed likely due to the degradation of the thiol group. In 2019, Claes *et al.* reported the detection of diethyl sulphide when the decarboxylation of cysteine was attempted (at 150 °C for 4 h or 24 h with 5 mol% isophorone loading) which may explain the degradation observed here as well. The use of the HCl salt of L-cysteine may also prevent the decarboxylation from occurring as discussed in section 4.3.6. Surprisingly, L-aspartic acid led to the formation of an orange brittle solid which did not form in the absence of isophorone. This plastic-like solid was also obtained when a catalytic amount of isophorone (20 mol%) was employed. This $CHCl_3$ and THF-insoluble solid could not be analysed by NMR spectroscopy nor GPC. However, FT-IR spectroscopy (see Appendix 15) a suggested poly(succinimide) formation when compared to previously reported spectra.[323] Although interesting, the obtention of primary amines was the focus of this chapter, and no further investigation on this product was undertaken.

Overall, the success of these initial decarboxylation reactions for some amino acids led to the trial of more substrates. Notably, in spite of the repeated literature reports on the inability to decarboxylate glutamic acid thermally, it was decided to investigate more in-depth its behaviour with the protocol developed here.

4.3.2 Specificity of glutamic acid regarding decarboxylation reactions

The abundance of glutamic acid residues in biomass protein and the microalgae studied in this work (Figure 58, p. 249) has naturally led to the assessment of its use as a platform molecule. Besides, It was included in the top-value added chemicals from biomass published by the DOE in 2004.[324]

Glutamic acid (Scheme 29, **53**) is one of the most produced amino acids (3.3 million $t.year^{-1}$ in 2016 globally) and is mainly used as a flavour enhancer (MSG) giving the well-

known “umami” taste.[325] It is possible to recover it from a protein hydrolysate at low pH specifically.[326] In fact, the original Ikeda method patented in 1909 to produce glutamic acid relied on the acid hydrolysis of protein-rich biomass, for instance, gluten. [326,327] Gluten is a co-product obtained during the industrial production of starch and is currently used as cattle feed [328].

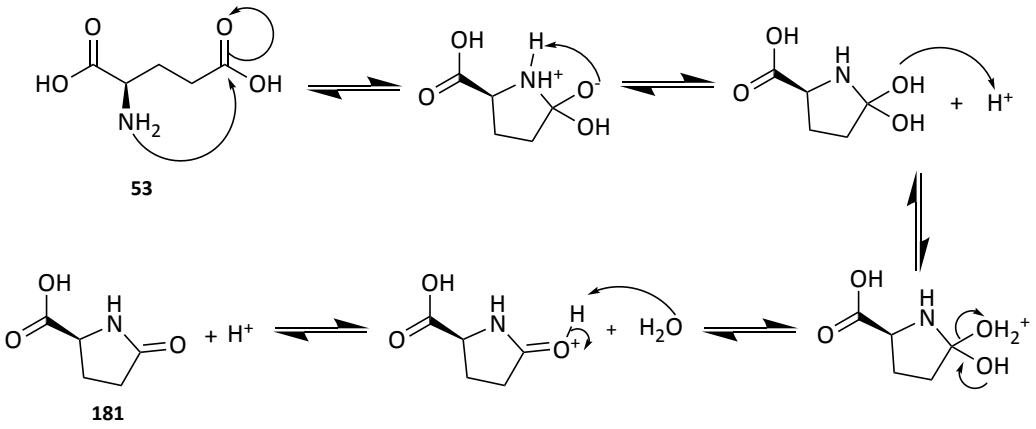

*Scheme 29 Mechanism of conversion of L-glutamic (**53**) to L-pyroglutamic acid (**181**)*

At high temperature (>120 °C) glutamic acid is thought to convert readily to pyroglutamic acid (Scheme 29, **181**), this being the dominant reported product.[286,309,329] Indeed, the decarboxylation at elevated temperature of glutamic acid is known to be particularly challenging relative to many of the other amino acids as a result of its preference to form **181**.

Glutamic acid decarboxylation to γ-aminobutyric acid (GABA, Scheme 30, **79**) has already been described using (immobilised) glutamic acid decarboxylase (GAD).[287,321] However, in most cases, the use of an expensive co-factor (pyridoxal phosphate, PLP) is necessary and additional costs of the enzymes and the immobilisation procedure are also required. Furthermore, despite the possibility to replace PLP with the much cheaper α-

ketoglutaric acid, the eventual deactivation of the GAD is unavoidable. [321] Recently, a solid-supported Pd/C catalysed decarboxylation of pyroglutamic acid (**181**), and glutamic acid via **181,** to 2-pyrrolidone (Scheme 30, **80**) was reported.[309] This method uses water as a solvent and does not require hydrogen peroxide or a halonium-giving species reducing the negative environmental impact.

Nevertheless, there is still interest in producing GABA more sustainably. Indeed, GABA contains a carboxylic acid and an amine group at the opposing ends of its carbon chain (ω-amino carboxylic acid). As such, it is a precursor for Nylon 4 (Scheme 30, **182**), N-alkyl pyrrolidone (Scheme 30, **183**) or pharmaceuticals (Scheme 30, **184**) and has been recently used for the synthesis of Racetams in a three-component Ugi reaction.[42,127,330–333]

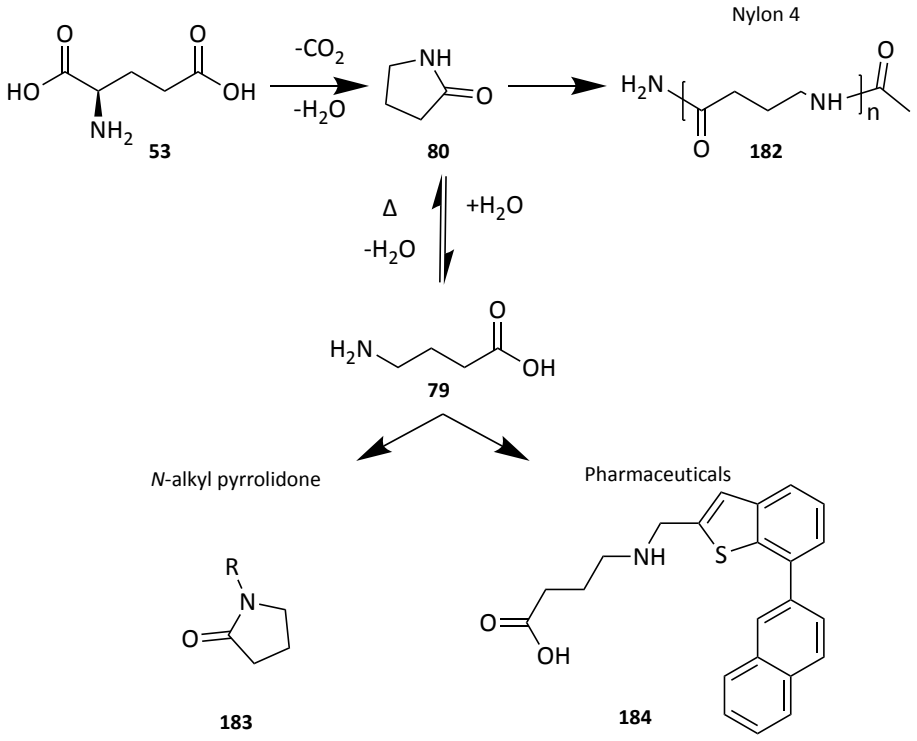

*Scheme 30 Use of GABA (**79**) for the production of pharmaceuticals, polymers or solvents*

4.3.3 Preliminary evidence of the possible glutamic acid thermal decarboxylation

First investigations into the decarboxylation of glutamic acid were conducted at a 2 mmol scale using two equivalent of the carbonyl inducer isophorone and heated in an *Anton Parr Monowave 400* microwave to 190 °C. Photographs were taken at regular time intervals to assess the completion of the reaction, as previously reported (Figure 59). [299,317,318] The reaction medium was observed to turn from an opaque suspension to a clear pale-yellow solution within 7-8 minutes (Figure 59, **C**-**H**). The yellow colouration was attributed to the imine formation (Figure 59, **185**) or isophorone-related impurities (dimer Figure 59, **186**) which are known to be present in impure isophorone samples.[334,335] The presence of compounds represented in Figure 59 could not be confirmed by GC-MS nor ^{1}H-NMR spectroscopy possibly due to the small concentration of these coloured side-products. A prolonged reaction time led to the browning of the reaction medium (Figure 59, **I**). This colouration was attributed to the further formation of impurities as above. Thus, 7 minutes was selected as the optimal reaction time for further optimisation.

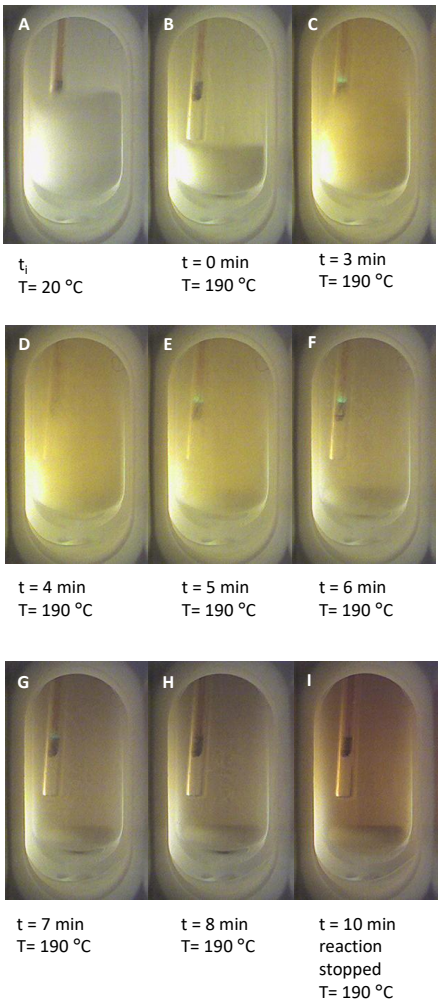

Figure 59 Photographs of the evolution of the reaction at different times. Possible structures leading to the yellowing of the reaction medium. Conditions: glutamic acid (2 mmol), isophorone (4 mmol), 3 mL n-propanol. Target temperature: 190 °C, 5 min ramping time.

Characterisation of the isolated product (HCl salt) was conducted with ^{1}H-NMR spectroscopy (Figure 60), and comparison with the ^{1}H-NMR (Figure 60) and FT-IR spectra (Figure 61) of the pure GABA HCl salt was made. This correlation confirmed the product was the expected primary amine and not pyroglutamic acid, its propyl ester, as described in earlier publications, or 2-pyrrolidone.[286,292,309] Zooming into specific regions of the IR spectra confirms the presence of both GABA and glutamic acid HCl in the final product. Two bands corresponding to the -C=O stretch of the carboxylic acids in glutamic acid (~1720 and 1625 cm^{-1}) whereas only one signal is present for GABA (~1725 cm^{-1}, Figure 61**A**). The

spectrum for the isolated product is a combination of both signals. Distinct peaks arising from the -C-N stretching in glutamic acid (1080 cm^{-1}, asymmetric stretch and 1000 cm^{-1}, symmetric stretch) are shifted to a lower frequency in GABA (-975 and 960 cm^{-1}, Figure 61**B**). This shift may be attributed to the higher probability for GABA to form hydrogen bond than glutamic acid due to the absence of the carboxylic acid α- to the amine. For similar reasons, the -N-H bending in glutamic acid appears as two distinct signals (870 and 825 cm^{-1}). In contrast, a broad peak probably due to signal overlapping is apparent in GABA's IR spectrum (780 cm^{-1}, Figure 61**B**). Further analysis (ESI-MS, CHN see experimental section) confirmed GABA presence in the decarboxylation product. Thus, the influence of two reaction parameters was subsequently investigated:

1. The HCl concentration used for the hydrolysis of the mixture during the second heating step (6 M or 2 M HCl solution as described by Jackson *et al.*) [318]
2. The isophorone loading (0, 0.1, 0.5, 1 or 2 equivalent)

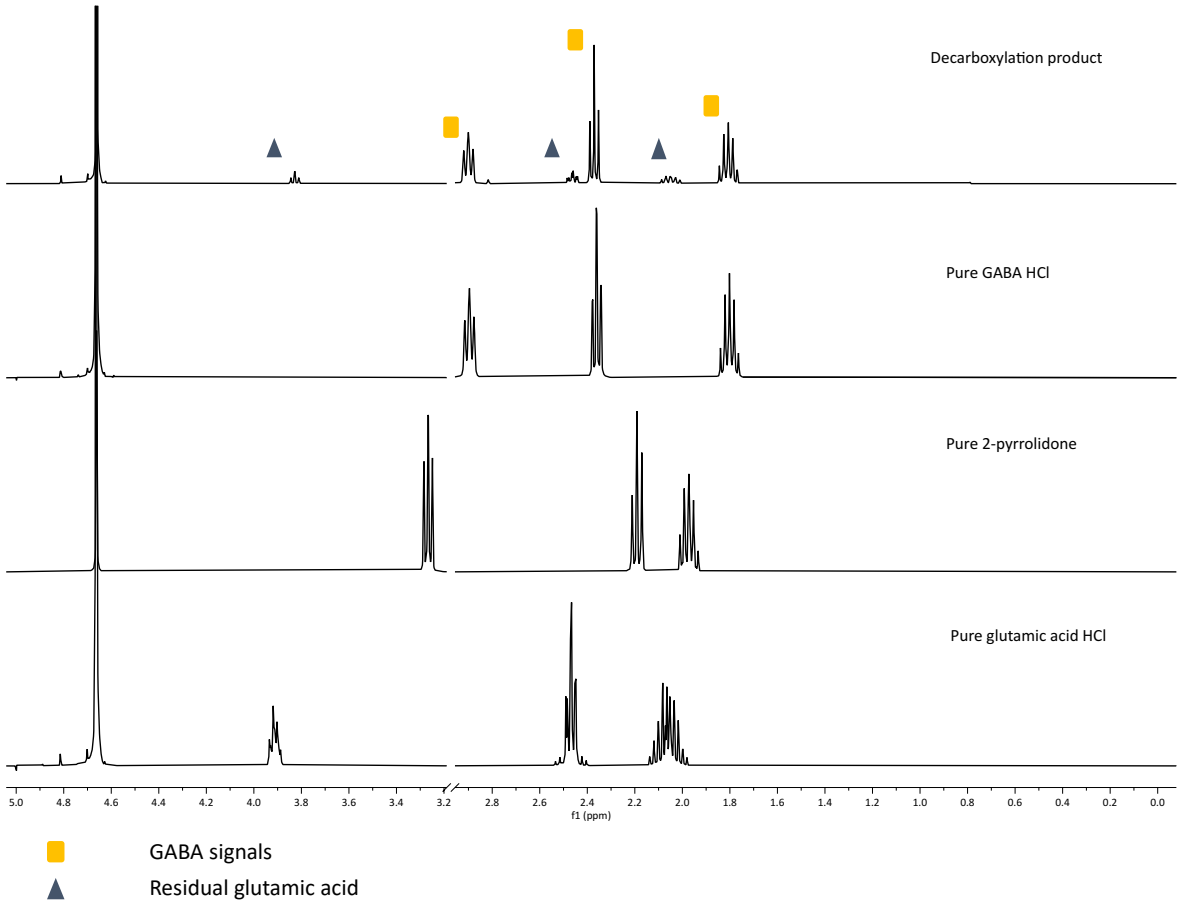

*Figure 60 Overlay of ^{1}H-NMR spectra of product of the reaction using glutamic acid (Table 22, entry 1, top spectrum), pure GABA HCl salt (**79** HCl salt, top middle spectrum), pure 2-pyrrolidone (**80**, middle bottom spectrum) and pure glutamic acid HCl salt (**53** HCl salt, bottom spectrum). Methylsulfone standard peak was cut for insert 3.1-3.18 ppm, NMR solvent = D_2O*

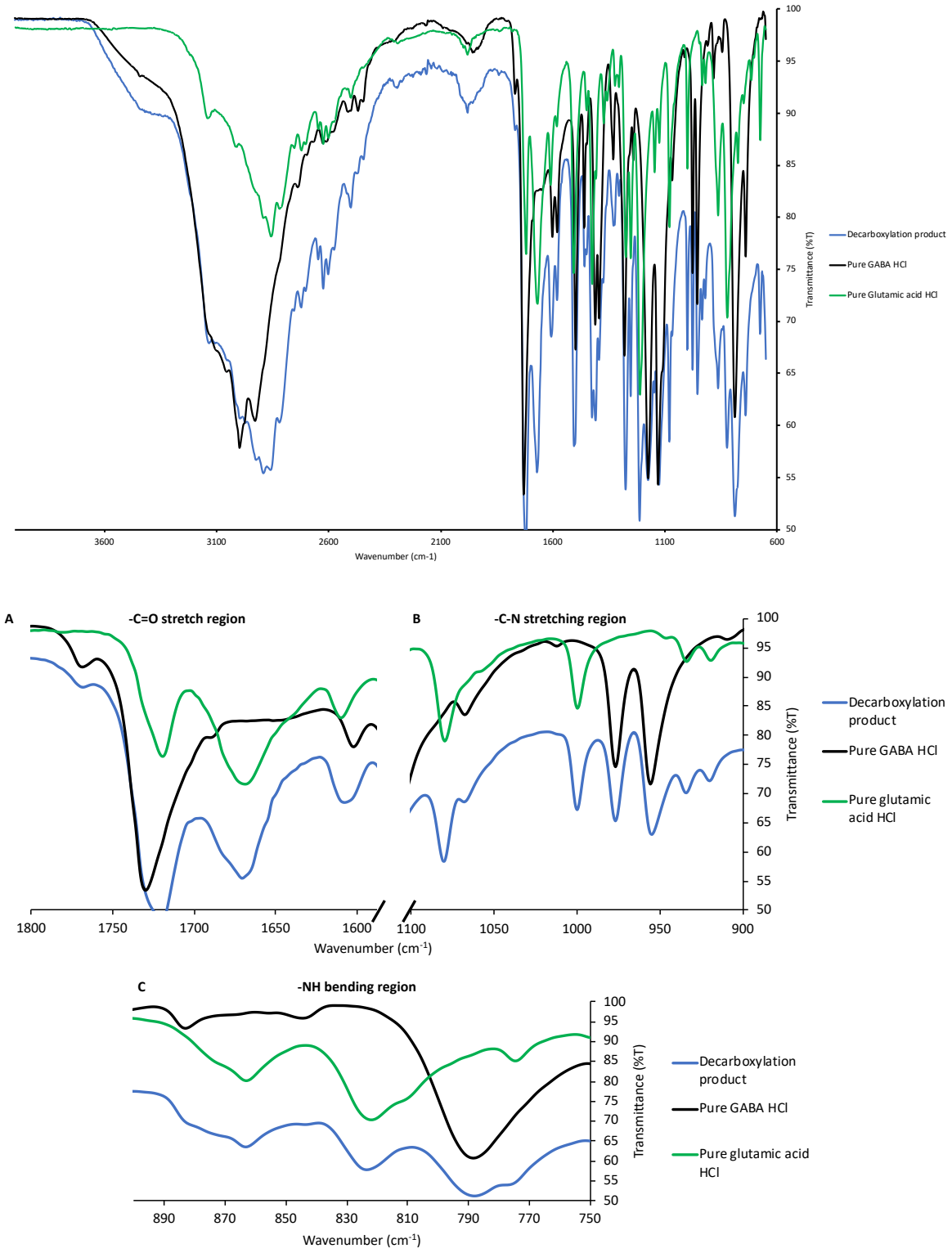

*Figure 61 Overlay of FT-IR spectra of pure glutamic acid HCl salt (**53** HCl salt, green line), pure GABA.HCl salt (**79** HCl salt, black line) and decarboxylation product (blue line). Conditions corresponding to Table 22, entry 1. Zoom on a specific region of the IR spectrum **A**: -C=O stretching region from carboxylic acid **B**: -C-N stretching region from primary amines **C**: -NH_2 bending region.*

4.3.4 Influence of the HCl concentration on GABA yield

The highest yields were obtained when heating for 20 min during the first reaction step, followed by using a 6 M HCl solution for the hydrolysis (entry 9, Table 22). However, a similar yield was obtained when heating for 7 min and using a 2 M HCl solution for hydrolysis (entry 5, Table 22). The ^{1}H-NMR (Figure 60, decarboxylation product spectrum, triplet signal ~3.8 ppm) and FT-IR spectra (Figure 61, green line, -C=O signal ~1680 cm^{-1}) show that residual glutamic acid (~20% by NMR spectroscopy) was also present. At 5 mmol scale, the concentration of the HCl solution did not appear to have a significant impact on the yield nor the mass ratio (Table 22, entries 5-10) of the final product.

Table 23 Summary of the decarboxylation reaction investigating the use of 6 M or 2 M HCl solution for the hydrolysis step at different scales and holding times.

Entry	Glutamic Acid	Time (min)	Isophorone loading (mmol)	HCl conc.	Mass ratio (%)	GABA Yield (%)*
1	2 mmol	7	4	2 M	76	56
2			4	6 M	59	49
3		13	4	2 M	57	51
4			4	6 M	21	21
5	5 mmol	7	10	2 M	79	63
6			10	6 M	70	53
7		13	10	2 M	61	48
8		20	10	2 M	67	50
9			10	6 M	69	65

*yield was calculated using the purity of the sample as described in experimental section, spectroscopy analysis.

Interestingly, the 2 mmol scale experiments displayed a different behaviour depending on the HCl concentration used. When the reaction was heated for 13 minutes, and a 6 M HCl solution was employed for the hydrolysis, a lower yield (21%, entry 4, Table 22) was obtained. On the other hand, no glutamic acid was detected in the collected product with ^{1}H-NMR spectroscopy (>98% purity using methyl sulfone as an internal standard).

However, when using the diluted 2 M HCl solution, glutamic acid was observed (purity between 70-85%, entries 1-3).

Reactions without a hydrolysis step but in the presence of glutamic acid and isophorone only resulted in 2-pyrrolidone, pyroglutamic acid (1:0.7 ratio) and isophorone (excess) detected in the crude product (Figure 62). This result confirms that the HCl hydrolysis step converts the initially formed 2-pyrrolidone product to GABA and that 2 M HCl is sufficient to separate impurities from the reaction medium. Thus, the use of a 2 M HCl solution and 7 min reaction time at 190 °C was used next to study the influence of isophorone loading on the reaction yield.

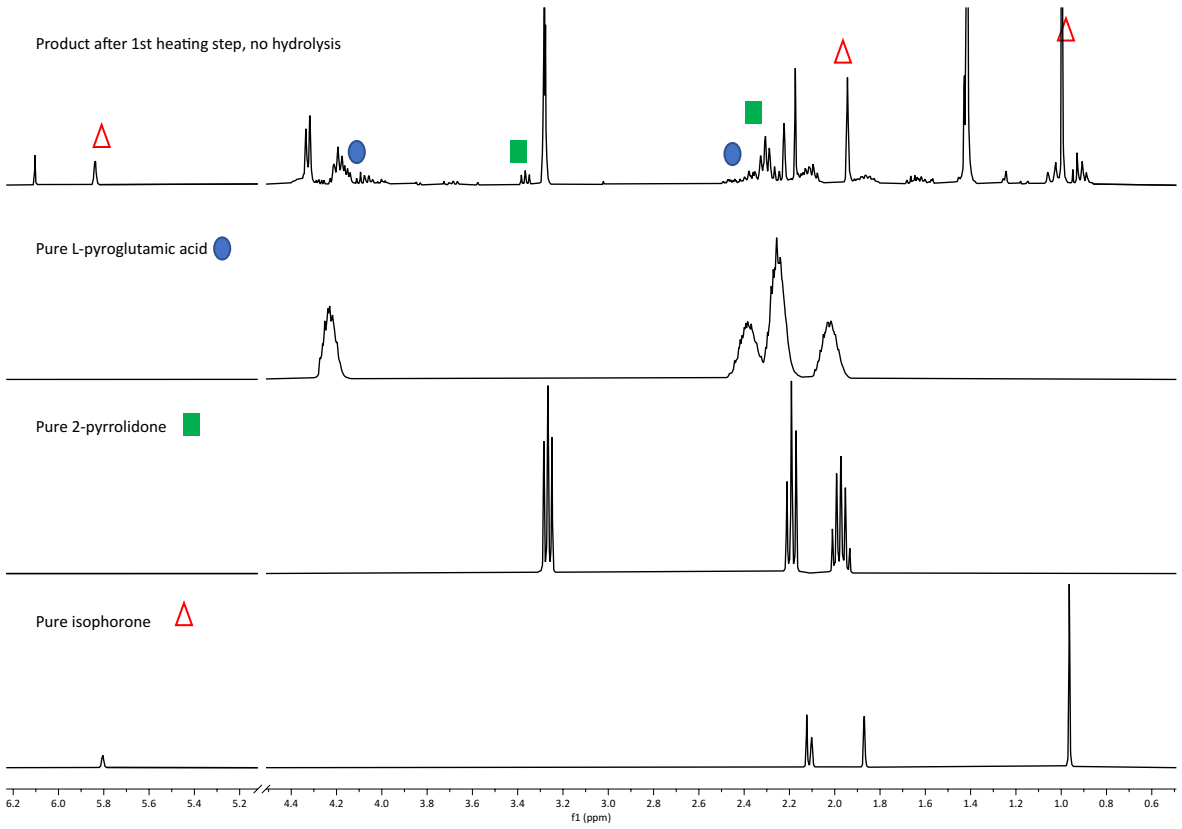

*Figure 62 ^{1}H-NMR spectra of the crude mixture after first reaction step (5 mmol, 2.2 eq. isophorone, bottom); pure 2-pyrrolidone (**80**, middle-bottom); pure pyroglutamic acid (**181**, middle-top); pure isophorone (**176**, top). Water peak was cut for insert 5-4.5 ppm, NMR solvent = D_2O for all except isophorone, $CDCl_3$*

4.3.5 Optimisation of the isophorone loading

No decarboxylation occurred in the absence of isophorone (Figure 63). After an aqueous work-up, the organic phase (0.125 g at 2 mmol scale) mainly contained pyroglutamic acid, *n*-propanol, and pyroglutamic acid propyl ester (~1:1.5:2) coming from the reaction between the former two, was confirmed with ^{1}H-NMR spectroscopy and GC-MS. After evaporation of the aqueous phase, the collected product was glutamic acid HCl salt (45% recovered), which further confirmed the conclusion made from Figure 63: the presence of isophorone is necessary for the decarboxylation to occur. Interestingly, under the same conditions (7 min hold at 190°C) a catalytic amount of isophorone (0.1 mmol, 2 mol%) led to a drop in GABA yield, the major product being glutamic acid HCl salt.

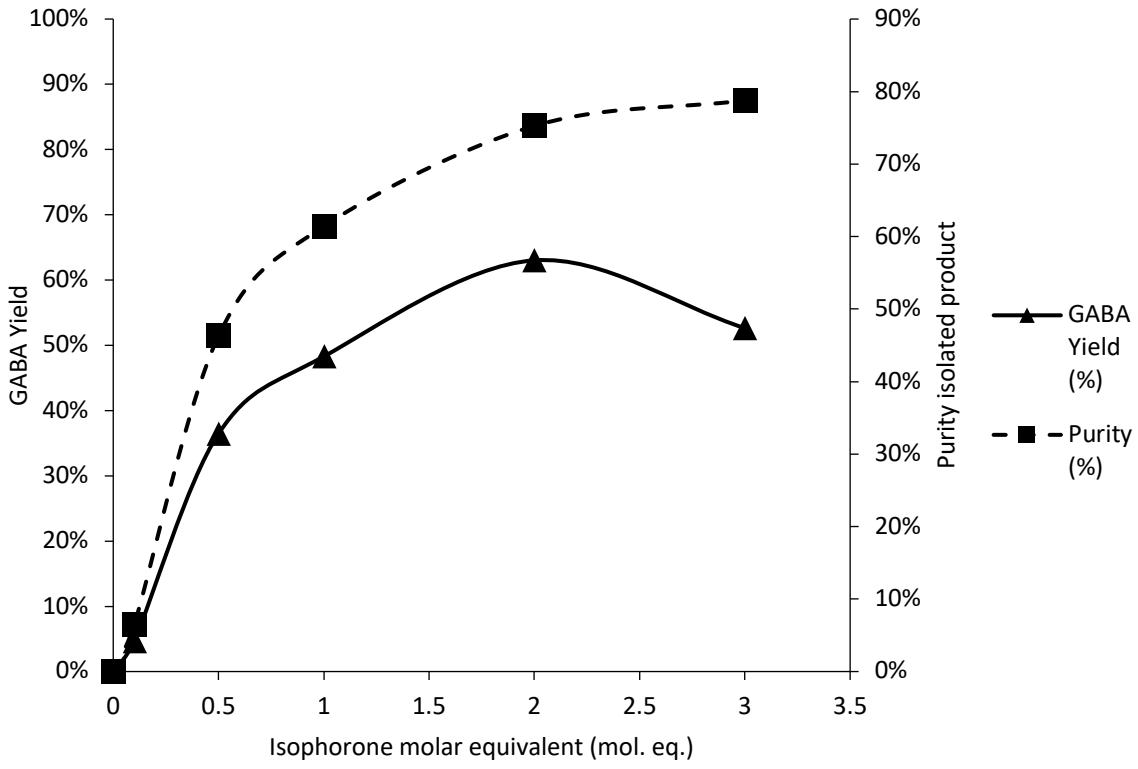

Figure 63 GABA yield and purity against molar equivalent of isophorone. Reaction conditions: 7 min holding time at 190°C, 5 mmol glutamic acid, 10 mL of 2 M HCl for the hydrolysis step

From Figure 63, it appeared that using more than a 2 molar equivalent of isophorone did not lead to a significant improvement in the yield nor purity of the isolated product. Using a catalytic amount of isophorone (0.1 mmol) for a prolonged reaction time (15 or 30 min), did not affect the final yield (7.5% and 4.5% respectively). From these observations, it can be concluded that using 2 molar equivalents of isophorone was necessary to obtain a good GABA yield. This result also suggests that, in this system, isophorone does not behave as a catalyst but as decarboxylation inducer. This conclusion further agrees with the results obtained by Claes *et al.* who did not observe any decarboxylation product with isophorone loadings of 5 mol%.[336]

Other impurities collected after the trituration step with acetone were analysed by GC-MS and were attributed to several side reactions (Figure 64). The formation of the impurity detected at 14.6 min is likely due to the reaction between 2-pyrrolidone and GABA to form 1-(4-aminobutanoyl)-2-pyrrolidone (Figure 64, i, **188**) (m/z = 171) or the esterification of pyroglutamic acid with propanol forming pyroglutamic n-propyl ester (Figure 64, ii, **187**) as reported before.[336] The other signals detected by GC-MS after 14.62 min are likely short oligomers of poly(glutamic acid) considering the regular spacing between the peaks.

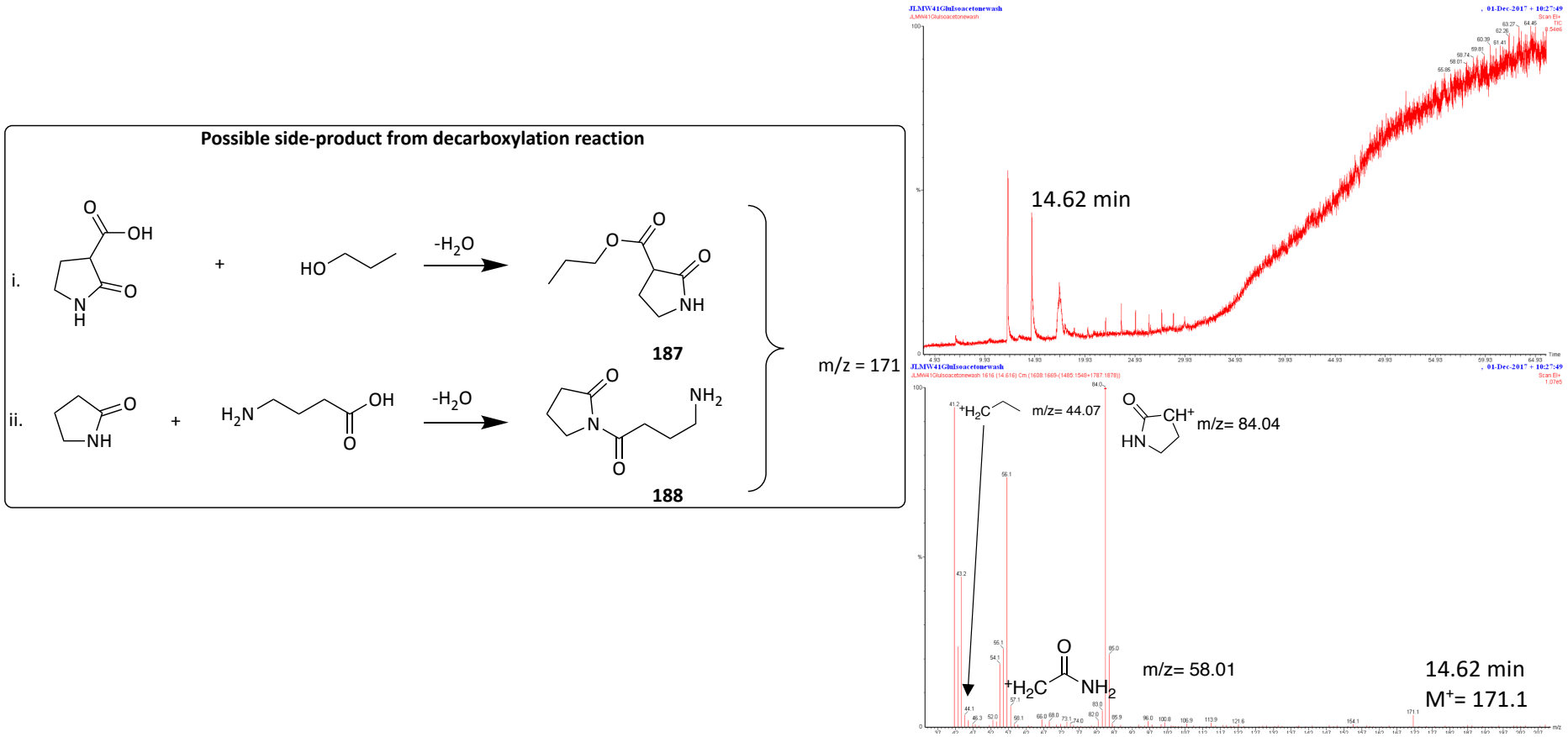

Figure 64 Possible structure of by-products obtained from acetone trituration residues as detected by GC-MS and attribution of some fragments for the detected m/z

A mechanistic investigation based on glutamic acid (protected) analogues and the reported products (pyroglutamic acid, 2- pyrrolidone and GABA) was performed to understand the thermal decarboxylation of glutamic acid.

4.3.6 Mechanistic investigation of the decarboxylation of glutamic acid

Since earlier studies stated that the pyroglutamic acid formation readily occurs at elevated temperature (>120 °C), the decarboxylation was attempted with this as the starting compound.[286] However, the main product obtained was instead glutamic acid with traces of GABA (93% mass ratio, 6% yield of GABA by ^{1}H-NMR spectroscopy). Because of the hydrolysis step, the lactam (Scheme 31, **181**) or Schiff base (Scheme 32 **189**) are hydrolysed back to the aliphatic amino acid (**53**). Therefore, the presence of GABA is likely due to the glutamic acid formation from pyroglutamic acid during the hydrolysis step. In turn, the former reacts with the isophorone remaining in the solution (Scheme 31).

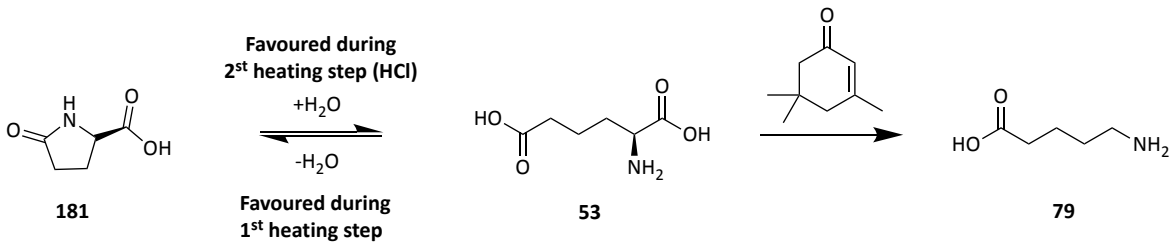

*Scheme 31 Possible GABA formation (**79**) using L-pyroglutamic acid (**181**) as a starting compound. L-pyroglutamic acid (5 mmol), isophorone (10 mmol), propan-1-ol (3 mL) i. MW 190 °C, 20 min, ii. 2 M HCl 190 °C no hold time.*

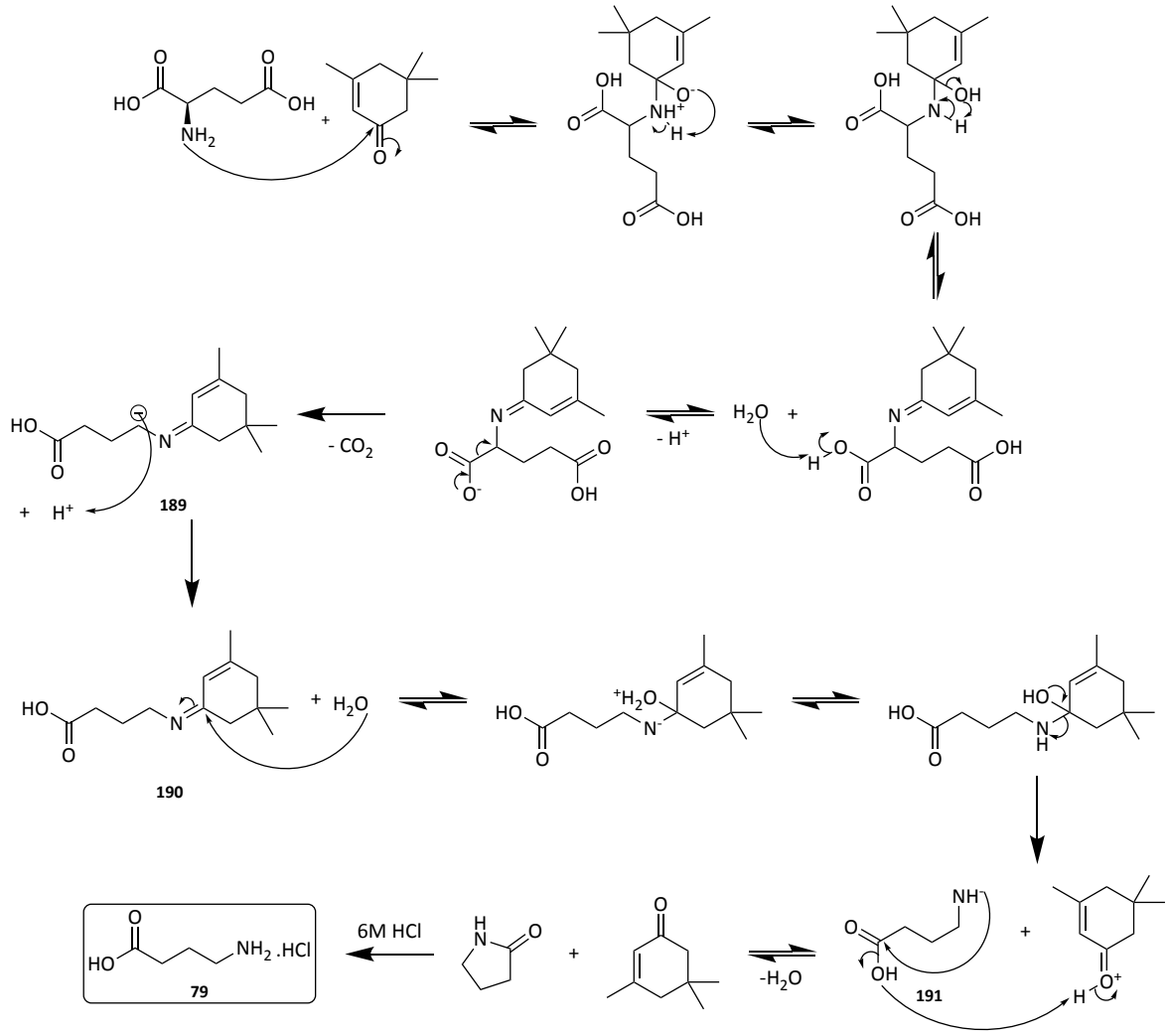

*Scheme 32 Proposed mechanism for the organocatalysed decarboxylation reaction of **53** to **79** (HCl salt) via HCl hydrolysis following Claes et al. suggested mechanism*[336]

This hypothesis could also explain the presence of glutamic acid as an impurity in the collected product from the standard reactions. In earlier studies by other groups, the pyroglutamic acid formation would occur before decarboxylation. This side-reaction could indeed lead to low yields for this particular amino acid.[287,309] As such, the protocol reported here seemingly reduces the pyroglutamic acid formation and represents an important step in the effective decarboxylation of glutamic acid.

The same protocol was also applied using GABA as a reagent. After the first heating step, the complete conversion of GABA to 2-pyrrolidone was observed by ^{1}H-NMR

spectroscopy (Figure 65). The second heating with HCl allowed its hydrolysis to form GABA, as confirmed when 2-pyrrolidone was used in the reaction system (GABA obtained with 90% mass ratio, 55%) for the previously indicated reason. Furthermore, using a protected version of glutamic acid (N-Fmoc, 5-OtBu, OH) did not afford any crystals, which again further agrees with Claes *et al.* when they attempted to used L-glutamic acid 5-methyl ester.[336] Traces of GABA could be detected by NMR spectroscopy likely due to the instability of these protecting group at high temperature and low pH. Using glutamic acid 5-methyl ester in the decarboxylation process resulted in a lower GABA yield (39 %).

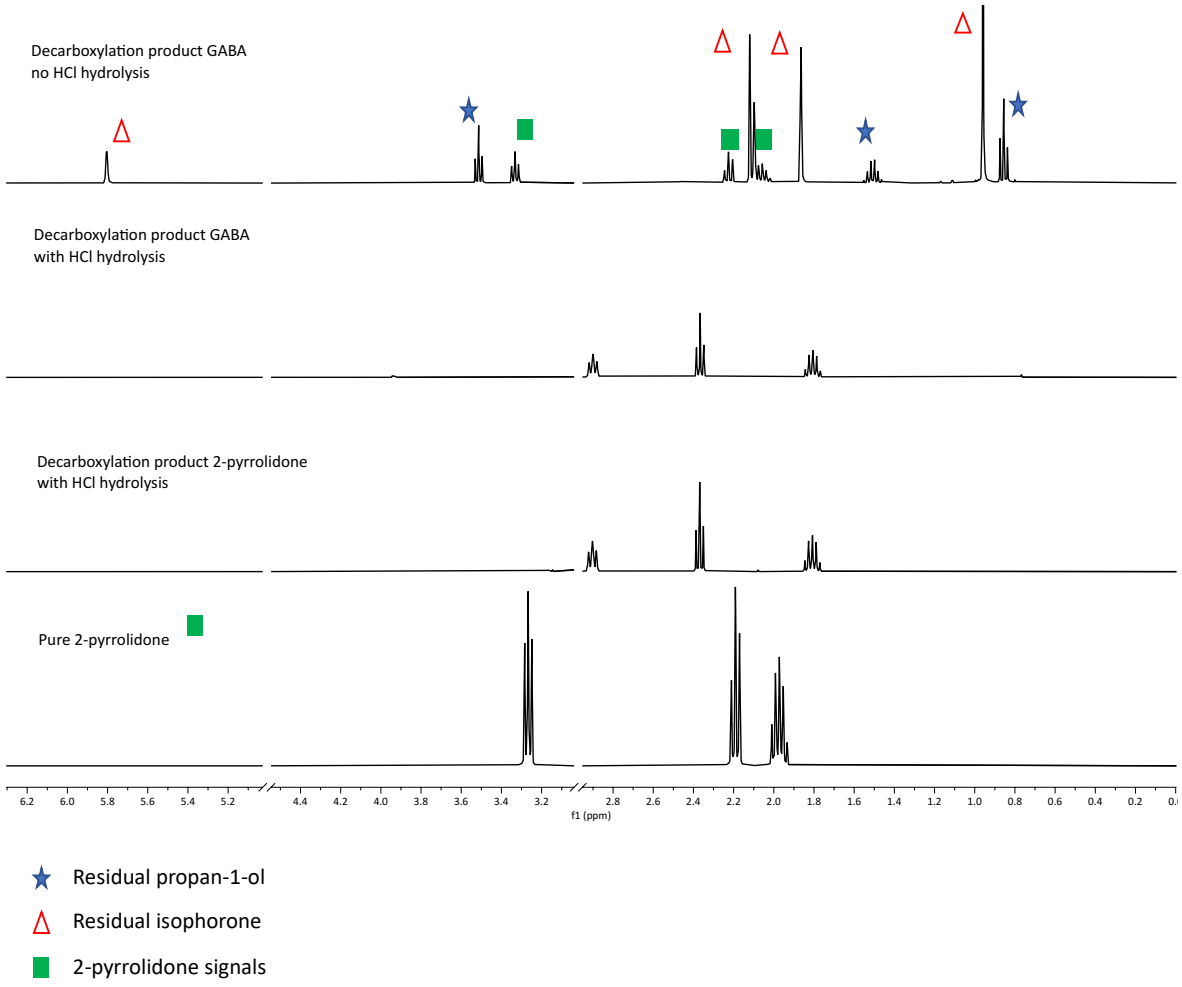

*Figure 65 Overlay of NMR spectra of decarboxylation product using GABA (**79**) as starting material without HCl hydrolysis step (top spectrum), with HCl hydrolysis (2 mmol scale, 10 mmol isophorone, middle top) or 2-pyrrolidone (**80**) with HCl hydrolysis (middle bottom) and pure 2-pyrrolidone (bottom). Water peak was cut for insert 5-4.5 ppm and methylsulfone standard peak for insert 3.1-3.16 ppm NMR solvent = D_2O. Conditions: GABA 2 mmol), isophorone (4 mmol), 2 mL n-propanol reaching 190 °C took longer ~10 min. 2-pyrrolidone (5 mmol), isophorone (10 mmol), 3 mL n-propanol.*

GC/MS confirmed the recovery of the excess isophorone. Commonly, 65% of the isophorone could be readily recovered according to GC-FID analysis. When the reaction was run at 5% molar equivalent of isophorone, glutamic acid was the main product (4 % GABA yield by ^{1}H-NMR spectroscopy), but 75% of the remaining isophorone could be

recovered. This result suggests that a side-reaction involving glutamic acid or its derivatives and isophorone can also influence the outcome of the decarboxylation.

Finally, it was proven possible to reuse the two organic fractions (containing both residual isophorone) obtained after an aqueous work up to run another reaction which afforded GABA at a reduced but still appreciable yield and purity (31% yield, 49.5% mass ratio). Higher yields were challenging to obtain due to the low mass ratio (Table 23, entry 4, p. 265). However, this represents a dramatic improvement compared to previous protocols where glutamic acid only afforded propyl pyroglutamate and none of the decarboxylated products GABA or 2-pyrrolidone.

From the result presented above, it appeared that two main competing reactions occurred: the formation of the Schiff base intermediate (Scheme 32, p. 271) and the conversion of glutamic acid (**53**) to pyroglutamic acid (**181**). Nevertheless, pyroglutamic acid hydrolysis could also happen during the reaction, which was promoted by the liberation of water during the imine formation. Overall, the reaction is driven towards the Schiff base formation due to the excess inducer used in this protocol. The presence of glutamic acid in the final product shows that the isomerisation into pyroglutamic acid could not be avoided entirely. However, Lee *et al.* showed that further purification using cation-exchange chromatography could afford GABA in high purity.[337] We postulated that the presence of 2-pyrrolidone in the reaction medium (prior to the hydrolysis step) is due to the rapid lactam formation from **191** also favoured by the high temperature herein employed.

This mechanism is similar to the one proposed by Claes *et al.* (reproduced Scheme 33) although no driving forces for the decarboxylation itself is identified. The decarboxylation happens spontaneously, and the intermediate carbanion (Scheme 33, **192**)

is stabilised by electron delocalisation via the aromatic amino acid pendants or α,β-unsaturated carbonyl catalysts, which is the driving force. This mechanism is supported by the facile decarboxylation of amino acids bearing an electron-rich moiety at the β-carbon (as observed in section 4.3.1). This proposed mechanism, similar to the PLP-dependent enzymatic decarboxylation mechanism, has the advantage of being a general mechanism valid for all amino acids that could be decarboxylated using this procedure.

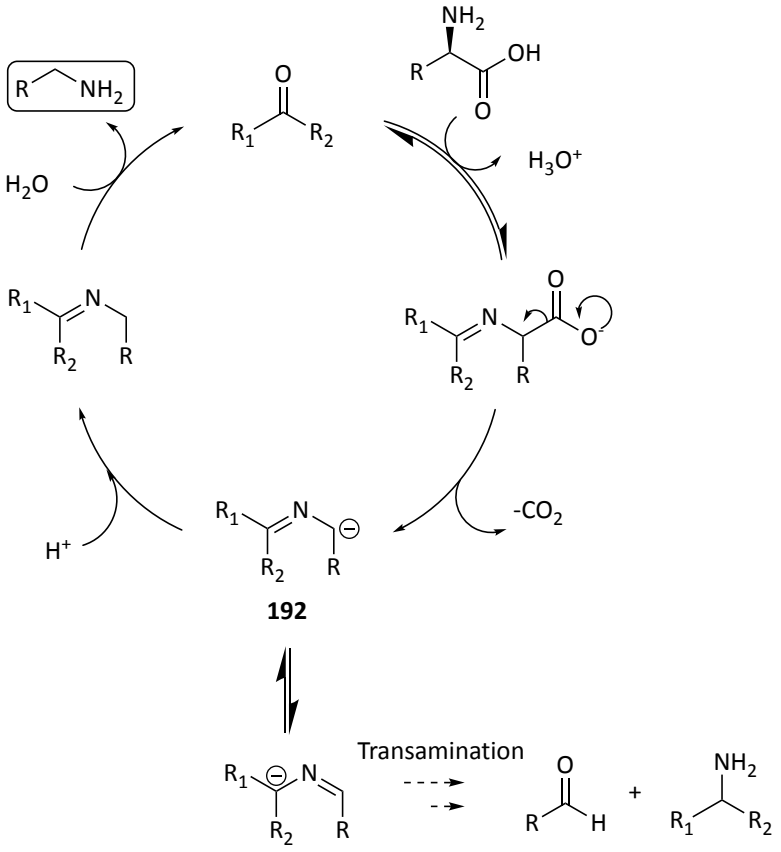

Scheme 33 Decarboxylation mechanism proposed by Claes et al. reproduced from [336]

Ultimately, the HCl hydrolysis step in the proposed mechanism for glutamic acid permitted the separation of the coloured impurities formed in the course of the reaction whilst also forming GABA HCl salt, the latter proving easier to isolate than its lactam counterpart 2-pyrrolidone.

It has recently been shown that microwaves promoted bubble-forming reactions.[338] This previous study suggests that bubbles disrupt the microwave field resulting in an over-heated zone in the vicinity of the bubbles, which can further drive the reaction.[338] Based on this recent observation, decarboxylation reactions are logically also likely to be promoted by microwaves. However, when conventional heating was applied, no significant difference was observed in yield (38%) or mass ratio (47% at 2 mmol scale) compared to our microwave reactions. Therefore, although benefits in using microwaves exist (improved efficiency, ability to stop heating instantly), the process is not reliant on this, thus showing the versatility of this approach, the conventional heating proving equally suitable. Ideally, the source of glutamic acid would be protein waste from protein-rich residues sourced from a biorefinery (Dried distillers grains with solubles – DDGS –, microalgae etc.). It was envisioned that using gluten derived glutamic acid as representative of DDGS-derived glutamic acid as reported by Sari *et al.* could demonstrate a possible way to valorise protein waste.

4.3.7 Production of glutamic acid from gluten

Originally, glutamic acid production was made by hydrolysing gluten in concentrated HCl as described in some patents.[309] Indeed, glutamic acid hydrochloride has a very low solubility at low pH (< 1). Furthermore, it has been postulated that the crystal system in which glutamic hydrochloride salts form prevents other amino acids from incorporating into it:

> "*In addition, the (glutamic acid hydrochloride) salt crystal itself has very high selectivity against other amino acids: L-glutamic acid molecules stack along the*

crystal's a-axis, linking α-amino N-H-Cl and γ-carboxyl O-H-Cl hydrogen bonds. Structurally, it is difficult for other amino acids to insert themselves into these growing crystals […]"[326,339]

Hence, after an HCl hydrolysis glutamic acid hydrochloride precipitates preferentially to the other amino acids. However, the need for a higher production capacity and a reduction of the hazards associated with HCl use led to a fermentation-based production.

Attempts to use the protein-rich aqueous phase left after CMF reaction work-up with microalgae, as described in chapter III.1, did not lead to any glutamic acid. Only inorganic salts could be isolated, likely NaCl from the marine microalgae. Thus, it was decided to try gluten in the CMF reaction and use the commonly discarded aqueous phase to obtain glutamic acid. In the context of a green economy using gluten as a feedstock, a co-product from the starch production industry (Figure 66) is pertinent.

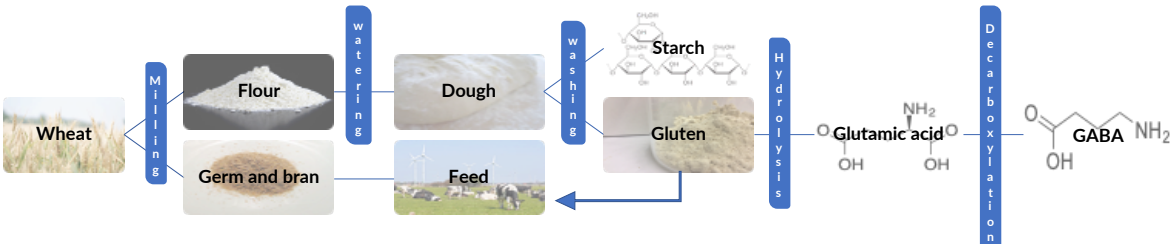

Figure 66 Valorisation of gluten from starch production as a feedstock for GABA synthesis

A low yield of CMF-lipid mixture was obtained ~5% mass yield (50 mg obtained from 1 g of gluten, Figure 67). However, since the gluten used had an advertised protein content of

>80% (TCI chemicals), this low CMF-lipid yield concords with the sugars and lipids remaining in this feedstock (likely< 20%).

After further hydrolysis of the aqueous phase and isolation, as described in experimental section p. 433, 110 mg of glutamic 90% pure could be obtained (assessed by ^{1}H-NMR spectroscopy Figure 67), 41% yield based on a glutamic acid content of 1.81 mmol per gram of gluten as reported by Sari *et al.*.[292]

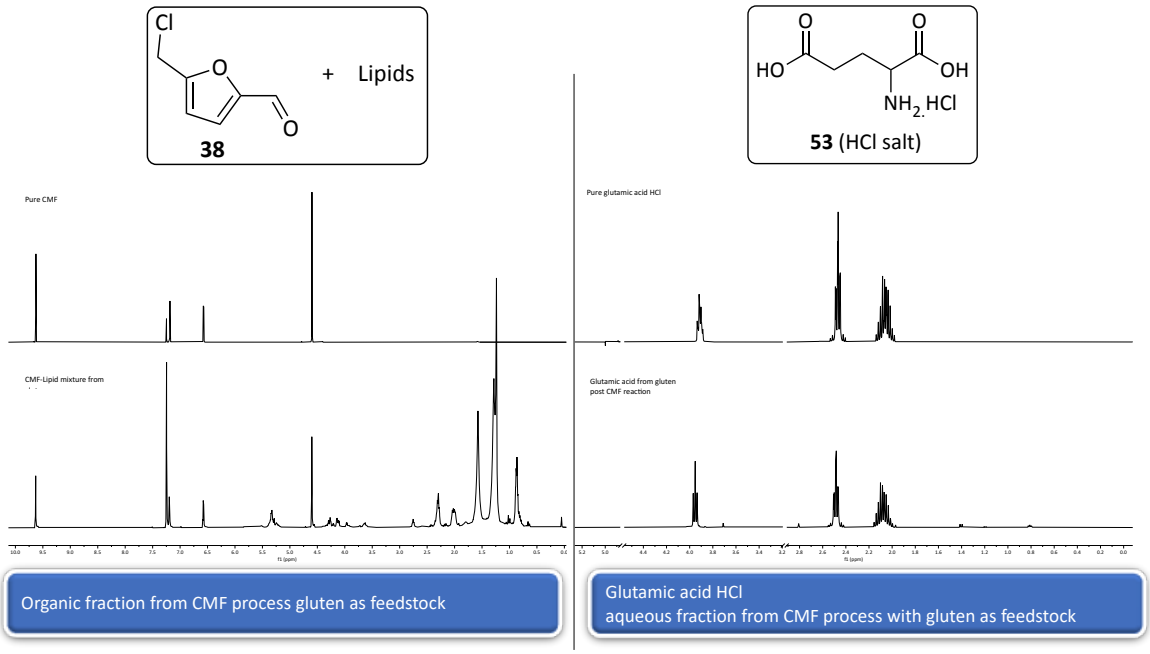

*Figure 67 NMR spectra overlay of pure CMF and collected organic product from CMF process using gluten as feedstock (left). ^{1}H-NMR spectra overlay of pure glutamic acid HCl and glutamic acid (**53** HCl salt) obtained from the aqueous phase obtained after CMF reaction work up and further hydrolysis (right). Methylsulfone standard peak was cut for insert 3.1-3.8 ppm, NMR solvent = D_2O was cut for insert 4.5-4.8 ppm*

This result showed that this method of obtaining glutamic acid could be a way to valorise the aqueous phase from the CMF process into a value-added product. Unfortunately, preliminary results of this method applied on aqueous phases of CMF reactions using

microalgae did not prove successful (no glutamic acid could be obtained). This valorisation approach requires further improvements based on each feedstock specificities.

To produce more gluten-derived glutamic acid, we envisioned that microwave heating could be used to isolate glutamic acid HCl from a protein hydrolysate. This heating method would also potentially streamline with the aforementioned decarboxylation.[106,340] Two different microwave conditions for gluten hydrolysis were compared (Table 24) that did not significantly differ in terms of glutamic acid yield, or the isolated product purity.

*Table 24 Summary of the glutamic acid (**53**) production from gluten using pressurised microwave vessel*

Temperature	150 °C	180 °C	110 °C (reflux)
Method	Microwave	Microwave	Conventional
Power	400 W	400 W	630 W
Time	30 min (+ 16 min ramping, 20 min cooling)	10 min (+20 min ramping, 20 min cooling)	24 h
Purity	86%	90%	94%
Isolated Yield	30%	34%	47%
mgGlutamic acid.W^{-1}.h^{-1}	1.49	1.73	0.01

• The yields were calculated assuming a glutamic acid content of 1.81 mmol.g^{-1} according to Sari *et al.*[292]

Compared to a conventional heating method (Table 23, far-right column), microwaves represent an excellent alternative to drastically reduce the hydrolysis time whilst maintaining a good yield and purity of the obtained product. When only the yield is considered, one may be tempted to think that conventional heating surpasses the microwave. However, when time and power are considered in the yield calculation, microwave heating appears ~10 times superior. This glutamic acid production method does

not require a neutralisation step which usually leads to a large amount of salt waste and necessitates further desalinisation either by dialysis or ion-exchange chromatography.

4.3.8 Decarboxylation of glutamic acid obtained from gluten

The decarboxylation reaction protocol described above was attempted with the glutamic acid hydrochloride salt isolated from gluten, though only a low yield of GABA (4%) could be obtained, the main product being residual glutamic acid (Figure 68, bottom spectrum). This result may indicate that the hydrochloride salts of other amino acids would not react as easily as their free bases. The presence of HCl in the first decarboxylation step, may lead to the protonated ammonium salt formation, which is not a nucleophile, unlike the amine free base. Assuming the rate-determining step in the mechanism involves the amine group (as discussed above), the suspected imine intermediate formation is disfavoured overall, during the decarboxylation.

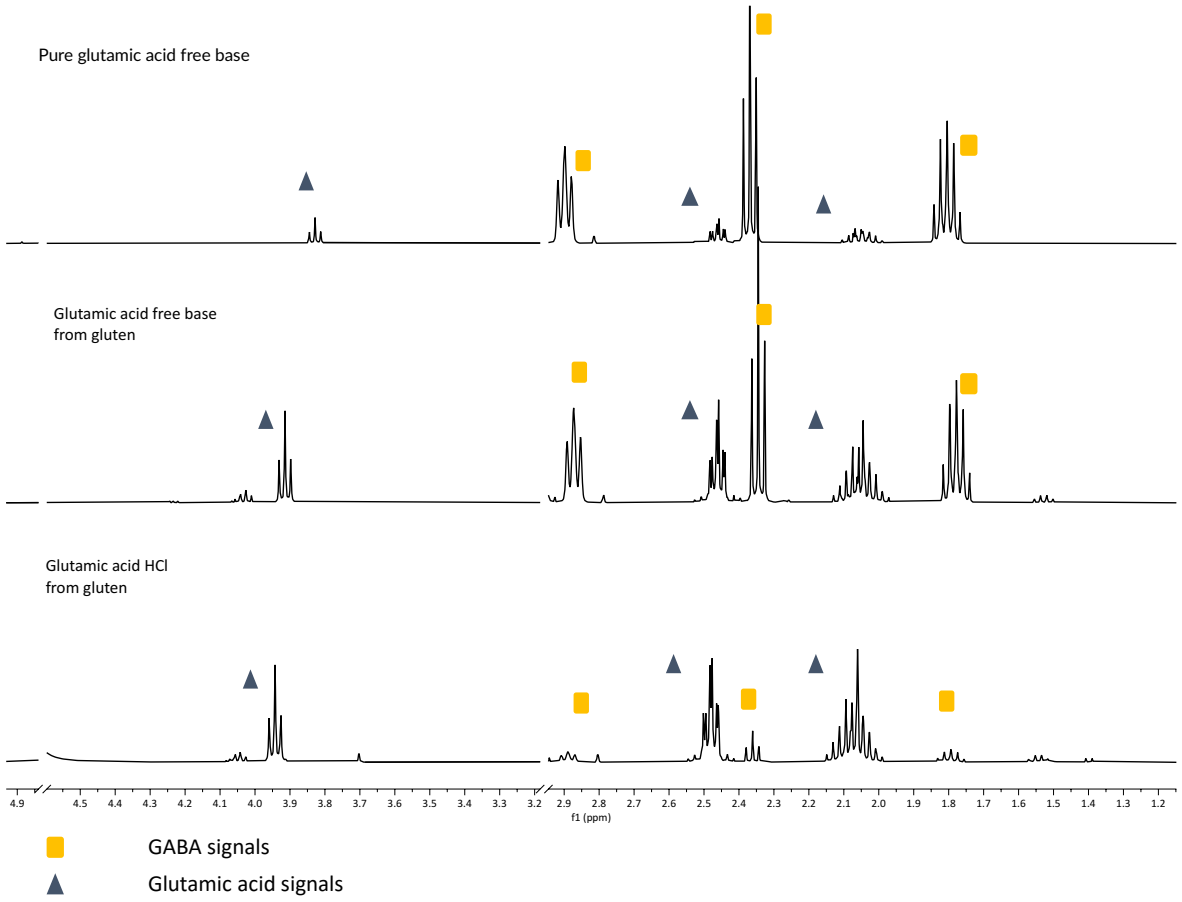

*Figure 68 Overlay of ^{1}H-NMR spectra of decarboxylation product obtained from pure L-glutamic acid free base (**53**, top), glutamic acid HCl from gluten (**53** HCl, middle) and glutamic acid free base from gluten (**53**, bottom). Methylsulfone standard peak was cut for insert 3.1-3.8 ppm, NMR solvent = D_2O was cut for insert 4.5-4.8 ppm*

To further improve the yield of GABA from gluten waste, the free base of glutamic acid was prepared from the gluten hydrolysate. Two commonly used methods exist to desalt amino acids, the first consist of eluting a solution of the amino acid hydrochloride over an anion exchange resin (*e.g.* Dowex50) to adsorb them. Subsequently, a second elution using a piperidine or ammonia solution allows the desorption of the amino acid free base. [341–344] The second technique uses electrodialysis with ion-exchange membranes.[284,288] However, both methods require specific equipment and large amounts of water/salt, resulting in significant waste. Glutamic acid, being a zwitterionic species, possess an isoelectric point (pI) at which its solubility in water is minimal. At this point, most of the glutamic acid

present in the solution is in the form of a free base.[326] The isolated glutamic acid HCl from gluten was thus converted into its free base following the procedure described in the experimental section p. 432. The success of the procedure was confirmed with NMR spectroscopy and CHN analysis (see experimental section p. 433). The obtained crystals were used in the decarboxylation process, and a much higher GABA yield could be obtained (26%, Figure 68, middle spectrum) than with the HCl salt. A way to further optimise the conditions would be to generate the free base *in situ* with a base such as NaOH, trimethylamine or piperidine and run the reaction but a substantial amount of salt may be generated.

4.4 Conclusion for chapter IV part 1

The abundance of glutamic acid protein-rich wastes from bio-refineries or the starch industry is increasingly attracting the green chemistry community's attention. The use of this potentially high-value platform chemical to produce solvents, polymers, or pharmaceutical is paramount, but a selective defunctionalisation must usually precede it. For instance, the decarboxylation of amino acids forming either their nitriles or amines equivalent is often necessary before their use in synthetic reactions. This defunctionalisation step also applies to glutamic acid.

For instance, chapter II exposes the selected example of the NMP synthesis from petrochemical or renewable resources. The *BioLogicTool* helped determine that the renewable route to NMP was preferable due to its higher rationality scores. However, a selective decarboxylation of glutamic acid was necessary to form either GABA or 2-pyrrolidone.

The successful decarboxylation of several amino acids, including glutamic acid, proved possible with the protocol developed here. It was even possible to extract glutamic acid from hydrolysed gluten proteins (optionally issued from the CMF reaction) and subsequently decarboxylate it. Unfortunately, no glutamic acid was obtained when microalgal hydrolysed proteins were used. The possible other materials present in microalgae (inorganic salts, other amino acids etc.) may prevent the selective precipitation of glutamic acid. Therefore, it is essential to pursue the efforts being made to separate amino acids cost-effectively to valorise protein wastes further.

One other way to valorise amino acids, in particular lysine, is to produce polymers. The following section focuses on the decarboxylation and use of this amino acid to make a non-isocyanate polyurethane replacement, namely polyhydroxyurethane.

Chapter IV
Use of proteinaceous waste from CMF-process

Part.2 Decarboxylation of L-lysine to 1,5-pentanediamine: synthesis of a polyurethane replacement[††]

[††] The following section is adapted from the article: Clark, J. H., Farmer, T. J., Ingram, I. D. V., Lie, Y. & North, M. Renewable Self-Blowing Non-Isocyanate Poly(urethane) Foams From Lysine And Sorbitol. *European J. Org. Chem.* **2018**, 4265–4271 (2018). Y. Lie performed the synthesis of the diamine linker and participated in the writing of the manuscript. Dr. Ian D. V. Ingram performed the synthesis of the bis-cyclic carbonates, polymerisation of thereof with diamines and characterisation of the polymers.
Part of the original text written by Prof. M. North, Dr. Farmer and Dr. Ian D. V. Ingram has been adapted for this chapter.

4.5 Introduction: Sustainability of polyurethanes and bio-based alternatives

4.5.1 Polyurethanes: production and uses

Polyurethanes are a class of polymers possessing carbamate (urethane) groups as their constitutive units (see Figure 69). Thanks to their versatility and depending on their formulations (additives, different pending groups, cross-linking etc.), these polymers are used in various sectors. For instance, the automotive industry utilises polyurethane foams for their interior parts. Polyurethane thermoplastics are used for sporting goods or phone cases, whereas water-borne formulations are employed as adhesive or sealant.[345] Akindoyo *et al.* estimated that 50% of the demand for polyurethanes is for foam applications.[345]

The current mega-tonne industrial synthesis uses isocyanate derivatives (2,4 or 5-toluene diisocyanate (TDI) or 4,4'-methylene diphenyl diisocyanate (MDI, Figure 69), which are CMRs (Carcinogenic, Mutagens, and Reprotoxic).[346] A particular type of isocyanate, methyl isocyanate (MIC) was the chemical involved in the Bhopal disaster that led to the death of thousands of people in 1984.[347] Moreover, isocyanates are produced using primary amines and phosgene, a highly hazardous material formerly used as a chemical weapon.

Classically, the di/tri-isocyanates are polymerised with polyols in the presence of a catalyst (metal-based- Pb, Zn, Sn - or amine catalyst – 1,4-diazabicyclo[2.2.2]octane (DABCO), *N,N*-dimethyl cyclohexylamine (DMCHA), Figure 69) or UV-light leading to polyurethane. Water is often voluntarily added to the polyols, which will react with the

residual isocyanates and generate amines and CO_2 bubbles, the latter generating a foamy material as the polymerisation proceeds.

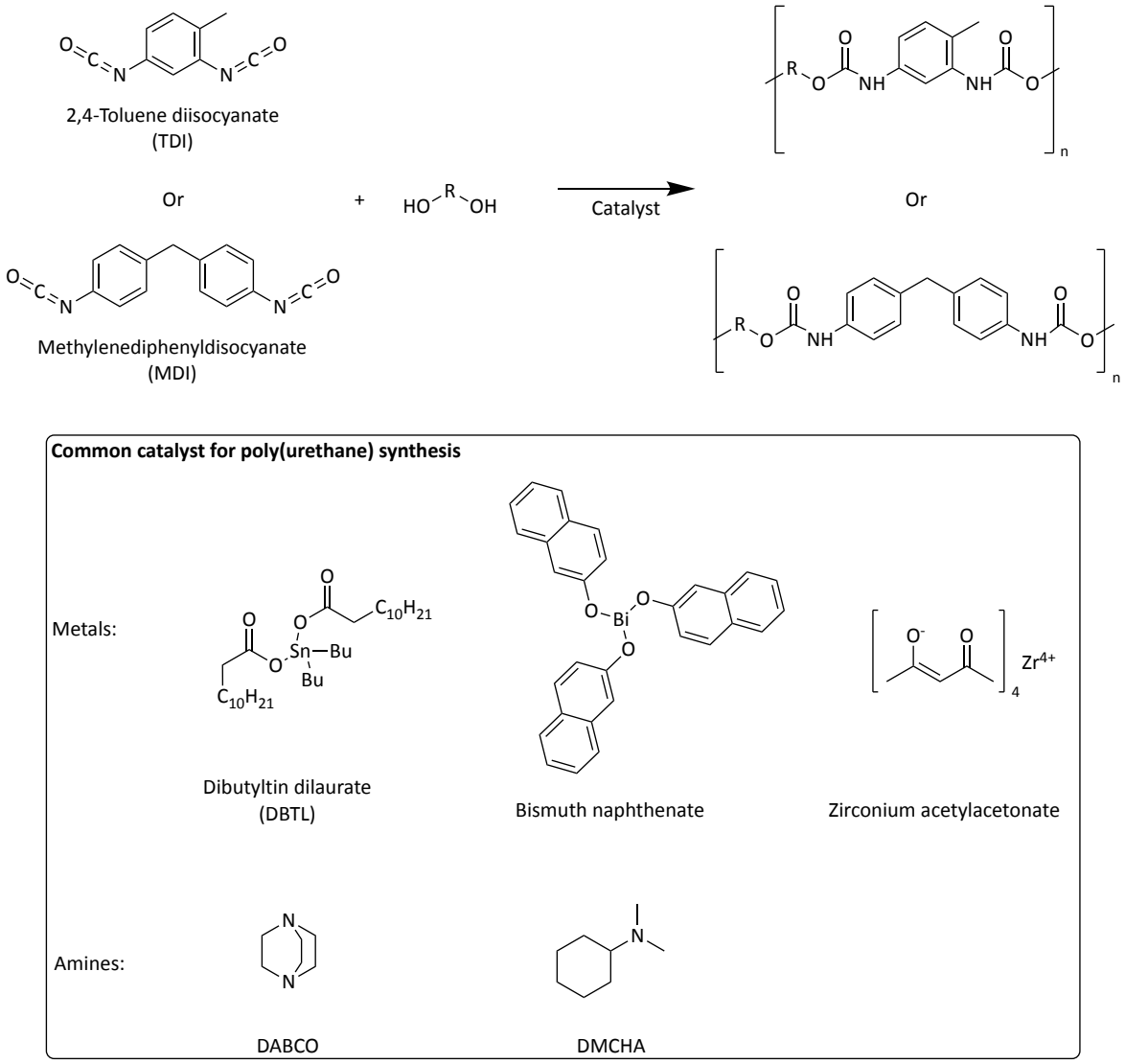

Figure 69 Typical diisocyanates used for the synthesis of polyurethanes and classically employed catalysts are represented below

4.5.2 Current efforts to improve the sustainability of polyurethanes

Due to a rise in environmental awareness, polyurethane manufacturers have begun to use vegetable oils to produce polyols. Castor oil from the plant *Ricinus communis* is one of the most studied plant-based oils due to its high ricinoleic acid (12-hydroxy-9-*cis*-octadecenoic

acid, Scheme 34, **193**) content. Indeed, it was found that up to 95% of the triglycerides are composed of this fatty acid.[348] The natural presence of a hydroxyl group on the 12th carbon makes it a good candidate for possible reactions with isocyanates to form a cross-linked network. Nevertheless, further reactions are needed to form polyols from vegetable oils prior to any polymerisation. These reactions include transesterification (with glycerol forming monoglycerides or diethanolamine forming diethanolamide, Scheme 34**A**), epoxidation and opening of the oxirane ring (Scheme 34**B**), reductive ozonolysis and reduction (Scheme 34**C**) and hydroformylation and reduction (Scheme 34**D**).[322,348,349]

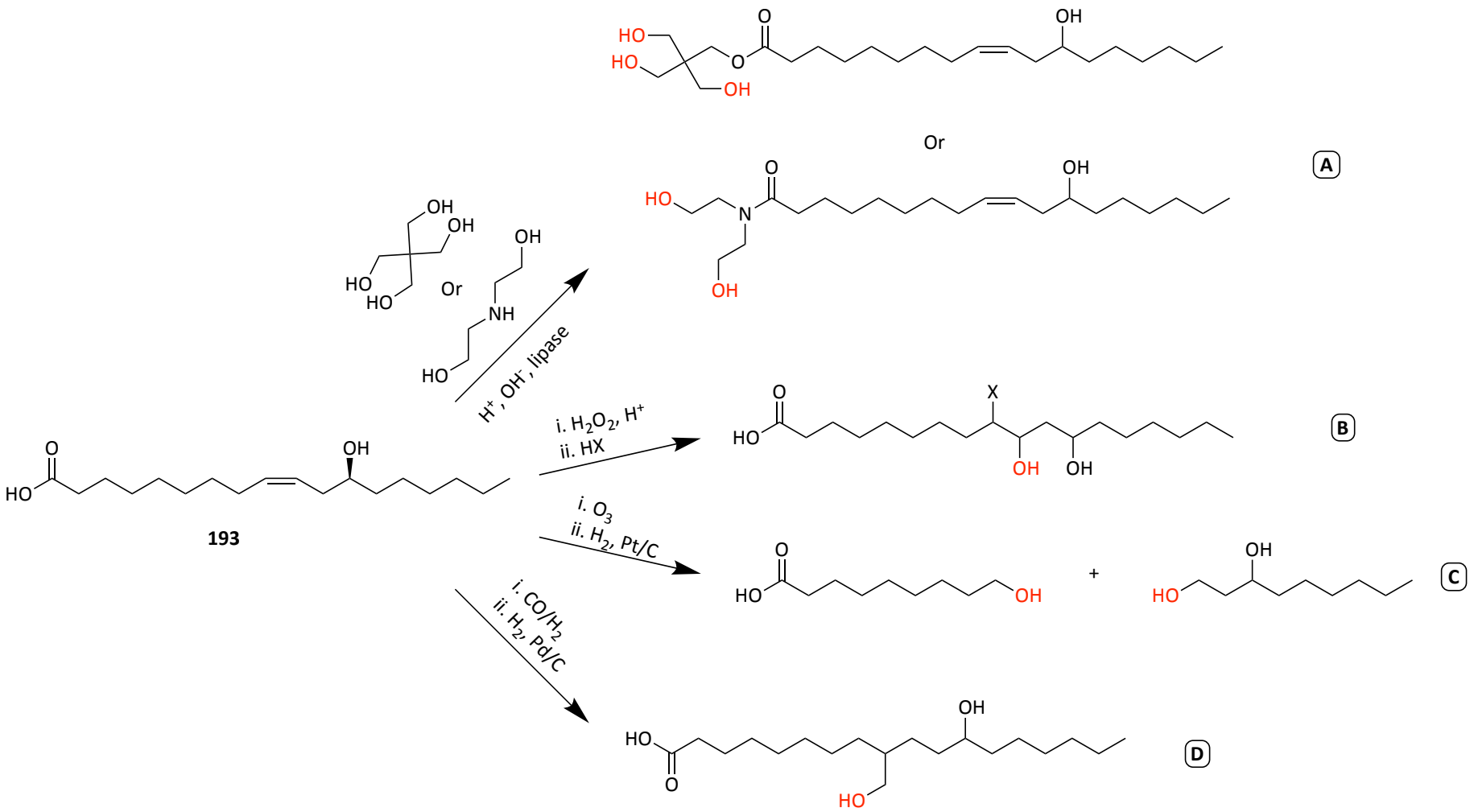

*Scheme 34 Different route to polyols from vegetable oils, example of ricinoleic acid (**193**). **A**: Transesterification/amidation **B**: Epoxidation, ring-opening, **C**: Ozonolysis, reduction **D**: Hydroformylation, reduction*

These efforts to use renewable resources for the production of polyols must be highlighted and encouraged. Unfortunately, the most significant hazard in the manufacture of polyurethanes, namely, isocyanates, remained an issue to be addressed.

Researchers are now focusing on finding safer, greener routes to non-isocyanate polyurethanes (NIPU). These were extensively reviewed in 2015 by Rokicki *et al*..[350] One promising NIPU candidates are polyhydroxyurethanes (PHUs, Scheme 35, **199**) obtained from the ring-opening aminolysis of bis-cyclic carbonates (Scheme 35, **198**) by aliphatic diamines. Described as early as 1957, by Grosznos and Drechsel, PHUs increasingly gain popularity.[351] Additionally, the low-toxicity of carbonates used as reagents (*e.g.* dimethyl carbonate, DMC) or solvent (*e.g.* racemic mixtures of propylene carbonate) have been repeatedly reported making them important chemicals to consider by green chemists.[352,353]

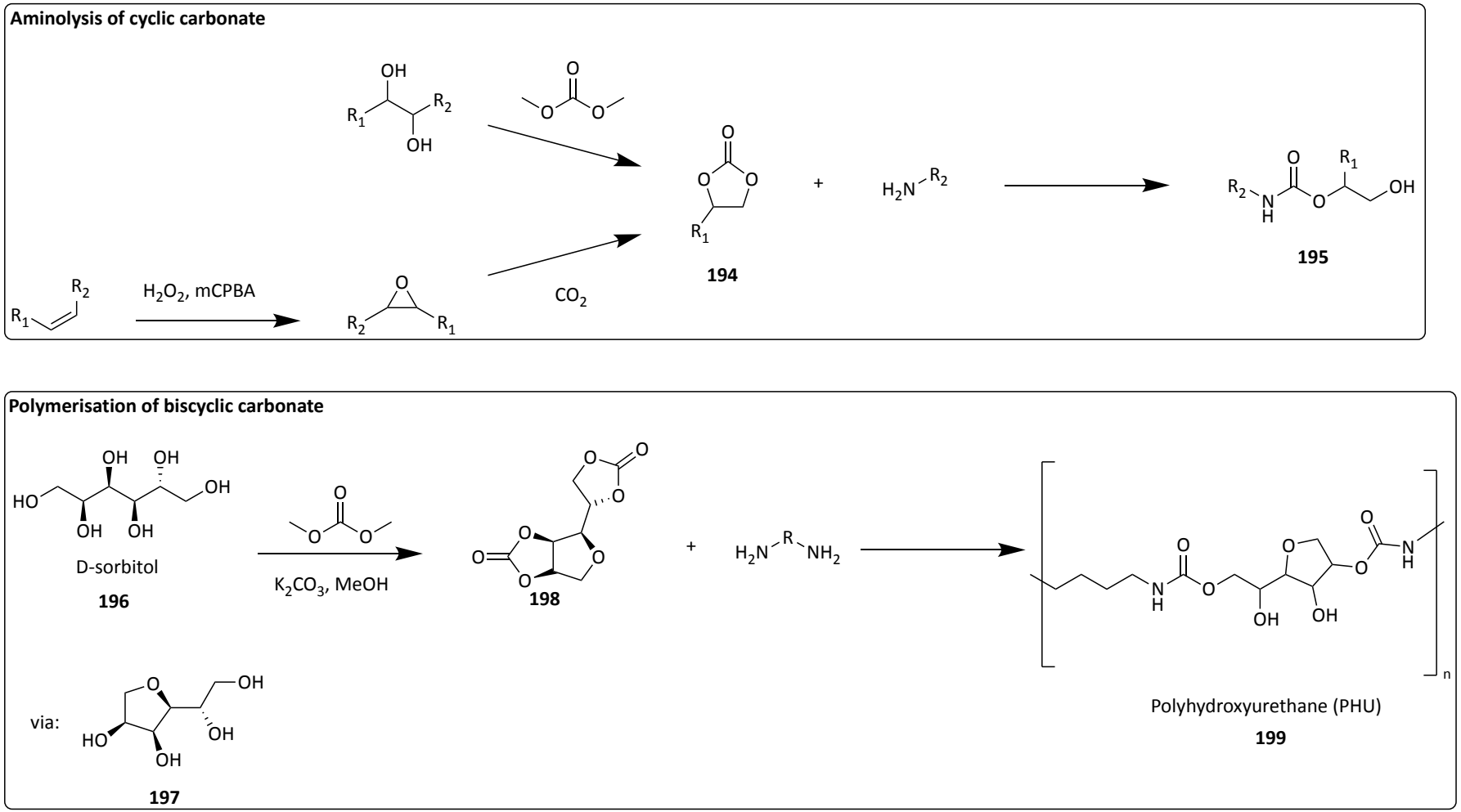

*Scheme 35 Production of carbamate from cyclic carbonate by aminolysis (top). Polymerisation of a bis-cyclic carbonate (bottom adapted from [354]) - [(1R,5R,6R)-6-[(4S)-1,3-dioxolan-2-one-4-yl]-3-oxo-2,4,7-trioxabicyclo[3.3.0]octane], **198**- obtained from sorbitol to non-isocyanate polyurethane (NIPU), polyhydroxyurethane (PHU). Due to the many possible isomers the stereochemistry of **199** is not represented.*

5-Membered ring cyclic carbonates are synthesised from CO_2 and epoxides in the presence of a Lewis acid.[355] However, epoxides are usually generated using hazardous precursors (chlorhydrins) or corrosive reagents (H_2O_2, *m*-CPBA) on alkenes. Fortunately, an alternative to the synthesis of 5 or 6-membered ring cyclic carbonate is the transesterification between vicinal diols and DMC. Notably, sugars such as sorbitol (Scheme 35, **196**), leads to the bis-cyclic carbonates **198** via intermediate sorbitan **197**, the aminolysis of which leads to PHUs.[346,356,357] The use of these sugars obtained from renewable resources (fructose or glucose) further increases the sustainability of the bis-cyclic carbonates obtained.

Although the PHU synthesis does avoid isocyanates, the origin of the diamines, employed for the aminolysis, is often dismissed when the polymer greenness is considered. Yet, the commonly used 1,6-hexanediamine (hexamethylenediamine, HMDA) is obtained from the hydrogenation of adiponitrile, a product issued form the hydrocyanation of butadiene with HCN.[358] Butadiene is a co-product of oil refining, and HCN is obtained from the reaction of methane, ammonia and oxygen at 1200 °C passed over a Pt catalyst.[359] Clearly, improvements to source renewable diamines with energy-efficient methods are necessary to improve the green credentials of PHU syntheses even more.

In this regard, 1,5-pentanediamine produced by non-oxidative decarboxylation of L-lysine may provide an answer to this issue. This amino acid is currently obtained by fermentation using genetically engineered *Corynebacterium glutamicum*. Yet, as was shown previously in chapter III.1 and IV.1, lysine is also an abundant amino acid in protein-rich residues and microalgae. Thus, the selective decarboxylation of L-lysine to 1,5-pentanediamine could add value to these feedstocks. However, this diamine production from its amino acid equivalent has been little studied due to its recalcitrance to decarboxylate under the

commonly employed thermal decarboxylation.[336] The diamine is often preferably produced directly by genetically engineered microorganism.[335,360]

4.6 Thermal decarboxylation of L-lysine to 1,5-pentanediamine

4.6.1 Production of a bio-derived diamine linker from L-lysine

Decarboxylation of L-lysine (**55**) to 1,5-pentadiamine (**200**) was studied with a similar approach to that described in chapter IV.1. Pictures were taken (Figure 70) to assess the transition of the reaction medium from a suspension to a clear solution, indicating completion of the reaction.[317,318] Unlike glutamic acid, yellowing appeared rapidly (0-1 min at 190 °C, Figure 70, **B**-**C**) and a solid brown residue was visible after 1.5 min (**D**). The reaction medium then turned clearer from 1.5 to 15 min (**D**-**P**) after which significant darkening of the reaction medium occurred (see picture **Q** after 27 min of reaction at 190 °C). The optimal reaction time for the decarboxylation was then chosen as 15 min.

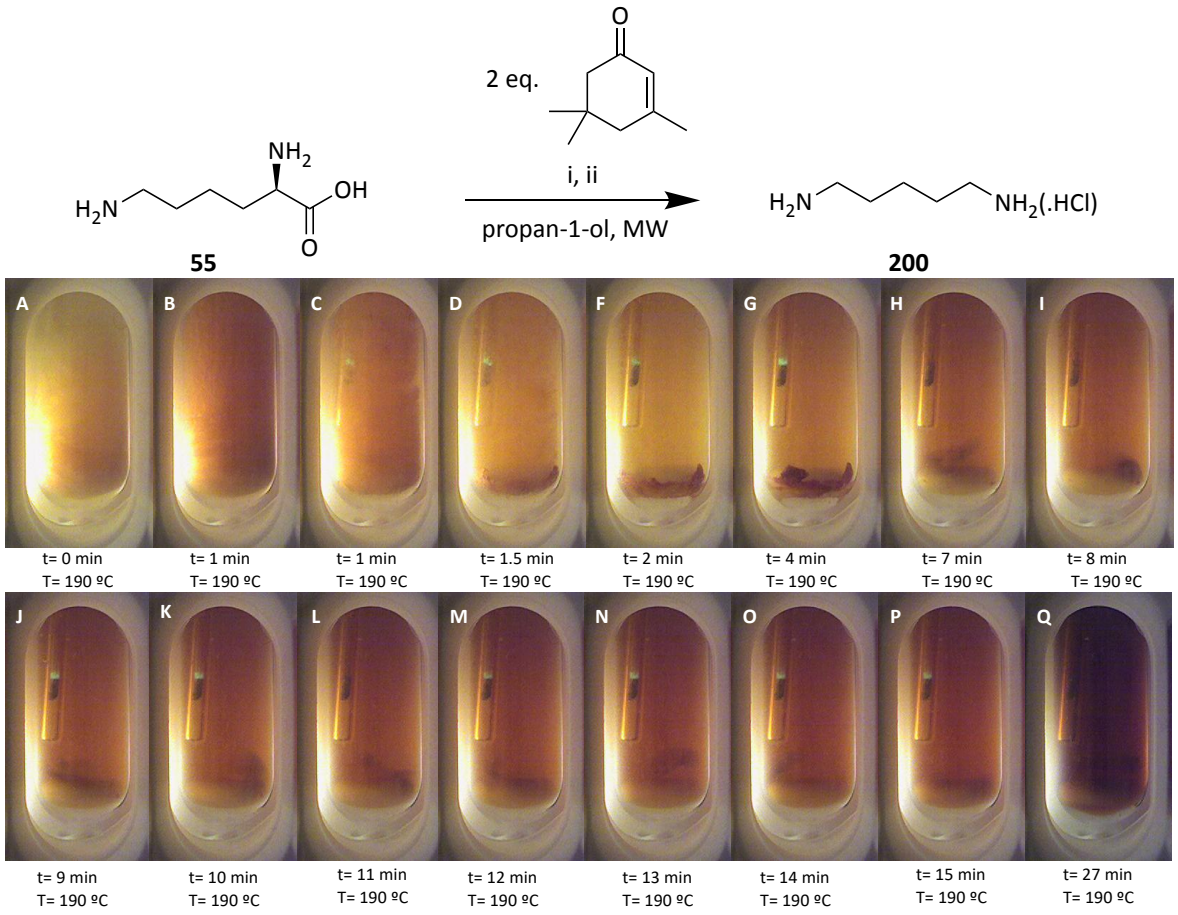

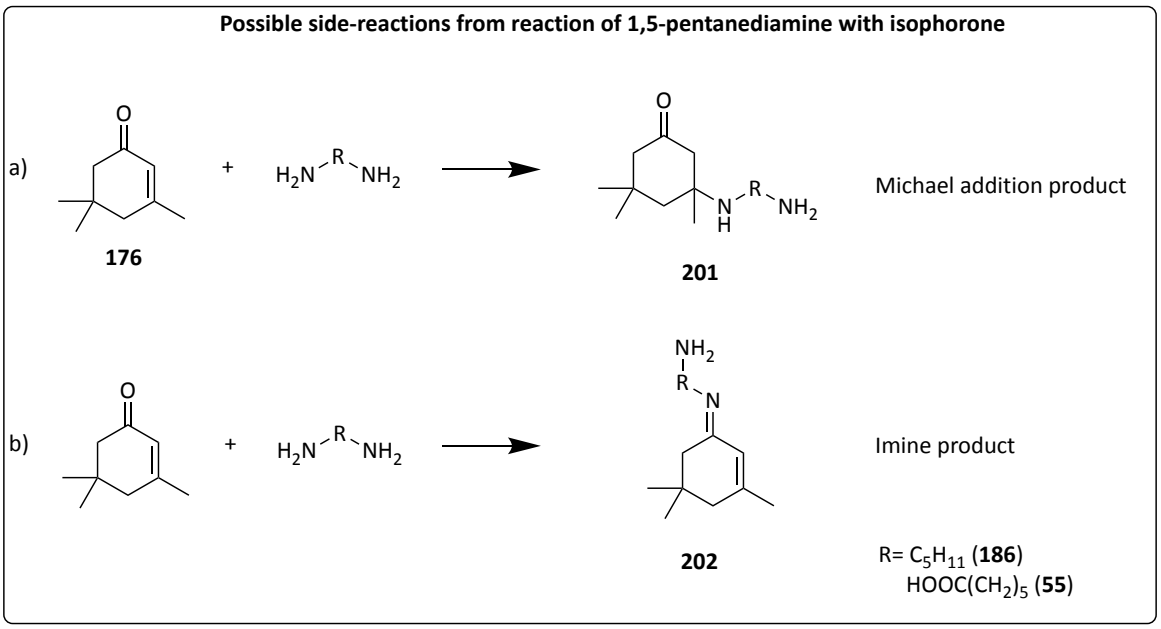

*Figure 70 Pictures taken during initial decarboxylation reaction of L-lysine (**55**) to 1,5-pentanediamine (**200**). Conditions: i. L-lysine (2 mmol), isophorone (4 mmol), n-propanol (3 mL), ii. 6 M HCl (8 mmol, 4 eq.), no hold time target temperature: 190 °C, ramp time to 190 °C was set to 5 min, microwave: Anton Paar Monowave 40, 15 mL vials. Structures of possible coloured side-products forming from the reaction of **55** or **200** with isophorone (**176**) are represented below.*

Similar to the glutamic acid decarboxylation, the colouring of the reaction was attributed to isophorone-related structures represented in Figure 59 p. 261. Additionally, L-lysine (or 1,5-pentanediamine) specific side-products are depicted in Figure 70, such as **201,** issued from the aza-Michael addition (with either 1,5-pentanediamine or L-lysine) or the imine formed between the diamine and isophorone, **202**. Finally, the observed solid residue may likely arise from further reaction such as self-polymerisation of lysine (Scheme 36, polymer B and B', **203** and **204** respectively), or even a combination of the reaction a) and b) represented Scheme 36 (polymer C, **205**).

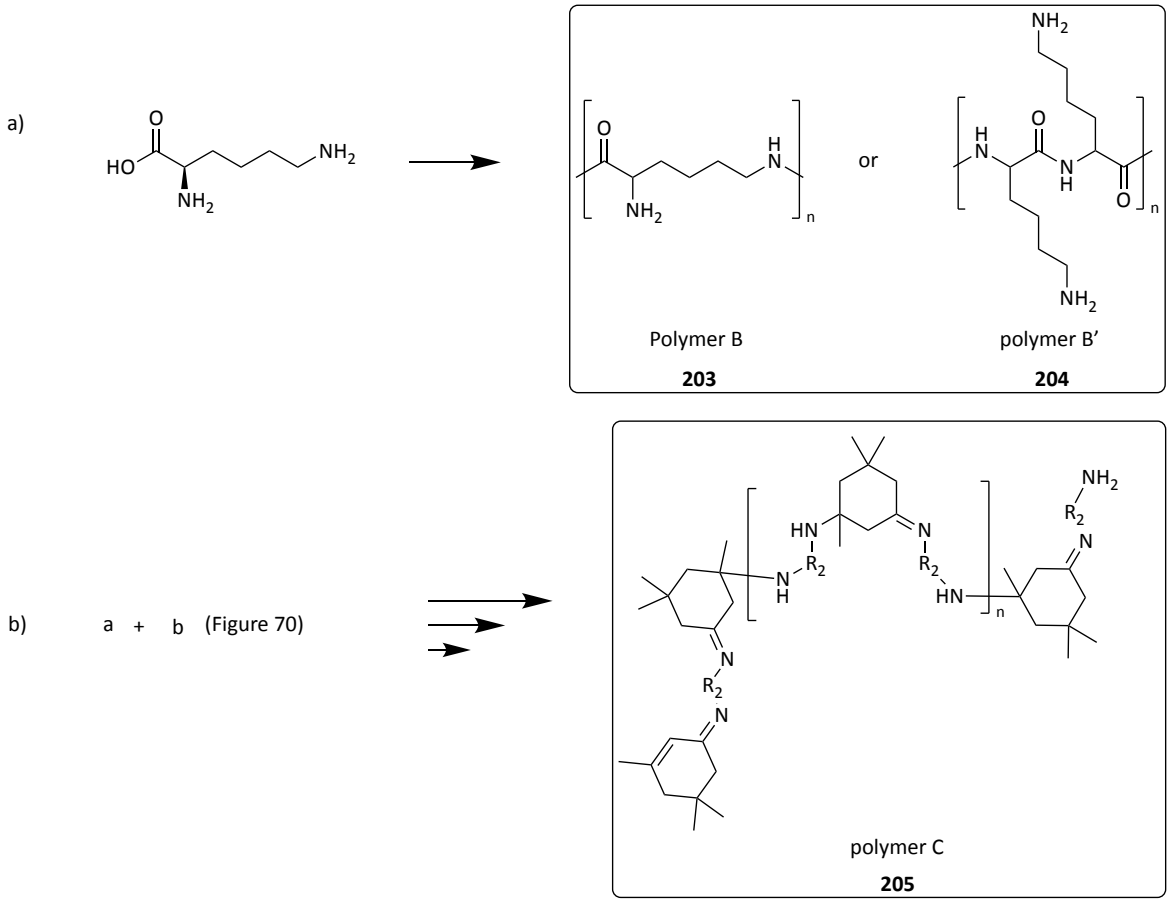

Scheme 36 Possible structure for solid precipitate formed during the decarboxylation reaction.

After work-up of the reaction, cadaverine hydrochloride could be isolated in excellent purity (>99% by ^{1}H-NMR spectroscopy), but only very low yields were obtained at first (~15%, Table 24). This observation is consistent with Claes *et al.*'s results which reported a GC-yield of 8% after 4 h and 28% after 24 h at 150 °C, using 5% of isophorone as a catalyst. Nonetheless, the yields obtained here and the one reported by Claes *et al.* were still almost half compared to the patent by Omeis *et al.* (56%) also using isophorone. Other reports using either (R)-carvone or 2-cyclohexen-1-one mention even higher **200** yields, 73% and 88% respectively.[299,318] For this reason, the comparison of the different inducers in our system was performed, using L-lysine and L-glutamic acid.

*Table 25 Comparison of the different cyclic enone inducers for the decarboxylation of L-lysine (**55**) or L-glutamic acid (**53**). Qualitative comments are given regarding the recyclability of the catalyst adapted from* [354].

	isophorone	R-carvone	2-cyclohexen-1-one
Yield 1,5-pentanediamine HCl (200, %)	15 (31)*	37	32
Yield of GABA HCl (79, %)	63	34	53
Catalyst recovery	Easy and straightforward	Possible but requires further steps (site-specific oxidation & hydrogenation/reduction)	No

*Yield obtained from freshly distilled isophorone.

Higher yields were obtained with the other cyclic enone inducers but could not match the previously reported values. The use of freshly distilled isophorone increased the yield of **200** up to 31%, which was in the same range as the yields obtained with (R)-carvone (37%) or 2-cyclohexen-1-one (32%). This result suggests that a disruptive impurity in older isophorone reagent likely prevents optimal yields of 1,5-pentanediamine. Using freshly distilled isophorone appears essential to ensure the reproducibility of such experience. Interestingly, the yield of GABA did not follow the same trend. Indeed, isophorone was a

better inducer (63% yield) than 2-cyclohexen-1-one (53%) and (R)-carvone (34%). This difference possibly suggested that the Brønsted acidity of the decarboxylated substrate influenced the outcome of the reaction. Due to the more basic character of lysine, (R)-carvone is less prone to isomerise to carvacrol (see Figure 71), whereas glutamic acid likely promotes it. The accumulation of amines (as 1,5-pentanediamine) in the reaction medium probably inhibits the inductive capacity of the cyclic enones by forming **201** or **202**, which explain the poor yields obtained overall when using lysine as a substrate. Finally, the recyclability of the excess carbonyl inducer was also considered. In this regard, (excess) isophorone was the only inducer that could be reused after the reaction, and a yield of 27% diamine was obtained without distillation of the recovered isophorone. (R)-carvone is almost entirely isomerised to carvacrol (Figure 71, **206**, 89% by GC-FID) due to the acidic work-up (Figure 71, FT-IR overlay and proposed mechanism). In contrast, the collected organic fraction of the reaction using 2-cylohexen-1-one only provided a black tar-like material which was not active anymore. Thus, from a sustainability perspective isophorone would be the inducer of choice for this reaction although additional purification may be necessary to ensure higher yields.

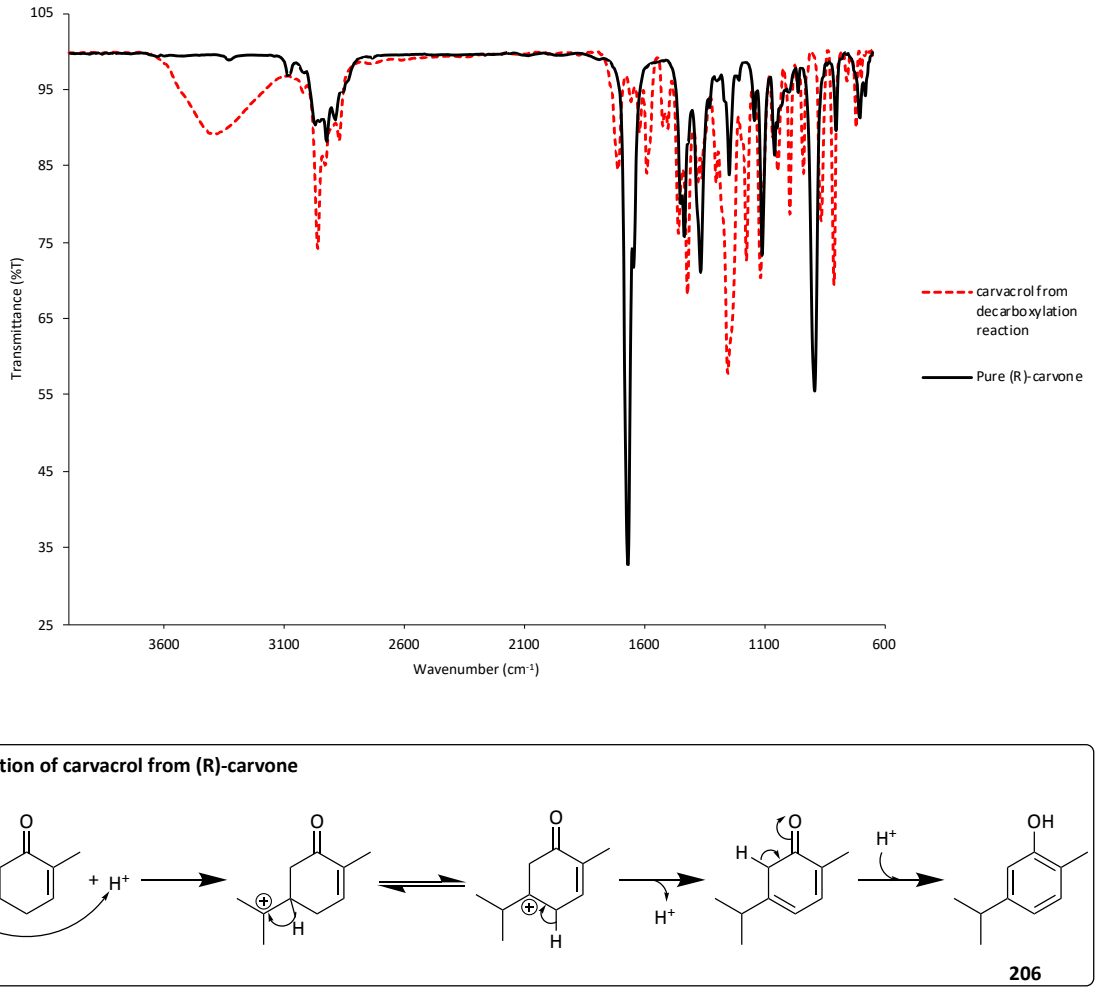

*Figure 71 FT-IR spectra overlay of pure (R)-carvone (**175**, black) and collected organic phases after decarboxylation reaction (red dotted line). Proposed mechanism for the formation of carvacrol (**206**) from **175***

The successful decarboxylation reactions provided enough material to attempt their use for the solvent-free polymerisation of the bis-cyclic carbonate **198** synthesised from sorbitol by Dr. Ian Ingram. Preliminary experiment using the commercial 1,5-pentanediamine free base (cadaverine) showed promising results that encouraged the utilisation of the lysine-derived diamine for the polymerisation.

4.6.2 Polymerisation of bis-cyclic carbonates with cadaverine

Dr. Ian D. V. Ingram synthesised the bis-cyclic carbonate obtained from sorbitol (**198**), following a procedure described by Tomczyk *et al.* in 2015, and further purified **198** by washing with acetone and recrystallisation from water.[361] The polymerisation of **198** and commercial 1,5-pentanediamine (performed by Dr. Ian D. V. Ingram) was tried in solvent-free conditions by simply grinding both compounds in a mortar and heating it at 100 °C for 20 hours. This reaction resulted in a rigid foam, the structure of which was confirmed by NMR spectroscopy (Figure 72) and MALDI-TOF analysis (Appendix 16). The ^{1}H-NMR spectra of **198** and the obtained polymer are represented in Figure 72.

Due to the diastereotopic nature of both *a* and *d* methylene protons, they appear as two distinct signals: two doublets of doublet for *a* and one doublet and a multiplet (likely another doublet) for *d*. The -NH- signals corresponding to the carbamate group formation are visible around 7.0 – 7.5 ppm (Figure 72). Unfortunately, most of the other signals for the opened bis-cyclic carbonate arose between 3.0 and 4.5 ppm which prevented any careful end-group analysis nor stereochemical considerations by ^{1}H-NMR spectroscopy.

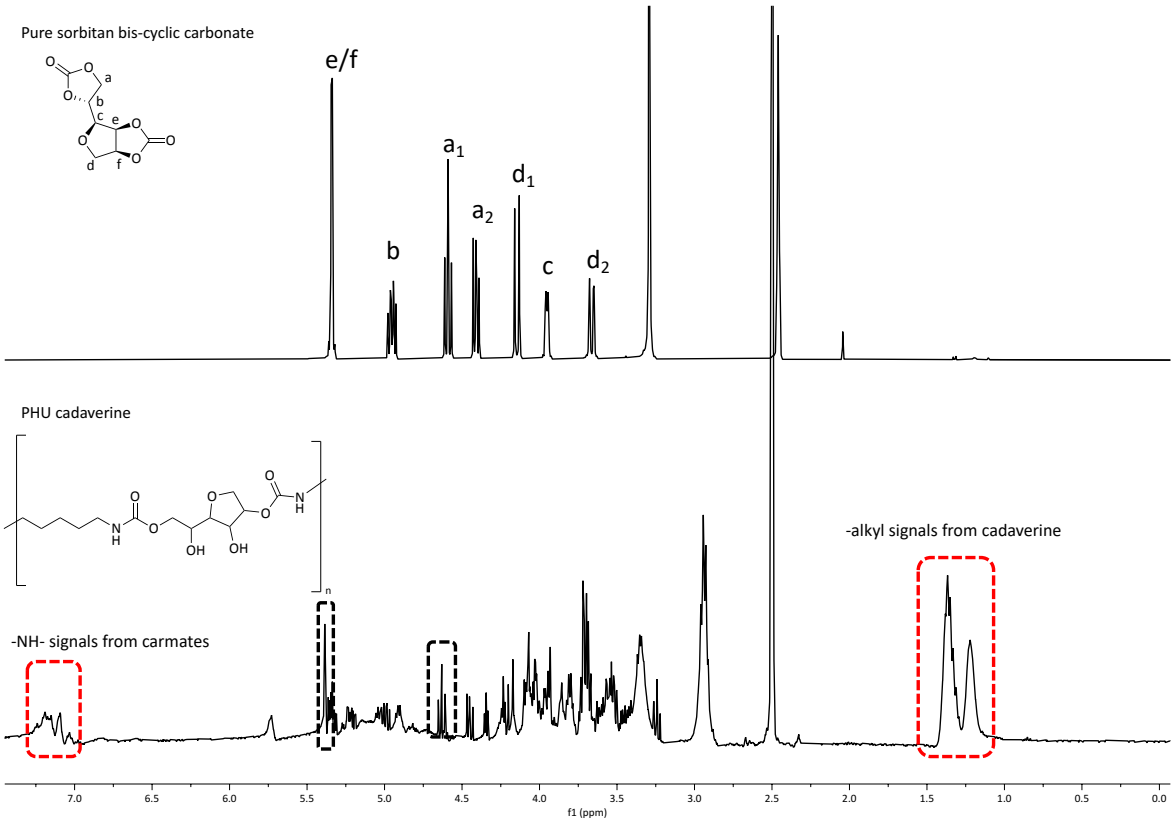

*Figure 72 ^{1}H-NMR spectra of **198** (top) and the obtained PHU with 1,5-pentanediamine (**199**, bottom). Black dotted squares represent the signals corresponding to residual carbonate left after polymerisation while red squares highlight signals corresponding to the urethane and alkyl group of the diamine. R= C_5H_{11}.*

The 4 different repeating units obtainable (Scheme 37) likely add to the complexity of the NMR spectrum. MALDI analysis suggests that only short oligomers could be obtained with a maximum average of M_w= 3.5 kDa (with m/z= 318.14 for the repeating unit).

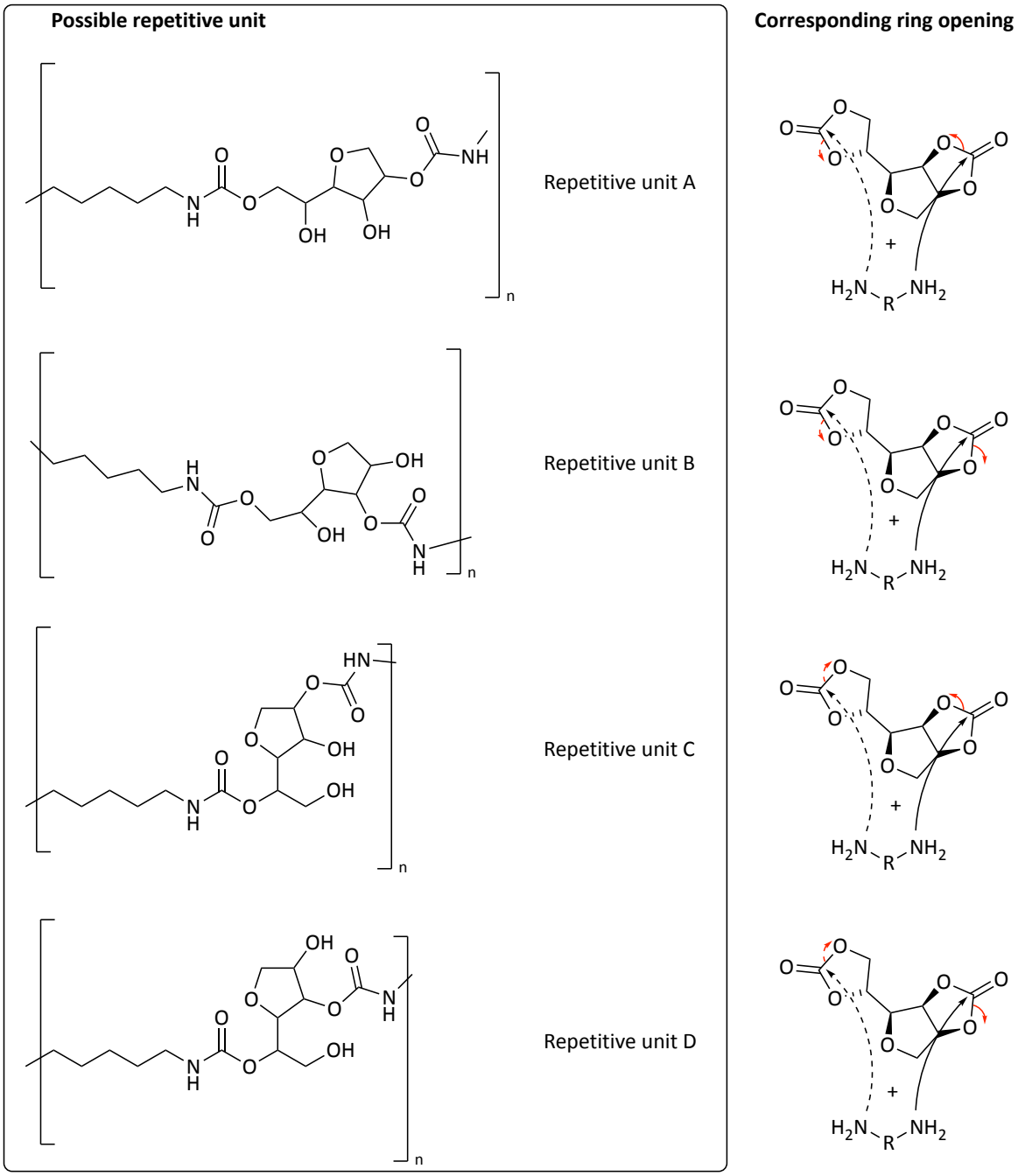

*Scheme 37 Possible repetitive units obtained during the aminolysis of **198** with a diamine (R= C_5H_{11} for 1,5-pentanediamine, **200**). Plain arrows and dotted arrows are consecutive events and not simultaneous.*

Thermal analysis (performed by Dr. Ian Ingram Figure 73) showed that the polymer had a $T_{10\%}$ of 193 °C, showing the thermal stability of this polymer. Previous TG-IR experiment employing hexamethylene diamine (HMDA) for the polymerisation of **198** displayed a close

$T_{10\%}$. Also, at temperatures similar to the polymerisation condition, the IR spectrum showed a signal corresponding to the emission of CO_2. A mechanism for the release of CO_2 was thus proposed to explain the self-blowing behaviour of this polymer. Likely, the formation of a primary diol from a first aminolysis reaction subsequently cyclises to form an isosorbide-like structure (Figure 73, **207**, pathway B) and releasing CO_2. The detection of compound **207** by ESI-MS, when the model compound n-dodecylamine was used in the reaction, further supported this mechanism. The secondary alcohol present in **207** is less likely to participate in further polymerisation reaction due to the reduced reactivity of such alcohols. Thus, the reaction leading to **207** with the tandem release of CO_2 is likely an end-capping reaction, although further polymerisation could not be entirely dismissed. Alternatively, an additional reaction of the intermediate with an amine can also lead to **207** with concomitant release of CO_2 (Figure 73, pathway **A**).

The reaction between **198** and HMDA was conducted in a TGA analyser (N_2 atmosphere, 100 °C) to prove that the formed polymer trapped the emitted CO2. Only a modest constant mass loss was observed for at least 20 h, which likely indicates that the emitted CO_2 is trapped within the polymer being formed and not immediately released. However, dissolving the previously prepared foams in methanol to release the trapped CO_2 and thoroughly removing the solvent did not lead to any consistent mass difference.

Concerning the PHU obtained with 1,5-pentanediamine, the FT-IR spectrum (Figure 73) showed carbonyl signals consistent with carbamates group (1688 cm^{-1}) and a small amount of residual carbonate (1779 cm^{-1}) which further confirmed the success of the polymerisation.

Differential scanning calorimetry displayed a high-temperature crystallisation event at 190 °C, and a small, low-temperature T_g-like feature at –31 °C (Appendix 17). However, this foam was rigid at room temperature, making a true T_g below room temperature unlikely.

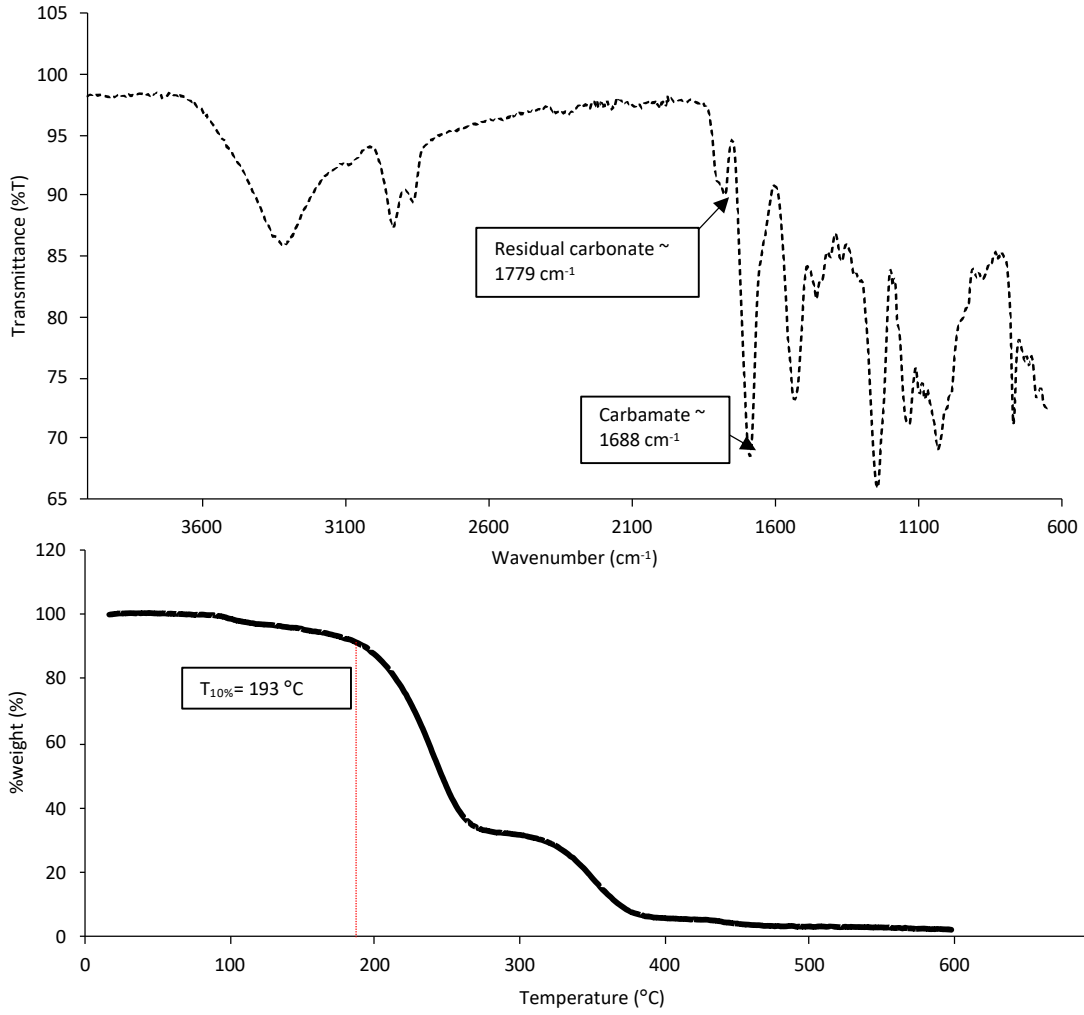

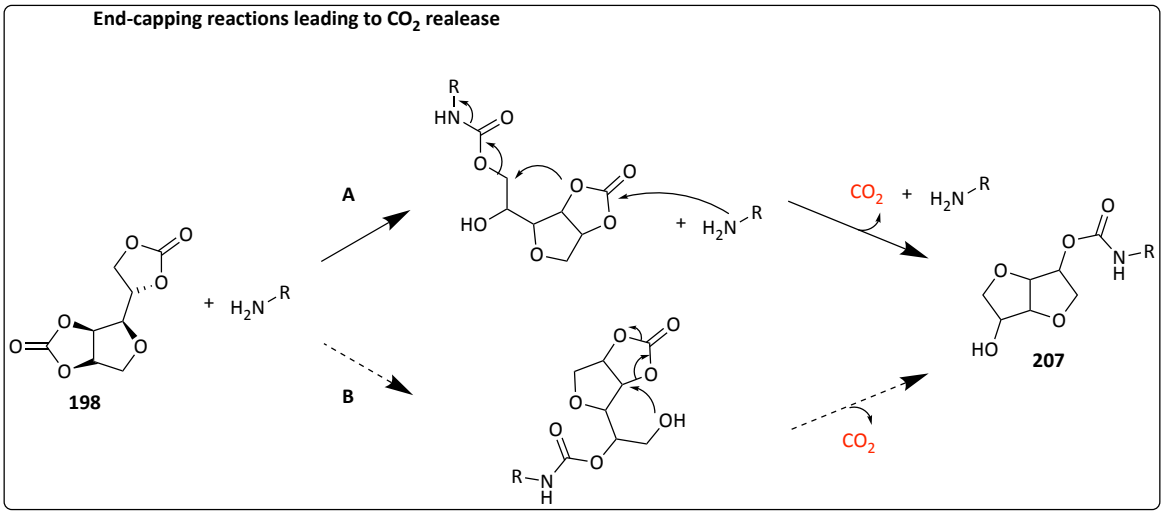

*Figure 73 FT-IR spectrum of the polymer obtained from **198** and 1,5-pentanediamine (**200**, top). TG trace of the PHU obtained from **198** and **200** (middle), the red dotted line indicates $T_{10\%}$. Proposed end-capping mechanisms with self-emission of CO_2* (bottom), *R= alkyl* (e.g. *dodecane*) adapted from [354]

Then, it was decided to use **200** obtained by decarboxylation. First, **200** prepared from L-lysine was desalted to ensure similar reactivity to the commercial reagent. The reaction of **200** HCl with excess sodium hydroxide and extraction with ethyl acetate led to 1,5-pentanediamine free base, which gave a result similar to that obtained using commercial **200**. This positive result pushed the preparation of a foam by directly reacting the **200** with sorbitan bis-carbonate **198** in the presence of a stoichiometric base (NaOH). This attempt also produced a rigid foam of similar appearance. Unfortunately, this material was particularly hygroscopic, likely due to the high amount of salt (NaCl) generated by the *in-situ* desalting process or NaOH employed in excess. This product formed a deliquescent foam that collapsed upon standing in moist air for a day, preventing any further characterisation.

4.7 *BioLogicTool* analysis of the PHU obtained from renewable resources

This PHU synthetic route presents the advantage of preserving a large proportion of the heteroatoms already present in the feedstock, as demonstrated by the *BioLogicTool* plots represented in Figure 74. The typical route to PU using TDI starts with the nitrosation-reduction of toluene to form 2,4-toluenediamine. Polymerisation with the chosen diol after the formation of isocyanates with phosgene leads to PU. The removal and incorporation of heteroatoms in this route dramatically reduce its rationality (Figure 74**A**). Consequently, the *BioLogicTool score* of this synthetic pathway is relatively high (2.23) and the *Total Length* (2.66). On the contrary, the bio-derived route (Figure 74**B**) has an excellent

BioLogicTool score (1.02) and lower *Total length* (1.45) than the route A, further underpinning the merits of this approach.

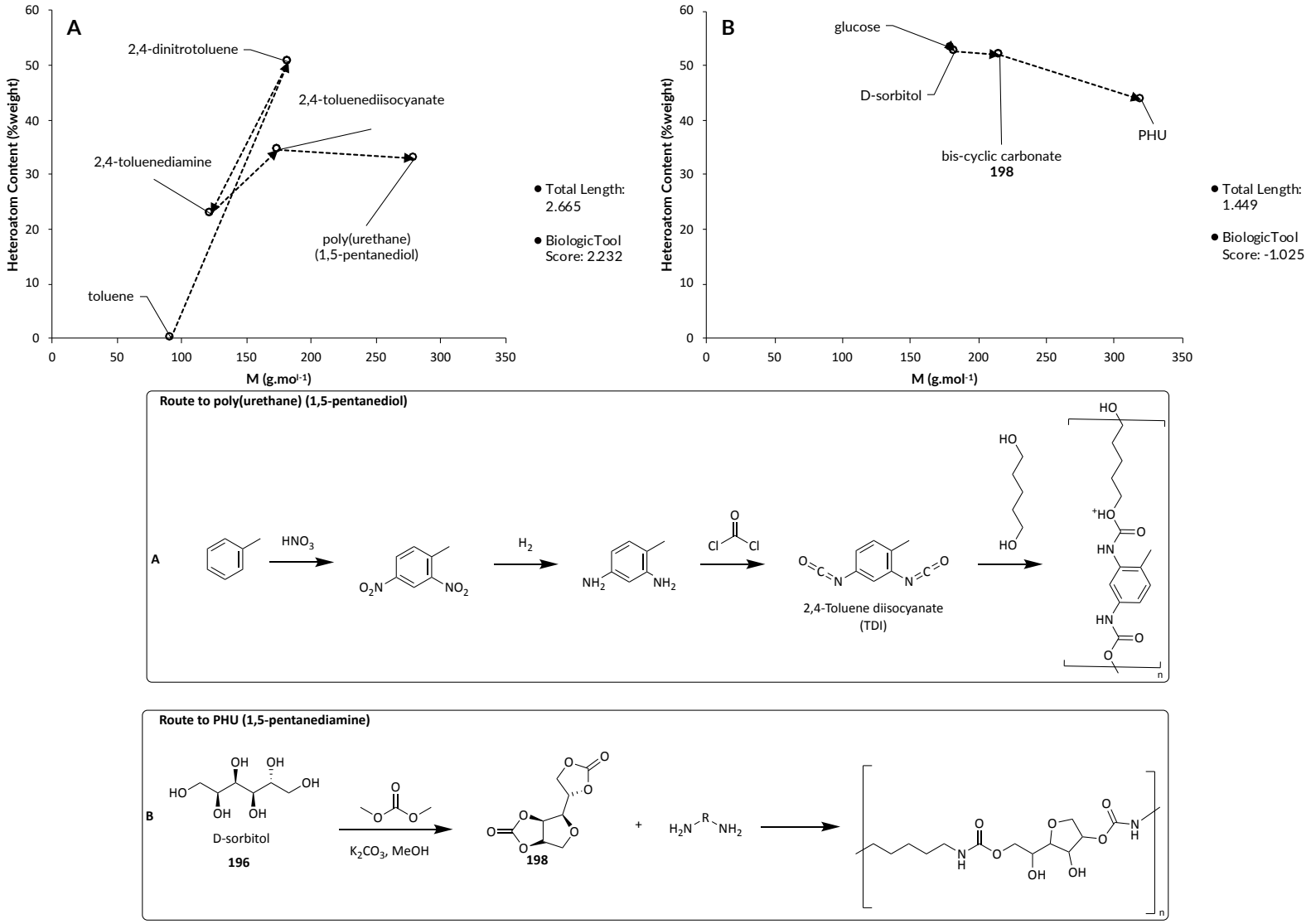

Figure 74 ***A****: BioLogicTool plot of polyurethane using 1,5-pentanediol as a diol;* ***B****: BioLogicTool plot of polyhydroxyurethane (PHU) with 1,5-pentanediamine*

4.8 Conclusion for chapter IV part 2

Polyurethanes are amongst the most commonly encountered polymers in our daily life. However, the isocyanate synthesis hazards are the reasons why alternatives have been sought after for several decades.

The first steppingstone towards a more sustainable polyurethane production was reached when the polyols necessary for polymerisation got produced from vegetable oils. Nevertheless, although the scientific community made remarkable efforts to enhance the greenness of this process, the real hazard, isocyanates, was remaining.

Non-isocyanate polyurethanes, PHUs, have recently progressed to the forefront of the scene as potentially excellent polyurethane replacement. PHU synthesis is based on the ring-opening polymerisation of bis-cyclic carbonates with diamines, both accessible from biomass. The resulting PHUs often displayed close if not better properties when compared to usual isocyanate-based polyurethane. This discovery led to a growing number of publications on this class of polymer. However, most studies do not consider the diamines being used when assessing the sustainability of the reaction. Yet, since most of them derive from fossil-based chemicals, finding renewable sources of diamines is particularly relevant in greener chemistry.

For these reasons, the use of L-lysine to produce 1,5-pentanediamine by decarboxylation, thus further valorising proteins residues, was conducted in this work. 1,5-pentanediamine dihydrochloride was obtained in yields up to 31% by employing the decarboxylation protocol developed for L-glutamic acid. Utilising other cyclic enone inducers did not

significantly improve yields but showed how the Brønsted acidity of the amino acid might impact the outcome of the reaction. Finally, although the highest yield was obtained using (R)-carvone as an inducer, it was proven impossible to reuse any excess of the inducer due to its conversion to carvacrol. Isophorone was thus deemed the most appropriate cyclic enone inducer for the thermal decarboxylation reaction of L-lysine.

The polymerisation of a bis-cyclic carbonate obtained from sorbitol with 1,5-pentanediamine was then conducted. The unexpected foamy appearance of the polymer obtained was attributed to the formation of an isosorbide-like structure concomitant with CO_2 emission. The CO_2 bubbles hence formed were proven to be trapped within the polymer, explaining the foam formation.

The L-lysine derived 1,5-pentanediamine utilisation in the ring-opening polymerisation was possible after desalting and led to similar foamy material. However, when the desalting was attempted *in situ*, the obtained foam was highly hygroscopic likely due to the high amount of salt formed and trapped within the polymer or the excess base employed.

Further challenges such as increasing the yield of the 1,5-pentanediamine, preventing salt formation or scaling-up of the polymerisation must be addressed. Nevertheless, this work represents an advancement in the utilisation of renewable resources for the production of NIPUs.

Chapter V
Conclusion

5.1 Concluding remarks

Humans deeply impacted their ecosystem, which led to the environmental emergency that the world is currently facing. The severe reduction of activity due to the COVID-19 pandemic further highlighted this impact. Indeed, a significant atmospheric pollution decrease (almost -50% of NO_2 in China) was observed in numerous places of the world as a lockdown side-effect.[362] This shows that extreme measures against GHG emission can, today, have a rapid, positive effect on our environment.

Yet, alarming reports were published early in the 1970s but remained mostly unheard by industries and policymakers.[3,363] Today, the current state of the ecological crisis is forcing all members of the society to take actions, and chemists must be part of it now more than ever.

Green chemistry was born in response to the rise in environmental awareness at the end of the millennium. The twelve principles, by which an ideal green chemical reaction should abide, still hold today but have also been significantly extended or improved with, for instance, the SDGs (see chapter I).[364] Intrinsic to green chemistry, several concepts of biorefineries have been developed to render the use of biomass a reality. However, both first and second-phases and generation biorefineries suffered from several drawbacks, notably, the need for arable lands to produce fuel or chemicals. In this context, microalgae were considered an alternative feedstock, hence giving birth to third-generation biorefineries.

The considerable rise in interest for microalgae by the scientific community in the previous decade rapidly dropped due to the many bottlenecks remaining to ensure the

financial viability of such biorefinery. The current challenges to address were presented in chapter III.1, together with the different solutions proposed. An increasing number of scientific analyses concord for the need of a *multi-component biorefinery* employing most biochemicals in the microorganisms for the production of multiple value-added products (phase II biorefinery).

Simultaneously, new metrics were developed to help chemists assessing the friendliness of a reaction from an environmental and productivity perspective. Although yields (by mass or mole) remained the most and sometimes only metrics to hold consideration amongst chemists, more and more "green" metrics are being considered such as E-factor, atom economy or biomass utilisation efficiency. No metrics developed so far could be used without a deep understanding of the reaction mechanism nor offered a visual representation.

The aim of this work was double:

- First, to develop a visual and quantitative tool to help to assess the rationality of a reaction.
- Second, to conceptually demonstrate the chemical possibilities enclosed in microalgal cells by synthesising different value-added products using molecules derivable from microalgae.

Main results presented in this thesis are summarised Figure 75 and 76:

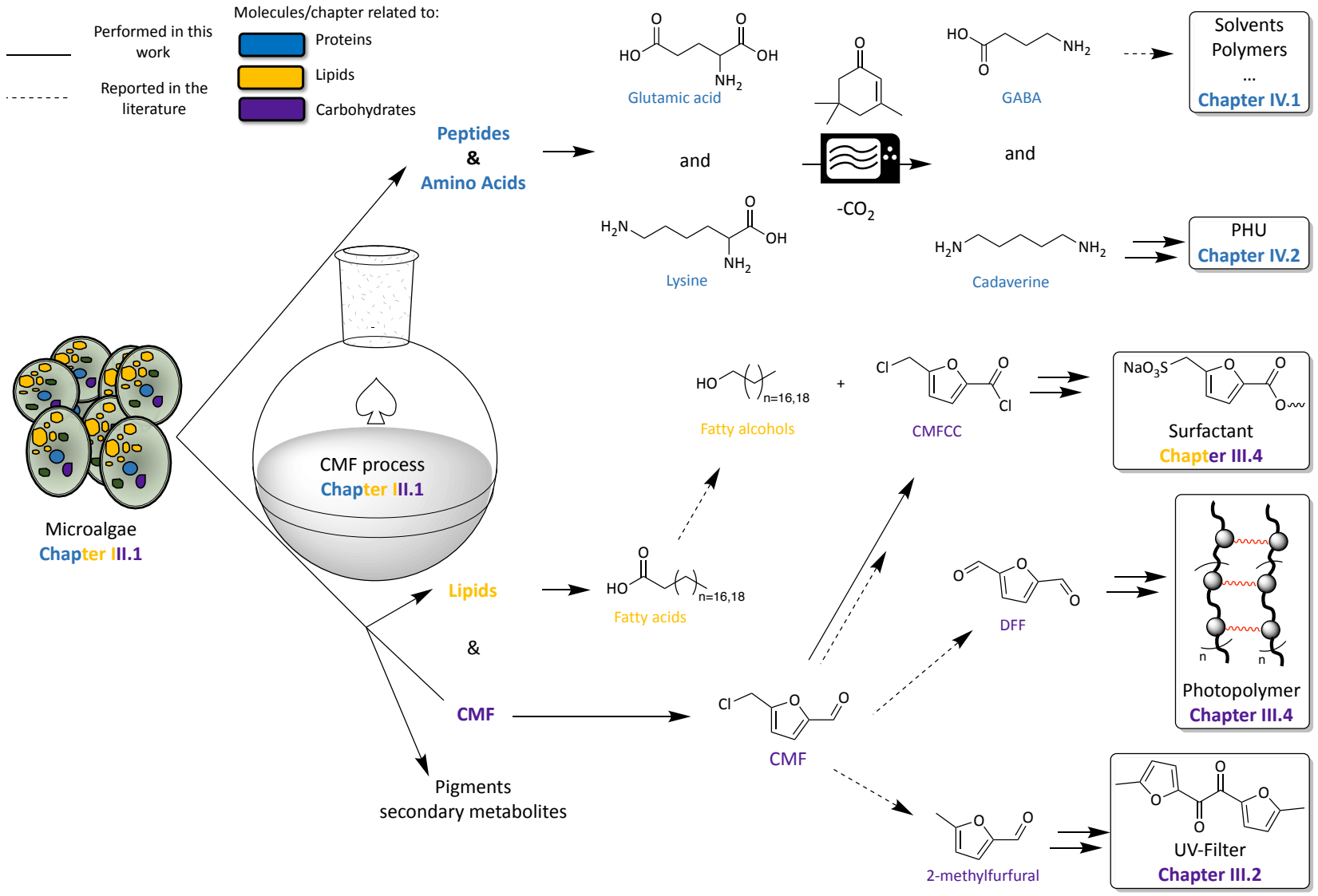

Figure 75 Summary of the synthetic work presented in this thesis, "Chemicalgal plant" concept

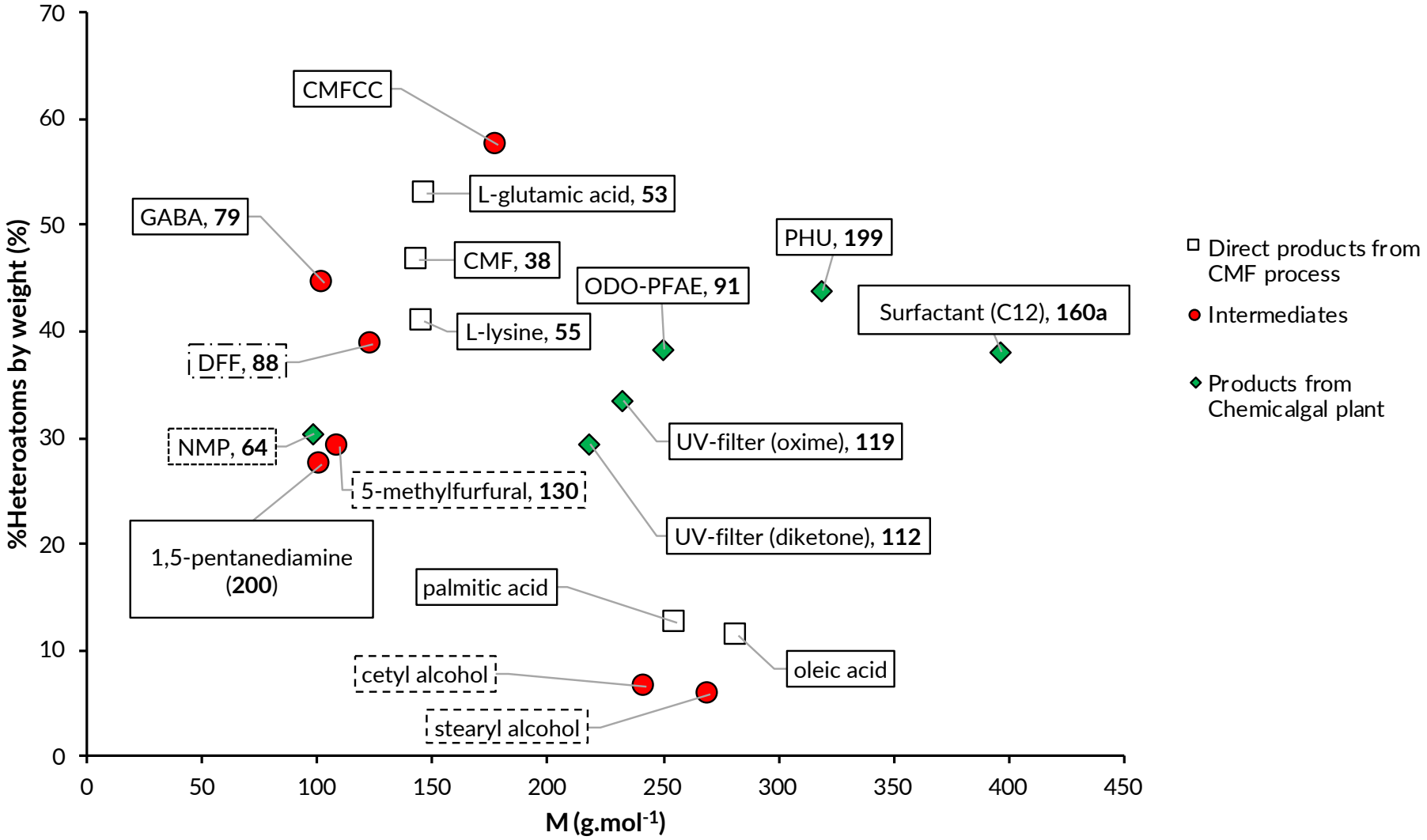

Figure 76 BioLogicTool mapping of products obtainable with the "Chemicalgal plant" concept

Chapter II focused on the first goal and introduced the *BioLogicTool* especially developed to compare bio-derived and fossil-derived routes. Starting from the van Krevelen diagram, different iterative modifications led to representing the %heteroatom by mass against the molar mass. These changes permitted to map chemicals simply based on the two parameters used. Starting material and intermediates could then be represented on this single plot using vectors to show the direction of each step of the chemical route to the target product. Finally, the length of the hence created vector was used to calculate rationality scores: *Total length* (of a chemical pathway) and *BioLogicTool score*. A case study using a monomer for photopolymers was employed to illustrate the use of the tool, and many examples were given throughout the chapters.

The remainder of this thesis was dedicated to the second aim presented before. Chapter III.1 was dedicated to the proximate and amino acid analysis of the biomass employed in this work. The impressive variations in composition between the microalgae species also highlighted the potential which resides in this type of feedstock.

The concept of a multi-component and multi-feedstock (phase III) microalgal biorefinery was herein called the "*Chemicalgal"* biorefinery. The CMF process was key to this concept, simultaneously converting carbohydrates into CMF (Figure 76 in purple), hydrolysing and extracting triglycerides to fatty acids (Figure 76 in yellow) and partially hydrolysing proteins to amino acids (Figure 76 in blue). The use of concentrated HCl avoids the need for microalgae harvesting, disruption and dewatering those three parameters being currently the principal operational expenses of a microalgae biorefinery. Until now, the CMF production from microalgae was not reported, and yet, it represents an ambitious solution to valorise every component of this biomass. Unfortunately, the low carbohydrate

content in our selected species did not lead to impressive yields of CMF despite careful optimisation. However, the successful production of CMF was encouraging and can, without a doubt, be significantly improved with the use of other(s), carbohydrate-rich microalga(e).

The following sub-sections of chapter III (III.2-4) demonstrated the use of polysaccharide-derived platform chemicals (furfural, CMF or HMF) for the production of higher-value chemicals: UV-filters for sunscreen application (Chapter III.2), photopolymers for photolithography/3D printing application (Chapter III.3) and surfactant for detergent application (Chapter III.4).

Chapter III.2 focused on the synthesis of bio-derived UV-filters for sunscreen application. The successful synthesis of nine UV-absorbing compounds (two of which scaled to several grams) bearing a potentially renewably derived furan ring core was reported. Unfortunately, their solubility in cosmetic oils and biodegradability were not deemed adequate for cosmetic applications. Besides, the photo-instability of most of the structures tested were not compatible with the standard conditions in which sunscreens are used. Nevertheless, this initial work demonstrated the possibility of tuning the UV-absorption spectrum of bio-derived molecules. Further work should focus on solving both solubility and photostability issues, as discussed in the following section.

The exceptionally high UV activity, and indeed instability, of one of the synthesised bifunctional structures, inspired its use as a monomer for polycondensation reactions. In chapter III.3, the necessary scale-up of the synthetic procedure used in chapter III.2, led to developing a semi-continuous method for producing the key intermediate DFF. Studies of

two different commercial sources of MnO_2 revealed structural and chemical differences which could explain the discrepancy in oxidative power. The following steps consisted of a Knoevenagel-Doebner condensation followed by esterification, which led to monomer **90** in good yield and high stereoselectivity. Chemo- and enzymatic catalytic polymerisation of this monomer with different diols were tried. In this work, iCaLB was preferred due to the higher M_n obtained, the use of critical-element free catalyst and the avoidance of untimely side reactions due to milder reaction conditions. Mechanical testing of a polymer film made of 1,8-octanediol and UV-active monomer as a constitutive unit before and after UV-curing was realised. Results showed an impressive increase in stiffness and a previously unseen work-hardening behaviour of the cross-linked photopolymer which can find application in photolithography or 3D printing.

Finally, chapter III.4 presented the synthesis of furan derived surfactants. Series of furan-derived sulfonated surfactant (FSS) structures were chosen with the help of an industrial partner to replace fossil-based sulfonated surfactant. One FSS family, bearing a sulfonate group α to the 5- position of the furan ring and an ester hydrophobic chain linker, could be satisfactorily sulfonated via the Strecker reaction and was made on a multi-gram scale. Amongst this family, two members with a branched hydrophobic chain appeared as a potential replacement for LAS. Their low Krafft temperature, CMC and good mildness often surpassed LAS performances, making them excellent surfactant for detergent application.

Additional surfactants were made also based on the previously mentioned motif to use the different biochemicals in microalgae. In this case, however, the hydrophobic chain attached to the surfactant was designed to mimic the potential mixture of fatty alcohols obtained from the hydrogenation of microalgal fatty acid. Thus, the low solubility of the

surfactant mixture made them unsuitable for detergency application, but they may find use as emulsifier or dispersant.

A step closer to a multi-component biorefinery was, at this point, conceptually reached since both microalgal sugars and lipids were valorised. Nevertheless, a major constituent of this biomass, proteins, remained. Chapter IV focused on the valorisation of proteins from microalgae. The aqueous phase left after the CMF process is mostly composed of hydrolysed free amino acids, short peptides and to a lesser extent, inorganic salts and unreacted sugars. The most abundant amino acids contained in the microalgae tested in this work, were L-glutamic acid and L-lysine as determined in chapter III.1. Thus, efforts were made to valorise these two amino acids to produce primary amines.

An extensive study on the non-oxidative decarboxylation of glutamic acid to GABA was presented in chapter IV.1. This amino acid was known for its recalcitrance to usual thermal decarboxylation conditions due to its propensity to isomerise to pyroglutamic acid before any reaction could occur. The decarboxylation product, GABA, has already found many applications for producing polymers, pharmaceuticals or solvents. Here, a judicious choice of cyclic enone inducer, isophorone, allowed the successful decarboxylation of glutamic acid to occur using microwaves as a greener heating method. The optimisation of the reaction conditions permitted to reach a yield of up to 63% in only 7 minutes. A mechanism explaining the presence of 2-pyrrolidone before work-up and the decarboxylation of glutamic acid was suggested.

A high purity glutamic acid was obtained from gluten after employing this feedstock in the CMF process or acid hydrolysis. Attempts to produce glutamic acid similarly with

microalgae failed likely due to other biocomponents preventing the selective precipitation of this amino acid. Nonetheless, glutamic acid derived from gluten could be decarboxylated in ~30 % after free base formation. Despite the poor yield obtained, this demonstrates the feasibility of such procedures to be applied on renewable feedstocks, in this case, gluten.

The second part of this chapter was dedicated to producing a linker for non-isocyanate polyurethane, NIPU, derived from renewable resources. In L-lysine, the presence of a primary amine group ω- to the carboxylic acid function made it a candidate of choice for the production of 1,5-pentanediamine, a potential linker for the synthesis of polyhydroxyurethanes, PHU. L-Lysine was thus decarboxylated using the protocol previously developed, and the comparison of different cyclic enone catalyst was also made. Isophorone appeared once again as the inducer of choice for non-oxidative L-lysine decarboxylation due to its reusability in further reaction. A bis-cyclic carbonate monomer was separately synthesised from sorbitol and successfully polymerised “in the melt”. Interestingly, the polymer thus obtained, had a foamy appearance that was later attributed to the release of CO_2 during the polymerisation. This self-blowing behaviour may be particularly of interest for insulation application and participated further to the greenness of this PHU by avoiding the addition of CO_2 or else as a foaming agent.

To conclude, this thesis represents a concept for a multi-component microalgal biorefinery (summarised in Figure 76). Every principal component of microalgae was proven to be of potential value, and a wide range of compounds was synthesised. Many improvements are required to ascertain financial viability or feasibility of this concept and are discussed in more details in the Future Work section exposed next.

5.2 Future work

Many aspects of the work conducted in this thesis are currently being or will be investigated in greater details. For instance, the *BioLogicTool* introduced in chapter II would be significantly enhanced by the inclusion of energy or environmental friendliness of the reactions. For example, it would be possible to add an additional axis by plotting the free Gibbs energy of each feedstock, intermediates and product at the ground state. A secondary set of vectors may be drawn with their direction indicating an endergonic reaction ($\Delta G>0$, positive vector, pointing upward) or exergonic ($\Delta G<0$, negative vector, pointing down). Inclusion of other metrics such as E-factor, biomass utilisation efficiency or atom economy within the *BioLogicTool* may further help assess the rationality of a chemical route.

Regarding the second part of this work, the microalgae used as feedstock for the CMF process were not suited to yield a high amount of CMF due to their low (poly)saccharide content. However, with carbohydrate-rich microalgae, much higher yield may be expected. For example, a species accumulating up to 60% (DW) starch was reported.[365] Using this microalga species would yield up to 0.48 $g_{CMF}.g_{microalgae}^{-1}$ (considering a CMF yield of 80% of available sugars), representing a great leap forward in the CMF production from microalgae. Humins (collected after filtration of the aqueous phase) inevitably produced during the reaction may be utilised as soil amendments or novel mesoporous material for catalysis.[117,366] Advantageously, the *Chemicalgal* plant may use multiple microalgae species to adjust the demand in lipid, protein or sugar-derived compounds by the market. A collaboration between a biotechnology laboratory or company to grow adequate

microalgae species under chosen conditions and chemists to explore this biomass in more details seems necessary.

The main parameter that remains an issue for the CMF process is the use of toxic 1,2-dichloroethane as a solvent (or DCM). Toluene and cyclohexane have been shown to tolerate the CMF process conditions but led to lower yields than when chlorinated solvents were used.[133] Xylenes derived from renewable resources may be a direct replacement for toluene, but their high boiling point (138 – 144 °C) may prevent their use in large-scale applications. Ionic liquids (ILs) may well represent an alternative to chlorinated or fossil-derived solvents in the CMF process which has little been explored.[117] However, the use of concentrated HCl may not be compatible with the common imidazolium salts employed as ionic liquids. ILs are also unlikely to be compatible with the biphasic nature of the reaction, which is one of the main advantages of this process. Development of novel bio-derived alternative solvents that would tolerate the CMF process conditions (conc. HCl, immiscible with water etc.) is essential to increase the sustainability of this reaction.

In chapter III.2 the low photostability and biodegradability of UV-filters possessing a furan core were the main issues to address. Many rearrangements of furan rings (Piancatelli, Achmatowicz, etc.) may advantageously preserve the UV activity of the subsequent compounds while improving their photostability. Notably, the photoreaction of furfural to produce 5-hydroxy-2[5H]-furanone (Scheme 38, **144**) is an exciting route to explore.

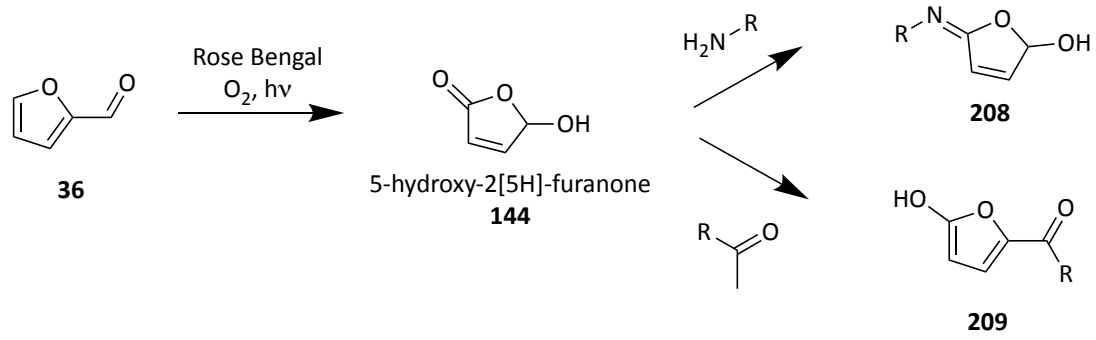

*Scheme 38 Possible UV-stable structures from furfural (**36**) for sunscreen applications*

This cyclic enone likely remains a good UV-absorber, the maximum absorption or solubility of which may be further tuned by using the ketone manifold (imine, aldol reaction) or the alkene manifold (Michael addition). Additionally, the less rigid ring, due to loss of the furan aromaticity, may increase the biodegradability of such molecules.

The photopolymer designed with renewable UV-active repeating units in chapter III.3 is worth investigating further. For instance, additional polymers with different diols or the synthesis of a copolymer (with fumaric/maleic acid) can be realised. This modification would offer a range of possibilities which will widen the possible application of such polyesters (adhesives, coatings etc.). Most importantly, the reversal of the [2+2] cycloaddition cross-linking should be possible using higher power UV-lamps. The mechanical or thermal "crack-healing" of this polymer may also be a potential route to explore. Finally, reusability of the immobilised enzymes is necessary to test and, if positive, would provide another argument favouring the use of this bio-catalyst.

The last section of chapter III (chapter III.4) employed platform molecules for the production of furan-derived sulfonated surfactants (FSS). The sulfonation/sulfation

reactions of furans remain a significant bottleneck to overcome to obtain larger arrays of FSS. Efforts to use sulfate/sulfite salts and avoid sulfur trioxide complexes would enhance the overall sustainability of the reactions by avoiding solvent-consuming ion-exchange chromatography. A path to explore is the catalytic sulfonation/sulfation using sulfite salts and copper-based catalysts.[367,368] Additionally, the synthetic procedure for the ester family may be improved by avoiding the Finkelstein reaction step and directly sulfonating the chloro- furan fatty esters. Tetrabutylammonium iodide, used as a phase transfer catalyst in the sulfonation reaction, may form the iodide intermediate before reacting with the sulfite ion, thus combining both steps in one. Other structures may also be obtained using the different furan rearrangement reaction as cited previously, but the loss of the furan aromaticity furan may be detrimental to the surfactant properties.

Chapter IV.1 and 2 focused on the valorisation of glutamic acid and lysine, respectively. First, it appeared evident that the selective isolation of single amino acids is far from trivial. Only glutamic acid could be selectively precipitated, but so far other methods of separation seem required for other amino acids. Alternatively, the development of a universal decarboxylation method may permit the separation (by fractional distillation for instance) of the different primary amines obtained. Besides, the synthesis of either:

1. a more active carbonyl inducer avoiding the high temperatures employed here or
2. the immobilisation of these cyclic enones would also be a possible improvement for this procedure to facilitate the recyclability of the carbonyl inducer and avoid using an excess reagent.

The low molecular weight of the self-blowing PHU obtained was likely problematic for insulation, automotive parts etc. Thus, this polymerisation method may benefit from using a catalyst that could help control the stereoisomerism of the polymer (using a chiral catalyst, for instance) and increase its molecular weight. Thiourea or TBD (1,5,7-triazabicyclo[4.4.0]dec-5-ene) have been proven to be excellent catalysts and is possible that a chiral derivative of these compounds may help control the stereoisomerism of PHU.[357]

To put in perspective the current stage of the microalgae industry with the petrol one, a *back-of-the-envelope* calculation based on the production of surfactant blend **160$_f$** follows (see also Figure 77).

Currently, 15 000 $t.y^{-1}$ of dry microalgal biomass is produced in the world (distributed among *c.a.* ten species) for an average retail price of 40 $€.kg^{-1}$.[69] If the entirety of the microalgal biomass produced (corresponding to 600 M€) were to be used for CMF production, approximately 7,200 tonnes of this platform molecules could be made (with a hypothetical production of 0.48 $g_{CMF}.g_{microalgae}^{-1}$). If, for instance, the surfactant mix **160$_f$** synthesised in chapter III.4 were the target molecule, ~7200 tonnes could be obtained (with the current overall yield of 31% from CMF). The retail price of this surfactant should thus be at least 83 $€.kg^{-1}$ to solely compensate the cost of the feedstock needed (600 M€/$7.2x10^6$ kg) and much higher to be profitable taking the CAPEX/OPEX into account. In comparison, LAS production volume is 3.5 $Mt.y^{-1}$ sold for 1.5 $\$.kg^{-1}$, far from the hypothetical numbers herein obtained.[227] To reach this production volume ~7 Mt of dry microalgae would be required (with the current numbers). Improvements on the different synthetic step yields could reduce the amount of biomass needed to 2.3 Mt (with a 98%

overall yield from CMF) still requiring a 150-fold biomass production increase. This simple calculation further demonstrates the need for a microalgal biorefinery to diversify its target compounds to be more profitable. However, the emerging microalgae industry will undoubtedly grow but is unlikely to reach the multi-billion-ton production volume like the petrol-based industry.

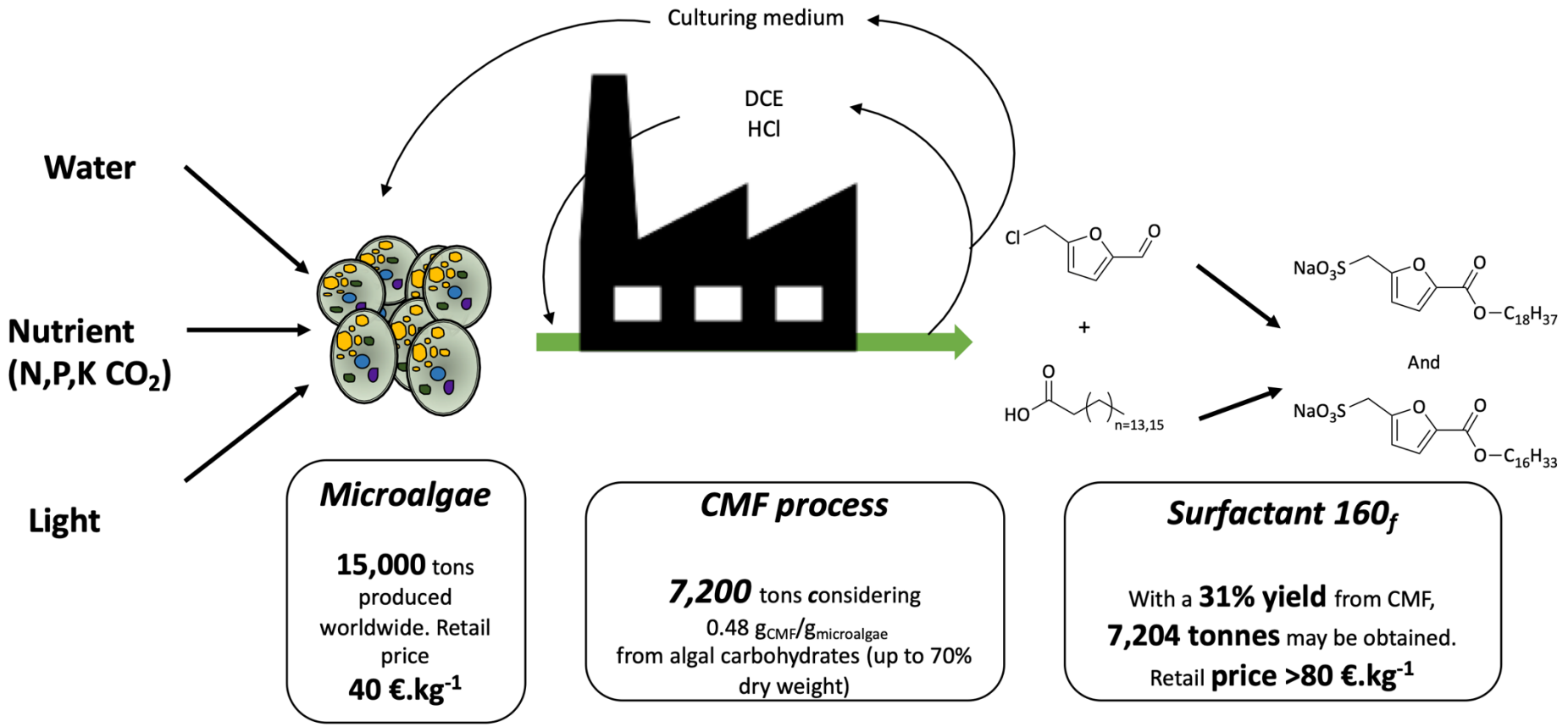

*Figure 77 Schematic representation of the production of surfactant **160_f** from microalgae employing the CMF process*

The proposed improvements discussed above can enhance the different reactions (or tool) developed in this thesis leading to a financially viable *Chemicalgal* plant. The future bio-society may rely on this concept together with the myriad of other existing and under-development technologies based on lignocellulosic residues (estimated to represent 4.6 billion tonnes globally).[369] Encouraging incentives to find more innovative ideas and challenge the dogma found in fossil-based chemistry is paramount to preserve the level of comfort we currently have in our society. However, adopting these novel technologies must go hand in hand with a profound change in the current consumerist-driven economy.

The terrible environmental damage seen since the beginning of this century has already forced us to question the economic model in place. Surely, chemical industries will realise profound changes in the following years that will help mitigate and, hopefully, solve some of the existing and future challenges.

Experimental Section

Materials and chemicals

All chemicals and reagents were purchased from commercial sources and used without further purification unless stated otherwise. Deionised (DI) water was obtained from an internal laboratory system using Centra Elga filtration apparatus. Chromatography grade water was used for HPLC was purchased from Fischer Scientific. Anhydrous CH_2Cl_2, THF, Et_2O, DMF and toluene were obtained from Innovative Technology Inc. PureSolv® solvent purification system and stored under Ar or N_2 with 3Å activated molecular sieves. Molecular sieves were activated at 300 °C overnight and stored in an open drying oven (80 °C). Furfural was purified by vacuum distillation using a Kugelrohr apparatus and stored under Ar at -20 °C. HMF was purified by active filtration using a 6 cm diameter sintered funnel filled with, from bottom to top: Celite 545 filtration agent (1 cm height), activated carbon (Honeywell, 1 cm height), Silica gel 0.0015-0.0045 mm (Merck, 4 cm height) and $MgSO_4$ (1 cm height). The hence prepared column was filled with DCM and allowed to elute until the solvent started to drip (DCM was added if necessary). The crude HMF was then dissolved in a minimum amount of DCM, and the resulting solution was loaded onto the column. The column was allowed to run until the eluting solution was colourless. The collected fractions were evaporated under reduced pressure to afford pure HMF, which was further dried under high vacuum and stored at 2 °C under Ar. *N*-Bromo succinimide and triphenylphosphine were recrystallised from water and isopropanol respectively, dried under high vacuum and stored in a vacuum desiccator before use. *Candida antarctica* lipase B (CaLB) immobilised onto acrylic resin (iCaLB) was purchased from Sigma-Merck and lyophilised 48 h in a vacuum oven at 40 °C before use. Silica gel 60 Å (Sigma-Merck) was used for flash column chromatography using a slight positive pressure of N_2. Silica gel

0.0015-0.0045 mm (Merck) was used for active filtration purification of HMF, CMF and Guerbet alcohol bromo-derivatives. Aluminium TLC plates, silica gel coated with fluorescent indicator F254 were used for TLC analysis with the indicated solvent system. Glassware was washed with commercial detergent (Teepol™), rinsed with tap and DI water and dried with acetone before storing in a drying oven (60-80 °C).

Microalgae *Nannochloropsis occulata* and *Spirulina sp.* were obtained from commercial sources: Varicon Acqua and myprotein.com respectively.[100,370] *Tetraselmis suecica* was a gift from Dr. Hubert Bonnefond (Inalve company). *Spirulina sp.* and *Tetraselmis s.* were obtained as a freeze-dried powder and directly used without further purification unless specified. *Nannochloropsis o.* was received as a frozen concentrated paste and washed as follow: ~7 g of microalgae paste was placed in a centrifuge tube, washed three times with distilled water (60 mL) and centrifuged (3600 rpm, 30 min) to removed excess culturing medium. The supernatants were discarded, and remaining solids dried in an oven at 60 °C until constant weight. The dried solids were then finely ground with a mortar and pestle until particle size was less than 1 mm. The obtained powder was used for the CMF reaction and characterisation.

Analytical instruments and methods

High-performance liquid chromatography

An Agilent HPLC Infinity 1200 was used to perform liquid chromatography. It comprised a quaternary pump (Agilent G7111B) to pump eluents through the column (see below for column specifications), a DAD detector (see amino acid analysis and UV-filter analysis,

Agilent G7115A) or a refractive index detector (see total sugar analysis). Sampler (Agilent G7129A) was used for the automated derivatisation procedure.

- *Total amino acid HPLC analysis*

This protocol was adapted from a previously reported procedure.[108] A Poroshell 120 EC-C18 4.6 x 100 mm, 2.7 μm diameter column was used for amino acids analysis. The temperature of the oven was set at 45 °C, with a pressure limit of 600 bar and a flow set at 0.4 mL.min^{-1}. Detection (DAD) was set at wavelength 263 nm (FMOC derivatives) and 338 nm (OPA derivatives). Sampler settings were the following: draw speed-200 μL.min^{-1}, eject speed-400 μL.min^{-1}. The following eluent gradient was used (Table 25):

Table 26 Eluent profile used for amino acid analysis by HPLC

Time (min)	A* (%)	B* (%)
12	80	20
13	65	35
17	60	40
19	55	45
21	44.7	55.3
25	40	60
28	30.0	70
29	25	75
30	15	85
32	10	90
34	5	95
36	0	100
37	40	60
40	80	20

*Compositions of eluents A and B are described below.

Eluent **A** (2 L) was prepared as follows: 2.84 g of $NaHPO_4$ and 4.02 g of NaB_4O_7 were dissolved chromatography grade water (2 L) and adjusted to pH 7.9 with conc. HCl (37%) and 1 M HCl. Eluent **B** (1 L) consisted of a MeOH: MeCN: H_2O (2:6:2) solution. Borate Buffer

(BB) solution was made by dissolving 1.24 g of boric acid and 1.49 g of KCl in DI water (50 mL) adjusted to pH 10.5 with NaOH ground pellets. Ethanethiol (ET) solution consisted of ethanethiol (500 μL), BB (20 mL)and MeOH (80 mL , ethanethiol has a strong, pungent smell and care must be taken to open the ethanethiol bottle under a fumehood). Fluorenylmethyloxycarbonyl (FMOC) solution was prepared by dissolving 25 mg of FMOC chloride in MeCN (10 mL). o*rtho*-Phthalaldehyde (OPA) /ET solution was made by dissolving 40 mg of OPA in ET solution (10 mL). Diluent was prepared by mixing eluent A (48.5 mL) with concentrated phosphoric acid (1.5 mL). The internal standard solution consisted ($ISTD_{sol}$) in a 1.5 mM Norleucine solution. The pre-column derivatisation was done in the HPLC needle by an automated procedure as follows (Table 26):

Table 27 Auto-sampler program for pre-column derivatisation

Function	Parameter
Draw	Draw 50 µL from location "P2-A1" with default speed using default offset
Draw	Draw 1 µL from air with default speed
Draw	Draw 2 µL from location "P2-A2" with default speed using default offset
Draw	Draw 2 µL from sample with default speed using default offset
Draw	Draw 12 µL from air with default speed
Mix	Mix 4 µL from air with default speed for 5 times
Wait	Wait 1 min
Eject	Eject 12 µL to seat with default speed
Wash	Wash needle in flushport for 5 s
Draw	Draw 2 µL from location "P2-A3" with default speed using default offset
Draw	Draw 12 µL from air with default speed
Mix	Mix 6 µL from air with default speed for 5 times
Wait	Wait 0.15 min
Eject	Eject 12 µL to seat with default speed
Wash	Wash needle in flushport for 5 s
Draw	Draw 4 µL from location "P2-A4" with default speed using default offset
Draw	Draw 12 µL from air with default speed
Mix	Mix 10 µL from air with default speed for 5 times
Eject	Eject 12 µL to seat with default speed
Inject	Inject

Hydrolysis of the samples was done as follow: 10 mg of biomass were suspended in 6 M HCl (25 mL with 1% w/v phenol) and heated at 150 °C for 30 min in a sealed 30 mL tube placed in an Anton Paar Monowave 300 microwave chamber. The resulting mixture was filtered and evaporated under reduced pressure. The resulting solid was re-suspended in a water:MeOH:$ISTD_{sol}$ solution (5:4:1, 30 mL). The suspension was sonicated for 10 s and filtrated through 0.22 µm Whatmann filters before analysis.

- *Total carbohydrate content HPLC analysis*

HPLC analyses were carried out with an Agilent Infinity 1260 using a Hi-Plex column (300 x 7.7 mm, H^+ form), an isocratic gradient of 0.005 M H_2SO_4 for 30 min, a column oven temperature of 60 °C and a refractive index (RI) detector set at 55 °C. A 2-steps hydrolysis procedure was adapted from an NREL protocol.[371] 25 mg of microalgae biomass was hydrolysed with 72% H_2SO_4 (0.25 mL) at 30 °C in a water bath for 1 h with vortex agitation every 15 min. The samples were then diluted with DI water (7 mL) and placed in a microwave (Anton Paar Monowave 300) for the indicated time and temperature. The samples were filtered, and an aliquot of the hydrolysate (3 mL) was neutralised to pH 7 with $CaCO_3$. Finally, the samples were filtered through 0.22 um pores diameter filters before submitting to the HPLC. Alternatively, total carbohydrates content (TCC) was obtained following the equation:

$$TCC=TSC-(TAC+TLC+TPC_{HPLC}) \quad \text{(eq. vi)}$$

Gel permeation chromatography (analysis realised by Dr. Ian D.V. Ingram)

Gel permeation chromatography of the THF soluble polymers was carried out by Dr. Ian Ingram using a PSS SDV High set composed of 3 analytical columns (300 × 8 mm, particle diameter 5 µm) of 1000, 105 and 106 Å pore sizes, plus guard column (Polymer Standards Service GmbH, PSS) installed in a PSS SECcurity SEC system. Elution was performed with THF at 1 $mL.min^{-1}$ with a column temperature of 23 °C and detection by refractive index. 20 µL of a ~2 $mg.mL^{-1}$ sample, adding a drop of toluene as a reference standard, was injected for each measurement and eluted for 50 min. GPC of $CHCl_3$ soluble polymers was carried out at 30 °C on an Agilent Technologies HPLC System (Agilent Technologies 1260 Infinity) connected to a 17369 6.0 mm ID × 40 mm L HHR-H, 5 µm Guard column and a 18055 7.8 mm ID × 300 mm L GMHHR-N, 5 µm TSKgel liquid chromatography column (Tosoh Bioscience, Tessenderlo, Belgium) using 1 $mL.min^{-1}$ $CHCl_3$ as mobile phase. An Agilent Technologies G1362A refractive index detector was employed for detection. The molecular weights of the polymers were calculated using linear polystyrene calibration standards 250-70000 Da (Sigma-Merck).

Gas chromatography

GC-FID was recorded on an Agilent GC7890B or Agilent 6890 equipped with a Rxi-5HT column. The general GC method used was as followed: initial temperature 50 °C, no hold time, ramp rate 30 $°C.min^{-1}$, final temperature: 300 °C, holding 5 min, split ratio 5:1, injector temperature 300 °C. Total lipid analysis was run using the following method: initial temperature 60 °C, hold 1 min, ramp rate 8 min, set temperature: 340 °C, hold 30 min, split ratio 5:1, injector temperature 340 °C. The same method was used for GC-MS (Perkin Elmer

Clarus 500, 560S) analysis. The identity of the detected compounds was assessed using the NIST library. Samples were diluted in the appropriate solvent and filtered through cotton wool plug before injection.

Spectroscopy analysis

^{1}H- and ^{13}C-NMR spectroscopy were run on a Jeol-400 MHz instrument using the NMR solvent peak (D_2O, $CDCl_3$, DMSO-d_6, MeOD-d_4) as reference. Samples were dissolved in the appropriate solvent (indicated in brackets in the procedure and characterisation section). Experiments were run with 8 up to 64 scans for ^{1}H (400 MHz) and 256-1024 scan for ^{13}C (100 MHz). Coupling constants (J) are reported in Hertz (Hz) and are quoted to the nearest 0.1 Hz. Multiplicity abbreviations are as follows: s, singlet; d, doublet; t, triplet; q, quartet; m, multiplet; dd, doublet of doublets; td, triplet of doublets; ddd, doublet of doublets of doublets; br indicates a broad signal. All NMR spectra were acquired at 298 K in non-disposable NMR tubes. When needed, DEPT, COSY and HMQC experiments were run to confirm signals attribution. Fourier Transformation Infrared Spectroscopy (FT-IR) analysis was performed on a PerkinElmer 400 spectrometer using neat product and the attenuated total reflectance setting. FT-IR spectroscopy experiments were run with 8 up to 16 scans at 1 cm^{-1} resolution. Qualitative comments are given next to selected relevant signals: very strong (vs), strong (s), weak (w), very weak (vw). TG-IR (run by Dr. Ian V. Ingram) was carried out using a Netsch STA409 linked to a gas cell in a Bruker Equinox 55 Infra-red spectrometer by a heated gas line. Pre-weighed samples were heated from 20 °C to 600 °C under N_2 atmosphere using a ramp of 10 °C/min. UV-Vis spectra were recorded on a Jasco 550-UV-vis spectrophotometer in a 1 cm quartz cuvettes. 50 μM solutions in EtOH, 1,4 dioxane or $CHCl_3$ were analysed at 1 nm resolution.

The purity (Px) of GABA obtained by microwave decarboxylation of glutamic acid was assessed by ^{1}H-NMR spectroscopy using 32 scans, a delay time d_1 of 10 seconds and methylsulfone (Sigma Aldrich 98% purity) as an internal standard. The following equation was used for purity calculation:

$$P\text{x} = \left(\frac{Ix}{Istd}\right) * \left(\frac{Nstd}{Nx}\right) * \left(\frac{Mx}{Mstd}\right) * \left(\frac{Wstd}{Wx}\right) * Pstd \qquad \text{(eq. xix)}^{372}$$

Where I,N,M,W and P are the integrated area, number of nuclei, molecular weight and mass of methylsulfone (std) and product(x) respectively. Yields for GABA reported were then calculated according to the following equation:

$$y = \frac{\frac{mass\ isolated\ product * Px}{Mw\ product}}{Moles\ of\ starting\ compound} \qquad \text{(eq. xx)}$$

Where Px is the purity calculated from (1).

Spectrometry analysis

MALDI-TOF MS analyses were carried out using a Bruker Solarix-XR FTICR mass spectrometer and the relative software package for the acquisition and the processing of the data. An acceleration voltage of 25 kV, using DCTB as a matrix (for PFAE analysis) and KTFA as ionisation agent were used. 10 µL of sample were mixed with the matrix solution (40 mg.mL^{-1} DCTB in $CHCl_3$, 10 μL) and KTFA (5 mg.mL^{-1}, 3 μL). 0.3 µL of the mixture were applied on the plate, and the measurement was conducted in positive mode with the detector set in reflector mode. ESI-MS analyses were obtained from a University of York service employing the following procedure: samples were dissolved in the appropriate

solvents and further diluted in MeOH. The hence prepared solution was injected (injection volume: 1 μL) in a Bruker "compact" time-of-flight mass spectrometer with an Agilent 1260 Infinity LC at 0.2 mL.min^{-1} using a MeOH:water (1:1) eluent. Low mass data were collected in mass range (m/z) 50 to 1200. Sodium formate was used as calibrant and was injected prior to the sample during each acquisition.

Solid-state analytical methods and instruments

Powder XRD was performed by Yang Gao using a Bruker AXS D8 Advance controlled by XRD Commander software, with scan type set at locked coupled, operating voltage of 40 kV (current, 40 mA), scan speed of 2 s.step^{-1} and the scan scope from 0 θ to 90 θ. Single-crystal XRD experiments were recorded on an Oxford Diffraction SuperNova apparatus equipped with dual Mo & Cu sources. Data were acquired, and structures were resolved by Rachel R. Parker or Dr. Adrian Whitwood. Porosimetry analyses were performed by Konstantina Sotiriou using a Micromeritics ASAP 2010. Samples were degassed under vacuum (0.007 mbar) for at least 6 h at 130 °C prior to analysis. The Brunauer-Emmett-Teller (BET) theory was used to determine the surface area, and data processed using the MicroActive software provided with the instrument. EDX-SEM data were recorded by Jaspreet Kaur on a JEOL 7800F Prime SEM, equipped with a Schottky (field-assisted) thermionic emitter. Solid-state ^{13}C-NMR was performed by the University of York on a Jeol solid-state magic angle spinning spectrometer 400 MHz (^{1}H frequency).

Thermogravimetric, differential scanning calorimetry analysis

- *Total solid content of microalgae*

The total solid content was determined following an NREL protocol.[94] In tared pre-conditioned crucibles (575 °C, 24 h cooled to 130 °C in the furnace and further to room temperature in a vacuum desiccator) were weighed microalgae samples to the nearest 0.1 mg. The crucibles containing the samples were then placed in a high-vacuum oven (15 mbar) and dried at 40 °C for 24 h. The samples were then allowed to cool to room temperature in a vacuum desiccator containing activated silica gel and weighed. The following formulas were used to calculate the total solid, oven-dry weight (ODW) and moisture content:

$$TSC = \frac{Weight_{crucible+dry\ sample} - Weight_{crucible}}{Weight_{sample\ before\ drying}} x100 \qquad \text{(eq. iv)}$$

$$Moisture = 100 - \left(\frac{Weight_{crucible+dry\ sample} - Weight_{crucible}}{Weight_{sample\ before\ drying}}\right)x100 \qquad \text{(eq. xxi)}$$

$$ODW = \frac{Weight_{air\ dried\ sample} \times \%TotalSolids}{100} \qquad \text{(eq. v)}$$

- *Total lipids*

The total lipids were determined gravimetrically after Soxhlet extraction.[91,113] In a cellulose thimble (Waters, 10 x 50 mm) was weighed 200 mg (to the nearest 0.5 mg) of microalgae sample. The thimble was then covered with a filter paper and placed in a Soxhlet apparatus. A 250 mL round bottom flask was added $CHCl_3$:MeOH (2:1, 210 mL) and external heating

was set at 80 °C ± 5°C. The system was left to heat for 24 h at a siphoning rate of ~20 flushes per hour. The resulting extract was transferred quantitatively into a 250 mL round bottom flask and brought up to 250 mL with $CHCl_3$:MeOH (2:1, 40 mL, used to wash the Soxhlet and round bottom flask). The solvent was thoroughly evaporated under reduced pressure before weighing the flask

- *Simultaneous thermogravimetric analysis & total ash content*

TGA was performed on a PL Thermal Sciences STA 625 thermal analyser. 10 mg of accurately weighed sample in an aluminium sample cup was placed into the furnace with an N_2 flow of 100 mL.min^{-1} and heated from room temperature to 625 °C at a heating rate of 10 °C.min^{-1}. From the TGA profiles, the temperatures at 10% and 50% mass loss (Td_{10} and Td_{50}) were subsequently determined for polymers. A specific ramp procedure adapted from reported methods was used for the total ash determination of biomass.[94]

- Ramp from room temp to 105 °C
- Hold at 105 °C for 12 minutes
- Ramp to 250 °C at 10 °C.min^{-1}
- Hold at 250 °C for 30 minutes
- Ramp to 575 °C at 20 °C.min^{-1}
- Hold at 575 °C for 180 minutes

- *Differential scanning calorimetry (analysis performed by Dr. Alessandro Pellis)*

DSC experiments were performed on a TA Instruments Q2000 DSC under an inert gas atmosphere (N_2). Heating and cooling rates were set to 5 °C.min^{-1} over the T range of -60-

200 °C. Sample mass was between 5-10 mg for all measured samples. The Tg values were calculated from the second heating scan.

Elemental analysis

CHN elemental analysis was realised by a service from the University of York and run on an Exeter Analytical Inc. CE-440 analyser.

Melting points

Melting points were measured using a Stuart SMP10 Digital Melting Point apparatus.

Krafft temperature (analysis performed by Dr. Craig Fairgrieve, Unilever R&D)

The Krafft temperature was determined by looking at the Correlogram and identifying the transition temperature using the following procedure. 10 $g.L^{-1}$ solutions of the surfactants were prepared in deionised water. These solutions were filtered through an 0.45 µm nylon filter into a dynamic light scattering disposable cuvette. Using a Malvern Zetasizer the particle size was measured as a function of temperature from 40 to 1 °C in 1 °C step decrement with the following parameters:

- Material: polystyrene latex
- Dispersant: water
- Cell: disposable cuvette
- Equilibration time: 900 s
- Number of measurements: 3.

Surface tension (analysis performed by Dr. Craig Fairgrieve, Unilever R&D)

The surface tension was determined using the following procedure. 2 $g.L^{-1}$ samples of each surfactant were prepared in 4 solvents; 0.1 M NaCl, 3 French Hardness (FH) water, 12 FH water and 24 FH water. These were then serially diluted (1/2) using a Hamilton Liquid handler across a 96 well plate giving a concentration range of 2-0.000977 $g.L^{-1}$. The surface tension was measured using a Kibron Delta 8 surface tensiometer, 4 repeats were carried out for each sample and averaged to generate the results presented in chapter III.4.

Mildness (analysis performed by Dr. Craig Fairgrieve, Unilever R&D)

The mildness of the surfactant samples was tested by a colourimetric assay of their solubilisation of zein (corn protein) mixed with a blue dye and dried to the bottom of a 96 well plate, the greater the solubility, the greater the absorbance. Measurements were made at 10, 5 & 1 $g.L^{-1}$, sodium dodecyl sulfate (SDS) was used as a positive control (harsh) while rhamnolipid (RL) and water were used as negative controls (mild). Samples were mixed, incubated at 40 °C for 30 minutes with agitation then the absorbance was read at 590 nm on a UV-Vis spectrophotometer.

Software and packages

Agilent Chemstation was used to process GC-FID and HPLC data. FT-IR spectra were analysed using the Perkin Elmer Spectrum available with the machine and ACD labs spectrus (V2018.2.5) software. All spectra were processed using the automated baseline correction, and the data auto-tune functions. MestReNova (version, 14.0.0, MestReLab Research) and iNMR (version 6.2) was used for NMR spectra processing. Deconvolution was

carried out using Mnova Global Spectral Deconvolution as described here: https://resources.mestrelab.com/gsd.

Microsoft Excel for Mac (version 16.35) was used for the VBA coding of the *BioLogicTool* and processing UV-vis, FT-IR and powder XRD data. HSPip version 5.2.06 was used to compute Hansen solubility parameters and calculate solubility spheres in chapter III.1. OriginLab2019 (V9.6.5.169, 2019b) was used to compute the full width at height maximum (FWHM) used to calculate the domain frame by the Scherrer equation:

$$\alpha = \frac{K \times \lambda}{FWHM \times \cos\left(\frac{2\theta}{2}\right)} \qquad \text{(eq. xxii)}$$

Where α is the domain frame or crystallite size (in nm), K is the Scherrer constant taken as 0.9, λ the wavelength used for analysis, here 0.15406 nm, FWMH, the full width at height maximum and θ the peak position. The asymptotic exponential fitted curved for the photochemical conversion followed by FT-IR spectroscopy was computed with OriginLab using the automatic aymptot1 exponential model available in the software. CMC calculations were performed with OriginLab using the package function developed by Soufi *et al.* for the OriginLab software.[264] Data Warrior (version 5.2.1) was used to create a surfactant library, compute the cLogP, relative polar surface area RSPA and shape index and map the surfactants.

TD-DFT calculations (performed by Dr. Ignacio Funès-Ardoiz) were carried out in Gaussian16 (A.03) program package.[373] Optimisations and frequency calculations were performed without symmetry restrictions at wB97XD/6-31+G(d,p) level due to the good agreement with the experimental UV-VIS absorption of monomer.[374] Solvation was

introduced by the CPCM implicit solvent method (chloroform).[375] All the stationary points were characterised as minima or transition state (0 or 1 imaginary frequency) in the corresponding electronic state (ground or excited state), and thermochemistry corrections at standard conditions were added to obtain the corresponding free energies. Both potential energies and free energies (in parentheses) are included in the manuscript in kcal.mol^{-1}.

Additional equipment

Microwaves

Decarboxylation reactions were conducted in a CEM Discover microwave in 30 mL vials and an Anton Paar Monowave 400 equipped with ruby probe thermometer fitted with an integrated camera in 30 mL vials. Small scale protein hydrolysis was performed in an Anton Paar Monowave 300 fitted with a ruby probe in 30 mL vials. Large scale protein hydrolysis (gluten) was performed in a Mars 6 CEM microwave.

UV-curing material

UV-lamps used for curing were custom-built by the electronic workshop of the University of York. The 365 nm UV LED gen2 emitter, 1250 mW (max output), LZ1-00UV00 was purchased from LED engine and the 5 W, 253 nm fluorescent lamp (PLS5/TUV 2 Pin 5W Germicidal UVC) from Lamp Specs website. The 22 mm diameter biconvex quartz lens used to collimate the 235 nm beam was purchased from UQG optics.

General synthetic procedures and compound characterisation

a. Synthetic procedures for chapter III.1 – part. 2 (p. 97-123)

5-(chloromethyl)furfural (38), from microalgae (conventional heating)

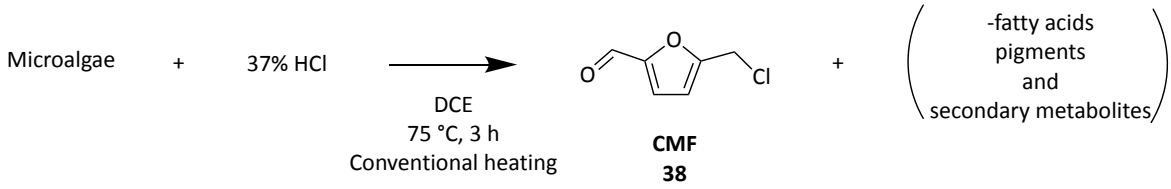

250 mg of microalgal biomass, 37% conc. HCl (35 mL), and 1,2-dichloroethane (70 mL) were introduced into a 250 mL Ace glass pressure flask with a large stirrer bar, and the flask was inserted into a heating block pre-heated at 80 °C (unless specified). The temperature was then set at 75 °C (measured on the block), and the reaction mixture was heated for 1 h with moderate stirring (~120 rpm). After 1 h the reaction was allowed to cool to room temperature, and the organic layer was separated with a 40 mL pipette. An additional 70 mL of solvent was added, the flask was capped, carefully shaken, and the organic layer separated. *Cycle 2*: A third portion of solvent (70 mL) was added to the aqueous layer, and the vessel was closed and heated for another hour as described above. The extraction process was repeated (fourth 70 mL solvent portion). *Cycle 3 and workup*: A fifth portion of solvent (70 mL) was added to the aqueous layer, and the vessel was sealed, heated for an additional 1 h, followed by a final extraction (sixth portion). The aqueous phase was filtered, and the solid washed with some distilled water and allowed to dry in air. The combined organic extracts were dried over $MgSO_4$ or Na_2SO_4, filtered and the solvent was removed *in vacuo*. After re-suspension with 50 mL of DCM, the solution

was filtrated through silica gel (~1 g), and additional DCM (4 x 50 mL) was used to rinse the silica plug. Evaporation of the filtrate gave the CMF-lipid mixture as a viscous, pale yellow oil (typically ~20 mg with *Spirulina sp.*, ~10% mass yield). The same procedure was used when gluten (1 g) was employed as a starting material.

^{1}H-NMR (400 MHz, [$CDCl_3$]): δ (ppm) 9.64 (s, 1H, $ClCH_2$-(C_4H_2O)-C<u>H</u>O), 7.20 (d, *J* = 3.6 Hz, 1H, $ClCH_2$-(COC<u>H</u>C_2H)-CHO), 6.59 (d, *J* = 3.6 Hz, 1H, CHO-(C_2HC<u>H</u>OC)-CH_2Cl), 4.61 (s, 2H,-Cl<u>CH_2</u>-(C_4H_2O)-CHO).

^{13}C-NMR (100 MHz, [$CDCl_3$]): δ (ppm) 177.9 ($ClCH_2$-(C_4H_2O)-<u>C</u>HO), 156.1 ($ClCH_2$-(C_3H_2O<u>C</u>)-CHO), 153.0 $ClCH_2$-(<u>C</u>OC_3H_2)-CHO), 121.9 $ClCH_2$-(C_2H<u>C</u>HOC)-CHO, 112.0 $ClCH_2$-(CO<u>C</u>HC_2H)-CH_2Cl), 36.6 (Cl<u>C</u>H_2-(C_4H_2O)-CHO). Chemical shift obtained by NMR spectroscopy are in accordance with reported values.[133]

FT-IR 3123 (vw); 2835 (vw); 1672 (vs); 1585 (vw); 1519 (vs); 1430 (vw); 1399 (s); 1363 (vw); 1279 (s); 1261 (vs); 1198 (vs); 1140 (w); 1021 (vs); 978 (vs); 969 (vs); 893 (vw); 806 (vs); 770 (vs); 754 (vs); 720 (vs); 692 (vs).

5-(chloromethyl)furfural from fructose (microwave heating)

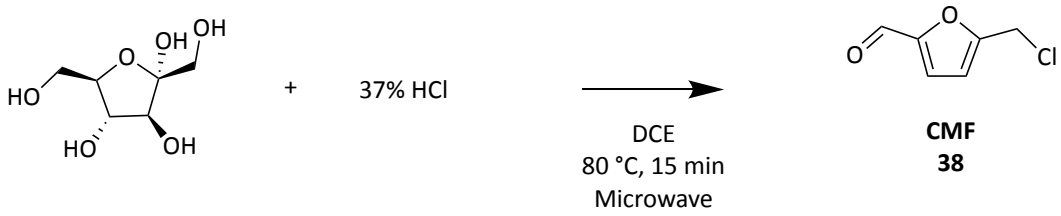

CMF
38

In a 30 mL microwave vessel (Anton Paar Monowave 300), 250 mg of D-fructose were dissolved in concentrated 37% HCl (5 mL) and the indicated organic solvent (see Table 7, p. 115, typically DCE, 10 mL) and a magnetic stirrer bar was added. The vessel was then placed in an Anton Paar Monowave 300 microwave and heated at 80 °C (ramping time 2 min) and held for 15 min with a high stirring rate (600 rpm). The cooled reaction mixture was then washed with the indicated solvent (3 x 30 mL). The collected organic phases were dried over $MgSO_4$ or Na_2SO_4, and evaporated to afford CMF (107 mg, 53 % yield obtained using DCE as solvent) as a brown oil. Characterisation corresponded to the previous product.

b. Synthetic procedures for chapter III.2 (p. 124-148)

Synthesis of 1,2-bis(5-methylfuran-2-yl)ethanedione (from 2-methylfuran), 112

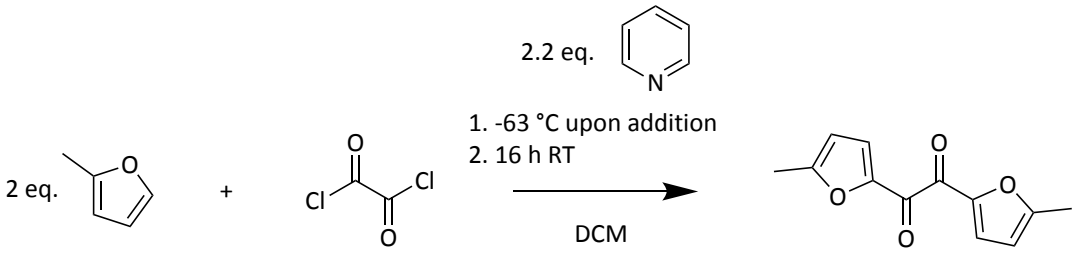

112

Protocol adapted from the literature.[152] A dried 500 mL two-necked round bottom flask was cooled to -63 °C ($CHCl_3/N_2$ slush bath) and charged with oxalyl chloride (75 mmol from a 2 M solution in DCM, 37.5 mL) and dry DCM (60.0 mL). Pyridine (13.051 g, 165 mmol, in dry DCM, 60.0 mL) was added followed by a dropwise addition of 2-methyl furan (12.315 g, 150 mmol, in dry DCM, 60.0 mL). After the addition, the cooling bath was removed, and the solution was stirred for 18 h (overnight) at room temperature. The resulting mixture was carefully added to a separating funnel and washed with 1 M HCl (2 x 250 mL) and brine (250 mL). The collected aqueous phases were back-extracted with DCM (100 mL). The collected organic phases were dried over Na_2SO_4 and filtered. Activated charcoal (~5 g) was added to the filtrate, and the slurry was stirred for 10 min. Thereafter, filtration of the slurry through cotton wool afforded a clear solution which was evaporated under reduced pressure to afford a brown residue (12.328 g, 75 % crude yield). Recrystallization from propan-2-ol twice afforded **112** as yellow needles (8.159 g, 50%).

^{1}H-NMR (400 MHz; [$CDCl_3$]): δ (ppm) 7.52 (d, *J* = 3.6 Hz, 2H, CH_3-(C_2HCHOC)-C(=O)-C(=O)- x2, *i.e.* identical proton on both sides of the ring), 6.25 (d, *J* = 3.6 Hz, 2H CH_3-(COCHC_2H)-C(=O)-C(=O)- x2)), 2.44 (s, 6H, CH_3-(C_4H_2O)-C(=O)-C(=O)- x2)).

^{13}C-NMR (101 MHz; [$CDCl_3$]): δ (ppm) 176.8 (CH_3-(C_4H_2O)-<u>C</u>(=O)-<u>C</u>(=O)-), 161.4 CH_3-(C_3H_2<u>C</u>O)-C(=O)-C(=O)-), 148.7 (CH_3-(<u>C</u>OC_3H_2)-C(=O)-C(=O)-), 126.9 (CH_3-(C_2H<u>C</u>HOC)-C(=O)-C(=O)-), 110.29 (CH_3-(CO<u>C</u>HC_2H)-C(=O)-C(=O)-), 14.4 (<u>C</u>H_3-(C_4H_2O)-C(=O)-<u>C</u>(=O)-). Data are in accordance with previously reported chemical shifts.[376]

FT-IR 3110 (w); 2340 (vw); 1622 (s); 1577 (w); 1558 (w); 1496 (s); 1454 (w); 1370; (w); 1343 (vw); 1287 (w); 1220 (vw); 1208 (w); 1041 (w); 1030 (s); 1012 (w); 969 (w); 959 (w); 948 (w); 844 (w); 823 (w); 807 (s); 749 (s); 732 (s); 669 (vw).

ESI-MS $C_{12}H_{10}NaO_4$, theoretical (m/z): 241.0471 [M+], measured: 241.0471 [M+].

Melting point 167-169 °C (lit. 166.5–167 °C)[152]

Single-crystal XRD structure is available on the CCDC database deposition number **2055845,** DOI: 10.5517/ccdc.csd.cc2708l4.

Synthesis of 5,5'-dimethylfuroin (131)

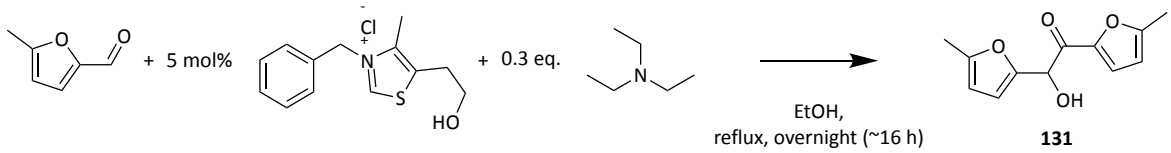

A 100 mL two-necked round-bottom flask equipped with a waterless condenser was charged with 5-methylfurfural (5.000 g, 45.4 mmol), 3-benzyl-5-(2-hydroxyethyl)-4-methyl-1,3-thiazolium chloride catalyst (0.612 g, 2.30 mmol) and EtOH (75 mL). Triethylamine (1.380 g, 13.6 mmol) was added rapidly from the side-neck using a syringe and needle with stirring, and the reaction mixture was refluxed overnight (16 h). After cooling to room temperature, the reaction mixture's volume was reduced to ~20 mL and placed in the freezer at -20 °C for 2 h. The resulting yellow precipitate was collected via vacuum filtration and recrystallised from EtOH/H_2O. Crystals were dried under high vacuum to afford **131** as a pale-yellow powder (1.487 g, 15% yield).

^{1}H-NMR (400 MHz; [$CDCl_3$]): δ (ppm) 7.11 (d, *J* = 3.5 Hz, 1H, CH_3-($C_2HC\underline{H}OC$)-C(=O)-CH(-OH)-), 6.24 (d, *J* = 3.1 Hz, 1H, CH_3-($C_2HC\underline{H}OC$)-CH(-OH)-C(=O)-), 6.14 (d, *J* = 3.6 Hz, 1H, CH_3-($C\underline{H}C_2HOC$)-C(=O)-CH(-OH)-), 5.90 (d, *J* = 3.1 Hz, 1H, CH_3-($C\underline{H}C_2HCO$)-CH(-OH)-C(=O)-), 5.64 (d, *J* = 6.3 Hz, 1H, CH_3-(C_4H_2O)-$C\underline{H}$(-OH)-C(=O)-(C_4H_2O)-CH_3), 4.21 (d, *J* = 6.4 Hz, 1H, CH_3-(C_4H_2O)-CH(-$O\underline{H}$)-C(=O)-(C_4H_2O)-CH_3), 2.37 (s, 3H, CH_3-(C_4H_2O)-CH(-OH)-C(=O)-(C_4H_2O)-$C\underline{H_3}$), 2.23 (s, 3H, $C\underline{H_3}$-(C_4H_2O)-CH(-OH)-C(=O)-(C_4H_2O)-CH_3).

^{13}C-NMR (101 MHz; [$CDCl_3$]): δ (ppm) 183.7 (CH_3-(C_4H_2O)-CH(-OH)-$\underline{C}$(=O)-(C_4H_2O)-CH_3), 159.4 (CH_3-($C_3H_2\underline{C}O$)-C(=O)-CH(-OH)-), 153.2 (CH_3-($C_3H_2\underline{C}O$)-C(-OH)-CH(=O)-), 149.9 (CH_3-($\underline{C}OC_3H_2O$)-C(=O)-CH(-OH)-), 148.3 (CH_3-($\underline{C}OC_3H_2$)-C(-OH)-CH(=O)-), 122.4 (CH_3-($C_2H\underline{C}HOC$)-C(=O)-CH(-OH)-), 110.1 (CH_3-($C_2H\underline{C}HOC$)-C(-OH)-CH(=O)-), 109.6 (CH_3-($\underline{C}HC_2HOC$)-C(=O)-

CH(-OH)-), 106.8 (CH_3-(<u>C</u>HC_2HOC)-C(-OH)-CH(=O)-), 69.0 CH_3-(C_4H_2O)-<u>C</u>H(-OH)-C(=O)-(C_4H_2O)-CH_3), 14.2 (<u>C</u>H_3-(C_4H_2O)-C(=O)-CH(-OH)-), 13.7 (<u>C</u>H_3-(C_4H_2O)-C(-OH)-CH(=O)-). Data are in accordance with previously reported chemical shifts.[377]

FT-IR wavenumber (cm^{-1}) 3413 (w); 3110.75 (vw); 2925 (vw); 1671 (vs); 1627 (s); 1578 (w); 1555 (w); 1511 (vs); 1451.14 (w); 1390 (w); 1282 (s); 1242 (w); 1209 (vs); 1182 (s); 1101 (w); 1029 (vs) 996.61 (s); 982 (s); 968 (s); 951 (s); 915 (w); 889 (vw); 858 (vw); 844 (vw); 827 (s); 799 (s); 784 (vs); 750 (s); 711 (vs); 670 (vw).

ESI-MS $C_{12}H_{12}NaO_4$, theoretical (m/z): 243.0628 [M+] measured: 243.0630 [M+].

Melting point 93.1–96.2 °C (lit. 91.5–93 °C)[377]

Synthesis of 1,2-bis(5-methylfuran-2-yl)ethanedione (from 5,5'-dimethylfuroin)

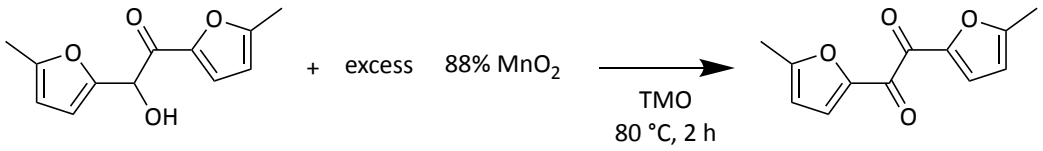

131 **112**

A 100 mL conical flask was charged with 5,5'-(dimethyl)furoin (**131**) (1.487 g, 6.76 mmol), excess MnO_2 (22.020 g, 253 mmol) and TMO (80 mL) and heated to 80 °C for 2 h. The resulting solution was filtered through a Celite pad further washed with TMO and evaporated under reduced pressure. Recrystallisation from propan-2-ol of the obtained yellow solid afforded **112** as pale-yellow needles (0.738 g, 59% yield). Characterisation data corresponded to the 1,2-bis(5-methylfuran-2-yl)ethanedione data described above.

Synthesis of 2-(5-methylfuran-2-yl)2-oxoacetic acid (111_a)

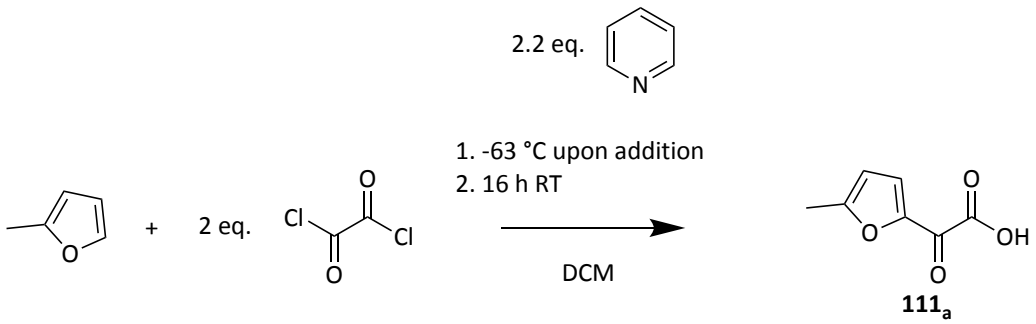

111_a

A dried 500 mL two-necked round bottom flask was cooled to -63 °C ($CHCl_3/N_2$ slush bath) and charged with oxalyl chloride (40 mmol from a 2 M solution in DCM, 20 mL) and dry DCM (40 mL). Pyridine (1.740 g, 22 mmol, in dry DCM, 20 mL) was added followed by a dropwise addition of 2-methyl furan (1.642 g, 20 mmol, in dry DCM, 60 mL). After the addition, the cooling bath was removed, and the solution was stirred for 16 h (overnight) at room temperature. The resulting mixture was carefully added to a separating funnel and washed with 1 M HCl (2 x 250 mL) and brine (250 mL). The collected organic phases were dried over Na_2SO_4, filtered and evaporated under reduced pressure to afford the crude product as a brown solid (2.230 g,). This crude product was purified by column chromatography (silica gel, DCM) to afford **111_a** (1.636 g, 53% yield) as small yellow needles. Analytical samples were obtained from partial recrystallisation from toluene forming white needles.

^{1}H-NMR (400 MHz, [$CDCl_3$]): δ (ppm) 8.17 (d, *J* = 3.6 Hz, 1H, CH_3-(C_2HCHOC)-C(=O)-COOH), 6.35 (d, *J* = 3.6 Hz, 1H, CH_3-($COCHC_2H$)-C(=O)-COOH), 2.49 (s, 3H, CH_3-(C_4H_2O)-C(=O)-COOH).

^{13}C-NMR (101 MHz; [$CDCl_3$]): δ (ppm) 168.3 (CH_3-(C_4H_2)-C(=O)-COOH), 164.1 (CH_3-(C_4H_2O)-C(=O)-COOH), 159.2 (CH_3-(C_3H_2CO)-C(=O)-COOH), 147.5 (CH_3-(COC_3H_2)-C(=O)-COOH),

131.7 (CH_3-($C_2H\underline{C}HOC$)-C(=O)-COOH), 111.5 (CH_3-($CO\underline{C}HC_2H$)-C(=O)-COOH), 14.6 ($\underline{C}H_3$-(C_4H_2O)-C(=O)-COOH).

FT-IR wavenumber (cm^{-1}): 3307 (br, s); 3159 (vw); 1756 (s); 1633 (vs); 1561 (w); 1508 (s); 1382 (w); 1359 (s); 1291 (s); 1204 (s); 1159 (s); 1052 (s); 1016.44 (s); 973 (w); 954 (w); 900 (w); 802 (s); 722 (s).

ESI-MS $C_7H_6NaO_4$, theoretical: 177.0158 [M+], measured: 177.0158 [M+].

Melting point 92.0-95.6 °C (lit. 90–91 °C)[378]

Single-crystal XRD structure is available on the CCDC database deposition number **2055862**, DOI: 10.5517/ccdc.csd.cc27094q

Synthesis of methyl 2-(5-methyl-furan-2-yl)2-oxo-acetate (111_b)

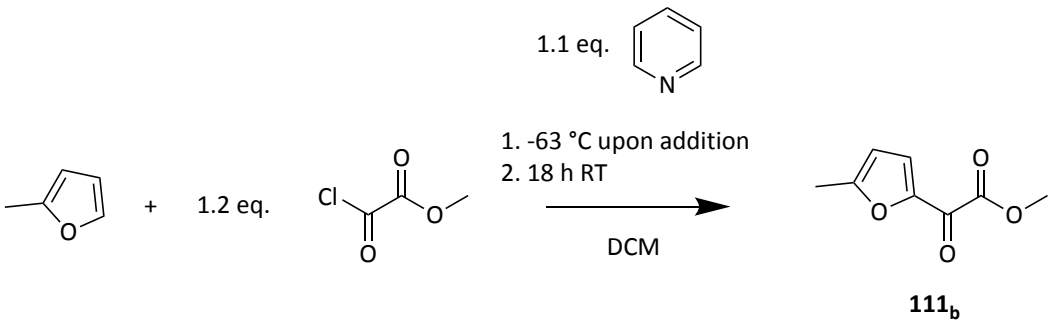

111_b

A dried 500 mL two-necked round bottom flask was cooled to -63 °C ($CHCl_3/N_2$ slush bath) and charged with oxalyl chloride (36 mmol from a 2 M solution in DCM, 18 mL) and dry DCM (47 mL). Pyridine (2.610 g, 33 mmol, in dry DCM, 50 mL) was added followed by a dropwise addition of 2-methyl furan (2.640 g, 30.0 mmol, in dry DCM, 50 mL). After the addition, the cooling bath was removed, and the solution was stirred for 18 h (overnight) at room temperature. The resulting mixture was carefully added to a separating funnel and washed with 1 M HCl (2 x 100 mL) and brine (100 mL). Collected organic phases were dried over Na_2SO_4, filtered and evaporated under reduced pressure to afford **111_b** (2.367 g, 47%) as yellow crystals over 95% pure (determined by ^{1}H-NMR spectroscopy). Purification of 2.095 g of these crystals by Kugelrohr distillation (90 °C, <1 mbar) afforded **111_b** (1.795 g) as white crystals. Colouration from possible decomposition occurred after storage in air at room temperature for one month.

^{1}H-NMR (400 MHz, [$CDCl_3$]): δ (ppm) 7.64 (d, *J* = 3.9 Hz, 1H, CH_3-(C_2HCHOC)-C(=O)-COOMe), 6.24 (d, *J* = 3.5 Hz, 1H, CH_3-($COCHC_2H$)-C(=O)-COOMe), 3.90 (d, *J* = 3.4 Hz, 3H, CH_3-(C_4H_2O)-C(=O)-COOMe), 2.41 (d, *J* = 3.7 Hz, 3H, CH_3-(C_4H_2O)-C(=O)-COOMe),

^{13}C-NMR (101 MHz; [$CDCl_3$]): δ (ppm) 169.7 (CH_3-(C_4H_2O)-C(=O)-COOMe), 162.0 (CH_3-(C_4H_2O)-C(=O)-COOMe), 161.7 (CH_3-(C_3H_2CO)-C(=O)-COOMe), 148.8 (CH_3-(COC_3H_2)-C(=O)-

COOMe), 127.4 (CH_3-($C_2H\underline{C}HOC$)-C(=O)-COOMe), 110.5 (CH_3-($CO\underline{C}HC_2H$)-C(=O)-COOMe), 53.1 (CH_3-(C_4H_2O)-C(=O)-COO<u>Me</u>), 14.4 (<u>C</u>H_3-(C_4H_2O)-C(=O)-COOMe).

FT-IR wavenumber (cm^{-1}): 3176 (vw); 3132 (vw); 6 (vw); 2925.72 (vw); 1730 (vs); 1655 (vs); 1578 (s); 1508 (vs); 1432 (vs); 1370 (s); 1336 (vs); 1248 (vs); 1217 (vs); 1195 (vs); 1049 (vs), 1027 (vs); 986 (vs); 965 (vs); 944 (s); 876 (s) 820 (vs); 807 (vs); 792 (vs); 692 (vw); 662 (vw).

ESI-MS $C_8H_8NaO_4$, theoretical (m/z): 191.0315 [M+], measured (m/z): 191.0318 [M+]

Melting point 56.1-60.4 °C (lit. 56–57 °C)[152]

Single-crystal XRD structure is available on the CCDC database deposition number **2055866**, DOI: 10.5517/ccdc.csd.cc27098v

Synthesis of ethyl 2-(5-methyl-furan-2-yl)2-oxoacetate (111_c)

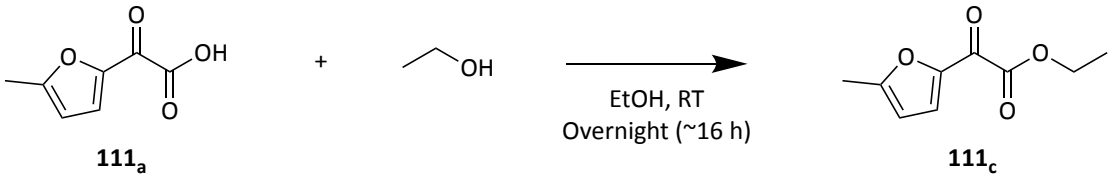

111_a **111_c**

A 50 mL conical flask was charged with crude **111_a** (1.500 g, 9.7 mmol), EtOH (20 mL), and stirred overnight at room temperature. The resulting solution was evaporated under reduced pressure and the obtained residue was purified via column chromatography (silica gel, DCM, Rf=0.4) to afford **111_c** as a yellow oil which crystallised upon storing at 2 °C in the fridge (1. 406 g, 7.7 mmol, 80% yield).

^{1}H-NMR (400 MHz, [$CDCl_3$]): δ (ppm) 7.61 (d, *J* = 3.6 Hz, 1H, CH_3-(C_2HCHOC)-C(=O)-COOEt), 6.23 (d, *J* = 3.6 Hz, 1H, CH_3-($COCHC_2H$)-C(=O)-COOEt), 4.36 (q, *J* = 7.2 Hz, 2H, CH_3-(C_4H_2O)-C(=O)-COO-CH_2-CH_3), 2.40 (s, 3H CH_3-(C_4H_2O)-C(=O)-COO-CH_2-CH_3), 1.37 (t, *J* = 7.2 Hz, 3H, CH_3-(C_4H_2O)-C(=O)-COO-CH_2-CH_3).

^{13}C-NMR (101 MHz; [$CDCl_3$]): δ (ppm) 170.2 (CH_3-(C_4H_2O)-C(=O)-COO-CH_2-CH_3), 161.8 (CH_3-(C_4H_2O)-C(=O)-COO-CH_2-CH_3), 161.4 (CH_3-(C_3H_2CO)-C(=O)-COO-CH_2-CH_3), 148.9 (CH_3-(COC_3H_2)-C(=O)-COO-CH_2-CH_3), 127.2 (CH_3-(C_2HCHOC)-C(=O)-COO-CH_2-CH_3), 110.3 (CH_3-($COCHC_2H$)-C(=O)-COO-CH_2-CH_3), 62.6 (CH_3-(C_4H_2O)-C(=O)-COO-CH_2-CH_3), 14.3 (CH_3-(C_4H_2O)-C(=O)-COO-CH_2-CH_3), 14.1 (CH_3-(C_4H_2O)-C(=O)-COO-CH_2-CH_3.

FT-IR wavenumber (cm^{-1}): 2985 (vw); 1732 (vs); 1663 (vs); 1577 (vw); 1507 (vs); 1447 (vw); 1368 (w); 1319 (vw); 1241 (vs); 1202 (vs); 1096 (vw); 1047 (vs); 1026 (vs); 979 (vw); 957 (w); 920 (vw); 861 (vw); 798 (w); 657 (vw).

ESI-MS $C_8H_8NaO_4$, theoretical (m/z): 182.06 [M+], measured (m/z):182.06 [M+].

Melting point 25.6-26.7°C

Single-crystal XRD structure is available on the CCDC database deposition number **2055863**, DOI: 10.5517/ccdc.csd.cc27095r

Synthesis of (E)-3-(5-methylfuran-2-yl)acrylic acid

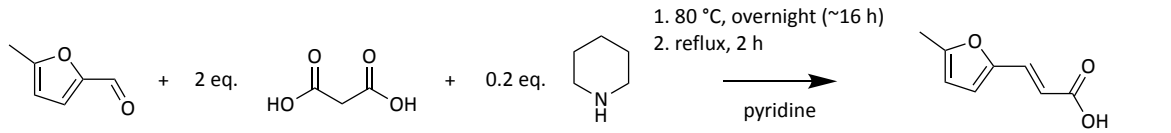

130 **(E)-3-(5-methylfuran-2-yl)acrylic acid**

A 250 mL two-neck round bottom flask equipped with a water-less condenser and a magnetic stirrer flea was charged with 5-methylfurfural (**130**, 8.00 g, 72.6 mmol). Malonic acid (15.12 g, 145.3 mmol) was added, followed by pyridine (80 mL). Piperidine (1.24 g, 14.5 mmol) was rapidly added, and the reaction mixture was heated to 80 °C 16 h (overnight) then to reflux 2 h with stirring. The vessel was allowed to cool to room temperature then placed in ice. 1 M HCl (100 mL) was added, followed by 37% HCl until the pH drop under 1 (~25 mL). The mixture was left to precipitate overnight, and solids were filtrated under vacuum (9.16 g crude). Recrystallisation from propan-2-ol/H_2O afforded (E)-3-(5-methylfuran-2-yl)acrylic acid as bright yellow needle-shaped crystals that were further dried under high vacuum (8.32 g, 75% yield).

^{1}H-NMR (400 MHz,[$CDCl_3$]): δ (ppm) 7.44 (d, J = 15.6 Hz, 1H, HOOC-CH=C<u>H</u>-(C_4H_2O)-CH_3), 6.56 (d, J = 3.4 Hz, 1H, HOOC-CH=CH-(COC<u>H</u>C_2H)-CH_3), 6.21 (d, J = 15.5 Hz, 1H, HOOC-C<u>H</u>=CH-(C_4H_2O)-CH_3), 6.09 (d, J = 3.3 Hz, 1H, HOOC-CH=CH-(C_3HC<u>H</u>OC)-CH_3), 2.35 (s, 3H, HOOC-CH=CH-(C_4H_2O)-C<u>H</u>$_3$).

^{13}C-NMR (101 MHz, [$CDCl_3$]): δ (ppm) 172.95 (HOO<u>C</u>-CH=CH-(C_4H_2O)-CH_3), 156.32 (HOOC-CH=CH-(<u>C</u>OC_3H_2)-CH_3), 149.39 HOOC-CH=CH-(C_3H_2<u>C</u>O)-CH_3), 133.17 (HOOC-CH=<u>C</u>H-(C_4H_2O)-CH_3), 117.74 HOOC-CH=CH-(CO<u>C</u>HC_2H)-CH_3), 112.98 (HOOC-<u>C</u>H=CH-(C_4H_2O)-CH_3), 109.18 HOOC-CH=CH-(C_3H<u>C</u>HO)-CH_3), 14.04 HOOC-CH=CH-(C_4H_2O)-<u>C</u>H_3). Data are in accordance with previously reported chemical shifts.[379]

FT-IR wavenumber (cm^{-1}): 2601 (s); 1674 (vs); 1622 (vs); 1575 (vs); 1530 (vs); 1450 (w); 1415 (vs); 1365 (s); 1309 (vs); 1285 (vs); 1273 (s); 1257 (vs); 1204 (vs); 1181 (vs); 1161 (s); 1022 (s); 1007 (vs); 978 (s); 964 (vs); 934 (vs); 872 (s); 850 (vs); 794 (vs); 741 (w); 733 (w); 725 (w); 678 (s)

ESI-MS $C_8H_9O_3$ theoretical: 153.0546 [M+], measured: 153.0547 [M+]

$C_8H_8NaO_3$ theoretical: 175.0366 [M+], measured: 175.0369 [M+]

Melting point 155.3-156.4 °C (lit. 154–156 °C)[380]

Single-crystal XRD structure is available on the CCDC database deposition number **2055860**, DOI: 10.5517/ccdc.csd.cc27092n

Synthesis of (E)-methyl 2-(5-methylfuran-2-yl)2-acrylate (113)

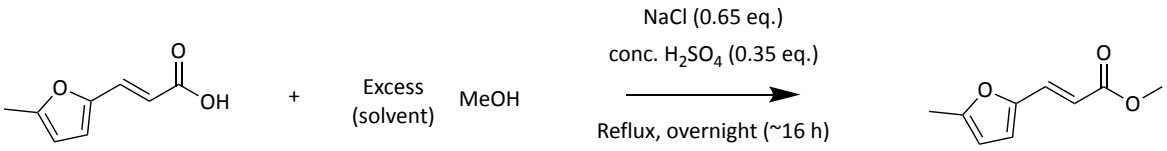

113

A 50 mL round-bottom flask equipped with a water-less condenser and a magnetic stirrer flea was charged with (E)-3-(5-methylfuran-2-yl)acrylic acid (2.00 g, 13.15 mmol) and MeOH (20 mL). The mixture was stirred until complete dissolution (heating may be applied to help solubilise the compound). Subsequently, NaCl (500 mg, 8.56 mmol, 0.65 eq.) was added to reduce the ester solubility followed by rapid addition of 98 % H_2SO_4 (250 µL, 4.66 mmol, 0.35 eq.). The mixture was refluxed with stirring overnight then left to cool to room temperature with stirring and further cooled in ice. Excess methanol was evaporated under reduced pressure, and the resulting solids were taken up in EtOAc (20 mL), and the solution was washed with 1 M HCl (2 x 40 mL) and brine (40 mL). The organic phase was dried with $MgSO_4$, filtered, and the solvent was removed under reduced pressure to afford crude **113** (2.356 g). Sublimation by Kugelrohr sublimation afforded **113** as white crystals. After one month of storage in air, crystals turned yellow/brown.

^{1}H-NMR (400 MHz,[$CDCl_3$]): δ (ppm) 7.34 (d, J = 15.6 Hz, 1H, MeOOC-CH=C<u>H</u>-(C_4H_2O)-CH_3), 6.49 (d, J = 3.3 Hz, 1H, MeOOC-CH=CH-(COC<u>H</u>C_2HOC)-CH_3), 6.21 (d, J = 15.8 Hz, 1H, MeOOC-C<u>H</u>=CH-(C_4H_2O)-CH_3), 6.05 (d, J = 3.3 Hz, 1H, MeOOC-CH=CH-(C_3HC<u>H</u>O)-CH_3), 3.75 (s, 3H, <u>Me</u>OOC-CH=CH-(C_4H_2O)-CH_3), 2.33 (s, 3H, MeOOC-CH=CH-(C_4H_2O)-C<u>H</u>$_3$).

^{13}C-NMR (101 MHz, [$CDCl_3$]): δ (ppm) 167.91 (MeOO<u>C</u>-CH=CH-(C_4H_2O)-CH_3), 155.60 (MeOOC-CH=CH-(<u>C</u>OC_3H_2)-CH_3), 149.57 (MeOOC-CH=CH-(C_3H_2<u>C</u>O)-CH_3), 131.38 (MeOOC-CH=<u>C</u>H-(C_4H_2)-CH_3), 116.66 (MeOOC-CH=CH-(<u>C</u>OHC_2H)-CH_3, 113.58 (MeOOC-<u>C</u>H=CH-

(C_4H_2)-CH_3), 108.90 (MeOOC-CH=CH-($OC_3H\underline{C}H$)-CH_3), 51.64 ($\underline{Me}$OOC-CH=CH-(C_4H_2)-CH_3), 13.98 (MeOOC-CH=CH-(C_4H_2)-$\underline{C}H_3$). Data are in accordance with previously reported chemical shifts. [379]

FT-IR wavenumber (cm^{-1}): 2990 (vw); 2947 (vw); 1705 (s); 1669 (vw); 1631 (s); 1578 (s); 1527 (w); 1491 (vw); 1455 (vw); 1438 (w); 1364 (w); 1304 (s); 1283 (w); 1260 (s); 1238 (w); 1224 (w); 1198 (s); 1187 (vs); 1164 (vs); 1122 (s); 1116 (s); 1110 (w); 1080 (w); 1066 (w); 1046 (vw); 1034 (vw); 1011 (s); 993 (vs); 971 (w); 941 (vw); 930 (w); 906 (vw); 897 (vw); 893 (vw); 885 (vw); 870 (vw); 857 (vw); 844 (w); 788 (s); 778 (s); 750 (vw); 741 (vw); 734 (vw); 696 (vw)

Melting point 39.4-42.5 °C (lit. 39–40 °C)[381]

ESI-MS $C_9H_{11}O_3$ theoretical: 167.0703 [M+], measured: 167.0701 [M+]

$C_9H_{10}NaO_3$ theoretical: 189.0522 [M+], measured: 189.0522 [M+]

Single-crystal XRD structure is available on the CCDC database deposition number **2055864**, DOI: 10.5517/ccdc.csd.cc27096s

Synthesis of (2E,2'E)-3,3'-(2,5-furandiyl)bisacrylic acid (89) also used for chapter III.3

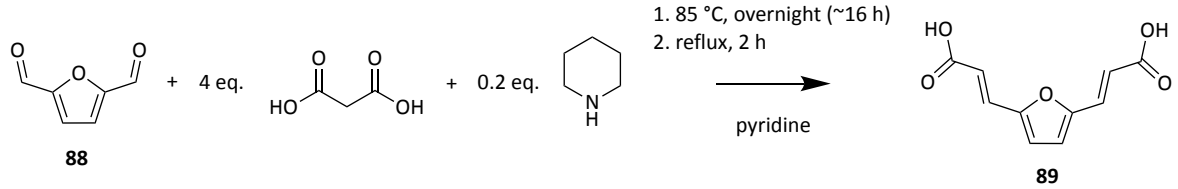

88 **89**

Protocol adapted from the literature.[187] An oven-dried 250 mL 2-necked round bottom flask equipped with a waterless condenser and a magnetic stirrer flea, was charged with 2,5-diformylfuran (12.566 g, 101 mmol), malonic acid (42.146 g, 405 mmol, 4 eq.) and anhydrous pyridine (150 mL, stored under 3 Å molecular sieves) consecutively. After complete dissolution, piperidine (1.724 g, 20.2 mmol, 0.2 eq.) was added, and the system was heated to 85 °C overnight (16 h). Thereafter, the reaction mixture was brought to reflux for 2 h. After cooling to room temperature, the solution was poured in a 500 mL beaker and neutralised with the careful addition of 37% conc. HCl (~150 mL) and 1 M HCl (~300 mL) until the pH dropped below 1. The reaction mixture was placed on an ice bath, and the resulting precipitate was collected via vacuum filtration over a fritted funnel. The beige solid was further washed with cold 1 M HCl and dried at 80 °C in a vacuum oven overnight to afford **89** (17.250 g, 82.9 mmol, 82% yield).

^{1}H-NMR (400 MHz, [DMSO-d_6]): δ (ppm) 7.34 (d, J = 15.8 Hz, 2H, HOOC-CH=C<u>H</u>-(C_4H_2O)-x2), 6.97 (s, 2H,-HOOC-CH=CH-($C_2\underline{H}_2C_2O$)-), 6.34 (d, J = 15.8 Hz, 2H, HOOC-C<u>H</u>=CH-(C_4H_2O)-x2).

^{13}C-NMR (101 MHz; [DMSO-d_6]): δ (ppm) 167.7 (HOO<u>C</u>-CH=CH-(C_4H_2O)-x2), 152.6 (HOOC-CH=CH-($\underline{C}_2OC_2H_2$)-), 130.5 (HOOC-CH=<u>C</u>H-(C_4H_2O)-x2), 118.9 HOOC-<u>C</u>H=CH-(C_4H_2O)-x2), 118.1 (HOOC-CH=CH-($C_2O\underline{C}_2H_2$)-). Chemical shifts are in accordance with previously reported values.[187]

FT-IR wavenumber (cm^{-1}): 2850 (vs); 2540.0758 (vs); 1655 (vs); 1627 (vs); 1550 (vs); 1428 (vs); 1298 (vs); 1280 (vs); 1243 (vs); 1200 (vs); 1165 (vs); 1018 (s); 992 (w); 966 (vs); 893 (vs); 871 (vs); 799 (vs); 742 (vs); 667 (vs).

ESI-MS $C_{10}H_8NaO_5$, theoretical: 231.0264 [M^+], measured: 231.0271 [M^+].

Melting point Decomposes >200 °C.

Synthesis of dimethyl (2E,2'E)-3,3'-(2,5-furandiyl)-diacrylate (90)

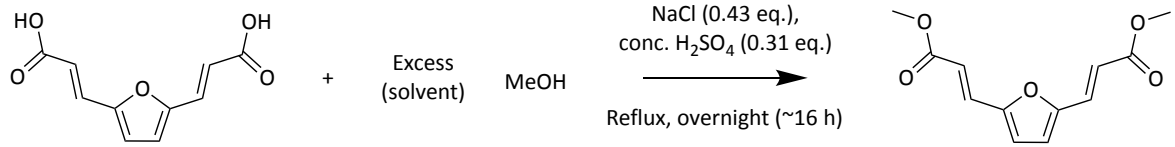

89 **90**

Protocol adapted from the literature also used for chapter III.3.[187] **89** (9.000 g, 43 mmol) was suspended in MeOH (150 mL) in a two-necked 250 mL round bottom flask fitted with a condenser. Thereafter, NaCl (1.090 g, 19 mmol, 0.43 eq.) was added to decrease the solubility of the diester in the methanolic solution and 98 % H_2SO_4 (730 µL, 13 mmol, 0.31 eq.) was added. The mixture was refluxed overnight (~16 h), and the slurry turned into a dark solution with crystalline solids in it. The solution was allowed to cool to room temperature with stirring and then further cooled with stirring on ice. Solids were filtrated under vacuum and recrystallised from propan-2-ol to afford **90** as shiny flakes (8.550 g, 84%). Overall 69% yield from 2,5-(diformyl)furan.

^{1}H-NMR (400 MHz, [$CDCl_3$]): δ (ppm) 7.40 (d, J = 15.7 Hz, 2H, MeOOC-CH=C<u>H</u>-(C_4H_2O)-x2), 6.65 (s, 2H, MeOOC-CH=CH-($C_4\underline{H_2}O$)-), 6.43 (d, J = 15.8 Hz, 2H, MeOOC-C<u>H</u>=CH-($C_4\underline{H_2}O$)-x2), 3.80 (s, 6H, <u>Me</u>OOC-CH=CH-(C_4H_2O)-x2).

^{13}C-NMR (101 MHz; [$CDCl_3$]): δ (ppm) 167.2 (MeOO<u>C</u>-CH=CH-(C_4H_2O)-), 152.5 (MeOOC-CH=CH-($\underline{C_2}OC_2H_2$)-), 130.4 (MeOOC-CH=<u>C</u>H-(C_4H_2O)-), 117.6 MeOOC-<u>C</u>H=CH-(C_4H_2O)-), 116.9 (MeOOC-CH=CH-($C_2O\underline{C_2}H_2$)-), 52.0 (<u>Me</u>OOC-CH=CH-(C_4H_2O)-). Data are in accordance with previously reported chemical shifts.[187]

FT-IR wavenumber (cm^{-1}): 2968 (vw); 1994 (vw); 1721 (vs); 1634 (vs); 1554 (s); 1505 (s); 1434 (s); 1386 (s); 1302 (vs); 1241 (vs); 1189 (s); 1163.37 (vs); 1015 (w); 1001 (w); 990 (w); 958 (vs); 920 (s); 858 (s); 792 (vs); 750 (s); 732 (w); 695 (vw); 659 (vw).

ESI-MS $C_{12}H_{12}NaO_5$, theoretical (m/z): 259.0577 [M+] measured (m/z): 259.0759 [M+].

Melting point 153.7–155.9 °C (lit. 152-153 °C)[189]

Single-crystal XRD structure is available on the CCDC database deposition number **2055861**, DOI: 10.5517/ccdc.csd.cc27093p

Synthesis of tetramethyl 2,2'-(furan-2,5-diylbis(methaneylylidene))dimalonate (117)

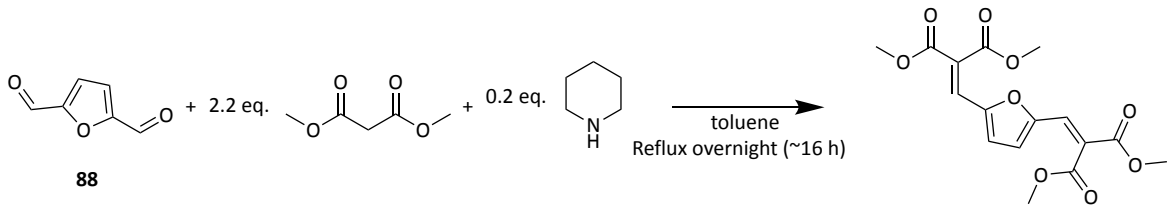

88 **117**

An oven-dried 250 mL two-necked round bottom flask equipped with a Dean-Stark apparatus fitted with a water-less condenser and a stirrer flea was charged with 2,5-diformylfuran (**88**, 0.496 g, 4.0 mmol). The system was flushed with N_2 (3 x times vacuum/filled cycle). A solution of dimethylmalonate (1.162 g, 8.8 mmol) in toluene (10 mL) was added, followed by a solution of piperidine (68 mg, 0.8 mmol) in toluene (10 mL). The reaction mixture was refluxed overnight with stirring. After the reaction, the solvent was removed under reduced pressure, and the crude mixture was diluted in EtOAc (80 mL). The resulting solution was washed with 1 M HCl (2 x 40 mL), deionised water (40 mL), and brine (40 mL). The collected organic phases were dried over Na_2SO_4 and evaporated under reduced pressure to afford crude **117** as a brown residue (1.275 g). The crude **117** was purified by column chromatography (EtOAc: *n*-hexane, 75:25, R_f= 0.6) to afford **117**, which was recrystallised from propan-2-ol (0.129 g, 9% yield).

^{1}H-NMR (400 MHz, [$CDCl_3$]): δ (ppm) 7.44 (s, 2H, -($C_4\underline{H}_2O$)-), 6.84 (s, 2H, -(C_4H_2O)-C$\underline{H}$=C(-$COOMe)_2$x2), 3.92 (s, 6H, -(C_4H_2O)-CH=C(-COO$\underline{Me}$)$_2$ (close to furan ring) x2), 3.83 (s, 6H, -(C_4H_2O)-CH=C(-COO$\underline{Me}$)$_2$ (far from furan ring)x2).

^{13}C-NMR (101 MHz; [$CDCl_3$]): δ (ppm) 166.0 (-(C_4H_2O)-CH=C-($\underline{C}OOMe)_2$- (close to furan rings) x2), 164.1 (-(C_4H_2O)-CH=C-($\underline{C}OOMe)_2$- (far from furan ring)x2)), 151.3 (-($C_3H_2\underline{C}O$)-

CH=C-(COOMe)$_2$-x2), 127.8 ((-(C$_2$HCHOC)-CH=C-(COOMe)$_2$-x2), 124.1 (-C=CH-CO=CH- x2), 119.1 (-CO=CH-CH=CO-), 53.08 (‘CH$_3$-COO-C=CH- (close to furan rings) x2) , 52.96 (CH$_3$-COO-C=CH (far from furan ring)x2)) .

FT-IR wavenumber (cm^{-1}): 2960 (vw); 1725 (vs); 1625 (s); 1434 (w); 1384 (w); 1351 (w); 1275 (s); 1249 (s); 1207 (vs); 1191 (vs); 1170 (vs); 1065 (s); 1036 (s); 995 (w); 963 (w); 930 (s); 834 (vw); 806 (w); 772 (w); 757 (w); 703 (vw); 688 (vw).

ESI-MS $C_{16}H_{16}NaO_9$, theoretical (m/z): 375.0678 [M+] measured (m/z): 375.0870 [M+].

Melting point 120.2–125.0 °C.

Synthesis of tetraethyl 2,2'-(furan-2,5-diylbis(methaneylylidene))dimalonate (118)

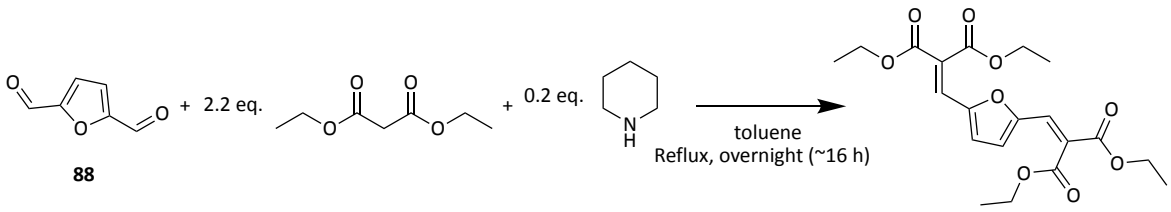

88 **118**

A 100 mL oven-dried round bottom flask was fitted with a Dean-Stark apparatus and a waterless condenser and the system was flushed with Ar (3 x times vacuum/filled cycle). Thereafter, 40 mL of TMO was added and heated to reflux to start the Dean-Stark apparatus. 2,5-diformylfuran (**88**, 0.500 g, 4.03 mmol) was then added, followed by diethylmalonate (1.42 g, ,8.9 mmol, 2 eq. in 10 mL TMO). A solution of piperidine (680 mg, 0.8 mmol in TMO, 10 mL) was then added and the reaction mixture was refluxed overnight with stirring. Thereafter, the solvent was removed under reduced pressure, and the crude mixture was taken up in EtOAc (15 mL). The resulting solution was washed with 1 M HCl (2x20 mL) and brine (50 mL). Collected organic phases were dried over $MgSO_4$ and evaporated under reduced pressure. The resulting residue was purified by column chromatography (EtOAc:*n*-hexane, 1:2, R_f=0.4) to afford **118** as a yellow oil which crystallised in EtOH (0.137 g, 8 % yield).

^{1}H-NMR (400 MHz, [$CDCl_3$]): δ (ppm) 7.38 (s, 2H, -($C_4\underline{H_2}O$)-CH=C(-$COOEt)_2$), 6.82 (s, 2H, -(C_4H_2O)-C<u>H</u>=C(-$COOEt)_2$x2), 4.37 (q, *J* = 7.2 Hz, 4H, -(C_4H_2O)-CH=C(-COO-C<u>H_2</u>-$CH_3)_2$ (close to furan rings) x2), 4.17 (q, *J* = 7.0 Hz, 4H, -(C_4H_2O)-CH=C(-COO-C<u>H_2</u>-$CH_3)_2$ (furthest from furan ring)x2), 1.33 (t, *J* = 7.2 Hz, 6H, -(C_4H_2O)-CH=C(-COO-CH_2-C<u>H_3</u>)$_2$ (close to furan rings) x2), 1.24 (t, *J* = 7.1 Hz, 6H, -(C_4H_2O)-CH=C(-COO-CH_2-C<u>H_3</u>)$_2$ (far from furan ring)x2)

^{13}C-NMR (101 MHz; [$CDCl_3$]): δ (ppm) 166.7 (-(C_4H_2O)-CH=C(-<u>C</u>OO-CH_2-CH_3)$_2$ (close to furan rings) x2), 163.76 (-(C_4H_2O)-CH=C(-<u>C</u>OO-CH_2-CH_3)$_2$ (far from furan ring)x2)), 151.33 (-(C_3H_2<u>C</u>O)-CH=C(-COO-CH_2-CH_3)$_2$), 127.15 (-(C_4H_2O)-<u>C</u>H=C(-COO-CH_2-CH_3)$_2$x2), 124.82 (-(C_4H_2O)-CH=<u>C</u>(-COO-CH_2-CH_3)$_2$x2), 118.77 (<u>C</u>$_2H_2C_2O$), 62.08 (-(C_4H_2O)-CH=C(-COO-<u>C</u>H_2-CH_3)$_2$ (close to furan rings) x2), 61.93 (-(C_4H_2O)-CH=C(-COO-<u>C</u>H_2-CH_3)$_2$ (far from furan ring)x2)), 14.17 (-(C_4H_2O)-CH=C(-COO-CH_2-<u>C</u>H_3)$_2$ (close to furan rings) x2), 14.15 (-(C_4H_2O)-CH=C(-COO-CH_2-<u>C</u>H_3)$_2$ (far from furan ring)x2)).

FT-IR wavenumber (cm^{-1}): 687 (vw); 704 (vw); 744 (w); 762 (w); 798 (vw); 828 (s); 837 (w); 870 (w); 935 (w); 967 (w); 1013 (vs); 1024 (vs); 1069 (vs); 1100 (w); 1116 (w); 1176 (vs); 1205 (vs); 1244 (vs); 1271 (s); 1352 (w); 1377 (w); 1395 (vw); 1451 (vw); 1456 (vw); 1468 (vw); 1485 (vw); 1545 (vw); 1635 (vs); 1720 (vs); 2935 (vw); 2981 (vw); 3049 (vw); 3125 (vw).

ESI-MS $C_{16}H_{16}NaO_9$, theoretical (m/z): 375.0678 [M+] measured (m/z): 375.0870 [M+].

Melting point 88.4–90.7 °C (lit. 90-91 °C)[189]

Single-crystal XRD structure is available on the CCDC database deposition number **2055865**, DOI:

Synthesis of 2-(hydroxyimino)-1,2-bis(5-methyfuran-2-diyl)-ethan-1-one (119)

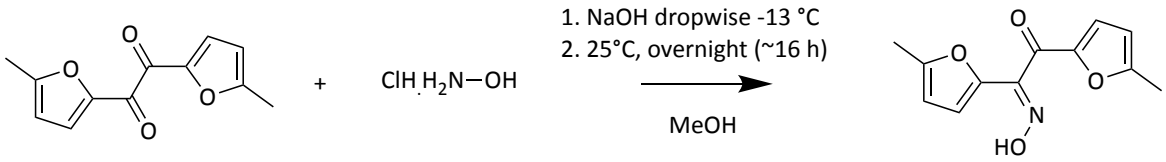

112 **119**

Protocol adapted from the literature.[153] A 100 mL flask equipped with a magnetic stirring bar was charged with 6.546 grams of **112** (30 mmol) and methanol (50 mL). A solution of 2.085 g hydroxylamine hydrochloride (30 mmol in deionized water, 6 mL) was added to the flask and then cooled to -13 ° C in NaCl/ice bath. A solution of 3.610 g sodium hydroxide (90 mmol, 3 eq., deionized water, 15 mL) was added to the flask dropwise, and the resulting mixture was stirred for 1 h. The solution was warmed up to 25 °C (room temperature) and stirred overnight (18 h). Thereafter, acetic acid (3.607 g) was added in the reaction mixture followed by brine (100 mL). The mixture was poured in a separatory funnel, and DCM (200 mL) was added. The organic layer was then washed with 1 M Na_2CO_3 (150 mL), and the collected aqueous phase was back-extracted with DCM (100 mL). The collected organic phases were then dried over anhydrous $MgSO_4$ and clarified with activated charcoal (~2 g). The resulting DCM solution was filtered and evaporated under reduced pressure to afford 5.643 g of **119** as a yellow solid which was then recrystallised from toluene. The white to off-white crystals (3.051 g, 44 %) were collected via vacuum filtration and dried in high vacuum.

^{1}H-NMR (400 MHz, [$CDCl_3$]): δ (ppm) 9.23 (s (broad), 1H, CH_3-(C_4H_2O)-C(=N-O<u>H</u>)-C(=O)-(C_4H_2O)-CH_3), 7.31 (d, *J* = 3.5 Hz, 1H, CH_3-(C_4H_2O)-C(=N-OH)-C(=O)-(COC<u>H</u>C_2H)-CH_3), 7.21 (d, *J* = 3.5 Hz, 1H, CH_3-(C_2HC<u>H</u>OC)-C(=N-OH)-C(=O)-(C_4H_2O)-CH_3), 6.20 (d, *J* = 3.6 Hz, 1H, CH_3-(C_4H_2O)-C(=N-OH)-C(=O)-(C_2HC<u>H</u>OC)-CH_3), 6.15 (d, *J* = 3.6 Hz, 1H, CH_3-(COC<u>H</u>C_2H)-C(=N-

OH)-C(=O)-(C_4H_2O)-CH_3), 2.44 (s, 3H, CH_3-(C_4H_2O)-C(=N-OH)-C(=O)-(C_4H_2O)-CH_3), 2.30 (s, 3H, CH_3-(C_4H_2O)-C(=N-OH)-C(=O)-(C_4H_2O)-CH_3).

^{13}C-NMR (101 MHz; [$CDCl_3$]): δ (ppm) 175.3 (CH_3-(C_4H_2O)-C(=N-OH)-C(=O)-(C_4H_2O)-CH_3) 160.6 (CH_3-(C_4H_2O)-C(=N-OH)-C(=O)-(C_4H_2O)-CH_3), 154.8 (=CH_3-(C_4H_2O)-C(=N-OH)-C(=O)-(COC_3H_2)-CH_3), 150.5 (CH_3-(C_3H_2OC)-C(=N-OH)-C(=O)-(C_4H_2O)-CH_3), 145.3 (CH_3-(C_4H_2O)-C(=N-OH)-C(=O)-(C_3H_2OC)-CH_3), 141.3 (CH_3-(COC_3H_2)-C(=N-OH)-C(=O)-(C_4H_2O)-CH_3), 125.6 (CH_3-(C_4H_2O)-C(=N-OH)-C(=O)-(COCHC_2HO)-CH_3), 121.7 (CH_3-(C_2HCHOC)-C(=N-OH)-C(=O)-(C_4H_2O)-CH_3), 109.8 (CH_3-(C_4H_2O)-C(=N-OH)-C(=O)-(C_2HCHOC)-CH_3), 108.8 (CH_3-(COCHC_2H)-C(=N-OH)-C(=O)-(C_4H_2O)-CH_3), 14.3 (CH_3-(C_4H_2O)-C(=N-OH)-C(=O)-(C_4H_2O)-CH_3) , 13.9 (CH_3-(C_4H_2O)-C(=N-OH)-C(=O)-(C_4H_2O)-CH_3)

FT-IR wavenumber (cm^{-1}): 3359 (vw); 1657 (s); 1583 (vw); 1507 (vs); 1446 (vw); 1364 (w); 1326 (w); 1253 (vw); 1204 (s); 1127 (vw); 1020 (s); 994 (w); 981 (w); 969 (w); 955 (w); 874 (vw); 824 (s); 812 (s); 796 (s); 758 (w); 709 (w); 680 (vw).

ESI-MS $C_{12}H_{11}NaO_4N$, theoretical (m/z): 256.0580 [M+] measured (m/z): 256.0582 [M+].

Melting point 133.8-136.5 °C.

Single-crystal XRD structure is available on the CCDC database deposition number **2055851**, DOI: 10.5517/ccdc.csd.cc2708sb

c. Synthetic procedures for chapter III.3 (p. 149-191)

Synthesis of 2,5-diformylfuran (88)

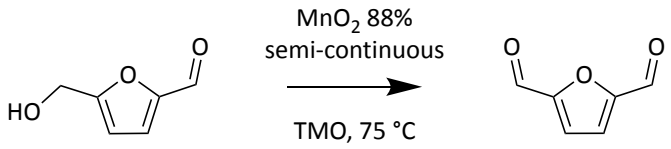

37 **88**

A spent HPLC column (25 mm length, 4 mm internal diameter) was emptied, cleaned then re-packed with 88% MnO_2 (6.20 g) with vacuum connected to one end of the column to ensure effective packing. The column was then connected to a JASCO HPLC pump PU 980 and clamped in a custom-made heating block and heated to 75 °C. A heating tape was applied to the tubing at the exit of the column to avoid clogging of the capillaries. Thereafter, neat TMO preheated to 75 °C was passed through the column at a flow rate of 1 $mL.min^{-1}$. Once the first drop of TMO exited the column, a 1% (w/v) HMF solution in TMO (1.00 g HMF, 7.9 mmol, in 100 mL TMO) was preheated to 75 °C and then passed through the system. The solution at the exit of the column was evaporated to afford 2,5-diformylfuran (DFF, **88**) as a white solid (0.771 g, 6.2 mmol, 78% yield). The evaporated TMO was recovered and reused after distillation through a Vigreux column, drying over $MgSO_4$ and stored over 3 Å activated molecular sieves.

^{1}H-NMR (400 MHz, [$CDCl_3$]): δ (ppm) 9.86 (s, 2H, C<u>H</u>O-(C_4H_2O)-C<u>H</u>O), 7.33 (s, 2H, CHO-($C_4\underline{H_2}O$)-CHO)).

^{13}C-NMR (101 MHz, [$CDCl_3$]): δ (ppm) 179.33 (<u>C</u>HO-(C_4H_2O)-<u>C</u>HO), 154.29 (CHO-($C_2H_2\underline{C_2}O$)-CHO), 119.34 (triplet like signals, CHO-($\underline{C_2}H_2C_2O$)-CHO). Data are in accordance with previously reported chemical shifts.[187]

FT-IR wavenumber (cm^{-1}): 3141 (w); 3127 (w); 3105 (w); 2974 (vw); 2875 (w); 2750 (vw); 1673 (vs); 1662 (vs); 1565 (vs); 1523 (s); 1512 (s); 1410 (vs); 1390 (s); 1350 (vw); 1265 (vs); 1238 (vs); 1188 (vs); 1172 (vs); 1043 (w); 1021 (vs); 1002 (s); 976 (vs); 958 (vs); 909 (w); 826 (vs); 804; (vs); 795 (vs).

Chemo-catalytic polycondensation 90 with 1,8-octanediol (ODO-PFAE, 91)

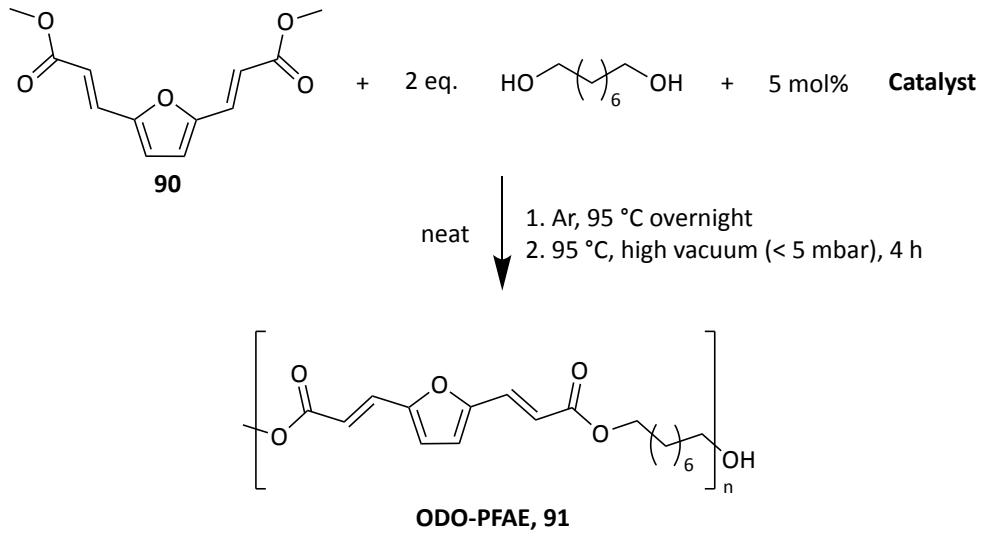

Catalyst: (t-BuO)$_4$Ti **or** (i-PrO)$_4$Zr .i-PrOH **or** (AcO)$_2$Zn **or** K_2CO_3

In a custom-made polymerisation flask, consisting of a round-bottom cylindrical flask adapted with a short-path distillation side neck were added consecutively, **90** (1.000 g, 4.23 mmol), 1,8-octane diol (1.24 g, 8.47 mmol) and 5 mol% of the catalyst (K_2CO_3, Zr(IV) isopropoxide isopropanol complex, Zn(II) acetate or Ti(IV) *tert*-butoxide e.g. for Ti(IV) *tert*-butoxide: 72.04 mg, 0.05 eq.) with a large egg-shaped rare earth magnetic stirring bar. The vessel was surmounted with a short-path distillation arm, to continuously remove the produced methanol, connected to a Schlenk line and the system was purged and filled with Ar or N_2 3 times before heating under Ar or N_2 at 95 °C overnight. High-vacuum was then applied whilst maintaining the heating, for 4 h to remove any excess diol and the crude material was analysed by GPC. Crude ^{1}H-NMR spectra are represented with annotated details in chapter III.3.

Enzymatic polymerizations in high boiling organic media (made by Dr. Alessandro Pellis)

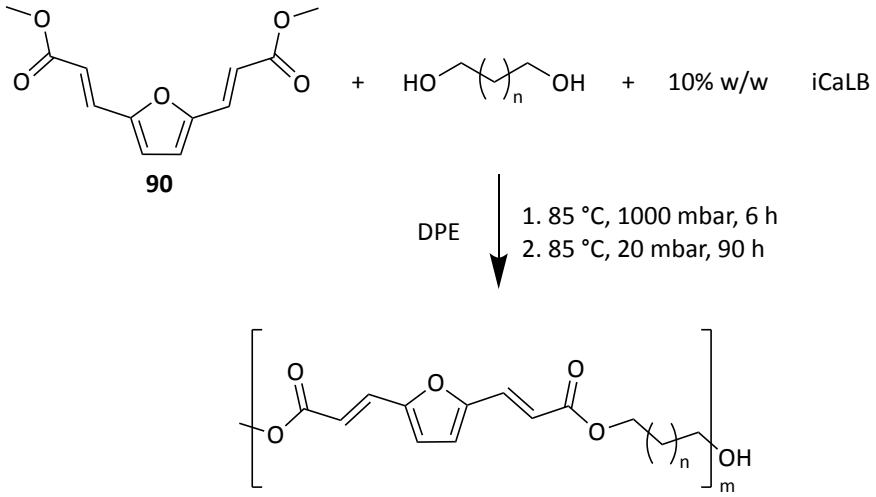

Protocol adapted from the literature.[205] In a 25 mL round bottom flask were added consecutively, **90** (8.0 mmol, 0.2 M), the indicated diol (8.0 mmol, 0.2 M, see Figure 43 p. 176, diester:diol ratio= 1:1) and diphenyl ether (DPE, 4 mL). The mixture was then stirred at 85 °C until complete dissolution of the monomers in the solvent. 10% $w.w^{-1}$ (calculated on the total amount of the monomers) of iCaLB was then added and the mixture was heated for 6 h at 85 °C, 1000 mbar. The reaction system was covered with aluminium foil to avoid light-induced side reactions of the reaction components. A vacuum of 20 mbar was subsequently applied for an additional 90 h while maintaining the reaction temperature at 85 °C. Thereafter, warm chloroform was added to the reaction mixture to solubilise the polymer product and the biocatalyst was filtered off through a sintered funnel. The chloroform was then removed under vacuum. The polymer-DPE mixture was subsequently crashed out in ice-cold methanol achieving precipitation of the products. Three methanol triturations were subsequently performed in order to remove the residual

DPE. The reactions led to a light-yellow powdery polymerisation product. All reactions were conducted in duplicates.

^{1}H-NMR (400 MHz, [$CDCl_3$], with 1,8-octanediol): δ (ppm) 7.36 (d, *J* = 15.8 Hz, 2H, (-(C_4H_2O)-C<u>H</u>=CH-COO-)x2), 6.63 (s, 2H, (-(C_4<u>H_2</u>O)-CH=CH-COO-)), 6.41 (d, *J* = 15.8 Hz, 2H, (-(C_4H_2O)-CH=C<u>H</u>-COO-)x2), 4.17 (t, *J* = 6.7 Hz, 2H, -(C_4H_2O)-CH=CH-COO-C<u>H_2</u>-), 1.68 (p, *J* = 6.8 Hz, 2H, -(C_4H_2O)-CH=CH-COO-CH_2-C<u>H_2</u>-CH_2-), 1.36 (s, br, 2H (8H), -C<u>H_2</u>-).

^{13}C-NMR (101 MHz; [$CDCl_3$], with 1,8-octanediol): δ (ppm), 166.83 (-<u>C</u>OO-alkyl), 152.54 (-(C_3H_2O<u>C</u>)-CH=CH-COO-), 130.13 (-(C_4H_2O)-<u>C</u>H=CH-COO-), 118.08 (-(C_4H_2O)-CH=<u>C</u>H-COO-), 116.78 (-(CO<u>C_2</u>H_2C)-CH=CH-COO-), 64.89 (-(C_4H_2O)-CH=CH-COO-<u>C</u>H_2-alkyl-), 29.25, 28.75, 25.97 (-(C_4H_2O)-CH=CH-COO-CH_2-<u>alkyl</u>-).

FT-IR wavenumber (cm^{-1}), qualitative comment very strong (vs), strong (s), weak (w), very weak (vw), with 1,8-octanediol: 2929 (vw); 2854 (vw); 1703 (vs); 1630 (vs); 1553 (vw); 1500 (vw); 1488 (vw); 1465 (vw); 1389 (vw); 1302 (s); 1243 (vs); 1168 (vs); 1157 (vs); 1072 (vw); 1062 (vw); 1044 (vw); 1020 (w); 983 (w); 967 (s); 958 (s); 920 (vw); 896 (vw); 863 (vw); 813 (w); 796 (w); 752 (vw); 736 (vw); 726 (vw); 690 (vw).

MALDI-TOF $C_{18}H_{22}O_5$ (repeating unit) theoretical (m/z): 318.1467 measured (m/z): 318.1512 average over 8 repeating unit.

Melting point ~110 °C (DSC)

Enzymatic polymerizations in low boiling organic media (made by Dr. Alessandro Pellis)

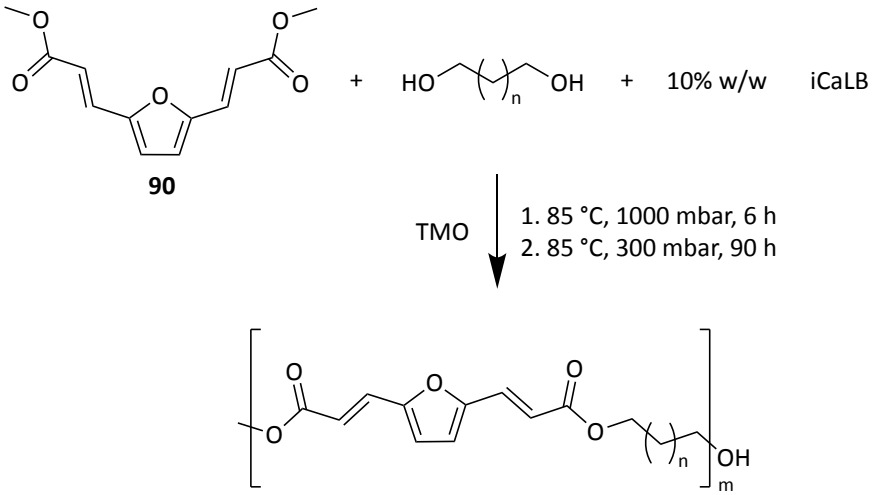

Enzymatic polycondensation reactions were conducted in a similar manner to that previously described for other polyesters. Briefly, a 100 mL round bottom flask was charged with **90** (0.8 mmol, 0.2 M) the indicated diol (0.8 mmol, 0.2 M, see Figure 43 p. 176), diester:diol ratio= 1:1) and TMO (4 mL) as a low boiling point organic solvent. The mixture was then stirred at 85 °C until complete dissolution of the monomers in the solvent. 10% w/w (calculated on the total amount of the monomers) of iCaLB was then added and the reaction was run for 6 h at 85 °C, 1000 mbar. The reaction system was covered with aluminium foil to avoid light-induced side-reactions of the mixture components. A 300 mbar vacuum was subsequently applied for an additional 90 h while maintaining the reaction temperature at 85 °C. At the end of the reaction, the biocatalyst was filtered, and the TMO was then removed under vacuum. The reactions led to yellow powdery polymerisation products. Characterisation data matched the ones described above.

ODO-PFAE (91) polymer film casting

The synthesized polymer **91** was dissolved in chloroform (10 mg.mL^{-1}) and the solution casted on a Kapton polyimide film placed inside a glass petri dish. The solvent was slowly removed at 21 °C keeping the casting system in the dark. The obtained thin film (thickness of 50 µm) was then peeled off the polyimide film and mechanically tested and cured as described below.

UV-irradiation of synthesised material

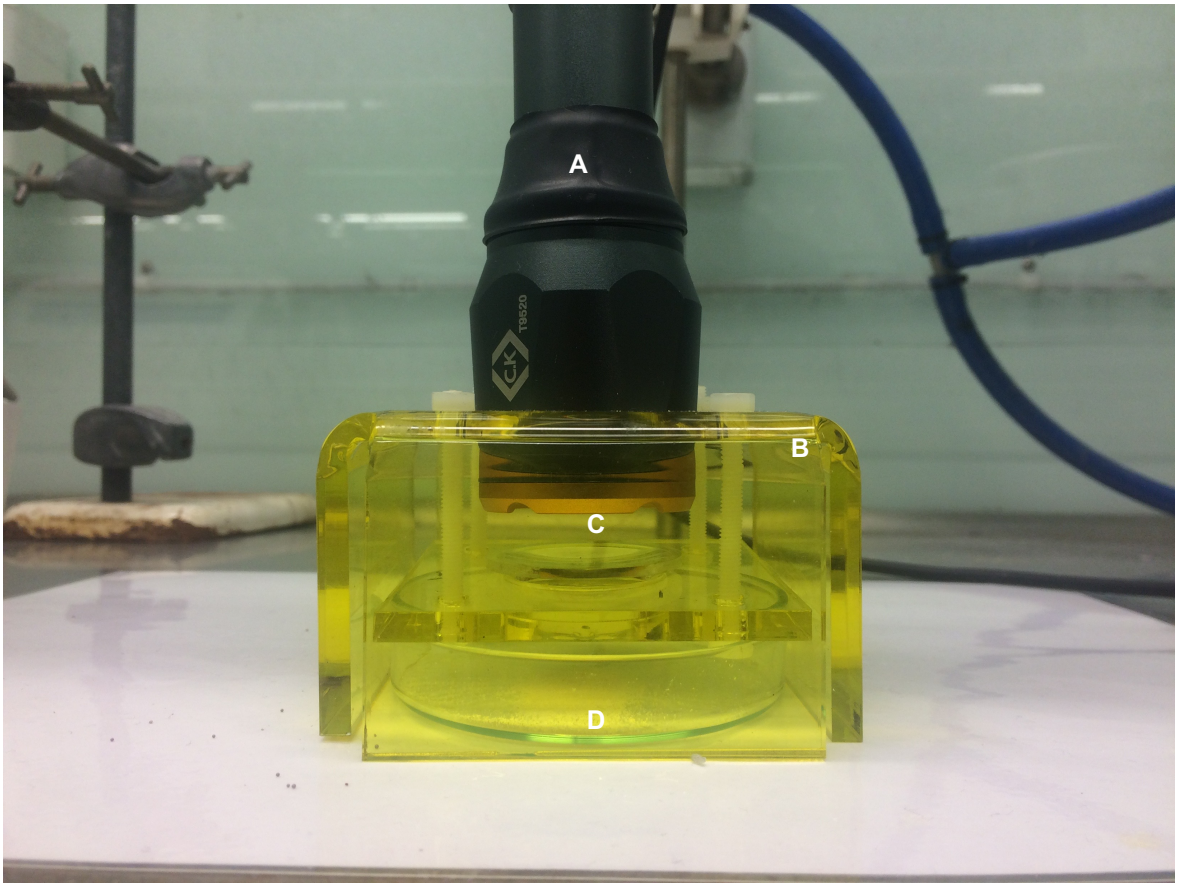

Custom made apparatus for UV-irradiation of samples. A: LED torch (maximum emission at 365 nm, 1250 mW flux output), B: Plastic casing coated with UV-protecting filter, C: Quartz lens, D: Irradiated sample in petri dish.

The beam of a custom-made LED torch or fluorescent lamp maximum emission at 365 nm, 1250 mW maximum flux output for the LED and 253 nm, 5 W for the fluorescent lamp) was

collimated with a biconvex plastic lens (for irradiation at 365 nm) and a biconvex quartz lens (for irradiation at 253 nm) on the sample layer (typically 100 mg neat for monomer 1 and **91**, 2.5 cm long, 0.5 cm wide strips for film, <1 mm thick, distance from lens ~5 cm for 365 nm lamp, < 2 cm for 253 nm lamp) placed on a glass petri dish. The reaction was monitored by FT-IR spectroscopy and mixing with a spatula (for powdery/crystalline) or change of irradiated faces (for film strips) was done every 24 h to assure homogeneous curing. Typically, UV-curing of a sample was stopped after 72 h of continuous irradiation unless specified otherwise.

d. Synthetic procedures for chapter III.4 (p. 192-242)

Synthesis of 1-(furan-2-yl)-1-hydroxytridecane(163$_a$)

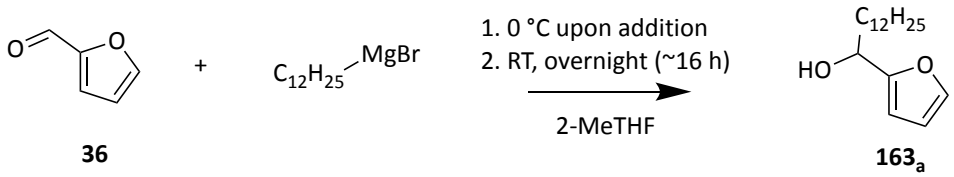

36 **163$_a$**

An oven-dried two-necked 250 mL round bottom flask was charged with furfural (8.270 g, 35.0 mmol), 2-MeTHF (30 mL, dried with 3Å molecular sieves, stored under Ar) and a dried stirrer flea. The mixture was cooled to ~0 °C (ice/water bath) and 35.5 mmol of dodecyl magnesium bromide (71 mL, 1.01 eq. 2 M solution in 2-MeTHF) was slowly added. After addition, the reaction was allowed to warm up to room temperature and was further stirred overnight. The reaction was quenched with a saturated ammonium chloride solution (100 mL). The phases were separated, and the organic phase was washed again with saturated ammonium chloride solution (100 mL) and brine (100 mL). The collected aqueous phases were back extracted with EtOAc (100 mL), and the collected organic phases were then dried over $MgSO_4$ and the solvent was evaporated under reduced pressure. Silica gel flash column chromatography (*n*-hexane:EtOAc, 4:1, R_f= 0.34) afforded **163$_a$** (9.310 g, >99% yield) as a white solid.

^{1}H-NMR (400 MHz, [$CDCl_3$]): δ (ppm) 7.36 (d, *J* = 1.7 Hz, 1H, ($\underline{H}COC_3H_2$)-CH(-OH)-$C_{12}H_{25}$), 6.35–6.28 (m, 1H, ($C_3H_2C\underline{H}OC$)-CH(-OH)-$C_{12}H_{25}$), 6.22 (d, *J* = 3.2 Hz, 1H, ($HCOC\underline{H}C_2H$)-CH(-OH)-$C_{12}H_{25}$), 4.66 (t, *J* = 6.8 Hz, 1H, (C_4H_3O)-C$\underline{H}$(-OH)-$C_{12}H_{25}$), 1.91–1.76 (m, 2H, (C_4H_3O)-CH(-OH)-C$\underline{H_2}$-$C_{11}H_{23}$), 1.24 (s, 20H, (C_4H_3O)-CH(-OH)-CH_2-$C_{10}H_{20}$-CH_3), 0.87 (t, *J* = 6.7 Hz, 3H, (C_4H_3O)-CH(-OH)-CH_2-$C_{10}H_{20}$-C$\underline{H_3}$).

^{13}C-NMR (101 MHz; [$CDCl_3$]): δ (ppm) 157.00 (($\underline{C}HOC_3H_2$)-CH(-OH)-$C_{12}H_{25}$), 141.97 (($C_3H_2O\underline{C}$)-CH(-OH)-$C_{12}H_{25}$), 110.19 (($CHO\underline{C}HC_2H$)-CH(-OH)-$C_{12}H_{25}$), 105.86 (($C_2H_2\underline{C}HOC$)-CH(-OH)-$C_{12}H_{25}$) , 67.95 ((C_4H_3O)-$\underline{C}$H(-OH)-$C_{12}H_{25}$), 35.65, 32.02, 29.77, 29.74, 29.67, 29.62, 29.50, 29.45, 25.64, 22.79 ((C_4H_3O)-CH(-OH)-$\underline{C_{12}}H_{25}$), 14.23 (C_4H_3O)-CH(-OH)-$C_{11}H_{22}$-$\underline{C}H_3$). Data are in accordance with previously reported chemical shifts.[382]

FT-IR wavenumber (cm^{-1}): 3340 (vw); 3334 (vw); 3321 (vw); 3309 (vw); 3300 (vw); 3278 (vw); 3259 (vw); 3239 (vw); 2953(w); 2914 (vs); 2873 (w); 2849 (vs); 1507 (vw); 1466 (s); 1430 (vw); 1329 (vw); 1319 (vw); 1235 (vw); 1229 (vw); 1222 (vw); 1147 (s); 1114 (vw); 1092 (w); 1067 (s); 1037 (vw); 1027 (vw); 1007 (s);978 (vw); 962 (w); 941 (vw); 930 (vw); 910 (vw); 884 (vw); 876 (vw); 810 (vw); 769 (vw); 729 (vs)

ESI-MS $C_{17}H_{30}NaO_2$ theoretical (m/z): 289.2138 [M+] measured (m/z): 289.2140 [M+].

Melting point 48.5–50.1 °C (lit. 44 °C)[382]

Synthesis of 1-(furan-2-yl)tridecan-1-one (164_a)

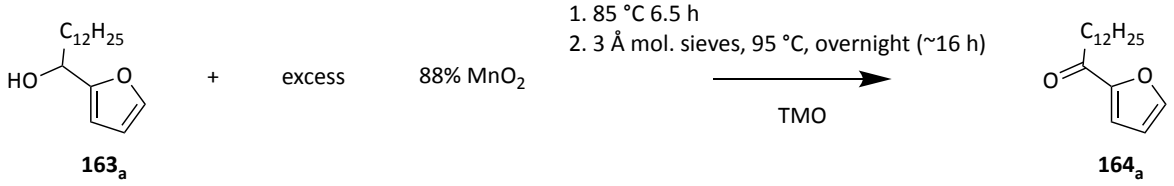

163_a **164_a**

A 100 mL conical flask was charged with 2-hydroxyalkylfuran (1.50 g, 5.6 mmol), 88% MnO_2 electrolytically precipitated (3.00 g, 4.5 mmol) and TMO (50 mL). A cork ring pierced with the temperature probe was placed on top of the conical flask, and the reaction mixture was vigorously stirred at 85 °C. Progression of the reaction was monitored by TLC (*n*-hexane:EtOAc, 9:1) and after 8 h of reaction, an extra 3.00 g of MnO_2 was added together with 3 Å Molecular sieves and heated to 95 °C overnight. After filtration through Celite of the reaction mixture, the filtrate was evaporated under reduced pressure, and the residue was purified by chromatography (silica gel, *n*-hexane:EtOAc 9:1, R_f=0.36) to afford **164_a** as a white solid (0.633 g, 45% yield).

^{1}H-NMR (400 MHz, [$CDCl_3$]): δ (ppm) 7.54 (s, 1H, , ($\underline{H}COC_3H_2$)-C(=O)-$C_{12}H_{25}$)), 7.14 (d, *J* = 3.5 Hz, 1H, (HCOC$\underline{H}C_2H$)-C(=O)-$C_{12}H_{25}$)), 6.49 (d, *J* = 3.6 Hz, 1H, ($C_2H_2C\underline{H}OC$)-C(=O)-$C_{12}H_{25}$)), 2.78 (t, *J* = 7.5 Hz, 2H, (C_4H_3O)-C(=O)-C$\underline{H_2}$- $C_{11}H_{23}$)), 1.68 (p, *J* = 7.3 Hz, 2H, (C_4H_3O)-C(=O)-CH_2-C$\underline{H_2}$-$C_{10}H_{21}$)), 1.22 (s (br), 18H (20H calc.), (C_4H_3O)-C(=O)-CH_2-CH_2-$C_9\underline{H_{18}}$-CH_3)), 0.85 (t, *J* = 6.6 Hz, 3H, (C_4H_3O)-C(=O)-CH_2-CH_2-C_9H_{18}-C$\underline{H_3}$)).

^{13}C-NMR (101 MHz; [$CDCl_3$]): δ (ppm) 189.92 ((C_4H_3O)-$\underline{C}$(=O)-$C_{12}H_{25}$), 152.94 (($H\underline{C}OC_3H_2$)-C(=O)-$C_{12}H_{25}$), 146.23 ($HCH_2O\underline{C}$)-C(=O)-$C_{12}H_{25}$), 116.86 (HCO$\underline{C}HC_2H$)-C(=O)-$C_{12}H_{25}$), 112.18 (($C_2H_2\underline{C}HOC$)-C(=O)-$C_{12}H_{25}$), 38.60 ((C_4H_3O)-C(=O)-$\underline{C}H_2$-$C_{11}H_{23}$), 32.00 ((C_4H_3O)-C(=O)-CH_2-$\underline{C}H_2$-$C_{10}H_{21}$) , 29.74, 29.69, 29.57, 29.49, 29.43, 24.43, 22.77 ((C_4H_3O)-C(=O)-CH_2-CH_2-$\underline{C}_9H_{18}$-

CH_3), 14.19 ((C_4H_3O)-C(=O)-CH_2-CH_2-C_9H_{18}-$\underline{C}H_3$)). Data are in accordance with previously reported chemical shifts.[383]

FT-IR wavenumber (cm^{-1}): 2952 (vw); 2914 (vs); 2872 (vw); 2849 (s); 1673 (vs); 1634 (vw); 1565 (vw); 1471 (vs); 1410 (w); 1397 (w); 1384 (vw); 1340 (vw); 1292 (vw); 1270 (vw); 1245 (vw); 1236 (vw); 1223 (vw); 1168 (w); 1094 (vw); 1084 (vw); 1060 (vw); 1048 (vw); 1026 (w); 1014 (vw); 995 (vw); 970 (s); 918 (w); 896 (vw); 884 (vw); 877 (vw); 832 (vw); 757 (vs); 728; (vw); 717 (w).

Melting point 44.2–45.8 °C (lit. 38.5–40 °C)[383]

Bromination of fatty alcohols (166$_{a-c}$)

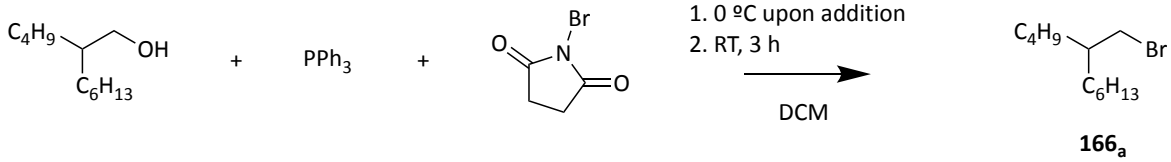

166$_a$

Protocol adapted from the literature.[384] A 250 mL two-necked round bottom flask was charged with the fatty alcohol (*e.g.* 2-butyl-1-octanol, 15.00 g, 80.5 mmol), triphenylphosphine (*e.g.* 21.110 g, 80.5 mmol) and anhydrous DCM (200 mL). After dissolution, the mixture was cooled in an ice bath (~0 °C) with stirring. Thereafter N-bromosuccinimide (*e.g.* 14.47 g, 81.3 mmol, 1.01 eq.) was gradually added and the mixture was left to stir at room temperature for 3 h. The solvent was then thoroughly removed under reduced pressure and *n*-hexane was added. The obtained solids were filtered and washed with *n*-hexane and the collected filtrate was concentrated. The bromo-derivative was obtained as a clear oil after dry vacuum column chromatography through silica (silica gel, Merck, 0.015-0.040 mm) topped with a layer of $MgSO_4$ (*e.g.* 14.43 g, 74% yield).

Fatty alcohol	Reaction time (h)	Yield (%)	Product
hexadecan-1-ol	3	94	$C_{16}H_{33}$–Br
2-butyl-1-octanol	3	74	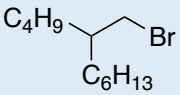
tetradecan-2-ol	overnight	80	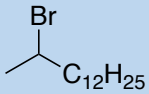

2-butyl-1-bromooctane (166_a)

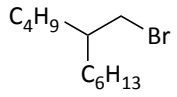

166_a

^{1}H-NMR (400 MHz, [$CDCl_3$]): δ (ppm) 3.41 (d, *J* = 4.9 Hz, 2H, Br-C$\underline{H_2}$-CH(-C_3H_6-CH_3)-C_5H_{10}-CH_3), 1.55 (m, *J* = 6.1 Hz, 1H, Br-CH_2-C$\underline{H}$(-C_3H_6-CH_3)-C_5H_{10}-CH_3), 1.48–1.04 (m, 16H, Br-CH_2-CH(-$C_3\underline{H_6}$-CH_3)-$C_5\underline{H_{10}}$-CH_3), 1.04–0.64 (m, 6H, Br-CH_2-CH(-C_3H_6-C$\underline{H_3}$)-C_5H_{10}-C$\underline{H_3}$). Data are in accordance with previously reported chemical shifts.[385]

FT-IR wavenumber (cm^{-1}): 2956 (w); 2925 (vs); 2872 (vw); 2856 (w); 1466 (vw); 1458 (vw); 1445; (vw); 1379 (vw); 1285 (vw); 1254 (vw); 1235 (vw); 726 (vw).

2-methyl-1-bromotetradecane(166_b)

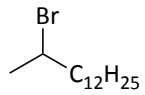

166_b

^{1}H-NMR (400 MHz, [$CDCl_3$]): δ (ppm) 4.25–4.05 (m, 1H, CH_3-C$\underline{H}$(-Br)-CH_2-$C_{10}H_{20}$-CH_3), 1.87–1.58 (m, 5H, C$\underline{H_3}$-CH(-Br)-C$\underline{H_2}$-$C_{10}H_{20}$-CH_3), 1.37–1.14 (m, 20H, CH_3-CH(-Br)-CH_2-$C_{10}\underline{H_{20}}$-CH_3), 0.87 (t, *J* = 6.7 Hz, 3H, CH_3-CH(-Br)-CH_2-$C_{10}H_{20}$-C$\underline{H_3}$).

^{13}C-NMR (101 MHz; [$CDCl_3$]): δ (ppm) 52.03 (CH_3-C$\underline{H}$(-Br)-CH_2-$C_{10}H_{20}$-CH_3), 41.29 (CH_3-CH(-Br)-C$\underline{H_2}$-$C_{10}H_{20}$-CH_3), 32.02 (C$\underline{H_3}$-CH(-Br)-CH_2-$C_{10}H_{20}$-CH_3), 31.69, 29.77, 29.74, 29.67, 29.64, 29.59, 29.46, 29.10, 27.88, 26.54, 22.79 (C$\underline{H_3}$-CH(-Br)-CH_2-C$\underline{_{10}}H_{20}$-CH_3), 14.21 (CH_3-CH(-Br)-CH_2-$C_{10}H_{20}$-C$\underline{H_3}$). Data are in accordance with previously reported chemical shifts.[386]

FT-IR wavenumber (cm^{-1}): 2956 (vw); 2921 (vs); 2852 (vs); 1466 (w); 1441 (vw); 1254 (vw); 1245; (vw); 721 (vw).

GC-MS (EI) No molecular ion (fragmentation). Main fragment (m/z): 197.2285, 141.1653, 113.1337, 99.1179, 85.1021, 71.0863, 57.0707, 43.0550, 29.0392

1-bromohexadecane (166$_c$)

$C_{16}H_{33}$—Br

166$_c$

^{1}H-NMR (400 MHz, [$CDCl_3$]): δ (ppm) 3.39 (t, *J* = 6.9 Hz, 2H, Br-C$\underline{H_2}$-$C_{15}H_{31}$), 1.84 (dt, *J* = 14.6, 6.9 Hz, 2H, Br-CH_2-C$\underline{H_2}$-$C_{14}H_{29}$), 1.25 (s, 26H, Br-CH_2-CH_2-$C_{13}\underline{H_{26}}$-CH_3), 0.87 (t, *J* = 6.8 Hz, 3H, Br-CH_2-CH_2-$C_{13}H_{26}$-C$\underline{H_3}$).

^{13}C-NMR (101 MHz; [$CDCl_3$]): δ (ppm) 34.12 (Br-CH_2-$\underline{C}H_2$-$C_{13}H_{26}$-CH_3), 32.95 (Br-$\underline{C}H_2$-CH_2-$C_{13}H_{26}$-CH_3), 32.03, 31.70, 29.79, 29.77, 29.73, 29.65, 29.55, 29.47, 28.88, 28.29, 22.80, 22.76 (Br-CH_2-CH_2-$\underline{C}_{13}H_{26}$-CH_3), 14.22 (Br-CH_2-CH_2-$C_{13}H_{26}$-$\underline{C}H_3$). Data are in accordance with previously reported chemical shifts.[387]

FT-IR wavenumber (cm^{-1}): 2956 (vw); 2921 (vs); 2852 (vs); 1466 (w); 1441 (vw); 1254 (vw); 1245; (vw); 721 (vw).

GC-MS (EI) $C_{16}H_{33}Br$, theoretical (m/z): 304.1760 [M+] measured (m/z): [M+] 304.1754

Synthesis of 1-(furan-2-yl)2 -butyloctan-1-ol (163_b)

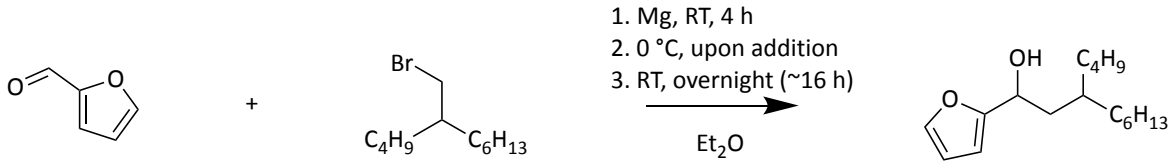

36 **166_a** **163_b**

A flame-dried 3-necked 250 mL round bottom flask was charged with 0.365 g of magnesium (15.0 mmol, 3 eq.) and anhydrous Et_2O (5 mL) under Ar. 1,2-Dibromoethane (~3 drops, ~0.2 mL) was added to the suspension and left to stir vigorously for 1 h. Thereafter a solution of alkyl halide (1.25 g, 5 mmol, in Et_2O, 35 mL) was slowly added making sure the Grignard formation initiated (constant Et_2O boiling) before adding the whole alkyl halide solution. The reaction mixture was then left to stir for 4 h at room temperature. The hence prepared Grignard reagent solution was cooled to 0 °C in ice and furfural was added (0.319 g, 3.32 mmol, in Et_2O, 20 mL). The resulting mixture was stirred overnight at room temperature. Thereafter, the reaction mixture was transferred via a cannula to a cooled (0 °C, ice) saturated ammonium chloride solution (100 mL). The phases were separated, and the organic phase was washed with saturated ammonium chloride (100 mL) and brine (100 mL). The aqueous phases were back extracted with EtOAc (100 mL). The collected organic phases were dried over $MgSO_4$, filtered, and the filtrate was evaporated under reduced pressure. The resulting product was purified by column chromatography over silica gel (*n*-hexane:EtOAc, 4:1, R_f= 0.4) to afford **163_b** as a pale yellow oil (242 mg, 27% yield).

^{1}H-NMR (400 MHz, [$CDCl_3$]): δ (ppm) 7.36 (dd, *J* = 1.8, 0.7 Hz, 1H, (HCOC_3H_2O)-CH(-OH)-CH_2-CH(-C_4H_9)-C_6H_{13}), 6.31 (dd, *J* = 3.2, 1.8 Hz, 1H, (C_2H_2C<u>H</u>OC)-CH(-OH)-CH_2-CH(-C_4H_9)-C_6H_{13}), 6.22 (d, *J* = 3.2 Hz, 1H, (HCOC<u>H</u>C_2H)-CH(-OH)-CH_2-CH(-C_4H_9)-C_6H_{13}), 4.79–4.70 (m,

1H, (C_4H_3O)-C<u>H</u>(-OH)-CH_2-CH(-C_4H_9)-C_6H_{13}), 1.82–1.68 (m, 2H, (C_4H_3O)-CH(-OH)-C<u>H_2</u>-CH(-C_4H_9)-C_6H_{13}), 1.34–1.18 (m, 17H, (C_4H_3O)-CH(-OH)-CH_2-C<u>H</u>(-C_3<u>H_6</u>-CH_3)-C_5<u>H_{10}</u>-CH_3), 0.91–0.80 (m, 6H, (C_4H_3O)-CH(-OH)-CH_2-CH(-C_3H_6-C<u>H_3</u>)-C_5H_{10}-C<u>H_3</u>).

^{13}C-NMR (101 MHz; [$CDCl_3$]): δ (ppm) 157.21 ((H<u>C</u>OC_3H_2)-CH(-OH)-CH_2-CH(-C_4H_9)-C_6H_{13}), 141.96 ((C_3H_3O<u>C</u>)-CH(-OH)-CH_2-CH(-C_4H_9)-C_6H_{13}), 110.20 ((HCO<u>C</u>HC_2H)-CH(-OH)-CH_2-CH(-C_4H_9)-C_6H_{13}), 105.88 ((C_2H_2<u>C</u>HOC)-CH(-OH)-CH_2-CH(-C_4H_9)-C_6H_{13}), 66.11 ((C_4H_3O)-<u>C</u>H(-OH)-CH_2-CH(-C_4H_9)-C_6H_{13}), 40.08 ((C_4H_3O)-CH(-OH)-<u>C</u>H_2-CH(-C_4H_9)-C_6H_{13}), 34.13 ((C_4H_3O)-CH(-OH)-CH_2-<u>C</u>H(-C_4H_9)-C_6H_{13}), 33.98, 33.91, 33.81, 33.66, 33.35, 33.02, 31.98, 29.81, 28.72, 28.58, 26.66, 26.47, 26.32, 23.17, 23.03, 22.78 ((C_4H_3O)-CH(-OH)-CH_2-<u>C</u>H(-<u>C_3</u>H_6-CH_3)-<u>C_5</u>H_{10}-CH_3, 14.22 ((C_4H_3O)-CH(-OH)-CH_2-CH(-C_3H_6-<u>C</u>H_3)-C_5H_{10}-<u>C</u>H_3).

FT-IR wavenumber (cm^{-1}): 3366 (vw); 3358 (vw); 3351 (vw); 3340 (vw); 3334 (vw); 2956 (w); 2925; (vs); 2872 (w); 2857 (w); 1504 (vw); 1466 (vw); 1458 (vw); 1411 (vw); 1378 (vw); 1340 (vw); 1302 (vw); 1258 (vw); 1228 (vw); 1181 (vw); 1150 (vw); 1066 (vw); 1008 (w); 920 (vw); 885; (vw); 805 (vw); 728 (vs).

ESI-MS $C_{17}H_{29}O_2$, theoretical (m/z): 265.2162 [M+] measured (m/z): 265.2158 [M+].

$C_{17}H_{28}NaO_2$ theoretical (m/z): 287.1982 [M+] measured (m/z): 287.1977 [M+].

Synthesis of 1-(furan-2-yl)-1-hydroxyhexadecane(163$_c$)

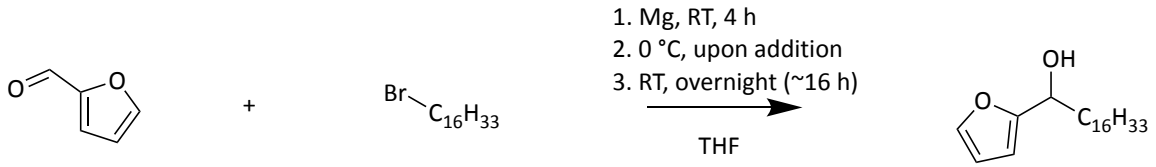

36 **166$_c$** **163$_c$**

A flame-dried 3-necked 250 mL round bottom flask was charged with 0.418 g of magnesium (17.0 mmol, 3 eq.) and anhydrous THF (5 mL) under Ar. 1,2-Dibromoethane (~3 drops, 0.2 mL) was added to the suspension until clear activation of Mg was observed (THF reflux) and the reaction mixture was left to stir for ~1 h until reflux ceased. Thereafter a solution of *n*-bromohexadecane (1.750 g, 5 mmol) in THF (35 mL) was slowly added making sure the Grignard formation initiated before adding the whole solution and the reaction mixture was stirred for 4 h at room temperature. The hence prepared Grignard reagent solution was cooled to 0 °C in an ice bath and a solution of furfural (0.500 g, 5.2 mmol, in THF, 50 mL) was added. The resulting mixture was stirred overnight at room temperature. Thereafter, the solution was transferred with a cannula to a cooled (0 °C, ice) saturated ammonium chloride solution (100 mL). The phases were separated, and the organic phase was washed with saturated ammonium chloride (100 mL) and brine (100 mL). The aqueous phases were back extracted with EtOAc (100 mL). The collected organic phases were dried over $MgSO_4$, filtered and the filtrate was evaporated under reduced pressure. The resulting product was purified by column chromatography over silica gel (EtOAc:*n*-hexane, 1:4, R_f= 0.35) to afford **163$_c$** as a pale yellow oil (570 mg, 51% yield).

^{1}H-NMR (400 MHz, [$CDCl_3$]): δ (ppm) 7.36 (dd, *J* = 1.8, 0.9 Hz, 1H, ($\underline{H}COC_3H_2$)-CH(-OH)-$C_{16}H_{33}$), 6.32 (dd, *J* = 3.2, 1.8 Hz, 1H, ($C_3H_2C\underline{H}OC$)-CH(-OH)-$C_{16}H_{33}$), 6.22 (d, *J* = 3.2 Hz, 1H, (HCOC$\underline{H}C_2H$)-CH(-OH)-$C_{16}H_{33}$), 4.66 (q, *J* = 6.7 Hz, 1H, (C_4H_3O)-C$\underline{H}$(-OH)-$C_{16}H_{33}$), 1.87–1.77

(m, 2H, , (C_4H_3O)-CH(-OH)-$C\underline{H_2}$-$C_{15}H_{31}$), 1.49–1.17 (m (br), 28H, (C_4H_3O)-CH(-OH)-CH_2-$C_{14}\underline{H_{28}}$-CH_3), 0.87 (t, *J* = 6.8 Hz, 3H, (C_4H_3O)-CH(-OH)-CH_2-$C_{14}H_{28}$-$C\underline{H_3}$).

^{13}C-NMR (101 MHz; [$CDCl_3$]): δ (ppm) 157.00 (($\underline{C}HOC_3H_2$)-CH(-OH)-$C_{16}H_{33}$), 141.98 (($C_3H_2O\underline{C}$)-CH(-OH)-$C_{16}H_{33}$), 110.20 (($CHO\underline{C}HC_2H$)-CH(-OH)-$C_{16}H_{33}$), 105.86 (($C_2H_2\underline{C}HOC$)-CH(-OH)-$C_{16}H_{33}$), 67.96 ((C_4H_3O)-$\underline{C}$H(-OH)-$C_{16}H_{33}$), 35.66 ((C_4H_3O)-CH(-OH)-$\underline{C}H_2$-$C_{14}H_{28}$-CH_3), 32.03, 29.79, 29.76, 29.67, 29.62, 29.50, 29.46, 25.64, 22.80 ((C_4H_3O)-CH(-OH)-CH_2-$\underline{C}_{14}H_{28}$-CH_3), 14.23 ((C_4H_3O)-CH(-OH)-CH_2-$C_{14}H_{28}$-$\underline{C}H_3$).

FT-IR wavenumber (cm^{-1}): 3335 (vw); 3255 (vw); 2954 (vw); 2915 (vs); 2873 (w); 2849 (vs); 1507; (vw); 1466 (s); 1225 (vw); 1148 (w); 1114 (vw); 1103 (vw); 1085 (vw); 1071 (w); 1055 (vw); 1043 (vw); 1031 (vw); 1007 (s); 987 (vw); 960 (vw); 942 (vw); 914 (vw); 892 (vw); 883 (vw); 822 (vw); 810 (vw); 771 (vw); 728 (vs).

ESI-MS $C_{21}H_{38}NaO_2$, theoretical (m/z): 345.2764 [M+] measured (m/z): 345.2747 [M+].

Synthesis of 1-(5-(hydroxymethyl)furan-2-yl)tridecan-1-ol (165)

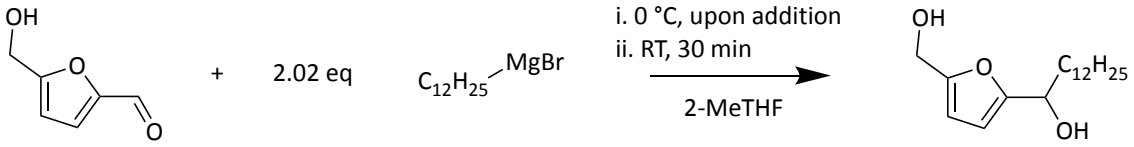

37 **165**

Protocol adapted from the literature.[388] In a 2-necked 250 mL round bottom flask were added consecutively, HMF (**37**, 4.040 g, 32.0 mmol), anhydrous 2-MeTHF (40 mL), 65.0 mmol of dodecyl magnesium bromide (130 mL, 2.02 eq., 0.5 M solution in 2-MeTHF) and the mixture was stirred for 30 min. The reaction was quenched with the addition of saturated ammonium chloride solution (100 mL) and poured in a separatory funnel. The organic phase was washed with saturated ammonium chloride solution (100 mL) and brine (100 mL) and the collected aqueous phases were back extracted EtOAc (100 mL). The collected organic phases were dried over $MgSO_4$, filtered and the filtrate was evaporated under reduced pressure to afford a pale yellow oil. The product **165** was obtained by precipitation from *n*-hexane as a white solid (5.370 g, 57% yield).

^{1}H-NMR (400 MHz, [$CDCl_3$]): δ (ppm) 6.22 (d, *J* = 3.2 Hz, 1H, HO-CH_2-($C_2HC\underline{H}OC$)-CH(-OH)-$C_{12}H_{25}$), 6.16 (d, *J* = 3.2 Hz, 1H, HO-CH_2-($COC\underline{H}C_2H$)-CH(-OH)-$C_{12}H_{25}$)), 4.63 (t, *J* = 6.8 Hz, 1H, HO-CH_2-(C_4H_2O)-C$\underline{H}$(-OH)-$C_{12}H_{25}$), 4.57 (s, 2H, HO-C$\underline{H_2}$-(C_4H_2O)-CH(-OH)-$C_{12}H_{25}$), 1.85–1.78 (m, 2H, HO-CH_2-(C_4H_2O)-CH(-OH)-C$\underline{H_2}$- $C_{11}H_{23}$), 1.55–1.12 (m, 20H, HO-CH_2-(C_4H_2O)-CH(-OH)-CH_2- $C_{10}\underline{H_{20}}$-CH_3), 0.93–0.83 (m, 3H, HO-CH_2-(C_4H_2O)-CH(-OH)-CH_2- $C_{10}H_{20}$-C$\underline{H_3}$).

^{13}C-NMR (101 MHz; [$CDCl_3$]): δ (ppm) 157.15 (HO-CH_2-($C_3H_2\underline{C}O$)-CH(-OH)-$C_{12}H_{25}$), 153.42 (HO-CH_2-($\underline{C}OC_3H_2$)-CH(-OH)-$C_{12}H_{25}$), 108.52 (HO-CH_2-($C_2HC\underline{H}OC$)-CH(-OH)-$C_{12}H_{25}$), 106.62 (HO-CH_2-($COC\underline{H}C_2H$)-CH(-OH)-$C_{12}H_{25}$), 67.96 (HO-CH_2-(C_4H_2O)-$\underline{C}$H(-OH)-$C_{12}H_{25}$), 57.66 (HO-$\underline{C}H_2$-(C_4H_2O)-CH(-OH)-$C_{12}H_{25}$), 35.55 (HO-CH_2-(C_4H_2O)-CH(-OH)-$\underline{C}H_2$-$C_{11}H_{23}$), 32.02, 29.77,

29.74, 29.68, 29.63, 29.49, 29.45, 25.68, 22.79 (HO-CH_2-(C_4H_2O)-CH(-OH)-CH_2-$\underline{C}_{10}H_{20}$-CH_3), 14.23 (HO-CH_2-(C_4H_2O)-CH(-OH)-CH_2-$C_{10}H_{20}$-$\underline{C}H_3$).

FT-IR wavenumber (cm^{-1}): 3293 (w); 3287 (w); 3222 (w); 3191 (w); 3184 (w); 3177 (w); 3167 (w); 2953 (w); 2920 (vs); 2870 (w); 2850 (vs); 1557 (vw); 1465 (s); 1443 (vw); 1434 (vw); 1399; (w); 1377 (vw); 1370 (vw); 1358 (w); 1335 (vw); 1303 (w); 1242 (vw); 1216 (vw); 1203 (w); 1185 (w); 1118 (vw); 1094 (w); 1070 (s); 1026 (vs); 1009 (vs); 984 (w); 963 (s); 952 (w); 943; (w); 917 (w); 875 (vw); 803 (w); 791 (s); 780 (s); 740 (vw); 722 (w); 676 (vw); 671 (vw); 666 (vw).

ESI-MS $C_{21}H_{38}NaO_2$, theoretical (m/z): 319.2244 [M+] measured (m/z): 319.2241 [M+].

Melting point 58.6–60.1 °C

Synthesis of the sulfonated Grignard derivative obtained from HMF

Protocol adapted from the literature.[389] A 100 mL round bottom flask was charged with **165** (1.000g, 3.4 mmol), and anhydrous DMF (50 mL). After complete dissolution, a solution of SO_3•pyridine complex (728 mg, 4.6 mmol, 1.3 eq., in anhydrous DMF, 10 mL), was added dropwise with a syringe and the solution was heated at 40 °C. Completion of the reaction was assessed by TLC (~16 h, DCM:MeOH R_f=0.46). The reaction mixture was then cooled in an ice bath and quenched by addition of 10% Na_2CO_3 (5 mL). The resulting mixture was allowed to warm up at room temperature and heated at 50 °C for 10 min. The resulting solution was poured in a separatory funnel, and brine (60 mL) was added together with *n*-butanol (30 mL). The aqueous phase was separated, and the washes repeated twice. The collected organic phases were dried over Na_2SO_4, filtered and the filtrate was evaporated under reduced pressure. Salt precipitates appearing during evaporation were filtrated over cotton wool. After evaporation, the residue was purified by column chromatography over silica gel to afford a pale yellow oil (DCM:MeOH 8.5:1.5, 765 mg, 50% yield).

^{1}H-NMR (400 MHz, [DMSO-d_6]): δ (ppm) 9.21–9.08 (m, 2H), 8.68–8.56 (m, 1H), 8.23–8.09 (m, 2H), 6.84 (d, *J* = 3.4 Hz, 1), 6.51 (d, *J* = 3.4 Hz, 1H), 6.13 (t, *J* = 7.7 Hz, 1H), 4.59 (s, 2H), 2.43–2.19 (m, 2H), 1.44–1.11 (m, 20H), 0.85–0.77 (m, 3H).

^{13}C-NMR (101 MHz; [DMSO-d_6]): δ (ppm) 153.41, 149.61, 147., 143.87, 129.45, 112.77, , 68.19, 60.04, 32.82, 31.82, 29.55, 29.48, 29.40, 29.23, 29.15, 28.75, 25.75, 22., 14.50.

FT-IR wavenumber (cm^{-1}): 3540 (vw); 3532 (vw); 3516 (vw); 3495 (vw); 3482 (vw); 3470 (vw); 3462; (vw); 3449 (vw); 3431 (vw); 2955 (vw); 2923 (s); 2853 (w); 1630 (vw); 1484 (w); 1467 (w); 1377 (vw); 1363 (vw); 1341 (vw); 1229 (vs); 1164 (w); 1137 (w); 1085 (vw); 1058 (vs); 1026; (w); 974 (vs); 905 (vw); 890 (vw); 875 (vw); 807 (vs); 719 (vs); 683 (vs).

ESI-MS $C_{23}H_{36}NO_5S$, theoretical (m/z): 438.2309 [M+] measured (m/z): 438.2312 [M+]. $C_{23}H_{35}NNaO_5S$, theoretical (m/z): 460.2128 [M+] measured (m/z): 460.2128 [M+].

Synthesis of 5-(chloromethyl)furfural from 5-(hydroxymethyl)furfural

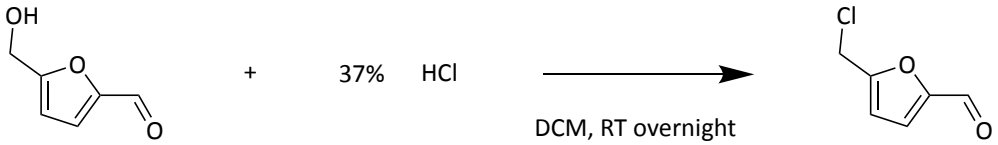

37 **38**

A 500 mL conical flask was charged with HMF (25.00 g, 198 mmol) and DCM (250 mL) and stirred until complete dissolution. Thereafter, ~37% HCl (125 mL, 1.51 mol, 7.6 eq.) was added and the biphasic solution was left to stir overnight. The mixture was then added to a separatory funnel and the organic layer was separated and washed with 1 M HCl (125 mL) and brine (125 mL). The aqueous phases were back extracted with DCM (125 mL) and the collected organic phases were dried over Na_2SO_4 and filtered. After evaporation of the filtrate, the obtained dark oil was purified through active filtration (Celite, activated charcoal, silica gel Merck 0.015 mm–0.040 mm and $MgSO_4$, eluted with DCM) to afford pure CMF as pale yellow oil (26.84 g, 94% yield). Analytical data were identical to the CMF previously obtained.

Synthesis of tert-butyl hypochlorite

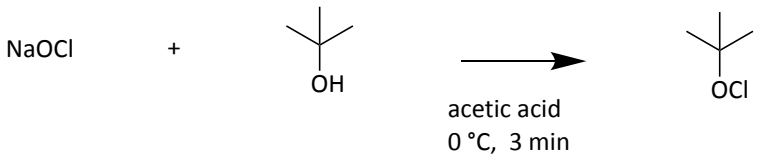

Protocol adapted from the literature.[390] A 500-mL Erlenmeyer flask was charged with 14% sodium hypochlorite (564.2 mmol, 300 mL), a large magnetic stirrer bar and placed on an ice bath wrapped with aluminium foil. Thereafter a solution of *tert*-butanol (38.18 g, 515.04 mmol in acetic acid, 35 mL) was added to the sodium hypochlorite solution and the resulting mixture was stirred for 3 min. The solution was poured in a 1 L separatory funnel and the aqueous phase was discarded. The pale yellow organic phase was washed with 10% Na_2CO_3 solution (50 mL) and DI water (50 mL). The organic phase was further dried over $MgSO_4$ and filtered to afford *tert*-BuOCl (43.72 g, 78.2%) without further purification.

^{1}H-NMR (400 MHz, [$CDCl_3$]): δ (ppm) 1.31 (s, 9H,($C\underline{H}_3$)$_3$-COCl).

^{13}C-NMR (101 MHz; [$CDCl_3$]): δ (ppm) 83.98 ((CH_3)$_3$-$\underline{C}$OCl), 26.87 (($\underline{C}H_3$)$_3$-COCl). Data are in accordance with previously reported chemical shifts.[391]

Synthesis of 5-(chloromethyl)furan-2-carbonyl chloride (170)

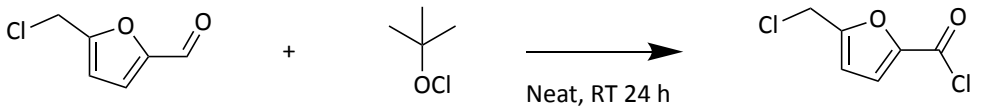

38 **170**

Protocol adapted from the literature.[192] A 500 mL round bottom flask was charged with **38** (25.000 g, 172.9 mmol), *tert*-BuOCl (93.350 g, 859.8 mmol, 5 eq.) and the mixture was stirred rapidly at room temperature overnight. The volatiles were evaporated at 35 °C (under reduced pressure) to afford the crude CMFCC (**170**, 38.508 g, 72% yield by ^{1}H-NMR using 1,4-dioxane as internal standard) which was used without further purification.

^{1}H-NMR (400 MHz, [$CDCl_3$]): δ (ppm) 7.41 (d, *J* = 3.7 Hz, 1H, Cl-CH_2-(C_2HCHOC)-C(=O)-Cl), 6.58 (d, *J* = 3.7 Hz, 1H, Cl-CH_2-($COCHC_2H$)-C(=O)-Cl), 4.56 (s, 2H, Cl-CH_2-(C_4H_2O)-C(=O)-Cl).

^{13}C-NMR (101 MHz; [$CDCl_3$]): δ (ppm) 158.08 (Cl-CH_2-(COC_3H_2)-C(=O)-Cl), 155.37 (Cl-CH_2-(C_4H_2O)-C(=O)-Cl), 146.05 (Cl-CH_2-(C_3H_2OC)-C(=O)-Cl), 125.57 (Cl-CH_2-($COCHC_2H$)-C(=O)-Cl), 112.54 (Cl-CH_2-(C_2HCHOC)-C(=O)-Cl, 36.37 (Cl-CH_2-(C_4H_2O)-C(=O)-Cl).

Synthesis of alkyl 5-(chloromethyl)furan-2-carboxylate (171_{a-f})

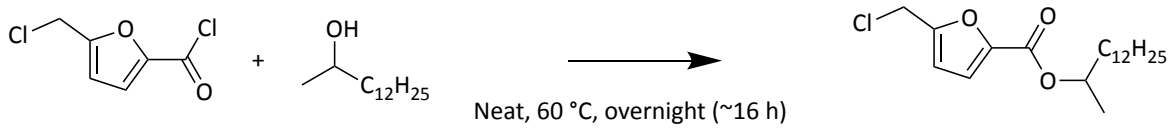

170 **171_d**

Protocol adapted from the literature.[192] CMFCC (*e.g.* 9.620 g of 62% CMFCC w/w, 5.960 g, 33.3 mmol) was mixed with the pre-heated (60 °C) fatty alcohol (*e.g.* tetradecan-2-ol, 10.720 g, 50.0 mmol, 1.5 eq.) in a 50 mL round bottom flask equipped with a drying tube (3 Å activated mol. sieves). The mixture was stirred overnight at 60 °C and completion of the reaction was monitored by TLC. The resulting dark residue was purified by column chromatography (silica gel, *n*-hexane:EtOAc, 9:1, R_f= 0.3 for all compounds of this series) to afford **171** as a pale yellow oil (*e.g.* 7.650 g, 64% yield for **171_d**).

dodecyl 5-(chloromethyl)furan-2-carboxylate (171_a)

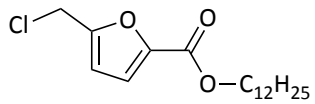

171_a

Yield: 90%

^{1}H-NMR (400 MHz, [$CDCl_3$]): δ (ppm) 7.04 (d, *J* = 3.5 Hz, 1H, Cl-CH_2-(COC<u>H</u>C_2H)-COO-$C_{12}H_{25}$), 6.43 (d, *J* = 3.3 Hz, 1H, Cl-CH_2-(HC_2C<u>H</u>OC)-COO-$C_{12}H_{25}$), 4.54 (s, 2H, Cl-C<u>H_2</u>-(C_4H_2O)-COO-$C_{12}H_{25}$), 4.23 (t, *J* = 6.8 Hz, 2H, Cl-CH_2-(C_4H_2O)-COO-C<u>H_2</u>-$C_{11}H_{23}$), 1.68 (p, *J* = 6.8 Hz, 2H, Cl-CH_2-(C_4H_2O)-COO-CH_2-C<u>H_2</u>-$C_{10}H_{21}$), 1.22 (s (br), *J* = 14.5 Hz, 18H, Cl-CH_2-(C_4H_2O)-COO-CH_2-CH_2-C_9<u>H_{18}</u>-CH_3), 0.82 (t, *J* = 6.8 Hz, 3H, Cl-CH_2-(C_4H_2O)-COO-CH_2-CH_2-C_9H_{18}-C<u>H_3</u>).

^{13}C-NMR (101 MHz; [$CDCl_3$]): δ (ppm) 158.51 (Cl-CH_2-(<u>C</u>OC_3H_2)-COO-$C_{12}H_{25}$), 154.14 (Cl-CH_2-(C_4H_2O)-<u>C</u>OO-$C_{12}H_{25}$), 145.15 (Cl-CH_2-(C_3H_2O<u>C</u>)-COO-$C_{12}H_{25}$), 118.54 (Cl-CH_2-(CO<u>C</u>HC_2H)-COO-$C_{12}H_{25}$), 111.37 (Cl-CH_2-(C_2H<u>C</u>HOC)-COO-$C_{12}H_{25}$), 65.29 (Cl-CH_2-(C_4H_2O)-COO-<u>C</u>H_2-$C_{11}H_{23}$), 36.72 (Cl-<u>C</u>H_2-(C_4H_2O)-COO-CH_2-$C_{11}H_{23}$), 31.97 (Cl-CH_2-(C_4H_2O)-COO-CH_2-<u>C</u>H_2-C_9H_{18}-CH_3), 29.69, 29.63, 29.57, 29.41, 29.30, 28.72, 25.97, 25.93, 22.74 (Cl-CH_2-(C_4H_2O)-COO-CH_2-CH_2-<u>C</u>$_9H_{18}$-CH_3), 14.15 (Cl-CH_2-(C_4H_2O)-COO-CH_2-CH_2-C_9H_{18}-<u>C</u>H_3).

FT-IR wavenumber (cm^{-1}): 2955 (vw); 2923 (vs); 2854 (s); 1720 (vs); 1595 (vw); 1534 (vw); 1521 (vw); 1466 (vw); 1393 (vw); 1379 (vw); 1297 (vs); 1266 (s); 1245 (w); 1211 (vs); 1157 (vs); 1124 (vs); 1080 (vw); 1071 (vw); 1061 (vw); 1051 (vw); 1018 (s); 973 (w); 950 (vw); 937; (vw); 927 (vw); 918 (vw); 895 (vw); 889 (vw); 879 (vw); 810 (w); 792 (vw); 785 (vw); 778; (vw); 761 (vs); 746 (vw); 713 (s).

tetradecyl 5-(chloromethyl)furan-2-carboxylate (171$_b$)

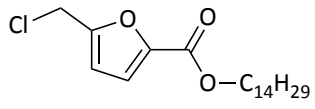

171$_b$

Yield: >99 %

^{1}H-NMR (400 MHz, [$CDCl_3$]): δ (ppm) 7.04 (d, *J* = 3.4 Hz, 1H, Cl-CH_2-(COC<u>H</u>C_2H)-COO-$C_{14}H_{29}$), 6.42 (d, *J* = 3.3 Hz, 1H, Cl-CH_2-(HC_2C<u>H</u>OC)-COO-$C_{14}H_{29}$), 4.53 (s, 2H, Cl-C<u>H$_2$</u>-(C_4H_2O)-COO-$C_{14}H_{29}$), 4.23 (t, *J* = 7.2 Hz, 2H, Cl-CH_2-(C_4H_2O)-COO-C<u>H$_2$</u>-$C_{13}H_{27}$), 1.67 (p, *J* = 6.9 Hz, 2H, Cl-CH_2-(C_4H_2O)-COO-CH_2-C<u>H$_2$</u>-$C_{12}H_{25}$), 1.20 (s (br), 22H, Cl-CH_2-(C_4H_2O)-COO-CH_2-CH_2-C_{11}<u>H$_{22}$</u>-CH_3), 0.81 (t, *J* = 6.6 Hz, 3H, Cl-CH_2-(C_4H_2O)-COO-CH_2-CH_2-$C_{11}H_{22}$-C<u>H$_3$</u>).

^{13}C-NMR (101 MHz; [$CDCl_3$]): δ (ppm) 158.51 (Cl-CH_2-(<u>C</u>OC_3H_2)-COO-$C_{14}H_{29}$), 154.15 (Cl-CH_2-(C_4H_2O)-<u>C</u>OO-$C_{14}H_{29}$), 145.14 (Cl-CH_2-(C_3H_2O<u>C</u>)-COO-$C_{14}H_{29}$), 118.54 (Cl-CH_2-(CO<u>C</u>HC_2H)-COO-$C_{14}H_{29}$), 111.36 (Cl-CH_2-(C_2H<u>C</u>HOC)-COO-$C_{14}H_{29}$), 65.28 (Cl-CH_2-(C_4H_2O)-COO-<u>C</u>H_2-$C_{13}H_{27}$), 36.71 (Cl-<u>C</u>H_2-(C_4H_2O)-COO-CH_2-$C_{13}H_{27}$), 31.99 (Cl-CH_2-(C_4H_2O)-COO-CH_2-<u>C</u>H_2-$C_{11}H_{22}$-CH_3), 29.75, 29.73, 29.72, 29.64, 29.57, 29.43, 29.31, 28.72, 25.94, 22.75 (Cl-CH_2-(C_4H_2O)-COO-CH_2-CH_2-<u>C</u>$_{11}H_{22}$-CH_3), 14.15 (Cl-CH_2-(C_4H_2O)-COO-CH_2-CH_2-$C_{11}H_{22}$-<u>C</u>H_3).

FT-IR wavenumber (cm^{-1}): 2988 (vw); 2959 (w); 2915 (vs); 2871 (w); 2848 (vs); 1726 (vs); 1711 (vs); 1598 (vw); 1539 (w); 1519 (w); 1471 (w); 1464 (w); 1446 (vw); 1441 (vw); 1426 (vw); 1396; (w); 1384 (vw); 1365 (vw); 1341 (vw); 1305 (vs); 1292 (vs); 1263 (vs); 1245 (w); 1216 (vs); 1176 (s); 1161 (vs); 1135 (vs); 1126 (vs); 1101 (w); 1075 (w); 1066 (w); 1049 (w); 1037 (w); 1025 (vs); 989 (w); 973 (vs); 947 (vw); 935 (w); 924 (w); 908 (vw); 890 (w); 856 (vw); 840; (vw); 821 (s); 813 (s); 785 (vw); 761 (vs); 746 (w); 728 (s); 720 (s); 703 (vs).

ESI-MS $C_{20}H_{34}ClO_3$, theoretical (m/z): 357.2191 [M+] measured (m/z): 357.2196 [M+]. $C_{20}H_{33}NaClO_3$ theoretical (m/z): 379.2010 [M+] measured (m/z): 379.2010 [M+].

2-butyl-octan-1-yl 5-(chloromethyl)furan-2-carboxylate (171$_c$)

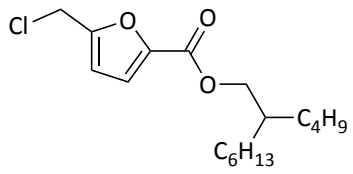

171$_c$

Yield: 69 %

^{1}H-NMR (400 MHz, [$CDCl_3$]): δ (ppm) 7.07 (d, *J* = 3.5 Hz, 1H, Cl-CH_2-(COC<u>H</u>C_2H)-COO-CH_2-CH(-C_4H_9)-C_6H_{13}), 6.47 (d, *J* = 3.5 Hz, 1H, Cl-CH_2-(HC_2C<u>H</u>OC)-COO-CH_2-CH(-C_4H_9)-C_6H_{13}), 4.58 (s, 2H, Cl-C<u>H$_2$</u>-(C_4H_2O)-COO-CH_2-CH(-C_4H_9)-C_6H_{13}), 4.18 (d, *J* = 5.8 Hz, 2H, Cl-CH_2-(C_4H_2O)-

COO-C$\underline{H_2}$-CH(-C_4H_9)-C_6H_{13}), 1.77–1.68 (m, 1H, Cl-CH_2-(C_4H_2O)-COO-CH_2-C$\underline{H}$(-C_4H_9)-C_6H_{13}), 1.35–1.23 (m (br), 16H, Cl-CH_2-(C_4H_2O)-COO-CH_2-CH(-$C_3\underline{H_6}$-CH_3)-$C_5\underline{H_{10}}$-CH_3), 0.87 (m, *J* = 6.7 Hz, 6H, Cl-CH_2-(C_4H_2O)-COO-CH_2-CH(-C_3H_6-C$\underline{H_3}$)-C_5H_{10}-C$\underline{H_3}$).

^{13}C-NMR (101 MHz; [$CDCl_3$]): δ (ppm) 158.74 (Cl-CH_2-(C$\underline{O}C_3H_2$)-COO-CH_2-CH(-C_4H_9)-C_6H_{13}), 154.19 (Cl-CH_2-(C_4H_2O)-C$\underline{O}$O-CH_2-CH(-C_4H_9)-C_6H_{13}), 145.18 (Cl-CH_2-(C_3H_2OC$\underline{}$)-COO-CH_2-CH(-C_4H_9)-C_6H_{13}), 118.48 (Cl-CH_2-(CO$\underline{C}$HC_2H)-COO-CH_2-CH(-C_4H_9)-C_6H_{13}), 111.40 (Cl-CH_2-(C_2H$\underline{C}$HOC)-COO-CH_2-CH(-C_4H_9)-C_6H_{13}), 68.04 (Cl-CH_2-(C_4H_2O)-COO-$\underline{C}H_2$-CH(-C_4H_9)-C_6H_{13}), 37.41 (Cl-$\underline{C}H_2$-(C_4H_2O)-COO-CH_2-CH(-C_4H_9)-C_6H_{13}), 36.80 (Cl-CH_2-(C_4H_2O)-COO-CH_2-$\underline{C}$H(-C_4H_9)-C_6H_{13}), 31.89, 31.37, 31.05, 29.68, 28.99, 26.75, 23.05, 22.74 (Cl-CH_2-(C_4H_2O)-COO-CH_2-CH(-$\underline{C}_3H_6$-CH_3)-$\underline{C}_5H_{10}$-CH_3), 14.19 (Cl-CH_2-(C_4H_2O)-COO-CH_2-CH(-C_3H_6-$\underline{C}H_3$)-C_5H_{10}-CH_3), 14.14 (Cl-$\underline{C}H_2$-(C_4H_2O)-COO-CH_2-CH(-C_3H_6-CH_3)-C_5H_{10}-$\underline{C}H_3$).

FT-IR wavenumber (cm^{-1}): 2956 (w); 2927 (s); 2871 (vw); 2858 (w); 1721 (vs); 1595 (vw); 1533 (vw); 1521 (w); 1466 (w); 1393 (vw); 1380 (vw); 1296 (vs); 1266 (s); 1245 (vw); 1211 (vs); 1158; (vs); 1124 (vs); 1019 (s); 984 (w); 973 (w); 946 (vw); 808 (w); 786 (vw); 761 (vs); 723 (s); 713 (s).

ESI-MS $C_{18}H_{29}ClNaO_3$, theoretical (m/z): 351.1697 [M+] measured (m/z): 351.1696 [M+].

tetradecan-2-yl 5-(chloromethyl)furan-2-carboxylate (171$_d$)

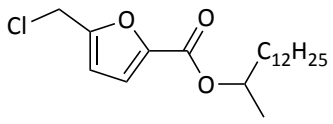

171$_d$

Yield: 64%

^{1}H-NMR (400 MHz, [$CDCl_3$]): δ (ppm) 7.07 (d, *J* = 3.5 Hz, 1H, Cl-CH_2-(COC<u>H</u>C_2H)-COO-CH(-CH_3)-$C_{12}H_{25}$), 6.46 (d, *J* = 3.3 Hz, 1H, Cl-CH_2-(HC_2C<u>H</u>OC)-COO-CH(-CH_3)-$C_{12}H_{25}$), 5.11 (h, *J* = 12.7, 6.2 Hz, 1H, Cl-CH_2-(C_4H_2O)-COO-C<u>H</u>(-CH_3)-$C_{12}H_{25}$), 4.58 (s, 2H, Cl-C<u>H_2</u>-(C_4H_2O)-COO-CH(-CH_3)-$C_{12}H_{25}$), 1.76–1.64 (m, 1H), 1.62–1.49 (m, 1H) **both** (Cl-CH_2-(C_4H_2O)-COO-CH(-CH_3)-C<u>H_2</u>-$C_{11}H_{23}$) 1.30 (d, *J* = 6.3 Hz, 3H, Cl-CH_2-(C_4H_2O)-COO-CH(-C<u>H_3</u>)-CH_2-$C_{11}H_{23}$), 1.23 (s (br), 20H, Cl-CH_2-(C_4H_2O)-COO-CH(-CH_3)-CH_2-C_{10}<u>H_{20}</u>-CH_3), 0.86 (t, *J* = 6.8 Hz, 3H, Cl-CH_2-(C_4H_2O)-COO-CH(-CH_3)-CH_2-$C_{10}H_{20}$-C<u>H_3</u>).

^{13}C-NMR (101 MHz; [$CDCl_3$]): δ (ppm) 158.32 (Cl-CH_2-(<u>C</u>OC_3H_2)-COO-CH(-CH_3)-$C_{12}H_{25}$), 154.02 (Cl-CH_2-(C_4H_2O)-<u>C</u>OO-CH(-CH_3)-$C_{12}H_{25}$), 145.51 (Cl-CH_2-(C_3H_2O<u>C</u>)-COO-CH(-CH_3)-$C_{12}H_{25}$), 118.36 (Cl-CH_2-(CO<u>C</u>HC_2H)-COO-CH(-CH_3)-$C_{12}H_{25}$), 111.39 (Cl-CH_2-(C_2H<u>C</u>HOC)-COO-CH(-CH_3)-$C_{12}H_{25}$), 72.36 (Cl-CH_2-(C_4H_2O)-COO-<u>C</u>H(-CH_3)-$C_{12}H_{25}$), 43.92 (Cl-<u>C</u>H_2-(C_4H_2O)-COO-CH(-CH_3)-$C_{12}H_{25}$), 36.84 (Cl-CH_2-(C_4H_2O)-COO-CH(-CH_3)-<u>C</u>H_2-$C_{11}H_{23}$), 36.01, 32.01, 29.95, 29.73, 29.66, 29.60, 29.52, 29.50, 29.44, 29.27, 25.48, 23.96, 22.78 (Cl-CH_2-(C_4H_2O)-COO-CH(-CH_3)-CH_2-<u>C</u>$_{10}H_{22}$-CH_3, unclear peaks), 20.14 (Cl-CH_2-(C_4H_2O)-COO-CH(-<u>C</u>H_3)-CH_2-$C_{10}H_{22}$-CH_3), 14.22 (Cl-CH_2-(C_4H_2O)-COO-CH(-<u>C</u>H_3)-CH_2-$C_{10}H_{22}$-<u>C</u>H_3).

FT-IR wavenumber (cm^{-1}): 2923 (vs); 2854 (s); 1716 (s); 1534 (vw); 1521 (vw); 1466 (vw); 1379 (vw); 1356 (vw); 1297 (vs); 1266 (w); 1246 (vw); 1211 (s); 1160 (s); 1120 (s); 1042 (vw); 1018 (w); 1001 (vw); 972 (w); 851 (vw); 809 (vw); 762 (s); 713 (s).

ESI-MS $C_{20}H_{33}ClNaO_3$, theoretical (m/z): 379.2010 [M+] measured (m/z): 379.2009 [M+].

hexadecyl 5-(chloromethyl)furan-2-carboxylate (171$_e$)

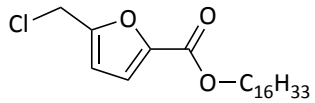

171$_e$

Yield: 73%

^{1}H-NMR (400 MHz, [$CDCl_3$]): δ (ppm) 7.08 (d, *J* = 3.5 Hz, 1H, Cl-CH_2-(COC<u>H</u>C_2H)-COO-$C_{16}H_{33}$), 6.46 (d, *J* = 3.5 Hz, 1H, Cl-CH_2-(HC_2C<u>H</u>OC)-COO-$C_{16}H_{33}$), 4.57 (s, 2H, Cl-C<u>H_2</u>-(C_4H_2O)-COO-$C_{16}H_{33}$), 4.26 (t, *J* = 6.8 Hz, 2H, Cl-CH_2-(C_4H_2O)-COO-C<u>H_2</u>-$C_{15}H_{31}$), 1.71 (dt, *J* = 14.5, 6.8 Hz, 2H, Cl-CH_2-(C_4H_2O)-COO-CH_2-C<u>H_2</u>-$C_{14}H_{29}$), 1.23 (s (br), 26H, Cl-CH_2-(C_4H_2O)-COO-CH_2-CH_2-C_{13}<u>H_{26}</u>-CH_3), 0.85 (t, *J* = 6.8 Hz, 3H, Cl-CH_2-(C_4H_2O)-COO-CH_2-CH_2-$C_{13}H_{26}$-C<u>H_3</u>).

^{13}C-NMR (101 MHz; [$CDCl_3$]): δ (ppm) 158.60 (Cl-CH_2-(<u>C</u>OC_3H_2)-COO-$C_{16}H_{33}$), 154.14 (Cl-CH_2-(C_4H_2O)-<u>C</u>OO-$C_{16}H_{33}$), 145.18 (Cl-CH_2-(C_3H_2O<u>C</u>)-COO-$C_{16}H_{33}$), 118.59 (Cl-CH_2-(CO<u>C</u>HC_2H)-COO-$C_{16}H_{33}$), 111.41 (Cl-CH_2-(C_2H<u>C</u>HOC)-COO-$C_{16}H_{33}$), 65.38 (Cl-CH_2-(C_4H_2O)-COO-<u>C</u>H_2-$C_{15}H_{31}$), 36.77 (Cl-<u>C</u>H_2-(C_4H_2O)-COO-CH_2-$C_{15}H_{31}$), 32.02 (Cl-CH_2-(C_4H_2O)-COO-CH_2-<u>C</u>H_2-$C_{13}H_{26}$-CH_3), 29.79, 29.76, 29.67, 29.60, 29.46, 29.34, 28.74, 25.96, 22.78 (Cl-CH_2-(C_4H_2O)-COO-CH_2-CH_2-<u>C_{13}</u>H_{26}-CH_3), 14.20 (Cl-CH_2-(C_4H_2O)-COO-CH_2-CH_2-$C_{13}H_{26}$-<u>C</u>H_3).

FT-IR wavenumber (cm^{-1}): 2958 (w); 2915 (vs); 2871 (w); 2848 (vs); 1727 (s); 1712 (vs); 1598 (vw); 1541 (w); 1519 (vw); 1472 (w); 1463 (w); 1448 (vw); 1397 (vw); 1340 (vw); 1321 (w); 1307; (vs); 1296 (vs); 1263 (vs); 1244 (w); 1217 (vs); 1177 (s); 1161 (vs); 1135 (s); 1057 (vw); 1047; (vw); 1037 (vw); 1025 (w); 1011 (vw); 997 (vw); 983 (vw); 973 (w); 933 (vw); 922 (vw); 821; (vw); 812 (w); 761 (vs); 729 (w); 720 (s); 704 (vs).

ESI-MS $C_{22}H_{38}ClO_3$, theoretical (m/z): 385.2504 [M+] measured (m/z): 385.2510 [M+]. $C_{22}H_{37}NaClO_3$ theoretical (m/z): 407.2323 [M+] measured (m/z): 407.2322 [M+].

Equimolar mixture of hexadecyl 5-(chloromethyl)furan-2-carboxylate and octadecyl 5-(chloromethyl)furan-2-carboxylate (171_f)

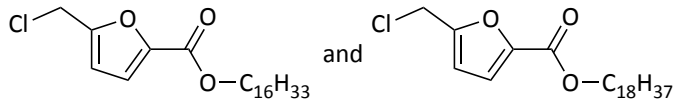

171_f

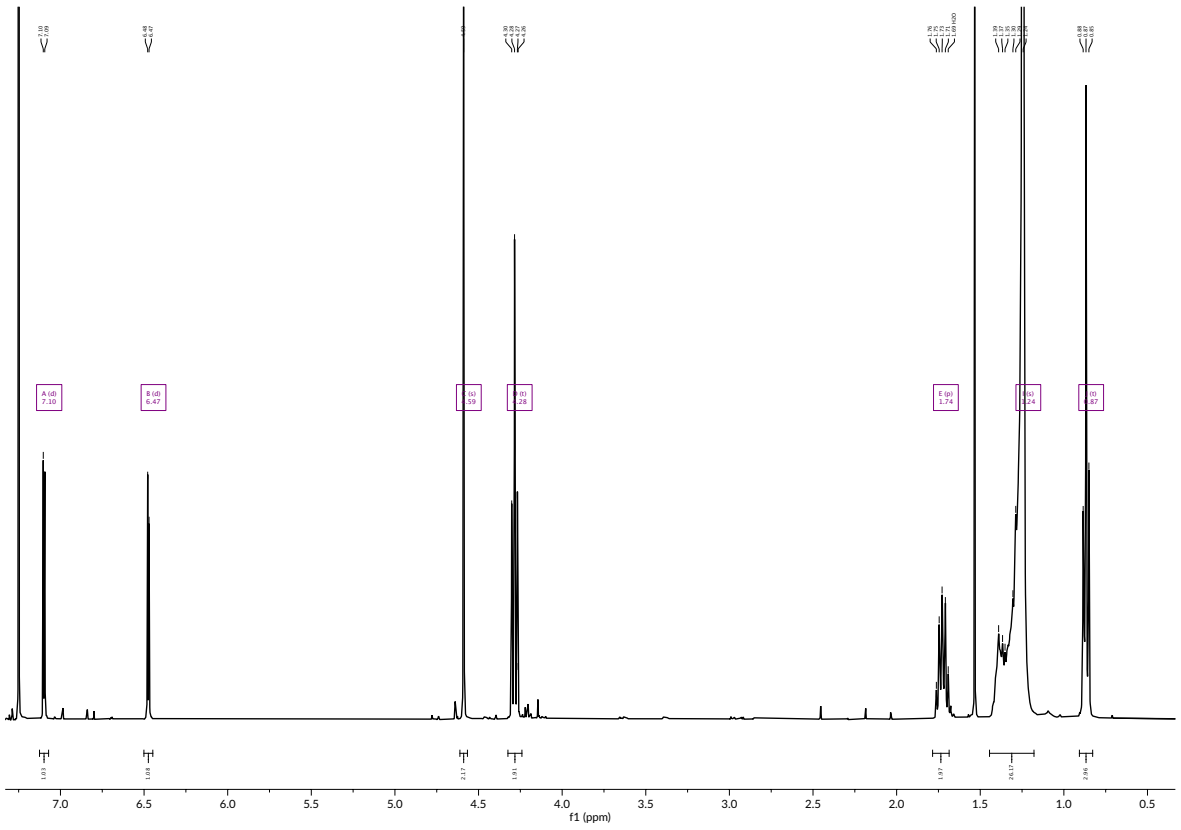

GC-FID confirmed the presence of 1:1 mixture of ester, 47.9 : 52.1 %total area)

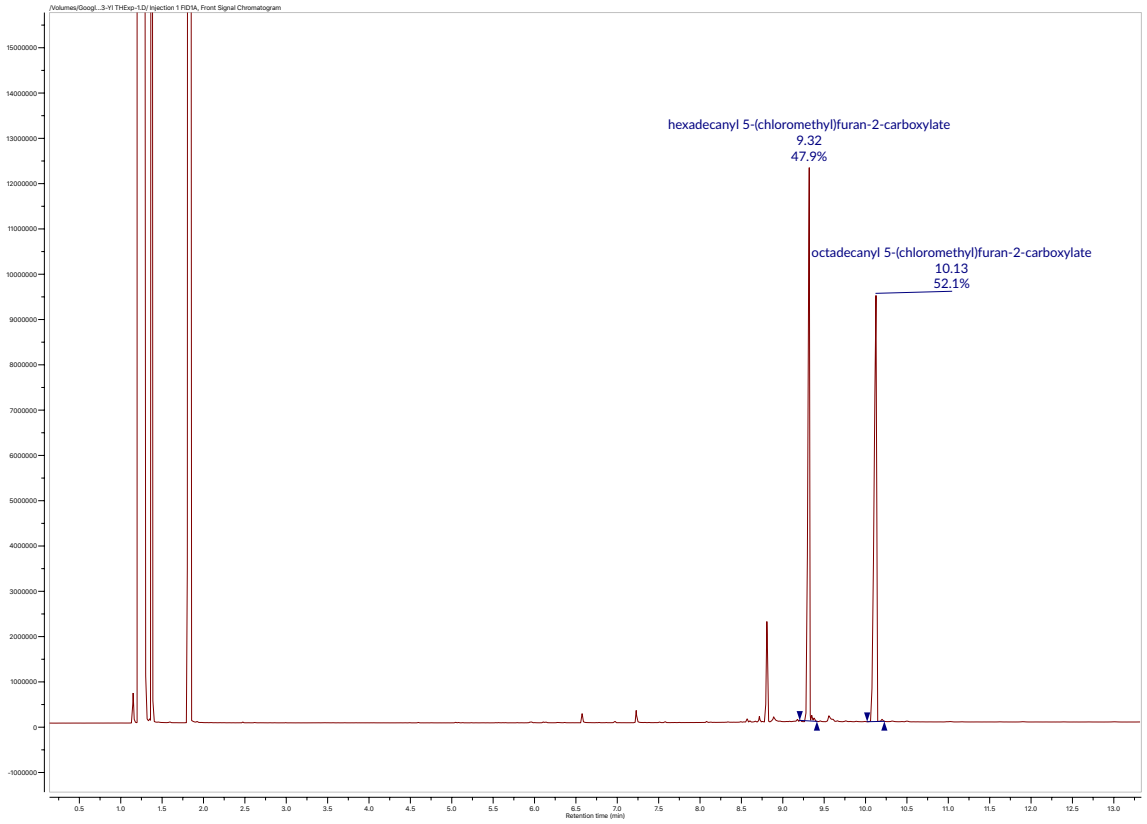

Yield: 67%

^{1}H-NMR (400 MHz, [$CDCl_3$]): Mixture, similar chemical shifts than previous compounds, esters cannot be distinguished.

^{13}C-NMR (101 MHz; [$CDCl_3$]): Mixture, similar chemical shifts than previous compounds, esters cannot be distinguished

FT-IR wavenumber (cm^{-1}): 2958 (vw); 2916 (vs); 2872 (vw); 2848 (s); 1723 (w); 1713 (s); 1540 (vw); 1519 (vw); 1472 (vw); 1463 (vw); 1397 (vw); 1323 (vw); 1308 (s); 1264 (w); 1245 (vw); 1217; (w); 1195 (vw); 1177 (w); 1162 (s); 1135 (w); 1080 (vw); 1049 (vw); 1025 (w); 995 (vw); 973; (w); 935 (vw); 922 (vw); 821 (vw); 813 (vw); 761 (w); 729 (vw); 720 (w); 704 (s).

ESI-MS $C_{22}H_{37}NaClO_3$ theoretical (m/z): 407.2323 [M+] measured (m/z): 407.2319 [M+]. $C_{24}H_{41}NaClO_3$ theoretical (m/z): 435.2636 [M+] measured (m/z): 435.2632 [M+].

Synthesis of alkyl 5-(iodomethyl)furan-2-carboxylate (172)

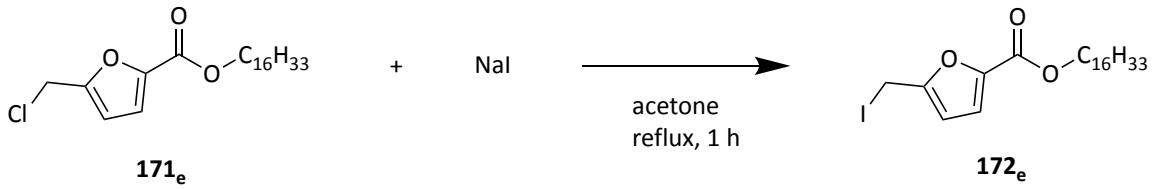

171_e **172_e**

Protocol adapted from the literature.[392] A 50 mL round bottom flask was charged with **171** (*e.g.* ***171_e*** 2.000 g, 5.20 mmol), NaI (*e.g.* ***171_e*** 1.560 g, 10.39 mmol, 2 eq.), acetone (20 mL) and the system was brought to reflux and stirred for 1 h. Thereafter, the solution was filtrated over a short path of Celite and the filtrate was evaporated. The resulting orange residue was triturated with EtOAc (50 mL), filtrated over Celite and the resulting solution was washed with $Na_2S_2O_5.5H_2O$ (10 % w/w in DI water, 2 x 50 mL), after which the organic phase lost most its deep orange colour, DI water (50 mL) and brine (50 mL). The collected organic phases were dried over $MgSO_4$, filtrated and the filtrate was evaporated to afford **172** as a yellow solid or oil (*e.g.* ***172_e*** 2.310 g, 93% yield).

dodecyl 5-(iodomethyl)furan-2-carboxylate (172_a)

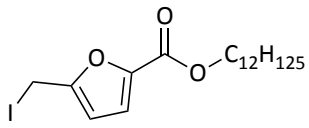

172_a

Yield: 93%

^{1}H-NMR (400 MHz, [$CDCl_3$]): δ (ppm) 7.06 (d, *J* = 3.6 Hz, 1H, I-CH_2-(COC<u>H</u>C_2H)-COO-$C_{12}H_{25}$), 6.45 (d, *J* = 3.3 Hz, 1H, I-CH_2-(HC_2C<u>H</u>OC)-COO-$C_{12}H_{25}$), 4.43 (s, 2H, I-C<u>H_2</u>-(C_4H_2O)-COO-$C_{12}H_{25}$), 4.27 (t, *J* = 6.8 Hz, 2H, I-CH_2-(C_4H_2O)-COO-C<u>H_2</u>-$C_{11}H_{23}$), 1.78–1.66 (m, 2H, I-CH_2-

(C_4H_2O)-COO-CH_2-C$\underline{H_2}$-$C_{10}H_{21}$), 1.44–1.14 (s (br), 18H, I-CH_2-(C_4H_2O)-COO-CH_2-CH_2-$C_9\underline{H_{18}}$-CH_3), 0.86 (t, *J* = 6.8 Hz, 3H, I-CH_2-(C_4H_2O)-COO-CH_2-CH_2-C_9H_{18}-C$\underline{H_3}$).

^{13}C-NMR (101 MHz; [$CDCl_3$]): δ (ppm) 158.68 (I-CH_2-($\underline{C}OC_3H_2$)-COO-$C_{12}H_{25}$), 155.72 (I-CH_2-(C_4H_2O)-$\underline{C}OO$-$C_{12}H_{25}$), 144.57 (I-CH_2-($C_3H_2O\underline{C}$)-COO-$C_{12}H_{25}$), 119.20 (I-CH_2-(CO$\underline{C}HC_2H$)-COO-$C_{12}H_{25}$), 110.39 (I-CH_2-($C_2H\underline{C}HOC$)-COO-$C_{12}H_{25}$), 65.37 (I-CH_2-(C_4H_2O)-COO-$\underline{C}H_2$-$C_{11}H_{23}$), 32.00 (I-CH_2-(C_4H_2O)-COO-CH_2-$\underline{C}H_2$-C_9H_{18}-CH_3), 29.74, 29.72, 29.68, 29.66, 29.60, 29.44, 29.33, 28.75, 25.97, 22.78 (I-CH_2-(C_4H_2O)-COO-CH_2-CH_2-$\underline{C}_9H_{18}$-CH_3), 14.22 (I-CH_2-(C_4H_2O)-COO-CH_2-CH_2-C_9H_{18}-$\underline{C}H_3$), -7.86 (I-$\underline{C}H_2$-(C_4H_2O)-COO-CH_2-$C_{11}H_{23}$).

FT-IR wavenumber (cm^{-1}): 2953 (vw); 2922 (vs); 2853 (s); 1718 (vs); 1590 (vw); 1527 (vw); 1515 (w); 1466 (vw); 1392 (vw); 1379 (vw); 1295 (vs); 1243 (vw); 1215 (vs); 1142 (vs); 1083 (vw); 1064 (vw); 1050 (vw); 1017 (w); 969 (w); 803 (vw); 760 (vs); 721 (vw); 707 (vw); 664 (vw).

tetradecyl 5-(iodomethyl)furan-2-carboxylate (172$_b$)

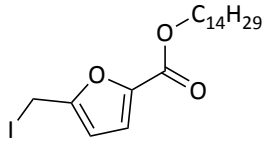

172$_b$

Yield: 91%

^{1}H-NMR (400 MHz, [$CDCl_3$]): δ (ppm) 7.06 (d, *J* = 3.5 Hz, 1H, I-CH_2-(COC$\underline{H}C_2H$)-COO-$C_{14}H_{29}$), 6.45 (d, *J* = 3.5 Hz, 1H, I-CH_2-($HC_2C\underline{H}OC$)-COO-$C_{14}H_{29}$), 4.43 (s, 2H, I-C$\underline{H_2}$-(C_4H_2O)-COO-C-$_{14}H_{29}$), 4.27 (t, *J* = 6.8 Hz, 2H, , I-CH_2-(C_4H_2O)-COO-C$\underline{H_2}$-$C_{13}H_{27}$), 1.78–1.68 (m, 2H, I-CH_2-(C_4H_2O)-COO-CH_2-C$\underline{H_2}$-$C_{12}H_{25}$), 1.42–1.20 (m (br), 22H, I-CH_2-(C_4H_2O)-COO-CH_2-CH_2-$C_{11}\underline{H_{22}}$-CH_3), 0.86 (t, *J* = 6.9, 6.5 Hz, 3H, I-CH_2-(C_4H_2O)-COO-CH_2-CH_2-$C_{11}H_{22}$-C$\underline{H_3}$).

^{13}C-NMR (101 MHz; [$CDCl_3$]): δ (ppm) 158.68 (I-CH_2-(<u>C</u>OC_3H_2)-COO-$C_{14}H_{29}$), 155.72 (I-CH_2-(C_4H_2O)-<u>C</u>OO-$C_{14}H_{29}$), 144.57 (I-CH_2-(C_3H_2O<u>C</u>)-COO-$C_{14}H_{29}$), 119.20 (I-CH_2-(CO<u>C</u>HC_2H)-COO-$C_{14}H_{29}$), 110.40 (I-CH_2-(C_2H<u>C</u>HOC)-COO-$C_{14}H_{29}$), 65.37 (I-CH_2-(C_4H_2O)-COO-<u>C</u>H_2-$C_{13}H_{27}$), 32.02 (I-CH_2-(C_4H_2O)-COO-CH_2-<u>C</u>H_2-$C_{11}H_{22}$-CH_3), 29.78, 29.76, 29.75, 29.67, 29.61, 29.46, 29.34, 28.75, 25.97, 22.79 (I-CH_2-(C_4H_2O)-COO-CH_2-CH_2-<u>C</u>$_{11}$$H_{22}$-$CH_3$), 14.23 (I-$CH_2$-($C_4H_2$O)-COO-$CH_2$-$CH_2$-$C_{11}H_{22}$-<u>C</u>$H_3$), -7.86 (I-<u>C</u>$H_2$-($C_4H_2$O)-COO-$CH_2$-$C_{13}H_{27}$).

FT-IR wavenumber (cm^{-1}): 2954 (vw); 2921 (vs); 2852 (s); 1716 (vs); 1591 (vw); 1528 (vw); 1515 (w); 1466 (w); 1392 (vw); 1378 (vw); 1294 (vs); 1241 (w); 1215 (vs); 1142 (vs); 1083 (vw); 1047; (vw); 1017 (s); 969 (w); 935 (vw); 814 (vw); 802 (w); 759 (vs); 722 (vw); 706 (vw); 663 (vw).

ESI-MS $C_{20}H_{34}IO_3$, theoretical (m/z): 449.1547 [M+] measured (m/z): 449.1541 [M+]. $C_{20}H_{33}INaO_3$, theoretical (m/z): 471.1367 [M+] measured (m/z): 471.1354 [M+].

2-butyl-octan-1-yl 5-(iodomethyl)furan-2-carboxylate (172$_c$)

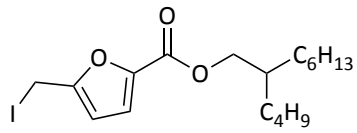

172$_c$

Yield: 93%

^{1}H-NMR (400 MHz, [$CDCl_3$]): δ (ppm) 7.04 (d, *J* = 3.5 Hz, 1H, I-CH_2-(COC<u>H</u>C_2H)-COO-CH_2-CH(-C_4H_9)-C_6H_{13}), 6.45 (d, *J* = 3.5 Hz, 1H, I-CH_2-(HC_2C<u>H</u>OC)-COO-CH_2-CH(-C_4H_9)-C_6H_{13}), 4.43 (s, 2H, I-C<u>H$_2$</u>-(C_4H_2O)-COO-CH_2-CH(-C_4H_9)-C_6H_{13}), 4.18 (d, *J* = 5.9 Hz, 2H, I-CH_2-(C_4H_2O)-COO-C<u>H$_2$</u>-CH(-C_4H_9)-C_6H_{13}), 1.73 (q, *J* = 5.6 Hz, 1H, I-CH_2-(C_4H_2O)-COO-CH_2-C<u>H</u>(-C_4H_9)-C_6H_{13}), 1.41–1.20 (m (br), 16H, I-CH_2-(C_4H_2O)-COO-CH_2-CH(-C_3<u>H$_6$</u>-CH_3)-C_5<u>H$_{10}$</u>-CH_3), 0.93–0.83 (m, 6H, I-CH_2-(C_4H_2O)-COO-CH_2-CH(-C_3H_6-C<u>H$_3$</u>)-C_5H_{10}-C<u>H$_3$</u>).

^{13}C-NMR (101 MHz; [$CDCl_3$]): δ (ppm) 158.78 (I-CH_2-(<u>C</u>OC_3H_2)-COO-CH_2-CH(-C_4H_9)-C_6H_{13}), 155.76 (I-CH_2-(C_4H_2O)-<u>C</u>OO-CH_2-CH(-C_4H_9)-C_6H_{13}), 144.57 (I-CH_2-(C_3H_2O<u>C</u>)-COO-CH_2-CH(-C_4H_9)-C_6H_{13}), 119.06 (I-CH_2-(CO<u>C</u>HC_2H)-COO-CH_2-CH(-C_4H_9)-C_6H_{13}), 110.36 (I-CH_2-(C_2H<u>C</u>HOC)-COO-CH_2-CH(-C_4H_9)-C_6H_{13}), 68.03 (I-CH_2-(C_4H_2O)-COO-<u>C</u>H_2-CH(-C_4H_9)-C_6H_{13}), 37.41 (I-CH_2-(C_4H_2O)-COO-CH_2-<u>C</u>H(-C_4H_9)-C_6H_{13}), 31.90, 31.39, 31.07, 29.70, 28.99, 26.76, 23.06, 22.75 (I-CH_2-(C_4H_2O)-COO-CH_2-CH(-<u>C</u>$_3H_6$-CH_3)-<u>C</u>$_5H_{10}$-CH_3), 14.21 (I-CH_2-(C_4H_2O)-COO-CH_2-CH(-C_3H_6-<u>C</u>H_3)-C_5H_{10}-CH_3), 14.16 (I-<u>C</u>H_2-(C_4H_2O)-COO-CH_2-CH(-C_3H_6-CH_3)-C_5H_{10}-<u>C</u>H_3), -7.86 (I-<u>C</u>H_2-(C_4H_2O)-COO-CH_2-CH(-C_4H_9)-C_6H_{13}).

ESI-MS $C_{18}H_{29}INaO_3$, theoretical (m/z): 443.1054 [M+] measured (m/z): 443.1052 [M+].

tetradec-2-yl 5-(iodomethyl)furan-2-carboxylate (172$_d$)

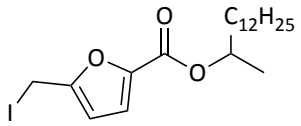

172$_d$

Yield: 97%

^{1}H-NMR (400 MHz, [$CDCl_3$]): δ (ppm) 7.03 (d, *J* = 3.5 Hz, 1H, I-CH_2-(COC<u>H</u>C_2H)-COO-CH(-CH_3)-$C_{12}H_{25}$), 6.44 (d, *J* = 3.4 Hz, 1H, I-CH_2-(HC$_2$C<u>H</u>OC)-COO-CH(-CH_3)-$C_{12}H_{25}$), 5.10 (h, *J* = 7.3, 6.2, 5.8, 5.6 Hz, 1H, I-CH_2-(C_4H_2O)-COO-C<u>H</u>(-CH_3)-$C_{12}H_{25}$), 4.43 (s, 2H, I-C<u>H$_2$</u>-(C_4H_2O)-COO-CH(-CH_3)-$C_{12}H_{25}$), 1.76–1.63 (m, 1H), 1.62–1.49 (m, 1H) **both** (I-CH_2-(C_4H_2O)-COO-CH(-CH_3)-C<u>H$_2$</u>-$C_{11}H_{23}$), 1.30 (d, *J* = 6.2 Hz, 3H, I-CH_2-(C_4H_2O)-COO-CH(-C<u>H$_3$</u>)-CH_2-$C_{11}H_{23}$), 1.28–1.19 (m (br), 20H, I-CH_2-(C_4H_2O)-COO-CH(-CH_3)-CH_2-C_{10}<u>H$_{20}$</u>-CH_3), 0.86 (t, *J* = 6.8 Hz, 3H, I-CH_2-(C_4H_2O)-COO-CH(-CH_3)-CH_2-$C_{10}H_{20}$-C<u>H$_3$</u>).

^{13}C-NMR (101 MHz; [$CDCl_3$]): δ (ppm) 158.35 (I-CH_2-(<u>C</u>OC_3H_2)-COO-CH(-CH_3)-$C_{12}H_{25}$), 155.60 (I-CH_2-(C_4H_2O)-<u>C</u>OO-CH(-CH_3)-$C_{12}H_{25}$), 144.90 (I-CH_2-(C_3H_2O<u>C</u>)-COO-CH(-CH_3)-$C_{12}H_{25}$),

118.92 (I-CH_2-(CO<u>C</u>HC_2H)-COO-CH(-CH_3)-$C_{12}H_{25}$), 110.37 (I-CH_2-(C_2H<u>C</u>HOC)-COO-CH(-CH_3)-$C_{12}H_{25}$), 72.29 (I-CH_2-(C_4H_2O)-COO-<u>C</u>H(-CH_3)-$C_{12}H_{25}$), , 36.02 (I-CH_2-(C_4H_2O)-COO-CH(-CH_3)-<u>C</u>H_2-$C_{11}H_{23}$), 32.01, 29.96, 29.76, 29.74, 29.70, 29.67, 29.61, 29.57, 29.53, 29.50, 29.45, 29.28, 25.48, 23.97, 22.79 (I-CH_2-(C_4H_2O)-COO-CH(-CH_3)-CH_2-<u>C</u>$_{10}H_{22}$-CH_3, unclear peaks), 20.15 (I-CH_2-(C_4H_2O)-COO-CH(-<u>C</u>H_3)-CH_2-$C_{10}H_{22}$-CH_3), 14.22 (I-CH_2-(C_4H_2O)-COO-CH(-<u>C</u>H_3)-CH_2-$C_{10}H_{22}$-<u>C</u>H_3), -7.74 (I-<u>C</u>H_2-(C_4H_2O)-COO-CH(-CH_3)-$C_{12}H_{25}$).

FT-IR wavenumber (cm^{-1}): 2923 (vs); 2853 (s); 1715 (vs); 1527 (vw); 1515 (vw); 1465 (vw); 1414 (vw); 1379 (vw); 1357 (vw); 1296 (vs); 1243 (w); 1216 (vs); 1148 (vs); 1122 (s); 1083 (vw); 1045 (vw); 1017 (w); 988 (vw); 967 (w); 948 (vw); 908 (vw); 886 (vw); 851 (vw); 802 (vw); 761 (s); 721 (vw); 707 (vw); 664 (vw);.

ESI-MS $C_{20}H_{33}INaO_3$, theoretical (m/z): [M+] 471.1367 measured (m/z): 471.1366 [M+].

hexadecyl 5-(iodomethyl)furan-2-carboxylate (172_e)

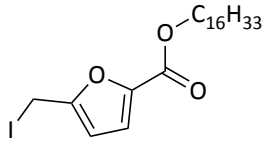

172_e

Yield: 93%

^{1}H-NMR (400 MHz, [$CDCl_3$]): δ (ppm) 7.06 (d, *J* = 3.5 Hz, 1H, I-CH_2-(COC<u>H</u>C_2H)-COO-$C_{16}H_{33}$), 6.45 (d, *J* = 3.5 Hz, 1H, I-CH_2-(HC_2C<u>H</u>OC)-COO-$C_{16}H_{33}$), 4.44 (s, 2H, I-C<u>H_2</u>-(C_4H_2O)-COO-C-$_{16}H_{33}$), 4.28 (t, *J* = 6.8 Hz, 2H, I-CH_2-(C_4H_2O)-COO-C<u>H_2</u>-$C_{15}H_{31}$), 1.72 (p (dt), *J* = 6.8 Hz, 2H, I-CH_2-(C_4H_2O)-COO-CH_2-C<u>H_2</u>-$C_{14}H_{29}$), 1.24 (s (br), 26H, I-CH_2-(C_4H_2O)-COO-CH_2-CH_2-C_{13}<u>H_{26}</u>-CH_3), 0.87 (t, *J* = 7.0, 6.6 Hz, 3H, I-CH_2-(C_4H_2O)-COO-CH_2-CH_2-$C_{13}H_{26}$-C<u>H_3</u>).

^{13}C-NMR (101 MHz; [$CDCl_3$]): δ (ppm) 155.72 (I-CH_2-(<u>C</u>OC_3H_2)-COO-$C_{16}H_{33}$), 147.84 (I-CH_2-(C_3H_2O<u>C</u>)-COO-$C_{16}H_{33}$), 119.20 (I-CH_2-(CO<u>C</u>HC_2H)-COO-$C_{16}H_{33}$), 110.40 (I-CH_2-(C_2H<u>C</u>HOC)-COO-$C_{16}H_{33}$), 65.39 (I-CH_2-(C_4H_2O)-COO-<u>C</u>H_2-$C_{15}H_{31}$), 32.02 (I-CH_2-(C_4H_2O)-COO-CH_2-<u>C</u>H_2-$C_{13}H_{26}$-CH_3), 29.79, 29.68, 29.61, 29.47, 29.35, 28.75, 25.98, 24.64, 22.80 (I-CH_2-(C_4H_2O)-COO-CH_2-CH_2-<u>C</u>$_{13}H_{26}$-CH_3), 14.23 (I-CH_2-(C_4H_2O)-COO-CH_2-CH_2-$C_{13}H_{26}$-<u>C</u>H_3),-7.85 (I-<u>C</u>H_2-(C_4H_2O)-COO-CH_2-$C_{15}H_{31}$).

ESI-MS $C_{22}H_{37}INaO_3$, theoretical (m/z): 499.1680 [M+] measured (m/z): 499.1675 [M+].

Melting point 52.6–55.3 °C

Mixture of hexadecyl 5-(iodomethyl)furan-2-carboxylate and octadecyl 5-(iodomethyl)furan-2-carboxylate (172$_f$)

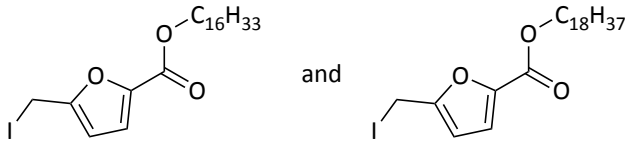

172$_f$

Yield: 93%

^{1}H-NMR (400 MHz, [$CDCl_3$]): δ (ppm) Mixture, similar chemical shifts than previous compounds, esters cannot be distinguished.

^{13}C-NMR (101 MHz; [$CDCl_3$]): δ (ppm) Mixture, similar chemical shifts than previous compounds, esters cannot be distinguished.

FT-IR wavenumber (cm^{-1}): 2954 (vw); 2921 (vs); 2852 (s); 1716 (vs); 1591 (vw); 1528 (vw); 1515 (w); 1466 (w); 1392 (vw); 1378 (vw); 1294 (vs); 1241 (w); 1215 (vs); 1142 (vs); 1083 (vw); 1047; (vw); 1017 (s); 969 (w); 935 (vw); 814 (vw); 802 (w); 759 (vs); 722 (vw); 706 (vw); 663 (vw)

ESI-MS $C_{22}H_{38}IO_3$, theoretical (m/z): 477.1860 [M+] measured (m/z): 477.1847 [M+]; $C_{22}H_{37}INaO_3$ theoretical (m/z): 499.1680 [M+] measured (m/z): 499.1668 [M+]; $C_{24}H_{42}IO_3$ theoretical (m/z): 505.2173 [M+] measured (m/z): 505.2164 [M+]; $C_{24}H_{42}INaO_3$ theoretical (m/z): 527.1993 [M+] measured (m/z): 527.1986 [M+].

Synthesis of alkyl 5-(methylsulfonate)furan-2-carboxylate (160)

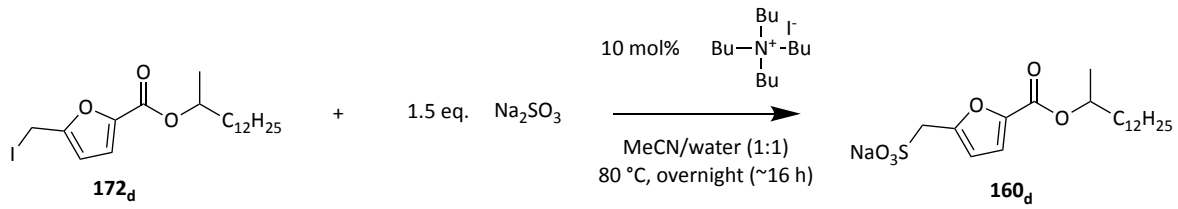

172$_d$ **160$_d$**

A 100 mL round-bottom flask equipped with a water condenser was charged with **172** (*e.g.* ***172$_d$***, 9.28 g, 20.7 mmol), Na_2SO_3 (*e.g.* ***172$_d$***, 3.91 g, 31.0 mmol, 1.5 eq.), tetrabutyl-ammonium Iodide (*e.g. for 2-tetradecanyl ester* 764 mg, 2.07 mmol, 0.1 eq.) and MeCN/water mixture (1:1, v:v, 50 mL). After stirring overnight at 80 °C, the solvent was removed under reduced pressure (vacuum must be applied carefully as intense foaming will occur, a splash guard is recommended), and the resulting product was extracted with methanol (100 mL) and sonicated at 50 °C for 5 min. The suspension was centrifuged (3500 rpm, 5 min) and the supernatant, carefully collected in a round bottom flask. The methanol extraction was repeated twice. The collected methanol fractions were evaporated to dryness and the resulting solid was washed with EtOAc (100 mL) and collected via filtration to afford **160** as white solid after drying in a vacuum oven at 80 °C overnight (*e.g.* ***160$_d$***, 5.50 g, 57% yield).

dodecyl 5-(sodium methanesulfonate)furan-2-carboxylate (160$_a$)

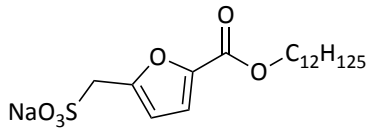

160$_a$

Yield: 72%

^{1}H-NMR (400 MHz, [D_2O]): δ (ppm) 6.95 (d, *J* = 3.4 Hz, 1H, , $NaSO_3$-CH_2-(COC<u>H</u>C_2H)-COO-$C_{12}H_{25}$), 6.44 (d, *J* = 3.4 Hz, 1H, $NaSO_3$-CH_2-(HC_2C<u>H</u>OC)-COO-$C_{12}H_{25}$), 4.13 (s, 2H, $NaSO_3$-C<u>H_2</u>-(C_4H_2O)-COO-$C_{12}H_{25}$), 4.04 (t, *J* = 6.6 Hz, 2H, $NaSO_3$-CH_2-(C_4H_2O)-COO-C<u>H_2</u>-$C_{11}H_{23}$), 1.50 (p, *J* = 6.8 Hz, 2H, $NaSO_3$-CH_2-(C_4H_2O)-COO-CH_2-C<u>H_2</u>-$C_{10}H_{21}$), 1.07 (s (br), 18H, $NaSO_3$-CH_2-(C_4H_2O)-COO-CH_2-CH_2-C_9<u>H_{18}</u>-CH_3), 0.68 (t, *J* = 6.7 Hz, 3H, $NaSO_3$-CH_2-(C_4H_2O)-COO-CH_2-CH_2-C_9H_{18}-C<u>H_3</u>).

^{13}C-NMR (101 MHz; [D_2O]): δ (ppm) 158.24 ($NaSO_3$-CH_2-(<u>C</u>OC_3H_2)-COO-$C_{12}H_{25}$), 143.11 ($NaSO_3$-CH_2-(C_3H_2O<u>C</u>)-COO-$C_{12}H_{25}$), 119.90 ($NaSO_3$-CH_2-(CO<u>C</u>HC_2H)-COO-$C_{12}H_{25}$), 111.04 ($NaSO_3$-CH_2-(C_2H<u>C</u>HOC)-COO-$C_{12}H_{25}$), 71.46 ($NaSO_3$-CH_2-(C_4H_2O)-COO-<u>C</u>H_2-$C_{11}H_{23}$), 51.03 ($NaSO_3$-<u>C</u>H_2-(C_4H_2O)-COO-CH_2-$C_{11}H_{23}$), 35.84 ($NaSO_3$-CH_2-(C_4H_2O)-COO-CH_2-<u>C</u>H_2-C_9H_{18}-CH_3), 31.83, 29.54, 29.43, 29.31, 29.25, 25.41, 22.64, 20.48 ($NaSO_3$-CH_2-(C_4H_2O)-COO-CH_2-CH_2-<u>C</u>$_9H_{18}$-CH_3), 14.51 ($NaSO_3$-CH_2-(C_4H_2O)-COO-CH_2-CH_2-C_9H_{18}-<u>C</u>H_3).

FT-IR wavenumber (cm^{-1}): 3482 (vw); 3435 (vw); 2957 (w); 2918 (vs); 2872 (vw); 2849 (s); 1714 (vs); 1516 (s); 1466 (w); 1397 (vw); 1384 (vw); 1321 (w); 1303 (vs); 1251 (w); 1220 (vs); 1208 (vs); 1178 (vs); 1164 (vs); 1122 (s); 1059 (vs); 1048 (vs); 1032 (s); 1020 (s); 985 (w); 972 (s); 937 (vw); 818 (w); 762 (vs); 721 (w); 655 (w).

ESI-MS $C_{18}H_{30}NaO_6S$, theoretical (m/z): 397.1655 [M+] measured (m/z): 397.1651 [M+]. $C_{18}H_{29}Na_2O_6S$ theoretical (m/z): 419.1475 [M+] measured (m/z): 419.1474 [M+].

Melting point Decomposes >190 °C

tetradecyl 5-(sodium methanesulfonate)furan-2-carboxylate (160_b)

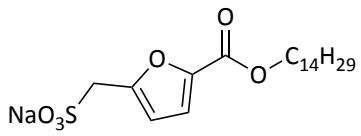

160_b

Yield: 64%

^{1}H-NMR (400 MHz, [MeOD-d_4]): δ (ppm) 7.16 (d, *J* = 2.4 Hz, 1H, $NaSO_3$-CH_2-(COC<u>H</u>C_2H)-COO-$C_{14}H_{29}$), 6.56 (d, *J* = 3.0 Hz, 1H, $NaSO_3$-CH_2-(HC_2C<u>H</u>OC)-COO-$C_{14}H_{29}$), 4.25 (t, *J* = 6.4 Hz, 2H, $NaSO_3$-CH_2-(C_4H_2O)-COO-C<u>H_2</u>-$C_{13}H_{27}$), 4.18 (s, 2H, $NaSO_3$-C<u>H_2</u>-(C_4H_2O)-COO-$C_{14}H_{29}$), 1.71 (p, *J* = 7.6 Hz, 2H, $NaSO_3$-CH_2-(C_4H_2O)-COO-CH_2-C<u>H_2</u>-$C_{12}H_{25}$), 1.27 (s (br), 22H, $NaSO_3$-CH_2-(C_4H_2O)-COO-CH_2-CH_2-C_{11}<u>H_{22}</u>-CH_3), 0.88 (t, *J* = 6.6 Hz, 3H, $NaSO_3$-CH_2-(C_4H_2O)-COO-CH_2-CH_2-$C_{11}H_{22}$-C<u>H_3</u>)

FT-IR wavenumber (cm^{-1}): 3487 (vw); 3478 (vw); 3462 (vw); 3451 (vw); 3438 (vw); 3432 (vw); 2956; (w); 2917 (vs); 2873 (vw); 2851 (vs); 1720 (vs); 1709 (vs); 1622 (vw); 1616 (vw); 1603 (vw); 1533 (w); 1516 (w); 1470 (w); 1398 (vw); 1385 (vw); 1323 (vw); 1302 (vs); 1251 (w); 1217; (vs); 1205 (vs); 1186 (vs); 1160 (vs); 1135 (s); 1113 (s); 1065 (vs); 1022 (s); 989 (vw); 972; (w); 937 (vw); 818 (vw); 809 (w); 800 (w); 776 (w); 762 (vs); 747 (vw); 720 (w); 656 (w).

ESI-MS $C_{20}H_{34}NaO_6S$, theoretical (m/z): 425.1968 [M+] measured (m/z): 425.1971 [M+]. $C_{20}H_{33}Na_2O_6S$ theoretical (m/z): 447.1788 [M+] measured (m/z): 447.1793 [M+].

Melting point Decomposition >200 °C

2-butyl-octan-1-yl 5-(sodium methylsulfonate)furan-2-carboxylate (160$_c$)

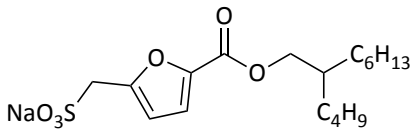

160$_c$

Yield: 71%

^{1}H-NMR (400 MHz, [DMSO-d_6]): δ (ppm) 7.14 (d, *J* = 3.4 Hz, 1H, $NaSO_3$-CH_2-(COC<u>H</u>C_2H)-COO-CH_2-CH(-C_4H_9)-C_6H_{13}), 6.41 (d, *J* = 3.5 Hz, 1H, $NaSO_3$-CH_2-(HC_2C<u>H</u>OC)-COO-CH_2-CH(-C_4H_9)-C_6H_{13}), 4.08 (d, *J* = 5.8 Hz, 2H, $NaSO_3$-CH_2-(C_4H_2O)-COO-C<u>H_2</u>-CH(-C_4H_9)-C_6H_{13}), 3.82 (s, 2H, $NaSO_3$-C<u>H_2</u>-(C_4H_2O)-COO-CH_2-CH(-C_4H_9)-C_6H_{13}), 1.71–1.60 (m, 1H, $NaSO_3$-CH_2-(C_4H_2O)-COO-CH_2-C<u>H</u>(-C_4H_9)-C_6H_{13}), 1.32–1.18 (m (br), 16H, $NaSO_3$-CH_2-(C_4H_2O)-COO-CH_2-CH(-C_3<u>H_6</u>-CH_3)-C_5<u>H_{10}</u>-CH_3), 0.86–0.77 (m, 6H, $NaSO_3$-CH_2-(C_4H_2O)-COO-CH_2-CH(-C_3H_6-C<u>H_3</u>)-C_5H_{10}-C<u>H_3</u>).

^{13}C-NMR (101 MHz; [DMSO-d_6]): δ (ppm) 158.58 ($NaSO_3$-CH_2-(<u>C</u>OC_3H_2)-COO-CH_2-CH(-C_4H_9)-C_6H_{13}), 155.55 ($NaSO_3$-CH_2-(C_4H_2O)-<u>C</u>OO-CH_2-CH(-C_4H_9)-C_6H_{13}), 142.83 ($NaSO_3$-CH_2-(C_3H_2O<u>C</u>)-COO-CH_2-CH(-C_4H_9)-C_6H_{13}), 119.96 ($NaSO_3$-CH_2-(CO<u>C</u>HC_2H)-COO-CH_2-CH(-C_4H_9)-C_6H_{13}), 111.11 ($NaSO_3$-CH_2-(C_2H<u>C</u>HOC)-COO-CH_2-CH(-C_4H_9)-C_6H_{13}), 67.17 ($NaSO_3$-CH_2-(C_4H_2O)-COO-<u>C</u>H_2-CH(-C_4H_9)-C_6H_{13}), 50.99 ($NaSO_3$-<u>C</u>H_2-(C_4H_2O)-COO-CH_2-CH(-C_4H_9)-C_6H_{13}), 37.27 ($NaSO_3$-CH_2-(C_4H_2O)-COO-CH_2-<u>C</u>H(-C_4H_9)-C_6H_{13}), 31.72, 31.17, 30.85, 29.49, 28.83, 26.54, 23.62, 22.93, 22.59 ($NaSO_3$-CH_2-(C_4H_2O)-COO-CH_2-CH(-<u>C</u>$_3H_6$-CH_3)-<u>C</u>$_5H_{10}$-CH_3), 14.50 ($NaSO_3$-CH_2-(C_4H_2O)-COO-CH_2-CH(-C_3H_6-<u>C</u>H_3)-C_5H_{10}-CH_3), 14.46 ($NaSO_3$-<u>C</u>H_2-(C_4H_2O)-COO-CH_2-CH(-C_3H_6-CH_3)-C_5H_{10}-<u>C</u>H_3).

FT-IR wavenumber (cm^{-1}): 3429 (vw); 2956 (w); 2927 (s); 2871 (w); 2858 (w); 1705 (s); 1522 (s); 1465 (w); 1399 (w); 1380 (w); 1311 (vs); 1250 (s); 1209 (vs); 1171 (vs); 1122 (s); 1047 (vs); 1020 (s); 973 (w); 941 (vw); 923 (vw); 822 (w); 777 (w); 763 (vs); 735 (vw); 727 (vw).

ESI-MS $C_{18}H_{30}NaO_6S$, theoretical (m/z): 397.1655 [M+] measured (m/z): 397.1650 [M+]. $C_{18}H_{29}Na_2O_6S$ theoretical (m/z): 419.1475 [M+] measured (m/z): 419.1469 [M+].

tetradecan-2-yl 5-(sodium methylsulfonate)furan-2-carboxylate (160_d)

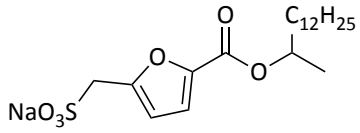

160_d

Yield: 63%

^{1}H-NMR (400 MHz, [DMSO-d_6]): δ (ppm) 7.13 (d, *J* = 3.5 Hz, 1H, $NaSO_3$-CH_2-(COC<u>H</u>C_2H)-COO-CH(-CH_3)-$C_{12}H_{25}$), 6.38 (d, *J* = 3.6 Hz, 1H, $NaSO_3$-CH_2-(HC$_2$C<u>H</u>OC)-COO-CH(-CH_3)-$C_{12}H_{25}$), 5.02–4.89 (m, 1H, $NaSO_3$-CH_2-(C_4H_2O)-COO-C<u>H</u>(-CH_3)-$C_{12}H_{25}$), 3.80 (s, 2H, $NaSO_3$-C<u>H$_2$</u>-(C_4H_2O)-COO-CH(-CH_3)-$C_{12}H_{25}$), 1.61–1.45 (m, 2H, $NaSO_3$-CH_2-(C_4H_2O)-COO-CH(-CH_3)-C<u>H$_2$</u>-$C_{11}H_{23}$), 1.34–1.09 (m (br), 23H, $NaSO_3$-CH_2-(C_4H_2O)-COO-CH(-C<u>H$_3$</u>)-CH_2-C_{10}<u>H$_{20}$</u>-CH_3), 0.81 (t, *J* = 6.8 Hz, 3H, $NaSO_3$-CH_2-(C_4H_2O)-COO-CH(-CH_3)-CH_2-$C_{10}H_{20}$-C<u>H$_3$</u>).

^{13}C-NMR (101 MHz; [DMSO-d_6]): δ (ppm) 158.24 ($NaSO_3$-CH_2-(<u>C</u>OC_3H_2)-COO-CH(-CH_3)-$C_{12}H_{25}$), 143.11 ($NaSO_3$-CH_2-(C_3H_2O<u>C</u>)-COO-CH(-CH_3)-$C_{12}H_{25}$), 119.90 ($NaSO_3$-CH_2-(CO<u>C</u>HC$_2$H)-COO-CH(-CH_3)-$C_{12}H_{25}$), 111.04 ($NaSO_3$-CH_2-(C_2H<u>C</u>HOC)-COO-CH(-CH_3)-$C_{12}H_{25}$), 71.46 ($NaSO_3$-CH_2-(C_4H_2O)-COO-<u>C</u>H(-CH_3)-$C_{12}H_{25}$), 51.03 ($NaSO_3$-<u>C</u>H_2-(C_4H_2O)-COO-CH(-CH_3)-$C_{12}H_{25}$), 35.84 ($NaSO_3$-CH_2-(C_4H_2O)-COO-CH(-CH_3)-<u>C</u>H_2-$C_{11}H_{23}$), 31.83, 29.54, 29.43, 29.31, 29.25, 25.41, 22.64 ($NaSO_3$-CH_2-(C_4H_2O)-COO-CH(-CH_3)-CH_2-<u>C</u>$_{10}H_{22}$-CH_3, unclear

peaks), 20.48 ($NaSO_3$-CH_2-(C_4H_2O)-COO-CH(-$\underline{C}H_3$)-CH_2-$C_{10}H_{22}$-CH_3), 14.51 ($NaSO_3$-CH_2-(C_4H_2O)-COO-CH(-$\underline{C}H_3$)-CH_2-$C_{10}H_{22}$-$\underline{C}H_3$).

FT-IR wavenumber (cm^{-1}): 3504 (w); 3496 (w); 3490 (w); 3474 (w); 3458 (w); 3433 (w); 3428 (w); 3138 (vw); 2957 (w); 2919 (vs); 2873 (vw); 2850 (s); 1715 (vs); 1683 (vw); 1650 (w); 1623; (vw); 1608 (vw); 1535 (vw); 1518 (w); 1467 (w); 1387 (w); 1303 (s); 1250 (vs); 1228 (vs); 1211 (vs); 1174 (vs); 1157 (vs); 1128 (w); 1117 (s); 1094 (vw); 1058 (vs); 1031 (vs); 970 (s); 841 (w); 818 (vw); 779 (w); 768 (s); 721 (vw); 655 (w).

ESNaSO3-MS $C_{20}H_{34}NaO_6S$, theoretical (m/z): 425.1968 [M+] measured (m/z): 425.1969 [M+]. $C_{20}H_{33}Na_2O_6S$ theoretical (m/z): 447.1788 [M+] measured (m/z): 447.1790 [M+].

Melting point Decomposes >150 °C

hexadecyl 5-(sodium methylsulfonate)furan-2-carboxylate (160_e)

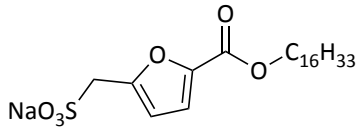

160_e

Yield: 94%

^{1}H-NMR (400 MHz, [DMSO-d_6]): δ (ppm) 7.16 (d, *J* = 3.4 Hz, 1H, $NaSO_3$-CH_2-(COC$\underline{H}C_2H$)-COO-$C_{16}H_{33}$), 6.39 (d, *J* = 3.6 Hz, 1H, $NaSO_3$-CH_2-($HC_2C\underline{H}OC$)-COO-$C_{16}H_{33}$), 4.16 (t, *J* = 6.7 Hz, 2H, $NaSO_3$-CH_2-(C_4H_2O)-COO-C$\underline{H_2}$-$C_{15}H_{31}$), 3.80 (s, 2H, $NaSO_3$-C$\underline{H_2}$-(C_4H_2O)-COO-$C_{16}H_{33}$), 1.61 (p, *J* = 6.7 Hz, 2H, $NaSO_3$-CH_2-(C_4H_2O)-COO-CH_2-C$\underline{H_2}$-$C_{14}H_{29}$), 1.20 (s (br), 26H, $NaSO_3$-CH_2-(C_4H_2O)-COO-CH_2-CH_2-$C_{13}\underline{H_{26}}$-CH_3), 0.82 (t, *J* = 7.0, 6.3 Hz, 3H, $NaSO_3$-CH_2-(C_4H_2O)-COO-CH_2-CH_2-$C_{13}H_{26}$-C$\underline{H_3}$).

^{13}C-NMR (101 MHz; [DMSO-d_6]): δ (ppm) 158.24 ($NaSO_3$-CH_2-(<u>C</u>OC_3H_2)-COO-$C_{16}H_{33}$), 143.11 ($NaSO_3$-CH_2-(C_3H_2O<u>C</u>)-COO-$C_{16}H_{33}$), 119.90 ($NaSO_3$-CH_2-(CO<u>C</u>HC_2H)-COO-$C_{16}H_{33}$), 111.04 ($NaSO_3$-CH_2-(C_2H<u>C</u>HOC)-COO-$C_{16}H_{33}$), 71.46 ($NaSO_3$-CH_2-(C_4H_2O)-COO-<u>C</u>H_2-$C_{15}H_{31}$), 51.03 ($NaSO_3$-<u>C</u>H_2-(C_4H_2O)-COO-CH_2-$C_{15}H_{31}$), 35.84, 31.83, 29.54, 29.43, 29.31, 29.25, 25.41, 22.64, 20.48 ($NaSO_3$-CH_2-(C_4H_2O)-COO-CH_2-CH_2-<u>C_{13}</u>H_{26}-CH_3), 14.51 ($NaSO_3$-CH_2-(C_4H_2O)-COO-CH_2-CH_2-$C_{13}H_{26}$-<u>C</u>H_3).

FT-IR wavenumber (cm^{-1}): 2956 (vw); 2917 (vs); 2873 (vw); 2850 (vs); 1720 (vs); 1650 (vw); 1520; (w); 1471 (w); 1397 (vw); 1383 (vw); 1304 (vs); 1268 (vw); 1251 (s); 1222 (vs); 1209 (vs); 1190 (vs); 1177 (vs); 1156 (vs); 1129 (s); 1116 (w); 1060 (vs); 1029 (s); 996 (vw); 972 (w); 944 (vw); 937 (vw); 839 (vw); 819 (vw); 811 (w); 779 (w); 767 (s); 718 (w); 656 (vw)

ESI-MS $C_{22}H_{38}NaO_6S$, theoretical (m/z): 453.2281 [M+] measured (m/z): 453.2288 [M+]. $C_{22}H_{37}Na_2O_6S$ theoretical (m/z): 475.2101 [M+] measured (m/z): 475.2109 [M+].

Mixture of hexadecyl 5-(sodium methylsulfonate)furan-2-carboxylate and octadecyl 5-(sodium methylsulfonate)furan-2-carboxylate (160$_f$)

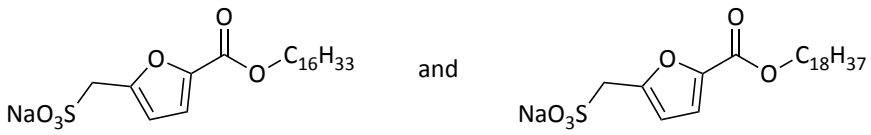

160$_f$

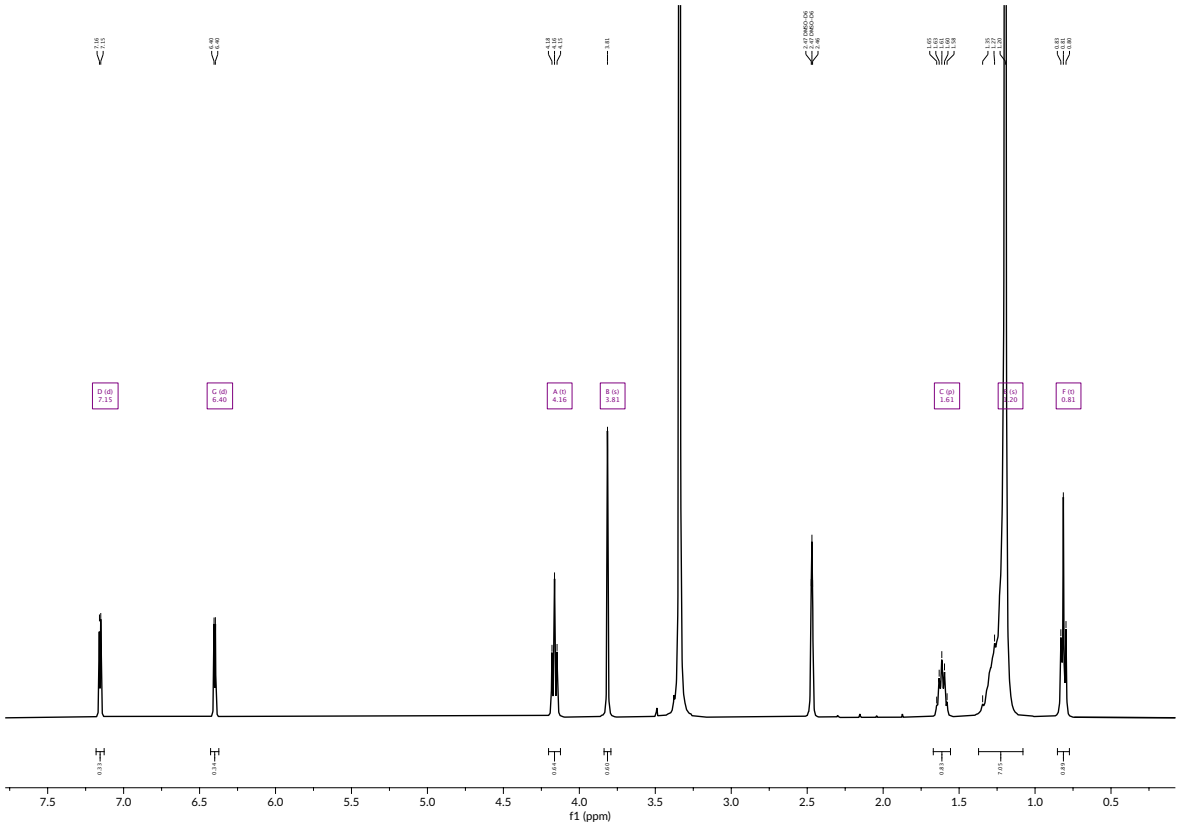

Yield: 69%

^{1}H-NMR (400 MHz, [DMSO-d_6]): δ (ppm) Mixture, similar chemical shifts than previous compounds, esters cannot be distinguished.

^{13}C-NMR (101 MHz; [DMSO-d_6]): δ (ppm) Mixture, similar chemical shifts than previous compounds, esters cannot be distinguished.

ESNaSO3-MS $C_{22}H_{38}NaO_6S$, theoretical (m/z): 453.2281 [M+] measured (m/z): 453.2286 [M+]. $C_{22}H_{37}Na_2O_6S$ theoretical (m/z): 475.2101 [M+] measured (m/z): 475.2105 [M+]. $C_{24}H_{42}NaO_6S$, theoretical (m/z): 481.2594 [M+] measured (m/z): 481.2595 [M+]. $C_{24}H_{41}Na_2O_6S$ theoretical (m/z): 503.2414 [M+] measured (m/z): 503.2413 [M+].

e. Synthetic procedures for chapter IV part.1 and 2 (p. 243 – 309)

Synthesis of primary amine hydrochlorides from L-amino acids (177-180)

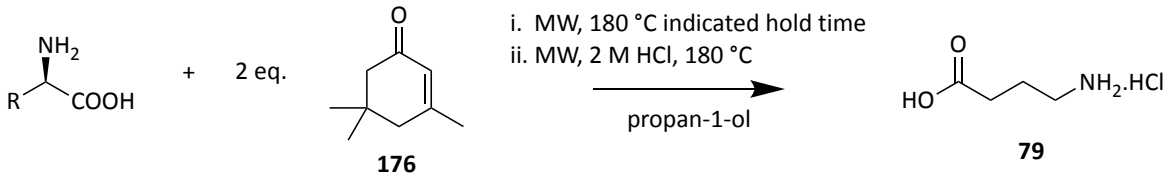

176 **79**

R: see Table 22, p. 256

Protocol adapted from the literature.[318] In a typical experiment, a 30 mL microwave vial was charged with 5.0 mmol of amino acid, propan-1-ol (3.00 mL) and 10 mmol of isophorone (1.50 mL). A magnetic stirrer was then added, and the vial was placed in the microwave chamber. The target temperature was set at 180 °C, (typically reached within 5 min) and held for the indicated time (see Table 22 p. 256). After this first heating, the reaction mixture was left to cool and 4 eq. of 2 M HCl (10 mL) was added in a one-pot fashion. The vial was returned to the microwave chamber and a second heating step of a ramp to 180 °C (i.e. no hold time) was set. The reaction mixture was then allowed to cool to room temperature and washed with diethyl ether or preferably ethyl acetate (1 x 25.0 mL). The aqueous phase was collected, and the organic phase was washed with 2 M HCl (10.0 mL) and water (10.0 mL). The collected aqueous phases were washed with diethyl ether or preferably ethyl acetate (2 x 25.0 mL) and evaporated under reduced pressure. The resulting light yellow oil was triturated with acetone (for L-phenylalanine), ethanol (for D,L-tryptophan and L-histidine) or propan-1-ol (for L-lysine) to afford the HCl salt of the corresponding primary amine which was filtered and dried under vacuum (72 mbar) at 80 °C for 2 h prior to analysis.

2-phenylethylamine hydrochloride (177)

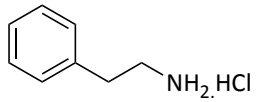

177

Yield: 68% (10 mol% isophorone used)

^{1}H-NMR (400 MHz, [D_2O]): δ (ppm) 7.32–7.24 (m, 2H ($C_3H_3C_2\underline{H_2}C$)-$CH_2$-$CH_2$-$NH_2$.HCl), 7.23–7.16 (m, 3H, ($C_3\underline{H_3}C_2H_2C$)-$CH_2$-$CH_2$-$NH_2$.HCl), 3.14 (t, *J* = 7.3 Hz, 2H, ($C_3H_3C_2H_2C$)-$C\underline{H_2}$-CH_2-NH_2.HCl), 2.86 (t, *J* = 7.3 Hz, 2H, $C_3H_3C_2H_2C$)-CH_2-$C\underline{H_2}$-NH_2.HCl).

^{13}C-NMR (101 MHz; [D_2O]): δ (ppm) 136.63 (($C_3H_3C_2H_2\underline{C}$)-$CH_2$-$CH_2$-$NH_2$.HCl), 129.09 (($C_3H_3\underline{C_2}H_2C$)-$CH_2$-$CH_2$-$NH_2$.HCl), 128.90 (($CH\underline{C_2}H_2C_2H_2C$)-$CH_2$-$CH_2$-$NH_2$.HCl), 127.38 (($\underline{C}HC_2H_2C_2H_2C$)-$CH_2$-$CH_2$-$NH_2$.HCl), 40.60 (($CHC_2H_2C_2H_2C$)-$\underline{C}H_2$-$CH_2$-$NH_2$.HCl), 32.75 (($CHC_2H_2C_2H_2C$)-$CH_2$-$\underline{C}H_2$-$NH_2$.HCl). Data are in accordance with previously reported chemical shifts.[318,336]

FT-IR wavenumber (cm^{-1}): 2968 (vs); 2874 (vs); 2614 (w); 2564 (w); 2534 (w); 2443 (vw); 1732 (vs); 1694 (w); 1604 (s); 1573 (w); 1559 (w); 1497 (s); 1481 (vs); 1466 (vs); 1455 (vs); 1448 (vs); 1423 (s); 1392 (w); 1359 (w); 1343 (w); 1286 (w); 1260 (w); 1225 (vs); 1209 (vs); 1201 (vs); 1154 (s); 1137 (vs); 1116 (s); 1100 (vs); 1080 (vs); 1050 (s); 1030 (s); 1017 (w); 1004 (w); 974 (w); 961 (w); 939 (s); 924 (s); 901 (s); 857 (vs); 823 (vs); 784 (vs); 759 (s); 743 (vs); 731; (vs); 697 (vs).

ESI-MS $C_8H_{12}N$, theoretical (m/z): 122.0964 [M+] measured (m/z): 122.0965 [M+]; $C_8H_{11}NNa$ theoretical (m/z): 144.0784 [M+] measured (m/z): 144.0790 [M+].

Melting point Decomposes 223.5–227.3 °C (lit. 217 -220 °C)[318]

methylamine hydrochloride (178)

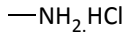

178

Yield: 47%

^{1}H-NMR (400 MHz, [D_2O]): δ (ppm) 2.44 (s, 3H, C<u>H</u>$_3$-NH_2.HCl).

^{13}C-NMR (101 MHz; [D_2O]): δ (ppm) 24.56 (<u>C</u>H_3-NH_2.HCl). Data are in accordance with previously reported chemical shifts.[318,336]

FT-IR wavenumber (cm^{-1}): 3088 (s); 2980 (s); 2883 (vs); 2847 (vs); 2604 (w); 2478 (w); 1739 (w); 1672 (vw); 1655 (vw); 1620 (w); 1594 (w); 1580 (w); 1558 (vw); 1526 (w); 1474 (s); 1448; (w); 1437 (w); 1410 (w); 1391 (w); 1355 (w); 1323 (vw); 1277 (vw); 1262 (vw); 1236 (s); 1225 (s); 1194 (w); 1179 (vw); 1150 (w); 1126 (w); 1089 (s); 1068 (vw); 1031 (vw); 989 (vw); 958 (w); 930 (w); 903 (w); 853 (vs); 818 (vs); 809 (vs); 783 (s); 774 (s); 732 (w); 700 (vw).

Melting point Decomposes >220 °C (lit. 235 -237 °C)[318]

histamine dihydrochloride (179)

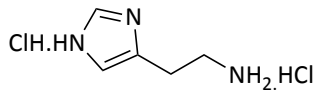

179

Yield: 59%

^{1}H-NMR (400 MHz, [D_2O]): δ (ppm) 8.51 (s, 1H, (HCl.HNC<u>H</u>NCCH)-CH_2-CH_2-NH_2.HCl), 7.24 (s, 1H, , (HCl.HNCHNCC<u>H</u>)-CH_2-CH_2-NH_2.HCl), 3.19 (t, *J* = 7.4 Hz, 2H, , (HCl.HNCHNCCH)-C<u>H$_2$</u>-CH_2-NH_2.HCl), 3.01 (t, *J* = 7.4 Hz, 2H, , (HCl.HNCHNCCH)-CH_2-C<u>H$_2$</u>-NH_2.HCl).

^{13}C-NMR (101 MHz; [D_2O]): δ (ppm) 133.94 ((HCl.HN<u>C</u>HNCCH)-CH_2-CH_2-NH_2.HCl), 128.43 ((HCl.HNCHN<u>C</u>CH)-CH_2-CH_2-NH_2.HCl), 117.05 ((HCl.HNCHNC<u>C</u>H)-CH_2-CH_2-NH_2.HCl), 38.03 ((HCl.HNCHNCCH)-<u>C</u>H_2-CH_2-NH_2.HCl), 22.20 ((HCl.HNCHNCCH)-CH_2-<u>C</u>H_2-NH_2.HCl). Data are in accordance with previously reported chemical shifts.[318,336]

FT-IR wavenumber (cm^{-1}): 3085 (s); 2946 (vs); 2844 (vs); 2782 (vs); 2665 (s); 2633 (s); 2603 (s); 2478; (w); 1626 (s); 1558 (w); 1526 (s); 1474 (s); 1448 (w); 1438 (s); 1410 (w); 1348 (vw); 1325; (vw); 1294 (vw); 1237 (w); 1184 (vw); 1168 (vw); 1149 (w); 1111 (w); 1090 (s); 1031 (w); 987 (vw); 957 (s); 932 (vw); 906 (w); 853 (vs); 805 (vs); 782 (s); 732 (w).

ESI-MS $C_5H_{10}N_3$ theoretical (m/z): 112.0869 [M+] measured (m/z): 112.0869 [M+];

Melting point 248.5–250.5 (lit. 239 -244 °C) [318]

tryptamine hydrochloride (180)

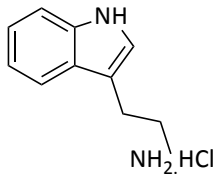

180

Yield: 69%

^{1}H-NMR (400 MHz, [D_2O]): δ (ppm) 7.54 (d, *J* = 7.9 Hz, 1H, ($C_2H_2CHCH<u>C</u>_2NHCHC$)-$CH_2$-$CH_2$-$NH_2$.HCl), 7.39 (d, *J* = 8.0 Hz, 1H, ($C_2H_2CH<u>C</u>HC_2NHCHC$)-$CH_2$-$CH_2$-$NH_2$.HCl), 7.16 (s, 1H, ($C_6H_4NHCH<u>C</u>$)-$CH_2$-$CH_2$-$NH_2$.HCl), 7.13 (t, *J* = 7.7 Hz, 1H, ($CHCH<u>C</u>_2H_2C_2NHCHC$)-$CH_2$-$CH_2$-$NH_2$.HCl), 7.05 (t, *J* = 7.0 Hz, 1H, ($CHCHC_2H_2C_2NHCHC$)-CH_2-CH_2-NH_2.HCl), 3.18 (t, *J* = 6.9 Hz, 2H, (C_8H_6N)-C<u>H</u>$_2$-CH_2-NH_2.HCl), 3.02 (t, *J* = 7.0 Hz, 2H, (C_8H_6N)-CH_2-C<u>H</u>$_2$-NH_2.HCl).

^{13}C-NMR (101 MHz; [D_2O]): δ (ppm) 136.40 (($C_2H_2CHCHC\underline{C}NHCHC$)-$CH_2$-$CH_2$-$NH_2$.HCl), 126.37 (($C_2H_2CHCH\underline{C}CNHCHC$)-$CH_2$-$CH_2$-$NH_2$.HCl), 124.31 (($C_2H_2CHCHCCNH\underline{C}HC$)-$CH_2$-$CH_2$-$NH_2$.HCl), 122.16 (($C_2H_2CH\underline{C}HC_2NHCHC$)-$CH_2$-$CH_2$-$NH_2$.HCl), 119.40 (($C_2H_2\underline{C}HCHC_2NHCHC$)-$CH_2$-$CH_2$-$NH_2$.HCl), 118.26 (($CH\underline{C}HC_2H_2C_2NHCCH$)-$CH_2$-$CH_2$-$NH_2$.HCl), 112.03 (($\underline{C}HCHC_2H_2C_2NHCCH$)-$CH_2$-$CH_2$-$NH_2$.HCl), 109.00 (($C_6H_4NHCH\underline{C}$)-$CH_2$-$CH_2$-$NH_2$.HCl, 39.72 ($C_8H_6N$)-$\underline{C}H_2$-$CH_2$-$NH_2$.HCl), 22.61 (($C_8H_6N$)-$CH_2$-$\underline{C}H_2$-$NH_2$.HCl). Data are in accordance with previously reported chemical shifts.[318,336]

FT-IR wavenumber (cm^{-1}): 3287 (w); 2983 (w); 2909 (w); 2808 (w); 2709 (vw); 2598 (vw); 2448; (vw); 1607 (vw); 1577 (vw); 1552 (vw); 1503 (vw); 1458 (vw); 1428 (vw); 1381 (vw); 1351; (vw); 1339 (vw); 1312 (vw); 1262 (vw); 1238 (vw); 1127 (vw); 1103 (vw); 1094 (vw); 1059; (vw); 1010 (vw); 949 (vw); 939 (vw); 889 (vw); 876 (vw); 850 (vw); 817 (vw); 742 (vw); 675 (vw).

ESI-MS $C_{10}H_{10}N$ theoretical (m/z): 144.0808 [M+] measured (m/z): 144.0807 [M+];

$C_{10}H_{13}N_2$ theoretical (m/z): 161.1073 [M+] measured (m/z): 161.1074 [M+];

$C_{10}H_{12}N_2Na$ theoretical (m/z): 183.0893 [M+] measured (m/z): 183.0892 [M+].

Melting point Decomposes >255 °C (lit. 245–248 °C) [318]

Synthesis of γ-Aminobutyric acid (GABA) hydrochloride (79)

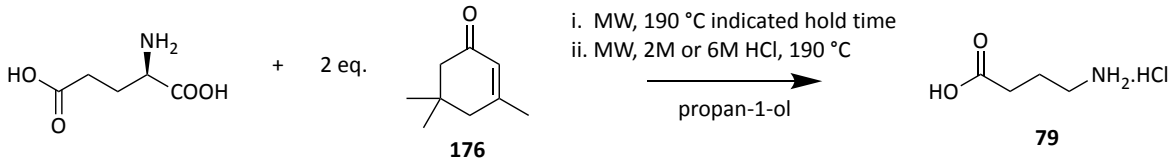

The same procedure as described above was used for L-glutamic acid decarboxylation with minor modifications. Briefly, in a typical 2 mmol scale experiment, a 30 mL microwave vial was charged with 2 mmol of L-glutamic acid, propan-1-ol (3.00 mL) and 4 mmol of isophorone (600 μL). A magnetic stirrer was then added, and the vial was placed in the microwave chamber. The target temperature was set at 190 °C (typically reached within 5 min) and held for the indicated time (see Table 23 p. 265). After this first heating, the reaction mixture was left to cool and 4 eq. of 2 M HCl (5 mL) or 6 M HCl (1.33 mL) was added in a one-pot fashion. The vial was returned to the microwave chamber and a second heating step of a ramp to 190 °C (i.e. no hold time) was set. The reaction mixture was then allowed to cool and washed with diethyl ether or preferably ethyl acetate (1 x 25.0 mL), the water phase collected, and the organic phase was washed with 2 M HCl (10.0 mL) and water (10.0 mL). The collected aqueous phases were washed with diethyl ether or preferably ethyl acetate (2 x 25.0 mL) and evaporated under reduced pressure. The resulting light yellow oil was triturated with acetone and crystals of **79** started to appear. After filtration, **79** (see yields Table 23, p. 265, purity assessed by ^{1}H-NMR spectroscopy) was obtained as white crystals which were dried under vacuum (72 mbar) at 80 °C for 2 h prior to analysis.

For recycling experiments, the organic phases were collected, dried over $MgSO_4$, filtrated and the filtrate was evaporated under reduced pressure to afford the recycled inducer as a brown oil which was used without further purification.

The conventional heating comparison was performed in an Anton Paar Monowave 50 in which only the 2 mmol scale experiments could be carried out (limited by reactor size). Target temperatures and hold times were identical to the aforementioned methodology. All work-up and characterisation were carried out as described above, GABA was obtained in 38%.

^{1}H-NMR (400 MHz, [D_2O]): δ (ppm) 2.90 (t, *J* = 7.6 Hz, 2H, HOOC-C$\underline{H_2}$-CH_2-CH_2-NH_2.HCl), 2.37 (t, *J* = 7.3 Hz, 2H, HOOC-CH_2-CH_2-C$\underline{H_2}$-NH_2.HCl), 1.81 (p (dt), *J* = 7.4 Hz, 2H, HOOC-CH_2-C$\underline{H_2}$-CH_2-NH_2.HCl).

^{13}C-NMR (101 MHz; [D_2O]): δ (ppm) 177.07 (HOO$\underline{C}$-CH_2-CH_2-CH_2-NH_2.HCl), 38.71 (HOOC-CH_2-CH_2-$\underline{C}H_2$-NH_2.HCl), 30.60 (HOOC-$\underline{C}H_2$-CH_2-CH_2-NH_2.HCl), 22.02 (HOOC-CH_2-$\underline{C}H_2$-CH_2-NH_2.HCl).

FT-IR wavenumber (cm^{-1}): 3056 (vs); 2997 (vs); 2926 (vs); 2736 (w); 2624 (w); 2513 (vw); 2468 (vw); 2446 (vw); 2163 (vw); 1959 (vw); 1768 (vw); 1728 (vs); 1601; (w); 1581 (w); 1497 (vs); 1459 (s); 1411 (vs); 1393 (vs); 1330 (w); 1279 (vs); 1241; (vw); 1172 (vs); 1129 (vs); 1067 (s); 977 (s); 954 (vs); 882 (w); 844 (vw); 788 (vs); 740 (s); 666 (vw).

ESI-MS $C_4H_{10}O_2$ theoretical (m/z): 104.0706 [M+] measured (m/z): 104.0704 [M+].

CHN $C_4H_{10}NO_2$ Calculated (Found): %C 34.42 (33.71), %H 7.22 (6.585), %N 10.04 (9.181)

Melting point 116- 125 °C

Synthesis of 1,5-pentanediamine dihydrochloride (200 HCl salt)

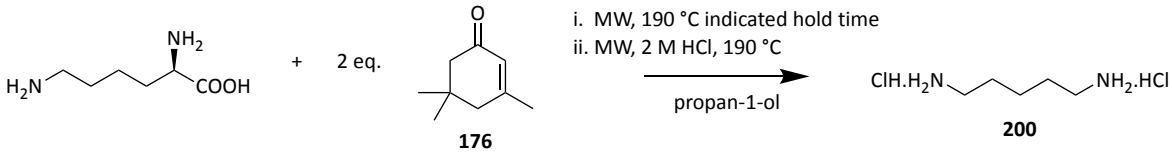

The same procedure as described for L-glutamic acid decarboxylation was employed for L-lysine. Reactions were run at 5 mmol scale using freshly distilled isophorone (purified using a Kugelrohr apparatus). Propan-1-ol was used for the trituration step and afforded 1,5-pentanediamine in 31% yield.

^{1}H-NMR (400 MHz, [D_2O]): δ (ppm) 3.01 (t, *J* = 7.6 Hz, 4H, ClH.H_2N-CH_2-CH_2-CH_2-CH_2-CH_2-NH_2.HCl), 1.71 (quintet, *J* = 7.7 Hz, 4H, ClH.H_2N-CH_2-CH_2-CH_2-CH_2-CH_2-NH_2.HCl), 1.46 (quintet, *J* = 7.9 Hz, 2H, ClH.H_2N-CH_2-CH_2-CH_2-CH_2-CH_2-NH_2.HCl).

^{13}C-NMR (101 MHz; [D_2O]): δ (ppm) 39.2 (ClH.H_2N-CH_2-CH_2-CH_2-CH_2-CH_2-NH_2.HCl, 26.3 (ClH.H_2N-CH_2-CH_2-CH_2-CH_2-CH_2-NH_2.HCl, 22.7 (ClH.H_2N-CH_2-CH_2-CH_2-CH_2-CH_2-NH_2.HCl)

FT-IR wavenumber (cm^{-1}): 2928 (vs); 2521 (w); 1568 (s); 1521 (vs); 1484 (s); 1400 (w); 1321 (w); 1295 (w); 1175 (w); 1125 (w); 1018 (w); 999 (w); 929 (w); 825 (w); 738 (vw)

ESI-MS $C_5H_{15}N_2$ theoretical (m/z): 103.1230 [M+] measured (m/z): 103.1229 [M+].

Melting point Decomposes >250 °C (lit. 249-256 °C)

Formation of amino acids hydrochloride salts

The amino acid (2 mmol) was dissolved in a 2 M HCl solution (1 mL, 1 eq. HCl) stirred for 10 min and evaporated under reduced pressure to afford the HCl salt of the corresponding amino acid.

Glutamic acid hydrochloride (53 HCl salt)

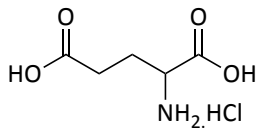

^{1}H-NMR (400 MHz, [D_2O]): δ (ppm) 4.06-4.01 (m, 1H HOOC-CH_2-CH_2-C<u>H</u>(-NH_2.HCl)-COOH), 2.66-2.53 (m, 2H, HOOC-C<u>H_2</u>-CH_2-CH(-NH_2.HCl)-COOH)), 2.26-2.11 (m, 2H, HOOC-CH_2-C<u>H_2</u>-CH(-NH_2.HCl)-COOH)).

^{13}C-NMR (101 MHz; [D_2O]): δ (ppm) 192.1 (HOOC-CH_2-CH_2-CH(-NH_2.HCl)-<u>C</u>OOH), 176.4 (HOO<u>C</u>-CH_2-CH_2-CH(-NH_2.HCl)-COOH), 52.3 (HOOC-CH_2-CH_2-<u>C</u>H(-NH_2.HCl)-COOH), 29.4 (HOOC-<u>C</u>H_2-CH_2-CH(-NH_2.HCl)-COOH), 24.9 (HOOC-CH_2-<u>C</u>H_2-CH(-NH_2.HCl)-COOH).

FT-IR wavenumber (cm^{-1}): 3140 (vw); 2856 (w); 2819 (w); 2721 (vw); 2646 (vw); 2624 (vw); 2601; (vw); 2501 (vw); 2292 (vw); 1980 (vw); 1719 (w); 1668 (s); 1609 (w); 1582 (vw); 1507 (s); 1449 (vw); 1424 (s); 1407 (w); 1372 (vw); 1357 (vw); 1322 (vw); 1305 (vw); 1274 (w); 1252; (w); 1211 (vs); 1146 (w); 1125 (vw); 1079 (w); 999 (w); 934 (vw); 919 (vw); 863 (w); 821 (s); 774 (vw); 749 (vw); 715 (vw); 675 (vw).

CHN $C_5H_9NO_4$.HCl Calculated (Found): %C 32.71 (33.19), %H 5.49 (5.38), %N 7.54 (7.63)

Melting point Decomposes 199–201 °C (lit. >200 °C)[393]

γ-Aminobutyric acid (GABA) hydrochloride (79 HCl salt)

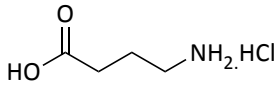

^{1}H-NMR (400 MHz, [D_2O]): δ (ppm) 3.03 (t, J = 7.7 Hz, 2H, HOOC-C$\underline{H_2}$-CH_2-CH_2-NH_2.HCl), 2.49 (t, J = 7.3 Hz, 2H, HOOC-CH_2-CH_2-C$\underline{H_2}$-NH_2.HCl), 1.93 (quintet, J = 7.5 Hz, 2H, HOOC-CH_2-C$\underline{H_2}$-CH_2-NH_2.HCl).

^{13}C-NMR (101 MHz; [D_2O]): δ (ppm) 177.1 (HOO$\underline{C}$-CH_2-CH_2-CH_2-NH_2.HCl), 38.7 (HOOC-CH_2-CH_2-$\underline{C}H_2$-NH_2.HCl), 30.7 (HOOC-$\underline{C}H_2$-CH_2-CH_2-NH_2.HCl), 22.1 (HOOC-CH_2-$\underline{C}H_2$-CH_2-NH_2.HCl).

FT-IR wavenumber (cm^{-1}): 2998 (vs); 2928 (s); 2736 (w); 2623 (vw); 2515 (vw); 2468 (vw); 1954 (vw); 1769 (vw); 1730 (s); 1601 (w); 1579 (w); 1498 (s); 1459 (w); 1410 (s); 1394 (s); 1331 (vw); 1280 (w); 1241 (vw); 1174 (vs); 1130 (vs); 1068 (vw); 1013 (vw); 976 (w); 956 (w); 883 (vw); 843 (vw); 787 (s); 739 (w).

ESI-MS $C_4H_{10}NO_2$ theoretical (m/z): 104.0706 [M+] measured (m/z): 104.0707 [M+].

CHN $C_4H_{10}NO_2$.HCl Calculated (Found): %C 34.42 (34.34), %H 7.22 (7.08), %N 10.04 (9.924)

Melting point 124.5–129.6 °C

Isolation of glutamic HCl from gluten

Gluten (1.00 g) and 6 M HCl (50 mL) were heated at 150 °C or 180 °C in a CEM Mars microwave reactor for 30 min or 10 min respectively with a 16 min or 20 min ramping time respectively. Power was set at 400 W and cooling allowed for 20 min after the reaction was complete. For the conventional heating method, a 100 mL round bottom flask was charged with 1.00 g of gluten and 6 M HCl (50 mL). The suspension was heated at reflux for 24 h with vigorous magnetic stirring. After hydrolysis, the humin residues were filtered and washed with a small amount of 6 M HCl. Activated carbon (~250 mg) was added to the hydrolysate and the slurry was stirred for 30 min. After filtration through cotton wool, the clear filtrate was reduced to a viscous liquid under reduced pressure and subsequently dissolved in 6 M HCl (3 mL). This solution was left to crystallise in a fridge (2-4 °C) overnight. The resulting crystals were separated from the supernatant, washed with a few drops of n-propanol and left to dry in air to afford **53** as small white crystals (see yields Table 24, p. 279)

A procedure, similar to the conventional one, was employed with the aqueous phase collected after the CMF reaction using gluten. Characterisation matched the pure glutamic acid HCl data as described above.

Obtention of glutamic acid free base

A 30 mL glass vial was charged with glutamic acid HCl (784 mg) obtained from gluten following the method described above and dissolved in deionised water (10 mL). The pH of the solution (originally ~1) was adjusted to 3.2 with pure NaOH and 0.1 M NaOH. The

solution started to crash and was left in a fridge overnight. The obtained crystals were collected via filtration and washed with few drops of n-propanol (46% yield). The success of the procedure was assessed by comparing CHN values between commercial glutamic acid free base and the one obtained by the method described above.

Glutamic acid free base from gluten

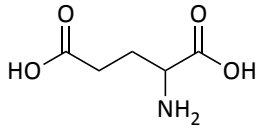

Yield: 46%

^{1}H-NMR (400 MHz, [D_2O]): δ (ppm) 3.63 (t, *J* = 6.3 Hz, 1H, HOOC-CH_2-CH_2-C<u>H</u>(-NH_2)-COOH), 2.46–2.28 (m, 2H, HOOC-C<u>H_2</u>-CH_2-CH(-NH_2)-COOH)), 2.06–1.88 (m, 2H, HOOC-CH_2-CH_2-CH(-NH_2.HCl)-COOH)).

^{13}C-NMR (101 MHz; [D_2O]): δ (ppm) 177.31 (HOOC-CH_2-CH_2-CH(-NH_2)-<u>C</u>OOH, 173.94 (HOO<u>C</u>-CH_2-CH_2-CH(-NH_2)-COOH), 53.91 (HOOC-CH_2-CH_2-<u>C</u>H(-NH_2)-COOH), 30.20 (HOOC-<u>C</u>H_2-CH_2-CH(-NH_2)-COOH), 25.60 (HOOC-CH_2-<u>C</u>H_2-CH(-NH_2)-COOH).

FT-IR wavenumber (cm^{-1}):2910 (vw); 2738 (vw); 2697 (vw); 2651 (vw); 2545 (vw); 2124 (vw); 1946; (vw); 1680 (vw); 1657 (vw); 1635 (vw); 1572 (w); 1553 (w); 1530 (w); 1517 (w); 1455 (vw); 1420 (vw); 1373 (vw); 1342 (vw); 1306 (w); 1254 (w); 1237 (w); 1180 (vw); 1160 (w); 1137; (w); 1092 (vw); 1076 (w); 1056 (vw); 1041 (vw); 1019 (w); 1006 (w); 986 (vw); 947 (vw); 911 (vw); 860 (vw); 818 (w); 810 (vw); 781 (vw); 742 (vw); 714 (vw); 702 (vw); 671 (vw).

CHN : $C_5H_9NO_4$ Calculated (Found): %C 40.82 (40.49), %H 6.17 (6.11), %N 9.52 (9.434)

Synthesis of (3aR,4R,6aS)-4-((S)-2-oxo-1,3-dioxolan-4-yl)tetrahydrofuro[3,4-d][1,3]dioxol-2-one (198, synthesis performed by Dr. Ian Ingram (analysed by Yann Lie)

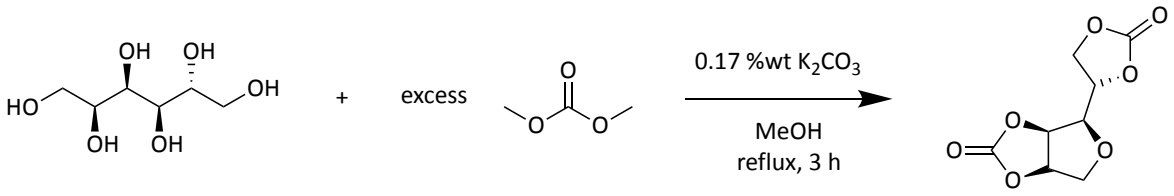

196 **198**

Protocol adapted from the literature.[356] Methanol (200 mL) was placed in a 1 L round bottom flask and heated to 60 °C. Then D-sorbitol (**196**) was gradually added (120.02 g, 0.659 mol) along with the catalyst (potassium carbonate, 0.17 %wt in respect to D-sorbitol) and dimethyl carbonate, also added gradually (627.46 g, 6.96 mol, 10.5 eq.). The reaction mixture was refluxed with stirring for almost 3 h. Methanol was carefully evaporated under reduced pressure. After 24 h no traces of the solvent could be found in the mixture. After vacuum filtration, the filtrate was concentrated, and the residue was washed with methanol. The obtained product was recrystallised from water to give **198 (**40 % yield) white needle crystals and dried thoroughly under vacuum before use.

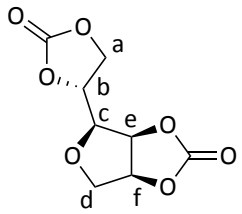

198

^{1}H-NMR (400 MHz, [D_2O]): δ (ppm) 5.38–5.30 (m, 2H,$H_{e\ \&\ f}$), 5.00–4.90 (m, 1H, H_b), 4.59 (d, *J* = 8.6 Hz, 1H, H_{a1}), 4.41 (dd, *J* = 8.4, 6.5 Hz, 1H, H_{a2}), 4.15 (d, *J* = 11.8 Hz, 1H, H_{d1}), 3.98–3.92 (m, 1H, H_c), 3.70–3.63 (m, 1H, H_{d2}).

FT-IR wavenumber (cm^{-1}):1771 (vs); 1722 (w); 1662 (vw); 1552 (vw); 1539 (vw); 1484 (vw); 1457; (vw); 1410 (w); 1377 (w); 1369 (w); 1348 (vw); 1330 (w); 1313 (vw); 1289 (vw); 1226 (w); 1192 (vs); 1175 (vs); 1132 (s); 1100 (vs); 1081 (vs); 1066 (s); 1052 (vs); 1040 (vs); 1005 (vs); 989 (s); 948 (w); 930 (s); 903 (w); 874 (vw); 852 (vw); 828 (vw); 772 (vs); 747 (s); 720 (w); 692 (vs); 668 (w).

Synthesis of polyhydroxyurethane with a diamine

The diamine (1.0 mmol) and sorbitan bis-carbonate **198** (1.0 mmol) were placed into a small agate mortar and ground together thoroughly for several minutes until a completely homogeneous gummy mixture was formed. This mixture was transferred to a glass vial and heated for 20 h at 100 °C, giving a rigid, colourless, foamy material which was characterised without further purification. The NMR spectra could not be assigned due to overlapping signals.

^{1}H-NMR

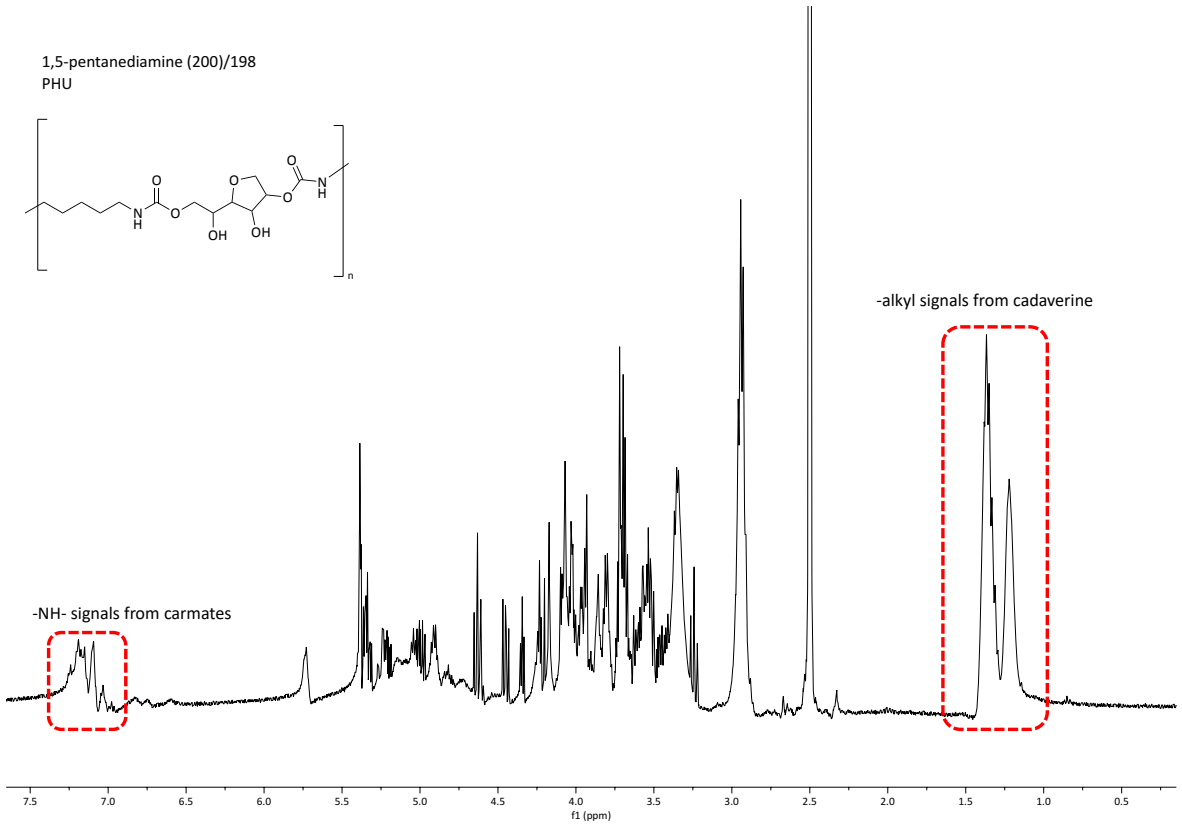

FT-IR 3318 (s); 2934 (s); 2865 (w); 1779 (w); 1693 (vs); 1533 (s); 1458 (w); 1443 (w); 1410; (w); 1370 (w); 1247 (s); 1192 (w); 1138 (s); 1100 (w); 1082 (w); 1039 (s); 772 (w).

MALDI-TOF Repeating unit m/z= 318.14 with 1,5 pentanediamine

References

1. Department for Business Energy & Industrial Strategy. *Growing The Bioeconomy*. (2018) Available at: https://bit.ly/2X7IrCs (Accessed: 29 July 2020).
2. Rebellion, N. E. About Us. (2019) Available at: https://rebellion.earth/the-truth/about-us/ (Accessed: 14 August 2019).
3. The World Commission on Environment and Development. *Our Common Future*. (Oxford University Press, 1987).
4. United Nation Development Program. *Sustainable Development Goals*. (2015) Available at: https://bit.ly/309m01F (Accessed: 29 July 2020).
5. Erisman, J. W., Sutton, M. A., Galloway, J., Klimont, Z. & Winiwarter, W. How A Century Of Ammonia Synthesis Changed The World. *Nat. Geosci.* **1**, 636–639 (2008) doi:10.1038/ngeo325.
6. Laval, G. & Golding, B. T. One-Pot Sequence For The Decarboxylation Of α-Amino Acids. *Synlett* **4**, 0542–0546 (2003) doi:10.1055/s-2003-37512.
7. Araceli Fernandez, P. & Levi, P. *The Future Of Petrochemicals*. *The Future Of Petrochemicals* (11 October 2018) Available at: https://bit.ly/2De4dNS (Accessed: 26 May 2020) doi:10.1787/9789264307414-en.
8. Araceli Fernandez, P. & Levi, P. *The Future Of Petrochemicals Towards More Sustainable Plastics And Fertilisers Together Secure Sustainable Executive Summary*. (2018) Available at: https://bit.ly/2P59GJz (Accessed: 15 May 2020).
9. Lewis, S. L. & Maslin, M. A. Defining The Anthropocene. *Nature* **519**, 171–180 (2015) doi:10.1038/nature14258.
10. Clark, J. H. & Deswarte, F. E. I. The Biorefinery Concept-An Integrated Approach. In *Introduction To Chemicals From Biomass* 1–20 (John Wiley & Sons, Ltd, 2008). doi:10.1002/9780470697474.ch1.
11. Sekulova, F., Kallis, G., Rodríguez-Labajos, B. & Schneider, F. Degrowth: From Theory To Practice. *J. Clean. Prod.* **38**, 1–6 (2013) doi:10.1016/j.jclepro.2012.06.022.
12. Cosme, I., Santos, R. & O'Neill, D. W. Assessing The Degrowth Discourse: A Review And Analysis Of Academic Degrowth Policy Proposals. *J. Clean. Prod.* **149**, 321–334 (2017) doi:10.1016/j.jclepro.2017.02.016.
13. Matharu, A. S. & Lokesh, K. Chapter 1. Green Chemistry Principles And Global Drivers For Sustainability – An Introduction. In *Driving Climate Change* 1–17 (2019). doi:10.1039/9781788012997-00001.
14. Chisti, Y. Biodiesel From Microalgae. *Biotechnol. Adv.* **25**, 294–306 (2007) doi:10.1016/j.biotechadv.2007.02.001.
15. Farmer, T. J. & Mascal, M. Platform Molecules. In *Introduction To Chemicals From Biomass* 89–155 (John Wiley & Sons, Ltd, 2014). doi:10.1002/9781118714478.ch4.
16. Mascal, M. Across The Board: Mark Mascal On The Challenges Of Lignin Biorefining. *ChemSusChem* **13**, 274–277 (2020) doi:10.1002/cssc.201903042.
17. Liao, Y., Koelewijn, S.-F., Van den Bossche, G., Van Aelst, J., Van den Bosch, S., Renders, T., Navare, K., Nicolaï, T., Van Aelst, K., Maesen, M., Matsushima, H., Thevelein, J. M., Van Acker, K., Lagrain, B., Verboekend, D. & Sels, B. F. A Sustainable Wood Biorefinery For Low–Carbon Footprint Chemicals Production. *Science (80-.).* **367**, 1385–1390 (2020) doi:10.1126/science.aau1567.
18. Yan, N. & Wang, Y. Catalyst: Is The Amino Acid A New Frontier For Biorefineries? *Chem* **5**, 739–741 (2019) doi:10.1016/j.chempr.2019.03.016.

19. Hülsey, M. J., Yang, H. & Yan, N. Sustainable Routes For The Synthesis Of Renewable Heteroatom-Containing Chemicals. *ACS Sustain. Chem. Eng.* **6**, 5694–5707 (2018) doi:10.1021/acssuschemeng.8b00612.
20. Anastas, P. T. & Warner, J. C. *Green Chemistry: Theory And Practice*. (Oxford University Press, 1998).
21. Trost, B. The Atom Economy--A Search For Synthetic Efficiency. *Science (80-.).* **254**, 1471–1477 (1991) doi:10.1126/science.1962206.
22. Sheldon, R. A. Catalysis, The Atom Utilization Concept And Waste Minimization. In *Industrial Environmental Chemistry* 99–119 (Springer US, 1992). doi:10.1007/978-1-4899-2320-2_9.
23. Tobiszewski, M., Marć, M., Gałuszka, A. & Namieśnik, J. Green Chemistry Metrics With Special Reference To Green Analytical Chemistry. *Molecules* **20**, 10928–10946 (2015) doi:10.3390/molecules200610928.
24. Phan, T. V. T., Gallardo, C. & Mane, J. Green Motion: A New And Easy To Use Green Chemistry Metric From Laboratories To Industry. *Green Chem.* **17**, 2846–2852 (2015) doi:10.1039/c4gc02169j.
25. Gonzalez, M. A. & Smith, R. L. A Methodology To Evaluate Process Sustainability. *Environ. Prog.* **22**, 269–276 (2003) doi:10.1002/ep.670220415.
26. Van Aken, K., Strekowski, L. & Patiny, L. EcoScale, A Semi-Quantitative Tool To Select An Organic Preparation Based On Economical And Ecological Parameters. *Beilstein J. Org. Chem.* **2**, 1–7 (2006) doi:10.1186/1860-5397-2-3.
27. Clark, J. The 12 Misunderstandings Of Green Chemistry. *Environmental Science & Engineering Magazine* 6–7 (2012).
28. Winterton, N. Green Chemistry: Deliverance Or Distraction? *Clean Technol. Environ. Policy* **18**, 991–1001 (2016) doi:10.1007/s10098-016-1118-y.
29. Supanchaiyamat, N. & Hunt, A. J. Conservation Of Critical Elements Of The Periodic Table. *ChemSusChem* **12**, 397–403 (2019) doi:10.1002/cssc.201802556.
30. BASF. Verbund Concept. Available at: https://on.basf.com/30WSfAy (Accessed: 12 February 2019).
31. Van Krevelen, D. W. Graphical-Statistical Method For The Study Of Structure And Reaction Processes Of Coal. *Fuel* **29**, 269–284 (1950).
32. Kim, S., Kramer, R. W. & Hatcher, P. G. Graphical Method For Analysis Of Ultrahigh-Resolution Broadband Mass Spectra Of Natural Organic Matter, The Van Krevelen Diagram. *Anal. Chem.* **75**, 5336–5344 (2003) doi:10.1021/ac034415p.
33. Dusselier, M., Mascal, M. & Sels, B. F. Top Chemical Opportunities From Carbohydrate Biomass: A Chemist's View Of The Biorefinery. In *Selective Catalysis For Renewable Feedstocks And Chemicals* 1–40 (2014). doi:10.1007/128_2014_544.
34. Rivas-Ubach, A., Liu, Y., Bianchi, T. S., Tolić, N., Jansson, C. & Paša-Tolić, L. Moving Beyond The Van Krevelen Diagram: A New Stoichiometric Approach For Compound Classification In Organisms. *Anal. Chem.* **90**, 6152–6160 (2018) doi:10.1021/acs.analchem.8b00529.
35. Froidevaux, V., Negrell, C., Caillol, S., Pascault, J.-P. & Boutevin, B. Biobased Amines: From Synthesis To Polymers; Present And Future. *Chem. Rev.* **116**, 14181–14224 (2016) doi:10.1021/acs.chemrev.6b00486.
36. Chang, F., Hsu, W.-H. & Mascal, M. Synthesis Of Anti-Inflammatory Furan Fatty Acids From Biomass-Derived 5-(Chloromethyl)Furfural. *Sustain. Chem. Pharm.* **1**, 14–18 (2015) doi:10.1016/j.scp.2015.09.002.

37. Mascal, M. & Dutta, S. Synthesis Of The Natural Herbicide δ-Aminolevulinic Acid From Cellulose-Derived 5-(Chloromethyl)Furfural. *Green Chem.* **13**, 40–41 (2011) doi:10.1039/C0GC00548G.
38. Mascal, M. & Dutta, S. Synthesis Of Ranitidine (Zantac) From Cellulose-Derived 5-(Chloromethyl)Furfural. *Green Chem.* **13**, 3101 (2011) doi:10.1039/c1gc15537g.
39. Chang, F., Dutta, S., Becnel, J. J., Estep, A. S. & Mascal, M. Synthesis Of The Insecticide Prothrin And Its Analogues From Biomass-Derived 5-(Chloromethyl)Furfural. *J. Agric. Food Chem.* **62**, 476–480 (2014) doi:10.1021/jf4045843.
40. Saska, J., Li, Z., Otsuki, A. L., Wei, J., Fettinger, J. C. & Mascal, M. Butenolide Derivatives Of Biobased Furans: Sustainable Synthetic Dyes. *Angew. Chemie Int. Ed.* **58**, 17293–17296 (2019) doi:10.1002/anie.201911387.
41. Lie, Y., Farmer, T. J. & Macquarrie, D. J. Facile And Rapid Decarboxylation Of Glutamic Acid To γ-Aminobutyric Acid Via Microwave-Assisted Reaction: Towards Valorisation Of Waste Gluten. *J. Clean. Prod.* **205**, (2018) doi:10.1016/j.jclepro.2018.09.151.
42. Lammens, T. M., Franssen, M. C. R., Scott, E. L. & Sanders, J. P. M. Synthesis Of Biobased N-Methylpyrrolidone By One-Pot Cyclization And Methylation Of γ-Aminobutyric Acid. *Green Chem.* **12**, 1430 (2010) doi:10.1039/c0gc00061b.
43. Court, G. R., Lawrence, C. H., Warwick, D. & Anthony, J. Method For Converting Lignocellulosic Materials Into Useful Chemicals. (2011) Available at: https://bit.ly/2P2vuWa (Accessed: 1 May 2020) Patent Number: *WO2011/000030 Al*.
44. Mouterde, L. M. M., Allais, F. & Stewart, J. D. Enzymatic Reduction Of Levoglucosenone By An Alkene Reductase (OYE 2.6): A Sustainable Metal- And Dihydrogen-Free Access To The Bio-Based Solvent Cyrene®. *Green Chem.* **20**, 5528–5532 (2018) doi:10.1039/C8GC03146K.
45. Park, D. S., Joseph, K. E., Koehle, M., Krumm, C., Ren, L., Damen, J. N., Shete, M. H., Lee, H. S., Zuo, X., Lee, B., Fan, W., Vlachos, D. G., Lobo, R. F., Tsapatsis, M. & Dauenhauer, P. J. Tunable Oleo-Furan Surfactants By Acylation Of Renewable Furans. *ACS Cent. Sci.* **2**, 820–824 (2016) doi:10.1021/acscentsci.6b00208.
46. Montero, M. F., Aristizábal, M. & García Reina, G. Isolation Of High-Lipid Content Strains Of The Marine Microalga Tetraselmis Suecica For Biodiesel Production By Flow Cytometry And Single-Cell Sorting. *J. Appl. Phycol.* **23**, 1053–1057 (2011) doi:10.1007/s10811-010-9623-6.
47. Guihéneuf, F., Khan, A. & Tran, L.-S. P. Genetic Engineering: A Promising Tool To Engender Physiological, Biochemical, And Molecular Stress Resilience In Green Microalgae. *Front. Plant Sci.* **7**, 400 (2016) doi:10.3389/fpls.2016.00400.
48. Halim, R., Danquah, M. K. & Webley, P. A. Extraction Of Oil From Microalgae For Biodiesel Production: A Review. *Biotechnol. Adv.* **30**, 709–732 (2012) doi:10.1016/j.biotechadv.2012.01.001.
49. Liang, M.-H. & Jiang, J.-G. Advancing Oleaginous Microorganisms To Produce Lipid Via Metabolic Engineering Technology. *Prog. Lipid Res.* **52**, 395–408 (2013) doi:10.1016/j.plipres.2013.05.002.
50. Alma, M. H. & Salan, T. A Review On Novel Bio-Fuel From Turpentine Oil. *Process. Petrochemistry Oil Refin.* **18**, 1–12 (2017).
51. Crivello, J. V. & Reichmanis, E. Photopolymer Materials And Processes For Advanced Technologies. *Chem. Mater.* **26**, 533–548 (2014) doi:10.1021/cm402262g.
52. Fujimoto, K., Takeda, H. & Kunugi, T. Catalytic Oxidation Of Ethylene To

Acetaldehyde. Palladium Chloride-Active Charcoal Catalyst. *Ind. Eng. Chem. Prod. Res. Dev.* **13**, 237–242 (1974) doi:10.1021/i360052a005.

53. Jira, R. Acetaldehyde From Ethylene-A Retrospective On The Discovery Of The Wacker Process. *Angew. Chemie Int. Ed.* **48**, 9034–9037 (2009) doi:10.1002/anie.200903992.
54. Jiang, Y., Yang, X., Bian, P., Feng, J., Dong, J., He, H., Li, Y., Zhang, Y. & Huang, L. Method Of Preparing Pentaerythritol. (2010) Available at: https://bit.ly/3g9htlC (Accessed: 1 May 2020) Patent Number: *US20100152500A1*.
55. Ma, X., Zhou, Z., Jin, E., Sun, Q., Zhang, B., Tang, J. & Shen, Y. Facile Synthesis Of Polyester Dendrimers As Drug Delivery Carriers. *Macromolecules* **46**, 37–42 (2013) doi:10.1021/ma301849a.
56. Vogel, A. I., Tatchell, A. R., Furnis, B. S., Hannaford, A. J. & Smith, P. W. G. *Vogel's Textbook Of Practical Organic Chemistry*. (Prentice Hall, 1989).
57. Fan, D., Dai, D.-J. & Wu, H.-S. Ethylene Formation By Catalytic Dehydration Of Ethanol With Industrial Considerations. *Materials (Basel).* **6**, 101–115 (2012) doi:10.3390/ma6010101.
58. Krishnan, M. S., Ho, N. W. Y. & Tsao, G. T. Fermentation Kinetics Of Ethanol Production From Glucose And Xylose By Recombinant Saccharomyces 1400(PLNH33). *Appl. Biochem. Biotechnol.* **78**, 373–388 (1999) doi:10.1385/ABAB:78:1-3:373.
59. Moore, C. M., Staples, O., Jenkins, R. W., Brooks, T. J., Semelsberger, T. A. & Sutton, A. D. Acetaldehyde As An Ethanol Derived Bio-Building Block: An Alternative To Guerbet Chemistry. *Green Chem.* **19**, 169–174 (2017) doi:10.1039/c6gc02507b.
60. Hufendiek, A., Lingier, S. & Du Prez, F. E. Thermoplastic Polyacetals: Chemistry From The Past For A Sustainable Future? *Polym. Chem.* **10**, 9–33 (2019) doi:10.1039/C8PY01219A.
61. Dai, J., Ma, S., Wu, Y., Han, L., Zhang, L., Zhu, J. & Liu, X. Polyesters Derived From Itaconic Acid For The Properties And Bio-Based Content Enhancement Of Soybean Oil-Based Thermosets. *Green Chem.* **17**, 2383–2392 (2015) doi:10.1039/C4GC02057J.
62. Teleky, B. E. & Vodnar, D. C. Biomass-Derived Production Of Itaconic Acid As A Building Block In Specialty Polymers. *Polymers (Basel).* **11**, (2019) doi:10.3390/polym11061035.
63. Cousinet, S., Ghadban, A., Fleury, E., Lortie, F., Pascault, J.-P. & Portinha, D. Toward Replacement Of Styrene By Bio-Based Methacrylates In Unsaturated Polyester Resins. *Eur. Polym. J.* **67**, 539–550 (2015) doi:10.1016/j.eurpolymj.2015.02.016.
64. Burgard, A. P., Burk, M. J., Osterhout, R. E. & Pharkya, P. Microorganisms For The Production Of Methacrylic Acid. (2012) Available at: https://bit.ly/312eIvS (Accessed: 1 May 2020) Patent Number: *US8241877B2*.
65. Pawlowski, G., Chen, C., Oberlander, J. & Plass, R. Negative Photoresist Compositions. (2009) Available at: https://bit.ly/30Vy7id (Accessed: 1 May 2020) Patent Number: *US7601482B2*.
66. Bhattacharya, D. & Medlin, and L. Algal Phylogeny And The Origin Of Land Plants. *Plant Physiol.* **116**, 9–15 (1998) doi:10.1104/pp.116.1.9.
67. Minoda, A., Sawada, H., Suzuki, S., Miyashita, S., Inagaki, K., Yamamoto, T. & Tsuzuki, M. Recovery Of Rare Earth Elements From The Sulfothermophilic Red Alga Galdieria Sulphuraria Using Aqueous Acid. *Appl. Microbiol. Biotechnol.* **99**, 1513–1519 (2015)

doi:10.1007/s00253-014-6070-3.
68. Chisti, Y. Large-Scale Production Of Algal Biomass: Raceway Ponds. In *Algae Biotechnology* 21–40 (2016). doi:10.1007/978-3-319-12334-9_2.
69. Bonnefond, H., Combe, C., Cadoret, J.-P., Sciandra, A., Bernard, O. & Baumberger, S. Potentiel Des Microalgues. In *Chimie Verte Et Industries Agroalimentaires - Vers Une Bioéconomie Durable* (Lavoisier).
70. Pérez-Rama, M. Cadmium Removal By Living Cells Of The Marine Microalga Tetraselmis Suecica. *Bioresour. Technol.* **84**, 265–270 (2002) doi:10.1016/S0960-8524(02)00045-7.
71. Tredici, M. R., Rodolfi, L., Biondi, N., Bassi, N. & Sampietro, G. Techno-Economic Analysis Of Microalgal Biomass Production In A 1-Ha Green Wall Panel (GWP®) Plant. *Algal Res.* **19**, 253–263 (2016) doi:10.1016/j.algal.2016.09.005.
72. Bonnefond, H., Grimaud, G., Rumin, J., Bougaran, G., Talec, A., Gachelin, M., Boutoute, M., Pruvost, E., Bernard, O. & Sciandra, A. Continuous Selection Pressure To Improve Temperature Acclimation Of Tisochrysis Lutea. *PLoS One* **12**, e0183547 (2017) doi:10.1371/journal.pone.0183547.
73. Diraman, H., Koru, E. & Dibeklioglu, H. Fatty Acid Profile Of Spirulina Platensis Used As A Food Supplement. *Isr. J. Aquac.* **61**, 134–142 (2009).
74. Barry, A., Wolfe, A., English, C., Ruddick, C. & Lambert, D. *National Algal Biofuels Technology Review*. *Office Of Energy Efficiency And Renewable Energy, Bioenergy Technologies Office.* (2016) Available at: https://bit.ly/2BGk5bF (Accessed: 29 July 2020).
75. Wijffels, R. H. & Barbosa, M. J. An Outlook On Microalgal Biofuels. *Science (80-.).* **329**, 796–799 (2010) doi:10.1126/science.1189003.
76. Raheem, A., Prinsen, P., Vuppaladadiyam, A. K., Zhao, M. & Luque, R. A Review On Sustainable Microalgae Based Biofuel And Bioenergy Production: Recent Developments. *J. Clean. Prod.* **181**, 42–59 (2018) doi:10.1016/j.jclepro.2018.01.125.
77. Bleakley, S. & Hayes, M. Algal Proteins: Extraction, Application, And Challenges Concerning Production. *Foods* **6**, 33 (2017) doi:10.3390/foods6050033.
78. Chew, K. W., Yap, J. Y., Show, P. L., Suan, N. H., Juan, J. C., Ling, T. C., Lee, D.-J. & Chang, J.-S. Microalgae Biorefinery: High Value Products Perspectives. *Bioresour. Technol.* **229**, 53–62 (2017) doi:10.1016/j.biortech.2017.01.006.
79. Mata, T. M., Martins, A. A. & Caetano, N. S. Microalgae For Biodiesel Production And Other Applications: A Review. *Renew. Sustain. Energy Rev.* **14**, 217–232 (2010) doi:10.1016/j.rser.2009.07.020.
80. Gifuni, I., Pollio, A., Safi, C., Marzocchella, A. & Olivieri, G. Current Bottlenecks And Challenges Of The Microalgal Biorefinery. *Trends Biotechnol.* **37**, 242–252 (2019) doi:10.1016/j.tibtech.2018.09.006.
81. ’t Lam, G. P., Vermuë, M. H., Eppink, M. H. M., Wijffels, R. H. & van den Berg, C. Multi-Product Microalgae Biorefineries: From Concept Towards Reality. *Trends Biotechnol.* **36**, 216–227 (2018) doi:10.1016/j.tibtech.2017.10.011.
82. Laurens, L. M. L., Markham, J., Templeton, D. W., Christensen, E. D., Van Wychen, S., Vadelius, E. W., Chen-Glasser, M., Dong, T., Davis, R. & Pienkos, P. T. Development Of Algae Biorefinery Concepts For Biofuels And Bioproducts; A Perspective On Process-Compatible Products And Their Impact On Cost-Reduction. *Energy Environ. Sci.* **10**, 1716–1738 (2017) doi:10.1039/C7EE01306J.
83. Odjadjare, E. C., Mutanda, T. & Olaniran, A. O. Potential Biotechnological Application

Of Microalgae: A Critical Review. *Crit. Rev. Biotechnol.* **37**, 37–52 (2017) doi:10.3109/07388551.2015.1108956.
84. Fernandes, T. V., Suárez-Muñoz, M., Trebuch, L. M., Verbraak, P. J. & Van de Waal, D. B. Toward An Ecologically Optimized N:P Recovery From Wastewater By Microalgae. *Front. Microbiol.* **8**, 1–6 (2017) doi:10.3389/fmicb.2017.01742.
85. Melis, A. Solar Energy Conversion Efficiencies In Photosynthesis: Minimizing The Chlorophyll Antennae To Maximize Efficiency. *Plant Sci.* **177**, 272–280 (2009) doi:10.1016/j.plantsci.2009.06.005.
86. de Mooij, T., Janssen, M., Cerezo-Chinarro, O., Mussgnug, J. H., Kruse, O., Ballottari, M., Bassi, R., Bujaldon, S., Wollman, F.-A. & Wijffels, R. H. Antenna Size Reduction As A Strategy To Increase Biomass Productivity: A Great Potential Not Yet Realized. *J. Appl. Phycol.* **27**, 1063–1077 (2015) doi:10.1007/s10811-014-0427-y.
87. Radakovits, R., Jinkerson, R. E., Darzins, A. & Posewitz, M. C. Genetic Engineering Of Algae For Enhanced Biofuel Production. *Eukaryot. Cell* **9**, 486–501 (2010) doi:10.1128/EC.00364-09.
88. Wilson, M. H. H., Groppo, J., Placido, A., Graham, S., Morton, S. A., Santillan-Jimenez, E., Shea, A., Crocker, M., Crofcheck, C. & Andrews, R. CO2 Recycling Using Microalgae For The Production Of Fuels. *Appl. Petrochemical Res.* **4**, 41–53 (2014) doi:10.1007/s13203-014-0052-3.
89. Bougaran, G., Rouxel, C., Dubois, N., Kaas, R., Grouas, S., Lukomska, E., Le Coz, J.-R. & Cadoret, J.-P. Enhancement Of Neutral Lipid Productivity In The Microalga Isochrysis Affinis Galbana (T-Iso) By A Mutation-Selection Procedure. *Biotechnol. Bioeng.* **109**, 2737–2745 (2012) doi:10.1002/bit.24560.
90. Laurens, L. M. L. *Summative Mass Analysis Of Algal Biomass - Integration Of Analytical Procedures: Laboratory Analytical Procedure (LAP)*. (13 January 2016) Available at: https://bit.ly/39OH9Sh (Accessed: 29 July 2020) doi:10.2172/1118072.
91. Laurens, L. M. L., Dempster, T. A., Jones, H. D. T., Wolfrum, E. J., Van Wychen, S., McAllister, J. S. P., Rencenberger, M., Parchert, K. J. & Gloe, L. M. Algal Biomass Constituent Analysis: Method Uncertainties And Investigation Of The Underlying Measuring Chemistries. *Anal. Chem.* **84**, 1879–1887 (2012) doi:10.1021/ac202668c.
92. Tokuşoglu, O. and Ü. M. K. Biomass Nutrient Profiles Of Three Microalgae: *J. Food Sci.* **68**, 1144–1148 (2003).
93. Agustini, T. W., Suzery, M., Sutrisnanto, D., Ma'ruf, W. F. & Hadiyanto. Comparative Study Of Bioactive Substances Extracted From Fresh And Dried Spirulina Sp. *Procedia Environ. Sci.* **23**, 282–289 (2015) doi:10.1016/j.proenv.2015.01.042.
94. Van Wychen, S. & Laurens, L. M. L. *Determination Of Total Solids And Ash In Algal Biomass: Laboratory Analytical Procedure (LAP)*. (13 January 2016) Available at: https://bit.ly/30Y9SzJ (Accessed: 29 July 2020) doi:10.2172/1118077.
95. Wilde, E. W. & Benemann, J. R. Bioremoval Of Heavy Metals By The Use Of Microalgae. *Biotechnol. Adv.* **11**, 781–812 (1993) doi:10.1016/0734-9750(93)90003-6.
96. Templeton, D. W. & Laurens, L. M. L. Nitrogen-To-Protein Conversion Factors Revisited For Applications Of Microalgal Biomass Conversion To Food, Feed And Fuel. *Algal Res.* **11**, 359–367 (2015) doi:10.1016/j.algal.2015.07.013.
97. Safi, C., Charton, M., Pignolet, O., Silvestre, F., Vaca-Garcia, C. & Pontalier, P.-Y. Influence Of Microalgae Cell Wall Characteristics On Protein Extractability And Determination Of Nitrogen-To-Protein Conversion Factors. *J. Appl. Phycol.* **25**, 523–

529 (2013) doi:10.1007/s10811-012-9886-1.
98. Boisen, S., Bech-Andersen, S. & Eggum, B. O. A Critical View On The Conversion Factor 6.25 From Total Nitrogen To Protein. *Acta Agric. Scand.* **37**, 299–304 (1987) doi:10.1080/00015128709436560.
99. Safi, C. M. *Microalgae Biorefinery : Proposition Of A Fractionation Process*. (2013) Available at: https://bit.ly/3hKF2S2 (Accessed: 1 May 2020).
100. Organic Spirulina Powder | MYPROTEIN™. Available at: https://bit.ly/337Rfwe (Accessed: 13 November 2019).
101. Campanella, L., Russo, M. V. & Avino, P. Free And Total Amino Acid Composition In Blue-Green Algae. *Ann. Chim.* **92**, 343–52 (2002).
102. Brown, M. R. The Amino-Acid And Sugar Composition Of 16 Species Of Microalgae Used In Mariculture. *J. Exp. Mar. Bio. Ecol.* **145**, 79–99 (1991) doi:10.1016/0022-0981(91)90007-J.
103. Fountoulakis, M. & Lahm, H.-W. Hydrolysis And Amino Acid Composition Analysis Of Proteins. *J. Chromatogr. A* **826**, 109–134 (1998) doi:10.1016/S0021-9673(98)00721-3.
104. Marconi, E. ., Panfili, G., Bruschi, L., Vivanti, V. & Pizzoferrato, L. Comparative Study On Microwave And Conventional Methods For Protein Hydrolysis In Food. *Amino Acids* **8**, 201–208 (1995) doi:10.1007/BF00806493.
105. Margolis, S. A., Jassie, L. & Kingston, H. M. The Hydrolysis Of Proteins By Microwave Energy. *J. Automat. Chem.* **13**, 93–95 (1991) doi:10.1155/S1463924691000172.
106. de la Hoz, A., Díaz-Ortiz, A. & Prieto, P. Chapter 1. Microwave-Assisted Green Organic Synthesis. In *Alternative Energy Sources For Green Chemistry* 1–33 (The Royal Society of Chemistry, 2016). doi:10.1039/9781782623632-00001.
107. Hanczkó, R., Jámbor, A., Perl, A. & Molnár-Perl, I. Advances In The O-Phthalaldehyde Derivatizations. *J. Chromatogr. A* **1163**, 25–42 (2007) doi:10.1016/j.chroma.2007.06.013.
108. Meussen, B. J., van Zeeland, A. N. T., Bruins, M. E. & Sanders, J. P. M. A Fast And Accurate UPLC Method For Analysis Of Proteinogenic Amino Acids. *Food Anal. Methods* **7**, 1047–1055 (2014) doi:10.1007/s12161-013-9712-7.
109. Spahr, P. F. & Edsall, J. T. Amino Acid Composition Of Human And Bovine Serum Mercaptalbumins. *J. Biol. Chem.* **239**, 850–4 (1964).
110. Lammens, T. M., Franssen, M. C. R., Scott, E. L. & Sanders, J. P. M. Availability Of Protein-Derived Amino Acids As Feedstock For The Production Of Bio-Based Chemicals. *Biomass And Bioenergy* **44**, 168–181 (2012) doi:10.1016/j.biombioe.2012.04.021.
111. Joergensen, L. & Thestrup, H. N. Determination Of Amino Acids In Biomass And Protein Samples By Microwave Hydrolysis And Ion-Exchange Chromatography. *J. Chromatogr. A* **706**, 421–428 (1995) doi:10.1016/0021-9673(94)01107-P.
112. Weiss, M., Manneberg, M., Juranville, J.-F., Lahm, H.-W. & Fountoulakis, M. Effect Of The Hydrolysis Method On The Determination Of The Amino Acid Composition Of Proteins. *J. Chromatogr. A* **795**, 263–275 (1998) doi:10.1016/S0021-9673(97)00983-7.
113. Sahasrabudhe, M. R. & Smallbone, B. W. Comparative Evaluation Of Solvent Extraction Methods For The Determination Of Neutral And Polar Lipids In Beef. *J. Am. Oil Chem. Soc.* **60**, 801–805 (1983) doi:10.1007/BF02787431.
114. Fenton, H. J. H. & Gostling, M. LXXXV.—Derivatives Of Methylfurfural. *J. Chem. Soc.,*

Trans. **79**, 807–816 (1901) doi:10.1039/CT9017900807.
115. Mascal, M. & Nikitin, E. B. Direct, High-Yield Conversion Of Cellulose Into Biofuel. *Angew. Chemie Int. Ed.* **47**, 7924–7926 (2008) doi:10.1002/anie.200801594.
116. Mascal, M. & Nikitin, E. B. Dramatic Advancements In The Saccharide To 5-(Chloromethyl)Furfural Conversion Reaction. *ChemSusChem* **2**, 859–861 (2009) doi:10.1002/cssc.200900136.
117. Mascal, M. 5-(Chloromethyl)Furfural (CMF): A Platform For Transforming Cellulose Into Commercial Products. *ACS Sustain. Chem. Eng.* **7**, 5588–5601 (2019) doi:10.1021/acssuschemeng.8b06553.
118. Delidovich, I., Leonhard, K. & Palkovits, R. Cellulose And Hemicellulose Valorisation: An Integrated Challenge Of Catalysis And Reaction Engineering. *Energy Environ. Sci.* **7**, 2803 (2014) doi:10.1039/C4EE01067A.
119. Rosatella, A. a., Simeonov, S. P., Frade, R. F. M. & Afonso, C. a. M. 5-Hydroxymethylfurfural (HMF) As A Building Block Platform: Biological Properties, Synthesis And Synthetic Applications. *Green Chem.* **13**, 754 (2011) doi:10.1039/c0gc00401d.
120. Mascal, M. & Nikitin, E. B. High-Yield Conversion Of Plant Biomass Into The Key Value-Added Feedstocks 5-(Hydroxymethyl)Furfural, Levulinic Acid, And Levulinic Esters Via5-(Chloromethyl)Furfural. *Green Chem.* **12**, 370–373 (2010) doi:10.1039/B918922J.
121. Lane, D. R., Mascal, M. & Stroeve, P. Experimental Studies Towards Optimization Of The Production Of 5-(Chloromethyl)Furfural (CMF) From Glucose In A Two-Phase Reactor. *Renew. Energy* **85**, 994–1001 (2016) doi:10.1016/j.renene.2015.07.032.
122. N/A-ECHA. Dichloromethane; Methylene Chloride. (2020) Available at: https://bit.ly/39Bz5UC (Accessed: 12 May 2020).
123. Hansen, C. M. The Three Dimensional Solubility Parameter And Solvent Diffusion Coefficient. Their Importance In Surface Coating Formulation. *DANISH TECHNICAL PRESS* vol. 14 (1967) Available at: https://www.hansen-solubility.com/Charles-Hansen/publications.php.
124. Blanks, R. F. & Prausnitz, J. M. Thermodynamics Of Polymer Solubility In Polar And Nonpolar Systems. *Ind. Eng. Chem. Fundam.* **3**, 1–8 (1964) doi:10.1021/i160009a001.
125. Hansen, C. M. *Hansen Solubility Parameters*. (CRC Press, 2007). doi:10.1201/9781420006834.
126. Yamamoto, H., Abbott, S. & Hansen, C. M. Consideration Of Hansen Solubility Parameters. Part 1 Dividing The Dispersion Term (ΔD) And New HSP Distance. *Hansen Solubility Parameters 50th Anniv. Conf.* 1–13 (2017).
127. Sherwood, J., Parker, H. L., Moonen, K., Farmer, T. J. & Hunt, A. J. N-Butylpyrrolidinone As A Dipolar Aprotic Solvent For Organic Synthesis. *Green Chem.* **18**, 3990–3996 (2016) doi:10.1039/C6GC00932H.
128. Yang, Y., Liu, W., Wang, N., Wang, H., Li, W. & Song, Z. Effect Of Different Ionic Liquids On 5-Hydroxymethylfurfural Preparation From Glucose In DMA Over AlCl3 : Experimental And Theoretical Study. *Chinese J. Chem.* **33**, 583–588 (2015) doi:10.1002/cjoc.201500030.
129. Ou, Y. J., Wang, X. M., Li, C. L., Zhu, Y. L. & Li, X. L. The Effects Of Alkali And Temperature On The Hydrolysis Rate Of N-Methylpyrrolidone. *IOP Conf. Ser. Earth Environ. Sci.* **100**, 012036 (2017) doi:10.1088/1755-1315/100/1/012036.

130. Mascal, M. & Nikitin, E. B. Co-Processing Of Carbohydrates And Lipids In Oil Crops To Produce A Hybrid Biodiesel. *Energy & Fuels* **24**, 2170–2171 (2010) doi:10.1021/ef9013373.
131. Dutta, S. & Mascal, M. Novel Pathways To 2,5-Dimethylfuran Via Biomass-Derived 5-(Chloromethyl)Furfural. *ChemSusChem* **7**, 3028–3030 (2014) doi:10.1002/cssc.201402702.
132. Prat, D., Wells, A., Hayler, J., Sneddon, H., McElroy, C. R., Abou-Shehada, S. & Dunn, P. J. CHEM21 Selection Guide Of Classical- And Less Classical-Solvents. *Green Chem.* **18**, 288–296 (2016) doi:10.1039/C5GC01008J.
133. Breeden, S. W., Clark, J. H., Farmer, T. J., Macquarrie, D. J., Meimoun, J. S., Nonne, Y. & Reid, J. E. S. J. Microwave Heating For Rapid Conversion Of Sugars And Polysaccharides To 5-Chloromethyl Furfural. *Green Chem.* **15**, 72–75 (2013) doi:10.1039/C2GC36290B.
134. Körner, P., Jung, D. & Kruse, A. The Effect Of Different Brønsted Acids On The Hydrothermal Conversion Of Fructose To HMF. *Green Chem.* **20**, 2231–2241 (2018) doi:10.1039/C8GC00435H.
135. Norman, A. W. From Vitamin D To Hormone D: Fundamentals Of The Vitamin D Endocrine System Essential For Good Health. *Am. J. Clin. Nutr.* **88**, (2008) doi:10.1093/ajcn/88.2.491s.
136. Mead, M. N. Benefits Of Sunlight: A Bright Spot For Human Health. *Environ. Health Perspect.* **116**, (2008) doi:10.1289/ehp.116-a160.
137. Rhodes, L. E., Webb, A. R., Fraser, H. I., Kift, R., Durkin, M. T., Allan, D., O'Brien, S. J., Vail, A. & Berry, J. L. Recommended Summer Sunlight Exposure Levels Can Produce Sufficient (≥20 Ng.Ml-1) But Not The Proposed Optimal (≥32 Ng.Ml-1) 25(OH)D Levels At UK Latitudes. *J. Invest. Dermatol.* **130**, 1411–1418 (2010) doi:10.1038/jid.2009.417.
138. World Health Organization World Meteorologcal Organization United Enviroment Programme International Comission on Non-Ionizing Radiation Protection. *Global Solar UV Index: A Practical Guide*. (2002) Available at: http://www.who.int/uv/ (Accessed: 29 July 2020) doi:10.1506/car.25.4.4.
139. Lowry, T. H. & Richardson, K. S. *Mechanism And Theory In Organic Chemistry*. *Journal Of Chemical Education* vol. 59 (1987).
140. de Paula, J. & Atkin, P. *Atkin's Physical Chemistry*. (Oxford University Press, 2018).
141. Zumdahl, S. S. & DeCoste, D. J. *Chemistry Principles*. (2017).
142. Herzog, B., Mongiat, S., Deshayes, C., Neuhaus, M., Sommer, K. & Mantler, A. In Vivo And In Vitro Assessment Of UVA Protection By Sunscreen Formulations Containing Either Butyl Methoxy Dibenzoyl Methane, Methylene Bis-Benzotriazolyl Tetramethylbutylphenol, Or Microfine ZnO. *Int. J. Cosmet. Sci.* **24**, 170–185 (2002) doi:10.1046/j.1467-2494.2002.00137.x.
143. Hruza, L. L. & Pentland, A. P. Mechanisms Of UV-Induced Inflammation. *J. Invest. Dermatol.* **100**, 35S-41S (1993) doi:10.1111/1523-1747.ep12355240.
144. Shaath. *Sunscreens*. *Taylor And Francis* (CRC Press, 2005). doi:10.1201/b14170.
145. Herzog, B., Wehrle, M. & Quass, K. Photostability Of UV Absorber Systems In Sunscreens. *Photochem. Photobiol.* **85**, 869–878 (2009) doi:10.1111/j.1751-1097.2009.00544.x.
146. Danovaro, R., Bongiorni, L., Corinaldesi, C., Giovannelli, D., Damiani, E., Astolfi, P., Greci, L. & Pusceddu, A. Sunscreens Cause Coral Bleaching By Promoting Viral

Infections. *Environ. Health Perspect.* **116**, 441–447 (2008) doi:10.1289/ehp.10966.
147. Fong, H. C. H., Ho, J. C. H., Cheung, A. H. Y., Lai, K. P. & Tse, W. K. F. Developmental Toxicity Of The Common UV Filter, Benophenone-2, In Zebrafish Embryos. *Chemosphere* **164**, 413–420 (2016) doi:10.1016/j.chemosphere.2016.08.073.
148. Gilbert, E., Pirot, F., Bertholle, V., Roussel, L., Falson, F. & Padois, K. Commonly Used UV Filter Toxicity On Biological Functions: Review Of Last Decade Studies. *Int. J. Cosmet. Sci.* **35**, 208–219 (2013) doi:10.1111/ics.12030.
149. Ruszkiewicz, J. A., Pinkas, A., Ferrer, B., Peres, T. V., Tsatsakis, A. & Aschner, M. Neurotoxic Effect Of Active Ingredients In Sunscreen Products, A Contemporary Review. *Toxicol. Reports* **4**, 245–259 (2017) doi:10.1016/j.toxrep.2017.05.006.
150. van Es, D. S., Marinkovic, S., Oduber, X. & Estrine, B. Use Of Furandicarboxylic Acid And Its Decyl Ester As Additives In The Fischer's Glycosylation Of Decanol By D-Glucose: Physicochemical Properties Of The Surfactant Compositions Obtained. *J. Surfactants Deterg.* **16**, 147–154 (2013) doi:10.1007/s11743-012-1382-8.
151. Okada, M., Tachikawa, K. & Aoi, K. Biodegradable Polymers Based On Renewable Resources. II. Synthesis And Biodegradability Of Polyesters Containing Furan Rings. *J. Polym. Sci. Part A Polym. Chem.* **35**, 2729–2737 (1997) doi:10.1002/(SICI)1099-0518(19970930)35:13<2729::AID-POLA18>3.0.CO;2-D.
152. Behr, D., Brandänge, S., Lindström, B., Enzell, C. R. & Swahn, C.-G. Synthesis Of Some Aryl Alpha-Diketones And Aryl Glyoxylic Acid Derivatives By Acylation Of Electron-Rich Aromatics. *Acta Chemica Scandinavica* vol. 27 2411–2414 (1973) doi:10.3891/acta.chem.scand.27-2411.
153. Bush, R. D., Bissett, D. L. & Chatterjee, R. Chelator Compositions Comprising Oxime Compounds. (1994) Available at: https://bit.ly/3gc5Slw (Accessed: 1 May 2020) Patent Number: *USOO5364617A*.
154. Boethling, R. S., Sommer, E. & DiFiore, D. Designing Small Molecules For Biodegradability. *Chem. Rev.* **107**, 2207–2227 (2007) doi:10.1021/cr050952t.
155. Lasseuguette, E., Gandini, A. & Timpe, H.-J. Photoreactive Furan Derivatives. *J. Photochem. Photobiol. A Chem.* **174**, 222–228 (2005) doi:10.1016/j.jphotochem.2005.03.012.
156. Waig Fang, S., Joachim Timpe, H. & Gandini, A. Photocrosslinkable Polymers Bearing Pendant Conjugated Heterocyclic Chromophores. *Polymer (Guildf).* **43**, 3505–3510 (2002) doi:10.1016/S0032-3861(02)00072-1.
157. Lasseuguette, E., Gandini, A., Belgacem, M. N. & Timpe, H.-J. Synthesis, Characterization And Photocross-Linking Of Copolymers Of Furan And Aliphatic Hydroxyethylesters Prepared By Transesterification. *Polymer (Guildf).* **46**, 5476–5483 (2005) doi:10.1016/j.polymer.2005.05.032.
158. Cáceres, T., Encinas, M. V. & Lissi, E. A. Photocleavage Of Benzil. *J. Photochem.* **27**, 109–114 (1984) doi:10.1016/0047-2670(84)87075-6.
159. McGimpsey, W. G. & Scaiano, J. C. A Two-Photon Study Of The "Reluctant" Norrish Type I Reaction Of Benzil. *J. Am. Chem. Soc.* **109**, 2179–2181 (1987) doi:10.1021/ja00241a045.
160. Herzog, B., Hüglin, D., Borsos, E., Stehlin, A. & Luther, H. New UV Absorbers For Cosmetic Sunscreens – A Breakthrough For The Photoprotection Of Human Skin. *Chim. Int. J. Chem.* **58**, 554–559 (2004) doi:10.2533/000942904777677632.
161. Künkel, A., Becker, J., Börger, L., Hamprecht, J., Koltzenburg, S., Loos, R., Schick, M. B., Schlegel, K., Sinkel, C., Skupin, G. & Yamamoto, M. Polymers, Biodegradable. In

Ullmann's Encyclopedia Of Industrial Chemistry 1–29 (Wiley-VCH Verlag GmbH & Co. KGaA, 2016). doi:10.1002/14356007.n21_n01.pub2.
162. Díaz, E., Ferrández, A., Prieto, M. A. & García, J. L. Biodegradation Of Aromatic Compounds By Escherichia Coli. *Microbiol. Mol. Biol. Rev.* **65**, 523–569 (2001) doi:10.1128/MMBR.65.4.523-569.2001.
163. Yoshida, S., Hiraga, K., Takehana, T., Taniguchi, I., Yamaji, H., Maeda, Y., Toyohara, K., Miyamoto, K., Kimura, Y. & Oda, K. A Bacterium That Degrades And Assimilates Poly(Ethylene Terephthalate). *Science (80-.).* **351**, 1196–1199 (2016) doi:10.1126/science.aad6359.
164. Downs, C. A., Kramarsky-Winter, E., Fauth, J. E., Segal, R., Bronstein, O., Jeger, R., Lichtenfeld, Y., Woodley, C. M., Pennington, P., Kushmaro, A. & Loya, Y. Toxicological Effects Of The Sunscreen UV Filter, Benzophenone-2, On Planulae And In Vitro Cells Of The Coral, Stylophora Pistillata. *Ecotoxicology* **23**, 175–191 (2014) doi:10.1007/s10646-013-1161-y.
165. Horbury, M. D., Holt, E. L., Mouterde, L. M. M., Balaguer, P., Cebrián, J., Blasco, L., Allais, F. & Stavros, V. G. Towards Symmetry Driven And Nature Inspired UV Filter Design. *Nat. Commun.* **10**, 1–8 (2019) doi:10.1038/s41467-019-12719-z.
166. Peyrot, C., Mention, M. M., Brunissen, F., Balaguer, P. & Allais, F. Innovative Bio-Based Organic UV-A And Blue Light Filters From Meldrum's Acid. *Molecules* **25**, 1–15 (2020) doi:10.3390/molecules25092178.
167. Gandini, A., Lacerda, T. M., Carvalho, A. J. F. & Trovatti, E. Progress Of Polymers From Renewable Resources: Furans, Vegetable Oils, And Polysaccharides. *Chem. Rev.* **116**, 1637–1669 (2016) doi:10.1021/acs.chemrev.5b00264.
168. Fertier, L., Koleilat, H., Stemmelen, M., Giani, O., Joly-Duhamel, C., Lapinte, V. & Robin, J.-J. The Use Of Renewable Feedstock In UV-Curable Materials – A New Age For Polymers And Green Chemistry. *Prog. Polym. Sci.* **38**, 932–962 (2013) doi:10.1016/j.progpolymsci.2012.12.002.
169. Mendes-Felipe, C., Oliveira, J., Etxebarria, I., Vilas-Vilela, J. L. & Lanceros-Mendez, S. State-Of-The-Art And Future Challenges Of UV Curable Polymer-Based Smart Materials For Printing Technologies. *Adv. Mater. Technol.* **4**, 1–16 (2019) doi:10.1002/admt.201800618.
170. Zhang, J. & Xiao, P. 3D Printing Of Photopolymers. *Polym. Chem.* **9**, 1530–1540 (2018) doi:10.1039/C8PY00157J.
171. Thi, T. H., Matsusaki, M. & Akashi, M. Development Of Photoreactive Degradable Branched Polyesters With High Thermal And Mechanical Properties. *Biomacromolecules* **10**, 766–772 (2009) doi:10.1021/bm801203g.
172. Wu, L., Jin, C. & Sun, X. Synthesis, Properties, And Light-Induced Shape Memory Effect Of Multiblock Polyesterurethanes Containing Biodegradable Segments And Pendant Cinnamamide Groups. *Biomacromolecules* **12**, 235–241 (2011) doi:10.1021/bm1012162.
173. Jasinski, F., Rannée, A., Schweitzer, J., Fischer, D., Lobry, E., Croutxé-Barghorn, C., Schmutz, M., Le Nouen, D., Criqui, A. & Chemtob, A. Thiol–Ene Linear Step-Growth Photopolymerization In Miniemulsion: Fast Rates, Redox-Responsive Particles, And Semicrystalline Films. *Macromolecules* **49**, 1143–1153 (2016) doi:10.1021/acs.macromol.5b02512.
174. Lawrie, K., Blakey, I., Blinco, J., Gronheid, R., Jack, K., Pollentier, I., Leeson, M. J., Younkin, T. R. & Whittaker, A. K. Extreme Ultraviolet (EUV) Degradation Of

Poly(Olefin Sulfone)S: Towards Applications As EUV Photoresists. *Radiat. Phys. Chem.* **80**, 236–241 (2011) doi:10.1016/j.radphyschem.2010.07.038.

175. Fonseca, A. C., Lima, M. S., Sousa, A. F., Silvestre, A. J., Coelho, J. F. J. & Serra, A. C. Cinnamic Acid Derivatives As Promising Building Blocks For Advanced Polymers: Synthesis, Properties And Applications. *Polym. Chem.* **10**, 1696–1723 (2019) doi:10.1039/C9PY00121B.
176. Perkin, W. H. XI.—On The Formation Of Coumarin And Of Cinnamic And Of Other Analogous Acids From The Aromatic Aldehydes. *J. Chem. Soc.* **31**, 388–427 (1877) doi:10.1039/JS8773100388.
177. Nguyen, H. T. H., Reis, M. H., Qi, P. & Miller, S. A. Polyethylene Ferulate (PEF) And Congeners: Polystyrene Mimics Derived From Biorenewable Aromatics. *Green Chem.* **17**, 4512–4517 (2015) doi:10.1039/C5GC01104C.
178. Rao, B. S. & Palanisamy, A. Synthesis Of Bio Based Low Temperature Curable Liquid Epoxy, Benzoxazine Monomer System From Cardanol: Thermal And Viscoelastic Properties. *Eur. Polym. J.* **49**, 2365–2376 (2013) doi:10.1016/j.eurpolymj.2013.05.029.
179. Zhao, S. & Abu-Omar, M. M. Renewable Epoxy Networks Derived From Lignin-Based Monomers: Effect Of Cross-Linking Density. *ACS Sustain. Chem. Eng.* **4**, 6082–6089 (2016) doi:10.1021/acssuschemeng.6b01446.
180. Durand, P. L., Grau, E. & Cramail, H. Bio-Based Thermo-Reversible Aliphatic Polycarbonate Network. *Molecules* **25**, (2020) doi:10.3390/molecules25010074.
181. Sousa, A. F., Fonseca, A. C., Serra, A. C., Freire, C. S. R., Silvestre, A. J. D. & Coelho, J. F. J. New Unsaturated Copolyesters Based On 2,5-Furandicarboxylic Acid And Their Crosslinked Derivatives. *Polym. Chem.* **7**, 1049–1058 (2016) doi:10.1039/C5PY01702E.
182. Fonseca, A. C., Lopes, I. M., Coelho, J. F. J. & Serra, A. C. Synthesis Of Unsaturated Polyesters Based On Renewable Monomers: Structure/Properties Relationship And Crosslinking With 2-Hydroxyethyl Methacrylate. *React. Funct. Polym.* **97**, 1–11 (2015) doi:10.1016/j.reactfunctpolym.2015.10.002.
183. Gandini, A., Fang, S. W., Timpe, H.-J. & Baumann, H. Acetal Copolymers And Use Thereof In Photosensitive Compositions. (2001) Available at: https://bit.ly/3gdSKfR (Accessed: 1 May 2020) Patent Number: *US6270938B1*.
184. Liebert, T. F. & Heinze, T. Tailored Cellulose Esters: Synthesis And Structure Determination. *Biomacromolecules* **6**, 333–340 (2005) doi:10.1021/bm049532o.
185. Lange, J., Davidenko, N., Rieumont, J. & Sastre, R. Study Of Network Formation In Furfuryl Methacrylate Photopolymerisation At Different Temperatures. The Tobita Method Applied To The Polymerisation At Low Conversions. *Polymer (Guildf).* **43**, 1003–1011 (2002) doi:10.1016/S0032-3861(01)00619-X.
186. Zhang, Z., Yuan, Z., Tang, D., Ren, Y., Lv, K. & Liu, B. Iron Oxide Encapsulated By Ruthenium Hydroxyapatite As Heterogeneous Catalyst For The Synthesis Of 2,5-Diformylfuran. *ChemSusChem* **7**, 3496–3504 (2014) doi:10.1002/cssc.201402402.
187. Serum, E. M., Selvakumar, S., Zimmermann, N. & Sibi, M. P. Valorization Of 2,5-Furandicarboxylic Acid. Diels–Alder Reactions With Benzyne. *Green Chem.* **20**, 1448–1454 (2018) doi:10.1039/C8GC00308D.
188. Jia, X., Ma, J., Wang, M., Du, Z., Lu, F., Wang, F. & Xu, J. Promoted Role Of Cu(NO3)2 On Aerobic Oxidation Of 5-Hydroxymethylfurfural To 2,5-Diformylfuran Over VOSO4. *Appl. Catal. A Gen.* **482**, 231–236 (2014) doi:10.1016/j.apcata.2014.05.031.

189. Cooper, W. F. & Nuttall, W. H. CCVIII.—The Condensation Of Furan–2 : 5-Dialdehyde With Malonic Ester And Malonic Acid. *J. Chem. Soc., Trans.* **105**, 2218–2226 (1914) doi:10.1039/CT9140502218.
190. Richter, D. T. & Lash, T. D. Oxidation With Dilute Aqueous Ferric Chloride Solutions Greatly Improves Yields In The '4+1' Synthesis Of Sapphyrins. *Tetrahedron Lett.* **40**, 6735–6738 (1999) doi:10.1016/S0040-4039(99)01352-0.
191. Hui, Z. & Gandini, A. Polymeric Schiff Bases Bearing Furan Moieties. *Eur. Polym. J.* **28**, 1461–1469 (1992) doi:10.1016/0014-3057(92)90135-O.
192. Dutta, S., Wu, L. & Mascal, M. Production Of 5-(Chloromethyl)Furan-2-Carbonyl Chloride And Furan-2,5-Dicarbonyl Chloride From Biomass-Derived 5-(Chloromethyl)Furfural (CMF). *Green Chem.* **17**, 3737–3739 (2015) doi:10.1039/C5GC00936G.
193. Hopkins, K. T., Wilson, W. D., Bender, B. C., McCurdy, D. R., Hall, J. E., Tidwell, R. R., Kumar, A., Bajic, M. & Boykin, D. W. Extended Aromatic Furan Amidino Derivatives As Anti- Pneumocystis Carinii Agents. *J. Med. Chem.* **41**, 3872–3878 (1998) doi:10.1021/jm980230c.
194. Gaines, T., Garcia, F., Virani, S., Liang, Z., Yoon, Y., Oum, Y. H., Shim, H. & Mooring, S. R. Synthesis And Evaluation Of 2,5-Furan, 2,5-Thiophene And 3,4-Thiophene-Based Derivatives As CXCR4 Inhibitors. *Eur. J. Med. Chem.* **181**, 111562 (2019) doi:10.1016/j.ejmech.2019.111562.
195. Kucherov, F. A., Galkin, K. I., Gordeev, E. G. & Ananikov, V. P. Efficient Route For The Construction Of Polycyclic Systems From Bioderived HMF. *Green Chem.* **19**, 4858–4864 (2017) doi:10.1039/c7gc02211e.
196. Ke, Q., Jin, Y., Ruan, F., Ha, M. N., Li, D., Cui, P., Cao, Y., Wang, H., Wang, T., Nguyen, V. N., Han, X., Wang, X. & Cui, P. Boosting The Activity Of Catalytic Oxidation Of 5-Hydroxymethylfurfural To 2,5-Diformylfuran Over Nitrogen-Doped Manganese Oxide Catalysts. *Green Chem.* **21**, 4313–4318 (2019) doi:10.1039/C9GC01041F.
197. Wang, Q., Hou, W., Meng, T., Hou, Q., Zhou, Y. & Wang, J. Direct Synthesis Of 2,5-Diformylfuran From Carbohydrates Via Carbonizing Polyoxometalate Based Mesoporous Poly(Ionic Liquid). *Catal. Today* **319**, 57–65 (2019) doi:10.1016/j.cattod.2018.07.042.
198. Vidal, S. Safety First: A Recent Case Of A Dichloromethane Injection Injury. *ACS Cent. Sci.* **6**, 83–86 (2020) doi:10.1021/acscentsci.0c00100.
199. Hayashi, E., Yamaguchi, Y., Kamata, K., Tsunoda, N., Kumagai, Y., Oba, F. & Hara, M. Effect Of MnO 2 Crystal Structure On Aerobic Oxidation Of 5-Hydroxymethylfurfural To 2,5-Furandicarboxylic Acid. *J. Am. Chem. Soc.* **141**, 890–900 (2019) doi:10.1021/jacs.8b09917.
200. Hayashi, E., Komanoya, T., Kamata, K. & Hara, M. Heterogeneously-Catalyzed Aerobic Oxidation Of 5-Hydroxymethylfurfural To 2,5-Furandicarboxylic Acid With MnO 2. *ChemSusChem* **10**, 654–658 (2017) doi:10.1002/cssc.201601443.
201. Khrouf, A., Abid, M., Boufi, S., Gharbi, R. El & Gandini, A. Polyesters Bearing Furan Moieties, 2. A Detailed Investigation Of The Polytransesterification Of Difuranic Diesters With Different Diols. *Macromol. Chem. Phys.* **199**, 2755–2765 (1998) doi:10.1002/macp.1998.021991219.
202. Rossi, B., Prosperini, S., Pastori, N., Clerici, A. & Punta, C. New Advances In Titanium-Mediated Free Radical Reactions. *Molecules* **17**, 14700–14732 (2012) doi:10.3390/molecules171214700.

203. Versace, D. L., Soppera, O., Lalevée, J. & Croutxé-Barghorn, C. Influence Of Zirconium Propoxide On The Radical Induced Photopolymerisation Of Hybrid Sol-Gel Materials. *New J. Chem.* **32**, 2270–2278 (2008) doi:10.1039/b806056h.
204. Muñoz-Guerra, S., Lavilla, C., Japu, C. & Martínez de Ilarduya, A. Renewable Terephthalate Polyesters From Carbohydrate-Based Bicyclic Monomers. *Green Chem.* **16**, 1716–1739 (2014) doi:10.1039/C3GC42394H.
205. Pellis, A., Comerford, J. W., Weinberger, S., Guebitz, G. M., Clark, J. H. & Farmer, T. J. Enzymatic Synthesis Of Lignin Derivable Pyridine Based Polyesters For The Substitution Of Petroleum Derived Plastics. *Nat. Commun.* **10**, 1762 (2019) doi:10.1038/s41467-019-09817-3.
206. Vastano, M., Pellis, A., Botelho Machado, C., Simister, R., McQueen-Mason, S. J., Farmer, T. J. & Gomez, L. D. Sustainable Galactarate-Based Polymers: Multi-Enzymatic Production Of Pectin-Derived Polyesters. *Macromol. Rapid Commun.* **1900361**, 1–10 (2019) doi:10.1002/marc.201900361.
207. Fodor, C., Golkaram, M., Woortman, A. J. J., van Dijken, J. & Loos, K. Enzymatic Approach For The Synthesis Of Biobased Aromatic–Aliphatic Oligo-/Polyesters. *Polym. Chem.* **8**, 6795–6805 (2017) doi:10.1039/C7PY01559C.
208. Raza, S., Fransson, L. & Hult, K. Enantioselectivity In Candida Antarctica Lipase B: A Molecular Dynamics Study. *Protein Sci.* **10**, 329–338 (2001) doi:10.1110/ps.33901.
209. Pellis, A., Guarneri, A., Brandauer, M., Acero, E. H., Peerlings, H., Gardossi, L. & Guebitz, G. M. Exploring Mild Enzymatic Sustainable Routes For The Synthesis Of Bio-Degradable Aromatic-Aliphatic Oligoesters. *Biotechnol. J.* **11**, 642–647 (2016) doi:10.1002/biot.201500544.
210. Jiang, Y., Woortman, A. J. J., Alberda van Ekenstein, G. O. R. & Loos, K. A Biocatalytic Approach Towards Sustainable Furanic–Aliphatic Polyesters. *Polym. Chem.* **6**, 5198–5211 (2015) doi:10.1039/C5PY00629E.
211. Pellis, A., Comerford, J. W., Maneffa, A. J., Sipponen, M. H., Clark, J. H. & Farmer, T. J. Elucidating Enzymatic Polymerisations: Chain-Length Selectivity Of Candida Antarctica Lipase B Towards Various Aliphatic Diols And Dicarboxylic Acid Diesters. *Eur. Polym. J.* **106**, 79–84 (2018) doi:10.1016/j.eurpolymj.2018.07.009.
212. Chae, B., Lee, S. W., Kim, S. Bin, Lee, B. & Ree, M. Photoreaction And Molecular Reorientation In Films Of Novel Photosensitive Polyesters Containing N -Alkyl Side Groups And 1,4-Phenylenediacryloyl Units In The Backbone. *Langmuir* **19**, 6039–6049 (2003) doi:10.1021/la0340596.
213. Chung, C., Roh, Y., Cho, S. & Kim, J. Crack Healing In Polymeric Materials Via Photochemical [2 + 2] Cycloaddition. *Chem. Mater.* **16**, 3982–3984 (2004) doi:10.1021/cm049394+.
214. Sonoda, Y. Solid-State [2+2] Photodimerization And Photopolymerization Of α,ω-Diarylpolyene Monomers: Effective Utilization Of Noncovalent Intermolecular Interactions In Crystals. *Molecules* **16**, 119–148 (2011) doi:10.3390/molecules16010119.
215. Skloss, T. W. & Haw, J. F. Detection Of Cross-Link Formation By 2 + 2 Photocycloaddition In Poly(Vinyl Cinnamate) By 13C Solid-State NMR. *Macromolecules* **27**, 6998–6999 (1994) doi:10.1021/ma00101a046.
216. Jang, N. R., Kim, H. R., Hou, C. T. & Kim, B. S. Novel Biobased Photo-Crosslinked Polymer Networks Prepared From Vegetable Oil And 2,5-Furan Diacrylate. *Polym. Adv. Technol.* **24**, 814–818 (2013) doi:10.1002/pat.3147.

217. Mills, I., Cvita, T., Homann, K., Kallay, N. & Kozokuchitsu, K. *IUPAC Gren Book*. (Blackwell Science, 1993).
218. Holmberg, K. Surfactants. In *Ullmann's Encyclopedia Of Industrial Chemistry* vol. 16 1–56 (Wiley-VCH Verlag GmbH & Co. KGaA, 2019). doi:10.1002/14356007.a25_747.pub2.
219. Kosswig, K. Surfactants. In *Ullmann's Encyclopedia Of Industrial Chemistry* vol. 16 45–67 (Wiley-VCH Verlag GmbH & Co. KGaA, 2012). doi:10.1002/14356007.a25_747.
220. Kronberg, B., Castas, M. & Silvestonti, R. Understanding The Hydrophobic Effect. *J. Dispers. Sci. Technol.* **15**, 333–351 (1994) doi:10.1080/01932699408943561.
221. Nakama, Y. Surfactants. In *Cosmetic Science And Technology* 231–244 (Elsevier, 2017). doi:10.1016/B978-0-12-802005-0.00015-X.
222. Castle, R. L. *The Utilisation Of Bio-Platform Molecules In The Green Synthesis Of Renewable Surfactants*. (2016) Available at: https://bit.ly/33ubNgH (Accessed: 1 May 2020).
223. Yang, J. *Hair Care Cosmetics*. *Cosmetic Science And Technology: Theoretical Principles And Applications* (Elsevier Inc., 2017). doi:10.1016/B978-0-12-802005-0.00036-7.
224. Showell, M. *Handbook Of Detergents, Part D Formulation*. (Taylor and Francis Inc., 2006). doi:10.1201/9781420028713.
225. Foster, N. C. *Sulfonation And Sulfation Processes*. *Chemithon* (1997) Available at: https://bit.ly/3hOwV76 (Accessed: 29 July 2020).
226. Torres Ortega, J. A. Sulfonation/Sulfation Processing Technology For Anionic Surfactant Manufacture. *Adv. Chem. Eng.* (2012) doi:10.5772/32077.
227. Dado, G. & Bernhardt, R. Sulfonation And Sulfation. In *Kirk-Othmer Encyclopedia Of Chemical Technology* 1–30 (John Wiley & Sons, Inc., 2017). doi:10.1002/0471238961.1921120611140107.a01.pub3.
228. Cupery, M. E. Sulfamic Acid A New Industrial Chemical. *Ind. Eng. Chem.* **30**, 627–631 (1938) doi:10.1021/ie50342a005.
229. Malkemus, J. D., Allendale, J. R. & Potter, J. D. Catalyzed Sulfamic Acid Sulfation. (1946) Available at: https://bit.ly/3gbqRFg (Accessed: 1 May 2020) Patent Number: *US2452943A*.
230. Benson, G. A. & Spillane, W. J. Sulfamic Acid And Its N-Substituted Derivatives. *Chem. Rev.* **80**, 151–186 (1980) doi:10.1021/cr60324a002.
231. Flitsch, S. & Guilbert, B. Regioselective Sulfation. (1999) Available at: https://bit.ly/30SuNUY (Accessed: 1 May 2020) Patent Number: *US5874548A*.
232. Al-Horani, R. A. & Desai, U. R. Chemical Sulfation Of Small Molecules—Advances And Challenges. *Tetrahedron* **66**, 2907–2918 (2010) doi:10.1016/j.tet.2010.02.015.
233. Schrickel, J. Sulfur Trioxide Amine Complexes: Versatile Reagents In Organic Synthesis. *RSC Symp. Berlin* (2010).
234. Lavergne, A., Zhu, Y., Pizzino, A., Molinier, V. & Aubry, J.-M. Synthesis And Foaming Properties Of New Anionic Surfactants Based On A Renewable Building Block: Sodium Dodecyl Isosorbide Sulfates. *J. Colloid Interface Sci.* **360**, 645–653 (2011) doi:10.1016/j.jcis.2011.04.110.
235. Wang, Z. Strecker Reaction. In *Comprehensive Organic Name Reactions And Reagents* 2707–2709 (John Wiley & Sons, Inc., 2010). doi:10.1002/9780470638859.conrr608.
236. Gilbert, E. E. *Sulfonation And Related Reactions*. (R. E. Krieger Publishing Company,

1977).
237. Tomanová, M., Jedinák, L. & Cankař, P. Reductive Dehalogenation And Dehalogenative Sulfonation Of Phenols And Heteroaromatics With Sodium Sulfite In An Aqueous Medium. *Green Chem.* **21**, 2621–2628 (2019) doi:10.1039/C9GC00467J.
238. Gassama, A., Ernenwein, C., Youssef, A., Agach, M., Riguet, E., Marinković, S., Estrine, B. & Hoffmann, N. Sulfonated Surfactants Obtained From Furfural. *Green Chem.* **15**, 1558 (2013) doi:10.1039/c3gc00062a.
239. Deepika & Tyagi, V. K. Sulfosuccinates As Mild Surfactants. *J. Oleo Sci.* **55**, 429–439 (2006) doi:10.5650/jos.55.429.
240. Singh, V. & Tyagi, R. Surface And Aggregation Properties Of Synthesized Cetyl Alcohol Based Bis-Sulfosuccinate Gemini Surfactants In Aqueous Solution. *J. Surfactants Deterg.* **19**, 111–118 (2016) doi:10.1007/s11743-015-1759-6.
241. Adewuyi, A., Adesina, A. D. & Oderinde, R. A. Synthesis Of Disodium Salt Of Sulfosuccinate Monoester From The Seed Oil Of Terminalia Catappa And Its Inhibitive Effect On The Corrosion Of Aluminum Sheet In 1 M HCl . *Adv. Chem.* **2014**, 1–7 (2014) doi:10.1155/2014/896965.
242. Eyck, R. Ten & Danishefsky, I. The Addition Of Bisulfite To Unsaturated Acids And Their Derivatives. *J. Org. Chem.* **16**, 1683–1689 (1951) doi:10.1021/jo50005a004.
243. Robert, T. & Friebel, S. Itaconic Acid – A Versatile Building Block For Renewable Polyesters With Enhanced Functionality. *Green Chem.* **18**, 2922–2934 (2016) doi:10.1039/C6GC00605A.
244. Berglung, R. A. Purification Of Carboxaldehyde. vol. 47905 1–7 (2001) Available at: https://bit.ly/2X2omh1 (Accessed: 1 May 2020) Patent Number: *EP 1 075 480 B1*.
245. Kraus, G. A. & Lee, J. J. A Direct Synthesis Of Renewable Sulfonate-Based Surfactants. *J. Surfactants Deterg.* **16**, 317–320 (2013) doi:10.1007/s11743-012-1408-2.
246. Tropsch, J. G. A Journey To Standardization Of Bio-Based Surfactants In Europe. *Informmagazine* (2017).
247. Niikura, F., Omine, M., Kimura, Y., Konta, H., Kageyama, M., Tobori, N. & Araki, K. Coloration Process In The Sulfonation Of Fatty Acid Methyl Ester With Sulfur Trioxide. *JAOCS, J. Am. Oil Chem. Soc.* **90**, 903–909 (2013) doi:10.1007/s11746-013-2233-0.
248. Tobori, N. & Kakui, T. *Methyl Ester Sulfonate*. *Biobased Surfactants* (Elsevier Inc., 2019). doi:10.1016/b978-0-12-812705-6.00009-5.
249. Research, G. view. Fatty Methyl Ester Sulfonate Market Size, Share & Trends Analysis By End-Use (Personal Care, Detergents), By Region, Competitive Landscape, And Segment Forecasts, 2018 - 2025. (2017).
250. Hayes, D. G. & Smith, G. A. *Biobased Surfactants: Overview And Industrial State Of The Art*. *Biobased Surfactants* (Elsevier Inc., 2019). doi:10.1016/b978-0-12-812705-6.00001-0.
251. Scully, J. F. & Brown, E. V. The Sulfonation Of Furan And Furan Homologs. Preparation Of Furansulfonamides. *J. Org. Chem.* **19**, 894–901 (1954) doi:10.1021/jo01371a003.
252. Krumm, C., Joseph, K., Park, D. S., Dauenhauer, P. J. & Mahanthappa, M. Aromatic Surfactant. (2017) Available at: https://bit.ly/3hKF8Jp (Accessed: 1 May 2020) Patent Number: *WO2017/079719AI*.
253. West, R., Wu, R. & Silks III, L. A. Furan Based Composition. (2015) Available at: https://bit.ly/2P2aPSe (Accessed: 1 May 2020) Patent Number: *WO 2015/084813 AI*

11.
254. OECD. *Test No. 301: Ready Biodegradability*. (OECD, 1992). doi:10.1787/9789264070349-en.
255. Kipshagen, L., Vömel, L. T., Liauw, M. A., Klemmer, A., Schulz, A., Kropf, C., Hausoul, P. J. C. & Palkovits, R. Anionic Surfactants Based On Intermediates Of Carbohydrate Conversion. *Green Chem.* **21**, 3882–3890 (2019) doi:10.1039/C9GC01163C.
256. Galkin, K. I., Krivodaeva, E. A., Romashov, L. V., Zalesskiy, S. S., Kachala, V. V., Burykina, J. V. & Ananikov, V. P. Critical Influence Of 5-Hydroxymethylfurfural Aging And Decomposition On The Utility Of Biomass Conversion In Organic Synthesis. *Angew. Chemie Int. Ed.* **55**, 8338–8342 (2016) doi:10.1002/anie.201602883.
257. Ötles, S. & Pire, R. Fatty Acid Composition Of Chlorella And Spirulina.Pdf. *J. AOAC Int.* **84**, 1708–1714 (2001).
258. Colla, L. M., Bertolin, T. E. & Costa, J. A. V. Fatty Acids Profile Of Spirulina Platensis Grown Under Different Temperatures And Nitrogen Concentrations. *Zeitschrift Für Naturforsch. C* **59**, 55–59 (2004) doi:10.1515/znc-2004-1-212.
259. Tan, X., Wang, Y., Liu, Y., Wang, F., Shi, L., Lee, K.-H., Lin, Z., Lv, H. & Zhang, X. Highly Efficient Tetradentate Ruthenium Catalyst For Ester Reduction: Especially For Hydrogenation Of Fatty Acid Esters. *Org. Lett.* **17**, 454–457 (2015) doi:10.1021/ol503456j.
260. Takeda, Y., Nakagawa, Y. & Tomishige, K. Selective Hydrogenation Of Higher Saturated Carboxylic Acids To Alcohols Using A ReOx–Pd/SiO2 Catalyst. *Catal. Sci. Technol.* **2**, 2221 (2012) doi:10.1039/c2cy20302b.
261. Rozmysłowicz, B., Kirilin, A., Aho, A., Manyar, H., Hardacre, C., Wärnå, J., Salmi, T. & Murzin, D. Y. Selective Hydrogenation Of Fatty Acids To Alcohols Over Highly Dispersed ReO X /TiO 2 Catalyst. *J. Catal.* **328**, 197–207 (2015) doi:10.1016/j.jcat.2015.01.003.
262. Lin, H. & Lee, Y. K. Genetic Engineering Of Medium-Chain-Length Fatty Acid Synthesis In Dunaliella Tertiolecta For Improved Biodiesel Production. *J. Appl. Phycol.* **29**, 2811–2819 (2017) doi:10.1007/s10811-017-1210-7.
263. Krafft Point. In *IUPAC Compendium Of Chemical Terminology* (IUPAC). doi:10.1351/goldbook.K03415.
264. Al-Soufi, W., Piñeiro, L. & Novo, M. A Model For Monomer And Micellar Concentrations In Surfactant Solutions: Application To Conductivity, NMR, Diffusion, And Surface Tension Data. *J. Colloid Interface Sci.* **370**, 102–110 (2012) doi:10.1016/j.jcis.2011.12.037.
265. Hoffmann, H. & Ulbricht, W. The Formation Of Micelles. *Thermodyn. Data Biochem. Biotechnol.* **c**, 297–348 (1986) doi:10.1007/978-3-642-71114-5_12.
266. Yorkshire Water. Available at: https://bit.ly/2P5x3Td (Accessed: 18 May 2020).
267. Thames Water. (2020) Available at: https://bit.ly/2X59zlu (Accessed: 18 May 2020).
268. Thakur, V. K. & Kessler, M. R. *Green Biorenewable Biocomposites*. (Apple Academic Press, 2016). doi:10.1201/b18092.
269. IARC. *Atrazine*. *IARC Monographs* vol. 1990 (1997) Available at: https://bit.ly/2X7c3zY (Accessed: 15 May 2020).
270. Vallette, J. & Stamm, R. *N-Methylpyrrolidone (NMP) Technical Report On Production, Imports, Use, End Of Life, And Associated Environmental And Human Health Hazards.* (2017) Available at: https://bit.ly/39BAJFM (Accessed: 15 May 2020).

271. N/A. Acetonitrile: Global Market Trends, Share, Size, Growth, Opportunity And Forecast (2019-2024). (2019) Available at: https://prn.to/2BDl0JI (Accessed: 21 January 2020).
272. N/A. Research Report On China's Glyphosate Industry (2018-2022). Available at: https://prn.to/3gcgFw6 (Accessed: 21 January 2020).
273. Appl, M. Ammonia. In *Ullmann's Encyclopedia Of Industrial Chemistry* (Wiley-VCH Verlag GmbH & Co. KGaA, 2011). doi:10.1002/14356007.a02_143.pub2.
274. Soloveichik, G. Electrochemical Synthesis Of Ammonia As A Potential Alternative To The Haber–Bosch Process. *Nat. Catal.* **2**, 377–380 (2019) doi:10.1038/s41929-019-0280-0.
275. Brown, T. Ammonia Production Causes 1% Of Total Global GHG Emissions. (2016) Available at: https://bit.ly/2EnJyaC (Accessed: 21 January 2020).
276. Mehta, P., Barboun, P., Herrera, F. A., Kim, J., Rumbach, P., Go, D. B., Hicks, J. C. & Schneider, W. F. Overcoming Ammonia Synthesis Scaling Relations With Plasma-Enabled Catalysis. *Nat. Catal.* **1**, 269–275 (2018) doi:10.1038/s41929-018-0045-1.
277. Han, G.-F., Li, F., Chen, Z.-W., Coppex, C., Kim, S.-J., Noh, H.-J., Fu, Z., Lu, Y., Singh, C. V., Siahrostami, S., Jiang, Q. & Baek, J.-B. Mechanochemistry For Ammonia Synthesis Under Mild Conditions. *Nat. Nanotechnol.* (2020) doi:10.1038/s41565-020-00809-9.
278. Scott, E., Peter, F. & Sanders, J. Biomass In The Manufacture Of Industrial Products—The Use Of Proteins And Amino Acids. *Appl. Microbiol. Biotechnol.* **75**, 751–762 (2007) doi:10.1007/s00253-007-0932-x.
279. Harada, K. Asymmetric Synthesis Of α-Amino-Acids By The Strecker Synthesis. *Nature* **200**, 1201–1201 (1963) doi:10.1038/2001201a0.
280. Zuend, S. J., Coughlin, M. P., Lalonde, M. P. & Jacobsen, E. N. Scaleable Catalytic Asymmetric Strecker Syntheses Of Unnatural α-Amino Acids. *Nature* **461**, 968–970 (2009) doi:10.1038/nature08484.
281. Wendisch, V. F., Jorge, J. M. P., Pérez-García, F. & Sgobba, E. Updates On Industrial Production Of Amino Acids Using Corynebacterium Glutamicum. *World J. Microbiol. Biotechnol.* **32**, 105 (2016) doi:10.1007/s11274-016-2060-1.
282. Hayashi, M., Mizoguchi, H., Ohnishi, J., Mitsuhashi, S., Yonetani, Y., Hashimoto, S. & Ikeda, M. A LeuC Mutation Leading To Increased L-Lysine Production And Rel-Independent Global Expression Changes In Corynebacterium Glutamicum. *Appl. Microbiol. Biotechnol.* **72**, 783–789 (2006) doi:10.1007/s00253-006-0539-7.
283. Zhang, R., Yang, T., Rao, Z., Sun, H., Xu, M., Zhang, X., Xu, Z. & Yang, S. Efficient One-Step Preparation Of γ-Aminobutyric Acid From Glucose Without An Exogenous Cofactor By The Designed Corynebacterium Glutamicum. *Green Chem.* **16**, 4190–4197 (2014) doi:10.1039/C4GC00607K.
284. Sandeaux, J., Sandeaux, R., Gavach, C., Grib, H., Sadat, T., Belhocine, D. & Mameri, N. Extraction Of Amino Acids From Protein Hydrolysates By Electrodialysis. *J. Chem. Technol. Biotechnol.* **71**, 267–273 (1998) doi:10.1002/(SICI)1097-4660(199803)71:3<267::AID-JCTB835>3.0.CO;2-O.
285. Teng, Y., Scott, E. L., Witte-van Dijk, S. C. M. & Sanders, J. P. M. Simultaneous And Selective Decarboxylation Of L-Serine And Deamination Of L-Phenylalanine In An Amino Acid Mixture—A Means Of Separating Amino Acids For Synthesizing Biobased Chemicals. *N. Biotechnol.* **33**, 171–178 (2016) doi:10.1016/j.nbt.2015.04.006.
286. Teng, Y., Scott, E. L. & Sanders, J. P. M. Separation Of L-Aspartic Acid And L-Glutamic Acid Mixtures For Use In The Production Of Bio-Based Chemicals. *J. Chem. Technol.*

Biotechnol. **87**, 1458–1465 (2012) doi:10.1002/jctb.3769.
287. Teng, Y., Scott, E. L. & Sanders, J. P. M. The Selective Conversion Of Glutamic Acid In Amino Acid Mixtures Using Glutamate Decarboxylase-A Means Of Separating Amino Acids For Synthesizing Biobased Chemicals. *Biotechnol. Prog.* **30**, 681–688 (2014) doi:10.1002/btpr.1895.
288. Elisseeva, T. V., Shaposhnik, V. A. & Luschik, I. G. Demineralization And Separation Of Amino Acids By Electrodialysis With Ion-Exchange Membranes. *Desalination* **149**, 405–409 (2002) doi:10.1016/S0011-9164(02)00763-4.
289. Teng, Y., Scott, E. L., van Zeeland, A. N. T. & Sanders, J. P. M. The Use Of L-Lysine Decarboxylase As A Means To Separate Amino Acids By Electrodialysis. *Green Chem.* **13**, 624 (2011) doi:10.1039/c0gc00611d.
290. Widyarani, Bowden, N. a., Kolfschoten, R. C., Sanders, J. P. M. & Bruins, M. E. Fractional Precipitation Of Amino Acids From Agro-Industrial Residues Using Ethanol. *Ind. Eng. Chem. Res.* **55**, 7462–7472 (2016) doi:10.1021/acs.iecr.6b00054.
291. Kumar, M. B. A., Gao, Y., Shen, W. & He, L. Valorisation Of Protein Waste: An Enzymatic Approach To Make Commodity Chemicals. *Front. Chem. Sci. Eng.* **9**, 295–307 (2015) doi:10.1007/s11705-015-1532-4.
292. Sari, Y. W., Alting, A. C., Floris, R., Sanders, J. P. M. & Bruins, M. E. Glutamic Acid Production From Wheat By-Products Using Enzymatic And Acid Hydrolysis. *Biomass And Bioenergy* **67**, 451–459 (2014) doi:10.1016/j.biombioe.2014.05.018.
293. Metkar, P. S., Scialdone, M. A. & Moloy, K. G. Lysinol: A Renewably Resourced Alternative To Petrochemical Polyamines And Aminoalcohols. *Green Chem.* **16**, 4575–4586 (2014) doi:10.1039/C4GC01167H.
294. Verduyckt, J. & De Vos, D. E. Controlled Defunctionalisation Of Biobased Organic Acids. *Chem. Commun.* **53**, 5682–5693 (2017) doi:10.1039/C7CC01380A.
295. De Schouwer, F., Cuypers, T., Claes, L. & De Vos, D. E. Metal-Catalyzed Reductive Deamination Of Glutamic Acid To Bio-Based Dimethyl Glutarate And Methylamines. *Green Chem.* **19**, 1866–1876 (2017) doi:10.1039/C6GC03222B.
296. Choi, K.-Y. Non-Enzymatic PLP-Dependent Oxidative Deamination Of Amino Acids Induces Higher Alcohol Synthesis. *Biotechnol. Bioprocess Eng.* **20**, 988–994 (2015) doi:10.1007/s12257-015-0434-0.
297. Claes, L., Matthessen, R., Rombouts, I., Stassen, I., De Baerdemaeker, T., Depla, D., Delcour, J. A., Lagrain, B. & De Vos, D. E. Bio-Based Nitriles From The Heterogeneously Catalyzed Oxidative Decarboxylation Of Amino Acids. *ChemSusChem* **8**, 345–352 (2015) doi:10.1002/cssc.201402801.
298. Stevenson, G. W. G. W., Luck, J. M. & Luck, M. J. The Bromodecarboxylation Of Amino Acids: Formation Of Nitriles. *J. Biol. Chem.* **236**, 715–717 (1961).
299. Hashimoto, M., Eda, Y., Osanai, Y., Iwai, T. & Aoki, S. A Novel Decarboxylation Of α-Amino Acids. A Facile Method Of Decarboxylation By The Use Of 2-Cyclohexen-1-One As A Catalyst. *Chem. Lett.* **15**, 893–896 (1986) doi:10.1246/cl.1986.893.
300. Omeis, M., Koehler, G., Neumann, M. & Kuebelbaeck, T. Continuous Process For Decarboxylating Carboxylic Acids. vol. 1 (3 February 2009) Available at: https://bit.ly/3jPAXhe (Accessed: 1 May 2020) Patent Number: *US7485756 B2*.
301. Keisuke, Y., Masafumi, M., Yaegashi, K. & Mikami, M. Process For Preparing Amines. vol. 99 1–10 (29 May 2006) Available at: https://bit.ly/2X2pa5x (Accessed: 1 May 2020) Patent Number: *US 20050222430 A1*.
302. Bellale, E. V., Huddar, S. N., Mahajan, U. S. & Akamanchi, K. G. Oxidative

Decarboxylation Of α-Amino Acids To Nitriles Using O-Iodoxybenzoic Acid In Aqueous Ammonia. *Pure Appl. Chem.* **83**, 607–612 (2011) doi:10.1351/PAC-CON-10-09-15.
303. Dakin, H. D. On The Oxidation Of Amino-Acids And Of Related Substances With Chloramine-T. *Biochem. J.* **11**, 79–95 (1917) doi:10.1042/bj0110079.
304. Friedman, A. H. & Morgulis, S. The Oxidation Of Amino Acids With Sodium Hypobromite. *J. Am. Chem. Soc.* **58**, 909–913 (1936) doi:10.1021/ja01297a017.
305. Norman, M. F. The Oxidation Of Amino-Acids By Hypochlorite. *Biochem. J.* **30**, 484–496 (1936) doi:10.1042/bj0300484.
306. But, A., Le Nôtre, J., Scott, E. L., Wever, R. & Sanders, J. P. M. Selective Oxidative Decarboxylation Of Amino Acids To Produce Industrially Relevant Nitriles By Vanadium Chloroperoxidase. *ChemSusChem* **5**, 1199–1202 (2012) doi:10.1002/cssc.201200098.
307. Xu, X., But, A., Wever, R. & Hollmann, F. Towards Preparative Chemoenzymatic Oxidative Decarboxylation Of Glutamic Acid. *ChemCatChem* **12**, 2180–2183 (2020) doi:10.1002/cctc.201902194.
308. Matthessen, R., Claes, L., Fransaer, J., Binnemans, K. & De Vos, D. E. Decarboxylation Of A Wide Range Of Amino Acids With Electrogenerated Hypobromite. *European J. Org. Chem.* **2014**, 6649–6652 (2014) doi:10.1002/ejoc.201403112.
309. De Schouwer, F., Claes, L., Claes, N., Bals, S., Degrève, J. & De Vos, D. E. Pd-Catalyzed Decarboxylation Of Glutamic Acid And Pyroglutamic Acid To Bio-Based 2-Pyrrolidone. *Green Chem.* **17**, 2263–2270 (2015) doi:10.1039/C4GC02194K.
310. Hunt, A. J., Farmer, T. J. & Clark, J. H. *Element Recovery And Sustainability*. *Green Chem. (RSC)* vol. 17 (Royal Society of Chemistry, 2013). doi:10.1039/9781849737340.
311. Claes, L., Verduyckt, J., Stassen, I., Lagrain, B. & De Vos, D. E. Ruthenium-Catalyzed Aerobic Oxidative Decarboxylation Of Amino Acids: A Green, Zero-Waste Route To Biobased Nitriles. *Chem. Commun.* **51**, 6528–6531 (2015) doi:10.1039/C5CC00181A.
312. Verduyckt, J., Coeck, R. & De Vos, D. E. Ru-Catalyzed Hydrogenation–Decarbonylation Of Amino Acids To Bio-Based Primary Amines. *ACS Sustain. Chem. Eng.* **5**, 3290–3295 (2017) doi:10.1021/acssuschemeng.6b03140.
313. Strecker, A. Ueber Einige Neue Bestandtheile Der Schweinegalle. *Ann. Der Chemie Und Pharm.* **123**, 353–360 (1862) doi:10.1002/jlac.18621230310.
314. Dose, K. Catalytic Decarboxylation Of α-Amino-Acids. *Nature* **179**, 734–735 (1957) doi:10.1038/179734b0.
315. Obata, Y. & Ishikawa, Y. Thermal Decarboxylation Of Sulfur-Containing Amino Acids In The Presence Of Acetophenone, A Preparation Of 3-Methylthiopropylamine Hydrochloride. *Agric. Biol. Chem.* **30**, 706–708 (1966) doi:10.1080/00021369.1966.10858669.
316. Chatelus, G. La Decarboxylation Des Acides A-Amines. *Bull. Soc. Chim. Fr.* **10**, 2523 (1964).
317. Brandt, S. D., Mansell, D., Freeman, S., Fleet, I. A. & Alder, J. F. Analytical Characterisation Of The Routes By Thermolytic Decarboxylation From Tryptophan To Tryptamine Using Ketone Catalysts, Resulting In Tetrahydro-β-Carboline Formation. *J. Pharm. Biomed. Anal.* **41**, 872–882 (2006) doi:10.1016/j.jpba.2006.02.007.
318. Jackson, D. M., Ashley, R. L., Brownfield, C. B., Morrison, D. R. & Morrison, R. W.

Rapid Conventional And Microwave-Assisted Decarboxylation Of L-Histidine And Other Amino Acids Via Organocatalysis With R-Carvone Under Superheated Conditions. *Synth. Commun.* **45**, 2691–2700 (2015) doi:10.1080/00397911.2015.1100745.

319. Claes, L., Janssen, M. & De Vos, D. E. *Catalytic Decarboxylation Of Amino Acids : From Protein Waste To Bio-Based Amines , Amides And Carbamates*. (2017) Available at: https://bit.ly/3f4slzO (Accessed: 29 July 2020).
320. Lammens, T. M. *Biobased Industrial Chemicals From Glutamic Acid*. (2011) Available at: https://bit.ly/337ksaf (Accessed: 1 May 2020).
321. Lammens, T. M., De Biase, D., Franssen, M. C. R., Scott, E. L. & Sanders, J. P. M. The Application Of Glutamic Acid α-Decarboxylase For The Valorization Of Glutamic Acid. *Green Chem.* **11**, 1562 (2009) doi:10.1039/b913741f.
322. Nohra, B., Candy, L., Blanco, J.-F., Guerin, C., Raoul, Y. & Mouloungui, Z. From Petrochemical Polyurethanes To Biobased Polyhydroxyurethanes. *Macromolecules* **46**, 3771–3792 (2013) doi:10.1021/ma400197c.
323. Piatkowski, M., Bogdal, D. & Ondruschka, B. Microwave-Assisted Synthesis Of Poly(Aspartic Acid). *Polimery* **54**, 573–576 (2009) doi:10.14314/polimery.2009.573.
324. Werpy, T. & Petersen, G. *Top Value Added Chemicals From Biomass: Volume I -- Results Of Screening For Potential Candidates From Sugars And Synthesis Gas*. *U.S. Department Of Energy* (1 August 2004) Available at: https://bit.ly/2X7vFUN (Accessed: 15 May 2020) doi:10.2172/15008859.
325. Ikeda, M. & Takeno, S. Recent Advances In Amino Acid Production. In *Encyclopedia Of Food Microbiology* 175–226 (Elsevier, 2020). doi:10.1007/978-3-030-39267-3_7.
326. Sano, C. History Of Glutamate Production. *Am. J. Clin. Nutr.* **90**, 728S-732S (2009) doi:10.3945/ajcn.2009.27462F.
327. Ikeda, K. & Suzuki, S. Nutritive And Flavoring Substance And Process Of Making Same. 1–4 (1909) Available at: https://bit.ly/2D2mEoS (Accessed: 1 May 2020) Patent Number: *US1035591A*.
328. Sari, Y. W. *Biomass And Its Potential For Protein And Amino Acids; Valorizing Agricultural By-Products*. (2015) Available at: https://bit.ly/2ZGa2Mx (Accessed: 1 May 2020).
329. Budarin, V., Ross, a. B., Biller, P., Riley, R., Clark, J. H., Jones, J. M., Gilmour, D. J. & Zimmerman, W. Microalgae Biorefinery Concept Based On Hydrothermal Microwave Pyrolysis. *Green Chem.* **14**, 3251 (2012) doi:10.1039/c2gc36202c.
330. Zhao, L., Wei, J., Qian, J., MA, J. & Tang, X. Method For Preparing Environmentally-Friendly Nylon Polybutyrolactam. (14 July 2016) Available at: https://bit.ly/3g6amu2 (Accessed: 1 May 2020) Patent Number: *US010308764B2*.
331. Park, S. J., Kim, E. Y., Noh, W., Oh, Y. H., Kim, H. Y., Song, B. K., Cho, K. M., Hong, S. H., Lee, S. H. & Jegal, J. Synthesis Of Nylon 4 From Gamma-Aminobutyrate (GABA) Produced By Recombinant Escherichia Coli. *Bioprocess Biosyst. Eng.* **36**, 885–892 (2013) doi:10.1007/s00449-012-0821-2.
332. Hur, W., Rosen, H. & Gray, N. S. A Benzo[B]Thiophene-Based Selective Type 4 S1P Receptor Agonist. *Bioorg. Med. Chem. Lett.* **27**, 1–5 (2017) doi:10.1016/j.bmcl.2016.11.050.
333. Cioc, R., Schaepkens van Riempst, L., Schuckman, P., Ruijter, E. & Orru, R. Ugi Four-Center Three-Component Reaction As A Direct Approach To Racetams. *Synthesis (Stuttg).* **49**, 1664–1674 (2016) doi:10.1055/s-0036-1588672.

334. Gonçalves, H., Robinet, G., Barthelat, M. & Lattes, A. Supramolecularity And Photodimerization Of Isophorone: FTIR And Molecular Mechanics Studies. *J. Phys. Chem. A* **102**, 1279–1287 (1998) doi:10.1021/jp9729270.
335. Kind, S., Neubauer, S., Becker, J., Yamamoto, M., Völkert, M., Abendroth, G. von, Zelder, O. & Wittmann, C. From Zero To Hero – Production Of Bio-Based Nylon From Renewable Resources Using Engineered Corynebacterium Glutamicum. *Metab. Eng.* **25**, 113–123 (2014) doi:10.1016/j.ymben.2014.05.007.
336. Claes, L., Janssen, M. & De Vos, D. E. Organocatalytic Decarboxylation Of Amino Acids As A Route To Bio-based Amines And Amides. *ChemCatChem* **11**, 4297–4306 (2019) doi:10.1002/cctc.201900800.
337. Lee, S., Ahn, J., Kim, Y.-G., Jung, J.-K., Lee, H. & Lee, E. Gamma-Aminobutyric Acid Production Using Immobilized Glutamate Decarboxylase Followed By Downstream Processing With Cation Exchange Chromatography. *Int. J. Mol. Sci.* **14**, 1728–1739 (2013) doi:10.3390/ijms14011728.
338. De bruyn, M., Budarin, V. L., Sturm, G. S. J., Stefanidis, G. D., Radoiu, M., Stankiewicz, A. & Macquarrie, D. J. Subtle Microwave-Induced Overheating Effects In An Industrial Demethylation Reaction And Their Direct Use In The Development Of An Innovative Microwave Reactor. *J. Am. Chem. Soc.* **139**, 5431–5436 (2017) doi:10.1021/jacs.7b00689.
339. Zhang, Y. J., Shu, Z., Xu, W., Chen, G. & Li, Z.-G. L-Glutamic Acid Hydrochloride At 153 K. *Acta Crystallogr. Sect. E Struct. Reports Online* **64**, o446–o446 (2008) doi:10.1107/S1600536807068560.
340. Galema, S. a. Microwave Chemistry. *Chem. Soc. Rev.* **26**, 233 (1997) doi:10.1039/cs9972600233.
341. Takano, Y., Kashiyama, Y., Ogawa, N. O., Chikaraishi, Y. & Ohkouchi, N. Isolation And Desalting With Cation-Exchange Chromatography For Compound-Specific Nitrogen Isotope Analysis Of Amino Acids: Application To Biogeochemical Samples. *Rapid Commun. Mass Spectrom.* **24**, 2317–2323 (2010) doi:10.1002/rcm.4651.
342. Buchanan, D. L. Desalting Amino Acid Solutions By Displacement With Piperidine. *Anal. Chem.* **29**, 1877–1878 (1957) doi:10.1021/ac60132a012.
343. Piez, K. A., Tooper, E. B. & Fosdick, L. S. Desalting Of Amino Acid Solutions By Ion Exchange. *J. Biol. Chem.* **194**, 669–672 (1952).
344. Mueller, G. C., Bowman, G. & Herranen, A. Desalting Amino Acid Solutions By Ion Exchange. *Anal. Chem.* **27**, 1357–1358 (1955) doi:10.1021/ac60104a052.
345. Akindoyo, J. O., Beg, M. D. H., Ghazali, S., Islam, M. R., Jeyaratnam, N. & Yuvaraj, A. R. Polyurethane Types, Synthesis And Applications – A Review. *RSC Adv.* **6**, 114453–114482 (2016) doi:10.1039/C6RA14525F.
346. Cornille, A., Blain, M., Auvergne, R., Andrioletti, B., Boutevin, B. & Caillol, S. A Study Of Cyclic Carbonate Aminolysis At Room Temperature: Effect Of Cyclic Carbonate Structures And Solvents On Polyhydroxyurethane Synthesis. *Polym. Chem.* **8**, 592–604 (2017) doi:10.1039/C6PY01854H.
347. Eckerman, I. *The Bhopal Saga - Causes And Consequences Of The World's Largest Industrial Disaster*. (Universities Press (India) Private Limited 2005, 2004). doi:10.13140/2.1.3457.5364.
348. Sawpan, M. A. Polyurethanes From Vegetable Oils And Applications: A Review. *J. Polym. Res.* **25**, 184 (2018) doi:10.1007/s10965-018-1578-3.
349. Petrovic, Z. S. Polyurethanes From Vegetable Oils. *Polym. Rev.* **48**, 109–155 (2008)

doi:10.1080/15583720701834224.
350. Rokicki, G., Parzuchowski, P. G. & Mazurek, M. Non-Isocyanate Polyurethanes: Synthesis, Properties, And Applications. *Polym. Adv. Technol.* **26**, 707–761 (2015) doi:10.1002/pat.3522.
351. Groszos, S. J. & Drechsel, E. K. Method Of Preparing A Polyurethane. (1957) Available at: https://bit.ly/2Xop2O3 (Accessed: 1 May 2020) Patent Number: *US2802022A*.
352. Pyo, S. H., Park, J. H., Chang, T. S. & Hatti-Kaul, R. Dimethyl Carbonate As A Green Chemical. *Curr. Opin. Green Sustain. Chem.* **5**, 61–66 (2017) doi:10.1016/j.cogsc.2017.03.012.
353. Schäffner, B., Schäffner, F., Verevkin, S. P. & Börner, A. Organic Carbonates As Solvents In Synthesis And Catalysis. *Chem. Rev.* **110**, 4554–4581 (2010) doi:10.1021/cr900393d.
354. Clark, J. H., Farmer, T. J., Ingram, I. D. V., Lie, Y. & North, M. Renewable Self-Blowing Non-Isocyanate Polyurethane Foams From Lysine And Sorbitol. *European J. Org. Chem.* **2018**, 4265–4271 (2018) doi:10.1002/ejoc.201800665.
355. North, M. & Pasquale, R. Mechanism Of Cyclic Carbonate Synthesis From Epoxides And CO2. *Angew. Chemie Int. Ed.* **48**, 2946–2948 (2009) doi:10.1002/anie.200805451.
356. Mazurek-Budzyńska, M. M., Rokicki, G., Drzewicz, M., Guńka, P. A. & Zachara, J. Bis(Cyclic Carbonate) Based On D -Mannitol, D -Sorbitol And Di(Trimethylolpropane) In The Synthesis Of Non-Isocyanate Poly(Carbonate-Urethane)S. *Eur. Polym. J.* **84**, 799–811 (2016) doi:10.1016/j.eurpolymj.2016.04.021.
357. Blain, M., Yau, H., Jean-Gérard, L., Auvergne, R., Benazet, D., Schreiner, P. R., Caillol, S. & Andrioletti, B. Urea- And Thiourea-Catalyzed Aminolysis Of Carbonates. *ChemSusChem* **9**, 2269–2272 (2016) doi:10.1002/cssc.201600778.
358. Betke, T., Maier, M., Gruber-Wölfler, H. & Gröger, H. Biocatalytic Production Of Adiponitrile And Related Aliphatic Linear α,ω-Dinitriles. *Nat. Commun.* **9**, 5112 (2018) doi:10.1038/s41467-018-07434-0.
359. Gail, E., Gos, S., Kulzer, R., Lorösch, J., Rubo, A., Sauer, M., Kellens, R., Reddy, J., Steier, N. & Hasenpusch, W. Cyano Compounds, Inorganic. In *Ullmann's Encyclopedia Of Industrial Chemistry* vol. 10 673–710 (Wiley-VCH Verlag GmbH & Co. KGaA, 2011). doi:10.1002/14356007.a08_159.pub3.
360. Bhatia, S. K., Kim, Y. H., Kim, H. J., Seo, H.-M., Kim, J.-H., Song, H.-S., Sathiyanarayanan, G., Park, S.-H., Park, K. & Yang, Y.-H. Biotransformation Of Lysine Into Cadaverine Using Barium Alginate-Immobilized Escherichia Coli Overexpressing CadA. *Bioprocess Biosyst. Eng.* **38**, 2315–2322 (2015) doi:10.1007/s00449-015-1465-9.
361. Tomczyk, K. M., Guńka, P. A., Parzuchowski, P. G., Zachara, J. & Rokicki, G. Intramolecular Etherification Of Five-Membered Cyclic Carbonates Bearing Hydroxyalkyl Groups. *Green Chem.* **14**, 1749 (2012) doi:10.1039/c2gc35265f.
362. Chen, K., Wang, M., Huang, C., Kinney, P. L. & Anastas, P. T. Air Pollution Reduction And Mortality Benefit During The COVID-19 Outbreak In China. *Lancet Planet. Heal.* **2019**, 2019–2021 (2020) doi:10.1016/S2542-5196(20)30107-8.
363. Meadows, D. H., Meadows, D. L., Randers, J. & Ill, W. W. B. *The Limits To Growth*. (1972).
364. Erythropel, H. C., Zimmerman, J. B., de Winter, T. M., Petitjean, L., Melnikov, F., Lam, C. H., Lounsbury, A. W., Mellor, K. E., Janković, N. Z., Tu, Q., Pincus, L. N., Falinski, M.

M., Shi, W., Coish, P., Plata, D. L. & Anastas, P. T. The Green ChemisTREE: 20 Years After Taking Root With The 12 Principles. *Green Chem.* **20**, 1929–1961 (2018) doi:10.1039/C8GC00482J.

365. Bránykiková, I., Maršálková, B., Doucha, J., Brányik, T., Bišová, K., Zachleder, V. & Vítová, M. Microalgae-Novel Highly Efficient Starch Producers. *Biotechnol. Bioeng.* **108**, 766–776 (2011) doi:10.1002/bit.23016.
366. Budarin, V. L., Clark, J. H., Henschen, J., Farmer, T. J., Macquarrie, D. J., Mascal, M., Nagaraja, G. K. & Petchey, T. H. M. Processed Lignin As A Byproduct Of The Generation Of 5-(Chloromethyl)Furfural From Biomass: A Promising New Mesoporous Material. *ChemSusChem* **8**, 4172–4179 (2015) doi:10.1002/cssc.201501319.
367. Tian, Q., He, P. & Kuang, C. Copper-Catalyzed Arylsulfonylation Of N-Arylsulfonyl-Acrylamides With Arylsulfonohydrazides: Synthesis Of Sulfonated Oxindoles. *Org. Biomol. Chem.* **12**, 6349–6353 (2014) doi:10.1039/c4ob01231c.
368. Fu, H., Wang, S. S. & Li, Y. M. Copper-Mediated Oxidative Radical Addition/Cyclization Cascade: Synthesis Of Trifluoromethylated And Sulfonated Quinoline-2,4(1H,3H)-Diones. *Adv. Synth. Catal.* **358**, 3616–3626 (2016) doi:10.1002/adsc.201600693.
369. Dahmen, N., Lewandowski, I., Zibek, S. & Weidtmann, A. Integrated Lignocellulosic Value Chains In A Growing Bioeconomy: Status Quo And Perspectives. *GCB Bioenergy* **11**, gcbb.12586 (2018) doi:10.1111/gcbb.12586.
370. Rees.Mariculture. *Nanno 3600*. Available at: https://bit.ly/39EEmLc (Accessed: 29 July 2020).
371. Van Wychen, S. & Laurens, L. M. L. *Determination Of Total Carbohydrates In Algal Biomass: Laboratory Analytical Procedure (LAP)*. (13 January 2016) Available at: https://bit.ly/3f79ELX (Accessed: 29 July 2020) doi:10.2172/1118073.
372. Bharti, S. K. & Roy, R. Quantitative 1H NMR Spectroscopy. *TrAC Trends Anal. Chem.* **35**, 5–26 (2012) doi:10.1016/j.trac.2012.02.007.
373. Frisch, M. J. … Fox, D. J. Guaussian 16. (2016) Patent Number: *A.03*.
374. Chai, J. Da & Head-Gordon, M. Long-Range Corrected Hybrid Density Functionals With Damped Atom-Atom Dispersion Corrections. *Phys. Chem. Chem. Phys.* **10**, 6615–6620 (2008) doi:10.1039/b810189b.
375. Cossi, M., Rega, N., Scalmani, G. & Barone, V. Energies, Structures, And Electronic Properties Of Molecules In Solution With The C-PCM Solvation Model. *J. Comput. Chem.* **24**, 669–681 (2003) doi:10.1002/jcc.10189.
376. Hirapara, P., Riemer, D., Hazra, N., Gajera, J., Finger, M. & Das, S. CO 2 -Assisted Synthesis Of Non-Symmetric α-Diketones Directly From Aldehydes Via C–C Bond Formation. *Green Chem.* **19**, 5356–5360 (2017) doi:10.1039/C7GC02425H.
377. Lee, C. K., Kim, M. S., Gong, J. S. & Lee, I.-S. H. Benzoin Condensation Reactions Of 5-Membered Heterocyclic Compounds. *J. Heterocycl. Chem.* **29**, 149–153 (1992) doi:10.1002/jhet.5570290127.
378. Reichstein, T. & Zschokke, H. Über 5-Methyl-Furfuryl-Chlorid. *Helv. Chim. Acta* **15**, 249–253 (1932) doi:10.1002/hlca.19320150124.
379. Gorsline, B. J., Wang, L., Ren, P. & Carrow, B. P. C–H Alkenylation Of Heteroarenes: Mechanism, Rate, And Selectivity Changes Enabled By Thioether Ligands. *J. Am. Chem. Soc.* **139**, 9605–9614 (2017) doi:10.1021/jacs.7b03887.
380. Mohite, A. R. & Bhat, R. G. A Practical And Convenient Protocol For The Synthesis Of

(E)-α,β-Unsaturated Acids. *Org. Lett.* **15**, 4564–4567 (2013) doi:10.1021/ol402130t.
381. Jakopčić, K. & Karminski-Zamola, G. Photochemical Isomerizations Of Furylacrylic Acids. *Croat. Chem. Acta* **46**, 71–78 (1974).
382. Gypser, A. & Scharf, H.-D. The Solvent Dependence Of The Diastereoselective Hydrogenation Of 2- And 2,5-Substituted Furylcarbinols On A Raney Nickel Contact. *Synthesis (Stuttg).* **1996**, 349–352 (1996) doi:10.1055/s-1996-4210.
383. Miyakoshi, T. & Togashi, H. Synthesis Of 3-Alkylcatechols Via Intramolecular Cyclization. *Synthesis (Stuttg).* **1990**, 407–410 (1990) doi:10.1055/s-1990-26889.
384. Sato, H., Kashiwamura, T., Okamoto, T. & Yokota, K. Carbonyl Compound Containing Long-Chain Branched Alkyl Group. (2006) Available at: https://bit.ly/2EmB6sb (Accessed: 1 May 2020) Patent Number: *WO2005077876A1*.
385. Cohen, Y., Bodner, E., Richman, M., Afri, M. & Frimer, A. A. NMR-Based Molecular Ruler For Determining The Depth Of Intercalants Within The Lipid Bilayer. Part I. Discovering The Guidelines. *Chem. Phys. Lipids* **155**, 98–113 (2008) doi:10.1016/j.chemphyslip.2008.07.004.
386. Nishio, Y., Mifune, R., Sato, T., Ishikawa, S. & Matsubara, H. Preparation And Properties Of A Novel Solution Of Hydrogen Bromide (HBr) In 1,4-Dioxane: An Alternative Reagent To HBr Gas Without Protic Solvents. *Tetrahedron Lett.* **58**, 1190–1193 (2017) doi:10.1016/j.tetlet.2017.02.020.
387. Cruz, C. M., Ortega-Muñoz, M., López-Jaramillo, F. J., Hernández-Mateo, F., Blanco, V. & Santoyo-González, F. Vinyl Sulfonates: A Click Function For Coupling-And-Decoupling Chemistry And Their Applications. *Adv. Synth. Catal.* **358**, 3394–3413 (2016) doi:10.1002/adsc.201600628.
388. Rajmohan, R., Gayathri, S. & Vairaprakash, P. Facile Synthesis Of 5-Hydroxymethylfurfural: A Sustainable Raw Material For The Synthesis Of Key Intermediates Toward 21,23-Dioxaporphyrins. *RSC Adv.* **5**, 100401–100407 (2015) doi:10.1039/C5RA19400H.
389. Sagisaka, M., Kudo, K., Hida, M. & Shikauchi, Y. Surfactant For Stabilizing Water/Supercritical Carbon Dioxide Microemulsion. (2013) Available at: https://bit.ly/3gaoF0B (Accessed: 1 May 2020) Patent Number: *US20130023687A1*.
390. Mintz, M. J. & Walling, C. Tert-Butyl Hypochlorite. *Org. Synth.* **49**, 9 (1969) doi:10.15227/orgsyn.049.0009.
391. Emery, K., Young, A., Arokianathar, J., Tuttle, T. & Murphy, J. KOtBu As A Single Electron Donor? Revisiting The Halogenation Of Alkanes With CBr4 And CCl4. *Molecules* **23**, 1055 (2018) doi:10.3390/molecules23051055.
392. Darwish, T. A., Evans, R. A., James, M., Malic, N., Triani, G. & Hanley, T. L. CO 2 Triggering And Controlling Orthogonally Multiresponsive Photochromic Systems. *J. Am. Chem. Soc.* **132**, 10748–10755 (2010) doi:10.1021/ja1013322.
393. Weiss, I. M., Muth, C., Drumm, R. & Kirchner, H. O. K. Thermal Decomposition Of The Amino Acids Glycine, Cysteine, Aspartic Acid, Asparagine, Glutamic Acid, Glutamine, Arginine And Histidine. *BMC Biophys.* **11**, 2 (2018) doi:10.1186/s13628-018-0042-4.

List of abbreviations

- AE: Atom economy
- BB: Borate buffer
- BSA: Bovine serum albumin
- BUE: Biomass utilisation efficiency
- CMC: Critical micelle concentration
- CMR: Carcinogenic mutagen reprotoxic
- DI: Deionised (water)
- EPA: Environmental protection agency (USA)
- ET: Ethanethiol solution
- FDCA:2,5-furan dicarboxylic acid
- FMOC: Fluorenylmethyloxycarbonyl
- FSS: Furan-derived sulfonated surfactant
- GABA: γ-aminobutyric acid
- GHG: Greenhouse gases
- HLB: Hydrophilic lipophilic balance
- HSP(s): Hansen solubility parameter(s)
- ISTDsol: Internal standard solution
- LAP: Laboratory analytical procedures
- LAS: Linear alkyl benzene sulfonates
- MDI: 4,4'-methylenediphenyl diisocyanate
- NIPU: Non-isocyanates polyurethanes
- NOM: Natural organic matter
- MED: Minimal erythema dose
- MES: Fatty acid methyl ester sulfonates
- MIC: Methyl isocyanate
- NREL: National Renewable Energy Laboratory
- ODW: oven-dry weight
- OPA: *ortho*-phthalaldehyde
- RPSA: Relative polar surface area
- PFAE: Polyesters of furandiyl diacrylic esters
- PHU: Polyhydroxyurethane
- PITC: Phenylisothiocyanate
- SDG(s): Sustainable development goal(s)
- SPF: Sun protection factor
- STA: Simultaneous thermogravimetric analysis
- TAA: Total amino acid analysis
- TAC: Total ash content
- TCC: Total carbohydrate content
- TDI: Toluene diisocyanate
- TLiC: Total lipid content
- TPC: Total protein content
- TSC: Total solid content
- UNSDP: United Nations for Sustainable Development Program
- UV: ultraviolet

Appendices

Appendix 1 List of base chemicals and platform molecules used to plot original and modified van Krevelen diagrams*. Fully labelled version of graphic C represented in Figure 8

List of Petroleum-derived Base Chemicals and Accompanying Data

Base Chemical	No.	RMM ($g.mol^{-1}$)	C	C% (mass)	H	H% (mass)	O	O% (mass)	%hetero	Structure
ethene	**1**	28.05	2	85.6	4	14.4	0	0.0	0.0	
propene	**2**	42.08	3	85.6	6	14.4	0	0.0	0.0	
butadiene	**3**	54.09	4	88.8	6	11.2	0	0.0	0.0	
butenes	**4**	56.11	4	85.6	8	14.4	0	0.0	0.0	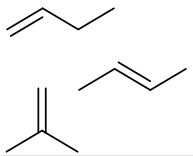
benzene	**5**	78.11	6	92.3	6	7.7	0	0.0	0.0	
toluene	**6**	92.14	7	91.2	8	8.8	0	0.0	0.0	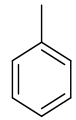
xylene (o-, m-, p-)	**7**	106.17	8	90.5	10	9.5	0	0.0	0.0	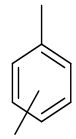
methanol	**8**	88.06	3	40.9	4	4.6	3	54.5	54.5	

* Reproduced from Lie, Y., Ortiz, P., Vendamme, R., Vanbroekhoven, K. & Farmer, T. J. *BioLogicTool* : A Simple Visual Tool For Assisting In The Logical Selection Of Pathways From Biomass To Products. *Ind. Eng. Chem. Res.* 58, 15945–15957 (2019), Supp. Information.

List of Biomass-derived Platform Molecules and Accompanying Data

Platform Molecule	RMM ($g.mol^{-1}$)	C	C% (mass)	H	H% (mass)	O	O% (mass)	%heteroo	Structure
methanol	32.04	1	37.5	4	12.6	1	49.9	49.9	
carbon dioxide	44.01	1	27.3	0	0.0	2	72.7	72.7	
formic acid	46.03	1	26.1	2	4.4	2	69.5	69.5	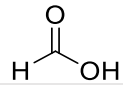
ethanol	46.07	2	52.1	6	13.1	1	34.7	34.7	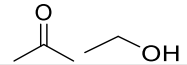
acetone	58.08	3	62.0	6	10.4	1	27.5	27.5	
isoprene	68.12	5	88.2	8	11.8	0	0.0	0.0	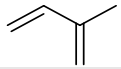
butanol (n-, iso-)	74.12	4	64.8	10	13.6	1	21.6	21.6	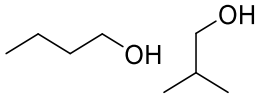
pyruvic acid	88.06	3	40.9	4	4.6	3	54.5	54.5	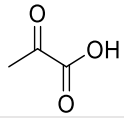
acetoin (3-hydroxybutanone)	88.11	4	54.5	8	9.2	2	36.3	36.3	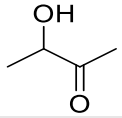
3-hydroxy-propionic acid	90.01	3	40.0	6	6.7	3	53.3	53.2	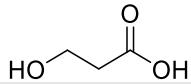
lactic acid	90.01	3	40.0	6	6.7	3	53.3	53.2	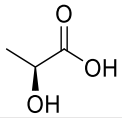

oxalic acid	90.03	2	26.7	2	2.2	4	71.1	71.1	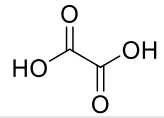
glycerol	92.09	3	39.1	8	8.8	3	52.1	52.1	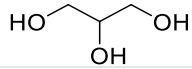
furfural	96.08	5	62.5	4	4.2	2	33.3	33.3	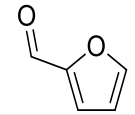
γ-valerolactone	100.12	5	60.0	8	8.1	2	32.0	32.0	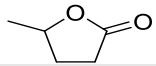
3-hydroxybutyro-lactone	102.09	4	47.1	6	5.9	3	47.0	47.0	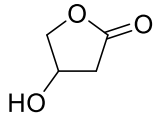
malonic acid	104.06	3	34.6	4	3.9	4	61.5	61.5	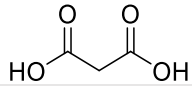
fumaric acid	116.07	4	41.4	4	3.5	4	55.1	55.1	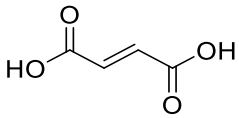
levulinic acid	116.12	5	51.7	8	6.9	3	41.3	41.3	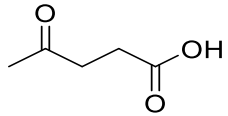
methylvinyl glycolate	116.12	5	51.7	8	6.9	3	41.3	41.3	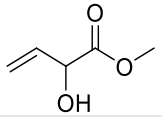
succinic acid	118.09	4	40.7	6	5.1	4	54.2	54.2	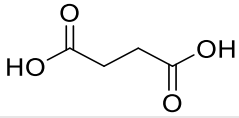

erythrose	120.1	4	40.0	8	6.7	4	53.3	53.3	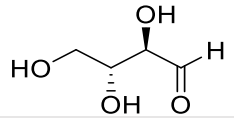
erythritol	122.12	4	39.3	10	8.3	4	52.4	52.4	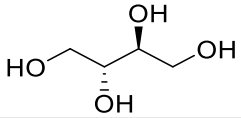
guaiacol	124.14	7	67.7	8	6.5	2	25.8	25.8	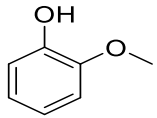
levoglucosenone	126.11	6	57.1	6	4.8	3	38.1	38.1	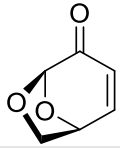
5-(hydroxymethyl) furfural	126.11	6	57.1	6	4.8	3	38.1	38.1	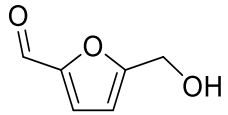
itaconic acid	130.1	5	46.2	6	4.6	4	49.2	49.2	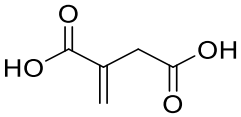
aspartic acid	133.1	4	36.1	7	5.3	4	48.1	58.6	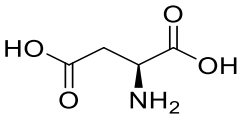
malic acid	134.09	4	35.8	6	4.5	5	59.7	59.7	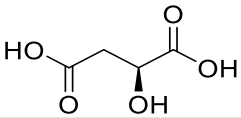

D-limonene and pinenes (monoterpenes)	136.24	10	88.2	16	11.8	0	0.0	0.0	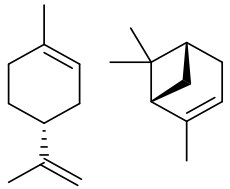
muconic acid	142.11	6	50.7	6	4.3	4	45.0	45.0	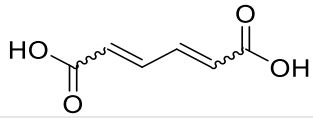
5-(chloromethyl) furfural	144.56	6	49.9	5	3.5	2	22.1	46.7	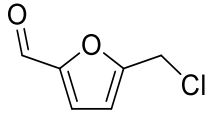
adipic acid	146.14	6	49.3	10	6.9	4	43.8	43.8	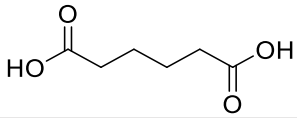
L-lysine	146.19	6	49.3	14	9.7	2	21.9	41.1	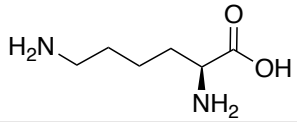
L-glutamic acid	147.13	5	40.8	9	6.2	4	43.5	53.0	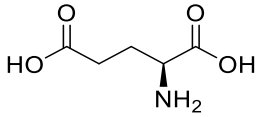
tartaric acid	150.09	4	32.0	6	4.0	6	64.0	64.0	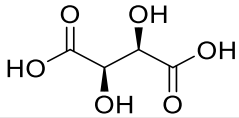
xylitol/arabitol	152.15	5	39.5	12	8.0	5	52.6	52.6	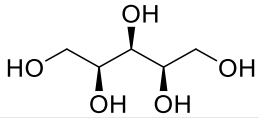

vanillin	152.15	8	63.2	8	5.3	3	31.5	31.5	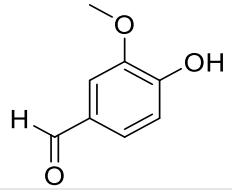
syringol	154.16	8	62.3	10	6.5	3	31.1	31.1	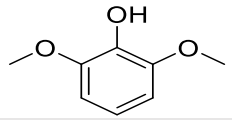
levoglucosan	162.14	6	44.4	10	6.2	5	49.3	49.3	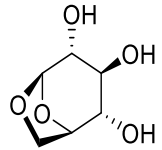
eugenol	164.2	10	73.1	12	7.4	2	19.5	19.5	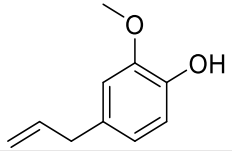
3-acetamido-5-acetylfuran	167.16	8	57.5	9	5.4	3	28.7	37.1	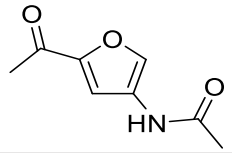
gallic acid	170.12	7	49.4	6	3.6	5	47.0	47.0	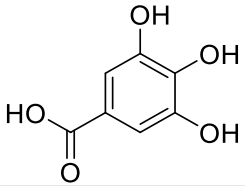
aconitic acid	174.11	6	41.4	6	3.5	6	55.1	55.1	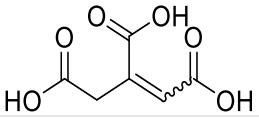

glucosamine	179.17	6	40.2	13	7.3	5	44.6	52.5	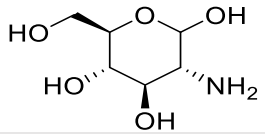
sorbitol/mannitol	182.17	6	39.6	14	7.7	6	52.7	52.7	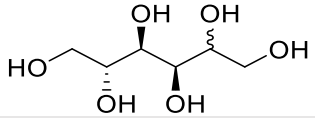
citric acid	192.12	6	37.5	8	4.2	7	58.3	58.3	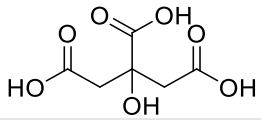
ferulic acid	194.18	10	61.9	10	5.2	4	33.0	33.0	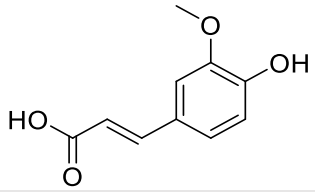
lauric acid	200.31	12	72.0	24	12.1	2	16.0	16.0	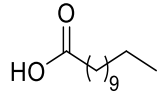
glucaric acid	210.14	6	34.3	10	4.8	8	60.9	60.9	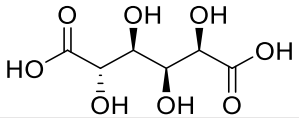
fatty acid alkyl esters (methyl laurate)	214.34	13	72.8	26	12.2	2	14.9	14.9	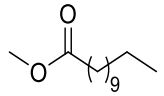
oleic acid	*282.47*	*18*	*76.5*	*34*	*12.1*	*2*	*11.3*	*11.3*	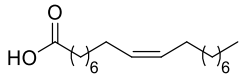
ricinoleic acid	*298.46*	*18*	*72.4*	*34*	*11.5*	*3*	*16.1*	*16.1*	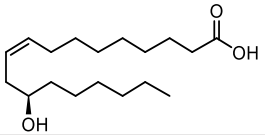

ancardic acid (C15:3)	*342.47*	*22*	*77.2*	*30*	*8.8*	*3*	*14.0*	*14.0*	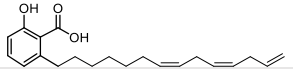
β-carotene	*536.89*	*40*	*89.5*	*56*	*10.5*	*0*	*0.0*	*0.0*	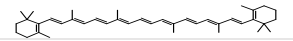
lutein (xanthophyll)	*568.87*	*40*	*84.5*	*56*	*9.9*	*2*	*5.6*	*5.6*	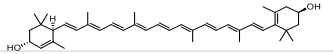

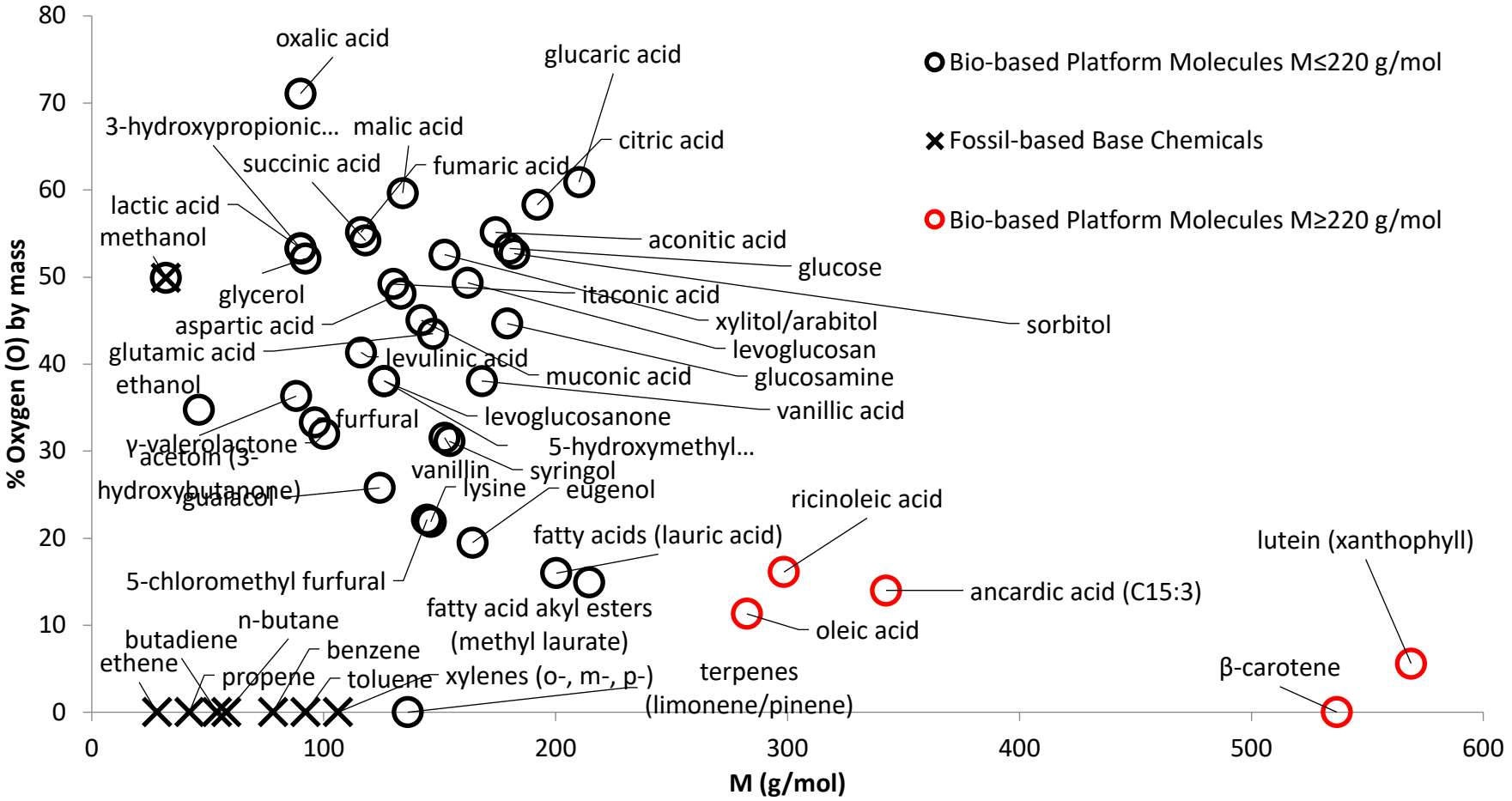

Fully labelled version of plot C represented in Figure 8, p. 52.

Appendix 2 Screenshot of the available *BioLogicTool* spreadsheet*

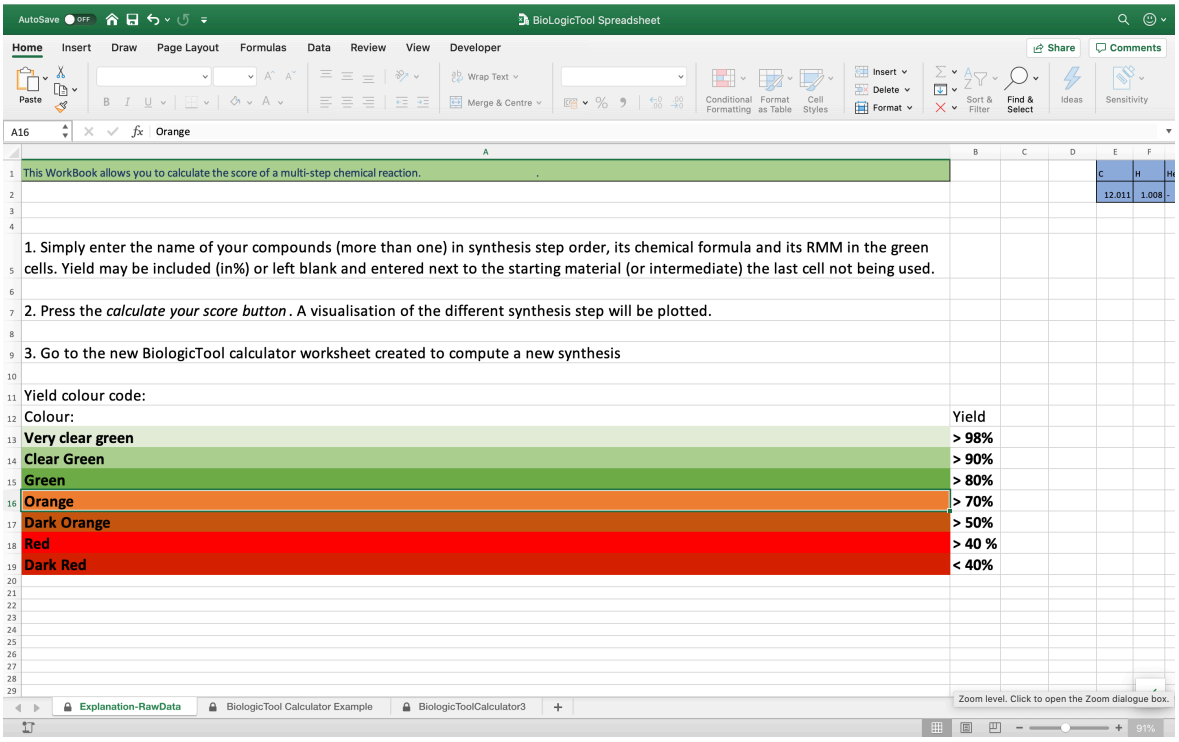

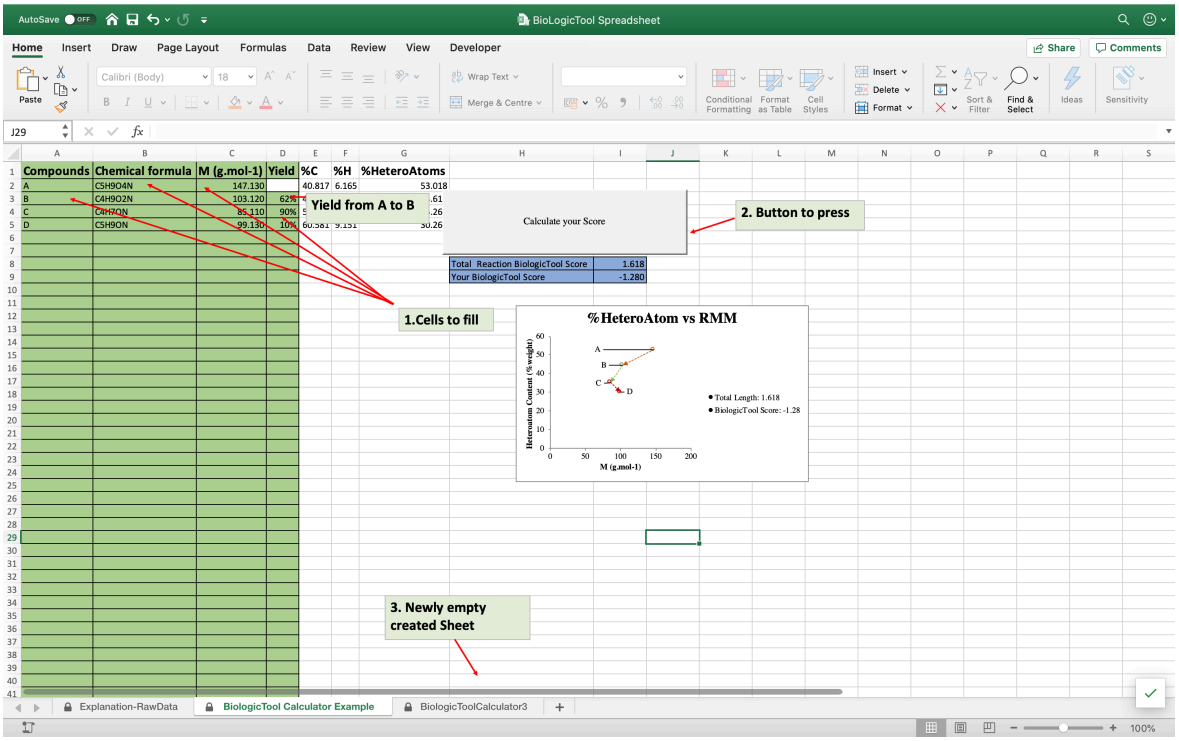

*Available at: https://pure.york.ac.uk/portal/en/datasets/biologictool-excel-spreadsheet-of-tool-linked-to-the-publication-biologictool-a-simple-visual-tool-for-assisting-in-the-logical-selection-of-pathways-from-biomass-to-products(64d80432-9929-4b74-bcb7-8e3226ec03ce).html

Appendix 3 Amino acid standard chromatogram (0.2 mM)

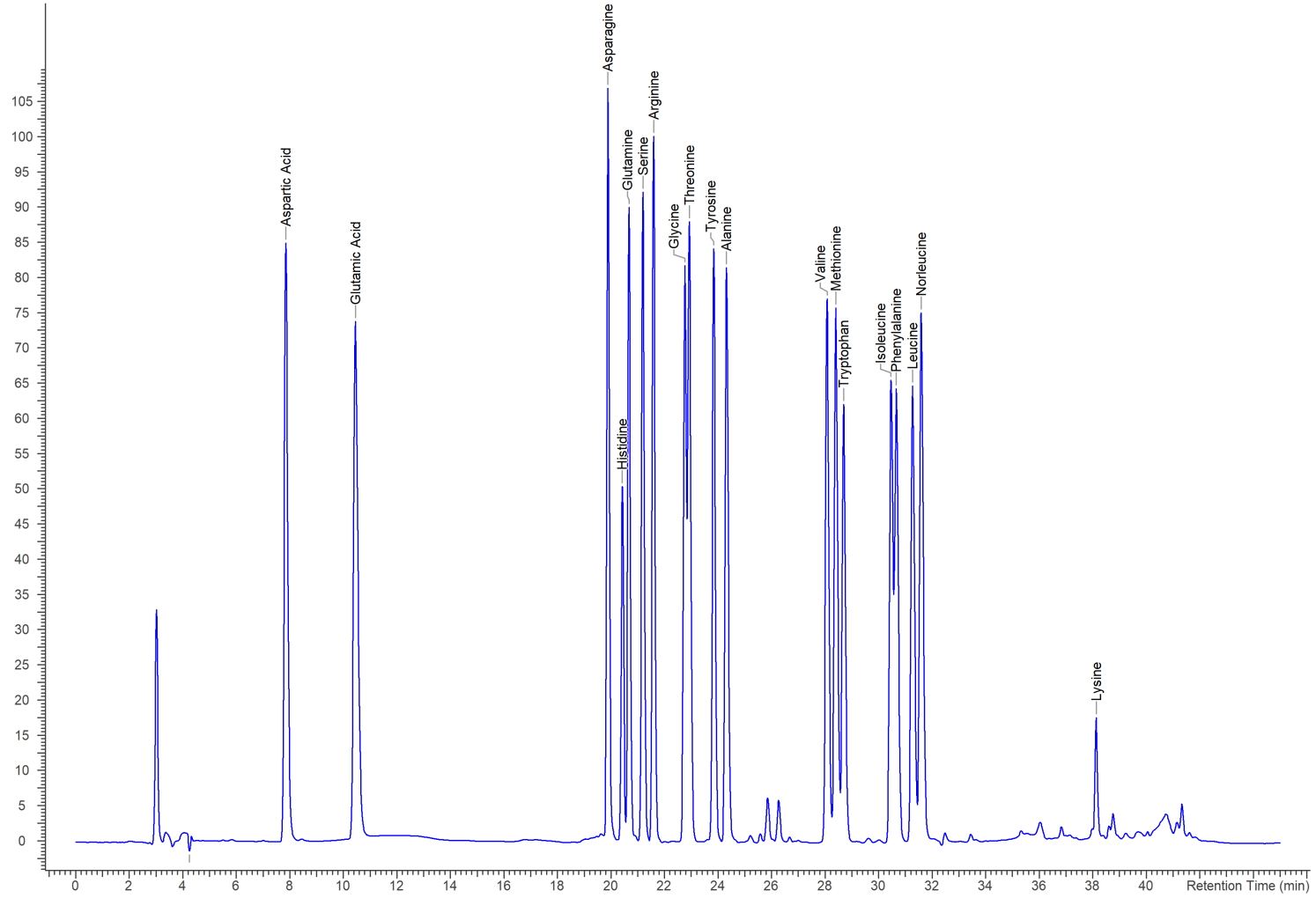

GABA is used as an internal standard. Conditions for elution and derivatisation can be found in Experimental section.

Appendix 4 Table of solvent blends optimised for HMF (37) computed HSP

Solvent 1	Solvent 2	Vol% 1	Vol% 2	dDmix	dPmix	dHmix	Solv-Distance	Distance HMF	Distance CMF
***N*-butyl pyrrolidone**	butan-1-ol	57	43	16.9	8.1	10.1	11.3	9.08	7.50
butan-2-ol	*N*-butyl pyrrolidone	40	60	16.8	8.2	9.3	10.2	9.413	7.24
ethylene dichloride	butan-1-ol	37	63	16.7	6.3	11.5	12.5	10.155	9.68
methylene dichloride (dichloromethane)	butan-1-ol	49	51	16.5	6.5	11.5	9.1	10.218	9.70
toluene	*N*-butyl pyrrolidone	0	100	17.5	9.9	5.8	9.4	10.267	4.95
***p*-xylene**	*N*-butyl pyrrolidone	0	100	17.5	9.9	5.8	9.3	10.267	4.95
isopropyl ether	*N*-butyl pyrrolidone	0	100	17.5	9.9	5.8	8.6	10.267	4.95
diethyl ether	*N*-butyl pyrrolidone	0	100	17.5	9.9	5.8	9.3	10.267	4.95
carbon tetrachloride (P By Group Cont.)	*N*-butyl pyrrolidone	0	100	17.5	9.9	5.8	6.6	10.267	4.95
***n*-hexane**	*N*-butyl pyrrolidone	0	100	17.5	9.9	5.8	12.6	10.267	4.95
***n*-pentane**	*N*-butyl pyrrolidone	0	100	17.5	9.9	5.8	12.9	10.267	4.95
benzene	*N*-butyl pyrrolidone	0	100	17.5	9.9	5.8	10.8	10.267	4.95
***n*-heptane**	*N*-butyl pyrrolidone	0	100	17.5	9.9	5.8	12.3	10.267	4.95
carbon tetrachloride (0 Dipole Moment)	*N*-butyl pyrrolidone	0	100	17.5	9.9	5.8	11.2	10.267	4.95
triethylamine	*N*-butyl pyrrolidone	0	100	17.5	9.9	5.8	11.4	10.267	4.95
cyclohexane	*N*-butyl pyrrolidone	0	100	17.5	9.9	5.8	11.5	10.267	4.95
methyl ethyl ketone (MEK)	*N*-butyl pyrrolidone	0	100	17.5	9.9	5.8	3.2	10.267	4.95
ethylene dichloride	*N*-butyl pyrrolidone	0	100	17.5	9.9	5.8	3.2	10.267	4.95
methylene dichloride (dichloromethane)	*N*-butyl pyrrolidone	0	100	17.5	9.9	5.8	3.1	10.267	4.95
ethyl acetate	*N*-butyl pyrrolidone	0	100	17.5	9.9	5.8	5.9	10.267	4.95
methyl ethyl ketone (MEK)	butan-1-ol	39	61	16	7	11.6	11.2	10.268	9.88
***N*-butyl pyrrolidone**	chloroform	99	1	17.5	9.8	5.8	6.8	10.302	5.04
***N*-butyl pyrrolidone**	*n*-butyl acetate	99	1	17.5	9.8	5.8	7.1	10.304	5.04

***N*-butyl pyrrolidone**	cyclopentyl methyl ether (Cpme)	99	1	17.5	9.8	5.8	6	10.312	5.04
***N*-butyl pyrrolidone**	methyl-*t*-butyl ether	99	1	17.5	9.8	5.8	7.8	10.316	5.04
***N*-butyl pyrrolidone**	chlorobenzene	99	1	17.5	9.8	5.8	7.4	10.319	5.04
butan-2-ol	methylene dichloride (dichloromethane)	50	50	16.4	6.5	10.8	7.9	10.502	9.51
butan-2-ol	ethylene dichloride	65	35	16.6	6.3	10.9	11.4	10.505	9.52
butan-2-ol	methyl ethyl ketone (MEK)	63	37	15.9	6.9	11	10	10.625	9.81
carbon tetrachloride (P By Group Cont.)	butan-1-ol	20	80	16	6.2	12.6	16	10.676	10.92
butan-1-ol	chlorobenzene	81	19	16.6	5.4	13.2	15.1	10.785	11.30
carbon tetrachloride (P By Group Cont.)	butan-2-ol	15	85	15.8	6.1	12.3	14.7	11.02	11.05
butan-2-ol	chlorobenzene	86	14	16.2	5.5	12.8	14.1	11.053	11.34
butan-1-ol	cyclopentyl methyl ether (Cpme)	90	10	16.1	5.6	14.7	11.7	11.088	12.40
butan-1-ol	chloroform	90	10	16.2	5.4	14.8	11	11.093	12.52
ethyl acetate	butan-1-ol	10	90	16	5.7	14.9	8.6	11.107	12.54
toluene	butan-1-ol	2	98	16	5.6	15.5	15	11.141	12.98
***p*-xylene**	butan-1-ol	0	100	16	5.7	15.8	14	11.143	13.12
isopropyl ether	butan-1-ol	0	100	16	5.7	15.8	13	11.143	13.12
diethyl ether	butan-1-ol	0	100	16	5.7	15.8	11.9	11.143	13.12
***n*-hexane**	butan-1-ol	0	100	16	5.7	15.8	16.9	11.143	13.12
***n*-pentane**	butan-1-ol	0	100	16	5.7	15.8	17.1	11.143	13.12
benzene	butan-1-ol	0	100	16	5.7	15.8	15.7	11.143	13.12
***n*-heptane**	butan-1-ol	0	100	16	5.7	15.8	16.9	11.143	13.12
carbon tetrachloride (0 Dipole Moment)	butan-1-ol	0	100	16	5.7	15.8	16.6	11.143	13.12
triethylamine	butan-1-ol	0	100	16	5.7	15.8	15.8	11.143	13.12
cyclohexane	butan-1-ol	0	100	16	5.7	15.8	16.7	11.143	13.12
butan-2-ol	butan-1-ol	0	100	16	5.7	15.8	1.4	11.143	13.12
butan-1-ol	*n*-butyl acetate	99	1	16	5.7	15.7	9.7	11.149	13.05

butan-1-ol	methyl-*t*-butyl ether	99	1	16	5.7	15.7	11.2	11.152	13.05
toluene	methylene dichloride (dichloromethane)	0	100	17	7.3	7.1	8.1	11.215	7.51
***p*-xylene**	methylene dichloride (dichloromethane)	0	100	17	7.3	7.1	7.6	11.215	7.51
isopropyl ether	methylene dichloride (dichloromethane)	0	100	17	7.3	7.1	6.8	11.215	7.51
diethyl ether	methylene dichloride (dichloromethane)	0	100	17	7.3	7.1	7.1	11.215	7.51
carbon tetrachloride (P By Group Cont.)	methylene dichloride (dichloromethane)	0	100	17	7.3	7.1	7.4	11.215	7.51
***n*-hexane**	methylene dichloride (dichloromethane)	0	100	17	7.3	7.1	11	11.215	7.51
***n*-pentane**	methylene dichloride (dichloromethane)	0	100	17	7.3	7.1	11.3	11.215	7.51
benzene	methylene dichloride (dichloromethane)	0	100	17	7.3	7.1	9.3	11.215	7.51
***n*-heptane**	methylene dichloride (dichloromethane)	0	100	17	7.3	7.1	10.7	11.215	7.51
carbon tetrachloride (0 Dipole Moment)	methylene dichloride (dichloromethane)	0	100	17	7.3	7.1	9.9	11.215	7.51
triethylamine	methylene dichloride (dichloromethane)	0	100	17	7.3	7.1	9.7	11.215	7.51
cyclohexane	methylene dichloride (dichloromethane)	0	100	17	7.3	7.1	10.1	11.215	7.51
methyl ethyl ketone (MEK)	methylene dichloride (dichloromethane)	0	100	17	7.3	7.1	3.3	11.215	7.51
ethylene dichloride	methylene dichloride (dichloromethane)	0	100	17	7.3	7.1	3.6	11.215	7.51
methylene dichloride (dichloromethane)	ethyl acetate	99	1	17	7.3	7.1	3.1	11.236	7.51
butan-2-ol	chloroform	98	2	15.8	5.6	14.3	10	11.238	12.43
butan-2-ol	cyclopentyl methyl ether (Cpme)	99	1	15.8	5.7	14.4	10.5	11.24	12.42
toluene	butan-2-ol	0	100	15.8	5.7	14.5	13.9	11.24	12.48
***p*-xylene**	butan-2-ol	0	100	15.8	5.7	14.5	13	11.24	12.48
isopropyl ether	butan-2-ol	0	100	15.8	5.7	14.5	11.7	11.24	12.48

diethyl ether	butan-2-ol	0	100	15.8	5.7	14.5	10.6	11.24	12.48
***n*-hexane**	butan-2-ol	0	100	15.8	5.7	14.5	15.7	11.24	12.48
***n*-pentane**	butan-2-ol	0	100	15.8	5.7	14.5	15.8	11.24	12.48
benzene	butan-2-ol	0	100	15.8	5.7	14.5	14.7	11.24	12.48
***n*-heptane**	butan-2-ol	0	100	15.8	5.7	14.5	15.6	11.24	12.48
carbon tetrachloride (0 Dipole Moment)	butan-2-ol	0	100	15.8	5.7	14.5	15.5	11.24	12.48
triethylamine	butan-2-ol	0	100	15.8	5.7	14.5	14.5	11.24	12.48
cyclohexane	butan-2-ol	0	100	15.8	5.7	14.5	15.5	11.24	12.48
butan-2-ol	ethyl acetate	99	1	15.8	5.7	14.4	7.3	11.242	12.42
methylene dichloride (dichloromethane)	chloroform	99	1	17	7.3	7.1	4.7	11.249	7.51
methylene dichloride (dichloromethane)	*n*-butyl acetate	99	1	17	7.3	7.1	4.4	11.253	7.51
butan-2-ol	*n*-butyl acetate	99	1	15.8	5.7	14.4	8.4	11.255	12.42
methylene dichloride (dichloromethane)	chlorobenzene	99	1	17	7.3	7	7.1	11.256	7.52
methylene dichloride (dichloromethane)	cyclopentyl methyl ether (Cpme)	99	1	17	7.3	7.1	4.1	11.256	7.51
butan-2-ol	methyl-*t*-butyl ether	99	1	15.8	5.7	14.4	9.8	11.26	12.42
methylene dichloride (dichloromethane)	methyl-*t*-butyl ether	99	1	17	7.3	7.1	5.7	11.264	7.51
methyl ethyl ketone (MEK)	ethylene dichloride	83	17	16.3	8.7	4.9	4.4	12.33	7.51
toluene	methyl ethyl ketone (MEK)	0	100	16	9	5.1	9.1	12.354	7.65
***p*-xylene**	methyl ethyl ketone (MEK)	0	100	16	9	5.1	9	12.354	7.65
isopropyl ether	methyl ethyl ketone (MEK)	0	100	16	9	5.1	6.4	12.354	7.65
diethyl ether	methyl ethyl ketone (MEK)	0	100	16	9	5.1	6.8	12.354	7.65
carbon tetrachloride (P By Group Cont.)	methyl ethyl ketone (MEK)	0	100	16	9	5.1	5.2	12.354	7.65
***n*-hexane**	methyl ethyl ketone (MEK)	0	100	16	9	5.1	10.6	12.354	7.65
***n*-pentane**	methyl ethyl ketone (MEK)	0	100	16	9	5.1	10.8	12.354	7.65
benzene	methyl ethyl ketone (MEK)	0	100	16	9	5.1	10.7	12.354	7.65
***n*-heptane**	methyl ethyl ketone (MEK)	0	100	16	9	5.1	10.4	12.354	7.65

carbon tetrachloride (0 Dipole Moment)	methyl ethyl ketone (MEK)	0	100	16	9	5.1	10.7	12.354	7.65
triethylamine	methyl ethyl ketone (MEK)	0	100	16	9	5.1	9.6	12.354	7.65
cyclohexane	methyl ethyl ketone (MEK)	0	100	16	9	5.1	10.4	12.354	7.65
methyl ethyl ketone (MEK)	ethyl acetate	99	1	16	9	5.1	4.3	12.359	7.65
methyl ethyl ketone (MEK)	chloroform	99	1	16	8.9	5.1	6.9	12.363	7.72
methyl ethyl ketone (MEK)	chlorobenzene	99	1	16	9	5.1	8.2	12.373	7.65
methyl ethyl ketone (MEK)	*n*-butyl acetate	99	1	16	8.9	5.1	5.4	12.373	7.72
methyl ethyl ketone (MEK)	cyclopentyl methyl ether (Cpme)	99	1	16	9	5.1	5	12.377	7.65
methyl ethyl ketone (MEK)	methyl-*t*-butyl ether	99	1	16	9	5.1	5.3	12.389	7.65
ethylene dichloride	ethyl acetate	76	24	17.5	6.9	4.8	5.8	12.788	7.87
toluene	ethylene dichloride	0	100	18	7.4	4.1	6.4	12.861	7.42
***p*-xylene**	ethylene dichloride	0	100	18	7.4	4.1	6.5	12.861	7.42
isopropyl ether	ethylene dichloride	0	100	18	7.4	4.1	7.2	12.861	7.42
diethyl ether	ethylene dichloride	0	100	18	7.4	4.1	8.3	12.861	7.42
carbon tetrachloride (P By Group Cont.)	ethylene dichloride	0	100	18	7.4	4.1	5.7	12.861	7.42
***n*-hexane**	ethylene dichloride	0	100	18	7.4	4.1	10.5	12.861	7.42
***n*-pentane**	ethylene dichloride	0	100	18	7.4	4.1	11	12.861	7.42
benzene	ethylene dichloride	0	100	18	7.4	4.1	7.7	12.861	7.42
***n*-heptane**	ethylene dichloride	0	100	18	7.4	4.1	10	12.861	7.42
carbon tetrachloride (0 Dipole Moment)	ethylene dichloride	0	100	18	7.4	4.1	8.2	12.861	7.42
triethylamine	ethylene dichloride	0	100	18	7.4	4.1	9.1	12.861	7.42
cyclohexane	ethylene dichloride	0	100	18	7.4	4.1	8.7	12.861	7.42
ethylene dichloride	*n*-butyl acetate	99	1	18	7.4	4.1	6.2	12.872	7.42
ethylene dichloride	chloroform	99	1	18	7.4	4.1	4.6	12.875	7.42
ethylene dichloride	methyl-*t*-butyl ether	99	1	18	7.4	4.1	7.2	12.881	7.42
ethylene dichloride	cyclopentyl methyl ether (Cpme)	99	1	18	7.4	4.1	4.1	12.882	7.42
ethylene dichloride	chlorobenzene	99	1	18	7.4	4.1	4.2	12.894	7.42

toluene	ethyl acetate	0	100	15.8	5.3	7.2	7.8	13.528	10.46
***p*-xylene**	ethyl acetate	0	100	15.8	5.3	7.2	7.2	13.528	10.46
isopropyl ether	ethyl acetate	0	100	15.8	5.3	7.2	4.7	13.528	10.46
diethyl ether	ethyl acetate	0	100	15.8	5.3	7.2	4.4	13.528	10.46
carbon tetrachloride (P By Group Cont.)	ethyl acetate	0	100	15.8	5.3	7.2	7.8	13.528	10.46
***n*-hexane**	ethyl acetate	0	100	15.8	5.3	7.2	9.1	13.528	10.46
***n*-pentane**	ethyl acetate	0	100	15.8	5.3	7.2	9.3	13.528	10.46
benzene	ethyl acetate	0	100	15.8	5.3	7.2	9.1	13.528	10.46
***n*-heptane**	ethyl acetate	0	100	15.8	5.3	7.2	9	13.528	10.46
carbon tetrachloride (0 Dipole Moment)	ethyl acetate	0	100	15.8	5.3	7.2	9.4	13.528	10.46
triethylamine	ethyl acetate	0	100	15.8	5.3	7.2	7.9	13.528	10.46
cyclohexane	ethyl acetate	0	100	15.8	5.3	7.2	9	13.528	10.46
ethyl acetate	chlorobenzene	99	1	15.8	5.3	7.1	8.3	13.534	10.46
ethyl acetate	chloroform	99	1	15.8	5.3	7.2	4.8	13.534	10.46
ethyl acetate	cyclopentyl methyl ether (Cpme)	99	1	15.8	5.3	7.2	3.6	13.542	10.46
ethyl acetate	*n*-butyl acetate	99	1	15.8	5.3	7.2	1.8	13.544	10.46
ethyl acetate	methyl-*t*-butyl ether	99	1	15.8	5.3	7.2	3.1	13.556	10.46
***n*-butyl acetate**	chloroform	26	74	17.3	3.3	5.9	4.1	14.884	11.14
carbon tetrachloride (P By Group Cont.)	chloroform	11	89	17.6	3.7	5.1	8.4	14.894	10.74
toluene	chloroform	0	100	17.8	3.1	5.7	4.1	14.922	11.15
***p*-xylene**	chloroform	0	100	17.8	3.1	5.7	3.3	14.922	11.15
isopropyl ether	chloroform	0	100	17.8	3.1	5.7	6	14.922	11.15
diethyl ether	chloroform	0	100	17.8	3.1	5.7	6.7	14.922	11.15
***n*-hexane**	chloroform	0	100	17.8	3.1	5.7	8.7	14.922	11.15
***n*-pentane**	chloroform	0	100	17.8	3.1	5.7	9.3	14.922	11.15
benzene	chloroform	0	100	17.8	3.1	5.7	5	14.922	11.15
***n*-heptane**	chloroform	0	100	17.8	3.1	5.7	8.2	14.922	11.15

carbon tetrachloride (0 Dipole Moment)	chloroform	0	100	17.8	3.1	5.7	6	14.922	11.15
triethylamine	chloroform	0	100	17.8	3.1	5.7	7.1	14.922	11.15
cyclohexane	chloroform	0	100	17.8	3.1	5.7	6.6	14.922	11.15
cyclopentyl methyl ether (Cpme)	chloroform	0	100	17.8	3.1	5.7	2.9	14.922	11.15
methyl-*t*-butyl ether	chloroform	0	100	17.8	3.1	5.7	6.2	14.922	11.15
chlorobenzene	chloroform	0	100	17.8	3.1	5.7	4.6	14.922	11.15
***n*-butyl acetate**	chlorobenzene	81	19	16.4	3.8	5.5	7.7	15.117	11.32
carbon tetrachloride (P By Group Cont.)	*n*-butyl acetate	11	89	15.8	4.2	5.6	7.8	15.163	11.50
cyclopentyl methyl ether (Cpme)	*n*-butyl acetate	25	75	16	3.9	5.8	2.8	15.172	11.54
toluene	*n*-butyl acetate	0	100	15.8	3.7	6.3	6.6	15.187	11.85
***p*-xylene**	*n*-butyl acetate	0	100	15.8	3.7	6.3	5.8	15.187	11.85
isopropyl ether	*n*-butyl acetate	0	100	15.8	3.7	6.3	3.4	15.187	11.85
diethyl ether	*n*-butyl acetate	0	100	15.8	3.7	6.3	3.2	15.187	11.85
***n*-hexane**	*n*-butyl acetate	0	100	15.8	3.7	6.3	7.5	15.187	11.85
***n*-pentane**	*n*-butyl acetate	0	100	15.8	3.7	6.3	7.8	15.187	11.85
benzene	*n*-butyl acetate	0	100	15.8	3.7	6.3	7.7	15.187	11.85
***n*-heptane**	*n*-butyl acetate	0	100	15.8	3.7	6.3	7.4	15.187	11.85
carbon tetrachloride (0 Dipole Moment)	*n*-butyl acetate	0	100	15.8	3.7	6.3	7.9	15.187	11.85
triethylamine	*n*-butyl acetate	0	100	15.8	3.7	6.3	6.3	15.187	11.85
cyclohexane	*n*-butyl acetate	0	100	15.8	3.7	6.3	7.4	15.187	11.85
methyl-*t*-butyl ether	*n*-butyl acetate	0	100	15.8	3.7	6.3	2.5	15.187	11.85
toluene	cyclopentyl methyl ether (Cpme)	0	100	16.7	4.3	4.3	4.5	15.312	10.89
***p*-xylene**	cyclopentyl methyl ether (Cpme)	0	100	16.7	4.3	4.3	4.1	15.312	10.89
isopropyl ether	cyclopentyl methyl ether (Cpme)	0	100	16.7	4.3	4.3	3.6	15.312	10.89
diethyl ether	cyclopentyl methyl ether (Cpme)	0	100	16.7	4.3	4.3	4.6	15.312	10.89
carbon tetrachloride (P By Group Cont.)	cyclopentyl methyl ether (Cpme)	0	100	16.7	4.3	4.3	6	15.312	10.89

***n*-hexane**	cyclopentyl methyl ether (Cpme)	0	100	16.7	4.3	4.3	7.1	15.312	10.89
***n*-pentane**	cyclopentyl methyl ether (Cpme)	0	100	16.7	4.3	4.3	7.5	15.312	10.89
benzene	cyclopentyl methyl ether (Cpme)	0	100	16.7	4.3	4.3	5.9	15.312	10.89
***n*-heptane**	cyclopentyl methyl ether (Cpme)	0	100	16.7	4.3	4.3	6.7	15.312	10.89
carbon tetrachloride (0 Dipole Moment)	cyclopentyl methyl ether (Cpme)	0	100	16.7	4.3	4.3	6.1	15.312	10.89
triethylamine	cyclopentyl methyl ether (Cpme)	0	100	16.7	4.3	4.3	5.6	15.312	10.89
cyclohexane	cyclopentyl methyl ether (Cpme)	0	100	16.7	4.3	4.3	5.9	15.312	10.89
cyclopentyl methyl ether (Cpme)	chlorobenzene	99	1	16.7	4.3	4.3	5.1	15.314	10.89
cyclopentyl methyl ether (Cpme)	methyl-*t*-butyl ether	99	1	16.7	4.3	4.3	3.9	15.318	10.89
methyl-*t*-butyl ether	chlorobenzene	50	50	16.9	4.3	3.5	8.9	15.74	10.99
carbon tetrachloride (P By Group Cont.)	chlorobenzene	40	60	17.8	5.9	1.2	7.3	16.099	10.24
carbon tetrachloride (P By Group Cont.)	methyl-*t*-butyl ether	39	61	15.3	5.9	3.1	6.9	16.136	11.34
diethyl ether	chlorobenzene	22	78	18	4	2.6	9.5	16.227	11.10
isopropyl ether	chlorobenzene	9	91	18.6	4.2	2.1	8	16.349	11.05
toluene	methyl-*t*-butyl ether	0	100	14.8	4.3	5	7.6	16.354	12.64
***p*-xylene**	methyl-*t*-butyl ether	0	100	14.8	4.3	5	7.1	16.354	12.64
isopropyl ether	methyl-*t*-butyl ether	0	100	14.8	4.3	5	2.2	16.354	12.64
diethyl ether	methyl-*t*-butyl ether	0	100	14.8	4.3	5	1.6	16.354	12.64
***n*-hexane**	methyl-*t*-butyl ether	0	100	14.8	4.3	5	6.6	16.354	12.64
***n*-pentane**	methyl-*t*-butyl ether	0	100	14.8	4.3	5	6.6	16.354	12.64
benzene	methyl-*t*-butyl ether	0	100	14.8	4.3	5	8.9	16.354	12.64
***n*-heptane**	methyl-*t*-butyl ether	0	100	14.8	4.3	5	6.7	16.354	12.64
carbon tetrachloride (0 Dipole Moment)	methyl-*t*-butyl ether	0	100	14.8	4.3	5	8.6	16.354	12.64
triethylamine	methyl-*t*-butyl ether	0	100	14.8	4.3	5	5.8	16.354	12.64
cyclohexane	methyl-*t*-butyl ether	0	100	14.8	4.3	5	7.6	16.354	12.64

toluene	chlorobenzene	0	100	19	4.3	2	3.5	16.365	11.02
***p*-xylene**	chlorobenzene	0	100	19	4.3	2	4.2	16.365	11.02
***n*-hexane**	chlorobenzene	0	100	19	4.3	2	9.5	16.365	11.02
***n*-pentane**	chlorobenzene	0	100	19	4.3	2	10.2	16.365	11.02
benzene	chlorobenzene	0	100	19	4.3	2	4.5	16.365	11.02
***n*-heptane**	chlorobenzene	0	100	19	4.3	2	8.8	16.365	11.02
carbon tetrachloride (0 Dipole Moment)	chlorobenzene	0	100	19	4.3	2	5.1	16.365	11.02
triethylamine	chlorobenzene	0	100	19	4.3	2	8.1	16.365	11.02
cyclohexane	chlorobenzene	0	100	19	4.3	2	6.4	16.365	11.02
***p*-xylene**	carbon tetrachloride (P By Group Cont.)	16	84	16.4	7.1	0.5	8.6	16.627	10.66
diethyl ether	carbon tetrachloride (P By Group Cont.)	18	82	15.8	7.3	0.8	7.8	16.628	10.93
toluene	carbon tetrachloride (P By Group Cont.)	2	98	16.1	8.2	0	8.1	16.685	10.61
isopropyl ether	carbon tetrachloride (P By Group Cont.)	0	100	16.1	8.3	0	6.3	16.686	10.55
carbon tetrachloride (P By Group Cont.)	benzene	99	1	16.1	8.2	0	9.7	16.688	10.61
carbon tetrachloride (P By Group Cont.)	carbon tetrachloride (0 Dipole Moment)	99	1	16.1	8.2	0	9	16.704	10.61
carbon tetrachloride (P By Group Cont.)	triethylamine	99	1	16.1	8.2	0	8.1	16.714	10.61
carbon tetrachloride (P By Group Cont.)	cyclohexane	99	1	16.1	8.2	0	8.4	16.714	10.61
carbon tetrachloride (P By Group Cont.)	*n*-heptane	99	1	16.1	8.2	0	8.5	16.725	10.61
carbon tetrachloride (P By Group Cont.)	*n*-hexane	99	1	16.1	8.2	0	8.6	16.728	10.61
carbon tetrachloride (P By Group Cont.)	*n*-pentane	99	1	16.1	8.2	0	8.9	16.73	10.61
***p*-xylene**	diethyl ether	38	62	15.8	2.2	4	7	17.61	13.53
toluene	diethyl ether	29	71	15.5	2.5	3.8	7.6	17.679	13.59
***p*-xylene**	isopropyl ether	37	63	16.1	2.4	3.2	5.8	17.754	13.33
diethyl ether	benzene	92	8	14.8	2.7	4.4	8.7	17.801	14.01
isopropyl ether	diethyl ether	16	84	14.6	2.9	4.4	1.9	17.813	14.08

diethyl ether	carbon tetrachloride (0 Dipole Moment)	99	1	14.5	2.9	4.6	8.2	17.826	14.16
toluene	isopropyl ether	21	79	15.7	2.8	2.9	6.2	17.834	13.41
diethyl ether	cyclohexane	99	1	14.5	2.9	4.6	7	17.838	14.16
diethyl ether	triethylamine	99	1	14.5	2.9	4.6	4.8	17.843	14.16
diethyl ether	*n*-heptane	99	1	14.5	2.9	4.6	5.7	17.853	14.16
diethyl ether	*n*-hexane	99	1	14.5	2.9	4.6	5.5	17.857	14.16
diethyl ether	*n*-pentane	99	1	14.5	2.9	4.6	5.4	17.861	14.16
isopropyl ether	benzene	99	1	15.1	3.2	3.2	7.4	17.884	13.58
isopropyl ether	carbon tetrachloride (0 Dipole Moment)	99	1	15.1	3.2	3.2	6.8	17.897	13.58
isopropyl ether	cyclohexane	99	1	15.1	3.2	3.2	5.5	17.908	13.58
isopropyl ether	triethylamine	99	1	15.1	3.2	3.2	3.6	17.911	13.58
isopropyl ether	*n*-heptane	99	1	15.1	3.2	3.2	4.5	17.921	13.58
isopropyl ether	*n*-hexane	99	1	15.1	3.2	3.2	4.5	17.925	13.58
isopropyl ether	*n*-pentane	99	1	15.1	3.2	3.2	4.7	17.928	13.58
toluene	*p*-xylene	0	100	17.8	1	3.1	1.2	18.134	13.75
***p*-xylene**	benzene	99	1	17.8	1	3.1	1.9	18.147	13.75
***p*-xylene**	triethylamine	99	1	17.8	1	3.1	5.1	18.157	13.75
***p*-xylene**	carbon tetrachloride (0 Dipole Moment)	99	1	17.8	1	3.1	2.7	18.157	13.75
***p*-xylene**	cyclohexane	99	1	17.8	1	3.1	3.7	18.162	13.75
***p*-xylene**	*n*-heptane	99	1	17.8	1	3.1	6	18.167	13.75
***p*-xylene**	*n*-hexane	99	1	17.8	1	3.1	6.7	18.168	13.75
***p*-xylene**	*n*-pentane	99	1	17.8	1	3.1	7.4	18.168	13.75
toluene	benzene	99	1	18	1.4	2	1.6	18.499	13.70
toluene	triethylamine	99	1	18	1.4	2	5.2	18.507	13.70
toluene	carbon tetrachloride (0 Dipole Moment)	99	1	18	1.4	2	2	18.509	13.70
toluene	cyclohexane	99	1	18	1.4	2	3.3	18.513	13.70

toluene	*n*-heptane	99	1	18	1.4	2	5.9	18.517	13.70
toluene	*n*-hexane	99	1	18	1.4	2	6.7	18.518	13.70
toluene	*n*-pentane	99	1	18	1.4	2	7.4	18.519	13.70
***n*-hexane**	benzene	0	100	18.4	0	2	7.3	19.507	14.95
***n*-pentane**	benzene	0	100	18.4	0	2	8.1	19.507	14.95
benzene	triethylamine	99	1	18.4	0	2	5.9	19.513	14.95
benzene	carbon tetrachloride (0 Dipole Moment)	99	1	18.4	0	2	1.8	19.516	14.95
benzene	cyclohexane	99	1	18.4	0	2	3.7	19.52	14.95
benzene	*n*-heptane	99	1	18.4	0	2	6.5	19.522	14.95
carbon tetrachloride (0 Dipole Moment)	triethylamine	89	11	17.5	0	0.6	4.6	20.488	15.66
***n*-hexane**	carbon tetrachloride (0 Dipole Moment)	0	100	17.8	0	0.6	5.8	20.494	15.58
***n*-pentane**	carbon tetrachloride (0 Dipole Moment)	0	100	17.8	0	0.6	6.6	20.494	15.58
***n*-heptane**	carbon tetrachloride (0 Dipole Moment)	0	100	17.8	0	0.6	5	20.494	15.58
carbon tetrachloride (0 Dipole Moment)	cyclohexane	99	1	17.8	0	0.6	2	20.499	15.58
triethylamine	cyclohexane	91	9	15.6	0.4	0.9	2.7	20.899	16.22
***n*-hexane**	triethylamine	0	100	15.5	0.4	1	1.6	20.901	16.26
***n*-pentane**	triethylamine	0	100	15.5	0.4	1	2.3	20.901	16.26
***n*-heptane**	triethylamine	0	100	15.5	0.4	1	1.1	20.901	16.26
***n*-hexane**	cyclohexane	0	100	16.8	0	0.2	3.8	21.049	16.11
***n*-pentane**	cyclohexane	0	100	16.8	0	0.2	4.6	21.049	16.11
***n*-heptane**	cyclohexane	0	100	16.8	0	0.2	3	21.049	16.11
***n*-hexane**	*n*-heptane	0	100	15.3	0	0	0.8	21.947	17.15
***n*-pentane**	*n*-heptane	0	100	15.3	0	0	1.6	21.947	17.15
***n*-hexane**	*n*-pentane	99	1	14.9	0	0	0.8	22.218	17.48

Appendix 5 ^{1}H-NMR spectrum of CMF (38) obtained using a DCM:DCE (1:1) organic solvent blend in microwave reaction

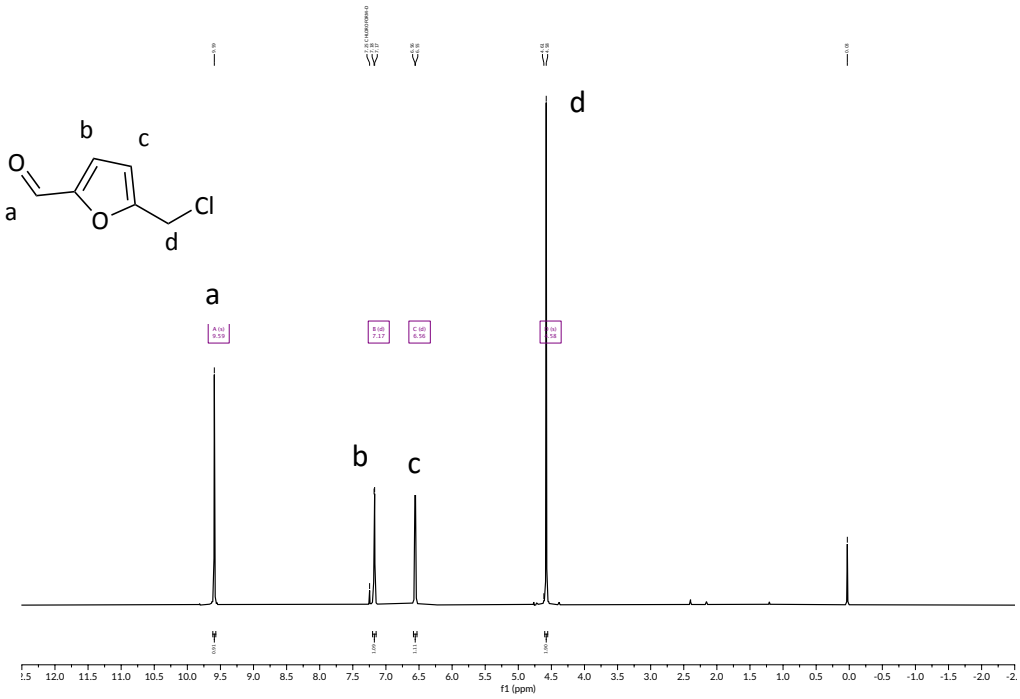

Fructose (250 mg), DCM:DCE (1:1, 10 mL), 37% HCl (5 mL), 80 °C 15 min, 1H-NMR (400 MHz, [CDCl3]): δ (ppm) 9.64 (s, 1H, ClCH2-(C4H2O)-CHO), 7.20 (d, *J* = 3.6 Hz, 1H, ClCH2-(COCHC2H)-CHO), 6.59 (d, *J* = 3.6 Hz, 1H, CHO-(C2HCHOC)-CH2Cl), 4.61 (s, 2H, - ClCH2-(C4H2O)-CHO).

Appendix 6 Computed (blue lines) and experimental (black dotted lines) spectra of selected bio-derived UV filter candidates.

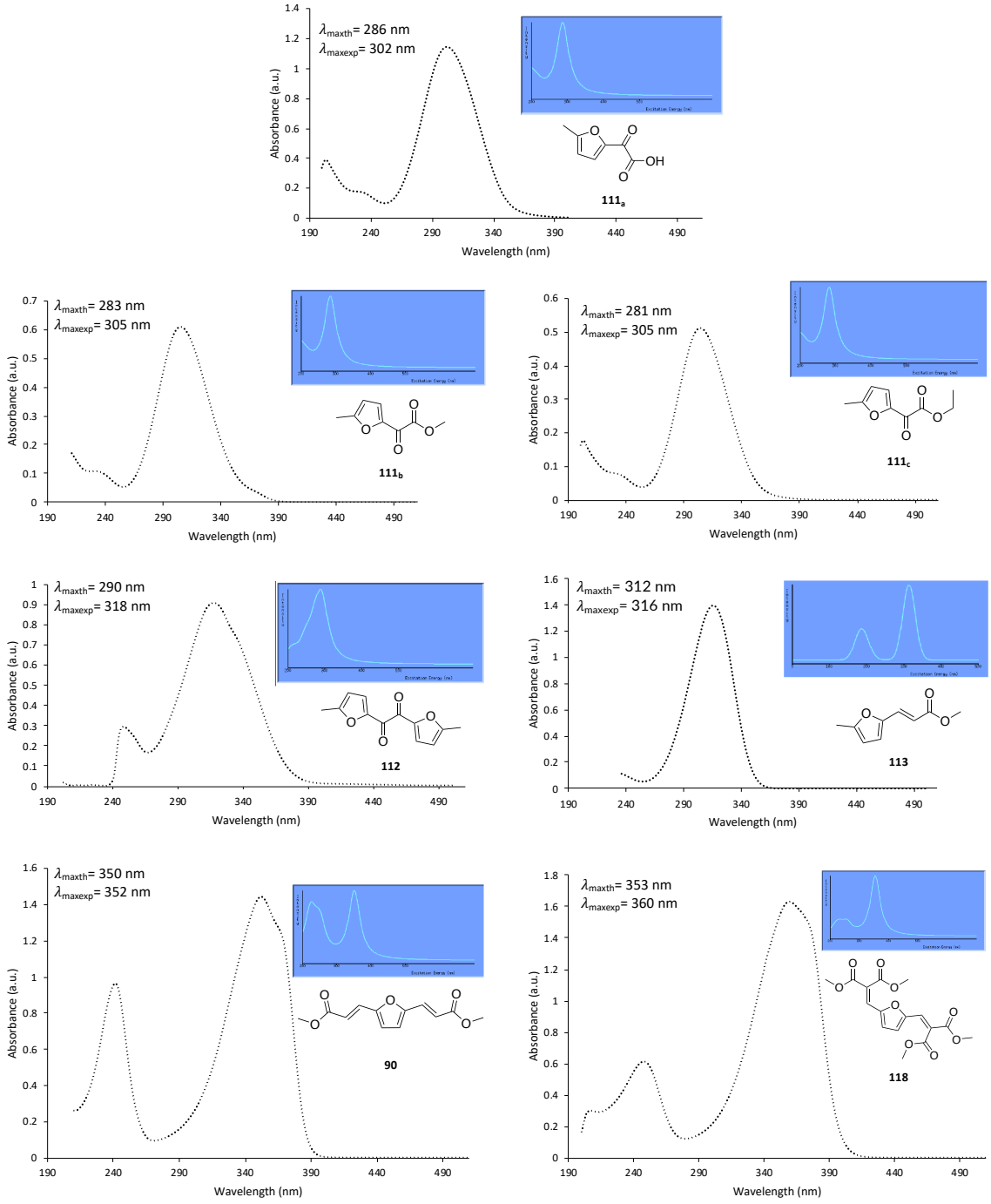

Appendix 7 Formulation used for the testing of UV-filter candidates.

Trade name	*INCI (includes)*	Compound **114** formulation
Amphisol K	*potassium cetyl phosphate*	1.80
Cutina GMS	*glyceryl stearate*	2.50
Lanette 18	*stearyl alcohol*	2.50
Myritol 318	*caprylic/capric triglyceride*	5.00
Cetiol AB	*c12-15 alkyl benzoate*	10.00
Water	***aqua***	**68.10**
1,2 Propane diol	*1-2 propane diol*	2.00
Rheocare XGN	*xanthan gum*	0.30
water		
Cetiol Ultimate	*undecane (and) tridecane*	5.00
Phenonip	*phenoxyethanol (and) methylparaben (and) ethylparaben (and) propylparaben (and) butylparaben (and) isobutylparaben*	0.80
NaOH solution 30%		If needed for neutralisation
TEA	*triethanolamine*	

Appendix 8 EDX-SEM images and XRD analysis for MnO_2 88% after reaction in TMO pre-calcination

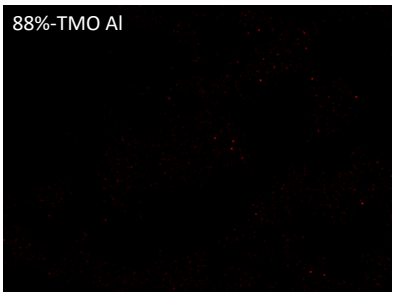

No Cl Detected

No Na Detected

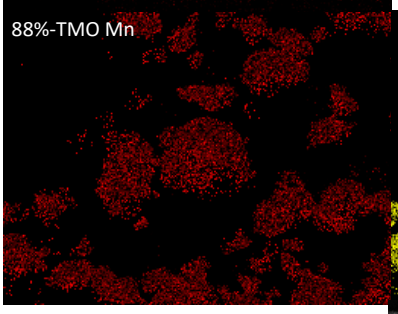

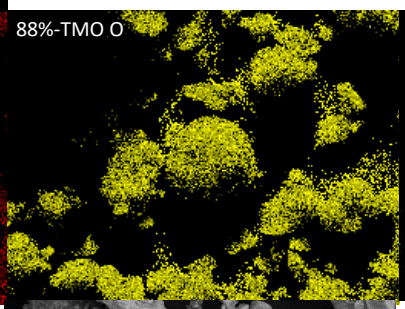

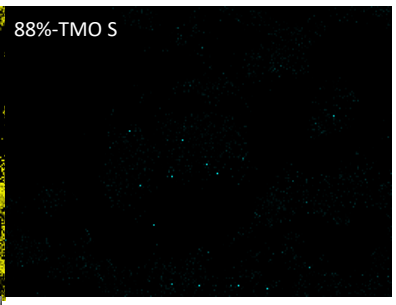

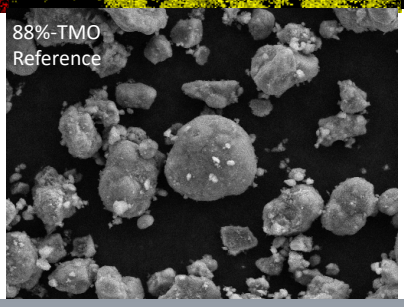

No Si Detected

Element	Base(1)		
	Net Counts	Weight %	Atom %
O K	44221	21.40	48.07
Al K	1205	0.53	0.71
S K	856	0.31	0.35
Mn K	63229	77.75	50.87
		100.00	100.00

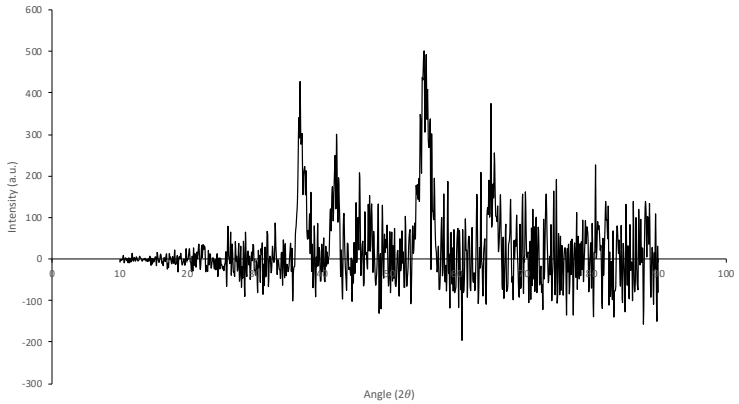

Appendix 8 (suite) EDX-SEM images and XRD analysis for MnO_2 88% after reaction in TMO post-calcination

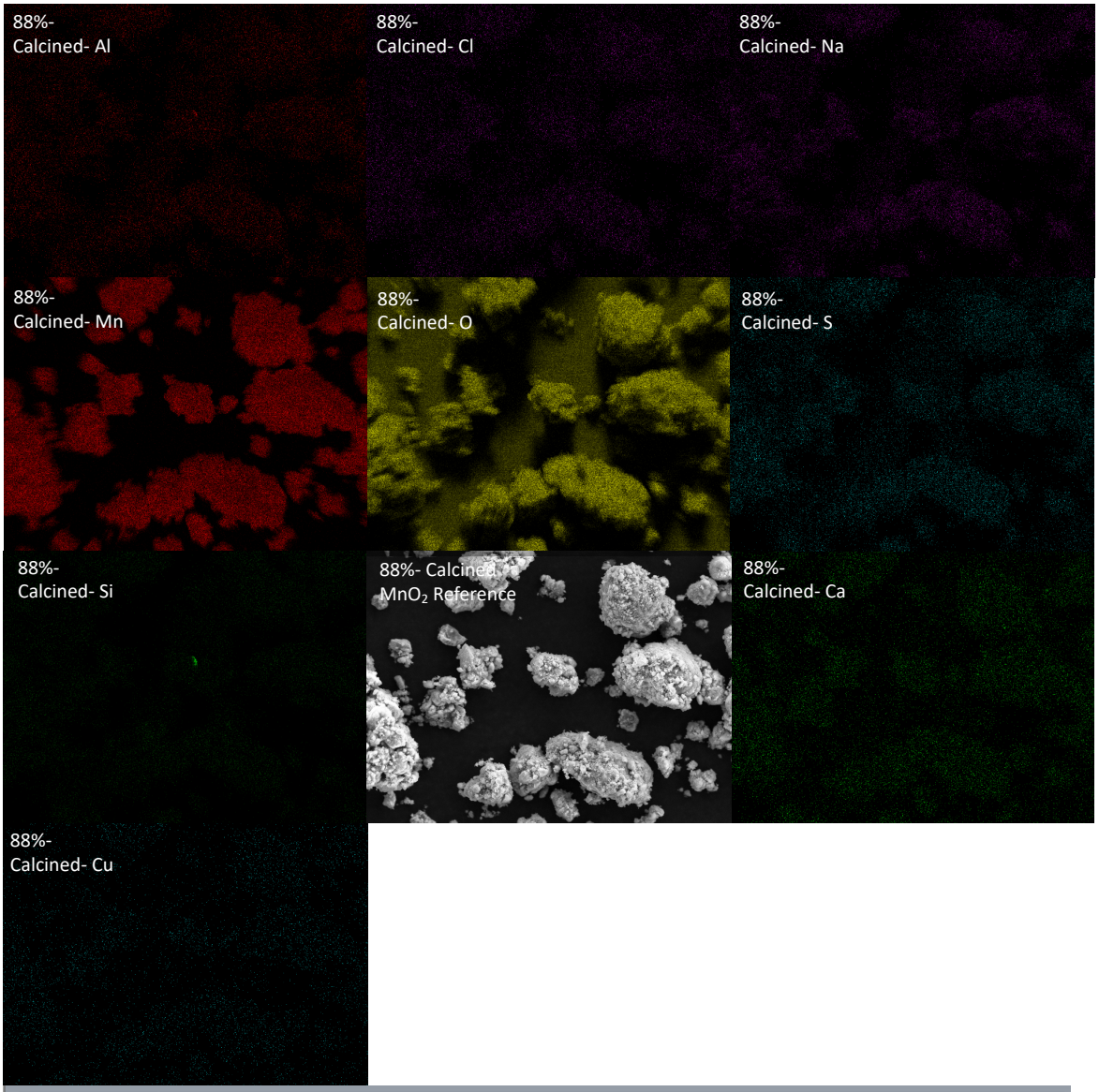

Element	expst(22)		
	Net Counts	Weight %	Atom %
O K	552833	18.96	44.14
Na K	4374	0.34	0.54
Al K	13348	0.41	0.57
Si K	6785	0.18	0.24
S K	11438	0.29	0.34
Cl K	1975	0.05	0.06
Ca K	5244	0.18	0.16
Mn K	933938	79.40	53.84
Cu K	900	0.19	0.11
		100.00	100.00

Appendix 9 Complete data of the enzymatically catalysed reactions in DPE (computed by Dr. Alessandro Pellis)

	^{1}H-NMR		Isolated yield [%][3]	GPC		
Diol	Monomers conversion [%][1]	Monomers conversion [%][2]		M_n [Da]	M_w [Da]	Đ
BDO	85	82	74	1300	3300	2.53
	86	86	75	1300	3300	2.48
ODO	97	97	89	3600	25700	5.95
	97	97	91	3500	22100	6.35
ODO[a]	88	89	71	3000	6600	2.16
CHDM	94	92	82	1600	5000	3.19
	93	92	77	1800	5100	2.80

[a] reaction conducted using double the reagent's concentration (0.4 M instead of 0.2 M).
[1] calculated from ^{1}H-NMR based on the diol component.
[2] calculated from ^{1}H-NMR based on the diester component.
[3] calculated after MeOH precipitation and three washing steps.

Appendix 10 Complete TGA analysis results for enzymatically-catalysed polymers

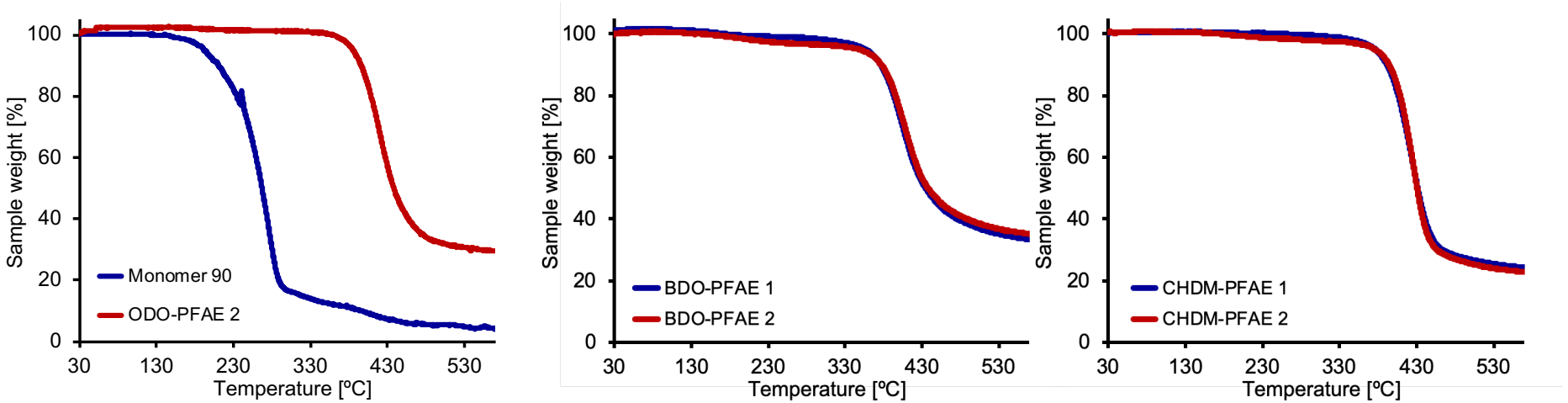

Diester	Diol	T_d5 (%)	T_d10 (%)	T_d50 (%)	Residue at 625 °C
90		192	211	267	3
90	BDO	356	376	435	32
		349	377	438	34
	ODO	382	389	434	13
		385	396	438	29
	ODO[a]	270	379	422	10
	CHDM	376	392	431	23
		375	394	430	22

[a] *reaction conducted using double the reagent's concentration (0.4 M instead of 0.2 M).*

Analysis performed by Dr. Alessandro Pellis

Appendix 11 Results of the DSC analysis for the different enzymatically-catalysed polyesters (top) and ODO-PFAE (91) after 6 cycles (bottom)

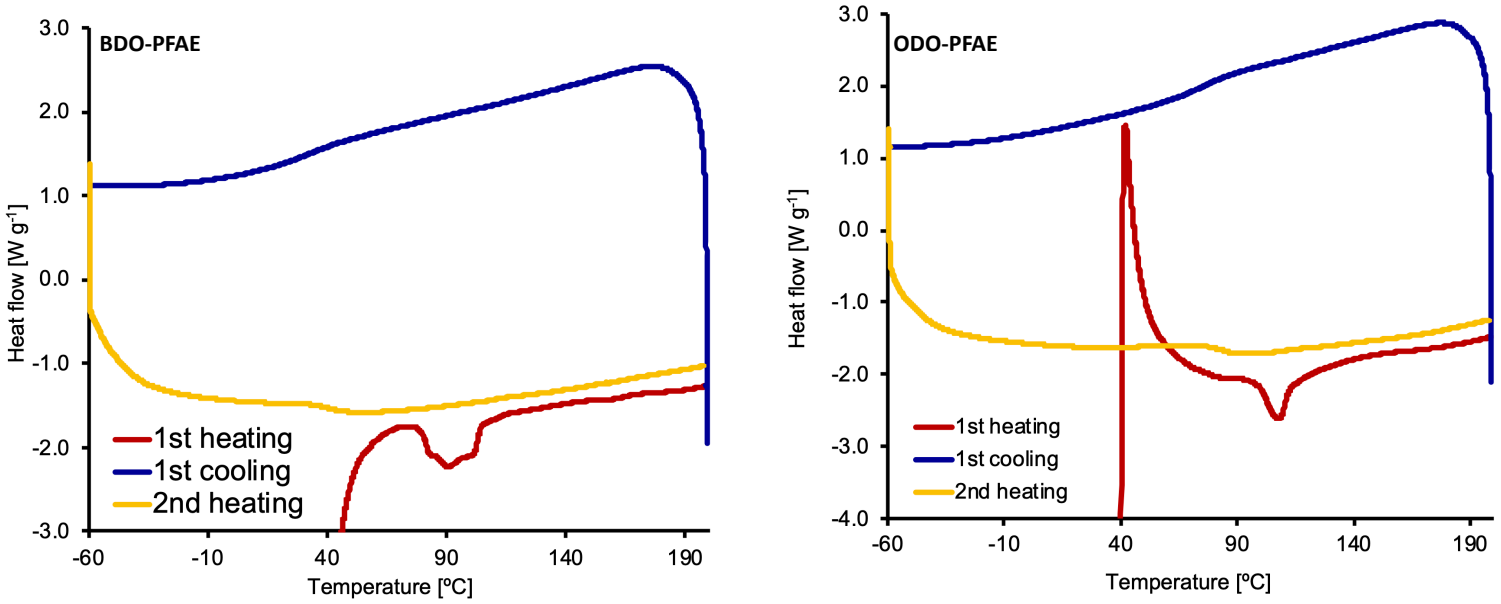

Diester	Diol	T_{m1} (°C)	T_g (°C)			ΔCp J/(g.°C^{-1})
90	BDO	101	35	47	39	0.17
		100	31	42	37	0.16
	ODO	59	16	23	19	0.18
		61	23	30	28	0.19
	ODO[a]	54	-3	2	-2	0.28
	CHDM	108	78	88	84	0.17
		107	75	81	80	0.05

Analysis performed by Dr. Alessandro Pellis

Appendix 11 (suite) Results of the DSC analysis for the ODO-PFAE after 6 cycles

Heating cycle	T_g (°C)			ΔCp J/(g.°C^{-1})
2nd	23	30	28	0.19
3rd	25	33	29	0.18
4th	26	34	31	0.15
5th	28	36	33	0.13
6th	29	37	34	0.13

Analysis performed by Dr. Alessandro Pellis

Appendix 12 MALDI-TOF analysis results for enzyme-catalysed polymer: ODO-PFAE (91)

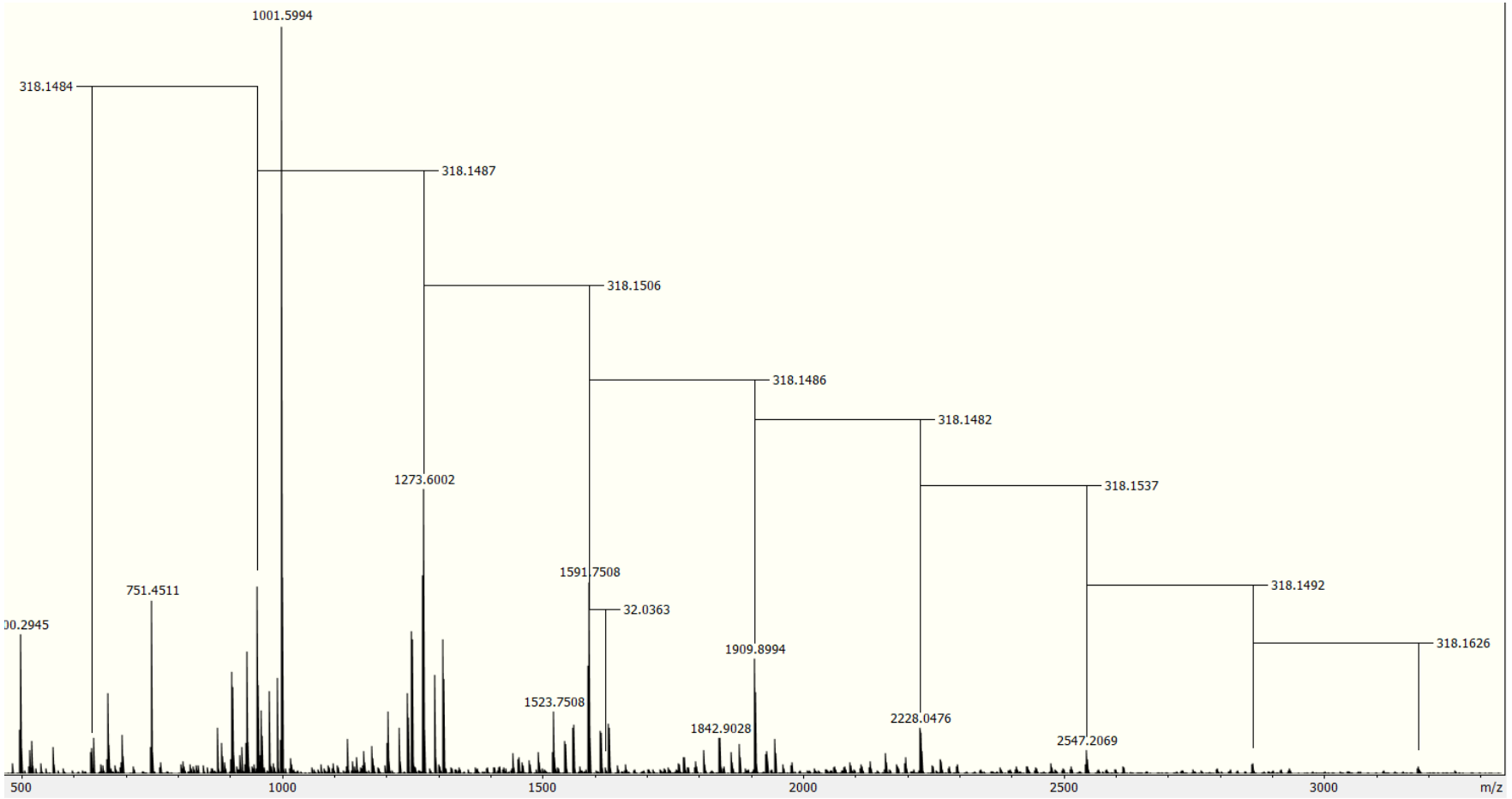

MALDI analysis of ODO-PFAE and assignment of the main repetitive unit, Analysis performed by Dr. Alessandro Pellis

Appendix 12 (suite) MALDI-TOF analysis results for enzyme-catalysed polymer: BDO-PFAE

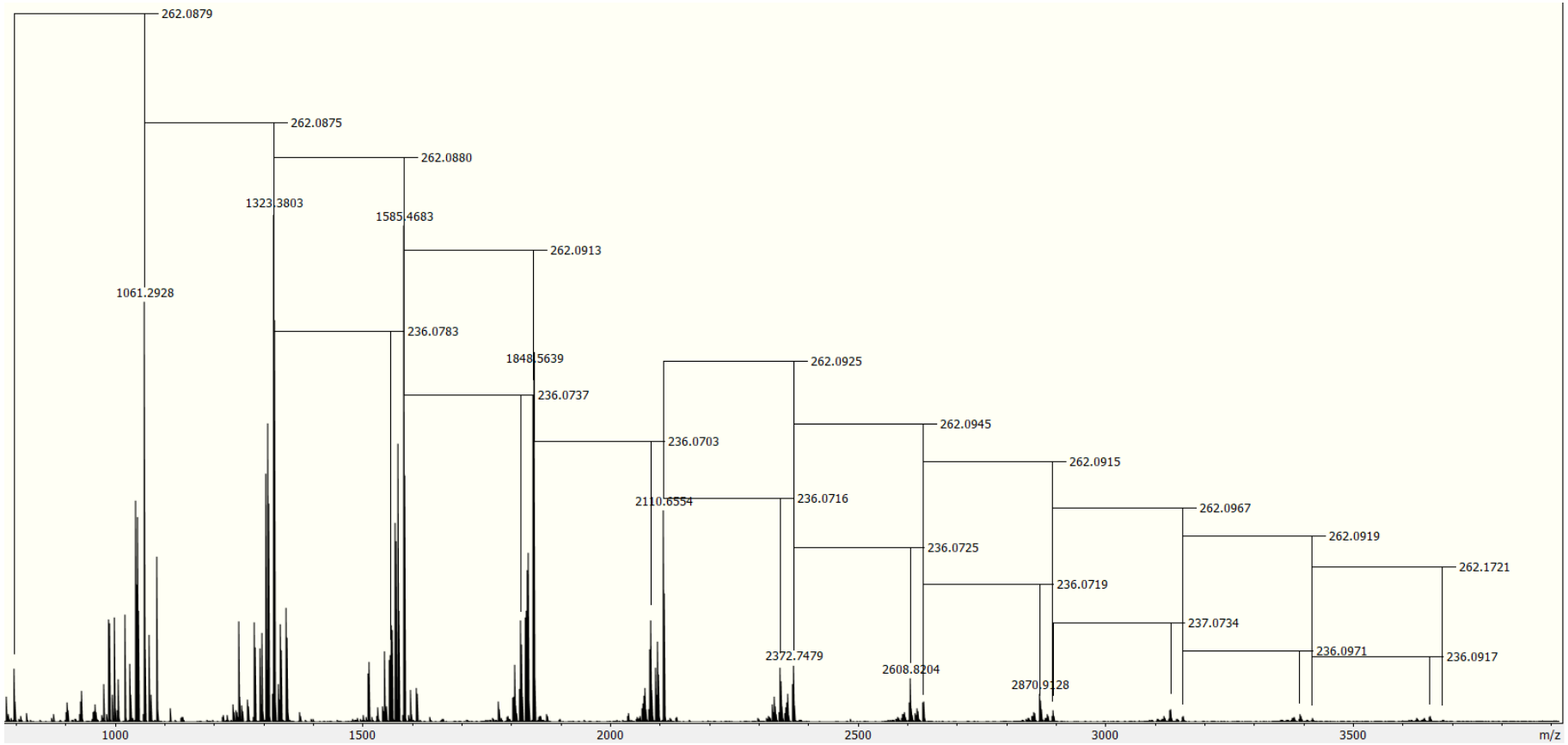

Analysis performed by Dr. Alessandro Pellis

Appendix 12 (suite) MALDI-TOF analysis results for enzyme-catalysed polymer: CHDM-PFAE

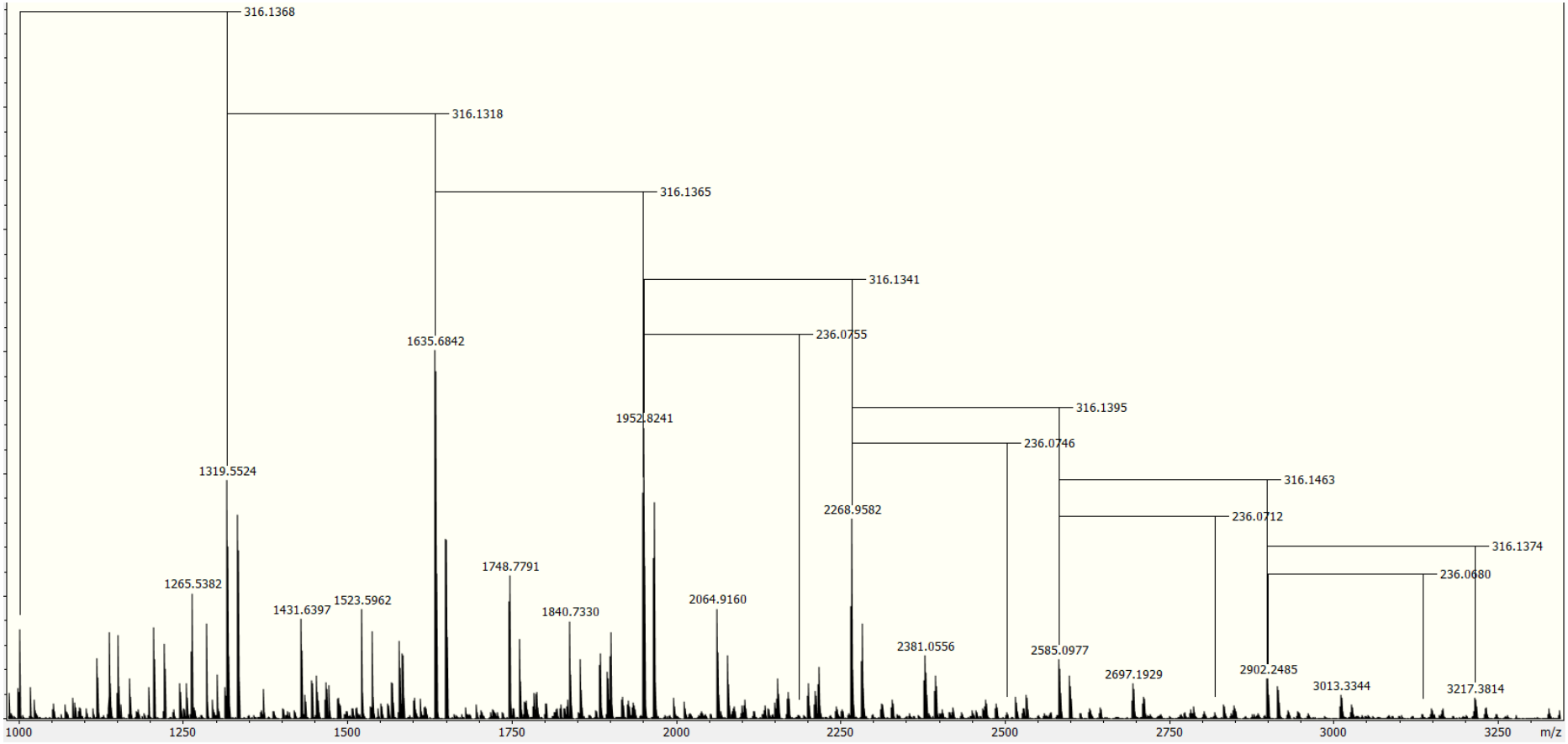

Analysis performed by Dr. Alessandro Pellis

Appendix 13 Grignard reaction optimisation using non-commercial long chain bromo-derivatives

Alkyl halide	Solvent	Mg : alkyl halide molar ratio	Magnesium activation conditions	Alkyl halide : furfural molar ratio	Furfural addition conditions	Yield (%)	General observations
$C_{16}H_{33}-Br$	2-MeTHF (Grignard formation)/THF (furfural solution)	2.5:1	- Iodine crystals (1-2) - vigorous stirring for 60 hours then 50 °C heating for 24 hours	1.1:1	- 0 °C upon addition - room temperature overnight (16 hours)	-	Activation of the magnesium was not successful (persistent yellow colouration)
	THF	3:1	- 1,2-dribromoethane (30 drops) - Reflux 4 hours	1.1:1	- 0 °C upon addition - room temperature (4 h, reaction stopped)	-	No conversion was observed by TLC (confirmed by ^{1}H-NMR spectroscopy)
	THF	3:1	- 1,2-dribromoethane (30 drops) - Reflux overnight	2:1 (HMF)	- 0 °C upon addition - room temperature (50 min)	-	No conversion using HMF as reagent
	THF	3:1	- 1,2-dribromoethane (0.8 mL) until reflux - Addition of alkyl halide to maintain reflux then refluxed for 1 h.	1.1:1	- 0 °C upon addition (furfural solution) - room temperature (24 h)	9	Use of large amount of activating agent explains low yield. Presence of linear hexadecane confirmed by ^{1}H-NMR spectroscopy
	THF	3:1	- 1,2-dribromoethane (5-10 drops) - 5 mL THF	1.1:1	- 0 °C upon addition - room temperature overnight (16 hours)	-	Flame-dried glassware Activation unsuccessful
	THF	3:1	- 1,2-dibromoethane (200 μL) - 5 mL THF - Vigorous stirring for 2 h before alkyl halide addition	1.1:1	- 0 °C upon addition - room temperature overnight (16 hours)	34	Successful activation, less than 200 μL of activating was likely enough
	THF	3:1	- 1,2-dibromoethane (200 μL) - 5 mL THF - Vigorous stirring for 2 h before alkyl halide addition	1.1:1	- 0 °C upon addition - room temperature overnight (16 hours)	-	Reaction done under N_2 may have prevented successful activation, alkyl halide recovered

Alkyl halide	Solvent	Mg : alkyl halide molar ratio	Magnesium activation conditions	Alkyl halide : furfural molar ratio	Furfural addition conditions	Yield (%)	General observations
	THF	3:1	- 1,2-dibromoethane (200 μL) - 5 mL THF - Vigorous stirring for 2 h before alkyl halide addition	1.1:1	- 0 °C upon addition - room temperature overnight (16 hours)	54	Reaction done under Ar, using freshly distilled furfural.
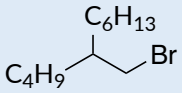	THF	6:1	- 1,2-dribromoethane (10 drops) added - Alkyl halide (5 mL 10 %w THF solution) to keep reflux	1.2:1	- room temperature addition - left overnight (16 h)	-	Addition of alkyl halide solution during Mg activation prevented good Grignard reagent formation
	THF	3:1	- 1,2-dibromoethane (200 μL) - 5 mL THF - Vigorous stirring for 2 h before alkyl halide addition	1.1:1	- room temperature addition - left overnight (16 h)	-	Alkyl halide recovered only. Probable unsuccessful activation
	THF	3:1	- 1,2-dibromoethane (100 μL) - 5 mL THF - Vigorous stirring for 2 h before alkyl halide addition	1.1:1	- room temperature addition - left overnight (16 h)	-	Unsuccessful activation
	Et_2O	3:1	- 1,2-dibromoethane (100 μL) - 5 mL THF Vigorous stirring for 2 h before alkyl halide addition	1.1:1	- room temperature addition - left overnight (16 h)	27	Use of Et_2O permitted effective Mg activation.

Appendix 14 C_{16} and C_{18} fatty acid profile of *Spirulina sp.*

	Otles *et al.* 2001			Diraman *et al* 2009							Ö. Tokus¸Oglu *et al* 2003		
Fatty acids	Spirulina platensis bio organic	Spirulina platensis-1	Spirulina platensis-2	Faculty of Fisheries	Bosdogan-1 Aydin	Seferihisar Izmir	Imported from china	Bosdogan-2 Aydin	EBILTEM Izmir	Menderes Izmir	Spirulina platensis-1	Spirulina platensis-2	Spirulina platensis-3
Palmitic	46.07	42.3	43.65	18.02	38.56	24.5	30.13	33.61	26.45	37.01	27.86	26.61	27.19
Palmitoleic	1.26	1	1.5	1.18	2.85	5.53	1.86	4.65	2.72	8.18	1.84	2.27	1.92
stearic	1.41	0.95	1.39	7.6	2.33	5.32	6.42	5.15	3.71	3.16	5.80	8.82	6.66
Oleic	5.23	1.97	2.05	5.82	2.52	20.35	5.95	6.55	2.93	4.74	32.86	34.71	35.74
linoleic	17.43	16.18	17.19	6.4	13.38	13.21	15.7	15.82	12.1	14.67	10.37	14.45	11.25
γ-Linoleic	8.87	20.06	21.73	4.07	22.51	7.12	14.65	19.15	10.77	18.91	4.60	3.64	5.52
Total fat	6.2	8.1	5.1	7.45	5.3	7.15	4.1	5.75	6.04	4.9	7.09	7.14	8.03

L Colla *et al* 2004								
Spiru platensis -1	Spiru platensis -2	Spiru platensis -3	Spiru platensis -4	Spiru platensis -5	Spiru platensis -6	Spiru platensis -7	Spiru platensis -8	Average all studies
45.92	44.89	45.97	44.59	45.78	48.27	45.57	45.31	37.54
2.74	2.54	1.67	1.81	2.83	2.46	2.12	2.01	2.62
0.89	0.95	0.9	0.86	1.57	0.91	1.09	1.24	3.20
7.77	8.57	6.84	8.56	9.29	7.5	8.34	8.02	10.78
11.95	11.93	12.29	12.73	13	12.3	14.54	14.68	13.41
20.63	20.1	20.38	20.92	18.51	18.34	19.53	19.51	15.22
								6.33
Average C_{16} fatty acids	40.15							
Average C_{18} fatty acids	42.60							

Appendix 15 FT-IR spectrum of the decarboxylation product obtained using L-aspartic acid as a starting material

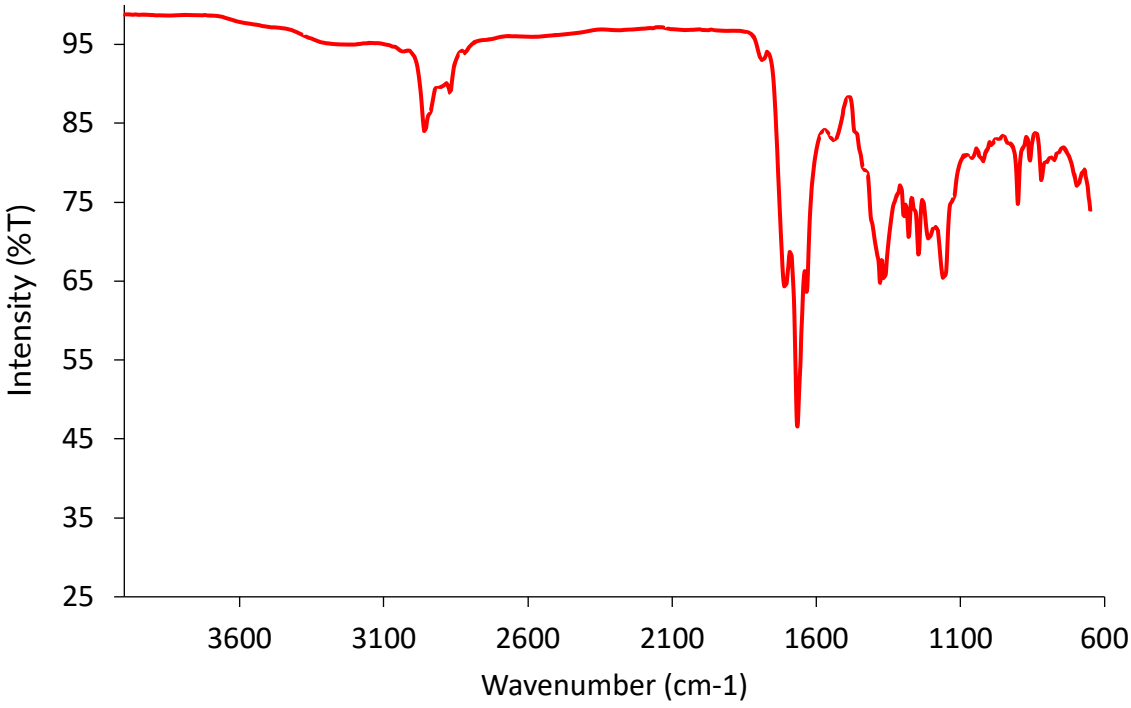

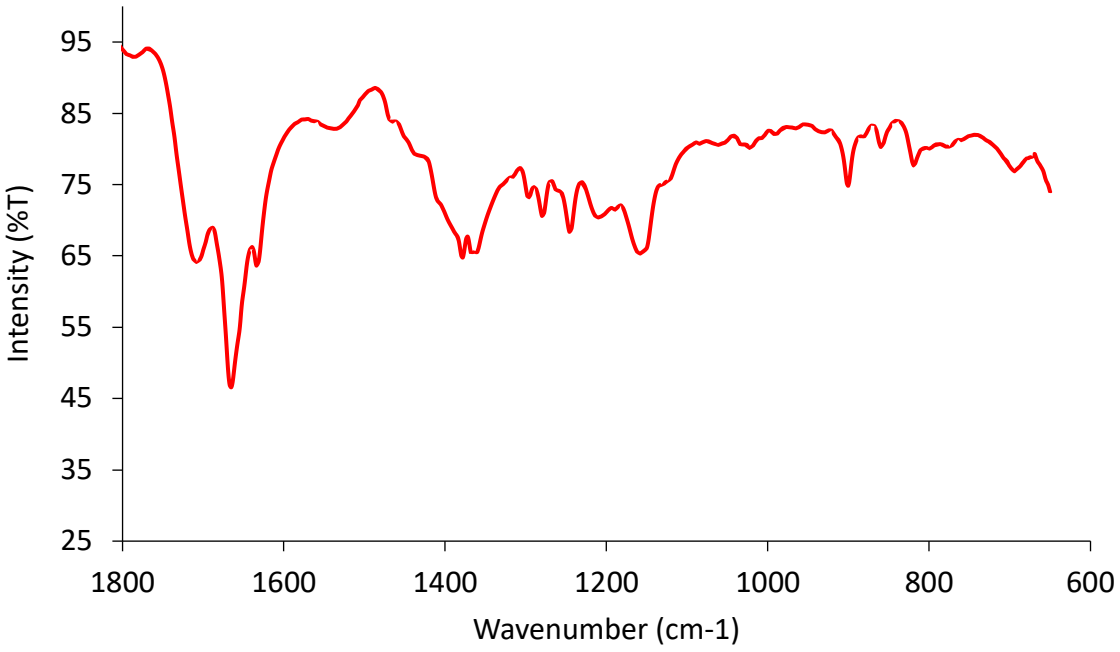

Appendix 16 MALDI-TOF analysis of PHU obtained with 1,5-pentanediamine (200)

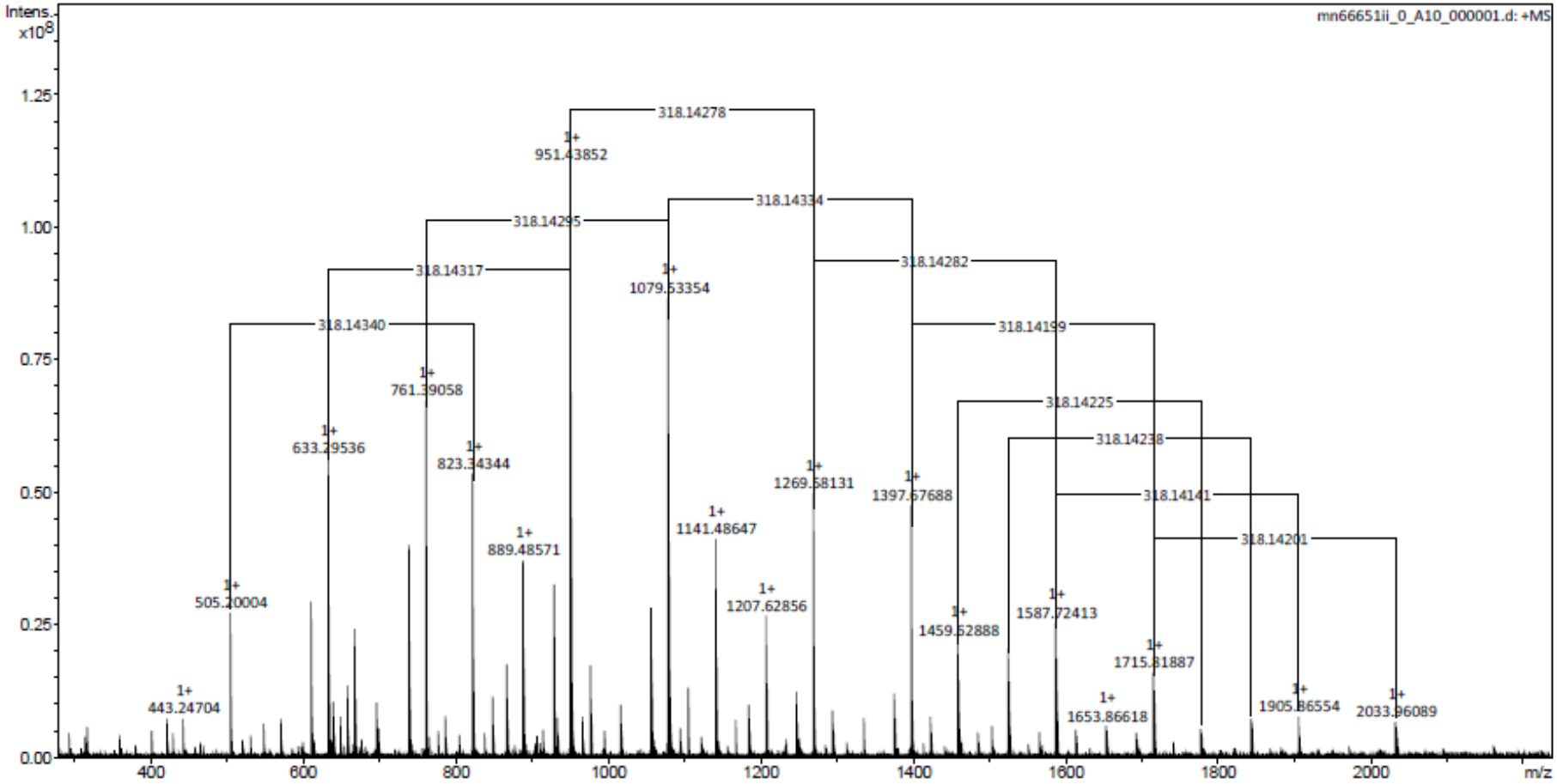

Analysis performed by Dr. Ian D. V. Ingram, Repeating unit m/z= 318.14

Appendix 17 DSC trace of PHU obtained from 198 and commercial 1,5-pentanediamine free base (200)

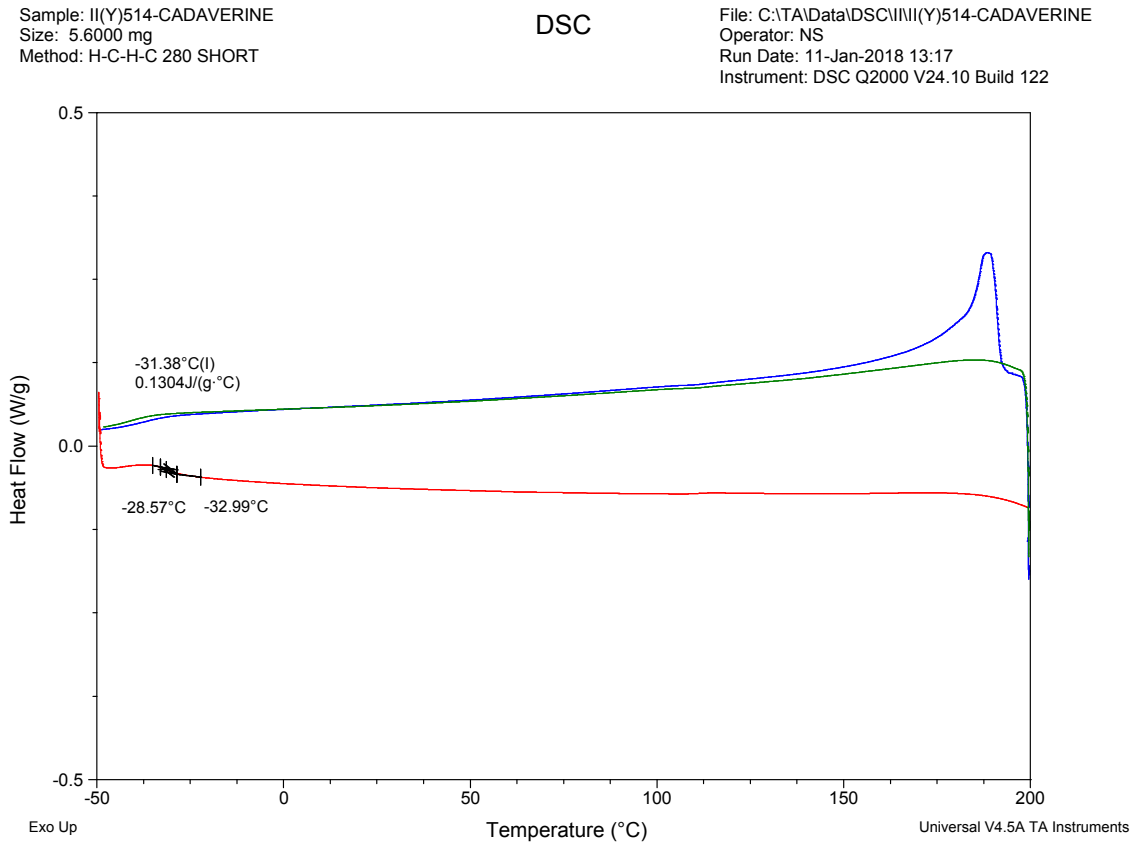

Analysis performed by Dr. Ian D. V. Ingram